

Advanced Textbooks in Control and Signal Processing

Nicola Mimmo

Analysis and Design of Control Laws for Advanced Driver-Assistance Systems

Theory and Applications



Springer

Advanced Textbooks in Control and Signal Processing

Series Editors

Michael J. Grimble, Electronic and Electrical Engineering Department, University of Strathclyde, Glasgow, UK

Lorenzo Marconi , Department of Electrical, Electronic, and Information Engineering, Università di Bologna, Bologna, Italy

Advanced Textbooks in Control and Signal Processing is a series designed to present ideas in these disciplines in a manner suitable for students and tutors involved in advanced-undergraduate and graduate courses. The subject matter may be theoretical or applied but must be suitable for learning at this level – these books do not often contain the latest cutting-edge research but take more of a long view of a subject as a whole and deal with general areas rather than specific niches.

Volumes in this series are designed to be adopted as classroom textbooks and are often augmented with accessory material available from the Web. This can be anything from MATLAB® files to pdf slides to be projected in class as teaching aids. Solutions manual pdfs available for download by class instructors are common additions and books are peer reviewed with view to the requirements of classroom tuition.

Titles in this series should be between 200 and 500 pages in length and should contain pedagogical material to assist the student: problems (preferably with solutions in a separate pdf); examples; learning plans; case studies; thorough background reference lists; etc.

Authors wishing to submit a proposal for this series should contact the

Series Editors

Professor **Michael J. Grimble** Department of Electronic and Electrical Engineering, Royal College Building, 204 George Street, Glasgow G1 1XW, United Kingdom

e-mail: m.j.grimble@strath.ac.uk

Professor **Lorenzo Marconi** of the Università di Bologna, Department of Electrical, Electronic, and Information Engineering “Guglielmo Marconi”, Via Zamboni 33, 40126 Bologna, Italy

e-mail: lorenzo.marconi@unibo.it

or the

In-house Editor

Mr. **Oliver Jackson** Springer London, 4 Crinan Street, London, N1 9XW, United Kingdom

e-mail: oliver.jackson@springer.com

Indexed by SCOPUS and Engineering Index.

Publishing Ethics:

Researchers should conduct their research from research proposal to publication in line with best practices and codes of conduct of relevant professional bodies and/or national and international regulatory bodies. For more details on individual ethics matters please see:

<https://www.springer.com/gp/authors-editors/journal-author/journal-author-help/publishing-ethics/14214>

Nicola Mimmo

Analysis and Design of Control Laws for Advanced Driver-Assistance Systems

Theory and Applications



Springer

Nicola Mimmo 

Department of Electrical, Electronic
and Information Engineering “G. Marconi”
University of Bologna
Bologna, Italy

ISSN 1439-2232 ISSN 2510-3814 (electronic)

Advanced Textbooks in Control and Signal Processing

ISBN 978-3-031-22519-2

ISBN 978-3-031-22520-8 (eBook)

<https://doi.org/10.1007/978-3-031-22520-8>

Mathematics Subject Classification: 93B05, 93B07, 93B10, 93B17, 93B18, 93B52, 93D05, 93D15

MATLAB is a registered trademark and Control System Toolbox is a trademark of The Mathworks, Inc.,
See <https://www.mathworks.com/trademarks> for a list of additional trademarks.

© The Editor(s) (if applicable) and The Author(s), under exclusive license to Springer Nature Switzerland AG 2023

This work is subject to copyright. All rights are solely and exclusively licensed by the Publisher, whether the whole or part of the material is concerned, specifically the rights of translation, reprinting, reuse of illustrations, recitation, broadcasting, reproduction on microfilms or in any other physical way, and transmission or information storage and retrieval, electronic adaptation, computer software, or by similar or dissimilar methodology now known or hereafter developed.

The use of general descriptive names, registered names, trademarks, service marks, etc. in this publication does not imply, even in the absence of a specific statement, that such names are exempt from the relevant protective laws and regulations and therefore free for general use.

The publisher, the authors, and the editors are safe to assume that the advice and information in this book are believed to be true and accurate at the date of publication. Neither the publisher nor the authors or the editors give a warranty, expressed or implied, with respect to the material contained herein or for any errors or omissions that may have been made. The publisher remains neutral with regard to jurisdictional claims in published maps and institutional affiliations.

This Springer imprint is published by the registered company Springer Nature Switzerland AG
The registered company address is: Gewerbestrasse 11, 6330 Cham, Switzerland

*To my daughter,
who makes my life happy.*

Series Editor's Foreword

The *Advanced Textbooks in Control and Signal Processing* series encourages a systematic textbook presentation of both fundamental and innovative topics in control engineering and signal processing disciplines. It is hoped that prospective authors will welcome the opportunity to publish a more rounded and structured presentation of some of the newer emerging control and signal processing technologies in this series. However, there is also a place in the series for contemporary presentations of foundational material in these important engineering topics.

There are not many areas of control applications that are advancing as rapidly as automotive systems. The work on driver-assistance systems that is the focus of this text has progressed rapidly and the evidence is to be seen in most new cars now launched. The text focuses on linear system models and design techniques and so the first chapter introduces linearization methods. The second chapter introduces the automotive problems of interest and describes the nonlinear equations that are linearized to obtain state equation models. This is representative of real industrial practice and is therefore needed in this textbook, although researchers now often explore the application of more demanding nonlinear control methods to such problems.

Methods for the analysis of these systems, described by linear time-invariant models, are covered in Chap. 3. Chapter 4, on control system architectures, is welcome since it is one of the topics that has a considerable influence on system design but is sometimes treated as though it were a given. The approach described includes very common and essential features such as integral action and feedforward control but is presented using an approach different from the classical ways of introducing such features.

Chapter 5 covers the perennial topics of optimal control and Kalman filtering that are so common and useful. It is important to understand the theory of such methods that is covered in the text. However, it may be comforting that modern control-design packages such as MATLAB[®] make the use of such methods very straightforward: hence their sustained popularity. The application examples illustrate the relatively simple design and tuning procedures involved.

Chapter 6 provides a brief overview of many advanced control ideas and design methods such as adaptive control, model predictive control, and extended Kalman

filtering. The most popular topic is probably model predictive control, which is dominating some other areas of research in automotive control engineering.

We welcome this contribution to the literature that should be helpful to students entering the field or design engineers already working on automotive systems. It covers several areas of basic system modeling and control fundamentals that should also be helpful to students and researchers in wider application areas. The author has useful experience in presenting the material in a master's degree course. The examples in the text and the exercises included at the end of chapters should be helpful to students of the topic. It represents a valuable contribution to the *Advanced Textbooks in Control and Signal Processing* series.

Glasgow, UK
October 2022

Michael J. Grimble

Preface

This textbook was conceived as a support for the course ‘Applied Automatic Control’, in the context of the master’s degree in “Advanced Automotive Electronic Engineering”, taught by me since the academic year 2017/2018 at the University of Bologna. It is addressed mainly to engineering school students with a background in linear algebra, mathematics, and physics.

The book provides engineering students with a procedural approach to designing control systems for automotive applications. To this end, I extract only the minimal, fundamental set of notions that are necessary for designing control systems applied to automotive plants from theoretical courses on “Advanced Controls” and “Optimal Controls”. On the other hand, the choice of the control design technique, based on linear optimal controls in the state space, is motivated by the following:

- *classic control theory*, based on design in the frequency domain, represents a handy tool to solve control problems but it is limited to simple plants characterized by single-input single-output representations. These methods are *stability-driven*, and often the fulfillment of the desired performance levels is hard. Moreover, the extension of this methodology to multi-input multi-output cases is non-trivial and represents a topic still under investigation.
- *modern control theory*, based on design in the state space, relies on fundamental tools like *reachability* and *observability* that give a clear, powerful insight into a plant and make clear what can be done and what cannot. From a more general point of view, students who understand these concepts can design the sensor and actuator suites to achieve prescribed control goals.
- *optimal control methods* exploit a *performance index* that represents an evaluation tool for designing the best solution, one that also guarantees the stability of the controlled plant. Moreover, linear quadratic optimal control has been chosen because of the inherent robustness that makes it attractive for real applications.
- in many engineering applications, control systems are designed to stabilize a plant around an equilibrium point and eventually to regulate it in the neighborhood of that point. Moreover, it is worth noting that, despite increasing on-board computational power, implementing simple static feedback gains often

represents the best one can do. This implies that nonlinear control techniques are more complex than the control goal requires. For these reasons, the control technique adopted in this textbook is linear and implementable by static feedback matrices.

This book shows readers how to design control systems through an incremental approach so as to achieve two control goals, introduced in Sect. 1.3.1: the first regarding the boundedness of signals (inherently associated with stability) and the second concerning the tracking of time-varying references. We treat control systems structures whose stability is associated with matrix \mathbf{A}_X , which is detailed in Sect. 4.1. This matrix is divided into three nested sub-matrices. Section 4.2 presents the inner layer, constituting the so-called *state feedback*, which achieves the signal boundedness goal. Section 4.3 completes the inner layer and improves state-feedback controllers by adding a dynamic system, that is, the *integral action*. The integral action makes the state feedback robust to constant disturbances and references. As for the mid-layer, Sect. 4.4 introduces the so-called *observer*, a further dynamic system making the state feedback implementable. The union of state feedback and observer represent the so-called *output-feedback controller*, detailed in Sect. 4.5. Finally, Sect. 4.6 introduces the so-called *feed-forward controller* as the outer layer and shows that it accomplishes the reference-tracking goal.

This book is self-contained thanks to the appendices, which recall the basics of linear algebra and basic MATLAB[®] instructions, which, in turn, help replicate, modify, and enhance the proposed simulation results. The organization of the concepts presented in this textbook is depicted in Fig. P.1, which I believe represent the *best practice* in the approach to the solution of any linear control problem applied to nonlinear plants.

Bologna, Italy

Nicola Mimmo

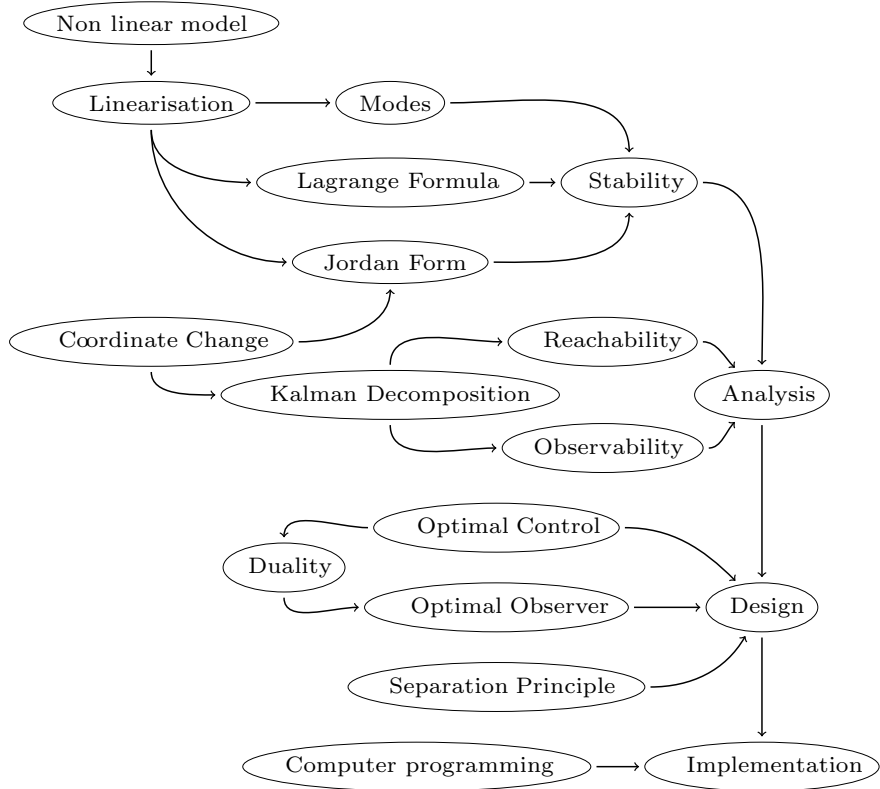


Fig.P.1 Control system design procedure

Acknowledgments

The idea of writing a textbook was born in 2018 when I was appointed to teach automatic controls to automotive engineers. Getting from that idea to the final realization was an exciting and demanding exercise that changed (and hopefully improved) my teaching approach. I am sure I would not have been able to make my initial idea real without the support of colleagues, students, friends, and family.

I thank colleagues of the research group I belong to. They helped me with their interesting points of view about the efficacy of teaching techniques. In particular, I am grateful to Lorenzo and Matteo for their always effective technical suggestions.

A special mention is due to Oliver for his incredible availability and professionalism. He was proactive throughout the editing process by proposing genial tips and tricks. He trusted in me and my work, and this has no price.

Students have directly influenced the contents of this book. I have each year updated examples and exercises they found interesting. I thank my students for their patience during this four-year-long improvement process.

Friends are fundamental while doing immersive works (in particular, those that are engineering-related). Andrea, Saskia, Francesco, Micaela, Alberto, Nadia, Serena, Marco, Michela, and Michele sustained my mood with sincere friendship and humor.

Writing a book requires time, time that I stole from my family. For this, I feel indebted to my parents, Emilia and Giovanni, my sister Anna, and my parents-in-law, Concetta and Luciano. I thank my wife, Ofelia, and my daughter, Penelope, for supporting me with unconditioned love and vital amounts of coffee.

Notation and Abbreviations

Notation

This book denotes sets of natural, real, and complex numbers by \mathbb{N} , \mathbb{R} , and \mathbb{C} . The elements of \mathbb{N} , \mathbb{R} , and \mathbb{C} are represented with lowercase letters, e.g., $x \in \mathbb{R}$. Sets are denoted by calligraphic letters, e.g., $\mathcal{X} \subseteq \mathbb{R}^n$ with $n \in \mathbb{N}$. Capital letters in outline, like $\mathbb{V}(\mathbb{C})$, are adopted to denote vector spaces. Vectors and matrices are denoted by bold lowercase and uppercase letters, e.g., let $n, m \in \mathbb{N}$, then $\mathbf{x} \in \mathbb{R}^n$ denotes a vector, whereas $\mathbf{X} \in \mathbb{R}^{n \times m}$ represents a matrix.

Let n matrices $\mathbf{X}_i \in \mathbb{R}^{n_i \times m}$ with $n, n_i, m \in \mathbb{N}$. Then, the column operator $\text{col}(\cdot) : \mathbb{R}^{n_1 \times m} \times \cdots \times \mathbb{R}^{n_n \times m} \rightarrow \mathbb{R}^{(\sum_{i=1}^n n_i) \times m}$ is defined as

$$\text{col}(\mathbf{X}_1, \dots, \mathbf{X}_n) = \begin{bmatrix} \mathbf{X}_1 \\ \vdots \\ \mathbf{X}_n \end{bmatrix}.$$

Let $\mathbf{x} \in \mathbb{R}^n$ with $\mathbf{x} = \text{col}(x_1, \dots, x_n)$ and $f : \mathbb{R}^n \mapsto \mathbb{R}^m$. Then, the Jacobian of f is denoted as $\nabla f_{\mathbf{x}} \in \mathbb{R}^{m \times n}$ with $\nabla f_{\mathbf{x}} := \begin{bmatrix} \frac{\partial f}{\partial x_1} & \cdots & \frac{\partial f}{\partial x_n} \end{bmatrix}$.

Let \mathbf{x} , \mathbf{y} , \mathbf{A} , and \mathbf{B} be two vectors and two matrices of proper dimensions. Then, to reduce the notation complexity, this book denotes the inner product $\langle \mathbf{x}, \mathbf{y} \rangle$ with $\mathbf{x}^\top \mathbf{y}$ and the dot products $\mathbf{A} \cdot \mathbf{x}$ and $\mathbf{A} \cdot \mathbf{B}$ with \mathbf{Ax} and \mathbf{AB} .

Let $\mathbf{x} \in \mathbb{R}^n$, then the norm of \mathbf{x} is denoted by $\|\mathbf{x}\| := \sqrt{\mathbf{x}^\top \mathbf{x}}$.

The lower and upper bounds of matrices are defined through $\underline{\sigma}, \bar{\sigma} : \mathbb{R}^{n \times m} \rightarrow \mathbb{R}^+$ such that, for any $\mathbf{X} \in \mathbb{R}^{n \times m}$, we have

$$\underline{\sigma}(\mathbf{X}) = \inf_{\mathbf{x} \in \mathbb{R}^m : \|\mathbf{x}\|=1} \frac{\|\mathbf{X}\mathbf{x}\|}{\|\mathbf{x}\|}, \bar{\sigma}(\mathbf{X}) = \sup_{\mathbf{x} \in \mathbb{R}^m : \|\mathbf{x}\|=1} \frac{\|\mathbf{X}\mathbf{x}\|}{\|\mathbf{x}\|}.$$

Abbreviations

ABS	Anti-lock Braking System
ACC	Adaptive Cruise Control
ADAS	Advanced Driver-Assistance Systems
AEB	Automatic Emergency Braking
AI	Artificial Intelligence
ARE	Algebraic Riccati Equation
AS	Active Suspensions
AST	Automatic Steering System
BIBS	Bounded-Input Bounded-State
BSD	Blind Spot Detection
CC	Cruise Control
DAC	Direct Adaptive Control
DRE	Differential Riccati Equation
EKF	Extended Kalman Filter
EPS	Electric Power Steering
ESP	Electonic Stability Program
FWD	Forward Collision Warning
4WS	Four-Wheel Steering
GNSS	Global Navigation Satellite Systems
GS	Gain Scheduling
IAC	Indirect Adaptive Control
ICE	Internal Combustion Engine
IMU	Inertial Measurement Unit
LaC	Launch Control
LC	Lane Changing
LDW	Lane Departure Warning
LK	Lane Keeping
LTI	Linear Time Invariant
LQ	Linear Quadratic
MIMO	Multi-Input Multi-Output
MISO	Multi-Input Single-Output
MPC	Model Predictive Control
MRAC	Model Reference Adaptive Control
NHTSA	National Highway Traffic Safety Administration
PID	Proportional-Integral-Derivative
SAE	Society of Automotive Engineers
SIMO	Single-Input Multi-Output.
SISO	Single-Input Single-Output
SLAM	Simultaneous Localisation And Mapping
SPA	Self-Park Assist
TC	Traction Control
TV	Torque Vectoring
2WS	Two-Wheel Steering

Contents

1	Introduction	1
1.1	Why ADAS?	1
1.1.1	Levels of Automation and ADAS	2
1.1.2	Brief Historical Notes	4
1.2	Plant Models	6
1.2.1	Linearization	10
1.3	Control via Linearization	14
1.3.1	Control Problem Formalization	14
1.3.2	Control System Architecture	16
1.3.3	Comparison with Classic PIDs	18
1.3.4	Limitations	19
1.4	Summary	20
References		21
2	Models and ADAS Control Goals	23
2.1	Active Suspensions	23
2.1.1	Single-Corner Model	24
2.1.2	Half-Car Model	28
2.2	Electro-mechanical Brakes	32
2.3	Wheel Speed Controls	35
2.4	Adaptive Cruise Control	41
2.5	Automatic Steering System	44
2.6	Latero-directional Controls	47
2.6.1	Lane Controls	52
2.6.2	Self-Park Assist	55
2.7	Summary	57
2.8	Exercises	58
References		63
3	LTI System Analysis	67
3.1	Jordan Canonical Form	67
3.1.1	Change of Coordinates	67
3.1.2	Eigenvalues and Eigenvectors	69

3.1.3	Jordan Transformation	73
3.2	Dynamics of LTI Systems	76
3.3	BIBS Stability	84
3.4	ADAS Analysis	86
3.4.1	Active Suspensions	86
3.4.2	Electro-mechanical Brakes	93
3.4.3	Wheel Speed Controls	96
3.4.4	Adaptive Cruise Control	100
3.4.5	Automatic Steering System	102
3.4.6	Latero-directional Controls	103
3.5	Summary	113
3.6	Exercises	114
	References	115
4	Control System Architecture	117
4.1	Closed-Loop System	117
4.2	State-Feedback Stabilizer	119
4.3	Integral Action	128
4.4	State Observer	130
4.5	Output-Feedback Stabilizer	138
4.5.1	Minimal Stabilizer	139
4.5.2	Robustness to Disturbance and Noise	145
4.5.3	Limitations on the Stabilization of Nonlinear Systems	147
4.6	Feed-Forward Control	149
4.7	ADAS Architecture	154
4.7.1	Active Suspensions	154
4.7.2	Electro-mechanical Brakes	158
4.7.3	Wheel Speed Controls	159
4.7.4	Adaptive Cruise Control	161
4.7.5	Automatic Steering System	163
4.7.6	Latero-directional Controls	164
4.8	Summary	174
4.9	Exercises	174
	References	176
5	Optimal Control and Kalman Filter	177
5.1	Robust Stationary Optimal Control	177
5.1.1	Gain Selection	186
5.2	Duality	188
5.3	Kalman Filter	191
5.4	ADAS Design	198
5.4.1	Active Suspensions	198
5.4.2	Electro-mechanical Brakes	210
5.4.3	Wheel Speed Controls	213
5.4.4	Adaptive Cruise Control	214
5.4.5	Automatic Steering System	216

5.4.6	Latero-directional Controls	218
5.5	Summary	229
5.6	Exercises	229
	References	230
6	ADAS Advanced Control Techniques	233
6.1	Gain Scheduling	233
6.2	Indirect and Direct Adaptive Control	235
6.3	Model Predictive Control	237
6.4	Feedback Linearization	238
6.5	Extended Kalman Filter	240
	References	241
7	Control Problems in Future Vehicles	251
	References	256
A	Linear Algebra	261
A.1	Matrices and Vectors	261
A.2	Matrix Sum and Product	263
A.3	Vector Products	265
A.4	Matrix Inverse	266
A.5	Matrix Pseudo-inverses (Moore–Penrose)	267
A.6	Vector Spaces	267
A.7	Linear Functions and Matrices	268
	References	268
B	Linear Control Theory Applied with MATLAB®	269
	References	270
C	Optimal Control Robustness	271
	References	273
Index	275



Introduction

1

After the description of the motivations that justify the presence of control systems onboard modern vehicles (Sect. 1.1), Sect. 1.2 introduces the terminologies and the models required to formalize any control problem. A linear system generated from the nonlinear model of the plant is the basis to describe the control technique described in this textbook. Section 1.2.1 describes the *linearization* technique, a method to develop the linear system mentioned earlier. The outcome of the linearization is exploited for the design of the elementary block constituting the control system architecture described in Sect. 1.3.2. Moreover, this control architecture is compared with the classic PIDs in Sect. 1.3.3 while Sect. 1.3.4 briefly discusses the limitations of the application of controls via linearization to nonlinear plants.

1.1 Why ADAS?

Automobiles and motorcycles have become some of the most used means of transport. Throughout their glorious history, they have been improved to reach the highest levels of safety and performance.

Passive mechanical and hydraulic components, designed to accomplish pre-defined tasks and whose behavior was inherently defined by their physical structure, predominantly characterized early vehicles. For example, cars with purely passive mechanical/hydraulic systems, such as the suspensions, steering, or braking systems, are designed to perform the best in nominal conditions. However, when these vehicles work in off-design conditions, performance is reduced, with a (possible) dangerous impact on stability and safety. Therefore, cars and motorbikes have been

equipped with more sophisticated systems that actively react to changed environmental conditions to keep the performance levels uniform, with remarkable benefits for stability and safety. These active systems are composed of three main elements: a sensor suite that is aware of the surrounding environment, a computational unit that processes the sensors' data to elaborate corrective actions, and an actuation suite, which implements the output of the computational unit. The set of criteria coded into the computational board, which represents the *logic* that manages the vehicle's behavior, constitutes the focus of the book and is formally identified as the set of *control laws*.

The availability of new sensors, actuators, and higher computational powers allows control algorithms to accomplish more complex tasks, ranging from stability augmentation to fully autonomous functions in which the pilot is no longer involved [3, 18]. This book focuses on the so-called Advanced Driver-Assistance Systems (ADAS) whose main task is to aid drivers in executing basic tasks, such as steering, acceleration, and braking, and to keep performance at their nominal values while guaranteeing the system's stability. Examples of these kind of systems are the Anti-lock Braking System (ABS), Adaptive Cruise Control (ACC), Electric Power Steering (EPS), Electronic Stability Program (ESP), and Active Suspensions (AS).

Accordingly to the National Highway Traffic Safety Administration (NHTSA) [19], introducing automatic control systems could improve safety, save lives, and reduce injuries by reducing human errors [24]. Moreover, automation may lead to economic and societal benefits because reducing accidents implies decreasing costs such as insurance, health care, and maintenance. On the other hand, collaborative vehicles could improve life quality by reducing the time spent in traffic congestion. Last but not least, automated cars could improve the mobility of aged people or those affected by disabilities.

1.1.1 Levels of Automation and ADAS

Mainly driven by safety needs, an increasing number of automatic control systems have been developed and adopted in modern vehicles. The level of automation can range from a pure warning system that aims to provide safety information to the drivers to a completely autonomous vehicle in which the driver represents just a payload. Accordingly to the NHTSA and to the Society of Automotive Engineers (SAE), vehicles can be classified into different levels of automation (see Fig. 1.1). In particular, the following clusters are defined:

- **Level 0—No Automation:** The human directly drives the vehicle. Examples are acceleration pedals mechanically linked to the throttle valve through a steel wire, brake pedals directly connected to a hydraulic cylinder that distributes the hydraulic pressure among the brake calipers, mechanical power windows, etc. On the other hand, all the warning and advisory systems, such as lane departure warnings, parking proximity sensors, blind spot information systems, forward-collision warnings,



Fig. 1.1 The automation levels as conceived by the NHTSA

traffic sign recognition, and many others, are automatic systems embedded in vehicles with this automation level.

- **Level 1—Driver Assistance:** The human driver still controls the vehicle, but automatic devices operating only in specific conditions support his or her actions. Examples of control systems equipping vehicles within this automation level are emergency braking assist, lane keeping, and adaptive cruise control. It is worth noting that, at this automation level, the systems mentioned do not operate concurrently.
- **Level 2—Partial Automation:** The main difference between Level 2 and Level 1 is the concurrent operability of the automatic control systems. The automated systems can fully control the vehicle for some specific driving conditions. Therefore, the driver is tasked with monitoring the environment and overriding/stopping the computerized systems when needed. Examples of systems installed on vehicles in this category are autonomous obstacle avoidance and autonomous parking.
- **Level 3—Conditional Automation:** Under certain circumstances, the driver leaves complete control of the vehicle to the automatic systems. He or she must be ready to take control when noticed by the automated system. Moreover, the driver does not need to monitor the environment when the computerized systems are working. For example, the highway chauffeur is an automated system for a vehicle of automation Level 3.
- **Level 4—High Automation:** In this class of vehicle, the driver should be ready to take back control and drive the car in all conditions in which the automatic systems are not designed to operate. When the control systems work, the driver does not need to monitor the systems and the environment. Automatic valet parking represents an example of automated systems featuring vehicles in this category.
- **Level 5—Fully Autonomous:** The driver represents a passenger at this automation level. High-level interfaces are provided to the driver, who can decide, for example, the destination and the stop-overs. At this level of automation, vehicles can perform all the driving tasks in any environmental condition (night, fog, crowded city centers, etc.).

In the context of the automation levels described in this section, ADAS are systems equipping vehicles from Level 0 to Level 2. This book focuses in more detail on the study and the design of the control laws of ADAS at Level 1 and Level 2. Indeed, the monitoring systems listed for Level 0 are usually designed by analytical tools (e.g., computer vision algorithms, if/then algorithms) different from those presented in this book.

1.1.2 Brief Historical Notes

The road to automation, which started in the early 1950s, is progressing hand in hand with the evolution of sensors [9] and embedded computation capabilities [2, 12, 25] (see Fig. 1.2). Roughly, the first historical period from 1950 to late 1990 saw the

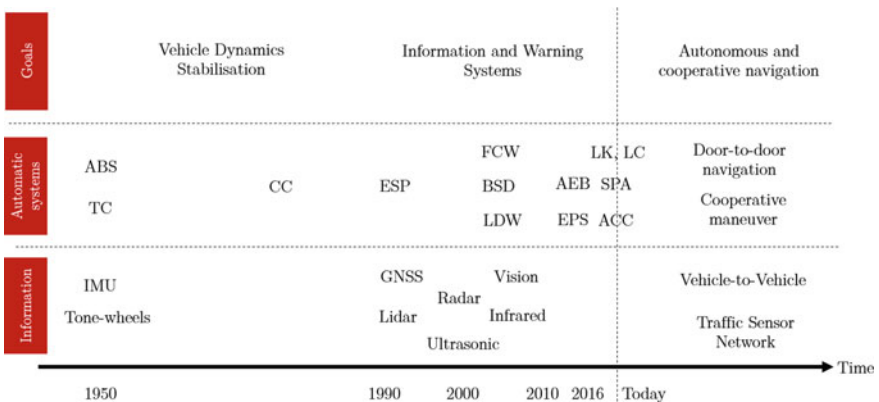


Fig. 1.2 Historical evolution of automatic control systems in automotive industry

development of systems for stabilizing vehicle dynamics based on proprioceptive sensors such as tone wheels and the Inertial Measurement Unit (IMU).

From the early 2000s to today, the focus has been placed on information and warning systems that rely on exteroceptive sensors such as Global Navigation Satellite Systems (GNSS), radar, and cameras.

The current trends seem to suggest that vehicles will be increasingly automated and cooperative in the future and that this goal is achievable through vehicle-to-vehicle connections and infrastructures like traffic sensor networks.

In more detail, it is not surprising that the first applications of automatic controls in automotive were the ABS [23] and the TC. Indeed, these systems rely only on a couple of tone wheels installed on the front and rear wheels, respectively. On the basis of ABS and TC, the Cruise Control (CC) came about as a natural consequence. These control systems represented the main driver assistance technologies from 1950 to 1990.

In early 1990, the integration of ABS/TC control policies (specialized in modifying the vehicle's yaw torque) with gyroscopes led to the development of the Electronic Stability Program (ESP).

The years from 2000 to 2010 saw the development of Forward Collision Warning (FWD), Blind Spot Detection (BSD) [22], and Lane Departure Warning (LDW), which rely on devices such as ultrasonic and infrared sensors, radar, lidar, and vision sensors, exploited to obtain awareness of the surrounding environment.

The development of obstacle detection systems and the functionalities of FWD and ABS were merged to create Automatic Emergency Braking (AEB), which represented the central technology for the years 2010–2016.

From 2016 on, new technologies were introduced [21]. Among them, ACC arose as a natural extension of CC, based on the more complex use of inter-vehicle distance sensors [5]. On the other hand, the introduction of torque meters installed on the steering column supported the evolution of EPS and so the ability to change vehicle direction. Thus, recent years have seen the affirmation of more complex control

systems such as Lane Keeping (LK), Lane Changing (LC), and Self-Park Assist (SPA) [4].

Future development of semi-automatic/autonomous navigation systems relying on GNSS and vehicle cooperation through vehicle-to-vehicle and ad hoc network connections is plausible. Examples of future technologies could be automated door-to-door driving and cooperative maneuvering.

In the context of a historical classification of ADAS (Levels 1 and 2), this textbook covers both past and current control systems where most of the ADAS from 1950 to today consist of the stabilization of a dynamic system around a nominal working point.

1.2 Plant Models

In the context of this textbook, an automotive system is conceived as a plant composed of a vehicle, a driver, actuators, and sensors (see Fig. 1.3). The suite of sensors collects information from both the plant (IMU, GNSS, etc.) and the driver (cameras, steering column torque meters, etc.). Information and warning systems elaborate these data to create higher-level information displayed to the driver (information messages, lamps, steering wheel vibrations, warning sounds, etc.). The driver, whose sensors are kinesthetic perception and senses, can control the vehicle directly and through the automatic control systems. On the other hand, these latter elaborate control actions on the basis of the information provided by the sensor suite and according to driver inputs. Dedicated actuators complete the automatic control system. They affect the vehicle's dynamics by applying the control inputs. It is worth noting that, for safety reasons, the control inputs of the driver and those of the automatic system

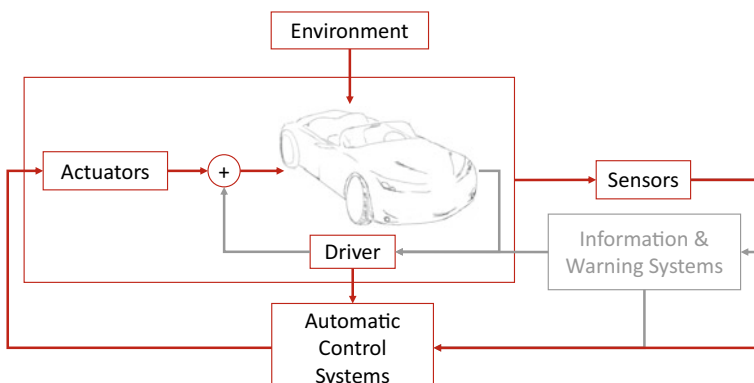


Fig. 1.3 Typical control system architecture for automotive applications. The gray parts are out of the scope of this textbook

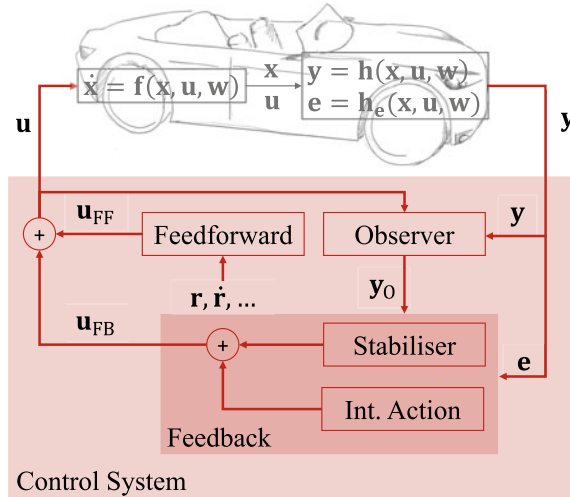


Fig. 1.4 Ground vehicles as a plant with inputs, disturbances, states, and outputs. The control system architecture consists of three blocks. First, the output y and the input u are elaborated through an observer that provides y_O which represents a proxy of x . This information and the couple (y, e) are passed to the feedback control which elaborates the control u_{FB} . On the other hand, the feed-forward control takes as input the reference r , and eventually its derivatives, and generates the signal u_{FF} . The two control signals are summed to create u

actuators are parallel. This parallelism lets the driver take over control in the case of malfunctions.

The goal of any control system is that of *modifying* the natural behavior of the **plant** under investigation [1, 11, 13, 20, 26, 27]. But, what does **plant** mean in the context of control systems?

We conceive the **plant** as a system, in which we have identified two groups of signals, namely **inputs** and **outputs**, as shown in Fig. 1.4. Therefore, the plant represents the link between inputs (causes) and outputs (effects). Moreover, the inputs can be further classified as **controls** and **exogenous signals**. The controls are manipulable input signals (exploitable to modify the system's behavior), whereas the exogenous signals cannot be governed to change the plant's behavior. Like the inputs, the outputs can also be divided into two clusters, namely **measurable outputs** (or simply outputs) and **controlled outputs**. The first group represents the set of all the data available thanks to the sensors installed in the plant. The second denotes the variables that should be modified through the control action (often, the controlled outputs are a subset of the measured outputs).

It is worth noting that the exogenous signals do not depend on the system's behavior. Instead, they collect disturbances, namely d , sensor noises, denoted by v , and the reference signal that the controlled output should track, identified by the symbol r .

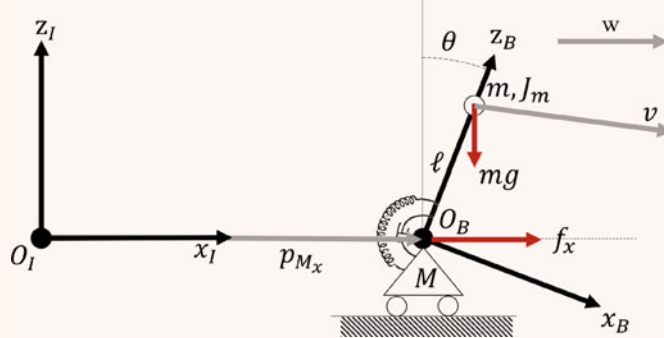
Let $p, r, q, m \in \mathbb{N}$ be positive integers, then declare with $\mathbf{u} \in \mathbb{R}^p$ the control vector, with $\mathbf{w} \in \mathbb{R}^r$ the exogenous vector, usually defined as $\mathbf{w} = \text{col}(\mathbf{d}, \mathbf{v}, \mathbf{r})$, with $\mathbf{y} \in \mathbb{R}^q$ the output vector of the plant, and with $\mathbf{e} \in \mathbb{R}^m$ the controlled outputs. Based on the dimensions of the input and output vectors, we classify the plants as Multi-Input Multi-Output (MIMO) if $p, q > 1$ and Single-Input Single-Output (SISO) if $p = q = 1$, with MISO and SIMO representing intermediate configurations.

A mathematical model, usually given by a set of ordinary differential nonlinear equations in the so-called Input-State-Output (or State Space) representation, describes the plant's behavior. In more detail, given the inputs \mathbf{u} , the exogenous \mathbf{w} , and the outputs \mathbf{y} and \mathbf{e} , the plant dynamics are modeled as

$$\begin{aligned}\dot{\mathbf{x}} &= \mathbf{f}(\mathbf{x}, \mathbf{u}, \mathbf{w}) & \mathbf{x}(t_0) &= \mathbf{x}_0 \\ \mathbf{y} &= \mathbf{h}(\mathbf{x}, \mathbf{u}, \mathbf{w}) \\ \mathbf{e} &= \mathbf{h}_e(\mathbf{x}, \mathbf{u}, \mathbf{w})\end{aligned}\tag{1.1}$$

where $\mathbf{x} \in \mathbb{R}^n$, $n \in \mathbb{N}$, is the **state** vector. For example, ground vehicles are systems whose inputs are the throttle, the steering angle, and the brake pressure, and whose exogenous signals are the wind field, the road inclination, the reference speed, the noises affecting the sensors, etc. On the other hand, the outputs are the measurements of the tachometer, GNSS receiver, accelerometers, gyroscopes, magnetometers, potentiometers, engine tone-wheels, engine pressures, airflow sensors, etc. Moreover, the controlled outputs could be the vehicle speed, the turning rate, the wheel speed, the chassis vibrations, etc. Finally, the state could (indeed it depends on the mathematical representation adopted for the description of the dynamics) be represented by inertial positions and speeds, attitude, angular speeds of the body, wheels, engine, etc.

Example 1.1 (*The cart-pole model*) This example aims to describe the identification process, which leads to the definition of the plant model. To achieve this goal identify the state \mathbf{x} , the control \mathbf{u} , the exogenous signals \mathbf{w} , the output \mathbf{y} as well as the functions $\mathbf{f}(\mathbf{x}, \mathbf{u}, \mathbf{w})$, $\mathbf{h}(\mathbf{x}, \mathbf{u}, \mathbf{w})$, and $\mathbf{h}_e(\mathbf{x}, \mathbf{u}, \mathbf{w})$. This example focuses on the cart-pole model obtained through a Lagrangian mechanics approach, see [8]. Introduce two reference frames, the first conceived as inertial and identified by the axes $x_I - O_I - z_I$, and the second attached to the base of the pole and denoted with $x_B - O_B - z_B$. The plant represents a cart of mass $M > 0$ and a pole of mass $m > 0$, and inertia $J_m > 0$. The link between these two masses is rigid, and its length is $\ell > 0$. The cart position is p_{M_x} , whereas the attitude of the pole to the vertical axis is θ . The system is subject to the gravitational acceleration g and two external forces. The first represents the aerodynamic drag acting on the pole. In contrast, f_x is a horizontal force applied to the cart. The aerodynamic drag is a function of the air density $\rho > 0$, the pole cross-section $S > 0$, and the drag coefficient $C_D > 0$. Finally, w denotes the horizontal wind speed.



The nonlinear system

$$\begin{bmatrix} m + M & m\ell \cos \theta \\ m\ell \cos \theta & J_m + m\ell^2 \end{bmatrix} \begin{bmatrix} \ddot{p}_{M_x} \\ \ddot{\theta} \end{bmatrix} = \begin{bmatrix} m\ell\dot{\theta}^2 \sin \theta + f_x - \frac{1}{2}\rho S v C_D (\dot{p}_{M_x} - w + \ell \cos \theta \dot{\theta}) \\ \ell g m \sin \theta - k\theta - \mu\dot{\theta} - \frac{1}{2}\rho S v C_D \ell (\cos \theta (\dot{p}_{M_x} - w) + \ell \dot{\theta}) \end{bmatrix} \quad (1.2)$$

represents the dynamics of the cart pole with

$$v = \sqrt{(\dot{p}_{M_x} + \cos \theta \ell \dot{\theta} - w)^2 + (\sin \theta \ell \dot{\theta})^2}.$$

Let $\dot{p}_{M_x} = v_{M_x}$ and $\dot{\theta} = \omega$ be changes of variables, then define the state $\mathbf{x} \in \mathbb{R}^4$ as the vector $\mathbf{x} := \text{col}(p_{M_x}, v_{M_x}, \theta, \omega)$, and the control input $u \in \mathbb{R}$ as $u := f_x$. The sensor suite is composed of an exteroceptive sensor providing p_{M_x} , an odometer measuring v_{M_x} , and a potentiometer providing θ . Moreover, we assume that the sensors are affected by the noises $v_p, v_v, v_\theta \in \mathbb{R}$. Let $\mathbf{v} := \text{col}(v_p, v_v, v_\theta)$, then the output vector $\mathbf{y} \in \mathbb{R}^3$ is defined as $\mathbf{y} := \text{col}(p_{M_x}, v_{M_x}, \theta) + \mathbf{v}$. Furthermore, the regulated output is $e = (p_{M_x} + v_p) + \ell \sin(\theta + v_\theta) - p_R$, where $p_{M_x} + \ell \sin \theta$ represents the horizontal position of the pole and p_R is the reference to be tracked. The exogenous $w \in \mathbb{R}^4$ is $\mathbf{w} := \text{col}(w, \mathbf{v}, p_R)$. Thanks to these definitions, Eq. (1.2) is rewritten as

$$\begin{bmatrix} 1 & 0 & 0 & 0 \\ 0 & m + M & 0 & m\ell \cos \theta \\ 0 & 0 & 1 & 0 \\ 0 & m\ell \cos \theta & 0 & J_m + m\ell^2 \end{bmatrix} \begin{bmatrix} \dot{p}_{M_x} \\ \dot{v}_{M_x} \\ \dot{\theta} \\ \dot{\omega} \end{bmatrix} = \begin{bmatrix} v_{M_x} \\ m\ell\dot{\theta}^2 \sin \theta + f_x - \frac{1}{2}\rho S v C_D (\dot{p}_{M_x} - w + \ell \cos \theta \dot{\theta}) \\ \omega \\ \ell g m \sin \theta - k\theta - \mu\dot{\theta} - \frac{1}{2}\rho S v C_D \ell (\cos \theta (\dot{p}_{M_x} - w) + \ell \dot{\theta}) \end{bmatrix}. \quad (1.3)$$

Define

$$\mathbf{F}(\mathbf{x}) = \begin{bmatrix} 1 & 0 & 0 & 0 \\ 0 & m+M & 0 & m\ell \cos \theta \\ 0 & 0 & 1 & 0 \\ 0 & m\ell \cos \theta & 0 & J_m + m\ell^2 \end{bmatrix}$$

and write (1.3) in the form (1.1) with

$$\mathbf{f}(\mathbf{x}, u, \mathbf{w}) :=$$

$$\mathbf{F}^{-1}(\mathbf{x}) \begin{bmatrix} v_{M_x} \\ m\ell\omega^2 \sin \theta + f_x - \frac{1}{2}\rho S v C_D (v_{M_x} - w + \ell \cos \theta \omega) \\ \omega \\ \ell g m \sin \theta - k\theta - \mu\omega - \frac{1}{2}\rho S v C_D \ell (\cos \theta (v_{M_x} - w) + \ell \omega) \end{bmatrix}$$

$$\mathbf{h}(\mathbf{x}, u, \mathbf{w}) := \begin{bmatrix} p_{M_x} + v_p \\ v_{M_x} + v_v \\ \theta + v_\theta \end{bmatrix},$$

$$h_e(\mathbf{x}, u, \mathbf{w}) := (p_{M_x} + v_p) + \ell \sin(\theta + v_\theta) - p_R,$$

and

$$\mathbf{F}^{-1}(\mathbf{x}) = \begin{bmatrix} 1 & 0 & 0 & 0 \\ 0 & \frac{J_m + m\ell^2}{\Delta} & 0 & -\frac{m\ell \cos \theta}{\Delta} \\ 0 & 0 & 1 & 0 \\ 0 & -\frac{m\ell \cos \theta}{\Delta} & 0 & \frac{m+M}{\Delta} \end{bmatrix}$$

with $\Delta = (J_m + m\ell^2)(m + M) - (m\ell \cos \theta)^2 > 0$.

1.2.1 Linearization

Let (1.1) be a nonlinear system. This textbook assumes that $\mathbf{f} : \mathbb{R}^n \times \mathbb{R}^p \times \mathbb{R}^r \rightarrow \mathbb{R}^n$ and $\mathbf{h} : \mathbb{R}^n \times \mathbb{R}^p \times \mathbb{R}^r \rightarrow \mathbb{R}^q$ are smooth and locally Lipschitz in \mathbf{x} (the latter assumption is needed to guarantee the existence and uniqueness of the solutions of (1.1)). Moreover, let $\mathbf{u}^* : \mathcal{T} \subset \mathbb{R} \rightarrow \mathbb{R}^p$ and $\mathbf{w}^* : \mathcal{T} \subset \mathbb{R} \rightarrow \mathbb{R}^r$ be the reference input and exogenous signals and assume that there exists a unique integral curve

$$\mathbf{x}^* : \mathcal{T} \subset \mathbb{R} \rightarrow \mathbb{R}^n \tag{1.4}$$

such that

$$\begin{aligned} \dot{\mathbf{x}}^* &= \mathbf{f}(\mathbf{x}^*, \mathbf{u}^*, \mathbf{w}^*) & \mathbf{x}^*(t_0) &= \mathbf{x}_0^* \\ \mathbf{y}^* &= \mathbf{h}(\mathbf{x}^*, \mathbf{u}^*, \mathbf{w}^*) \\ \mathbf{0} &= \mathbf{h}_e(\mathbf{x}^*, \mathbf{u}^*, \mathbf{w}^*). \end{aligned} \tag{1.5}$$

Let the functions $\mathbf{u} : \mathcal{T} \subset \mathbb{R} \rightarrow \mathbb{R}^p$, $\mathbf{w} : \mathcal{T} \subset \mathbb{R} \rightarrow \mathbb{R}^r$, the state \mathbf{x} , and the output \mathbf{y} be defined in agreement with (1.1), and introduce the errors

$$\begin{aligned} \tilde{\mathbf{x}} &= \mathbf{x} - \mathbf{x}^*, & \tilde{\mathbf{u}} &= \mathbf{u} - \mathbf{u}^* \\ \tilde{\mathbf{y}} &= \mathbf{y} - \mathbf{y}^*, & \tilde{\mathbf{w}} &= \mathbf{w} - \mathbf{w}^*. \end{aligned} \tag{1.6}$$

The dynamics of $\tilde{\mathbf{x}}$ is given by

$$\begin{aligned}\dot{\tilde{\mathbf{x}}} &= \dot{\mathbf{x}} - \dot{\mathbf{x}}^* = \\ &= \mathbf{f}(\mathbf{x}, \mathbf{u}, \mathbf{w}) - \mathbf{f}(\mathbf{x}^*, \mathbf{u}^*, \mathbf{w}^*) = \\ &= \mathbf{f}(\mathbf{x}^* + \tilde{\mathbf{x}}, \mathbf{u}^* + \tilde{\mathbf{u}}, \mathbf{w}^* + \tilde{\mathbf{w}}) - \mathbf{f}(\mathbf{x}^*, \mathbf{u}^*, \mathbf{w}^*).\end{aligned}\quad (1.7)$$

Since \mathbf{f} is differentiable, we can write

$$\begin{aligned}\mathbf{f}(\mathbf{x}^* + \tilde{\mathbf{x}}, \mathbf{u}^* + \tilde{\mathbf{u}}, \mathbf{w}^* + \tilde{\mathbf{w}}) &= \\ &= \mathbf{f}(\mathbf{x}^*, \mathbf{u}^*, \mathbf{w}^*) + \nabla \mathbf{f}_{\mathbf{x}} \tilde{\mathbf{x}} + \nabla \mathbf{f}_{\mathbf{u}} \tilde{\mathbf{u}} + \nabla \mathbf{f}_{\mathbf{w}} \tilde{\mathbf{w}} + O(\|\tilde{\mathbf{x}}\|^2, \|\tilde{\mathbf{u}}\|^2, \|\tilde{\mathbf{w}}\|^2).\end{aligned}\quad (1.8)$$

The substitution of (1.8) into (1.7) leads to

$$\dot{\tilde{\mathbf{x}}} = \nabla \mathbf{f}_{\mathbf{x}} \tilde{\mathbf{x}} + \nabla \mathbf{f}_{\mathbf{u}} \tilde{\mathbf{u}} + \nabla \mathbf{f}_{\mathbf{w}} \tilde{\mathbf{w}} + O(\|\tilde{\mathbf{x}}\|^2, \|\tilde{\mathbf{u}}\|^2, \|\tilde{\mathbf{w}}\|^2). \quad (1.9)$$

On the other hand, the output error $\tilde{\mathbf{y}}$ is defined as

$$\tilde{\mathbf{y}} = \mathbf{h}(\mathbf{x}^* + \tilde{\mathbf{x}}, \mathbf{u}^* + \tilde{\mathbf{u}}, \mathbf{w}^* + \tilde{\mathbf{w}}) - \mathbf{h}(\mathbf{x}^*, \mathbf{u}^*, \mathbf{w}^*) \quad (1.10)$$

where, as previously done for \mathbf{f} , \mathbf{h} can also be written via a Taylor polynomial as

$$\begin{aligned}\mathbf{h}(\mathbf{x}^* + \tilde{\mathbf{x}}, \mathbf{u}^* + \tilde{\mathbf{u}}, \mathbf{w}^* + \tilde{\mathbf{w}}) &= \\ &= \mathbf{h}(\mathbf{x}^*, \mathbf{u}^*, \mathbf{w}^*) + \nabla \mathbf{h}_{\mathbf{x}} \tilde{\mathbf{x}} + \nabla \mathbf{h}_{\mathbf{u}} \tilde{\mathbf{u}} + \nabla \mathbf{h}_{\mathbf{w}} \tilde{\mathbf{w}} + O(\|\tilde{\mathbf{x}}\|^2, \|\tilde{\mathbf{u}}\|^2, \|\tilde{\mathbf{w}}\|^2).\end{aligned}\quad (1.11)$$

The output error is then rewritten by substituting (1.11) into (1.10):

$$\tilde{\mathbf{y}} = \nabla \mathbf{h}_{\mathbf{x}} \tilde{\mathbf{x}} + \nabla \mathbf{h}_{\mathbf{u}} \tilde{\mathbf{u}} + \nabla \mathbf{h}_{\mathbf{w}} \tilde{\mathbf{w}} + O(\|\tilde{\mathbf{x}}\|^2, \|\tilde{\mathbf{u}}\|^2, \|\tilde{\mathbf{w}}\|^2). \quad (1.12)$$

Moreover, the regulated output error, i.e., $\tilde{\mathbf{e}} = \mathbf{e} - \mathbf{0}$, can also be formally expressed as

$$\tilde{\mathbf{e}} = \nabla \mathbf{h}_{e_x} \tilde{\mathbf{x}} + \nabla \mathbf{h}_{e_u} \tilde{\mathbf{u}} + \nabla \mathbf{h}_{e_w} \tilde{\mathbf{w}} + O(\|\tilde{\mathbf{x}}\|^2, \|\tilde{\mathbf{u}}\|^2, \|\tilde{\mathbf{w}}\|^2) \quad (1.13)$$

exploiting the same strategy used to obtain (1.12). For small values of errors (1.6), the linearization of (1.1) in the neighborhood of \mathbf{x}^* , is defined as [6]

$$\begin{aligned}\dot{\tilde{\mathbf{x}}} &= \mathbf{A}(\mathbf{x}^*, \mathbf{u}^*, \mathbf{w}^*) \tilde{\mathbf{x}} + \mathbf{B}_1(\mathbf{x}^*, \mathbf{u}^*, \mathbf{w}^*) \tilde{\mathbf{u}} + \mathbf{B}_2(\mathbf{x}^*, \mathbf{u}^*, \mathbf{w}^*) \tilde{\mathbf{w}} \\ \tilde{\mathbf{y}} &= \mathbf{C}(\mathbf{x}^*, \mathbf{u}^*, \mathbf{w}^*) \tilde{\mathbf{x}} + \mathbf{D}_1(\mathbf{x}^*, \mathbf{u}^*, \mathbf{w}^*) \tilde{\mathbf{u}} + \mathbf{D}_2(\mathbf{x}^*, \mathbf{u}^*, \mathbf{w}^*) \tilde{\mathbf{w}} \\ \mathbf{e} &= \mathbf{C}_e(\mathbf{x}^*, \mathbf{u}^*, \mathbf{w}^*) \tilde{\mathbf{x}} + \mathbf{D}_{e_1}(\mathbf{x}^*, \mathbf{u}^*, \mathbf{w}^*) \tilde{\mathbf{u}} + \mathbf{D}_{e_2}(\mathbf{x}^*, \mathbf{u}^*, \mathbf{w}^*) \tilde{\mathbf{w}} \\ \tilde{\mathbf{x}}(t_0) &= \tilde{\mathbf{x}}_0\end{aligned}\quad (1.14)$$

where

$$\begin{aligned}\mathbf{A}(\mathbf{x}^*, \mathbf{u}^*, \mathbf{w}^*) &:= \nabla \mathbf{f}_{\mathbf{x}}|_{\mathbf{x}^*, \mathbf{u}^*, \mathbf{w}^*} \\ \mathbf{B}_1(\mathbf{x}^*, \mathbf{u}^*, \mathbf{w}^*) &:= \nabla \mathbf{f}_{\mathbf{u}}|_{\mathbf{x}^*, \mathbf{u}^*, \mathbf{w}^*} \\ \mathbf{B}_2(\mathbf{x}^*, \mathbf{u}^*, \mathbf{w}^*) &:= \nabla \mathbf{f}_{\mathbf{w}}|_{\mathbf{x}^*, \mathbf{u}^*, \mathbf{w}^*} \\ \mathbf{C}(\mathbf{x}^*, \mathbf{u}^*, \mathbf{w}^*) &:= \nabla \mathbf{h}_{\mathbf{x}}|_{\mathbf{x}^*, \mathbf{u}^*, \mathbf{w}^*}, \quad \mathbf{C}_e(\mathbf{x}^*, \mathbf{u}^*, \mathbf{w}^*) := \nabla \mathbf{h}_{e_x}|_{\mathbf{x}^*, \mathbf{u}^*, \mathbf{w}^*} \\ \mathbf{D}_1(\mathbf{x}^*, \mathbf{u}^*, \mathbf{w}^*) &:= \nabla \mathbf{h}_{\mathbf{u}}|_{\mathbf{x}^*, \mathbf{u}^*, \mathbf{w}^*}, \quad \mathbf{D}_{e_1}(\mathbf{x}^*, \mathbf{u}^*, \mathbf{w}^*) := \nabla \mathbf{h}_{e_u}|_{\mathbf{x}^*, \mathbf{u}^*, \mathbf{w}^*} \\ \mathbf{D}_2(\mathbf{x}^*, \mathbf{u}^*, \mathbf{w}^*) &:= \nabla \mathbf{h}_{\mathbf{w}}|_{\mathbf{x}^*, \mathbf{u}^*, \mathbf{w}^*}, \quad \mathbf{D}_{e_2}(\mathbf{x}^*, \mathbf{u}^*, \mathbf{w}^*) := \nabla \mathbf{h}_{e_w}|_{\mathbf{x}^*, \mathbf{u}^*, \mathbf{w}^*}.\end{aligned}$$

Remark 1.1 It is worth noting that the matrices \mathbf{A} , \mathbf{B}_1 , etc. appearing in (1.14) are time-varying if at least one element of the triplet $(\mathbf{x}^*, \mathbf{u}^*, \mathbf{w}^*)$ is time-varying. Thus, the mentioned matrices are constant if and only if all the elements of the triplet $(\mathbf{x}^*, \mathbf{u}^*, \mathbf{w}^*)$ are constant. Let us assume that there exists $\mathbf{u}^* \equiv \mathbf{u}_0$ and $\mathbf{w}^* \equiv \mathbf{w}_0$ such that the integral curve $\mathbf{x}^* \equiv \mathbf{x}_0$ for all $t \in \mathcal{T}$, then

$$\begin{aligned}\mathbf{0} &= \mathbf{f}(\mathbf{x}_0, \mathbf{u}_0, \mathbf{w}_0) & \mathbf{x}(t_0) &= \mathbf{x}_0 \\ \mathbf{y}_0 &= \mathbf{h}(\mathbf{x}_0, \mathbf{u}_0, \mathbf{w}_0) \\ \mathbf{0} &= \mathbf{h}(\mathbf{x}_0, \mathbf{u}_0, \mathbf{w}_0).\end{aligned}\tag{1.15}$$

The triplet $(\mathbf{x}_0, \mathbf{u}_0, \mathbf{w}_0)$ is called an *equilibrium triplet* and the associated system (1.14) is called **Linear Time Invariant (LTI)**.

For the remainder of this book, the dependency on the triplet $(\mathbf{x}^*, \mathbf{u}^*, \mathbf{w}^*)$ is omitted and the notation of (1.14) is shortened as follows:

$$\begin{aligned}\dot{\tilde{\mathbf{x}}} &= \mathbf{A}\tilde{\mathbf{x}} + \mathbf{B}_1\tilde{\mathbf{u}} + \mathbf{B}_2\tilde{\mathbf{w}} & \tilde{\mathbf{x}}(t_0) &= \tilde{\mathbf{x}}_0 \\ \tilde{\mathbf{y}} &= \mathbf{C}\tilde{\mathbf{x}} + \mathbf{D}_1\tilde{\mathbf{u}} + \mathbf{D}_2\tilde{\mathbf{w}} \\ \tilde{\mathbf{e}} &= \mathbf{C}_e\tilde{\mathbf{x}} + \mathbf{D}_{e_1}\tilde{\mathbf{u}} + \mathbf{D}_{e_2}\tilde{\mathbf{w}}.\end{aligned}\tag{1.16}$$

Example 1.2 (*Linearization of the cart-pole model*) Given the nonlinear system of Example 1.1, assume that there exists an initial condition $\mathbf{x}_0 = \text{col}(p_0, v_0, \theta_0, 0)$ and a $u^*(t) : \mathbb{R} \rightarrow \mathbb{R}$ such that, for $\mathbf{w}^* \equiv \mathbf{0}$, the following equality holds for all $t \geq t_0$:

$$\begin{bmatrix} v_0 \\ 0 \\ 0 \\ 0 \end{bmatrix} = \mathbf{f}(\mathbf{x}_0, u^*, \mathbf{0}).$$

Then, there exists a reference trajectory $\mathbf{x}^* : \mathbb{R} \rightarrow \mathbb{R}^4$, which is defined as a solution of

$$\dot{\mathbf{x}}^* = \mathbf{f}(\mathbf{x}^*, u^*, \mathbf{0}) \quad \mathbf{x}^*(t_0) = \mathbf{x}_0$$

$$\mathbf{y}^* = \mathbf{h}(\mathbf{x}^*, u^*, \mathbf{0})$$

$$\mathbf{0} = \mathbf{h}_e(\mathbf{x}^*, u^*, \mathbf{0}).$$

Remark 1.2 In this simple case, we have $\dot{\mathbf{x}}^* = \text{col}(v_0, 0, 0, 0)$ and $\mathbf{x}^*(t) = \text{col}(p_0 + v_0(t - t_0), v_0, \theta_0, 0)$. Note that $\theta_0 \neq 0$ is due to the aerodynamic drag which creates a torque statically balanced by the rotational spring reaction.

The linearized system, obtained approximating the nonlinear dynamics (1.2) in the neighborhood of the reference trajectory \mathbf{x}^* is given by (1.14) in which the following matrices appear:

$$\mathbf{A} = \begin{bmatrix} 0 & 1 & 0 & 0 \\ 0 & A_{22} & A_{23} & A_{24} \\ 0 & 0 & 0 & 1 \\ 0 & A_{42} & A_{43} & A_{44} \end{bmatrix}, \quad \mathbf{B}_1 = \mathbf{F}^{-1}(\mathbf{x}^*) \begin{bmatrix} 0 \\ 1 \\ 0 \\ 0 \end{bmatrix}$$

$$\mathbf{B}_2 = \mathbf{F}^{-1}(\mathbf{x}^*) \begin{bmatrix} 0 & 0 & 0 & 0 & 0 \\ \rho S C_D v_0 & 0 & 0 & 0 & 0 \\ 0 & 0 & 0 & 0 & 0 \\ 0 & 0 & 0 & 0 & 0 \end{bmatrix}$$

$$\mathbf{C} = \begin{bmatrix} 1 & 0 & 0 & 0 \\ 0 & 1 & 0 & 0 \\ 0 & 0 & 1 & 0 \end{bmatrix}, \quad \mathbf{D}_1 = \begin{bmatrix} 0 \\ 0 \\ 0 \end{bmatrix}, \quad \mathbf{D}_2 = \begin{bmatrix} 0 & 1 & 0 & 0 & 0 \\ 0 & 0 & 1 & 0 & 0 \\ 0 & 0 & 0 & 1 & 0 \end{bmatrix}$$

$$\mathbf{C}_e = [1 \ 0 \ \ell \cos \theta^* \ 0], \quad D_{e1} = 0, \quad D_{e2} = [1 \ 0 \ \ell \cos \theta^* \ 0]$$

with

$$\begin{bmatrix} 1 \\ A_{22} \\ 0 \\ A_{42} \end{bmatrix} = \mathbf{F}^{-1}(\mathbf{x}^*) \begin{bmatrix} 1 \\ -\rho S C_D v_0 \\ 0 \\ -\rho S C_D v_0 \ell \cos \theta_0 \end{bmatrix}$$

$$\begin{bmatrix} 0 \\ A_{23} \\ 0 \\ A_{43} \end{bmatrix} = \mathbf{F}^{-1}(\mathbf{x}^*) \begin{bmatrix} 0 \\ 0 \\ 0 \\ \ell m g \cos \theta_0 - k + \frac{1}{2} \rho S C_D v_0^2 \sin \theta_0 \ell \end{bmatrix} + \frac{\partial \mathbf{F}^{-1}}{\partial \theta} \begin{bmatrix} v_0 \\ 0 + u^* - \frac{1}{2} \rho S v_0^2 C_D \\ 0 \\ \ell g m \sin \theta_0 - k \theta_0 - \frac{1}{2} \rho S v_0^2 C_D \ell \cos \theta_0 \end{bmatrix}$$

$$\begin{bmatrix} 0 \\ A_{24} \\ 1 \\ A_{44} \end{bmatrix} = \mathbf{F}^{-1}(\mathbf{x}^*) \begin{bmatrix} 0 \\ -\rho S C_D \ell \cos \theta_0 \\ 1 \\ -\mu - \frac{1}{2} \rho S C_D \ell^2 v_0 (1 + \cos^2 \theta_0) \end{bmatrix}$$

$$\frac{\partial \mathbf{F}^{-1}}{\partial \theta} = \begin{bmatrix} 0 & 0 & 0 & 0 \\ 0 & 0 & 0 & \frac{m \ell \sin \theta}{\Delta_0} \\ 0 & 0 & 0 & 0 \\ 0 & \frac{m \ell \sin \theta}{\Delta_0} & 0 & 0 \end{bmatrix}$$

$$+ 2m\ell \cos \theta_0 \sin \theta_0 \begin{bmatrix} 1 & 0 & 0 & 0 \\ 0 & -\frac{J_m + m\ell^2}{\Delta_0^2} & 0 & \frac{m\ell \cos \theta}{\Delta_0^2} \\ 0 & 0 & 1 & 0 \\ 0 & \frac{m\ell \cos \theta}{\Delta_0^2} & 0 & -\frac{m+M}{\Delta_0^2} \end{bmatrix}.$$

1.3 Control via Linearization

The control system's design can be successfully achieved via linearization when vehicles work in the neighborhood of a stationary point. This section aims to formalize the control problem and present the architecture of linear control systems [10, 15], specialization of Fig. 1.4. Then, this control architecture is compared with PID, which represents one of the most adopted industrial control systems. Finally, this section ends with some comments about the limitations of the control systems designed via linearization.

1.3.1 Control Problem Formalization

Assume the model (1.16) is known and time-invariant. Then, make the following assumptions to formalize the control problem.

Assumption 1.1 (Disturbance and reference)

1. The disturbance is not *observable*, i.e., it is not possible to reconstruct d . This assumption forces the creation of a control system that is *robust* to plant uncertainties;
2. The disturbance is bounded. This assumption is necessary to guarantee the existence of a bounded control action able to achieve the control goals G1 and G2 described later;
3. The reference $\mathbf{r}(t)$ and its time derivatives up to the order $r_{\max} > 0$ are known. Moreover, $d^i/dt^i \mathbf{r}(t)$ is continuous and bounded for all $i = 0, \dots, r_{\max}$.

Assumption 1.2 (Input redundancy) The number of inputs is greater than or equal to the number of regulated outputs, i.e., $p \geq m$. As described in Sect. 4.6, this assumption is necessary (but not sufficient) to determine a control input able to steer \mathbf{e} to zero in the presence of a time-varying reference \mathbf{r} .

Assumption 1.3 (Regulated output readability) The regulated output \mathbf{e} is *readable* from \mathbf{y} , i.e., a surjective map $\mathbf{E} : \mathbb{R}^q \rightarrow \mathbb{R}^m$ exists, with $q \geq m$, such that $\mathbf{e} = \mathbf{E}(\mathbf{y})$. Moreover, the q measurements are linearly independent. This assumption is necessary to solve the control problem G2, which is described later.

Then, the control system is designed to:

- (G1) assure the existence of a non-empty compact set $\mathcal{X}_0 \subset \mathbb{R}$ and $\bar{w} > 0$ such that, for any $\mathbf{x}_0 \in \mathcal{X}_0$ and $\|\mathbf{w}(t)\|_\infty < \bar{w}$, the state $\mathbf{x}(t)$, the regulated output $\mathbf{e}(t)$, and the control $\mathbf{u}(t)$ remain bounded for all times;
- (G2) ensures $\limsup_{t \rightarrow \infty} \|\tilde{\mathbf{e}}(t)\| = 0$ in the case of constant disturbances and the absence of measurement noises.

This book adopts the hybrid **closed/open-loop** control system architecture, highlighted in the light red-filled box in Fig. 1.4, to achieve G1 and G2. It comprises a feedback line that provides the outputs \mathbf{y} and \mathbf{e} to the controller. The latter generates a bounded control action \mathbf{u} that both limits \mathbf{x} and asymptotically steers \mathbf{e} close to zero.

The internal structure of the control system depicted in Fig. 1.4 is complex, but the presence of each block, i.e., the observer, the feedback, and the feed-forward, can be motivated as follows.

The observer represents a tool to gain knowledge about the plant, which is more than a possible direct inversion of $\mathbf{y} = \mathbf{h}(\mathbf{x}, \mathbf{u}, \mathbf{w})$. Indeed, assuming that the plant model (1.1) is known, the observer exploits the signals \mathbf{u} and \mathbf{y} to generate \mathbf{y}_O , which is supplementary information related to \mathbf{x} .

The information extracted from the plant through the observer is fused with the current controlled output \mathbf{e} via the feedback. This block aims to solve the first part of the control problem, i.e., keeping the state \mathbf{x} and the error \mathbf{e} bounded, at any time, through the stabilizer. Moreover, the presence of an integral action provides robustness against constant external disturbances.

On the other hand, the feed-forward exploits the knowledge of the reference and its time derivative to generate control actions needed to compensate for future variations of \mathbf{e} . In doing so, the feed-forward does not rely on either the current values of \mathbf{y} or the supplementary \mathbf{y}_O .

Note

Roughly, feedback and feed-forward are associated with the concepts of stability and robustness (the former) and performance (the latter). In the following, these intuitive connections are given through the description of the control actions we undertake while performing the same turn at higher and higher speeds in the presence of a lateral wind. Let us now assume the ideal trajectory is known (by experience).

Performing a turn at low speed can explain the correlation between feedback, stabilization, and robustness. In doing so, we turn the steering wheel, then we feel the acceleration, and we observe our vehicle's position and direction. The first implicit task is keeping the vehicle under control, i.e., avoiding the car from swerving off the road. While performing this task, we compensate for extra accelerations, drifts, and yaw (measured by our sensory apparatus). Second, we correct wrong vehicle positions and alignments to keep the difference between the actual and the ideal trajectory close to zero. Moreover, the wind induces a side speed which leads to a gradual drift. To compensate for this effect, we rotate the steering wheel to create a lateral force that cancels the wind effects and eliminates the trajectory tracking error accumulated (i.e., integrated) up to that time. As a result, the ideal trajectory is tracked with bounded errors whose upper values depend on our driving ability. In this experiment, we act as a feedback controller that tries to keep both the state and the tracking errors bounded.

Let us now repeat the turn at higher and higher speeds. Intuitively, we should act on the steering wheel more aggressively to keep the trajectory tracking errors confined within the same bounds. Moreover, performing this aggressive maneuver relying on a continuous feedback policy would require our senses and brain to be more responsive. Consequently, the inherent limitations of our sensory apparatus and the finite responsiveness of our brain imply that a pure feedback policy cannot guarantee good performance at high speeds.

On the other hand, let us assume we can foresee the evolution of the tracking error (through a model of the phenomenon we built by experience). Then, without waiting for the evidence of the tracking error, we anticipate our actions on the steering wheel to keep the tracking error at zero. With this control policy, we do not rely on the continuous check of the tracking error and do not require the brain to elaborate feedback based on this information. Then, in principle, this control policy, named feed-forward, may lead to a superior performance. However, the drawback of the feed-forward is that its reliability is directly associated with our ability to foresee the future, which, commonly, is questionable.

To conclude, feedback is necessary to assure stability and to face uncertainties (unknown vehicle mass and inertia, ground conditions, wind, etc.). Still, its trajectory tracking performances are constrained by the bounded ability to elaborate the output and the trajectory tracking error. On the other hand, feed-forward is necessary to guarantee high trajectory tracking performances, but a non-perfect knowledge of the process constrains its efficacy.

The design of observer, feedback, and feed-forward is the subject matter of automatic controls. Among all possible design strategies, this textbook focuses on the so-called design via linearization. The following section investigates the control architecture of Fig. 1.4 for creating linear observers and controllers.

1.3.2 Control System Architecture

In the context of linear systems, the controller is not directly designed on the model (1.1) but rather on its linear approximation (1.16). In more detail, the nonlinear control law \mathbf{u} is decomposed as the sum of the reference \mathbf{u}^* plus the linearized control $\tilde{\mathbf{u}}$, with the former designed on (1.5) and the latter designed on (1.14).

Since the controller is designed on the approximation (1.14), to implement it, it is necessary to make available to the controller the same outputs $\tilde{\mathbf{y}}$ and $\tilde{\mathbf{e}}$ of the system (1.14). For this reason, the feedback line consists in a subtraction node that, taking the values \mathbf{y} , \mathbf{e} , and \mathbf{y}^* , generates the signals $\tilde{\mathbf{y}}$ and $\tilde{\mathbf{e}}$. Then, $\tilde{\mathbf{y}}$ and $\tilde{\mathbf{e}}$ are sent to the controller to elaborate $\tilde{\mathbf{u}}$.

In the context of linear control systems, it is natural to conceive observer, feedback, and feed-forward algorithms as further linear systems [14]. In particular, let the observer be defined as

$$\begin{aligned}\dot{\mathbf{x}}_O &= \mathbf{A}_O \mathbf{x}_O + \mathbf{B}_O \tilde{\mathbf{u}} + \mathbf{K}_O \tilde{\mathbf{y}} \\ \mathbf{y}_O &= \mathbf{C}_O \mathbf{x}_O + \mathbf{D}_O \tilde{\mathbf{y}},\end{aligned}\tag{1.17a}$$

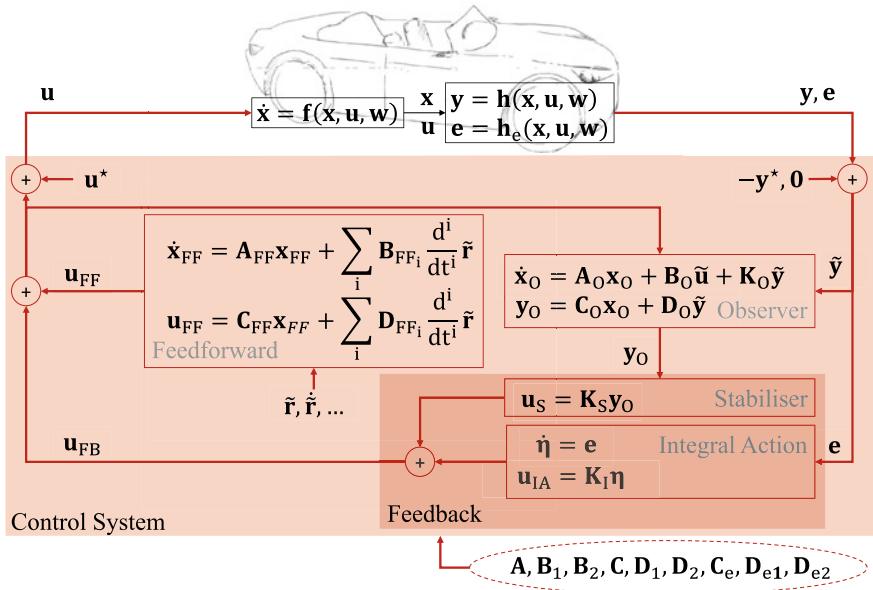


Fig. 1.5 This book deals with control systems based on the linearized model of the plant. The control system architecture comprises sum and subtraction nodes, reference signals, and linear dynamic systems

and let the feedback control law be

$$\mathbf{u}_{FB} := \mathbf{u}_S + \mathbf{u}_{IA} \quad (1.17b)$$

where \mathbf{u}_S denotes the stabilizer law

$$\mathbf{u}_S := \mathbf{K}_S \mathbf{y}_O. \quad (1.17c)$$

On the other hand, \mathbf{u}_{IA} defines the integral action, which represents the output of the dynamic system

$$\begin{aligned} \dot{\boldsymbol{\eta}} &= \mathbf{e} \\ \mathbf{u}_{IA} &= \mathbf{K}_I \boldsymbol{\eta}. \end{aligned} \quad (1.17d)$$

Let the feed-forward control law be defined as

$$\begin{aligned} \dot{\mathbf{x}}_{FF} &= \mathbf{A}_{FF} \mathbf{x}_{FF} + \sum_i^{r_{\max}} \mathbf{B}_{FFi} \frac{d^i}{dt^i} \mathbf{r} \\ \mathbf{u}_{FF} &= \mathbf{C}_{FF} \mathbf{x}_{FF} + \sum_i^{r_{\max}} \mathbf{D}_{FFi} \frac{d^i}{dt^i} \mathbf{r} \end{aligned} \quad (1.17e)$$

for some finite $r_{\max} \in \mathbb{N}$.

The architecture of a control system designed via linearization is depicted in Fig. 1.5 where the matrices, constituting the observer, the feedback, and the feed-forward, are designed by exploiting $\mathbf{A}, \mathbf{B}_1, \dots$ of (1.14). The rationale behind (1.17) will be evident in the next section where a comparison with classic PIDs is provided.

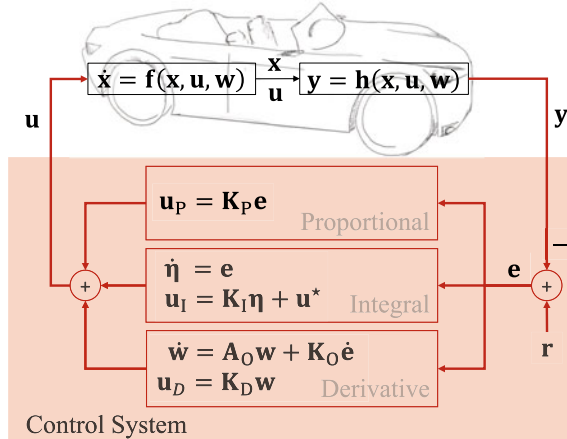


Fig. 1.6 Basic PID architecture. The control action is the sum of three parallel lines, the proportional, the derivative, and the integral

Important

A straight implementation of the control law (1.17c) would lead to an algebraic loop. Indeed, \mathbf{u}_S depends on \tilde{y} , which, in turn, depends on \mathbf{u}_S . Either $\mathbf{D}_1 = \mathbf{0}$ or $\mathbf{D}_O = \mathbf{0}$ break this algebraic loop. This section introduces \mathbf{D}_O to compare (1.17) with the classic PIDs (see the following section), although it is not necessary to achieve the control goals G1 and G2. As detailed in Sect. 4.4, the matrix $\mathbf{D}_O \neq \mathbf{0}$ is introduced when $\mathbf{D}_1 = \mathbf{0}$ to reduce the size of \mathbf{x}_O .

1.3.3 Comparison with Classic PIDs

The PID controller is widespread in industrial applications [7, 28]. It is composed of three parallel control actions, the proportional, the integral, and the derivative. They all elaborate the regulated output, arranged as in Fig. 1.6.

The classic time-domain formulation of a PID controller is given by

$$\dot{w} = A_O w + K_O \dot{e} \quad (1.18a)$$

$$u_{PID} = K_P e + K_D w + K_I \int_0^t e(\tau) d\tau + u^* \quad (1.18b)$$

where it is worth noting that w represents the output of the dynamic system necessary to let the control system be causal. Moreover, u^* denotes the initial condition of the integral action. To compare the PID control architecture with that proposed in Fig. 1.5, note that $e := r - y$, assume $r^* = y^*$, then subtract $r^* - y^*$ from e to obtain

$$e = r - y = \tilde{r} - \tilde{y}$$

where $\tilde{\mathbf{r}} := \mathbf{r} - \mathbf{r}^*$ and $\tilde{\mathbf{y}} := \mathbf{y} - \mathbf{y}^*$. Let $\mathbf{w} := \mathbf{x}_{\text{FF}} - \mathbf{x}_O$ and exploit the superposition principle to rewrite the dynamics of \mathbf{w} as

$$\begin{aligned}\dot{\mathbf{x}}_O &= \mathbf{A}_O \mathbf{x}_O + \mathbf{K}_O \dot{\tilde{\mathbf{y}}} \\ \dot{\mathbf{x}}_{\text{FF}} &= \mathbf{A}_O \mathbf{x}_{\text{FF}} + \mathbf{K}_O \dot{\tilde{\mathbf{r}}}.\end{aligned}\quad (1.19a)$$

Define

$$\dot{\boldsymbol{\eta}} = \mathbf{e}, \quad (1.19b)$$

let $\mathbf{K}_S := [-\mathbf{K}_P - \mathbf{K}_D]$, $\mathbf{y}_O := \text{col}(\tilde{\mathbf{y}}, \mathbf{x}_O)$, $\mathbf{C}_O := \text{col}(\mathbf{0}, \mathbf{I})$, and $\mathbf{D}_O := \text{col}(\mathbf{I}, \mathbf{0})$. Substitute all these terms in (1.18) to obtain

$$\mathbf{u}_{\text{PID}} = \mathbf{u}_{\text{FB}} + \mathbf{u}_{\text{FF}} \quad (1.19c)$$

where

$$\begin{aligned}\mathbf{u}_{\text{FF}} &:= \mathbf{K}_D \mathbf{x}_{\text{FF}} + \mathbf{K}_P \tilde{\mathbf{r}} \\ \mathbf{u}_{\text{FB}} &:= \mathbf{K}_S \mathbf{y}_O + \mathbf{K}_I \boldsymbol{\eta}.\end{aligned}\quad (1.19d)$$

The architecture of (1.19), depicted in Fig. 1.7, quasi-perfectly matches that proposed in Fig. 1.5 with four remarkable differences:

1. If \mathbf{y} depends on \mathbf{u} , the classic PID cannot be implemented due to the algebraic loop created by \mathbf{u}_P . On the other hand, the observer (1.17a) faces this issue by imposing $\mathbf{D}_O = \mathbf{0}$;
2. The derivative of $\tilde{\mathbf{y}}$ is needed to implement (1.19a). This is usually achieved via numerical approximations plus noise suppression filters. For this reason, the block above the feedback is not an observer in the sense of (1.17a). Contrarily, (1.17a) only relies on the signal $\tilde{\mathbf{y}}$;
3. The PID adopts only the first-order time derivative of the reference signal \mathbf{r} . As described in Sect. 4.6, the perfect tracking of a known trajectory may require higher-order derivatives of \mathbf{r} , as foreseen by the feed-forward (1.17e);
4. The dynamics of (1.19a), mimicking (1.18a), are driven by the need to make PID causal. Dissimilarly, the dynamics of the feed-forward (1.17e) and the observer (1.17a) are generic and, as detailed in Sect. 4, are designed with a different perspective.

In conclusion, we can conceive the controller (1.17) as a generalization of the classic PID without the issues associated with the derivative of \mathbf{y} . Moreover, looking at the PID from the perspective of Fig. 1.7 allows identifying the sub-parts responsible for the stability, those that make the control system robust, and those providing performance.

1.3.4 Limitations

Despite their simple structure and an attractive set of design tools, controls via linearization (PIPs included) are inherently limited by their local nature. In more detail,

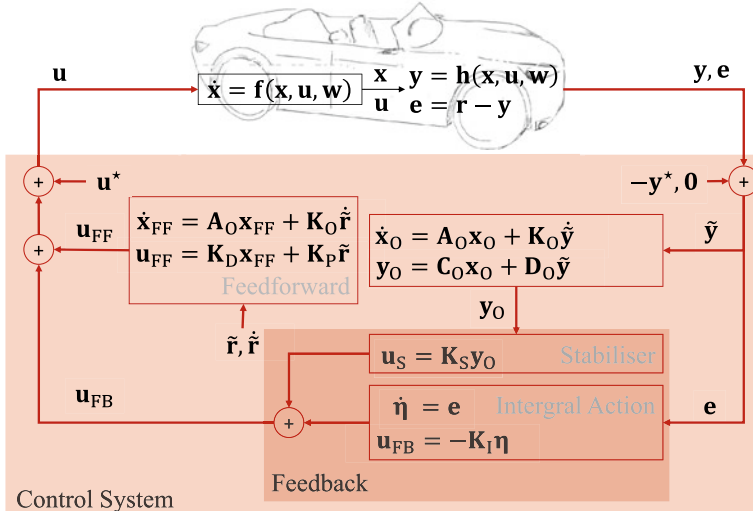


Fig. 1.7 The architecture of a PID after some manipulations. This control structure looks like that in Fig. 1.5

since they are tuned on a nominal design point, their performance may rapidly deteriorate in severe off-design conditions [16, 17].

As described in Sect. 4.5.3, when controls via linearization act on nonlinear plants, the boundedness of the state and control action can be guaranteed if the initial conditions and the exogenous signals belong to sufficiently small neighborhoods of the design point. In particular, Sect. 4.5.3 demonstrates that there are small sets of initial and exogenous conditions such that the nonlinear plant's trajectories remain in a bounded set. However, the maximization of the sets of initial and exogenous conditions that guarantee bounded evolutions of the closed-loop nonlinear system is non-trivial. Moreover, as depicted in Sect. 4.5.2, even for linear plants, increasing the magnitude of the controller gains cannot reduce the asymptotic bounds on the state and regulated output because of the measurement noise amplification.

In conclusion, the major limitation of linear control systems (applied to nonlinear plants) consists in the impossibility of arbitrarily enlarging the domain of initial conditions and exogenous signals with no compromises between disturbance attenuation, non-linearities ruling, and noise magnification.

1.4 Summary

This chapter has recalled the benefits associated with the use of automatic controls in ground vehicles. Undeniable advantages are safety improvement, pollution reduction, mobility increase, and better inclusion.

Section 1.1 identified the control systems representing this book's target among sets of automatic algorithms that make a vehicle autonomous. It also reviewed the six levels of automation to identify the so-called ADAS, i.e., some of the control systems of the second and third automation levels.

Then, Section 1.3.1 introduced the essential ingredients of any automotive control system architecture and defined the control problem formally. Section 1.2 described the control system architecture as the composition of sensors, computational units, and interfaces with the driver and actuators. It also modeled the plant (actuators+vehicle+sensors) as a generic nonlinear dynamic system whose state should be guaranteed as bounded through a bounded control action. The control laws should guarantee state boundedness despite bounded measurement noises and environmental disturbances. Moreover, the regulated output should be asymptotically vanishing in the case of constant disturbances.

Section 1.3.2 proposed a solution to the stated control problem, consisting of a linear dynamic system. Furthermore, the process of obtaining the design plant from the nonlinear system, called linearization, was described. The internal architecture of controls via linearization consists of an observer, static feedback, and integral action. Section 1.3.2 also included a feed-forward control to exploit the knowledge of the reference to be tracked.

Sections 1.3.3 and 1.3.4 described the proposed solution's limitations and similarities with standard PIDs. In more detail, Sect. 1.3.3 rearranged the time-domain formulation of PID to identify the same components of controls via linearization with two remarkable differences: the use of the derivatives of the output and the absence of higher-order derivatives of the reference signals. Then, Sect. 1.3.4 presented the limitations of linearized control systems applied to nonlinear plants.

References

1. Bakshi U, Bakshi V (2010) Control systems. Technical Publications
2. Bengler K, Dietmayer K, Farber B, Maurer M, Stiller C, Winner H (2014) Three decades of driver assistance systems: Review and future perspectives. IEEE Intell Transp Syst Mag 6(4):6–22
3. Blosseville J (2006) Driver assistance systems, a long way to ahs. In: 2006 IEEE intelligent vehicles symposium, pp 237–237
4. Bosh (2021) Automated valet parking. <https://www.bosch.com/stories/automated-valet-parking/>. Accessed 26 Sept 2021
5. Chen Y-L, Wang C-A (2007) Vehicle safety distance warning system: a novel algorithm for vehicle safety distance calculating between moving cars. In: 2007 IEEE 65th vehicular technology conference - VTC2007-Spring, pp 2570–2574
6. Cheng D, Hu X, Shen T (2010) Linearization of nonlinear systems. In: Analysis and design of nonlinear control systems. Springer, Berlin, pp 279–313
7. Dodds SJ et al (2015) Feedback control. Springer, London, p 5
8. Fantoni I, Lozano R (2002) The cart-pole system, volume non-linear control for underactuated mechanical systems. Communications and Control Engineering. Springer, London

9. Fleming W (2001) Overview of automotive sensors. *IEEE Sens J* 1(4):296–308
10. Fortmann TE, Hitz KL (1977) An introduction to linear control systems. Crc Press
11. Franklin GF, Powell JD, Emami-Naeini A, Powell JD (2002) Feedback control of dynamic systems, vol 4. Prentice hall Upper Saddle River
12. Galvani M (2019) History and future of driver assistance. *IEEE Instrum Meas Mag* 22(1):11–16
13. Gopal M (2002) Control systems: principles and design. McGraw-Hill Education (India) Pvt Limited
14. Grujitch LT (2013) Tracking control of linear systems. CRC Press
15. Hendricks E, Jannerup O, Sørensen PH (2008) Linear systems control: deterministic and stochastic methods. Springer, Berlin
16. Hu T, Lin Z (2001) Control systems with actuator saturation: analysis and design. Springer Science & Business Media
17. Li Y, Lin Z (2018) Stability and performance of control systems with actuator saturation. Springer, Berlin
18. Meyer G, Beiker S (2020) Road vehicle automation, vol 7. Springer International Publishing
19. NHTSA (2021) Automated vehicles for safety. <https://www.nhtsa.gov/technology-innovation/automated-vehicles-safety#topic-road-self-driving>. Accessed 26 Sept 2021
20. Phillips CL, Habor RD (1995) Feedback control systems. Simon & Schuster, Inc
21. PSA (2021) Highway chauffeur: autonomous driving on motorways. <https://www.groupe-psa.com/en/newsroom/automotive-innovation/highway-chauffeur/>. Accessed 26 Sept 2021
22. Racine DP, Cramer NB, Zadeh MH (2010) Active blind spot crash avoidance system: a haptic solution to blind spot collisions. In: 2010 IEEE International symposium on haptic audio visual environments and games, pp 1–5
23. Reif K (2014) Brakes, brake control and driver assistance systems. Springer Vieweg, Wiesbaden
24. Reimer B (2014) Driver assistance systems and the transition to automated vehicles: a path to increase older adult safety and mobility? *Public Policy Aging Rep* 24(1):27–31
25. Shaout A, Colella D, Awad S (2011) Advanced driver assistance systems—past, present and future. In: 2011 seventh international computer engineering conference (ICENCO’2011), pp 72–82
26. Sinha N (2008) Control systems. New Age International (P) Limited
27. Srivastava M, MC S, S B (2009) Control systems. Tata McGraw-Hill
28. Visioli A (2006) Practical PID control. Springer, London



Models and ADAS Control Goals

2

This chapter presents the control-oriented nonlinear models describing the dynamics of some automotive systems. More in detail, this chapter derives a set of differential equations for each application through Newtonian or Lagrangian approaches—the definitions of state, inputs, outputs, and exogenous complete these models. Then, the linearized models and the control goals are identified for each application scenario. Section 2.1 describes the suspension system and the Active Suspensions problem: Sect. 2.1.2 extends the model presented in Sect. 2.1.1 and introduces the Attitude Control problem. Section 2.2 depicts the Electro-mechanical Brake system and the associated control problem. Then, Sect. 2.3 introduces the wheel dynamics and the Anti-lock Braking System, Traction Control, and Launch Control problems. The Adaptive Cruise Control, as well as the longitudinal vehicle dynamics, are introduced in Sect. 2.4. The Automatic Steering System is presented in Sect. 2.5. Then, Sect. 2.6 describes the latero-directional dynamics and the associated control problems. Special extensions of these models represent the contents of Sects. 2.6.1 and 2.6.2 in which Lane Keeping, Lane Changing, and the Self-Park Assist are described.

2.1 Active Suspensions

In agreement with [34], Active Suspensions aim at (a) providing a good ride quality through the isolation of the cabin from vibrations due to road irregularities; (b) maintaining a constant tire load, thus keeping constant interaction between the road

and the tires; (c) providing good handling quality in terms of reduction of cabin roll and pitch.

Based on the goals, only a half-vehicle model or a single-corner model is considered [4]. On the one hand, when attention is on the vibrational behavior of the suspension, the full-car model is simplified to a single corner. On the other hand, the so-called half-car model lets us study the control of the attitude, such as for the cabin–road relative roll angle.

2.1.1 Single-Corner Model

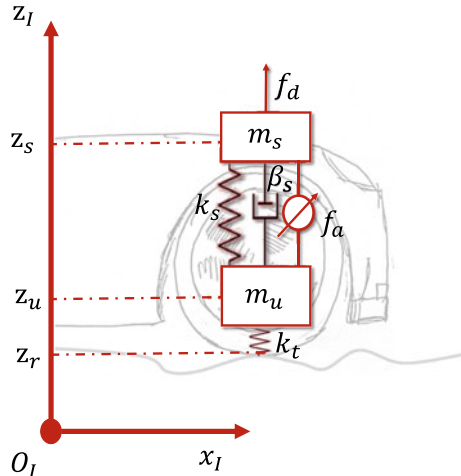
The model of a quarter car suspension is characterized by two masses, i.e., the *sprung* one ($m_s > 0$) and the *unsprung* one ($m_u > 0$), see Fig. 2.1. These two masses are linked through the suspension system. This latter is composed of a parallel arrangement of a spring (whose stiffness coefficient is $k_s > 0$), a damper (with viscous friction coefficient $\beta_s > 0$), and an active component that provides the force $f_a \in \mathbb{R}$. The suspension system interacts with the ground through the tire, here modeled as a spring of stiffness $k_t > 0$. The plant is equipped with two sensors, a potentiometer that measures the length of the suspension, and an accelerometer installed on the sprung mass.

The plant model is obtained through a composition of the dynamics of the sprung and the unsprung masses. These dynamics are connected via Newton's third law of motion. In more detail, let $z_s \in \mathbb{R}$ be the vertical position of the sprung mass. Then, its dynamics are described by

$$m_s \ddot{z}_s = -m_s g + f_s + f_d \quad (2.1a)$$

where $f_s \in \mathbb{R}$ denotes the force of the suspension, and f_d represents the aerodynamic downforce. Similarly, define with z_u the vertical position of the unsprung mass; then

Fig. 2.1 Quarter car active suspension model



its second-order derivative is described by the differential law

$$m_u \ddot{z}_u = -m_u g - f_s + f_t(z_u - z_r) \quad (2.1b)$$

where the tire force $f_t \geq 0$ is modeled as

$$f_t(z_u - z_r) = \begin{cases} 0 & z_u - z_r > \ell_t \\ -k_t(z_u - z_r - \ell_t) & z_u - z_r \leq \ell_t \end{cases} \quad (2.1c)$$

with $\ell_t > 0$ denoting the zero-load length of the tire. It is worth noting that, in agreement with Newton's third law of motion, in (2.1b), the force f_s has been pre-multiplied by -1 . The definition of the following suspension force constitutes the union of (2.1a) and (2.1b):

$$f_s := -k_s(z_s - z_u - \ell_s) - \beta_s(\dot{z}_s - \dot{z}_u) + f_a \quad (2.1d)$$

where $\ell_s > 0$ represents the length of the suspension at zero loads. The definition of f_d completes the description of forces. In particular, the classic aerodynamic approach models the downforce as

$$f_d = \frac{1}{2} \rho S v^2 C_z \quad (2.2)$$

where $\rho > 0$ denotes the air density, $S > 0$ represents a reference area (usually, the footprint or the cross-section), $v > 0$ defines the vehicle speed, and $C_z < 0$ is the downforce coefficient.

With these descriptions at hand, rewrite (2.1) in compact form as

$$\begin{aligned} m_s \ddot{z}_s &= -m_s g - k_s(z_s - z_u - \ell_s) - \beta_s(\dot{z}_s - \dot{z}_u) + f_a + f_d \\ m_u \ddot{z}_u &= -m_u g + k_s(z_s - z_u - \ell_s) + \beta_s(\dot{z}_s - \dot{z}_u) - f_a \\ &\quad + f_t(z_s - z_u), \end{aligned} \quad (2.3a)$$

and complete the model with the output

$$\begin{aligned} y_p &= z_s - z_u + \nu_p && \text{potentiometer} \\ y_a &= -g - \frac{k_s}{m_s}(z_s - z_u - \ell_s) - \frac{\beta_s}{m_s}(\dot{z}_s - \dot{z}_u) + \frac{f_a + f_d}{m_s} + \nu_a && \text{accelerometer} \end{aligned} \quad (2.3b)$$

where $\nu_a, \nu_p \in \mathbb{R}$ represent the noises affecting the accelerometer and potentiometer. Let $r \in \mathbb{R}$ be the reference rattle space, then the error the AS should control is

$$e = z_s - z_u - r. \quad (2.3c)$$

To define a control-oriented model in form (1.1), let $\dot{z}_s := v_s$ and $\dot{z}_u := v_u$ and rewrite (2.3a) as

$$\begin{aligned} \dot{z}_s &= v_s \\ m_s \dot{v}_s &= -m_s g - k_s(z_s - z_u - \ell_s) - \beta_s(v_s - v_u) + f_a + f_d \\ \dot{z}_u &= v_u \\ m_u \dot{v}_u &= -m_u g + k_s(z_s - z_u - \ell_s) + \beta_s(v_s - v_u) - f_a \\ &\quad + f_t(z_u - z_r). \end{aligned} \quad (2.4)$$

A detailed investigation of (2.4) suggests that the most important quantities are $z_s - z_u$ and $z_u - z_r$ (more important than every single term). For this reason, introduce a further change of coordinates

$$\begin{bmatrix} x_1 \\ x_2 \\ x_3 \\ x_4 \end{bmatrix} := \begin{bmatrix} z_s - z_u \\ v_s - v_u \\ z_u - z_r \\ v_u - \dot{z}_r \end{bmatrix}, \quad (2.5)$$

and rewrite (2.4), (2.3b), and (2.3c) as

$$\begin{aligned} \dot{x}_1 &= x_2 \\ \dot{x}_2 &= -\frac{m_s + m_u}{m_s m_u} k_s (x_1 - \ell_s) - \frac{m_s + m_u}{m_s m_u} \beta_s x_2 + \frac{m_s + m_u}{m_s m_u} f_a \\ &\quad + \frac{1}{m_s} f_d - \frac{1}{m_u} f_t(x_3) \end{aligned} \quad (2.6a)$$

$$\begin{aligned} \dot{x}_3 &= x_4 \\ \dot{x}_4 &= -g + \frac{k_s}{m_u} (x_1 - \ell_s) + \frac{\beta_s}{m_u} x_2 - \frac{f_a}{m_u} + \frac{1}{m_u} f_t(x_3) - \ddot{z}_r \end{aligned}$$

$$\begin{aligned} y_p &= x_1 \\ y_a &= -g - \frac{k_s}{m_s} (x_1 - \ell_s) - \frac{\beta_s}{m_s} x_2 + \frac{f_a + f_d}{m_s} \end{aligned} \quad (2.6b)$$

$$e = z_s - z_u - r. \quad (2.6c)$$

To obtain a system in the form

$$\begin{aligned} \dot{\mathbf{x}} &= \mathbf{f}(\mathbf{x}, \mathbf{u}, \mathbf{w}) \quad \mathbf{x}(t_0) = \mathbf{x}_0 \\ \mathbf{y} &= \mathbf{h}(\mathbf{x}, \mathbf{u}, \mathbf{w}) \\ \mathbf{e} &= \mathbf{h}_e(\mathbf{x}, \mathbf{u}, \mathbf{w}), \end{aligned} \quad (2.7)$$

define the state $\mathbf{x} = \text{col}(x_1, x_2, x_3, x_4)$, the input $u = f_a$, the disturbance $\mathbf{d} = \text{col}(\ddot{z}_r, f_d)$, the sensor noise $\boldsymbol{\nu} = \text{col}(\nu_p, \nu_a)$, the exogenous $\mathbf{w} = \text{col}(\mathbf{d}, \boldsymbol{\nu}, r)$, the output $\mathbf{y} = \text{col}(y_p, y_a)$, and the following functions:

$$\begin{aligned} \mathbf{f}(\mathbf{x}, u, \mathbf{w}) &= \begin{bmatrix} x_2 \\ \frac{m_s + m_u}{m_s m_u} (-k_s(x_1 - \ell_s) - \beta_s x_2 + u) + \frac{f_d}{m_s} - \frac{1}{m_u} f_t(x_3) \\ x_4 \\ -g + \frac{k_s}{m_u} (x_1 - \ell_s) + \frac{\beta_s}{m_u} x_2 - \frac{u}{m_u} + \frac{1}{m_u} f_t(x_3) - d \end{bmatrix} \\ \mathbf{h}(\mathbf{x}, u, \mathbf{w}) &= \begin{bmatrix} x_1 + \nu_p \\ -g - \frac{k_s}{m_s} (x_1 - \ell_s) - \frac{\beta_s}{m_s} x_2 + \frac{u + f_d}{m_s} + \nu_a \end{bmatrix} \\ h_e(\mathbf{x}, u, \mathbf{w}) &= x_1 - r. \end{aligned} \quad (2.8)$$

To linearize (2.7), assume $u_0 = 0$, $\mathbf{d}_0 = \mathbf{0}$, and determine the equilibrium state $\mathbf{x}_0 := \text{col}(x_{10}, x_{20}, x_{30}, x_{40})$, the equilibrium output $\mathbf{y}_0 := \text{col}(y_{p0}, y_{a0})$, and the reference r_0 by imposing $\dot{\mathbf{x}} = \mathbf{0}$

$$\begin{aligned} 0 &= x_{20} \\ 0 &= -\frac{m_s + m_u}{m_s m_u} k_s (x_{10} - \ell_s) + \frac{k_t}{m_u} (x_{30} - \ell_t) \\ 0 &= x_{40} \\ 0 &= -g + \frac{k_s}{m_u} (x_{10} - \ell_s) - \frac{k_t}{m_u} (x_{30} - \ell_t) \\ y_{p0} &= x_{10} \\ y_{a0} &= -g - \frac{k_s}{m_s} (x_{10} - \ell_s) \\ r_0 &= x_{10}, \end{aligned} \quad (2.9)$$

which leads to

$$\begin{bmatrix} x_{10} \\ x_{20} \\ x_{30} \\ x_{40} \end{bmatrix} = \begin{bmatrix} \ell_s - g \frac{m_s}{k_s} \\ 0 \\ \ell_t - g \frac{m_s + m_u}{k_t} \\ 0 \end{bmatrix} \quad (2.10)$$

$$\begin{bmatrix} y_{p0} \\ y_{a0} \end{bmatrix} = \begin{bmatrix} \ell_s - g \frac{m_s}{k_s} \\ 0 \end{bmatrix}$$

$$r_0 = \ell_s - g \frac{m_s}{k_s}.$$

Define the errors to the equilibrium point as

$$\begin{aligned} \tilde{\mathbf{x}} &:= \mathbf{x} - \mathbf{x}_0, \quad \tilde{u} := u - u_0, \quad \tilde{\mathbf{d}} := \mathbf{d} - \mathbf{d}_0, \quad \tilde{\boldsymbol{\nu}} = \boldsymbol{\nu} - \boldsymbol{\nu}_0, \quad \tilde{\mathbf{y}} := \mathbf{y} - \mathbf{y}_0 \\ \tilde{r} &:= r - r_0, \quad \tilde{\mathbf{w}} = \text{col}(\tilde{d}, \tilde{\boldsymbol{\nu}}, \tilde{\mathbf{r}}), \quad \tilde{e} := e - 0 \end{aligned}$$

and linearize (2.8) to obtain

$$\mathbf{A} = \begin{bmatrix} 0 & 1 & 0 & 0 \\ -k_s \frac{m_s + m_u}{m_s m_u} & -\beta_s \frac{m_s + m_u}{m_s m_u} & \frac{k_t}{m_u} & 0 \\ 0 & 0 & 0 & 1 \\ \frac{k_s}{m_u} & \frac{\beta_s}{m_u} & -\frac{k_t}{m_u} & 0 \end{bmatrix}$$

$$\mathbf{B}_1 = \begin{bmatrix} 0 \\ \frac{m_s + m_u}{m_s m_u} \\ 0 \\ -\frac{1}{m_u} \end{bmatrix}, \quad \mathbf{B}_2 = \begin{bmatrix} 0 & 0 & 0 & 0 & 0 \\ 0 & m_s^{-1} & 0 & 0 & 0 \\ 0 & 0 & 0 & 0 & 0 \\ -1 & 0 & 0 & 0 & 0 \end{bmatrix}$$

$$\mathbf{C} = \begin{bmatrix} 1 & 0 & 0 & 0 \\ -\frac{k_s}{m_s} & -\frac{\beta_s}{m_s} & 0 & 0 \end{bmatrix}, \quad \mathbf{C}_e = [1 \ 0 \ 0 \ 0]$$

$$\mathbf{D}_1 = \begin{bmatrix} 0 \\ m_s^{-1} \end{bmatrix}, \quad \mathbf{D}_2 = \begin{bmatrix} 0 & 0 & 1 & 0 & 0 \\ 0 & m_s^{-1} & 0 & 1 & 0 \end{bmatrix}$$

$$\mathbf{D}_{e2} = [0 \ 0 \ 0 \ 1 \ -1].$$

Then, the linearized model is

$$\begin{aligned} \dot{\tilde{\mathbf{x}}} &= \mathbf{A}\tilde{\mathbf{x}} + \mathbf{B}_1\tilde{u} + \mathbf{B}_2\tilde{\mathbf{w}} \\ \tilde{\mathbf{y}} &= \mathbf{C}\tilde{\mathbf{x}} + \mathbf{D}_1\tilde{u} + \mathbf{D}_2\tilde{\mathbf{w}} \\ \tilde{e} &= \mathbf{C}_e\tilde{\mathbf{x}} + \mathbf{D}_{e2}\tilde{\mathbf{w}}. \end{aligned} \quad (2.11)$$

Important

Model (2.3a) considers the ground infinitely rigid and implicitly defines the vertical force that the asphalt applies on the tire as $N = -k_t(z_u - z_r - \ell_t)$. Then, (2.11) is valid as far as $N \geq 0$, thus matching the physical intuition that the tire is kept “pressed” on the ground. Since the road cannot “pull down” the tire, the inequality $x_3(t) \leq \ell_t$ must be satisfied for any $t \geq t_0$.

2.1.2 Half-Car Model

The half-car model is composed of a *sprung* body modeled by the mass $m > 0$ and the inertia $J > 0$, see Fig. 2.2. The vertical location of the sprung body is denoted by $z \in \mathbb{R}$ while the rotation is $\phi \in \mathbb{R}$. The suspensions generate the forces $f_{s_l}, f_{s_r} \in \mathbb{R}$. In parallel, actuators add the manipulable forces $f_{a_l}, f_{a_r} \in \mathbb{R}$. The suspensions and the actuators are anchored to the sprung body at distances $d_l, d_r > 0$ from the center of gravity. Then, the suspensions transmit the wheel forces $f_{w_l}, f_{w_r} \in \mathbb{R}$ from the ground to the sprung mass. $\ell_l, \ell_r > 0$ denotes the distance from the point at which f_{w_l}, f_{w_r} are applied to the suspension strut mounts. The ground vertical displacements, at the tire-ground contact points, are denoted by p_r and p_l . Accordingly to Newton’s laws, the vertical and rotational dynamics of the sprung mass are

$$\begin{aligned} m\ddot{z} &= -mg + f_{s_l} + f_{s_r} + f_{a_l} + f_{a_r} \\ J\ddot{\phi} &= (f_{s_l} + f_{a_l})d_l - (f_{s_r} + f_{a_r})d_r + f_{w_l}\ell_l + f_{w_r}\ell_r \end{aligned} \quad (2.12a)$$

where $g > 0$ is the gravitational acceleration. Moreover, the superposition of a spring of stiffness $k > 0$ and a damper with friction coefficient $\beta > 0$ models the suspensions. The following expression approximates the length of the suspensions for small values of ϕ :

$$\ell_l = z + d_l \sin \phi - p_l, \quad \ell_r = z - d_r \sin \phi - p_r. \quad (2.12b)$$

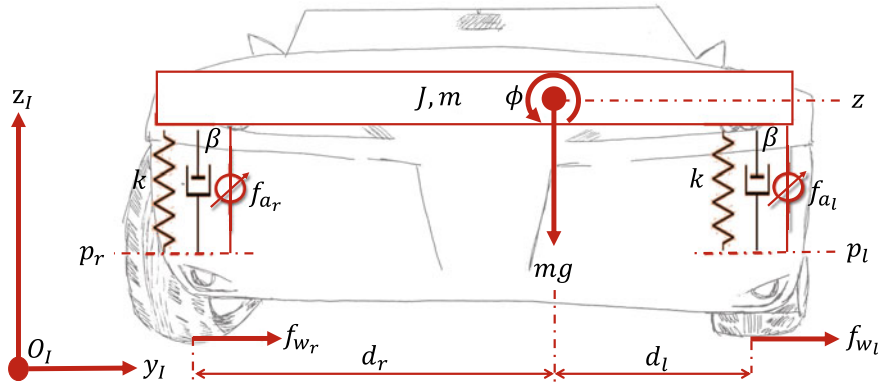


Fig. 2.2 This half-car model, exploited to describe the roll dynamics, has been simplified by neglecting the deflection of the tires. The body is considered rigid and described by its mass m and its inertia J . The right and left suspensions are modeled as in the quarter-car model. The vehicle interacts with the ground and is subject to the lateral forces f_{w_r} and f_{w_l} , which affect the roll angle

To model the ground, let $z_g, \phi_g \in \mathbb{R}$ be the road altitude and bank angle; it is then assumed that

$$p_l = z_g + d_l \sin \phi_g, \quad p_r = z_g - d_r \sin \phi_g. \quad (2.12c)$$

Let $\ell > 0$ be the zero-load length of the suspensions and define the suspension deflections as $s_1 = \ell_l - \ell$ and $s_3 = \ell_r - \ell$. Let $s_2 := \dot{s}_1$ and $s_4 := \dot{s}_3$ be the suspension speeds and define $f_s : \mathbb{R} \times \mathbb{R} \rightarrow \mathbb{R}$ with $f_s(p, v) = -kp - \beta v$. Then the suspension forces are defined as

$$f_{s_l} = f_s(s_1, s_2), \quad f_{s_r} = f_s(s_3, s_4). \quad (2.12d)$$

The kinematic chain describing road banking completes the model. Let $\omega_g, \alpha_g \in \mathbb{R}$ be the bank speed and acceleration, then

$$\dot{\phi}_g = \omega_g, \quad \ddot{\phi}_g = \alpha_g. \quad (2.13)$$

The system has two accelerometers that provide the vertical and lateral accelerations in the body frame, a gyroscope that measures the roll speed, and two potentiometers, one for each suspension, whose output represents the deflection of the suspension. These sensors are modeled as

$$\begin{aligned}
 y_y &= \sin \phi (\ddot{z} + g) + \frac{\cos \phi}{m} (f_{w_r} + f_{w_l}) + \nu_y && \text{y-axis accelerometer} \\
 y_z &= \cos \phi (\ddot{z} + g) - \frac{\sin \phi}{m} (f_{w_r} + f_{w_l}) + \nu_z && \text{z-axis accelerometer} \\
 y_g &= \dot{\phi} + \nu_g && \text{gyroscope} \\
 y_l &= s_1 + \nu_l && \text{left potentiometer} \\
 y_r &= s_3 + \nu_r && \text{right potentiometer}
 \end{aligned} \quad (2.14)$$

in which $\nu_z, \nu_g, \nu_r, \nu_l \in \mathbb{R}$ are the noises affecting the sensors.

The errors that the automatic control system should minimize represent the last part of the model. The active suspension system regulates the vehicle height as the first control goal. As for selecting the second regulated output, this section focuses on improving passenger comfort by defining an apparent roll angle, namely ϕ_a , directly proportional to the passengers' lateral acceleration. The roll angle ϕ_a is defined as a nonlinear combination of the accelerometer measurements. In detail, use y_y and y_z to define $\sin \phi_a = y_y / \sqrt{y_y^2 + y_z^2}$. Let $r_z, r_\phi \in \mathbb{R}$ be the reference height and apparent roll angle. Then, define

$$\mathbf{e} = \begin{bmatrix} y_l d_r + y_r d_l \\ d_r + d_l \\ \phi_a - r_\phi \end{bmatrix}. \quad (2.15)$$

Introduce $x_1 := z - z_g, x_2 := \dot{z} - \dot{z}_g, x_3 := \phi, x_4 := \dot{\phi}, x_5 := \ddot{\phi}_g, x_6 := \omega_g$, and identify the state as $\mathbf{x} := \text{col}(x_1, \dots, x_6)$. Let $u_1 := f_{a_l} + f_{a_r}, u_2 := f_{a_l} d_l - f_{a_r} d_r$, and define the control input as $\mathbf{u} := \text{col}(u_1, u_2)$. Moreover, denote the output with $\mathbf{y} := \text{col}(y_y, y_z, y_g, y_r, y_l)$, and let the reference be $\mathbf{r} := \text{col}(r_z, r_\phi)$. Finally, introduce the disturbance $\mathbf{d} := \text{col}(\ddot{z}_g, \alpha_g, f_{w_l}, f_{w_r})$, the sensor noises $\boldsymbol{\nu} := \text{col}(\nu_y, \nu_z, \nu_g, \nu_l, \nu_r)$, and the exogenous $\mathbf{w} := \text{col}(\mathbf{d}, \boldsymbol{\nu}, \mathbf{r})$. The system is rearranged as

$$\begin{aligned} \dot{\mathbf{x}} &= \mathbf{f}(\mathbf{x}, \mathbf{u}, \mathbf{w}) \\ \mathbf{y} &= \mathbf{h}(\mathbf{x}, \mathbf{u}, \mathbf{w}) \\ \mathbf{e} &= \mathbf{h}_e(\mathbf{x}, \mathbf{u}, \mathbf{w}) \end{aligned} \quad (2.16)$$

where (2.16) is built by exploiting

$$\begin{aligned} \begin{bmatrix} s_1 \\ s_3 \end{bmatrix} &= \begin{bmatrix} x_1 + d_l(\sin x_3 - \sin x_5) \\ x_1 - d_r(\sin x_3 - \sin x_5) \end{bmatrix} \\ \begin{bmatrix} s_2 \\ s_4 \end{bmatrix} &= \begin{bmatrix} x_2 + d_l(x_4 \cos x_3 - x_6 \cos x_5) \\ x_2 - d_r(x_4 \cos x_3 - x_6 \cos x_5) \end{bmatrix}. \end{aligned} \quad (2.17)$$

Now, define $\mathbf{f}(\mathbf{x}, \mathbf{u}, \mathbf{w}) = \text{col}(x_2, f_2 - \ddot{z}_g, x_4, f_4, x_6, \alpha_g)$, where

$$f_2 = -g + \frac{1}{m}(f_s(s_1, s_2) + f_s(s_3, s_4)) + \frac{u_1}{m} \quad (2.18)$$

$$f_4 = \frac{f_s(s_1, s_2)d_l - f_s(s_3, s_4)d_r}{J} + \frac{u_2}{J} + \frac{f_{w_l}\ell_l + f_{w_r}\ell_r}{J}, \quad (2.19)$$

and, as for the output map, let $\mathbf{h}(\mathbf{x}, \mathbf{u}, \mathbf{w}) := \text{col}(h_1, h_2, x_4, s_1, s_3) + \boldsymbol{\nu}$ where

$$h_1 = \sin x_3(f_2 + g) + \cos x_3(f_{w_r} + f_{w_l})/m$$

$$h_2 = \cos x_3(f_2 + g) - \sin x_3(f_{w_r} + f_{w_l})/m.$$

Finally, let

$$\mathbf{h}_e(\mathbf{x}, \mathbf{u}, \mathbf{w}) := \begin{bmatrix} \frac{y_l d_r + y_r d_l}{d_r + d_l} - r_z \\ \sin^{-1} \left(\frac{y_y}{\sqrt{y_y^2 + y_z^2}} \right) - r_\phi \end{bmatrix}. \quad (2.20)$$

To create the linearized model, first find the equilibrium point \mathbf{x}_0 assuming that the system is at rest on a level flat ground and subject to gravity effects only. In more detail, take \mathbf{u}_0 such that $\phi_0 = 0$, and let $\Delta_0 := -mg/(2k)$. This results in $\mathbf{x}_0 = \text{col}(\Delta_0, 0, 0, 0, 0, 0)$, $\mathbf{u}_0 = \text{col}(0, k\Delta_0(d_l - d_r))$, and $\mathbf{y}_0 = \text{col}(0, g, 0, \Delta_0, \Delta_0)$. Let $\mathbf{r}_0 := \text{col}(\Delta_0, 0)$ be the linearization reference and obtain $\mathbf{e}_0 = \mathbf{0}$. Define the errors $\tilde{\mathbf{x}} = \mathbf{x} - \mathbf{x}_0$, $\tilde{\mathbf{u}} = \mathbf{u} - \mathbf{u}_0$, $\tilde{\mathbf{w}} = \mathbf{w} - \mathbf{w}_0$, $\tilde{\mathbf{y}} = \mathbf{y} - \mathbf{y}_0$, and $\tilde{\mathbf{e}} = \mathbf{e} - \mathbf{e}_0$.

The dynamics of $\tilde{\mathbf{x}}$, obtained as the linearization of (2.16) at $(\mathbf{x}_0, \mathbf{u}_0, \mathbf{w}_0)$, is

$$\begin{aligned}\dot{\tilde{\mathbf{x}}} &= \mathbf{A}\tilde{\mathbf{x}} + \mathbf{B}_1\tilde{\mathbf{u}} + \mathbf{B}_2\tilde{\mathbf{w}} \quad \tilde{\mathbf{x}}(0) = \tilde{\mathbf{x}}_0 \\ \tilde{\mathbf{y}} &= \mathbf{C}\tilde{\mathbf{x}} + \mathbf{D}_1\tilde{\mathbf{u}} + \mathbf{D}_2\tilde{\mathbf{w}} \\ \tilde{\mathbf{e}} &= \mathbf{C}_e\tilde{\mathbf{x}} + \mathbf{D}_{e2}\tilde{\mathbf{w}}\end{aligned}\tag{2.21}$$

with

$$\begin{aligned}\mathbf{A} &= \begin{bmatrix} 0 & 1 & 0 & 0 & 0 & 0 \\ -\frac{2k}{m} & -\frac{2\beta}{m} & -\frac{k(d_l-d_r)}{m} & -\frac{\beta(d_l-d_r)}{m} & \frac{k(d_l-d_r)}{m} & \frac{\beta(d_l-d_r)}{m} \\ 0 & 0 & 0 & 1 & 0 & 0 \\ -\frac{k(d_l-d_r)}{J} & -\frac{\beta(d_l-d_r)}{J} & -\frac{k(d_l^2+d_r^2)}{J} & -\frac{\beta(d_l^2+d_r^2)}{J} & \frac{k(d_l^2+d_r^2)}{J} & \frac{\beta(d_l^2+d_r^2)}{J} \\ 0 & 0 & 0 & 0 & 0 & 1 \\ 0 & 0 & 0 & 0 & 0 & 0 \end{bmatrix} \\ \mathbf{B}_1 &= \begin{bmatrix} 0 & 0 \\ 1/m & 0 \\ 0 & 0 \\ 0 & 1/J \\ 0 & 0 \\ 0 & 0 \end{bmatrix}, \quad \mathbf{B}_2 = \begin{bmatrix} 0 & 0 & 0 & 0 & 0 & \mathbf{0} \\ -1 & 0 & 0 & 0 & 0 & \mathbf{0} \\ 0 & 0 & 0 & 0 & 0 & \mathbf{0} \\ 0 & 0 & (\Delta_0 + \ell)/J & (\Delta_0 + \ell)/J & 0 & \mathbf{0} \\ 0 & 0 & 0 & 0 & 0 & \mathbf{0} \\ 0 & 1 & 0 & 0 & 0 & \mathbf{0} \end{bmatrix} \\ \mathbf{C} &= \begin{bmatrix} 0 & 0 & g & 0 & 0 & 0 \\ -\frac{2k}{m} & -\frac{2\beta}{m} & -\frac{k(d_l-d_r)}{m} & -\frac{\beta(d_l-d_r)}{m} & \frac{k(d_l-d_r)}{m} & \frac{\beta(d_l-d_r)}{m} \\ 0 & 0 & 0 & 1 & 0 & 0 \\ 1 & 0 & d_l & 0 & -d_l & 0 \\ 1 & 0 & -d_r & 0 & d_r & 0 \end{bmatrix} \\ \mathbf{C}_e &= \begin{bmatrix} 1 & 0 & 0 & 0 & 0 & 0 \\ 0 & 0 & 1 & 0 & 0 & 0 \end{bmatrix} \\ \mathbf{D}_1 &= \begin{bmatrix} 0 & 0 \\ 1/m & 0 \\ 0 & 0 \\ 0 & 0 \\ 0 & 0 \end{bmatrix}, \quad \mathbf{D}_2 = \begin{bmatrix} 0 & 0 & 1/m & 1/m & 1 & 0 & 0 & 0 & 0 & 0 \\ 0 & 0 & 0 & 0 & 0 & 1 & 0 & 0 & 0 & 0 \\ 0 & 0 & 0 & 0 & 0 & 0 & 1 & 0 & 0 & 0 \\ 0 & 0 & 0 & 0 & 0 & 0 & 0 & 1 & 0 & 0 \\ 0 & 0 & 0 & 0 & 0 & 0 & 0 & 0 & 1 & 0 \end{bmatrix} \\ \mathbf{D}_{e2} &= \begin{bmatrix} 0 & 0 & 0 & 0 & 0 & 0 & \frac{d_r}{d_r+d_l} & \frac{d_l}{d_r+d_l} & -1 & 0 \\ 0 & 0 & \frac{1}{mg} & \frac{1}{mg} & \frac{1}{g} & 0 & 0 & 0 & 0 & -1 \end{bmatrix}.\end{aligned}$$

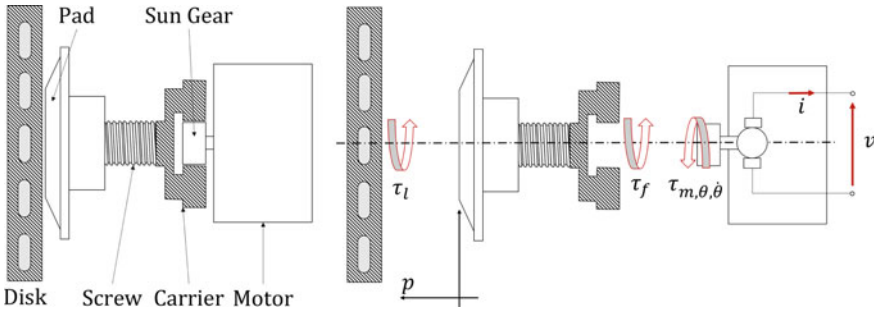


Fig. 2.3 Electro-mechanical Brake example. (Left) The system is composed of an electrical motor that drives a sun gear. The rotative movement is transformed into a linear one to move the pad. The interaction of this latter with the brake disk generates the brake torque. (Right) The assembly is exploded to highlight the terms of major interest. The motor is controlled by the voltage v and the internal current i is directly proportional to τ_m . This torque counteracts the internal friction τ_f and the pad-disk load τ_l

Important

Model (2.21) is valid only if both suspensions are compressed. Indeed, since the ground cannot “pull down” the wheels, the suspension forces $f_{sr} + f_{ar}$, $f_{sl} + f_{al}$ cannot be negative. Thanks to (2.12d), this physical constraint is translated into inequalities $f_{al} \geq ks_1 + \beta s_2$ and $f_{ar} \geq ks_3 + \beta s_4$.

2.2 Electro-mechanical Brakes

Electro-mechanical Brakes (EMB) represent valid options, especially for electric vehicles. They are composed of a brushless motor whose angular rotation is transformed into a linear translation through a planetary gear and a ball screw. Then, the screw moves the brake pads; see Fig. 2.3. As described in [13, 16, 17], the rotor and the gear are modeled as a unique lumped inertia $J > 0$ which is subject to three main torques, i.e., the control torque $\tau_m \in \mathbb{R}$, the torque induced by the braking caliper load $\tau_l \in \mathbb{R}$, and the torque due to internal friction $\tau_f \in \mathbb{R}$. Let $i \in \mathbb{R}$ and $k > 0$ be the motor current and the torque coefficient, then the control torque is

$$\tau_m := i k. \quad (2.22)$$

The torque induced by the caliper load is a nonlinear function of the ball screw displacement, denoted by $p \in \mathbb{R}$. This latter is obtained through the gearbox ratio $N > 0$, as $p = N\theta$, where $\theta \in \mathbb{R}$ is the motor angular position. Then, the torque induced by the caliper load is [29]

$$\tau_l(p) := \begin{cases} 0 & p < 0 \\ \alpha_0 + \alpha_1 p + \alpha_2 p^2 + \alpha_3 p^3 & p \geq 0 \end{cases} \quad (2.23)$$

where $\alpha_0, \dots, \alpha_3 \in \mathbb{R}$. The following Columb model gives the friction torque:

$$\tau_f(\dot{\theta}, \tau_m, \tau_l) = \begin{cases} \frac{\tau_m - \tau_l}{\dot{\theta} = 0} & (\dot{\theta} = 0) \cup (|\tau_m - \tau_l| \leq \tau_s + \beta_0 \tau_l) \\ \frac{\beta_1 \dot{\theta} + \frac{(\beta_2 + \beta_0 \tau_l) \kappa \dot{\theta}}{\sqrt{1 + (\kappa \dot{\theta})^2}}}{\dot{\theta} \neq 0} & \dot{\theta} \neq 0 \\ (\tau_s + \beta_0 \tau_l) \text{sign}(\tau_m - \tau_l) & \text{otherwise} \end{cases} \quad (2.24)$$

where $\kappa, \beta_0, \beta_1, \beta_2, \tau_s > 0$. Write the balance of torques acting on the motor shaft as

$$J \ddot{\theta} = \tau_m - \tau_f - \tau_l \quad (2.25)$$

in which τ_m, τ_f, τ_l are given in (2.22)–(2.24). The following permanent-magnet DC motor models the electric subsystem:

$$L \frac{d}{dt} i = v - Ri - k_{\text{emf}} \dot{\theta} \quad (2.26)$$

where $v \in \mathbb{R}$ denotes the input voltage, $L, R, k_{\text{emf}} > 0$ denote the inductance, resistance, and back-electromagnetic force coefficients. The following sensor suite, composed of a load-cell measuring the clamping force [12] and an incremental encoder providing $\dot{\theta}$, completes the system:

$$\begin{aligned} y_l &= \tau_l / N + \nu_l && \text{load cell} \\ y_\omega &= \dot{\theta} (1 + \nu_\omega) && \text{incremental encoder} \end{aligned} \quad (2.27)$$

where it is worth noting that the encoder output is corrupted by a multiplicative noise; see Infobox 2.1.

Infobox 2.1 (Incremental encoder) *Incremental encoders compute the speed as the ratio of the number of ticks over time. These ticks are usually falling or rising edges of electric signals provided by optical and magnetic/Hall-effect sensors. Then, a first internal counter collects the number of ticks, namely N . Usually, a second counter registers the time ΔT , exploiting a crystal oscillator. Finally, the speed is estimated as*

$$y_\omega = \frac{N + \nu_n}{\Delta T + \nu_t}$$

where $\nu_n, \nu_t \in \mathbb{R}$ denote the counter errors. There are two computation policies:

(a) counting the time to see a fixed number of ticks; (b) counting the number of ticks in a fixed amount of time. These two policies have different performance based on the speed regime. Indeed, let $\omega \in \mathbb{R}$ be the actual speed and $k_n, k_t > 0$ be two proportionality constants (associated with the number of teeth of a gear). Then, the first computation policy reads as

$$y_{\omega_1} = \frac{N + \nu_n}{\frac{k_t}{\omega} + \nu_t} = \omega \frac{N + \nu_n}{k_t + \omega \nu_t}$$

whereas the second one is

$$y_{\omega_2} = \frac{k_n \omega + \nu_n}{\Delta T + \nu_t}.$$

It is easy to see that y_{ω_1} is more reliable than y_{ω_2} at low-speed regimes. On the opposite, at high speeds, y_{ω_2} works better than y_{ω_1} . Petrella et al. [24] suggest mixing these two computation strategies. A first-order truncated Taylor expansion approximates the outputs y_{ω_1} , y_{ω_2} under the assumption of small noises. In particular, let $k_t = N$ and $k_n = \Delta T$, then

$$\begin{aligned} y_{\omega_1} &\approx \omega \left(1 + \frac{\nu_n}{N} - \frac{\omega}{N} \nu_t \right) \\ y_{\omega_2} &\approx \omega \left(1 + \frac{1}{\Delta T} \nu_t \right) + \frac{\nu_n}{\Delta T}. \end{aligned}$$

To conclude, in agreement with the speed regimes, for $\omega \ll \frac{N}{\nu_t}$

$$y_{\omega_1} \approx \omega \left(1 + \frac{\nu_n}{N} \right),$$

whereas for $\omega \gg \frac{\nu_n}{\Delta T}$

$$y_{\omega_2} \approx \omega \left(1 + \frac{\nu_t}{\Delta T} \right).$$

A typical goal of EMB control systems is to make the brake caliper load τ_l/N tracking a reference load $r \geq 0$ [17].

To formalize the plant as

$$\begin{aligned} \dot{\mathbf{x}} &= \mathbf{f}(\mathbf{x}, u, \mathbf{w}) & \mathbf{x}(t_0) &= \mathbf{x}_0 \\ \mathbf{y} &= \mathbf{h}(\mathbf{x}, u, \mathbf{w}) \\ e &= h_e(\mathbf{x}, u, \mathbf{w}), \end{aligned} \tag{2.28}$$

let $\omega := \dot{\theta}$ be the motor angular speed, $\mathbf{x} := \text{col}(\theta, \omega, i)$ be the state, $u := v$ be the control, $d := \tau_f$ be the disturbance, $\nu := \text{col}(\nu_l, \nu_\omega)$ be the sensor noises, $\mathbf{w} := \text{col}(d, \nu, r)$ be the exogenous signals, $\mathbf{y} := \text{col}(y_l, y_\omega)$ be the outputs, and $e := \tau_l/N - r$ be the regulated output. Then, define

$$\begin{aligned} \mathbf{f}(\mathbf{x}, u, \mathbf{w}) &= \begin{bmatrix} \omega \\ J^{-1}(i k - \tau_f(\omega, i k, \tau_l(N\theta)) - \tau_l(N\theta)) \\ L^{-1}(u - R i - k_{\text{emf}}\omega) \end{bmatrix} \\ \mathbf{h}(\mathbf{x}, u, \mathbf{w}) &= \begin{bmatrix} \tau_l(N\theta)/N + \nu_l \\ \omega(1 + \nu_\omega) \end{bmatrix} \\ h_e(\mathbf{x}, u, \mathbf{w}) &= \tau_l(N\theta)/N - r + \nu_l. \end{aligned} \tag{2.29}$$

Remark 2.1. The definition of $d = \tau_f$ as an exogenous signal, i.e.,

$$d(t) = \tau_f(\dot{\theta}(t), \tau_m(t), \tau_l(t))$$

as a function that only depends on t , hides the state dependency and thus creates a model mismatch that impacts the linearization. Indeed, friction phenomena dissipate energy and represent a “natural source of stabilization” for the open-loop plant.

Consequently, the linearization process and control system design neglect this natural stability. On the other hand, the friction force discontinuities represent strong non-linearities that limit the performance of a control system designed via linearization; see Sect. 5.4.2. The literature proposes systems dedicated to the control of discontinuous systems [6,31].

To linearize (2.28), let $(\mathbf{x}_0, u_0, \mathbf{w}_0, \mathbf{y}_0, e_0)$ be the equilibrium tuple. Impose $\dot{\mathbf{x}} = 0$, $r = r_0$, $d_0 = 0$, $\nu = \mathbf{0}$, and exploit (2.29) to define $\mathbf{x}_0 = \text{col}(\theta_0, 0, i_0)$, where $\theta_0 : \tau_l(N\theta_0)/N = r_0$ and $i_0 k = k^{-1} \tau_l(N\theta_0)$. Moreover, let $u_0 := R i_0$, $\mathbf{y}_0 := \text{col}(r_0, 0)$, $e_0 = 0$, and $\mathbf{w}_0 := \text{col}(0, \mathbf{0}, r_0)$. Then, define the errors $\tilde{\mathbf{x}} = \mathbf{x} - \mathbf{x}_0$, $\tilde{u} = u - u_0$, $\tilde{\mathbf{y}} = \mathbf{y} - \mathbf{y}_0$, $\tilde{\mathbf{w}} = \mathbf{w} - \mathbf{w}_0$, and $\tilde{e} = e - e_0$, and linearize (2.29) assuming $r_0 > 0$ (which implies $\theta_0, i_0 > 0$).

Let

$$\begin{aligned}\mathbf{A} &:= \begin{bmatrix} 0 & 1 & 0 \\ -N \frac{N\alpha_1 + 2\alpha_2 N^2 \theta_0 + 3N\alpha_3 (N\theta_0)^2}{J} & 0 & \frac{k}{J} \\ 0 & -L^{-1} k_{\text{emf}} & -L^{-1} R \end{bmatrix} \\ \mathbf{B}_1 &:= \begin{bmatrix} 0 \\ 0 \\ L^{-1} \end{bmatrix}, \quad \mathbf{B}_2 := \begin{bmatrix} 0 & 0 & 0 & 0 \\ -J^{-1} & 0 & 0 & 0 \\ 0 & 0 & 0 & 0 \end{bmatrix} \\ \mathbf{C} &:= \begin{bmatrix} N\alpha_1 + 2\alpha_2 N^2 \theta_0 + 3N\alpha_3 (N\theta_0)^2 & 0 & 0 \\ 0 & 1 & 0 \end{bmatrix}, \quad \mathbf{D}_2 := \begin{bmatrix} 0 & 1 & 0 & 0 \\ 0 & 0 & 1 & 0 \end{bmatrix} \\ \mathbf{C}_e &:= \begin{bmatrix} N\alpha_1 + 2\alpha_2 N^2 \theta_0 + 3N\alpha_3 (N\theta_0)^2 & 0 & 0 \end{bmatrix}, \quad \mathbf{D}_{e2} := \begin{bmatrix} 0 & 1 & 0 & -1 \end{bmatrix}.\end{aligned}$$

Then, the linearized system is given by

$$\begin{aligned}\dot{\tilde{\mathbf{x}}} &= \mathbf{A} \tilde{\mathbf{x}} + \mathbf{B}_1 \tilde{u} + \mathbf{B}_2 \tilde{\mathbf{w}} \quad \tilde{\mathbf{x}}(0) = \tilde{\mathbf{x}}_0 \\ \tilde{\mathbf{y}} &= \mathbf{C} \tilde{\mathbf{x}} + \mathbf{D}_2 \tilde{\mathbf{w}} \\ \tilde{\mathbf{e}} &= \mathbf{C}_e \tilde{\mathbf{x}} + \mathbf{D}_{e2} \tilde{\mathbf{w}}.\end{aligned}\tag{2.30}$$

Important

System (2.30) represents a valid linearization of (2.28) as long as $\tau_l(1) > 0$ for any $t \geq 0$. In particular, $\theta(t) \geq 0$, for any $t \geq 0$, fulfills this constraint.

2.3 Wheel Speed Controls

Vehicles are subject to forces generated by the interaction with the ground. These forces are mainly due to the ratio between the wheel angular speed and the vehicle speed [23]. Thus, manipulating the wheel speed represents one of the essential tools for stabilizing and controlling ground vehicles. This section presents the model of a 2D car [22].

Fig. 2.4 Graphical representation of the principal quantities involved in the design of wheel controls

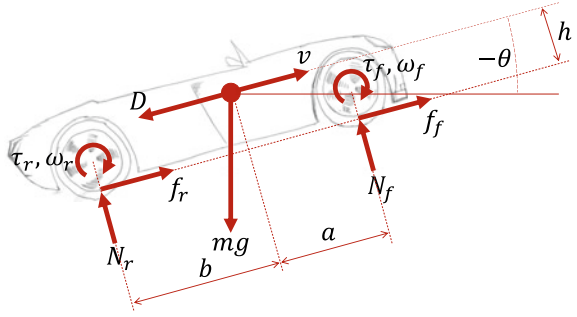


Figure 2.4 shows the plant, which is composed of two wheels and a main body. The subscripts f and r denote quantities associated with the front and rear wheels, respectively.

Rigid bodies, with inertia $J_r, J_f > 0$ and radius $r_r, r_f > 0$, rotating at speed $\omega_r, \omega_f \in \mathbb{R}$, model the rear and front wheels. The wheels are subject to shaft torques $\tau_r, \tau_f \in \mathbb{R}$ and friction forces generated by the contact with the ground. In particular, these two forces are due to rolling resistance and traction, later described. On the other hand, the vehicle is modeled as a point mass, of mass $m > 0$ inclusive of the wheels, whose inertial position and speed is $p, v \in \mathbb{R}$. The vehicle dynamics are influenced by the aerodynamic drag $D \in \mathbb{R}$.

Denote by $N_r, N_f \geq 0$ the forces normal to the ground and let $f_r, f_f \in \mathbb{R}$ be the rear and front friction forces, whose classical formulation [23, 28] is

$$\begin{aligned} f_r &= N_r(\mu(\lambda(v, \omega_r r_r), \Theta) - c_r(v)) \\ f_f &= N_f(\mu(\lambda(v, \omega_f r_f), \Theta) - c_r(v)) \end{aligned} \quad (2.31)$$

where $c_r : \mathbb{R} \rightarrow \mathbb{R}$ represents the rolling resistance coefficient, $\lambda : \mathbb{R}^2 \rightarrow [-1, 1]$ is the longitudinal slip ratio, and $\mu : [-1, 1] \times \mathbb{R}^3 \rightarrow \mathbb{R}$ is the traction coefficient. Commonly, semi-empirical functions model the traction coefficient. For example, the so-called “Burckhardt formula” reads as

$$\mu(\lambda, \Theta) = \text{sign}(\lambda)\theta_1 \left(1 - e^{-|\lambda|\theta_2}\right) - \lambda\theta_3 \quad (2.32)$$

where $\Theta := \text{col}(\theta_1, \theta_2, \theta_3) \in \mathbb{R}^3$ are coefficients depending on tire and road conditions.

As depicted in Fig. 2.5, the traction coefficient is null for $\lambda = 0$, reaches a maximum (minimum) at a specific $\lambda > 0 (< 0)$, and decreases to a less positive (negative) value for $\lambda = 1 (= -1)$. The longitudinal slip ratio is defined as

$$\lambda(v, \omega r) = \begin{cases} 0 & v = \omega r \quad (\text{rolling/at rest}) \\ \frac{\omega r - v}{\max\{|v|, |\omega r|, |\omega_r - v|\}} & \text{otherwise} \quad (\text{driving/braking}). \end{cases} \quad (2.33)$$

Commonly, polynomial functions of v model the rolling resistance coefficient. According to the standard SAE J2452, the following relation holds [8, 20]:

$$c_r(v) = c_{r0} + c_{r1}v + c_{r2}v^2 \quad (2.34)$$

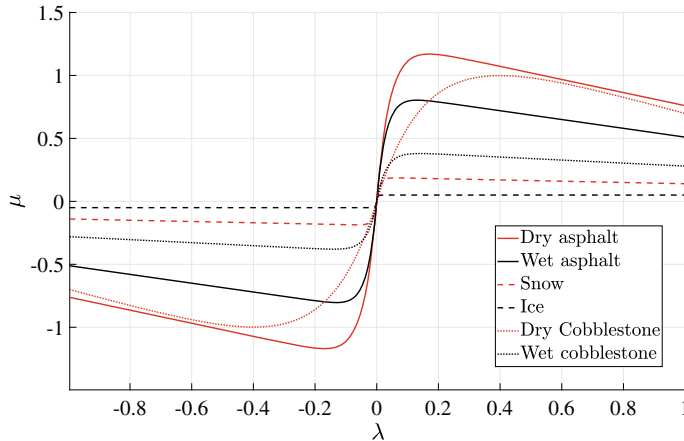


Fig. 2.5 Traction coefficient as a function of the longitudinal slip ratio. Positive values of μ correspond to driving, whereas a negative μ identifies braking

where $c_{r0}, c_{r1}, c_{r2} > 0$ depend on the tire geometry, the tire inflation pressure, and the road surface.

Assume rigid suspension and let $h, a, b > 0$ be the vertical and longitudinal distances from the center of gravity to the rear and front wheels' contact points. Then, the vehicle dynamics are obtained, via a Newtonian approach, by considering the longitudinal acceleration and the vertical and rotational equilibria

$$\begin{aligned} m\dot{v} &= -mg \sin \theta + f_f + f_r - D && \text{longitudinal} \\ 0 &= -mg \cos \theta + N_f + N_r && \text{vertical} \\ 0 &= -(f_f + f_r)h - N_f a + N_r b && \text{rotational.} \end{aligned} \quad (2.35)$$

Equations (2.35) contain the unknowns \dot{v}, N_r, N_f which, thanks to the linear dependence of f_f, f_r on N_f, N_r (see Eq. (2.31)), are found as solutions of a linear system. In more detail, let $\mu_r := \mu(\lambda(v, \omega_r r_r), \Theta)$, $\mu_f := \mu(\lambda(v, \omega_f r_f), \Theta)$, $\ell := a + b$, $\bar{h} := h/\ell$, $\bar{a} := a/\ell$, and $\bar{b} := b/\ell$, then

$$\dot{v} = -g \sin \theta + \frac{N_f}{m}(\mu_f - c_r) + \frac{N_r}{m}(\mu_r - c_r) - \frac{D}{m}, \quad (2.36a)$$

where

$$\begin{bmatrix} N_r \\ N_f \end{bmatrix} = \frac{mg \cos \theta}{1 - (\mu_r - \mu_f)\bar{h}} \begin{bmatrix} (\mu_f - c_r)\bar{h} + \bar{a} \\ -(\mu_r - c_r)\bar{h} + \bar{b} \end{bmatrix}. \quad (2.36b)$$

The aerodynamic effects are specialized to complete the description of (2.36). In more detail, the drag force is modeled as a nonlinear function of the vehicle speed. Let $w \in \mathbb{R}$ be the wind speed (supposed as parallel to v), then

$$D(v - w) = \frac{1}{2}\rho S \frac{(v - w)^3}{|v - w|} C_D \quad (2.37)$$

where $C_D > 0$ denotes the drag coefficient, $\rho > 0$ is the air density, and $S > 0$ represents a reference area (usually, the cross-section or the footprint).

As for the wheel dynamics, the following equations describe the rotational acceleration of the rear and front wheels:

$$\begin{aligned} J_r \dot{\omega}_r &= \tau_r - f_r r_r \\ J_f \dot{\omega}_f &= \tau_f - f_f r_f, \end{aligned} \quad (2.38)$$

where $\tau_f, \tau_r \in \mathbb{R}$ are the torques applied on the wheel shaft by the driveline and brakes.

The plant has a GNSS receiver providing v and two tonewheels sensing the wheel speed ω_r, ω_f . These sensors are affected by the noises $\nu_v, \nu_r, \nu_f \in \mathbb{R}$, respectively. Then,

$$\begin{aligned} y_v &= v + \nu_v && \text{GNSS receiver} \\ y_r &= \omega_r(1 + \nu_r) && \text{rear tonewheel} \\ y_f &= \omega_f(1 + \nu_f) && \text{front tonewheel.} \end{aligned} \quad (2.39)$$

The goal of speed control systems, such as the ABS, TC, and LaC, is to regulate ω_r, ω_f to a given reference $r_r(t), r_f(t)$ [26]. Define,

$$\begin{aligned} e_r &= \omega_r - r_r(t) \\ e_f &= \omega_f - r_f(t) \end{aligned} \quad (2.40)$$

and let $\mathbf{x} := \text{col}(v, \omega_r, \omega_f)$, $\mathbf{u} := \text{col}(\tau_r, \tau_f)$, $\mathbf{w} := \text{col}(\theta, w, \nu_v, \nu_r, \nu_f, r_r, r_f)$, $\mathbf{y} := \text{col}(v, \omega_r, \omega_f)$, and $\mathbf{e} := \text{col}(e_r, e_f)$. Then (2.36)–(2.40) can be compacted in the form

$$\begin{aligned} \dot{\mathbf{x}} &= \mathbf{f}(\mathbf{x}, \mathbf{u}, \mathbf{w}) & \mathbf{x}(t_0) &= \mathbf{x}_0 \\ \mathbf{y} &= \mathbf{h}(\mathbf{x}, \mathbf{u}, \mathbf{w}) \\ \mathbf{e} &= \mathbf{h}_e(\mathbf{x}, \mathbf{u}, \mathbf{w}) \end{aligned} \quad (2.41a)$$

by defining

$$\mathbf{f}(\mathbf{x}, \mathbf{u}, \mathbf{w}) = \begin{bmatrix} \frac{N_f(\mu_f - c_r) + N_r(\mu_r - c_r)}{m} - g \sin \theta - \frac{D}{m} \\ J_r^{-1} (\tau_r - N_r r_r (\mu_r - c_r)) \\ J_f^{-1} (\tau_f - N_f r_f (\mu_f - c_r)) \end{bmatrix} \quad (2.41b)$$

$$\mathbf{h}(\mathbf{x}, \mathbf{u}, \mathbf{w}) = \begin{bmatrix} v + \nu_v \\ \omega_r(1 + \nu_r) \\ \omega_f(1 + \nu_f) \end{bmatrix}, \quad \mathbf{h}_e(\mathbf{x}, \mathbf{u}, \mathbf{w}) = \begin{bmatrix} \omega_r(1 + \nu_r) - r_r \\ \omega_f(1 + \nu_f) - r_f \end{bmatrix}, \quad (2.41c)$$

where N_r, N_f are introduced in (2.36b).

The solutions to the following equation represent the traction coefficients needed to negotiate $\dot{v}_0 \in \mathbb{R}$:

$$N_f(\mu_f - c_r) + N_r(\mu_r - c_r) = \dot{v}_0 + D + mg \sin \theta, \quad (2.42)$$

where the speed dependence has been omitted to shorten the notation. Substitute

(2.36b) into (2.42) to eliminate N_r and N_f , then find μ_f as

$$\mu_f = \frac{mgc_r + \dot{v}_0 + D + mg \sin \theta}{mg\bar{b} - (\dot{v}_0 + D + mg \sin \theta)\bar{h}} - \mu_r \frac{(\dot{v}_0 + D + mg \sin \theta)\bar{h} + mg\bar{a}}{mg\bar{b} - (\dot{v}_0 + D + mg \sin \theta)\bar{h}}. \quad (2.43)$$

The latter equation describes the traction distribution (for front-wheel driving, set $\mu_r = 0$, whereas for rear-wheel driving, impose $\mu_f = 0$). Define

$$\mu'_r = \frac{mgc_r + \dot{v}_0 + D + mg \sin \theta}{(\dot{v}_0 + D + mg \sin \theta)\bar{h} + mg\bar{a}}, \quad (2.44)$$

which corresponds to the value of μ_r such that $\mu_f = 0$. Let $\mu^* > 0$ be the maximum traction coefficient according to the actual road and tire conditions. Then, the desired acceleration \dot{v}_0 is negotiated for any

$$\mu_r \in [0, \min\{\mu^*, \mu'_r\}]$$

and μ_f given by (2.43).

Important

Model (2.41) is valid as far as N_r and $N_f \geq 0$. In particular, the vehicle speed, acceleration, and rear wheel speed (through the traction coefficient) are bounded to avoid wheelies. Exploit (2.43) to constrain v, \dot{v} in a subdomain of \mathbb{R}^2 such that $mg\bar{b} - (\dot{v} + D + mg \sin \theta)\bar{h} > 0$. Therefore, the rear traction coefficient is bounded by using (2.36b) as $\mu_r < c_r + \bar{b}/\bar{h}$.

To define the linearization conditions, let $v_0 > 0$ be a constant equilibrium speed and assume $\mathbf{w} = \mathbf{0}$. Then, let (μ_{r0}, μ_{f0}) be an equilibrium couple with $\mu_{r0} \in [0, \min\{\mu^*, \mu'_{r0}\}]$. The coefficients μ'_{r0} and μ_{f0} are obtained from (2.44) and (2.43) and evaluated at $\dot{v} = 0, v = v_0, w = \theta = 0$, and $\mu_r = \mu_{r0}$. The equilibrium $(\lambda_{r0}, \lambda_{f0})$ are found as implicit solutions to (2.32) with $\mu_{r0} = \mu(\lambda_{r0})$ and $\mu_{f0} = \mu(\lambda_{f0})$. Moreover, the equilibrium $(\omega_{r0}, \omega_{f0})$ is found by exploiting (2.33) to solve $\lambda_{r0} = \lambda(v_0, \omega_{r0} r_r)$ and $\lambda_{f0} = \lambda(v_0, \omega_{f0} r_f)$. With these quantities at hand, define $\mathbf{x}_0 = \text{col}(v_0, \omega_{r0} r_r, \omega_{f0})$.

Let $\mathbf{u}_0 := \text{col}(\tau_{r0}, \tau_{f0})$ be the equilibrium control input whose entries are computed as

$$\begin{aligned} \tau_{r0} &= r_r(\mu_{r0} - c_r) \frac{mg((\mu_{f0} - c_r)\bar{h} + \bar{a})}{1 - (\mu_{r0} - \mu_{f0})\bar{h}} \\ \tau_{f0} &= r_f(\mu_{f0} - c_r) \frac{mg(-(\mu_{r0} - c_r)\bar{h} + \bar{b})}{1 - (\mu_{r0} - \mu_{f0})\bar{h}}. \end{aligned} \quad (2.45)$$

The equilibrium output is $\mathbf{y}_0 = \mathbf{x}_0$, whereas $(r_{r0}, r_{f0}) = (\omega_{r0}, \omega_{f0})$ leads to $\mathbf{e}_0 = \mathbf{0}$.

Then, define the errors $\tilde{\mathbf{x}} = \mathbf{x} - \mathbf{x}_0$, $\tilde{\mathbf{u}} = \mathbf{u} - \mathbf{u}_0$, $\tilde{\mathbf{y}} = \mathbf{y} - \mathbf{y}_0$, $\tilde{\mathbf{w}} = \mathbf{w} - \mathbf{w}_0$, $\tilde{\mathbf{e}} = \mathbf{e} - \mathbf{e}_0$, and linearize (2.41) by defining

$$\begin{aligned}\dot{\tilde{\mathbf{x}}} &= \mathbf{A}\tilde{\mathbf{x}} + \mathbf{B}_1\tilde{\mathbf{u}} + \mathbf{B}_2\tilde{\mathbf{w}} \quad \tilde{\mathbf{x}}(0) = \tilde{\mathbf{x}}_0 \\ \tilde{\mathbf{y}} &= \mathbf{C}\tilde{\mathbf{x}} + \mathbf{D}_2\tilde{\mathbf{w}} \\ \tilde{\mathbf{e}} &= \mathbf{C}_e\tilde{\mathbf{x}} + \mathbf{D}_{e2}\tilde{\mathbf{w}}\end{aligned}\tag{2.46}$$

with

$$\begin{aligned}\mathbf{A} &= \left[\begin{array}{ccc} \frac{1}{m} \left(\frac{\partial f_r + f_f}{\partial v} - \rho S v C_D \right) & \frac{1}{m} \frac{\partial f_r + f_f}{\partial \omega_r} & \frac{1}{m} \frac{\partial f_r + f_f}{\partial \omega_f} \\ -\frac{r_r}{J_r} \frac{\partial f_r}{\partial v} & -\frac{r_r}{J_r} \frac{\partial f_r}{\partial \omega_r} & -\frac{r_r}{J_r} \frac{\partial f_r}{\partial \omega_f} \\ -\frac{r_f}{J_f} \frac{\partial f_f}{\partial v} & -\frac{r_f}{J_f} \frac{\partial f_f}{\partial \omega_r} & -\frac{r_f}{J_f} \frac{\partial f_f}{\partial \omega_f} \end{array} \right]_{\mathbf{x}=\mathbf{x}_0} \\ \mathbf{B}_1 &= \begin{bmatrix} 0 & 0 \\ J_r^{-1} & 0 \\ 0 & J_f^{-1} \end{bmatrix}, \quad \mathbf{B}_2 = \begin{bmatrix} -g & \frac{1}{m} \rho S v_0 C_D & 0 & 0 & 0 & 0 & 0 \\ 0 & 0 & 0 & 0 & 0 & 0 & 0 \\ 0 & 0 & 0 & 0 & 0 & 0 & 0 \end{bmatrix} \\ \mathbf{C} &= \mathbf{I}, \quad \mathbf{D}_2 = \begin{bmatrix} 0 & 0 & 1 & 0 & 0 & 0 & 0 \\ 0 & 0 & 0 & \omega_{r0} & 0 & 0 & 0 \\ 0 & 0 & 0 & 0 & \omega_{f0} & 0 & 0 \end{bmatrix} \\ \mathbf{C}_e &= \begin{bmatrix} 0 & 1 & 0 \\ 0 & 0 & 1 \end{bmatrix}, \quad \mathbf{D}_{e2} = \begin{bmatrix} 0 & 0 & 0 & \omega_{r0} & 0 & -1 & 0 \\ 0 & 0 & 0 & 0 & \omega_{f0} & 0 & -1 \end{bmatrix}.\end{aligned}\tag{2.47}$$

The partial derivatives, appearing in (2.47), are detailed as:

$$\begin{aligned}\frac{\partial f_r}{\partial v} &= \left(\frac{\partial N_r}{\partial \mu_r} \frac{\partial \mu_r}{\partial \lambda_r} \frac{\partial \lambda_r}{\partial v} + \frac{\partial N_r}{\partial \mu_f} \frac{\partial \mu_f}{\partial \lambda_f} \frac{\partial \lambda_f}{\partial v} + \frac{\partial N_r}{\partial c_r} \frac{\partial c_r}{\partial v} + \frac{\partial N_r}{\partial c_r} \frac{\partial c_r}{\partial v} \right) (\mu_r - c_r) \\ &\quad + N_r \left(\frac{\partial \mu_r}{\partial \lambda_r} \frac{\partial \lambda_r}{\partial v} - \frac{\partial c_r}{\partial v} \right) \\ \frac{\partial f_f}{\partial v} &= \left(\frac{\partial N_f}{\partial \mu_r} \frac{\partial \mu_r}{\partial \lambda_r} \frac{\partial \lambda_r}{\partial v} + \frac{\partial N_f}{\partial \mu_f} \frac{\partial \mu_f}{\partial \lambda_f} \frac{\partial \lambda_f}{\partial v} + \frac{\partial N_f}{\partial c_r} \frac{\partial c_r}{\partial v} + \frac{\partial N_f}{\partial c_r} \frac{\partial c_r}{\partial v} \right) (\mu_f - c_r) \\ &\quad + N_f \left(\frac{\partial \mu_f}{\partial \lambda_f} \frac{\partial \lambda_f}{\partial v} - \frac{\partial c_r}{\partial v} \right) \\ \frac{\partial f_r}{\partial \omega_r} &= \left(\frac{\partial N_r}{\partial \mu_r} (\mu_r - c_r) + N_r \right) \frac{\partial \mu_r}{\partial \lambda_r} \frac{\partial \lambda_r}{\partial \omega_r} \\ \frac{\partial f_f}{\partial \omega_r} &= \frac{\partial N_f}{\partial \mu_r} \frac{\partial \mu_r}{\partial \lambda_r} \frac{\partial \lambda_r}{\partial \omega_r} (\mu_f - c_r) \\ \frac{\partial f_r}{\partial \omega_f} &= \frac{\partial N_r}{\partial \mu_f} \frac{\partial \mu_f}{\partial \lambda_f} \frac{\partial \lambda_f}{\partial \omega_f} (\mu_r - c_r) \\ \frac{\partial f_f}{\partial \omega_f} &= \left(\frac{\partial N_f}{\partial \mu_f} (\mu_f - c_r) + N_f \right) \frac{\partial \mu_f}{\partial \lambda_f} \frac{\partial \lambda_f}{\partial \omega_f}\end{aligned}$$

with

$$\begin{aligned}\frac{\partial N_r}{\partial \mu_r} &= mg \cos \theta \frac{\bar{a} + (\mu_f - c_r)\bar{h}}{(1 - (\mu_r - \mu_f)\bar{h})^2} \bar{h} \\ \frac{\partial N_r}{\partial \mu_f} &= mg \cos \theta \frac{1 - \bar{a} + (c_r - \mu_r)\bar{h}}{(1 - (\mu_r - \mu_f)\bar{h})^2} \bar{h} \\ \frac{\partial N_f}{\partial \mu_r} &= -mg \cos \theta \frac{1 - \bar{b} + (\mu_f - c_r)\bar{h}}{(1 - (\mu_r - \mu_f)\bar{h})^2} \bar{h} \\ \frac{\partial N_f}{\partial \mu_f} &= -mg \cos \theta \frac{\bar{b} - (\mu_r - c_r)\bar{h}}{(1 - (\mu_r - \mu_f)\bar{h})^2} \bar{h} \\ \frac{\partial N_r}{\partial c_r} &= -\frac{mg \cos \theta}{1 - (\mu_r - \mu_f)\bar{h}} \bar{h} \\ \frac{\partial N_f}{\partial c_r} &= \frac{mg \cos \theta}{1 - (\mu_r - \mu_f)\bar{h}} \bar{h}\end{aligned}$$

and

$$\begin{aligned}\frac{\partial \mu}{\partial \lambda} &= \text{sign}(\lambda) \theta_1 \theta_2 e^{-\lambda \theta_2} - \theta_3, \quad \frac{\partial c_r}{\partial v} = c_{r1} + 2c_{r2}v, \\ \frac{\partial \lambda}{\partial \omega} &= \begin{cases} 0 & v = \omega r \\ v/(\omega^2 r) & \omega r > v > 0 \\ r/v & v > \omega r > 0 \end{cases}, \quad \frac{\partial \lambda}{\partial v} = \begin{cases} 0 & v = \omega r \\ -(\omega r)^{-1} & \omega r > v > 0 \\ -\omega r/v^2 & v > \omega r > 0 \end{cases}.\end{aligned}$$

2.4 Adaptive Cruise Control

Driving for a long time in a queue on a highway represents a demanding task. The Adaptive Cruise Control (ACC) tracks the preceding vehicle's speed while keeping its safety distance to alleviate the driver's workload [14,21]. Three cars in a queue comprise the plant under investigation. Subscripts A, B, and C identify these vehicles. Assume A is the leader and B and C are the followers, then the vehicles B and C are modeled as points, with mass $m_B, m_C > 0$, subject to wind and road disturbances and driver control actions. Define by $p_A, p_B, p_C \in \mathbb{R}$ the inertial vehicle positions, denote by $v_A, v_B, v_C \in \mathbb{R}$ the inertial speeds, and use w and θ to describe the wind speed and the road slope. Then, in agreement with the kinematics and Newton's laws of dynamics, compute

$$\begin{aligned}\dot{p}_A &= v_A \\ \dot{p}_B &= v_B \\ \dot{v}_B &= g \sin \theta + \frac{1}{m_B} (f_B - D_B(v_B - w)) \\ \dot{p}_C &= v_C \\ \dot{v}_C &= g \sin \theta + \frac{1}{m_C} (f_C - D_C(v_C - w)),\end{aligned}\tag{2.48}$$

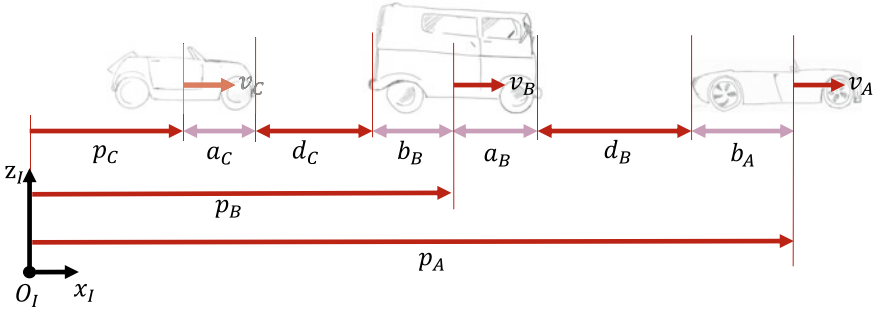


Fig. 2.6 Platoon of three heterogeneous vehicles

where $f_B, f_C \in \mathbb{R}$ are the driver-induced forces. The terms $D_B, D_C \in \mathbb{R}$ denote the aerodynamic drag forces (see Eq. (2.37))

$$\begin{aligned} D_B(v_B - w) &= \frac{1}{2}\rho S_B C_{D_B}(v_B - w)^2 \\ D_C(v_C - w) &= \frac{1}{2}\rho S_C C_{D_C}(v_C - w)^2, \end{aligned}$$

where $\rho > 0$ is the air density, $C_{D_B}, C_{D_C} > 0$ are the drag coefficients, and $S_B, S_C > 0$ denote the vehicle cross-sections. In the context of ACC, the followers (B and C) have to track the leader (A) whose acceleration, namely a_A , is unknown.

Define by $b_A, a_B, b_B, a_C > 0$ the longitudinal lengths of the three vehicles, as illustrated in Fig. 2.6, and let

$$\begin{aligned} d_B &:= p_A - p_B - b_A - a_B \\ d_C &:= p_B - p_C - b_B - a_C \end{aligned} \tag{2.49}$$

be the inter-vehicle distances A–B and B–C. Assume that vehicles B and C have a GNSS receiver and a device sensing the inter-vehicle distance (such as lidars or range finders). Then, the available measurements are

$$\begin{aligned} y_{dB} &= d_B + \nu_{dB} && \text{range sensor vehicle B} \\ y_{vB} &= v_B + \nu_{vB} && \text{GNSS vehicle B} \\ y_{dC} &= d_C + \nu_{dC} && \text{range sensor vehicle C} \\ y_{vC} &= v_C + \nu_{vC} && \text{GNSS vehicle C}, \end{aligned} \tag{2.50}$$

where $\nu_{dB}, \nu_{dC} \in \mathbb{R}$ denote noises affecting the distance measurement, and $\nu_{vB}, \nu_{vC} \in \mathbb{R}$ are noises on the GNSS receiver's output. According to the *Highway Code*, the speed of the follower defines the safety distance between two vehicles. Therefore

$$\begin{aligned} d_B^* &= d_{\min} + \frac{1}{k} v_B^2 \\ d_C^* &= d_{\min} + \frac{1}{k} v_C^2, \end{aligned} \tag{2.51}$$

where $k, d_{\min} > 0$, represent the safety distances. Then, define the following errors:

$$\begin{aligned} e_{dB} &= d_B - d_B^* \\ e_{dC} &= d_C - d_C^* \end{aligned} \quad (2.52)$$

and let $\mathbf{x} := \text{col}(d_B, v_B, d_C, v_C)$, $\mathbf{u} := \text{col}(f_B, f_C)$, $\mathbf{d} := \text{col}(v_A, \sin \theta, w)$, $\boldsymbol{\nu} := \text{col}(\nu_{dB}, \nu_{vB}, \nu_{dC}, \nu_{vC})$, $\mathbf{w} := \text{col}(\mathbf{d}, \boldsymbol{\nu})$, $\mathbf{y} := \text{col}(y_{dB}, y_{vB}, y_{dC}, y_{vC})$, and $\mathbf{e} := \text{col}(e_{dB}, e_{dC})$. The plant (2.48)–(2.52) is compacted as

$$\begin{aligned} \dot{\mathbf{x}} &= \mathbf{f}(\mathbf{x}, \mathbf{u}, \mathbf{w}) \quad \mathbf{x}(t_0) = \mathbf{x}_0 \\ \mathbf{y} &= \mathbf{h}(\mathbf{x}, \mathbf{u}, \mathbf{w}) \\ \mathbf{e} &= \mathbf{h}_e(\mathbf{x}, \mathbf{u}, \mathbf{w}) \end{aligned} \quad (2.53)$$

by defining

$$\begin{aligned} \mathbf{f}(\mathbf{x}, \mathbf{u}, \mathbf{w}) &= \begin{bmatrix} v_A - v_B \\ g \sin \theta + (f_B - 1/2\rho S_B C_{D_B} (v_B - w)^2) / m_B \\ v_B - v_C \\ g \sin \theta + (f_C - 1/2\rho S_C C_{D_C} (v_C - w)^2) / m_C \end{bmatrix} \\ \mathbf{h}(\mathbf{x}, \mathbf{u}, \mathbf{w}) &= \begin{bmatrix} d_B + \nu_{dB} \\ v_B + \nu_{vB} \\ d_C + \nu_{dC} \\ v_C + \nu_{vC} \end{bmatrix} \\ \mathbf{h}_e(\mathbf{x}, \mathbf{u}, \mathbf{w}) &= \begin{bmatrix} y_{dB} - d_{\min} - y_{vB}^2/k \\ y_{dC} - d_{\min} - y_{vC}^2/k \end{bmatrix}. \end{aligned} \quad (2.54)$$

Determine the linearization conditions as follows. Let $v_A = v_B = v_C = v_0 > 0$ and define $D_{B0} = D_B(v_0)$, and $D_{C0} = D_C(v_0)$. Impose $\dot{\mathbf{x}} = \mathbf{0}$, $\theta = 0$, $d_B = d_B^*$ and $d_C = d_C^*$, and let $\mathbf{d}_0 = \text{col}(v_0, 0, 0)$ be the equilibrium disturbance. Then, the equilibrium input is $\mathbf{u}_0 := \text{col}(D_{B0}, D_{C0})$. Moreover, let $\mathbf{x}_0 = \text{col}(d_{\min} + v_0^2/k, v_0, d_{\min} + v_0^2/k, v_0)$ be the equilibrium state. Assume $\boldsymbol{\nu}_0 = \mathbf{0}$, and define $\mathbf{w}_0 = \text{col}(\mathbf{d}_0, \boldsymbol{\nu}_0)$, $\mathbf{y}_0 = \mathbf{h}(\mathbf{x}_0, \mathbf{u}_0, \mathbf{w}_0)$, and $\mathbf{e}_0 = \mathbf{0}$.

To introduce the linearization of (2.53), define the errors $\tilde{\mathbf{x}} = \mathbf{x} - \mathbf{x}_0$, $\tilde{\mathbf{u}} = \mathbf{u} - \mathbf{u}_0$, $\tilde{\mathbf{y}} = \mathbf{y} - \mathbf{y}_0$, $\tilde{\mathbf{w}} = \mathbf{w} - \mathbf{w}_0$, and $\tilde{\mathbf{e}} = \mathbf{e} - \mathbf{e}_0$. Then, the linearization around the equilibrium is

$$\begin{aligned} \dot{\tilde{\mathbf{x}}} &= \mathbf{A}\tilde{\mathbf{x}} + \mathbf{B}_1\tilde{\mathbf{u}} + \mathbf{B}_2\tilde{\mathbf{w}} \quad \tilde{\mathbf{x}}(0) = \tilde{\mathbf{x}}_0 \\ \tilde{\mathbf{y}} &= \mathbf{C}\tilde{\mathbf{x}} + \mathbf{D}_2\tilde{\mathbf{w}} \\ \tilde{\mathbf{e}} &= \mathbf{C}_e\tilde{\mathbf{x}} + \mathbf{D}_{e_2}\tilde{\mathbf{w}} \end{aligned} \quad (2.55)$$

with

$$\mathbf{A} = \begin{bmatrix} 0 & -1 & 0 & 0 \\ 0 & -\rho S_B C_{D_B} v_0 / m_B & 0 & 0 \\ 0 & 1 & 0 & -1 \\ 0 & 0 & 0 & -\rho S_C C_{D_C} v_0 / m_C \end{bmatrix}$$

$$\mathbf{B}_1 = \begin{bmatrix} 0 & 0 \\ m_B^{-1} & 0 \\ 0 & 0 \\ 0 & m_C^{-1} \end{bmatrix}, \quad \mathbf{B}_2 = \begin{bmatrix} 1 & 0 & 0 & 0 & 0 & 0 \\ 0 & g & \rho S_B C_{D_B} v_0 / m_B & 0 & 0 & 0 \\ 0 & 0 & 0 & 0 & 0 & 0 \\ 0 & g & \rho S_C C_{D_C} v_0 / m_C & 0 & 0 & 0 \end{bmatrix}$$

$$\mathbf{C} = \begin{bmatrix} 1 & 0 & 0 & 0 \\ 0 & 1 & 0 & 0 \\ 0 & 0 & 1 & 0 \\ 0 & 0 & 0 & 1 \end{bmatrix}, \quad \mathbf{D}_2 = \begin{bmatrix} 0 & 0 & 0 & 1 & 0 & 0 & 0 \\ 0 & 0 & 0 & 0 & 1 & 0 & 0 \\ 0 & 0 & 0 & 0 & 0 & 1 & 0 \\ 0 & 0 & 0 & 0 & 0 & 0 & 1 \end{bmatrix}$$

$$\mathbf{C}_e = \begin{bmatrix} 1 & -2v_0/k & 0 & 0 \\ 0 & 0 & 1 & -2v_0/k \end{bmatrix}$$

$$\mathbf{D}_{e2} = \begin{bmatrix} 0 & 0 & 0 & 1 & -2v_0/k & 0 \\ 0 & 0 & 0 & 0 & 0 & 1 & -2v_0/k \end{bmatrix}.$$

2.5 Automatic Steering System

Automatic steering represents a mandatory low-level control system in autonomous driving and drive-by-wire vehicles. The primary purpose is steering the wheels to track a known time-varying reference. The plant represents the mechanical steering system composed of the rack, the tie rods, and the steering arms rigidly connected to the wheels [28]. The system is subject to the torque of an electric motor installed on the rack. Moreover, the torques generated by the interaction between the tires and the ground also influence the system.

The dynamics of this plant are modeled through a Lagrangian approach [2,25]. Only rack and wheel assemblies are assumed to possess mass and inertia to reduce the model complexity. Let $\delta_l, \delta_r \in \mathbb{R}$ be the toe angles of the left and right wheels, $s \in \mathbb{R}$ be the rack displacement, and let $\delta \in \mathbb{R}$ be the angular position of the steering column. The rack displacement is directly proportional to the motor rotation through the gear train ratio $r > 0$, i.e.,

$$s = r\delta. \quad (2.56)$$

With reference to Fig. 2.7, define $a, b, c, d, \ell, \gamma > 0$ and let $\overline{AB} = \overline{EF} := a$, $\overline{BF} := b$, $\overline{AD} = \overline{EH} := c$, $\overline{DC} = \overline{HG} := d$, and $\overline{CG} := \ell$. Then, the steering kinematics are described through the following trigonometric relations:

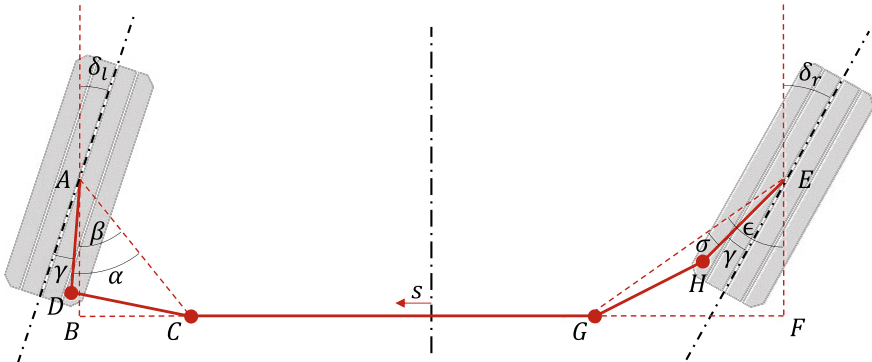


Fig. 2.7 Rack and pinion steering kinematics. The line \overline{CG} represents the rack that, moved by the pinion, slides to steer the wheels. The steering system consists of the tie rods \overline{CD} and \overline{GH} connecting the rack to the steering arms \overline{AD} and \overline{EH} . These arms are rigidly anchored to the wheel assemblies. The angle γ is fixed

$$\begin{aligned}
 \delta_l &= \beta - \gamma - \alpha & \delta_r &= -\epsilon + \gamma + \sigma \\
 \alpha &= \cos^{-1} \left(\frac{c^2 + \overline{AC}^2 - d^2}{2c \overline{AC}} \right) & \sigma &= \cos^{-1} \left(\frac{c^2 + \overline{EG}^2 - d^2}{2c \overline{EG}} \right) \\
 \beta &= \cos^{-1} \left(\frac{a^2 + \overline{AC}^2 - \overline{BC}^2}{2a \overline{AC}} \right) & \epsilon &= \cos^{-1} \left(\frac{a^2 + \overline{EG}^2 - \overline{FG}^2}{2a \overline{EG}} \right) \quad (2.57) \\
 \overline{AC} &= \sqrt{a^2 + \overline{BC}^2} & \overline{EG} &= \sqrt{a^2 + \overline{FG}^2} \\
 \overline{BC} &= b/2 - \ell/2 - s & \overline{FG} &= b/2 - \ell/2 + s.
 \end{aligned}$$

Let

$$\delta_l = f_l(\delta), \quad \delta_r = f_r(\delta), \quad (2.58)$$

where $f_l, f_r : \mathbb{R} \rightarrow \mathbb{R}$, representing the steering kinematics, are built exploiting (2.56) and (2.57). Let

$$J_l(\delta) := \frac{\partial f_l}{\partial \delta}, \quad J_r(\delta) := \frac{\partial f_r}{\partial \delta} \quad (2.59)$$

be the Jacobians of rotation of the wheels. Then, the angular wheel speeds and the linear rack speed are given by

$$\begin{aligned}
 \dot{\delta}_l &= J_l(\delta) \dot{\delta} \\
 \dot{\delta}_r &= J_r(\delta) \dot{\delta} \\
 \dot{s} &= r \dot{\delta}.
 \end{aligned} \quad (2.60)$$

Let $J, m > 0$ be the wheel inertia and the rack mass. Define $B(\delta) = J(J_l^2(\delta) + J_r^2(\delta)) + mr^2$ as the equivalent inertia and $K(\delta, \dot{\delta}) = 1/2B(\delta)\dot{\delta}^2$ as the kinetic energy. Let $\tau_l, \tau_r \in \mathbb{R}$ be the disturbance torques acting on the left and right wheels and $\tau \in \mathbb{R}$ be the torque delivered by the motor. Equations (1.4) and (1.5) in [23]

detail that τ_l, τ_r represent the so-called “aligning torques”. In particular, τ_l and τ_r are approximated, for small δ_r and δ_f , as

$$\tau_l = -c_\delta \delta_l + d_l, \quad \tau_r = -c_\delta \delta_r + d_r, \quad (2.61)$$

where $c_\delta > 0$ represents the so-called “aligning stiffness” and d_r and d_l are extra torques due to exogenous disturbances. Then, Lagrangian mechanics provide

$$dt \frac{\partial K}{\partial \dot{\delta}} - \frac{\partial K}{\partial \delta} = J_l(\delta)(d_l - c_\delta f_l(\delta)) + J_r(\delta)(d_r - c_\delta f_r(\delta)) + \tau, \quad (2.62)$$

which, exploiting the definition of $K(\delta, \dot{\delta})$, is written as

$$B(\delta) \ddot{\delta} = -\frac{1}{2} \frac{\partial B(\delta)}{\partial \delta} \dot{\delta}^2 + J_l(\delta)(d_l - c_\delta f_l(\delta)) + J_r(\delta)(d_r - c_\delta f_r(\delta)) + \tau. \quad (2.63)$$

The system is equipped with an encoder measuring the pinion angle

$$y = \delta + \nu, \quad (2.64)$$

where ν denotes the sensor noise. Let $r_\delta(t)$ be the reference steering angle, then the regulated output is defined as

$$e = \delta - r_\delta(t). \quad (2.65)$$

To write the plant in form (1.1), define $\omega = \dot{\delta}$, $\mathbf{x} = \text{col}(\delta, \omega)$, $u = \tau$, $\mathbf{d} = \text{col}(d_l, d_r)$, $\mathbf{w} = \text{col}(\mathbf{d}, \nu, r_\delta(t))$, and

$$\begin{aligned} \dot{\mathbf{x}} &= \mathbf{f}(\mathbf{x}, u, \mathbf{w}) & \mathbf{x}(t_0) &= \mathbf{x}_0 \\ y &= h(\mathbf{x}, u, \mathbf{w}) \\ e &= h_e(\mathbf{x}, u, \mathbf{w}) \end{aligned} \quad (2.66)$$

with

$$\begin{aligned} \mathbf{f}(\mathbf{x}, u, \mathbf{w}) &= \left[\begin{array}{c} \omega \\ B^{-1}(\delta) \left(-\frac{1}{2} \frac{\partial B(\delta)}{\partial \delta} \omega^2 + J_l(\delta)(d_l - c_\delta f_l(\delta)) + J_r(\delta)(d_r - c_\delta f_r(\delta)) + \tau \right) \end{array} \right] \\ h(\mathbf{x}, u, \mathbf{w}) &= \delta + \nu \\ h_e(\mathbf{x}, u, \mathbf{w}) &= \delta + \nu - r_\delta(t). \end{aligned} \quad (2.67)$$

Impose the system at equilibrium to find the linearization conditions. In particular, constrain $\dot{\mathbf{x}} = \mathbf{0}$ and let $\delta(t) = \delta_0 \in \mathbb{R}$. Conceive $d_{r0}, d_{l0} \in \mathbb{R}$ as disturbances and compute the equilibrium control input as

$$u_0 = -J_l(\delta_0)(d_{l0} - c_\delta \delta_0) - J_r(\delta_0)(d_{r0} - c_\delta \delta_0).$$

With $\nu = 0$ define $y_0 = \delta_0$ and $e_0 = 0$. Then, the equilibrium vectors are $\mathbf{x}_0 = \text{col}(\delta_0, 0)$, $\mathbf{d}_0 = \text{col}(d_{r0}, d_{l0})$, and $\mathbf{w}_0 = \text{col}(\delta_0, \mathbf{d}_0, 0)$. Introduce $\tilde{\mathbf{x}} := \mathbf{x} - \mathbf{x}_0$, $\tilde{u} := u - u_0$, $\tilde{y} := y - y_0$, $\tilde{\mathbf{w}} := \mathbf{w} - \mathbf{w}_0$, and $\tilde{e} := e - e_0$. Thanks to these definitions, the linear approximation of (2.66) is

$$\begin{aligned} \dot{\tilde{\mathbf{x}}} &= \mathbf{A}\tilde{\mathbf{x}} + \mathbf{B}_1\tilde{u} + \mathbf{B}_2\tilde{\mathbf{w}} & \tilde{\mathbf{x}}(0) &= \tilde{\mathbf{x}}_0 \\ \tilde{y} &= \mathbf{C}\tilde{\mathbf{x}} + \mathbf{D}_2\tilde{\mathbf{w}} \\ \tilde{e} &= \mathbf{C}_e\tilde{\mathbf{x}} + \mathbf{D}_{e_2}\tilde{\mathbf{w}}, \end{aligned} \quad (2.68)$$

where

$$\begin{aligned}\mathbf{A} &= \begin{bmatrix} 0 & 1 \\ A_{21} & 0 \end{bmatrix}, \quad \mathbf{B}_1 = \begin{bmatrix} 0 \\ B^{-1}(\delta_0) \end{bmatrix}, \\ \mathbf{B}_2 &= B^{-1}(\delta_0) \begin{bmatrix} 0 & 0 & 0 & 0 \\ J_r(\delta_0) & J_l(\delta_0) & 0 & 0 \end{bmatrix}, \\ \mathbf{C} &= [1 \ 0], \quad \mathbf{D}_2 = [0 \ 0 \ 1 \ 0] \\ \mathbf{C}_e &= [1 \ 0], \quad \mathbf{D}_{e2} = [0 \ 0 \ 1 \ -1]\end{aligned}$$

and

$$A_{21} = B^{-1}(\delta_0) \left(\frac{\partial J_r(\delta)}{\partial \delta} d_{r0} + \frac{\partial J_l(\delta)}{\partial \delta} d_{l0} - (J_r^2(\delta_0) + J_l^2(\delta_0)) c_\delta \right) \Big|_{\delta=\delta_0}.$$

2.6 Latero-directional Controls

The latero-directional motion represents one of the most critical dynamics of ground vehicles [1]. Through the action of brakes, differentials, and the steering wheel, the driver can steer the car to follow a reference path/trajectory (as for Lane Keeping (LK) [35], Lane Changing (LC) [10], and Self-Park Assist (SPA) [33]), improve the turning performance (as for Torque Vectoring (TV) [3]), or improve the stability (as for Electronic Stability Program (ESP) [19]). Some fundamental quantities are the tire forces and their close relationship to the load transfer. The generic model presented in this section represents the basis for those detailed in Sects. 2.6.1 and 2.6.2 for lane control and parking maneuvers.

The lumped mass $m > 0$ and the inertia $J > 0$ model the car. The suspensions are assumed to be rigid. The vehicle dynamics are constrained on the horizontal plane; thus the vertical displacement and the roll and pitch rotations are null. Concerning Fig. 2.8, let $v_x, v_y \in \mathbb{R}$ be the vehicle inertial speed expressed in the body axes, let $\omega \in \mathbb{R}$ be the yaw rate, and define $f_x, f_y \in \mathbb{R}$ and $\tau \in \mathbb{R}$ as the forces and torque created by the tires, represented in the body axes. The vehicle is subject to the aerodynamic drag $D : \mathbb{R} \rightarrow \mathbb{R}$ (see Eq. (2.37)). Standard Newtonian arguments lead to [7]

$$\begin{bmatrix} \dot{v}_x \\ \dot{v}_y \\ \dot{\omega} \end{bmatrix} = \begin{bmatrix} \omega v_y \\ -\omega v_x \\ 0 \end{bmatrix} + \begin{bmatrix} (f_x - D(v_x - w))/m \\ f_y/m \\ \tau/J \end{bmatrix} \quad (2.69)$$

where $w \in \mathbb{R}$ denotes the wind speed.

Take $\mu : [-1, 1] \times \mathbb{R}^3 \rightarrow \mathbb{R}$ as defined in (2.32) and let $\lambda_i, \beta_i \in [-1, 1]$, with $i = 1, \dots, 4$, be the wheels' longitudinal and side slip ratios. Define $\Theta_i \in \mathbb{R}^3$ as the parameters describing the friction coefficients for the i th wheel. Moreover, let $\delta_i \in [-\pi/2, \pi/2]$ be the wheel toe angle, with $i = 1, \dots, 4$. Define $N_i \geq 0$, with $i = 1, \dots, 4$, as the vertical tire forces, then the forces f_x, f_y and the torque τ are defined as

$$\begin{bmatrix} f_x \\ f_y \\ \tau \end{bmatrix} = \sum_{i=1}^4 N_i \mu(\lambda_i, \Theta_i) \begin{bmatrix} \cos \delta_i \\ \sin \delta_i \\ x_{w_i} \sin \delta_i - y_{w_i} \cos \delta_i \end{bmatrix} + \sum_{i=1}^4 N_i \mu(\beta_i, \Theta_i) \begin{bmatrix} -\sin \delta_i \\ \cos \delta_i \\ x_{w_i} \cos \delta_i + y_{w_i} \sin \delta_i \end{bmatrix}. \quad (2.70)$$

Denote with $r_w > 0$ the wheel radius and let $\omega_i \geq 0$, with $i = 1, \dots, n$, be the wheel speeds. Moreover, define $x_{w_i}, y_{w_i} \in \mathbb{R}$ as the coordinates of the i th wheel in the body reference frame. On the one hand, in agreement with (2.33), the longitudinal slip ratios are defined as $\lambda_i = \lambda(v_i, \omega_i r_w)$, with

$$v_i = \cos \delta_i (v_x - y_{w_i} \omega) + \sin \delta_i (v_y + x_{w_i} \omega). \quad (2.71)$$

On the other hand, the following equations describe the local sideslip ratios (see Fig. 2.8):

$$\beta_i = -\frac{2}{\pi} \sin^{-1} \left(\frac{\cos \delta_i (v_y + x_{w_i} \omega) - \sin \delta_i (v_x - y_{w_i} \omega)}{\sqrt{(v_y + x_{w_i} \omega)^2 + (v_x - y_{w_i} \omega)^2}} \right). \quad (2.72)$$

Finally, let $h > 0$ be the vertical distance from the ground to the cabin's center of gravity. The vertical forces N_i are found by imposing null vertical acceleration and null roll and pitch dynamics:

$$\sum_{i=1}^4 \begin{bmatrix} 1 \\ y_{w_i} + h(\mu(\beta_i, \Theta_i) \cos \delta_i + \mu(\lambda_i, \Theta_i) \sin \delta_i) \\ h(\mu(\lambda_i, \Theta_i) \cos \delta_i - \mu(\beta_i, \Theta_i) \sin \delta_i) + x_{w_i} \end{bmatrix} N_i = \begin{bmatrix} mg \\ 0 \\ 0 \end{bmatrix}. \quad (2.73)$$

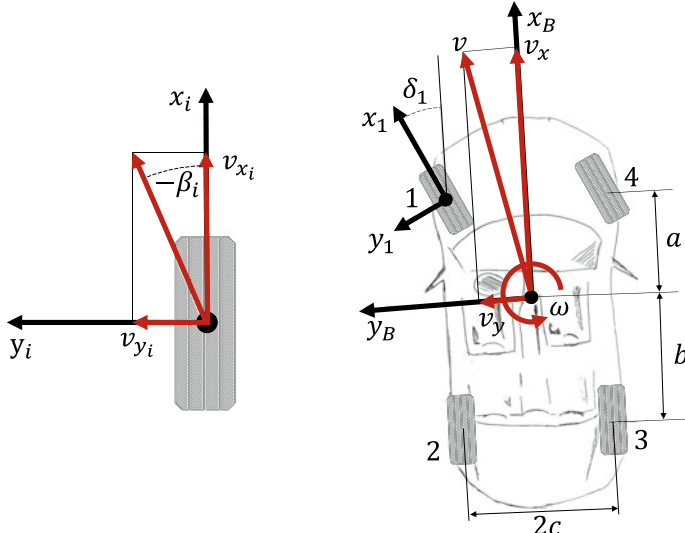


Fig. 2.8 3DOF (two translations and one rotation) model of a four-wheel vehicle for studying the latero-directional dynamics

If the wheel locations are non-collinear, Eq. (2.73) admits at least one solution. In particular, let

$$\mathbf{v}_i := \begin{bmatrix} 1 \\ y_{w_i} + h(\mu(\beta_i) \cos \delta_i + \mu(\lambda_i) \sin \delta_i) \\ h(\mu(\lambda_i) \cos \delta_i - \mu(\beta_i) \sin \delta_i) + x_{w_i} \end{bmatrix} \quad (2.74)$$

and $\mathbf{H} := [\mathbf{v}_1 \dots \mathbf{v}_n]$, then the solution of (2.73) is found through the right pseudo-inverse

$$\begin{bmatrix} N_1 \\ \vdots \\ N_4 \end{bmatrix} = \mathbf{H}^\top [\mathbf{H}\mathbf{H}^\top]^{-1} \begin{bmatrix} mg \\ 0 \\ 0 \end{bmatrix}. \quad (2.75)$$

Important

Model (2.69)–(2.75) is valid as far as $N_1, \dots, N_4 \geq 0$. Indeed, this constraint prevents both wheelies and rollovers.

In the context of latero-directional dynamics, information about the vehicle state comes from a gyroscope sensing the yaw rate. More specifically, let $\nu \in \mathbb{R}$ be the gyroscope noise, then the sensor model is

$$y = \omega + \nu. \quad (2.76)$$

The definition of the controlled output e completes the model. The control goal is tracking a reference yaw rate. In more detail, let $r(t) \in \mathbb{R}$ be the reference, then

$$e := \omega - r(t). \quad (2.77)$$

Finally, rearrange plant (2.69)–(2.77) in the form

$$\begin{aligned} \dot{\mathbf{x}} &= \mathbf{f}(\mathbf{x}, \mathbf{u}, \mathbf{w}) & \mathbf{x}(t_0) &= \mathbf{x}_0 \\ y &= h(\mathbf{x}, \mathbf{u}, \mathbf{w}) \\ e &= h_e(\mathbf{x}, \mathbf{u}, \mathbf{w}) \end{aligned} \quad (2.78)$$

through the following definitions. Let $\mathbf{x} := \text{col}(v_x, v_y, \omega)$,

$$\begin{aligned} \mathbf{u} &:= \text{col}(\delta_1, \dots, \delta_4, \omega_1, \dots, \omega_4), \\ \mathbf{d} &:= \text{col}(w, \Theta_1, \Theta_2, \Theta_3, \Theta_4), \mathbf{w} := \text{col}(\mathbf{d}, \nu, r), \text{ and} \\ h(\mathbf{x}, \mathbf{u}, \mathbf{w}) &:= \omega, \quad h_e(\mathbf{x}, \mathbf{u}, \mathbf{w}) := y - r(t). \end{aligned} \quad (2.79)$$

The function \mathbf{f} is

$$\mathbf{f}(\mathbf{x}, \mathbf{u}, \mathbf{w}) := \begin{bmatrix} \omega v_y \\ -\omega v_x \\ 0 \end{bmatrix} + \begin{bmatrix} (f_x - D(v_x - w))/m \\ f_y/m \\ \tau/J \end{bmatrix} \quad (2.80)$$

where f_x , f_y , and τ are given in (2.70).

Adopt the procedure detailed in Sect. 1.2.1 to linearize (2.78). The system is linearized around an equilibrium corresponding to a constant-speed straight trajectory.

Let $a, b > 0$ as the distance from the gravity center to the front and rear axle. Moreover, let $c > 0$ and assume $|y_{w_i}| = c$ for each $i = 1, \dots, 4$. Define the wheel from 1 to 4 as the front-left, the rear-left, the rear-right, and the front-right. It follows that $y_{w_1} = y_{w_2} = c$, $y_{w_3} = y_{w_4} = -c$, $x_{w_1} = x_{w_4} = a$, and $x_{w_2} = x_{w_3} = -b$. Define $\bar{a} = a/(a+b)$, $\bar{b} = b/(a+b)$, and $\bar{h} = h/(a+b)$, let $v_0 > 0$, and assume $\mathbf{x}_0 = \text{col}(v_0, 0, 0)$ and $\mathbf{d}_0 = \text{col}(0, \Theta_0, \Theta_0, \Theta_0, \Theta_0)$ for some $\Theta_0 \in \mathbb{R}^3$. Then, use (2.43) with $(\mu_r, \mu_f) = (\mu_{r0}, \mu_{f0})$ such that

$$\mu_{f0} = \frac{D(v_0)}{mg\bar{b} - D(v_0)\bar{h}} - \mu_{r0} \frac{D(v_0)\bar{h} + mg\bar{a}}{mg\bar{b} - D(v_0)\bar{h}} \quad (2.81)$$

from which the equilibrium control input is given by

$$\mathbf{u}_0 = \text{col} \left(0, 0, 0, 0, \frac{v_0}{r_w(1 - \lambda_{f0})}, \frac{v_0}{r_w(1 - \lambda_{r0})}, \frac{v_0}{r_w(1 - \lambda_{r0})}, \frac{v_0}{r_w(1 - \lambda_{f0})} \right)$$

with $\lambda_{r0}, \lambda_{f0} \in (0, 1)$ such that

$$\mu_{r0} = \mu(\lambda_{r0}, \Theta_0), \quad \mu_{f0} = \mu(\lambda_{f0}, \Theta_0). \quad (2.82)$$

In addition, the equilibrium output is $y_0 = 0$ under the assumption $\nu = 0$. As a consequence the equilibrium error is $e_0 = 0$. Let $\tilde{\mathbf{x}} := \mathbf{x} - \mathbf{x}_0$, $\tilde{\mathbf{u}} := \mathbf{u} - \mathbf{u}_0$, $\tilde{y} := y - y_0$, $\tilde{\mathbf{w}} := \mathbf{w} - \mathbf{w}_0$, and $\tilde{e} := e - e_0$. Thanks to these definitions, the linear approximation of (2.78) is

$$\begin{aligned} \dot{\tilde{\mathbf{x}}} &= \mathbf{A}\tilde{\mathbf{x}} + \mathbf{B}_1\tilde{\mathbf{u}} + \mathbf{B}_2\tilde{\mathbf{w}} \quad \tilde{\mathbf{x}}(0) = \tilde{\mathbf{x}}_0 \\ \tilde{y} &= \mathbf{C}\tilde{\mathbf{x}} + \mathbf{D}_2\tilde{\mathbf{w}} \\ \tilde{e} &= \mathbf{C}_e\tilde{\mathbf{x}} + \mathbf{D}_e\tilde{\mathbf{w}}, \end{aligned} \quad (2.83)$$

where

$$\begin{aligned} \mathbf{A} &= \begin{bmatrix} m^{-1}\rho SC_D v_0 & 0 & 0 \\ 0 & 0 & -v_0 \\ 0 & 0 & 0 \end{bmatrix} \\ &+ \begin{bmatrix} m^{-1} & 0 & 0 \\ 0 & m^{-1} & 0 \\ 0 & 0 & J^{-1} \end{bmatrix} \left(\sum_{i=1}^4 \mu(\lambda_{i0}, \Theta_i) \begin{bmatrix} 1 \\ 0 \\ -y_{w_i} \end{bmatrix} \frac{\partial N_i}{\partial \mathbf{x}} \right. \\ &+ \sum_{i=1}^4 N_{i0} \begin{bmatrix} 1 \\ 0 \\ -y_{w_i} \end{bmatrix} \frac{\partial \mu(\lambda_i, \Theta_i)}{\partial \lambda_i} \frac{\partial \lambda_i}{\partial \mathbf{x}} \\ &\left. + \sum_{i=1}^4 N_{i0} \begin{bmatrix} 0 \\ 1 \\ x_{w_i} \end{bmatrix} \frac{\partial \mu(\beta_i, \Theta_i)}{\partial \beta_i} \frac{\partial \beta_i}{\partial \mathbf{x}} \right)_{(\mathbf{x}, \mathbf{u}, \mathbf{w})=(\mathbf{x}_0, \mathbf{u}_0, \mathbf{w}_0)}, \end{aligned}$$

$$\begin{aligned}
\mathbf{B}_1 &= \left[\begin{array}{ccc} m^{-1} & 0 & 0 \\ 0 & m^{-1} & 0 \\ 0 & 0 & J^{-1} \end{array} \right] \left(\sum_{i=1}^4 \mu(\lambda_{i_0}, \Theta_i) \begin{bmatrix} 1 \\ 0 \\ -y_{w_i} \end{bmatrix} \frac{\partial N_i}{\partial \mathbf{u}} \right. \\
&\quad + \sum_{i=1}^4 N_{i_0} \begin{bmatrix} 1 \\ 0 \\ -y_{w_i} \end{bmatrix} \frac{\partial \mu(\lambda_i, \Theta_i)}{\partial \lambda_i} \frac{\partial \lambda_i}{\partial \mathbf{u}} \\
&\quad + \sum_{i=1}^4 N_{i_0} \begin{bmatrix} 0 \\ 1 \\ x_{w_i} \end{bmatrix} \frac{\partial \mu(\beta_i, \Theta_i)}{\partial \beta_i} \frac{\partial \beta_i}{\partial \mathbf{u}} \\
&\quad \left. + \sum_{i=1}^4 N_i \mu(\lambda_i, \Theta_i) \frac{\partial}{\partial \mathbf{u}} \begin{bmatrix} \cos \delta_i \\ \sin \delta_i \\ x_{w_i} \sin \delta_i - y_{w_i} \cos \delta_i \end{bmatrix} \right)_{(\mathbf{x}, \mathbf{u}, \mathbf{w}) = (\mathbf{x}_0, \mathbf{u}_0, \mathbf{w}_0)}, \\
\mathbf{B}_2 &= \left[\begin{array}{cc} -m^{-1} \rho S C_D v_0 & \mathbf{0} \\ 0 & \mathbf{0} \\ 0 & \mathbf{0} \end{array} \right] \\
&\quad + \left[\begin{array}{ccc} m^{-1} & 0 & 0 \\ 0 & m^{-1} & 0 \\ 0 & 0 & J^{-1} \end{array} \right] \left(\sum_{i=1}^4 \mu(\lambda_{i_0}, \Theta_i) \begin{bmatrix} 1 \\ 0 \\ -y_{w_i} \end{bmatrix} \frac{\partial N_i}{\partial \mathbf{w}} \right. \\
&\quad + \sum_{i=1}^4 N_{i_0} \begin{bmatrix} 1 \\ 0 \\ -y_{w_i} \end{bmatrix} \frac{\partial \mu(\lambda_i, \Theta_i)}{\partial \lambda_i} \frac{\partial \lambda_i}{\partial \mathbf{w}} \\
&\quad \left. + \sum_{i=1}^4 N_{i_0} \begin{bmatrix} 0 \\ 1 \\ x_{w_i} \end{bmatrix} \frac{\partial \mu(\beta_i, \Theta_i)}{\partial \beta_i} \frac{\partial \beta_i}{\partial \mathbf{w}} \right)_{(\mathbf{x}, \mathbf{u}, \mathbf{w}) = (\mathbf{x}_0, \mathbf{u}_0, \mathbf{w}_0)},
\end{aligned}$$

with $\lambda_{10} = \lambda_{40} = \lambda_{f0}$, $\lambda_{20} = \lambda_{30} = \lambda_{r0}$, and

$$\begin{bmatrix} N_{10} \\ N_{20} \\ N_{30} \\ N_{40} \end{bmatrix} = \frac{mg}{2(1 - (\mu_{r0} - \mu_{f0})\bar{h})} \begin{bmatrix} \bar{b} - \mu_{r0}\bar{h} \\ \mu_{f0}\bar{h} + \bar{a} \\ \mu_{f0}\bar{h} + \bar{a} \\ \bar{b} - \mu_{r0}\bar{h} \end{bmatrix}.$$

Moreover, the matrices \mathbf{C} and \mathbf{D} are given by

$$\mathbf{C} = [0 \ 0 \ 1], \quad \mathbf{D} = [\mathbf{0} \ 1 \ 0],$$

and the matrices \mathbf{C}_e and \mathbf{D}_e are

$$\mathbf{C}_e = [0 \ 0 \ 1], \quad \mathbf{D}_e = [\mathbf{0} \ 1 \ -1].$$

2.6.1 Lane Controls

Lane Keeping (LK) and Lane Changing (LC) are maneuvers in which the driver maintains the position within the lane according to reference values. These references can be constant (LK) or time-varying (LC).

As detailed in Fig. 2.9, define with $\mathbf{p}_L^I, \mathbf{p}_A^I, \mathbf{p}_B^I \in \mathbb{R}^2$ the inertial position of points L , A , and B . Let $\mathbf{p}_L^B, \mathbf{p}_A^B \in \mathbb{R}^2$ be the coordinates of L and A in the body axes with $\mathbf{p}_A^B := \text{col}(x_A, 0)$. Define with $\mathbf{R} : \mathbb{R} \rightarrow \text{SO}(2)$ the rotation matrix from inertial to body and let $\psi \in \mathbb{R}$ be the vehicle yaw angle. Moreover, let $\mathbf{h}_L : \mathbb{R}^2 \times \mathbb{R} \rightarrow \mathbb{R}^2$ be such that

$$\mathbf{p}_L^I = \mathbf{h}_L(\mathbf{p}_A^I, \psi), \quad (2.84)$$

where $\mathbf{p}_A^I = \mathbf{p}_B^I + \mathbf{R}^\top(\psi)\mathbf{p}_A^B$. Therefore, the projection of L on the body axes is

$$\begin{aligned} \mathbf{p}_L^B &= \mathbf{R}(\psi) (\mathbf{p}_L^I - \mathbf{p}_B^I) \\ &= \mathbf{R}(\psi) (\mathbf{h}_L(\mathbf{p}_B^I + \mathbf{R}^\top(\psi)\mathbf{p}_A^B, \psi) - \mathbf{p}_B^I). \end{aligned} \quad (2.85)$$

Define with $\rho \in \mathbb{R}$ the distance from A to L and let $\mathbf{e}_2 := \text{col}(0, 1)$, then $\rho = \mathbf{e}_2^\top \mathbf{p}_L^B$ by definition.

Let $\dot{\mathbf{p}}_\#^I, \mathbf{v}_\#^B \in \mathbb{R}^2$, with $\# \in \{A, B, L\}$, be the inertial speed of A , B , and L . Denote their projection on the body axes with $\mathbf{v}_\#^B = \mathbf{R}(\psi)\dot{\mathbf{p}}_\#^I$. Define $\omega = \dot{\psi}$ and let $\mathbf{S} : \mathbb{R} \rightarrow \mathfrak{so}(2)$ be such that $\dot{\mathbf{R}}(\psi) = -\mathbf{S}(\omega)\mathbf{R}(\psi)$. Note that $\dot{\mathbf{p}}_A^B = \mathbf{0}$ by definition.

Fig. 2.9 Key quantities for the description of lane control problems. The distance ρ is sensed by proprioceptive sensors like cameras and corresponds to the distance from point A to point L . The vehicle is controlled to track a desired reference position within the lane

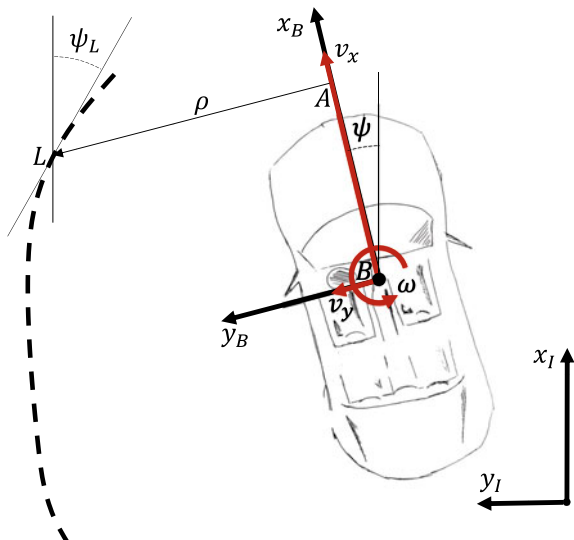
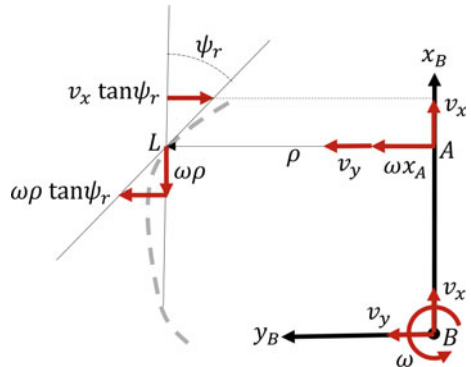


Fig. 2.10 The distance ρ varies according to the speeds depicted. The superposition of two phenomena describes the distance variation: the translation and rotation around A . Then, v_x , v_y , and ω define the linear speed of A



As a consequence,

$$\begin{aligned}\dot{\rho} &= -\mathbf{e}_2^\top (\mathbf{S}(\omega)\mathbf{p}_L^B + \mathbf{v}_B^B) + \mathbf{e}_2^\top \mathbf{v}_L^B \\ \mathbf{v}_L^B &= \mathbf{R}(\psi) \left[\frac{\partial \mathbf{h}_L(\mathbf{p}, \psi)}{\partial \mathbf{p}} \Big|_{\mathbf{p}=\mathbf{p}_A^I} \mathbf{R}^\top(\psi) \mathbf{v}_A^B + \frac{\partial \mathbf{h}_L(\mathbf{p}_A^I, s)}{\partial s} \Big|_{s=\psi} \omega \right].\end{aligned}\quad (2.86)$$

Let $\psi_L : \mathbb{R}^2 \rightarrow \mathbb{R}$ be the lane yaw angle at point L and define $\psi_r = \psi - \psi_L(\mathbf{p}_L^I)$. Then, with the support of Fig. 2.10 and some geometric arguments, we have

$$\begin{aligned}\mathbf{R}(\psi) \frac{\partial \mathbf{h}_L(\mathbf{p}, \psi)}{\partial \mathbf{p}} \Big|_{\mathbf{p}=\mathbf{p}_A^I} \mathbf{R}^\top(\psi) &= \begin{bmatrix} 1 & 0 \\ -\tan \psi_r & 0 \end{bmatrix}, \\ \mathbf{R}(\psi) \frac{\partial \mathbf{h}_L(\mathbf{p}, s)}{\partial s} \Big|_{s=\psi} &= \rho \begin{bmatrix} -1 \\ \tan \psi_r \end{bmatrix}.\end{aligned}\quad (2.87)$$

Denote with $\dot{\mathbf{p}}_B^I, \mathbf{v}_B^B \in \mathbb{R}^2$ the inertial speed of B . Its projection on the body axes is $\mathbf{v}_B^B = \mathbf{R}(\psi)\dot{\mathbf{p}}_B^I$ and, therefore, $\mathbf{v}_A^B = \mathbf{v}_B^B + \mathbf{S}(\omega)\mathbf{p}_A^B$. Moreover, let $\mathbf{v}_B^B := \text{col}(v_x, v_y)$ and use

$$\mathbf{S}(\omega) = \begin{bmatrix} 0 & -\omega \\ \omega & 0 \end{bmatrix}$$

to write the dynamics of (2.86) as

$$\dot{\rho} = -\tan \psi_r v_x - v_y + (\rho \tan \psi_r - x_A)\omega. \quad (2.88)$$

In addition, define $\chi : \mathbb{R}^2 \rightarrow \mathbb{R}$ as the lane curvature; then the time derivative of ψ_r is provided through the following algebraic system:

$$\begin{aligned}\dot{\psi}_r &= \omega - \dot{\psi}_L \\ \dot{\psi}_L &= \chi(\mathbf{p}_L^I)\dot{s}\end{aligned}\quad (2.89a)$$

where

$$\dot{s} := \frac{v_x - \rho\omega}{\cos \psi_r} \quad (2.89b)$$

represents the projection of $\dot{\mathbf{p}}_L^I$ on the tangent line at point L ; see Fig. 2.10.

A proprioceptive sensor, providing the distance ρ and the relative heading ψ_r , is modeled as

$$\begin{aligned} y_\rho &= \rho + \nu_\rho \\ y_\psi &= \psi_r + \nu_\psi \end{aligned} \quad (2.90)$$

where $\nu_\rho, \nu_\psi \in \mathbb{R}$ denote sensor noises. Also, let $r_L : \mathbb{R} \rightarrow \mathbb{R}$ be a time function representing the reference lane distance. Then, the goal of lane controls is to nullify the errors

$$\mathbf{e}_L := \begin{bmatrix} y_\rho - r_L(t) \\ y_\psi \end{bmatrix}. \quad (2.91)$$

The overall model is obtained by adding (2.88)–(2.91) to (2.78). Let $\mathbf{x}_L := \text{col}(\rho, \psi_r, \mathbf{x})$, $d_L := \chi$, $\boldsymbol{\nu}_L := \text{col}(\nu_\rho, \nu_\psi, \nu)$, $\mathbf{w}_L := \text{col}(d_L, \boldsymbol{\nu}_L, r_L)$, and $\mathbf{y}_L := \text{col}(y_\rho, y_\psi, y)$, then

$$\begin{aligned} \dot{\mathbf{x}}_L &= \mathbf{f}_L(\mathbf{x}_L, \mathbf{u}, \mathbf{w}_L) \quad \mathbf{x}_L(t_0) = \mathbf{x}_{L0} \\ \mathbf{y}_L &= \mathbf{h}_L(\mathbf{x}_L, \mathbf{u}, \mathbf{w}_L) \\ \mathbf{e}_L &= \mathbf{h}_{Le}(\mathbf{x}_L, \mathbf{u}, \mathbf{w}_L) \end{aligned} \quad (2.92)$$

where

$$\begin{aligned} \mathbf{f}_L(\mathbf{x}_L, \mathbf{u}, \mathbf{w}_L) &:= \begin{bmatrix} -\tan \psi_r v_x - v_y + (\rho \tan \psi_r - x_A) \omega \\ \omega - \chi(\mathbf{p}_L^T)(v_x - \rho \omega) / \cos \psi_r \\ \mathbf{f}(\mathbf{x}, \mathbf{u}, \mathbf{w}) \end{bmatrix} \\ \mathbf{h}_L(\mathbf{x}_L, \mathbf{u}, \mathbf{w}_L) &:= \begin{bmatrix} \rho + \nu_\rho \\ \psi_r + \nu_\psi \\ h(\mathbf{x}, \mathbf{u}, \mathbf{w}) \end{bmatrix} \\ \mathbf{h}_{Le}(\mathbf{x}_L, \mathbf{u}, \mathbf{w}_L) &:= \begin{bmatrix} \rho + \nu_\rho - r_\rho(t) \\ \psi_r + \nu_\psi \end{bmatrix}. \end{aligned}$$

The terms \mathbf{u} , $\mathbf{f}(\mathbf{x}, \mathbf{u}, \mathbf{w})$, and $h(\mathbf{x}, \mathbf{u}, \mathbf{w})$ are given in (2.78).

The remainder of this section deals with the linearization of (2.92). Assume the lane is straight and parallel to the reference trajectory adopted to linearize (2.78). These conditions lead to $\chi(\mathbf{p}_L^T(0)) = 0$. Let $\rho_0 \in \mathbb{R}$ and define $\mathbf{x}_{L0} = \text{col}(\rho_0, 0, v_0, 0, 0)$, $r_{L0} = \rho_0$, $d_{L0} = 0$, $\boldsymbol{\nu}_{L0} = \mathbf{0}$, $\mathbf{w}_{L0} = \text{col}(d_{L0}, \boldsymbol{\nu}_{L0}, r_{L0})$, $\mathbf{y}_{L0} = \text{col}(\rho_0, 0)$, and $\mathbf{e}_{L0} = \mathbf{0}$. As a consequence, the linearization errors are $\tilde{\mathbf{x}}_L := \mathbf{x}_L - \mathbf{x}_{L0}$, $\tilde{\mathbf{y}}_L := \mathbf{y}_L - \mathbf{y}_{L0}$, $\tilde{\mathbf{w}}_L := \mathbf{w}_L - \mathbf{w}_{L0}$, and $\tilde{\mathbf{e}}_L := \mathbf{e}_L - \mathbf{e}_{L0}$. The linearized dynamics read as

$$\begin{aligned} \dot{\tilde{\mathbf{x}}}_L &= \mathbf{A}_L \tilde{\mathbf{x}}_L + \mathbf{B}_L \tilde{\mathbf{u}} + \mathbf{B}_{L2} \tilde{\mathbf{w}}_L \quad \tilde{\mathbf{x}}_L(0) = \tilde{\mathbf{x}}_{L0} \\ \tilde{\mathbf{y}}_L &= \mathbf{C}_L \tilde{\mathbf{x}}_L + \mathbf{D}_L \tilde{\mathbf{w}}_L \\ \tilde{\mathbf{e}}_L &= \mathbf{C}_{Le} \tilde{\mathbf{x}}_L + \mathbf{D}_{Le} \tilde{\mathbf{w}}_L, \end{aligned} \quad (2.93)$$

in which $\tilde{\mathbf{u}}$ is provided by (2.83) and

$$\begin{aligned} \mathbf{A}_L &= \left[\begin{bmatrix} 0 & -v_0 \\ 0 & 0 \\ \mathbf{0} \end{bmatrix} \quad \begin{bmatrix} 0 & -1 & -x_A \\ 0 & 0 & 1 \\ \mathbf{A} \end{bmatrix} \right], \quad \mathbf{B}_{L1} = \begin{bmatrix} \mathbf{0} \\ \mathbf{B}_1 \end{bmatrix} \\ \mathbf{C}_L &= \begin{bmatrix} \mathbf{I} & \mathbf{0} \\ \mathbf{0} & \mathbf{C} \end{bmatrix}, \quad \mathbf{C}_{Le} = [\mathbf{I} \ \mathbf{0}], \end{aligned}$$

where \mathbf{A} , \mathbf{B}_1 , and \mathbf{C} are defined in (2.83). Lastly, the vectors associated with the exogenous are

$$\mathbf{B}_{L2} = \begin{bmatrix} 0 & 0 & 0 & 0 & 0 \\ v_0 & 0 & 0 & 0 & 0 \\ 0 & 0 & 0 & 0 & 0 \\ 0 & 0 & 0 & 0 & 0 \\ 0 & 0 & 0 & 0 & 0 \end{bmatrix}$$

and

$$\mathbf{D}_L = \begin{bmatrix} 0 & 1 & 0 & 0 & 0 \\ 0 & 0 & 1 & 0 & 0 \\ 0 & 0 & 0 & 1 & 0 \end{bmatrix}, \mathbf{D}_{Le} = \begin{bmatrix} 0 & 1 & 0 & 0 & -1 \\ 0 & 0 & 1 & 0 & 0 \end{bmatrix}.$$

2.6.2 Self-Park Assist

The description of the dynamics of the parking procedure (see Fig. 2.11) is based on (2.88)–(2.89) but with some simplifications. Indeed, the dynamic effects are neglected since this maneuver happens at low speed and low acceleration. In more detail, adopting the so-called *bicycle model* ([18], Sect. 13.3.1.3), assume $\lambda_r, \lambda_f \approx 0$, let $V \in \mathbb{R}$ be the tangential speed of the front wheel, and define $\delta \in \mathbb{R}$ as the front wheel toe angle. Adopt the kinematic triangle of Fig. 2.12 (also called *Ackermann steering* [30]) and write

$$\begin{aligned} v_x &= V \cos \delta \\ v_y &= 0 \\ \omega &= \frac{V}{\ell} \sin \delta \end{aligned} \tag{2.94}$$

where $\ell > 0$ denotes the wheelbase. Substitute (2.94) into (2.88)–(2.89) to obtain

$$\begin{aligned} \dot{\rho} &= V \left(\tan \psi_r \left(\frac{\rho}{\ell} \sin \delta - \cos \delta \right) - \frac{x_A}{\ell} \sin \delta \right) \\ \dot{\psi}_r &= V \left(\frac{\sin \delta}{\ell} \left(1 + \rho \frac{\chi(\mathbf{p}_L^I)}{\cos \psi_r} \right) - \chi(\mathbf{p}_L^I) \frac{\cos \delta}{\cos \psi_r} \right), \end{aligned}$$

where it is worth noting that the reference lane curvature $\chi(\cdot)$ is known and usually provided by a path planner [15, 32]. The control system relies on a Simultaneous Localisation And Mapping (SLAM) algorithm to localize the vehicle in the scene [9]. In more detail and without loss of generality, it is assumed that ρ is measured. This distance also represents the error to be minimized [5]. Let $\mathbf{x} := \text{col}(\rho, \psi_r)$, $u := \delta$, $d := \chi(\mathbf{p}_L^I)$, $\nu := \text{col}(\nu_\rho, \nu_\psi)$, $\mathbf{w} := \text{col}(d, \nu)$, $e := y_\rho$, and $\mathbf{y} := \text{col}(y_\rho, y_\psi)$, where y_ρ and y_ψ are given in (2.90). Then, the plant model is formalized as

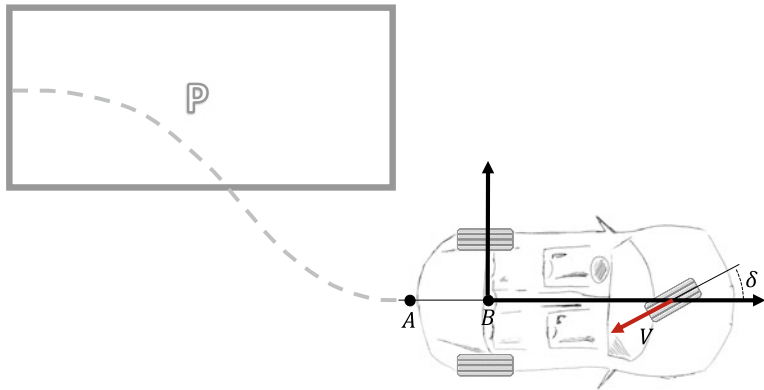


Fig. 2.11 Example of a parking maneuver. A planner generates the dashed path, and the controller uses the toe angle to make the point A stay on the reference path while moving the vehicle backward at a constant speed V

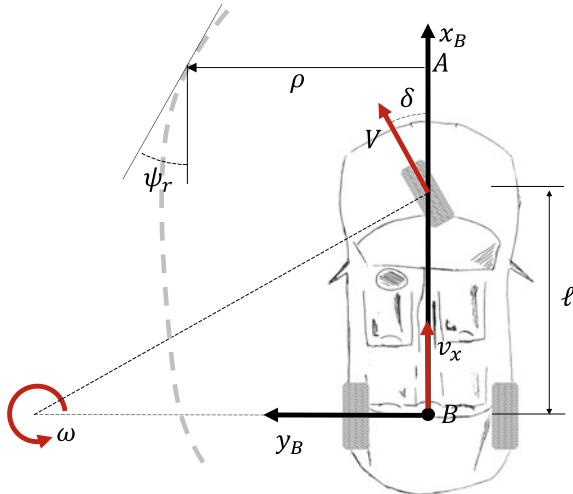


Fig. 2.12 Ackermann steering kinematics: at low speed, the vehicle rotates around a virtual fulcrum at the intersections between the rear axle line and the line perpendicular to the front wheels. The speed at the front wheel is assumed to be V while δ denotes the front wheel toe angle

$$\begin{aligned}\dot{\mathbf{x}} &= \mathbf{f}(\mathbf{x}, u, \mathbf{w}) & \mathbf{x}(t_0) &= \mathbf{x}_0 \\ \mathbf{y} &= \mathbf{h}(\mathbf{x}, u, \mathbf{w}) \\ e &= h_e(\mathbf{x}, u, \mathbf{w})\end{aligned}\tag{2.95}$$

in which (Fig. 2.12).

$$\mathbf{f}(\mathbf{x}, u, \mathbf{w}) := V \begin{bmatrix} \tan \psi_r \left(\frac{\rho}{\ell} \sin \delta - \cos \delta \right) - \frac{x_A}{\ell} \sin \delta \\ \frac{\sin \delta}{\ell} \left(1 + \rho \frac{\chi(\mathbf{p}_L^I)}{\cos \psi_r} \right) - \chi(\mathbf{p}_L^I) \frac{\cos \delta}{\cos \psi_r} \end{bmatrix},$$

where $\mathbf{h}(\mathbf{x}, u, \mathbf{w}) := \text{col}(\rho + \nu_\rho, \psi_r + \nu_\psi)$ and $h_e(\mathbf{x}, u, \mathbf{w}) := \rho + \nu_\rho$. Finally, linearize the plant around a straight path traveled at $V = v_0 \neq 0$ and $\rho = 0$, with $\mathbf{w}_0 = \mathbf{0}$. These conditions lead to $\mathbf{x}_0 = \text{col}(0, 0)$, $u_0 = 0$, $e_0 = 0$, and $\mathbf{y}_0 = \mathbf{0}$, from which the linearized quantities are $\tilde{\mathbf{x}} = \mathbf{x}$, $\tilde{u} = u$, $\tilde{\mathbf{w}} = \mathbf{w}$, $\tilde{\mathbf{y}} = \mathbf{y}$, and $\tilde{e} = e$. The linearized system is

$$\begin{aligned} \dot{\tilde{\mathbf{x}}} &= \mathbf{A}\tilde{\mathbf{x}} + \mathbf{B}_1\tilde{u} + \mathbf{B}_2\tilde{\mathbf{w}} \quad \tilde{\mathbf{x}}(0) = \tilde{\mathbf{x}}_0 \\ \tilde{\mathbf{y}} &= \mathbf{C}\tilde{\mathbf{x}} + \mathbf{D}_2\tilde{\mathbf{w}} \\ \tilde{e} &= \mathbf{C}_e\tilde{\mathbf{x}} + \mathbf{D}_{2e}\tilde{\mathbf{w}} \end{aligned} \tag{2.96}$$

in which

$$\begin{aligned} \mathbf{A} &= \begin{bmatrix} 0 & -v_0 \\ 0 & 0 \end{bmatrix}, \quad \mathbf{B}_1 = \begin{bmatrix} -v_0 x_A / \ell \\ v_0 / \ell \end{bmatrix}, \quad \mathbf{B}_2 = \begin{bmatrix} 0 & 0 & 0 \\ -v_0 & 0 & 0 \end{bmatrix} \\ \mathbf{C} &= \mathbf{I}, \quad \mathbf{C}_e = [1 \ 0], \quad \mathbf{D}_2 = \begin{bmatrix} 0 & 1 & 0 \\ 0 & 0 & 1 \end{bmatrix}, \quad \mathbf{D}_{2e} = [0 \ 1 \ 0]. \end{aligned}$$

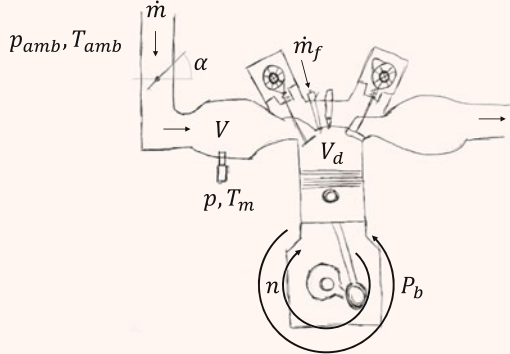
2.7 Summary

This chapter has collected the control-oriented models describing the dynamics of some vehicle subsystems of significant importance for ADAS. The main feature of these models is identifying essential quantities such as inputs, states, outputs, and nonlinear differential models representing the cause–effect flow. Based on the definition of these elements, the control designer can fill the blocks by modeling the plant of Fig. 1.5. Once the linearization equilibrium is defined, the linearization errors’ dynamics are described through LTI systems. They represent the base knowledge for the design of the controllers. At this stage, the controller interfaces are defined according to the definition of the linearized inputs and outputs.

The linearized models consist of matrices. In particular, the matrix \mathbf{A} is crucial for studying the dynamics outlined in Chap. 3. Moreover, the tuples $(\mathbf{A}, \mathbf{B}_1, \mathbf{C}_e)$ and (\mathbf{A}, \mathbf{C}) are used in Chap. 4 to identify the intra-controller signals and blocks according to the architecture of Fig. 1.5. Finally, the linearized models are exploited in Chap. 5 to design the controller’s tunable parameters.

2.8 Exercises

Exercise 2.1 (Mean value engine model) The following nonlinear ordinary differential equations describe the so-called mean value model of an internal combustion engine [11,27]:



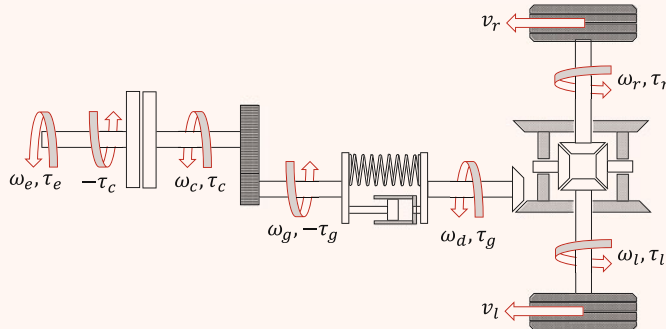
$$\begin{aligned}\dot{p} &= \frac{n V_d \eta_v p}{120V} + \frac{R T_{amb}(t)}{V} \dot{m} \\ \dot{n} &= -\frac{P_b(t)}{n J} + \frac{H_u \beta_b}{n J} \dot{m}_f(t) \\ \dot{m} &= C_t \frac{\pi}{4} D^2 \frac{p_{amb}(t)}{\sqrt{R T_{amb}(t)}} (1 - \cos(\alpha(t))) \beta(p)\end{aligned}$$

where p is the intake manifold pressure, n represents the crankshaft speed, \dot{m} and $\dot{m}_f(t)$ denote the intake manifold airflow and the fuel mass flow, $P_b(t)$ is the brake power, and $\alpha(t)$ is the throttle valve angle. The remaining parameters are H_u which represents the fuel energy constant, V_d and V denote the engine displacement and the manifold-port passage volume, η_v and η_b are the volumetric and brake thermal efficiency, p_{amb} and T_{amb} represent the environmental pressure and temperature respectively, R denotes the gas constant, D is the throttle bore diameter, and C_t represents the flow coefficient of the throttle valve. Moreover, assuming a non-choked air flow, the function $\beta(p)$ is given by

$$\beta(p) = \sqrt{\frac{2k}{k-1}} \sqrt{\left(\frac{p}{p_{amb}(t)}\right)^{\frac{2}{k}} - \left(\frac{p}{p_{amb}(t)}\right)^{\frac{k+1}{k}}}, \quad \frac{p(t)}{p_{amb}(t)} \geq \left(\frac{2}{k+1}\right)^{\frac{k}{k-1}},$$

where k is the ratio of the specific heats. The engine is equipped with a pressure sensor that provides a measurement of p and a speed sensor for n . Assuming that the sensors are affected by noises and given $n_r(t)$ is the reference engine speed, identify the state \mathbf{x} , the input \mathbf{u} , the exogenous \mathbf{w} , and the output \mathbf{y} . Represent the system in the form (1.1). Assume the engine is at equilibrium with constant speed $n_0 > 0$ and power $P_{b0} > 0$, then linearize the plant at this equilibrium condition.

Exercise 2.2 (Powertrain model) The dynamics of a powertrain, from the engine crankshaft to the wheels, are modeled using the following set of ordinary differential equations:



$$\begin{aligned} J_e \dot{\omega}_e &= \tau_e(t) - \tau_c \\ \dot{\theta}_g &= \frac{1}{n_g} \omega_c \\ (J_c + n_g^{-2} J_g) \dot{\omega}_c &= \tau_c - \frac{1}{n_g} \tau_g \\ \dot{\theta}_d &= \omega_d \\ J_w \dot{\omega}_l &= \alpha(t) \tau_g - \tau_l \\ J_w \dot{\omega}_r &= (1 - \alpha(t)) \tau_g - \tau_r \end{aligned}$$

where $J_e, J_c, J_g, J_w > 0$ are the inertia values of the engine group (engine crankshaft, utility loads, half of the clutch), the clutch group (half of the clutch, half of the gearbox), the gearbox group (gearbox and the propeller shaft), and the wheel group (the differential and the wheel shaft). Moreover, $n_g > 0$ represents the transmission gear ratio; $\omega_e, \omega_c, \omega_d, \omega_l$, and ω_r denote the angular speed of the engine group, the clutch group, the differential, and the two wheel groups. The terms θ_g and θ_d are the angular positions of the gearbox and differential shafts, $\tau_e(t)$ denotes the engine torque applied to the crankshaft, and $\tau_d(t)$ is the required torque at the differential input port. The following static relations complete the differential equations:

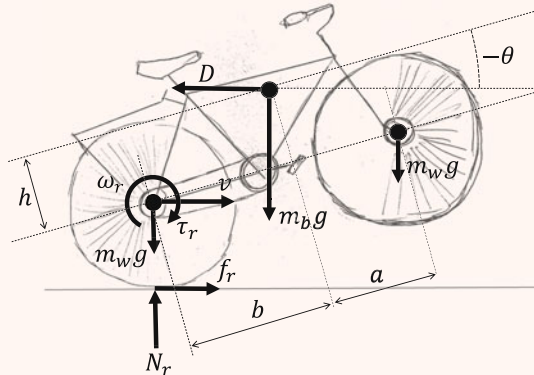
$$\begin{aligned} \omega_d &= (\omega_l + \omega_r)/2 \\ \tau_c &= P(t) \pi r^2 \mu (\omega_e - \omega_c) \\ \tau_g &= k_s (\theta_g - \theta_d) + \beta_s \left(\frac{1}{n_g} \omega_c - \omega_d \right) \\ \tau_l &= r_w N_l \mu_L (\lambda_l) \\ \tau_r &= r_w N_r \mu_L (\lambda_r) \\ \lambda_l &= 1 - \frac{v_l(t)}{\omega_l r_w}, \quad \omega_l r_w > v_l > 0 \\ \lambda_r &= 1 - \frac{v_r(t)}{\omega_r r_w}, \quad \omega_r r_w > v_r > 0, \end{aligned}$$

in which $P(t)$ represents the clutch pressure, r is the clutch radius, μ is the viscous friction coefficient of the clutch, k_s is the propeller shaft elasticity coefficient, and β_s denotes the shaft internal damping. Moreover, r_w is the wheel radius, N_l, N_r denote the left and right wheel load, λ_{sx} and λ_{dx} are the so-called longitudinal slip ratios, and $v_l(t)$, and $v_r(t)$ represent the wheel forward speeds. The friction coefficient is modeled through the function $\mu_L(\cdot)$.

Finally, the plant is equipped with a sensor suite composed of speed sensors for ω_e and ω_c and a torque meter that provides a measurement of τ_g . As for the wheel assemblies, it is assumed that speed sensors providing ω_l and ω_r are installed.

Assuming the sensors are affected by noises and taking $r_l, r_r > 0$ as the references that the wheel speeds should track. Identify the state \mathbf{x} , the input \mathbf{u} , the exogenous \mathbf{w} , and the output \mathbf{y} . Represent the system in the form (1.1). Moreover, linearize the plant on a constant-speed straight path.

Exercise 2.3 (Bike wheelie) The following set of ordinary differential equations describe the dynamics of a bike during a wheelie:



$$\begin{aligned} m\dot{v} &= -[m_b(h \cos \theta - b \sin \theta) - m_w \sin \theta(a + b)]\ddot{\theta} + f_r - D \\ &\quad + [m_b(b \cos \theta + h \sin \theta) + m_w \cos \theta(a + b)]\dot{\theta}^2 \\ I\ddot{\theta} &= -[m_b(h \cos \theta - b \sin \theta) - m_w \sin \theta(a + b)]\dot{v} \\ &\quad + [m_b(b \cos \theta + h \sin \theta) + m_w \cos \theta(a + b)]g \\ &\quad - D(h \cos \theta - b \sin \theta) - \tau_r \\ I_w \dot{\omega}_r &= \tau_r - f_r r \end{aligned}$$

where $m = m_b + 2m_w$ represents the total mass. This is the sum of m_b and m_w , which are the masses of the main body and wheels. Moreover, $I = I_b + (a + b)^2 m_w + (b^2 + h^2)m_b$ denotes the total inertia to the freehub of the rear wheel. This corresponds to the sum of the inertia of the main body I_b and the inertial momenta of masses m_b and m_w (with arms $b^2 + h^2$ and $(a + b)^2$). The bike's geometry is described through the lengths a , b , and h . The force created by the

contact between the rear tire and the ground, f_r , and the aerodynamic drag, D , are described as

$$f_r = N_r \mu(\lambda_r), \quad D = \frac{1}{2} \rho S C_D (v - w)^2.$$

The term

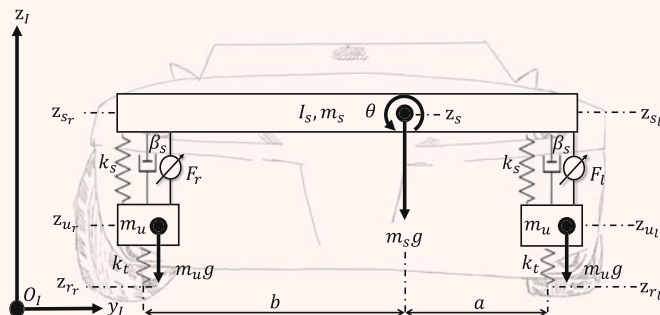
$$N_r = -[m_b(h \cos \theta - b \sin \theta) - (a + b)m_w \sin \theta] \ddot{\theta}^2 + m_b g + 2g m_w \\ - [m_b(b \cos \theta + h \sin \theta) + (a + b)m_w \cos \theta] \ddot{\theta}$$

represents the vincular reaction of the ground at the rear wheel contact point. The function $\mu_r(\cdot)$ models the friction coefficient, while the longitudinal slip ratio is λ_r .

$$\lambda_r = 1 - \frac{v}{\omega_r r} \quad \omega_r r > v > 0.$$

The aerodynamic resistance is modeled through the air density ρ , the cross-section S , the drag coefficient C_D , and the so-called air speed $v - w$. The term w denotes the wind speed. The system is equipped with a sensor suite composed of an odometer that measures v , one tonewheel that senses ω_r , and one gyroscope that measures $\dot{\theta}$. Assume the sensors are affected by noise and take r_θ as the reference wheelie angle the bike should track. Then, identify the state \mathbf{x} , the input \mathbf{u} , the exogenous \mathbf{w} , and the output \mathbf{y} . Represent the system in the form (1.1). Find the values of θ_0 such that, if $\theta = \theta_0$, there are $v_0, \omega_{r0}, \tau_{r0} > 0$ that keep the bike at equilibrium.

Exercise 2.4 (2D vehicle suspensions) The system's dynamics, depicted in the figure, are described by employing the following set of ordinary differential equations:



$$m_u \ddot{z}_{ur} = f_{tr} - m_u g - f_{sr} \\ m_u \ddot{z}_{ul} = f_{tl} - m_u g - f_{sl} \\ m_s \ddot{z}_s = f_{sr} + f_{sl} - m_s g \\ I_s \ddot{\theta} = f_{sl}a - f_{sr}b,$$

in which m_u , I_s , and m_s are the unsprung mass, the sprung inertia, and the sprung mass respectively. The forces created by the tires are denoted by f_{tr} and f_{tl} . The forces generated by the suspensions are f_{sr} and f_{sl} for the right and left side. These forces are described as

$$\begin{aligned} f_{tr} &= -k_t(z_{ur} - z_{r_r} - \ell_t) \\ f_{tl} &= -k_t(z_{ul} - z_{r_l} - \ell_t) \\ f_{sr} &= -k_s(z_{sr} - z_{ur} - \ell_s) - \beta_s(\dot{z}_{sr} - \dot{z}_{ur}) + F_r \\ f_{sl} &= -k_s(z_{sl} - z_{ul} - \ell_s) - \beta_s(\dot{z}_{sl} - \dot{z}_{ul}) + F_l \end{aligned}$$

in which k_t and k_s are the stiffness of the springs associated with the tires and suspensions, β_s is the suspension damping coefficient, and F_r and F_l are the active forces for the right and left side. The terms ℓ_s and ℓ_t denote the 0-load spring length for the suspension and the tire. The quantities z_{fr} , z_{ur} , and z_{sr} (z_{rl} , z_{ul} , and z_{sl}) represent the vertical position of the road, the unsprung mass, and the sprung mass of the right (left) side. Finally, the vertical displacement of the sprung mass, namely z_s , and its rotation θ , are linked to the variables z_{sr} and z_{sl} according to the relation

$$z_{sr} = z_s - b \sin \theta, \quad z_{sl} = z_s + a \sin \theta$$

in which a and b identify the location of the mass m_s on the wheelbase. This system is equipped with two potentiometers that measure the suspension deflections $z_{ur} - z_{sr} - \ell_s$ and $z_{ul} - z_{sl} - \ell_s$, and one gyroscope that senses $\dot{\theta}$. Define the vehicle clearance at the center of gravity and the road-relative roll angle with

$$\begin{aligned} \bar{z} &= \frac{(z_{sl} - z_{ul}) - (z_{sr} - z_{ur})}{a + b} b + (z_{sr} - z_{ur}) \\ \bar{\theta} &= \sin^{-1} \left(\frac{(z_{sl} - z_{ul}) - (z_{sr} - z_{ur})}{a + b} \right). \end{aligned}$$

Assume the sensors are affected by noises and take $\bar{\theta}_R$, \bar{z}_R as the reference roll angle and clearance that the sprung body should track. Then, identify the state \mathbf{x} , the input \mathbf{u} , the exogenous \mathbf{w} , and the output \mathbf{y} . Represent the system in the form (1.1). Finally, assume the plant is at rest, with no active forces, and linearize it at this equilibrium condition.

Exercise 2.5 (Hydraulic actuator) A double-rod hydraulic actuator is constituted of a cylinder in which a differential pressure $P \in \mathbb{R}$, acting on the piston of surface $A > 0$, creates a force that accelerates a mass $m > 0$ [36]. The displacement of a servo-valve regulates the differential pressure. Let $\beta > 0$ be a friction coefficient and define $d(\cdot) : \mathbb{R} \rightarrow \mathbb{R}$ as an external force acting on the mass. Then, the dynamics are modeled as

$$m\ddot{x}_p = PA - \beta\dot{x}_p + d(t),$$

in which $x_p \in \mathbb{R}$ denotes the piston displacement. In addition, the differential pressure P varies according to a differential equation hereafter reported. Let $V, \gamma, \delta > 0$ be the hydraulic volume, the oil bulk module, and the internal leakage coefficient. Then

$$\frac{V}{\gamma} \dot{P} = -A\dot{x}_p - \delta P + Q,$$

in which Q denotes the load flow rate. This latter is a nonlinear function of the differential pressure P and the servo valve displacement $x_v(\cdot) : \mathbb{R} \rightarrow \mathbb{R}$. In detail, let $k_q, P_s > 0$ be the flow-rate gain and the supply pressure, then

$$Q = k_q x_v(t) \sqrt{P_s - \text{sign}(x_v(t))) P}$$

with

$$\text{sign}(s) := \begin{cases} 1 & s > 0 \\ 0 & s = 0 \\ -1 & s < 0. \end{cases}$$

Assume the plant is equipped with a noisy potentiometer, measuring the piston displacement. Moreover, define $x_R(t)$ as the time-varying reference the piston displacement should track.

Write the plant model in the form (1.1) and linearize it assuming a constant disturbance $d > 0$.

References

1. Andrzejewski R, Awrejcewicz J (2006) Nonlinear dynamics of a wheeled vehicle, vol 10. Springer Science & Business Media
2. Brizard AJ (2014) Introduction to lagrangian mechanics. World Scientific Publishing Company, An
3. De Novellis L, Sorniotti A, Gruber P, Pennycott A (2014) Comparison of feedback control techniques for torque-vectoring control of fully electric vehicles. IEEE Trans Veh Technol 63(8):3612–3623
4. Desai R, Guha A, Seshu P (2021) A comparison of quarter, half and full car models for predicting vibration attenuation of an occupant in a vehicle. J Vib Eng Technol 9:983–1001
5. Fan Z, Chen H (2017) Study on path following control method for automatic parking system based on lqr. SAE Int J Passeng Cars-Electron Electr Syst 10(1):41–50
6. Filippov AF (2013) Differential equations with discontinuous righthand sides: control systems, vol 18. Springer Science & Business Media
7. Gillespie TD (1992) Fundamentals of vehicle dynamics, vol 400. Society of automotive engineers Warrendale, PA
8. Hall DE, Moreland JC (2001) Fundamentals of rolling resistance. Rubber Chem Technol 74(3):525–539
9. Han J, Kim J, Shim DH (2019) Precise localization and mapping in indoor parking structures via parameterized slam. IEEE Trans Intell Transp Syst 20(12):4415–4426

10. Hatipoglu C, Ozguner U, Redmill K (2003) Automated lane change controller design. *IEEE Trans Intell Transp Syst* 4(1):13–22
11. Heywood JB (2018) Internal combustion engine fundamentals. McGraw-Hill Education
12. Hoseinnezhad R, Bab-Hadiashar A, Rocco T (2008) Real-time clamp force measurement in electromechanical brake calipers. *IEEE Trans Veh Technol* 57(2):770–777
13. Jo C, Hwang S, Kim H (2010) Clamping-force control for electromechanical brake. *IEEE Trans Veh Technol* 59(7):3205–3212
14. Jones S et al (2013) Cooperative adaptive cruise control: human factors analysis. Technical report, United States. Federal Highway Administration. Office of Safety Research and..
15. Li B, Wang K, Shao Z (2016) Time-optimal maneuver planning in automatic parallel parking using a simultaneous dynamic optimization approach. *IEEE Trans Intell Transp Syst* 17(11):3263–3274
16. Li Y, Shim T, Shin D-H, Lee S, Jin S (2021) Control system design for electromechanical brake system using novel clamping force model and estimator. *IEEE Trans Veh Technol* 70(9):8653–8668
17. Line C, Manzie C, Good MC (2008) Electromechanical brake modeling and control: from pi to mpc. *IEEE Trans Control Syst Technol* 16(3):446–457
18. Lynch KM, Park FC (2017) Modern robotics: mechanics, planning, and control, 1st edn. Cambridge University Press
19. Manning W, Crolla D (2007) A review of yaw rate and sideslip controllers for passenger vehicles. *Trans Inst Meas Control* 29(2):117–135
20. Mars W, Luchini J (1999) An analytical model for the transient rolling resistance behavior of tires. *Tire Sci Technol* 27(3):161–175
21. Marsden G, McDonald M, Brackstone M (2001) Towards an understanding of adaptive cruise control. *Transp Res Part C: Emerg Technol* 9(1):33–51
22. Milliken WF, Milliken DL et al (1995) Race car vehicle dynamics, vol 400. Society of Automotive Engineers Warrendale, PA
23. Pacejka H (2012) Tire and vehicle dynamics, 3rd edn. Elsevier
24. Petrella R, Tursini M, Peretti L, Zigliotto M (2007) Speed measurement algorithms for low-resolution incremental encoder equipped drives: a comparative analysis. In: 2007 international aegean conference on electrical machines and power electronics, pp 780–787
25. Pila AW (2019) Introduction to lagrangian dynamics. Springer, Berlin
26. Pretagostini F, Ferranti L, Berardo G, Ivanov V, Shyrokau B (2020) Survey on wheel slip control design strategies, evaluation and application to antilock braking systems. *IEEE Access* 8:10951–10970
27. Rajamani R (2012) Vehicle dynamics and control. Springer, US
28. Reimpell J, Stoll H, Betzler JW (2001) The automotive chassis: engineering principles, 2nd edn. Elsevier
29. Riva G, Ruiz F, Formentin S, Savaresi SM (2021) Model-reference design of fixed-order controllers for brake-by-wire actuators. In: 2021 American control conference (ACC), pp 130–135
30. Simionescu P, Beale D (2002) Optimum synthesis of the four-bar function generator in its symmetric embodiment: the ackermann steering linkage. *Mech Mach Theory* 37(12):1487–1504
31. Stewart DE, Anitescu M (2010) Optimal control of systems with discontinuous differential equations. *Numerische Mathematik* 114(4):653–695
32. Vieira R, Argento E, Revoredo T (2022) Trajectory planning for car-like robots through curve parametrization and genetic algorithm optimization with applications to autonomous parking. *IEEE Lat Am Trans* 20(2):309–316
33. Wang W, Song Y, Zhang J, Deng H (2014) Automatic parking of vehicles: a review of literatures. *Int J Automot Technol* 15(6):967–978
34. Williams R (1997) Automotive active suspensions part 1: basic principles. *Proc Inst Mech Eng, Part D: J Automob Eng* 211(6):415–426

35. Wu S-J, Chiang H-H, Perng J-W, Chen C-J, Wu B-F, Lee T-T (2008) The heterogeneous systems integration design and implementation for lane keeping on a vehicle. *IEEE Trans Intell Transp Syst* 9(2):246–263
36. Yao J, Deng W, Sun W (2017) Precision motion control for electro-hydraulic servo systems with noise alleviation: a desired compensation adaptive approach. *IEEE/ASME Trans Mechatron* 22(4):1859–1868



This chapter introduces the study of the trajectories of linear systems. In particular, trajectory boundedness is linked to the eigenvalues of matrix A . In more detail, Sect. 3.1 introduces an instrumental mathematical tool called *Jordan canonical form*. This canonical form is then exploited in Sect. 3.2 to compute the solution of a set of linear ordinary differential equations. The section investigates these solutions and links them with the eigenvalues of A . Concerning the control goal G1, this link is exploited in Sect. 3.3 to state a stability criterion, which assures the boundedness of trajectories. Finally, these theoretical tools are exploited to investigate the linearized plants introduced in Chap. 2.

3.1 Jordan Canonical Form

This section presents the design of a change of coordinate suitable to study the behavior of the state of LTI systems [2]. This change of coordinates transforms the original linear plant into the so-called *Jordan canonical form*. Two ingredients are needed to achieve this result, i.e., a change of coordinates and a design criterion. As detailed in Sect. 3.1.2, the eigenvectors steer the design criterion. Section 3.1.1 defines the transformation of coordinates, while Sect. 3.1.3 specializes it to study the dynamics of LTI systems.

3.1.1 Change of Coordinates

Let $\mathbb{V}(\mathbb{C})$ be an n -dimensional vector space with $n \in \mathbb{N}$; see Sect. A.6. Then, a basis of $\mathbb{V}(\mathbb{C})$ is a finite set of vectors $\{\mathbf{b}_1, \dots, \mathbf{b}_n\}$, $\mathbf{b}_i \in \mathbb{V}(\mathbb{C})$, with $i = 1, \dots, n$, such that any vector $\mathbf{v} \in \mathbb{V}(\mathbb{C})$ can be represented as a linear combination of $\mathbf{b}_1, \dots, \mathbf{b}_n$. In other words, n constants $\beta_i \in \mathbb{C}$ exist such that

$$\mathbf{v} = [\mathbf{b}_1 \cdots \mathbf{b}_n] \begin{bmatrix} \beta_1 \\ \vdots \\ \beta_n \end{bmatrix}.$$

The term β_i means the i -th component of \mathbf{v} on $\{\mathbf{b}_1, \dots, \mathbf{b}_n\}$. Define $\mathbf{u} = \text{col}(\beta_1, \dots, \beta_n)$ and let $\{\mathbf{c}_1, \dots, \mathbf{c}_n\}$ be a second basis, such that the vector \mathbf{v} has components $\mathbf{w} := \text{col}(\gamma_1, \dots, \gamma_n)$ on $\{\mathbf{c}_1, \dots, \mathbf{c}_n\}$, i.e., such that $\mathbf{v} = [\mathbf{c}_1 \cdots \mathbf{c}_n] \mathbf{w}$. Vectors \mathbf{u} and \mathbf{w} are related through a linear function $\mathbf{T} : \mathbb{V}(\mathbb{C}) \rightarrow \mathbb{V}(\mathbb{C})$, called *change of coordinates*, such that

$$\mathbf{u} = \mathbf{T}\mathbf{w}.$$

The columns of \mathbf{T} represent the components of vectors $\mathbf{c}_1, \dots, \mathbf{c}_n$ on $\{\mathbf{b}_1, \dots, \mathbf{b}_n\}$. Since the representation of a vector on a given basis is unique, coordinate changes are bijections, and so they are invertible such that

$$\mathbf{w} = \mathbf{T}^{-1}\mathbf{u}.$$

Let $\mathbf{A} : \mathbb{V}(\mathbb{C}) \rightarrow \mathbb{V}(\mathbb{C})$ be a linear function with $\mathbf{A} \in \mathbb{C}^{n \times n}$. Let $\mathbf{x}, \mathbf{y} \in \mathbb{V}(\mathbb{C})$ be two vectors, both defined on the basis $\{\mathbf{c}_1, \dots, \mathbf{c}_n\}$ such that

$$\mathbf{y} = \mathbf{Ax}. \quad (3.1)$$

Then, let

$$\chi := \mathbf{T}\mathbf{x} \quad \mu := \mathbf{T}\mathbf{y},$$

pre-multiply both sides of (3.1) by \mathbf{T} , and exploit $\mathbf{x} = \mathbf{T}^{-1}\chi$ to obtain

$$\mu = \bar{\mathbf{A}}\chi$$

where $\bar{\mathbf{A}} := \mathbf{T}\mathbf{A}\mathbf{T}^{-1}$ represents \mathbf{A} described on $\{\mathbf{b}_1, \dots, \mathbf{b}_n\}$. This result is directly exploited in Sect. 3.1.3 to build the Jordan canonical form.

This section ends with some details, which are instrumental for the results proposed in Chap. 4.

Let $\mathbb{S}(\mathbb{C}) \subseteq \mathbb{V}(\mathbb{C})$ be a p -dimensional subspace of $\mathbb{V}(\mathbb{C})$ and let $\{\mathbf{s}_1, \dots, \mathbf{s}_p\}$ be a basis for $\mathbb{S}(\mathbb{C})$. Then, the orthogonal complement of $\mathbb{S}(\mathbb{C})$, denoted with $\mathbb{S}^\perp(\mathbb{C})$, is defined as a subspace of $\mathbb{V}(\mathbb{C})$ such that

$$\mathbb{V}(\mathbb{C}) = \mathbb{S}(\mathbb{C}) \oplus \mathbb{S}^\perp(\mathbb{C}),$$

where the symbol $(\cdot)^\perp$ denotes the *orthogonal complement*.

Remark 3.1 The direct sum \oplus means that $\mathbb{S}(\mathbb{C}) \cup \mathbb{S}^\perp(\mathbb{C}) = \mathbb{V}(\mathbb{C})$ and $\mathbb{S}(\mathbb{C}) \cap \mathbb{S}^\perp(\mathbb{C}) = 0$, or equivalently that $\mathbb{S}(\mathbb{C})$ and $\mathbb{S}^\perp(\mathbb{C})$ share only the origin but their union corresponds to $\mathbb{V}(\mathbb{C})$.

Moreover, let $\{s_1^*, \dots, s_q^*\}$, with $q = n - p$, be a basis for $\mathbb{S}^\perp(\mathbb{C})$. Then, the set $\{s_1, \dots, s_p, s_1^*, \dots, s_q^*\}$ represents a basis for $\mathbb{V}(\mathbb{C})$.

Let $\mathbb{X}(\mathbb{C})$ and $\mathbb{Y}(\mathbb{C})$ be two linear vector spaces and let $\mathbf{A} : \mathbb{X} \rightarrow \mathbb{Y}$ be a linear function. Then, the *image* of \mathbf{A} is the subspace of \mathbb{Y} defined as

$$\text{im}(\mathbf{A}) = \{\mathbf{y} \in \mathbb{Y} : \mathbf{y} = \mathbf{Ax}, \mathbf{x} \in \mathbb{X}\}$$

with $\text{im}(\mathbf{A}) \subseteq \mathbb{Y}$. The *kernel* of \mathbf{A} is the subspace of \mathbb{X} defined as

$$\ker(\mathbf{A}) = \{\mathbf{x} \in \mathbb{X} : \mathbf{0} = \mathbf{Ax}\}$$

with $\ker(\mathbf{A}) \subseteq \mathbb{X}$.

The kernel and the image are such that $\ker(\mathbf{A}) = (\text{im}(\mathbf{A}^\top))^\perp$. Finally, the following equalities hold true:

$$\begin{aligned}\mathbb{X} &= \ker(\mathbf{A}) \oplus (\ker(\mathbf{A}))^\perp = \ker(\mathbf{A}) \oplus \text{im}(\mathbf{A}^\top) \\ \mathbb{Y} &= \text{im}(\mathbf{A}) \oplus (\text{im}(\mathbf{A}))^\perp = \text{im}(\mathbf{A}) \oplus \ker(\mathbf{A}^\top).\end{aligned}$$

3.1.2 Eigenvalues and Eigenvectors

Let $\mathbf{A} \in \mathbb{R}^{n \times n}$ be a square matrix and let

$$\dot{\mathbf{x}} = \mathbf{Ax} \tag{3.2}$$

be an LTI system. It is interesting to find all the non-trivial solutions to (3.2) for which there exists $\lambda \in \mathbb{C}$ such that ([7], Sect. 3)

$$\dot{\mathbf{x}} = \mathbf{Ax} = \lambda \mathbf{x}, \tag{3.3}$$

i.e., those vectors whose direction does not change over time. Then, to solve this problem, rearrange $\mathbf{Ax} = \lambda \mathbf{x}$ as

$$(\mathbf{A} - \lambda \mathbf{I})\mathbf{x} = \mathbf{0} \tag{3.4}$$

where the non-trivial solutions are those belonging to $\ker(\mathbf{A} - \lambda \mathbf{I})$. Consequently, the values of λ that make $\mathbf{A} - \lambda \mathbf{I}$ singular (i.e., those making $\ker(\mathbf{A} - \lambda \mathbf{I})$ non-trivial) are needed. These particular λ , called **eigenvalues of \mathbf{A}** ([1], Sect. 2), are found as solutions to

$$\det(\mathbf{A} - \lambda \mathbf{I}) = 0$$

where $\det(\mathbf{A} - \lambda \mathbf{I})$ is a polynomial in λ , called **characteristic polynomial**. Let λ_i be the i -th eigenvalue, then the **algebraic multiplicity**, denoted with a_i , is defined as the order of the root λ_i . Thanks to this definition, and considering p distinct eigenvalues, it follows that

$$\det(\lambda \mathbf{I} - \mathbf{A}) = \prod_{i=1}^p (\lambda - \lambda_i)^{a_i}$$

with $\sum_{i=1}^p a_i = n$.

Remark 3.2 The eigenvalues of block triangular matrices correspond to those of the matrices on the main diagonal. Chapter 4 uses this result.

The vectors \mathbf{v} satisfying

$$(\mathbf{A} - \lambda_i \mathbf{I})^{a_i} \mathbf{v} = \mathbf{0} \quad (3.5)$$

are the **eigenvectors** associated with λ_i ([1], Sect. 2). The **geometric multiplicity** related to λ_i , denoted with g_i , corresponds to the dimension of $\ker(\mathbf{A} - \lambda_i \mathbf{I})$. To find the eigenvectors associated with \mathbf{A} , rewrite (3.5) through the recursive definition detailed hereafter. Let $\mathbf{v}_{i,j,0} := \mathbf{0}$ and $\mathbf{v}_{i,j,k-1} := (\mathbf{A} - \lambda_i \mathbf{I})\mathbf{v}_{i,j,k}$ for $i = 1, \dots, p$, $j = 1, \dots, g_i$, and $k = 1, \dots, q_{i,j}$ with $1 \leq q_{i,j} \leq a_i$ such that $\sum_{j=1}^{g_i} q_{i,j} = a_i$. Then, (3.5) is equivalent to

$$\begin{aligned} (\mathbf{A} - \lambda_i \mathbf{I})\mathbf{v}_{i,j,1} &= \mathbf{0} \\ (\mathbf{A} - \lambda_i \mathbf{I})\mathbf{v}_{i,j,2} &= \mathbf{v}_{i,j,1} \\ &\vdots \\ (\mathbf{A} - \lambda_i \mathbf{I})\mathbf{v}_{i,j,q_{i,j}} &= \mathbf{v}_{i,j,q_{i,j}-1}. \end{aligned} \quad (3.6)$$

The term $q_{i,j}$ denotes the **length of the chain of the eigenvectors** related to $\mathbf{v}_{i,j,1}$ and represents the largest integer such that the vectors $\mathbf{v}_{i,j,q_{i,j}}$ and $\mathbf{v}_{i,j,q_{i,j}-1}$ are linearly independent. For instance, Fig. 3.1 depicts the organization of the eigenvectors of \mathbf{A} .

Remark 3.3 The length of chains of eigenvectors is equal to 1 when the geometric multiplicity is equal to the algebraic multiplicity. Indeed, assuming $g_i = a_i$ and $q_{i,j} \geq 1$ we have $\sum_{j=1}^{a_i} q_{i,j} = a_i$ if and only if $q_{i,j} = 1$ for each $j = 1, \dots, g_i$.

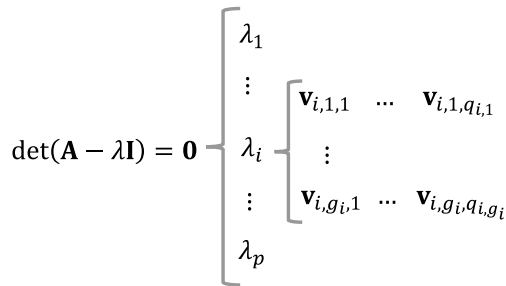


Fig. 3.1 Organization of eigenvectors of matrix \mathbf{A} . First, the p distinct eigenvalues are defined. Second, the g_i eigenvectors are associated with each eigenvalue. Third, a chain of eigenvectors of length $q_{i,j}$ is associated with each eigenvector $\mathbf{v}_{i,j,1}$

Example 3.1 (Eigenvalues and Eigenvectors) Let s_1, s_2, s_3 be real numbers such that $s_1 \neq s_2 \neq s_3 \neq 0$, and define

$$\mathbf{A} = \begin{bmatrix} s_1 & 0 & 0 & 0 & 0 \\ 0 & s_2 & 0 & 0 & 0 \\ 0 & 0 & s_2 & 0 & 0 \\ 0 & 0 & 0 & s_3 & 1 \\ 0 & 0 & 0 & 0 & s_3 \end{bmatrix}.$$

The eigenvalues of \mathbf{A} are the roots of $\det(\mathbf{A} - \lambda\mathbf{I}) = 0$, where

$$\begin{aligned} \det(\mathbf{A} - \lambda\mathbf{I}) &= \det \left(\begin{bmatrix} s_1 - \lambda & 0 & 0 & 0 & 0 \\ 0 & s_2 - \lambda & 0 & 0 & 0 \\ 0 & 0 & s_2 - \lambda & 0 & 0 \\ 0 & 0 & 0 & s_3 - \lambda & 1 \\ 0 & 0 & 0 & 0 & s_3 - \lambda \end{bmatrix} \right) \\ &= (s_1 - \lambda)(s_2 - \lambda)^2(s_3 - \lambda)^2. \end{aligned}$$

There are three independent eigenvalues (thus $p = 3$) which are $\lambda_1 = s_1$, $\lambda_2 = s_2$, and $\lambda_3 = s_3$. Their algebraic multiplicities are $a_1 = 1$, $a_2 = 2$, and $a_3 = 2$. Note that $\sum_{i=1}^3 a_i = 5$. The eigenvector associated with λ_1 is found by solving $(\mathbf{A} - \lambda_1\mathbf{I})\mathbf{v} = \mathbf{0}$. In particular, let $\mathbf{v} := \text{col}(x_1, \dots, x_5)$ and compute

$$\begin{aligned} (\mathbf{A} - \lambda_1\mathbf{I})\mathbf{v} &= \\ \begin{bmatrix} 0 & 0 & 0 & 0 & 0 \\ 0 & s_2 - s_1 & 0 & 0 & 0 \\ 0 & 0 & s_2 - s_1 & 0 & 0 \\ 0 & 0 & 0 & s_3 - s_1 & 1 \\ 0 & 0 & 0 & 0 & s_3 - s_1 \end{bmatrix} \begin{bmatrix} x_1 \\ x_2 \\ x_3 \\ x_4 \\ x_5 \end{bmatrix} &= \\ \begin{bmatrix} 0 \\ (s_2 - s_1)x_2 \\ (s_2 - s_1)x_3 \\ (s_3 - s_1)x_4 + x_5 \\ (s_3 - s_1)x_5 \end{bmatrix} &= \begin{bmatrix} 0 \\ 0 \\ 0 \\ 0 \\ 0 \end{bmatrix}. \end{aligned}$$

It is worth noting that the assumption $s_1 \neq s_2 \neq s_3 \neq 0$ implies $x_2 = x_3 = x_4 = x_5 = 0$. Then, the eigenvector associated with λ_1 is found as

$$\mathbf{v}_{1,1,1} = \begin{bmatrix} x_1 \\ 0 \\ 0 \\ 0 \\ 0 \end{bmatrix}$$

with $x_1 \neq 0$ free (one possible choice is $x_1 = 1$). The eigenvalues related to λ_2 are found by solving

$$\begin{aligned}
 & (\mathbf{A} - \lambda_2 \mathbf{I}) \mathbf{v} = \\
 & \begin{bmatrix} s_1 - s_2 & 0 & 0 & 0 & 0 \\ 0 & 0 & 0 & 0 & 0 \\ 0 & 0 & 0 & 0 & 0 \\ 0 & 0 & 0 & s_3 - s_2 & 1 \\ 0 & 0 & 0 & 0 & s_3 - s_2 \end{bmatrix} \begin{bmatrix} x_1 \\ x_2 \\ x_3 \\ x_4 \\ x_5 \end{bmatrix} = \\
 & \begin{bmatrix} (s_1 - s_2)x_1 \\ 0 \\ 0 \\ (s_3 - s_2)x_4 + x_5 \\ (s_3 - s_2)x_5 \end{bmatrix} = \begin{bmatrix} 0 \\ 0 \\ 0 \\ 0 \\ 0 \end{bmatrix}
 \end{aligned}$$

which leads to $x_1 = x_4 = x_5 = 0$ and $(x_2, x_3) \in \mathbb{R}^2 \setminus \{(0, 0)\}$. Then, it is possible to find two eigenvectors (geometric multiplicity $g_2 = 2$), namely $\mathbf{v}_{2,1,1}$ and $\mathbf{v}_{2,2,1}$ as

$$\mathbf{v}_{2,1,1} = \begin{bmatrix} 0 \\ x_2 \\ 0 \\ 0 \\ 0 \end{bmatrix}, \quad \mathbf{v}_{2,2,1} = \begin{bmatrix} 0 \\ 0 \\ x_3 \\ 0 \\ 0 \end{bmatrix}.$$

The eigenvectors associated with λ_3 are the solution to

$$\begin{aligned}
 & (\mathbf{A} - \lambda_3 \mathbf{I}) \mathbf{v} = \\
 & \begin{bmatrix} s_1 - s_3 & 0 & 0 & 0 & 0 \\ 0 & s_2 - s_3 & 0 & 0 & 0 \\ 0 & 0 & s_2 - s_3 & 0 & 0 \\ 0 & 0 & 0 & 0 & 1 \\ 0 & 0 & 0 & 0 & 0 \end{bmatrix} \begin{bmatrix} x_1 \\ x_2 \\ x_3 \\ x_4 \\ x_5 \end{bmatrix} = \\
 & \begin{bmatrix} (s_1 - s_3)x_1 \\ (s_2 - s_3)x_2 \\ (s_2 - s_3)x_3 \\ x_5 \\ 0 \end{bmatrix} = \begin{bmatrix} 0 \\ 0 \\ 0 \\ 0 \\ 0 \end{bmatrix}
 \end{aligned}$$

which leads to $x_1 = x_2 = x_3 = x_5 = 0$. These equalities imply the existence of only one eigenvector, namely $\mathbf{v}_{3,1,1}$, with geometric multiplicity $g_3 = 1$, given by

$$\mathbf{v}_{3,1,1} = \begin{bmatrix} 0 \\ 0 \\ 0 \\ x_4 \\ 0 \end{bmatrix}.$$

Since $a_3 - g_3 > 0$, there exists a chain of eigenvectors with length $q_{3,1} = 2$. These eigenvectors are found as the solution to $(\mathbf{A} - \lambda_3 \mathbf{I}) \mathbf{v}_{3,1,2} = \mathbf{v}_{3,1,1}$. In

detail, let $\mathbf{v}_{3,1,2} := \text{col}(y_1, \dots, y_5)$ and compute

$$\begin{aligned} & (\mathbf{A} - \lambda_3 \mathbf{I}) \mathbf{v}_{3,1,2} = \\ & \begin{bmatrix} s_1 - s_3 & 0 & 0 & 0 & 0 \\ 0 & s_2 - s_3 & 0 & 0 & 0 \\ 0 & 0 & s_2 - s_3 & 0 & 0 \\ 0 & 0 & 0 & 0 & 1 \\ 0 & 0 & 0 & 0 & 0 \end{bmatrix} \begin{bmatrix} y_1 \\ y_2 \\ y_3 \\ y_4 \\ y_5 \end{bmatrix} = \\ & \begin{bmatrix} (s_1 - s_3)y_1 \\ (s_2 - s_3)y_2 \\ (s_2 - s_3)y_3 \\ y_5 \\ 0 \end{bmatrix} = \begin{bmatrix} 0 \\ 0 \\ 0 \\ x_4 \\ 0 \end{bmatrix} \end{aligned}$$

which implies $y_1 = y_2 = y_3 = 0$ and $y_5 = x_4$ leading to

$$\mathbf{v}_{3,1,2} = \begin{bmatrix} 0 \\ 0 \\ 0 \\ y_4 \\ x_4 \end{bmatrix}.$$

3.1.3 Jordan Transformation

This section presents a change of coordinates, based on eigenvectors, to investigate the dynamics of LTI systems in the form $\dot{\mathbf{x}} = \mathbf{A}\mathbf{x}$ with $\mathbf{A} \in \mathbb{R}^{n \times n}$.

Define the set of distinct eigenvalues of \mathbf{A} with

$$\{\lambda_1, \dots, \lambda_p\} \quad p \leq n.$$

Let a_i and g_i be the algebraic and the geometric multiplicity associated with λ_i . On the one hand, let $q_{i,j}$ be the length of the chain of eigenvectors related to the eigenvector $\mathbf{v}_{i,j,1}$. Let

$$\mathbf{V}_{i,j} := [\mathbf{v}_{i,j,1} \ \mathbf{v}_{i,j,2} \ \cdots \ \mathbf{v}_{i,j,q_{i,j}}] \quad (3.7)$$

be the matrix obtained as the composition of the $q_{i,j}$ eigenvectors associated with $\mathbf{v}_{i,j,1}$. On the other hand, for each $i = 1, \dots, p$, the following relations are true (see Eq. (3.6)):

$$\mathbf{A}\mathbf{v}_{i,j,k} = \lambda_i \mathbf{v}_{i,j,k} + \mathbf{v}_{i,j,k-1} \quad j = 1, \dots, g_i, \quad k = 1, \dots, q_{i,j},$$

which can be written in compact form as

$$\mathbf{A}\mathbf{V}_{i,j} = \mathbf{V}_{i,j} \mathbf{J}_{i,j}$$

where

$$\mathbf{J}_{i,j} = \begin{bmatrix} \lambda_i & 1 & \dots & 0 & 0 \\ 0 & \lambda_i & \ddots & 0 & 0 \\ \vdots & \ddots & \ddots & \ddots & \vdots \\ 0 & 0 & \ddots & \lambda_i & 1 \\ 0 & 0 & \dots & 0 & \lambda_i \end{bmatrix} \in \mathbb{C}^{q_{i,j} \times q_{i,j}}.$$

Moreover, let

$$\mathbf{V}_i := [\mathbf{v}_{i,1} \ \mathbf{v}_{i,2} \ \dots \ \mathbf{v}_{i,g_i}]$$

be the compositions of all the chains of eigenvectors related to λ_i . Let

$$\mathbf{V} := [\mathbf{V}_1 \ \dots \ \mathbf{V}_p]$$

be the composition of all the eigenvectors of \mathbf{A} . It is worth noting that \mathbf{V} represents a basis for \mathbb{C}^n thanks to the linear independence of \mathbf{V}_i , \mathbf{V}_j for each $i, j \in \{1, \dots, p\}$ with $i \neq j$. Define

$$\mathbf{J}_i := \text{blkdiag}(\mathbf{J}_{i,1}, \dots, \mathbf{J}_{i,g_i}) \quad \mathbf{J} := \text{blkdiag}(\mathbf{J}_1, \dots, \mathbf{J}_p),$$

and use \mathbf{J} to write

$$\mathbf{AV} = \mathbf{V}\mathbf{J}.$$

Since \mathbf{V} is composed of linearly independent vectors, its inverse is well-posed. Consequently, it can be exploited to define the transformation

$$\mathbf{V}^{-1}\mathbf{AV} = \mathbf{J}, \tag{3.8}$$

called *Jordan canonical form* ([1], Sect. 2) and representing one of the primary tools for investigating LTI system dynamics.

The remainder of this section presents a procedure to reduce \mathbf{V} to a real-valued matrix.

Let λ be an eigenvalue of \mathbf{A} and \mathbf{v} be an eigenvector associated with λ . Assume $\lambda \in \mathbb{C}$ and $\mathbf{v} \in \mathbb{C}^n$. Then, there exists $\alpha, \beta \in \mathbb{R}$ and $\mathbf{a}, \mathbf{b} \in \mathbb{R}^n$ such that

$$\lambda = \alpha + i\beta \quad \lambda^* = \alpha - i\beta$$

$$\mathbf{v} = \mathbf{a} + i\mathbf{b} \quad \mathbf{v}^* = \mathbf{a} - i\mathbf{b}$$

where the starred quantities denote complex conjugates. The following relations hold:

$$\begin{aligned} [\mathbf{A} - \lambda\mathbf{I}]\mathbf{v} &= [\mathbf{A} - (\alpha + i\beta)\mathbf{I}][\mathbf{a} + i\mathbf{b}] \\ &= [\mathbf{A} - \alpha\mathbf{I} - i\beta\mathbf{I}]\mathbf{a} + [\mathbf{A} - \alpha\mathbf{I} - i\beta\mathbf{I}]i\mathbf{b} \\ &= [\mathbf{A} - \alpha\mathbf{I}]\mathbf{a} - i\beta_i\mathbf{I}\mathbf{a} + [\mathbf{A} - \alpha\mathbf{I}]i\mathbf{b} - i^2\beta_i\mathbf{I}\mathbf{b} \\ &= [\mathbf{A} - \alpha\mathbf{I}]\mathbf{a} + \beta_i\mathbf{I}\mathbf{b} + i\{[\mathbf{A} - \alpha\mathbf{I}]\mathbf{b} - \beta_i\mathbf{I}\mathbf{a}\} = 0. \end{aligned}$$

Split the latter equality into two parts, for real and complex terms, as

$$\begin{cases} [\mathbf{A} - \alpha\mathbf{I}]\mathbf{a} + \beta_i\mathbf{I}\mathbf{b} = 0 \\ [\mathbf{A} - \alpha\mathbf{I}]\mathbf{b} - \beta_i\mathbf{I}\mathbf{a} = 0 \end{cases} \iff \begin{cases} \mathbf{A}\mathbf{a} = \alpha\mathbf{a} - \beta\mathbf{b} \\ \mathbf{A}\mathbf{b} = \alpha\mathbf{b} + \beta\mathbf{a}, \end{cases}$$

which is compacted in this matrix form

$$\mathbf{A} [\mathbf{a} \ \mathbf{b}] = [\mathbf{a} \ \mathbf{b}] \begin{bmatrix} \alpha & \beta \\ -\beta & \alpha \end{bmatrix}.$$

Let $\lambda_i \in \mathbb{C}$ be an eigenvalue of \mathbf{A} and let $\alpha_i, \beta_i \in \mathbb{R}$ such that $\lambda_i = \alpha_i + i\beta_i$. Let $\mathbf{V}_{i,j}$ be the chain of eigenvectors defined in (3.7) and let $\mathbf{a}_{i,j,k}, \mathbf{b}_{i,j,k} \in \mathbb{R}^n$ such that for $j = 1, \dots, g_i$ and $k = 1, \dots, q_{i,j}$ we have $\mathbf{v}_{i,j,k} = \mathbf{a}_{i,j,k} + i\mathbf{b}_{i,j,k}$. Let

$$\bar{\mathbf{V}}_{i,j} := [\mathbf{a}_{i,j,1} \ \mathbf{b}_{i,j,1} \ \mathbf{a}_{i,j,2} \ \mathbf{b}_{i,j,2} \ \dots \ \mathbf{a}_{i,j,q_{i,j}} \ \mathbf{b}_{i,j,q_{i,j}}]$$

$$\bar{\mathbf{J}}_{i,j} := \begin{bmatrix} \alpha_i & \beta_i & & & & \mathbf{I} & \dots & \mathbf{0} \\ -\beta_i & \alpha_i & & & & & & \\ \mathbf{0} & & \alpha_i & \beta_i & \ddots & & \mathbf{0} \\ & & -\beta_i & \alpha_i & & & \\ \vdots & & \ddots & \ddots & & & \vdots \\ \mathbf{0} & & \mathbf{0} & & \dots & \alpha_i & \beta_i \\ & & & & & -\beta_i & \alpha_i \end{bmatrix},$$

then, $\mathbf{A}\bar{\mathbf{V}}_{i,j} = \bar{\mathbf{V}}_{i,j}\bar{\mathbf{J}}_{i,j}$ holds true.

Example 3.2 (Study of the cart-pole) Investigate the matrix \mathbf{A} , defined in Example 1.2, by assuming

$$(m, M, \ell, g, J_m, k, \mu) = (1000, 100, 1, 9.81, 100, 16000, 1000)$$

(these numerical values model the longitudinal dynamics of a car). Moreover, assume as a linearization triplet $(\mathbf{x}^*, u^*, d^*) = (\mathbf{0}, 0, 0)$. On the one hand, as a consequence of the latter assumption, the matrix becomes

$$\mathbf{A} = \begin{bmatrix} 0 & 1 & 0 & 0 \\ 0 & 0 & A_{23} & A_{24} \\ 0 & 0 & 0 & 1 \\ 0 & 0 & A_{43} & A_{44} \end{bmatrix}$$

with

$$A_{23} = \frac{\ell m(k - \ell mg)}{Mm\ell^2 + J_m(M+m)} \quad A_{24} = \frac{\ell km}{Mm\ell^2 + J_m(M+m)}$$

$$A_{43} = -\frac{(M+m)(k - \ell mg)}{Mm\ell^2 + J_m(M+m)} \quad A_{44} = -\frac{\mu(M+m)}{Mm\ell^2 + J_m(M+m)}.$$

The eigenvalues of this matrix and their algebraic multiplicity, obtained by solving the problem $\det(\mathbf{A} - \lambda\mathbf{I}) = \mathbf{0}$, are

$$\lambda_1 = 0 \quad a_1 = 2$$

$$\lambda_{2,3} = \frac{A_{44} \pm \sqrt{A_{44}^2 + 4A_{43}}}{2} \quad a_{2,3} = 1.$$

On the other hand, a numerical computation of the eigenvalues leads to $\lambda_{2,3}$ complex conjugate, i.e., $\lambda_2 = \lambda_3^*$. Moreover, it is easy to check that the geometric multiplicity of λ_1 is $g_1 = 1$, so there exists a chain of generalized eigenvectors (related to λ_1) of length $a_1 - g_1 = 1$. Let $\alpha_2, \beta_2 \in \mathbb{R}$ be such that $\lambda_2 = \alpha_2 + i\beta_2$. Then, eigenvalues and eigenvectors uniquely define the Jordan matrix as

$$\mathbf{J} = \begin{bmatrix} \mathbf{J}_1 & \mathbf{0} \\ \mathbf{0} & \bar{\mathbf{J}}_2 \end{bmatrix}, \quad \mathbf{J}_1 = \begin{bmatrix} 0 & 1 \\ 0 & 0 \end{bmatrix}, \quad \bar{\mathbf{J}}_2 = \begin{bmatrix} \alpha_2 & \beta_2 \\ -\beta_2 & \alpha_2 \end{bmatrix}.$$

3.2 Dynamics of LTI Systems

This section exploits the Jordan transformation to study the dynamics of LTI systems. The goal is to transform the system from the original coordinates to some particular coordinates in which the system dynamics correspond to a composition of independent sub-dynamics, for which an explicit description is available.

Let

$$\dot{\mathbf{x}} = \mathbf{Ax} + \mathbf{Bu} \quad \mathbf{x}(t_0) = \mathbf{x}_0 \quad (3.9)$$

be an LTI system, let \mathbf{V} be the set of the eigenvectors of \mathbf{A} , and assume \mathbf{V} is in the real form. Let $\mathbf{T} : \mathbb{R}^n \rightarrow \mathbb{R}^n$ be a change of coordinates such that $\mathbf{T} = \mathbf{V}^{-1}$. Define $\mathbf{z} = \mathbf{Tx}$. Then, the dynamics of \mathbf{z} are obtained by pre-multiplying both members of (3.9) by \mathbf{T} and by exploiting $\mathbf{x} = \mathbf{T}^{-1}\mathbf{z}$

$$\dot{\mathbf{z}} = \bar{\mathbf{A}}\mathbf{z} + \bar{\mathbf{B}}\mathbf{u} \quad \mathbf{z}(t_0) = \mathbf{T}\mathbf{x}_0, \quad (3.10)$$

where $\bar{\mathbf{A}} := \mathbf{T}\mathbf{A}\mathbf{T}^{-1}$ and $\bar{\mathbf{B}} = \mathbf{T}\mathbf{B}$.

Since the new coordinates are chosen according to the Jordan canonical form, matrix $\bar{\mathbf{A}}$ assumes the following block diagonal form:

$$\bar{\mathbf{A}} = \begin{bmatrix} \mathbf{J}_1 & 0 & \dots & 0 \\ 0 & \mathbf{J}_2 & \dots & 0 \\ \vdots & \vdots & \ddots & \vdots \\ 0 & 0 & 0 & \mathbf{J}_p \end{bmatrix}, \quad \mathbf{J}_i = \begin{bmatrix} \mathbf{J}_{i,1} & 0 & \dots & 0 \\ 0 & \mathbf{J}_{i,2} & \dots & 0 \\ \vdots & \vdots & \ddots & \vdots \\ 0 & 0 & 0 & \mathbf{J}_{i,g_i} \end{bmatrix}. \quad (3.11)$$

Redefine

$$\mathbf{z} := \text{col}(\mathbf{z}_{1,1}, \dots, \mathbf{z}_{1,g_1}, \mathbf{z}_{2,1}, \dots, \mathbf{z}_{2,g_2}, \dots, \mathbf{z}_{p,1}, \dots, \mathbf{z}_{p,g_p})$$

and exploit (3.11) to rewrite (3.10) as

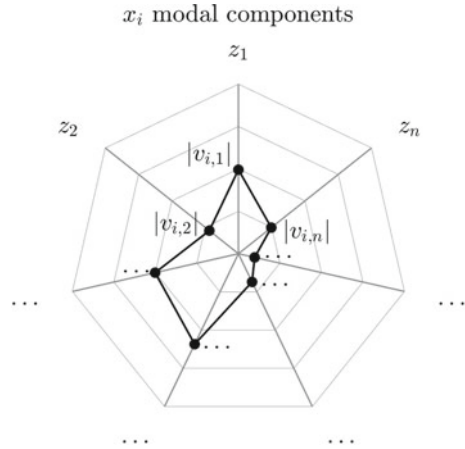
$$\begin{aligned} \dot{\mathbf{z}}_{i,j} &= \mathbf{J}_{i,j}\mathbf{z}_{i,j} + \bar{\mathbf{B}}_{i,j}\mathbf{u} & \mathbf{z}_{i,j}(t_0) &= \mathbf{V}_{i,j}\mathbf{x}_0 & i &= 1, \dots, p \\ \mathbf{y} &= \bar{\mathbf{C}}_{i,j}\mathbf{z}_{i,j} + \mathbf{D}\mathbf{u} & j &= 1, \dots, g_i, \end{aligned} \quad (3.12)$$

where $\bar{\mathbf{B}}_{i,j}$ and $\bar{\mathbf{C}}_{i,j}$ are proper sub-parts of $\bar{\mathbf{B}}$ and $\bar{\mathbf{C}}$.

The solution to (3.12) is [1, 7]

$$\mathbf{z}_{i,j}(t) = \exp(\mathbf{J}_{i,j}(t - t_0))\mathbf{z}_{i,j}(t_0) + \int_{t_0}^t \exp(\mathbf{J}_{i,j}(t - \tau))\bar{\mathbf{B}}_{i,j}\mathbf{u}(\tau)d\tau, \quad (3.13)$$

Fig. 3.2 The i th state dynamics are a linear combination of \mathbf{z} . This diagram provides graphical support to understand which, if any, are the components of \mathbf{z} that principally describe x_i



in which $\exp(\mathbf{J}_{i,j}t) := \sum_{k=0}^{\infty} \frac{1}{k!} \mathbf{J}_{i,j}^k t^k$ is called *transition matrix* ([1], Sect. 2).

Remark 3.4 With $\mathbf{z}(t)$ at hand, the solution to (3.9) is obtained as $\mathbf{x}(t) = \mathbf{V}\mathbf{z}(t)$, for all $t \geq t_0$. Let $\mathbf{z} := \text{col}(z_1, \dots, z_n)$ and assume \mathbf{V} is in the real form. Denote with $v_{i,j}$ the (i, j) -th entry of \mathbf{V} . Then, the time behavior of the i -th state component is obtained of as a linear combination of independent dynamics

$$x_i(t) = \sum_{j=1}^n v_{i,j} z_j(t), \quad (3.14)$$

where $x_i(t)$ is thought as a weighted mean of $\mathbf{z}(t)$ with weights $v_{i,j}$. Figure 3.2 provides a graphical representation of (3.14). With abuse of terminology, we define the elements of $\mathbf{z}(t)$ as *modes*.

It is interesting to note that the evolution of $\mathbf{z}_{i,j}(t)$ can be seen as a superposition of two parts [5]:

- *free evolution*, only dependent on the initial conditions,

$$\mathbf{z}_{i,j}^{\text{free}}(t) = \exp(\mathbf{J}_{i,j}(t - t_0)) \mathbf{z}_{i,j}(t_0);$$

- *forced evolution*, only dependent on the input history,

$$\mathbf{z}_{i,j}^{\text{forced}}(t) = \int_{t_0}^t \exp(\mathbf{J}_{i,j}(t - \tau)) \bar{\mathbf{B}}_{i,j} \mathbf{u}(\tau) d\tau.$$

The term $\mathbf{z}_{i,j}^{\text{free}}(t)$ is null if $\mathbf{z}_{i,j}(t_0) = \mathbf{0}$, whereas the term $\mathbf{z}_{i,j}^{\text{forced}}(t) = \mathbf{0}$ if $\mathbf{u}(\tau) \equiv \mathbf{0}$ $\forall \tau \in [t_0, t]$. To compute $\exp(\mathbf{J}_{i,j}t)$, note that

$$\mathbf{J}_{i,j} = \begin{bmatrix} \lambda_i & 1 & \dots & 0 & 0 \\ 0 & \lambda_i & \ddots & 0 & 0 \\ \vdots & \ddots & \ddots & \ddots & \vdots \\ 0 & 0 & \ddots & \lambda_i & 1 \\ 0 & 0 & \dots & 0 & \lambda_i \end{bmatrix}$$

can be written as $\mathbf{J}_{i,j} = \lambda_i \mathbf{I} + \mathbf{N}_{i,j}$ with

$$\mathbf{N}_{i,j} = \begin{bmatrix} 0 & 1 & \dots & 0 & 0 \\ 0 & 0 & \ddots & 0 & 0 \\ \vdots & \ddots & \ddots & \ddots & \vdots \\ 0 & 0 & \ddots & 0 & 1 \\ 0 & 0 & \dots & 0 & 0 \end{bmatrix}.$$

Then, the transition matrix is

$$\exp(\mathbf{J}_{i,j}t) = \exp((\lambda_i \mathbf{I} + \mathbf{N}_{i,j})t) = \exp(\lambda_i t) \exp(\mathbf{N}_{i,j}t)$$

and

$$\begin{aligned} \exp(\mathbf{N}_{i,j}t) &= \sum_{k=0}^{\infty} \frac{1}{k!} \tilde{\mathbf{N}}_{i,j}^k t^k = \mathbf{I} + \mathbf{N}_{i,j}t + \frac{1}{2} \mathbf{N}_{i,j}^2 t^2 + \dots \\ &= \begin{bmatrix} 1 & t & \frac{t^2}{2} & \dots & \frac{t^{q_{i,j}-2}}{(q_{i,j}-2)!} & \frac{t^{q_{i,j}-1}}{(q_{i,j}-1)!} \\ 0 & 1 & t & \ddots & \frac{t^{q_{i,j}-3}}{(q_{i,j}-3)!} & \frac{t^{q_{i,j}-2}}{(q_{i,j}-2)!} \\ 0 & 0 & 1 & \ddots & \frac{t^{q_{i,j}-4}}{(q_{i,j}-4)!} & \frac{t^{q_{i,j}-3}}{(q_{i,j}-3)!} \\ \vdots & \vdots & \ddots & \ddots & \ddots & \vdots \\ 0 & 0 & 0 & \ddots & 1 & t \\ 0 & 0 & 0 & \dots & 0 & 1 \end{bmatrix}. \end{aligned}$$

Infobox 3.1 (Powers of $\mathbf{N}_{i,j}$) *The k -th power of $\mathbf{N}_{i,j}$ is a null matrix with the k -th upper diagonal composed of "1" elements. For example,*

$$\mathbf{N}_{i,j}^2 = \begin{bmatrix} 0 & 0 & 1 & 0 & \dots & 0 & 0 \\ 0 & 0 & 0 & 1 & \dots & 0 & 0 \\ 0 & 0 & 0 & 0 & \ddots & 0 & 0 \\ \vdots & \vdots & \vdots & \ddots & \ddots & \ddots & \vdots \\ 0 & 0 & 0 & 0 & \ddots & 0 & 1 \\ 0 & 0 & 0 & 0 & \dots & 0 & 0 \\ 0 & 0 & 0 & 0 & \dots & 0 & 0 \end{bmatrix}, \quad \mathbf{N}_{i,j}^3 = \begin{bmatrix} 0 & 0 & 0 & 1 & \dots & 0 & 0 \\ 0 & 0 & 0 & 0 & \dots & 0 & 0 \\ 0 & 0 & 0 & 0 & \ddots & 0 & 0 \\ \vdots & \vdots & \vdots & \ddots & \ddots & \ddots & \vdots \\ 0 & 0 & 0 & 0 & \ddots & 0 & 0 \\ 0 & 0 & 0 & 0 & \dots & 0 & 0 \\ 0 & 0 & 0 & 0 & \dots & 0 & 0 \end{bmatrix}.$$

Let $q_{i,j}$ be the dimension of $\mathbf{N}_{i,j}$, then $\mathbf{N}_{i,j}^k = \mathbf{0}$ for all $k \geq q_{i,j}$. As a consequence, $\mathbf{N}_{i,j}$ is said to be **nilpotent** of order $q_{i,j}$.

In the case of complex conjugate eigenvalues, the Jordan block $\mathbf{J}_{i,j}$ is reformulated as

$$\mathbf{J}_{i,j} = \begin{bmatrix} \mathbf{M} & \mathbf{I} & \dots & \mathbf{0} & \mathbf{0} \\ \mathbf{0} & \mathbf{M} & \ddots & \mathbf{0} & \mathbf{0} \\ \vdots & \vdots & \ddots & \ddots & \vdots \\ \mathbf{0} & \mathbf{0} & \dots & \mathbf{M} & \mathbf{I} \\ \mathbf{0} & \mathbf{0} & \dots & \mathbf{0} & \mathbf{M} \end{bmatrix},$$

where $\mathbf{M} = \alpha_i \mathbf{I} + \beta_i \mathbf{S}$ with $\mathbf{S} = \begin{bmatrix} 0 & 1 \\ -1 & 0 \end{bmatrix}$. Therefore, $\mathbf{J}_{i,j} = \mathbf{D}_{i,j} + \mathbf{N}_{i,j}$ where

$$\mathbf{D}_{i,j} = \begin{bmatrix} \alpha_i \mathbf{I} + \beta_i \mathbf{S} & \mathbf{0} & \dots & \mathbf{0} \\ \mathbf{0} & \alpha_i \mathbf{I} + \beta_i \mathbf{S} & \dots & \mathbf{0} \\ \vdots & \vdots & \ddots & \vdots \\ \mathbf{0} & \mathbf{0} & \dots & \alpha_i \mathbf{I} + \beta_i \mathbf{S} \end{bmatrix}$$

and

$$\mathbf{N}_{i,j} = \begin{bmatrix} \mathbf{0} & \mathbf{I} & \dots & \mathbf{0} & \mathbf{0} \\ \mathbf{0} & \mathbf{0} & \ddots & \mathbf{0} & \mathbf{0} \\ \vdots & \ddots & \ddots & \ddots & \vdots \\ \mathbf{0} & \mathbf{0} & \ddots & \mathbf{0} & \mathbf{I} \\ \mathbf{0} & \mathbf{0} & \dots & \mathbf{0} & \mathbf{0} \end{bmatrix}.$$

The exponential of $\mathbf{D}_{i,j}$ is composed of the exponential of $\alpha_i \mathbf{I} + \beta_i \mathbf{S}$, where

$$\begin{aligned} \exp((\alpha_i \mathbf{I} + \beta_i \mathbf{S})t) &= \exp(\alpha_i \mathbf{I}t) \exp(\beta_i \mathbf{S}t) \\ &= \exp(\alpha_i t) \exp(\beta_i \mathbf{S}t). \end{aligned}$$

It can be demonstrated that

$$\exp(\beta_i \mathbf{S}t) = \begin{bmatrix} \cos(\beta_i t) & \sin(\beta_i t) \\ -\sin(\beta_i t) & \cos(\beta_i t) \end{bmatrix}$$

and

$$\exp(\mathbf{N}_{i,j}t) = \begin{bmatrix} \mathbf{I} & t\mathbf{I} & \frac{t^2}{2}\mathbf{I} & \dots & \frac{t^{q_{i,j}-2}}{(q_{i,j}-2)!}\mathbf{I} & \frac{t^{q_{i,j}-1}}{(q_{i,j}-1)!}\mathbf{I} \\ \mathbf{0} & \mathbf{I} & t\mathbf{I} & \ddots & \frac{t^{q_{i,j}-3}}{(q_{i,j}-3)!}\mathbf{I} & \frac{t^{q_{i,j}-2}}{(q_{i,j}-2)!}\mathbf{I} \\ \mathbf{0} & \mathbf{0} & \mathbf{I} & \ddots & \frac{t^{q_{i,j}-4}}{(q_{i,j}-4)!}\mathbf{I} & \frac{t^{q_{i,j}-3}}{(q_{i,j}-3)!}\mathbf{I} \\ \vdots & \ddots & \ddots & \ddots & \ddots & \vdots \\ \mathbf{0} & \mathbf{0} & \mathbf{0} & \ddots & \mathbf{I} & t\mathbf{I} \\ \mathbf{0} & \mathbf{0} & \mathbf{0} & \dots & \mathbf{0} & \mathbf{I} \end{bmatrix}.$$

In conclusion, the exponential of $\mathbf{J}_{i,j}$ in the case of complex conjugate eigenvalues is

$$\begin{aligned} \exp(\mathbf{J}_{i,j}t) &= \exp(\mathbf{D}_{i,j}t + \mathbf{N}_{i,j}t) = \exp(\mathbf{D}_{i,j}t) \exp(\mathbf{N}_{i,j}t) \\ &= [\exp(\alpha_i t) \mathbf{I} \otimes \exp(\beta_i St)] \exp(\mathbf{N}_{i,j}t). \end{aligned}$$

The following paragraphs investigate the time behavior associated with the transition matrix of a single block $\mathbf{J}_{i,j}$ for different eigenvalues.

Real eigenvalues

In the case of real λ_i , the transition matrix related to $\mathbf{J}_{i,j}$ is given by

$$\begin{aligned} \exp(\mathbf{J}_{i,j}t) &= \exp(\lambda_i t) \exp(\mathbf{N}_{i,j}t) \\ &= \begin{bmatrix} \exp(\lambda_i t) & t \exp(\lambda_i t) & \dots & \frac{t^{q_{i,j}-1}}{(q_{i,j}-1)!} \exp(\lambda_i t) \\ 0 & \exp(\lambda_i t) & \dots & \frac{t^{q_{i,j}-2}}{(q_{i,j}-2)!} \exp(\lambda_i t) \\ \vdots & \vdots & \ddots & \vdots \\ 0 & 0 & \dots & \exp(\lambda_i t) \end{bmatrix}. \end{aligned}$$

If $\mathbf{u} = \mathbf{0}$, the dynamics of $\mathbf{z}_{i,j}$ are given by

$$\mathbf{z}_{i,j}(t) = \exp(\mathbf{J}_{i,j}t)\mathbf{z}_{i,j}(t_0)$$

where, in particular, the dynamics of the first element of $\mathbf{z}_{i,j}$, namely $z_{i,j,1}$, are

$$z_{i,j,1}(t) = \exp(\lambda_i t) \sum_{k=0}^{q_{i,j}-1} \frac{t^k}{k!} z_{i,j,(k+1)}(t_0).$$

The dynamics are bounded if, for each k , there exists a finite real M_k such that

$$\lim_{t \rightarrow \infty} \exp(\lambda_i t) t^k < M_k \in \mathbb{R}, \forall k = 0, \dots, q_{i,j} - 1.$$

The latter inequality leads to the following conditions:

$$\mathbf{z}_{i,j}(t) \begin{cases} \text{exponentially convergent to zero} & \lambda_i < 0, q_{i,j} \geq 1 \\ \text{constant} & \lambda_i = 0, q_{i,j} = 1 \\ \text{polynomially divergent from } \mathbf{z}_{i,j}(t_0) & \lambda_i = 0, q_{i,j} > 1 \\ \text{exponentially divergent from } \mathbf{z}_{i,j}(t_0) & \lambda_i > 0, q_{i,j} \geq 1 \end{cases}.$$

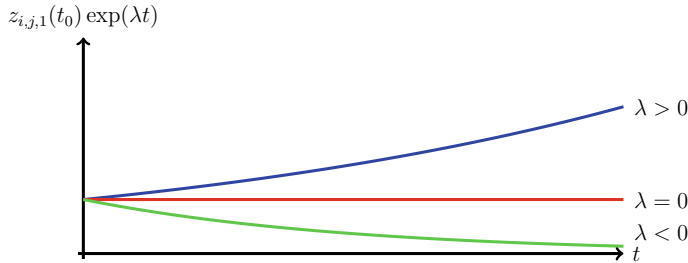


Fig. 3.3 Time behavior of $z_{i,j,1}(t_0) \exp(\lambda t)$

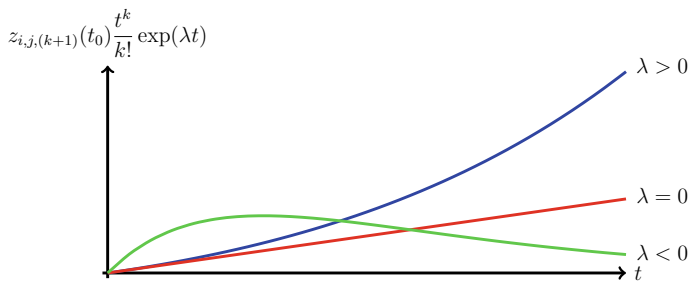


Fig. 3.4 Time behavior of $z_{i,j,(k+1)}(t_0) \frac{t^k}{k!} \exp(\lambda t)$ for $k > 0$

Figures 3.3 and 3.4 depict the time behavior of the term $\exp(\lambda_i t) \frac{t^k}{k!} z_{i,j,(k+1)}(t_0)$ in the case of real λ_i for $k = 0$ and $k > 0$ respectively.

Complex conjugate eigenvalues

In the case of complex conjugate eigenvalues, the exponential of $\mathbf{J}_{i,j} t$ becomes

$$\begin{aligned} \exp(\mathbf{J}_{i,j} t) &= [\exp(\alpha_i t) \mathbf{I} \otimes \exp(\beta_i \mathbf{S}t)] \exp(\mathbf{N}_{i,j} t) = \\ &= \exp(\alpha_i t) \mathbf{I} \otimes \begin{bmatrix} \cos(\beta_i t) & \sin(\beta_i t) \\ -\sin(\beta_i t) & \cos(\beta_i t) \end{bmatrix} \cdot \\ &\quad \begin{bmatrix} \mathbf{I} & t\mathbf{I} & \frac{t^2}{2}\mathbf{I} & \frac{t^3}{3!}\mathbf{I} & \dots & \frac{t^{q_{i,j}-2}}{(q_{i,j}-2)!}\mathbf{I} & \frac{t^{q_{i,j}-1}}{(q_{i,j}-1)!}\mathbf{I} \\ \mathbf{0} & \mathbf{I} & t\mathbf{I} & \frac{t^2}{2}\mathbf{I} & \dots & \frac{t^{q_{i,j}-3}}{(q_{i,j}-3)!}\mathbf{I} & \frac{t^{q_{i,j}-2}}{(q_{i,j}-2)!}\mathbf{I} \\ \mathbf{0} & \mathbf{0} & \mathbf{I} & t\mathbf{I} & \dots & \frac{t^{q_{i,j}-4}}{(q_{i,j}-4)!}\mathbf{I} & \frac{t^{q_{i,j}-3}}{(q_{i,j}-3)!}\mathbf{I} \\ \vdots & \vdots & \vdots & \vdots & \ddots & \vdots & \vdots \\ \mathbf{0} & \mathbf{0} & \mathbf{0} & \mathbf{0} & \dots & \mathbf{I} & t\mathbf{I} \\ \mathbf{0} & \mathbf{0} & \mathbf{0} & \mathbf{0} & \dots & \mathbf{0} & \mathbf{I} \end{bmatrix}. \end{aligned}$$

Assuming $\mathbf{u} = \mathbf{0}$, the dynamics of $\mathbf{z}_{i,j}$ are given by

$$\mathbf{z}_{i,j}(t) = \exp(\mathbf{J}_{i,j} t) \mathbf{z}_{i,j}(t_0)$$

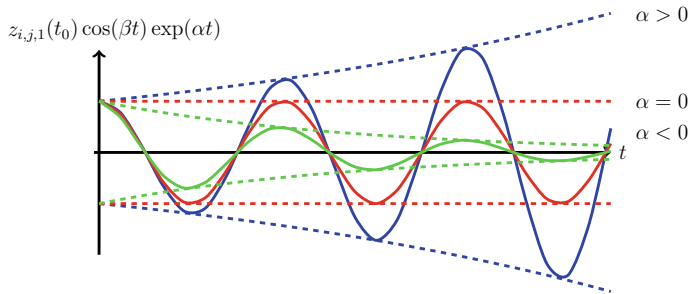


Fig. 3.5 Time behavior of $z_{i,j,1}(t_0) \cos(\beta t) \exp(\alpha t)$

where, in particular, the dynamics of the first two elements of $\mathbf{z}_{i,j}$, i.e., $\text{col}(z_{i,j,1}(t), z_{i,j,2}(t))$, are

$$\begin{bmatrix} z_{i,j,1}(t) \\ z_{i,j,2}(t) \end{bmatrix} = \exp(\alpha_i t) \begin{bmatrix} \cos(\beta_i t) & \sin(\beta_i t) \\ -\sin(\beta_i t) & \cos(\beta_i t) \end{bmatrix} \sum_{k=0}^{q_{i,j}-1} \frac{t^k}{k!} \begin{bmatrix} z_{i,j,2k+1}(t_0) \\ z_{i,j,2k+2}(t_0) \end{bmatrix}. \quad (3.15)$$

The elements of $\text{col}(z_{i,j,1}(t), z_{i,j,2}(t))$ are bounded if there exists finite $M > 0$ such that

$$\lim_{t \rightarrow \infty} \exp(\alpha_i t) t^k < M_k \in \mathbb{R}, \quad \forall k = 0, \dots, q_{i,j} - 1.$$

This inequality leads to the following conditions (Fig. 3.5):

$$\mathbf{z}_{i,j}(t) \left\{ \begin{array}{ll} \text{exponentially convergent to zero} & \alpha_i < 0, q_{i,j} \geq 1 \\ \text{constant} & \alpha_i = 0, q_{i,j} = 1 \\ \text{polynomially divergent from } \mathbf{z}_{i,j}(t_0) & \alpha_i = 0, q_{i,j} > 1 \\ \text{exponentially divergent from } \mathbf{z}_{i,j}(t_0) & \alpha_i > 0, q_{i,j} \geq 1. \end{array} \right.$$

Figures 3.6, 3.8, and 3.7 depict the time behavior of the terms appearing in (3.15) for both $k = 0$ and $k > 0$.

Infobox 3.2 Regarding the frequency analysis, the values α_i and β_i , representing the real and the imaginary part of a complex eigenvalue, are usually exploited to define the pulsation ω_i and the damping ratio δ_i as

$$\omega_i = \sqrt{\alpha_i^2 + \beta_i^2}, \quad \delta_i = \tan^{-1}(\alpha_i / \beta_i).$$

Example 3.3 (Cart-pole modes) Let \mathbf{J} be the Jordan matrix associated with the matrix \mathbf{A} of Exercise 3.2. Then, the plant trajectories are described by

$$\exp(\mathbf{J}t) = \begin{bmatrix} \exp(\mathbf{J}_1 t) & \mathbf{0} \\ \mathbf{0} & \exp(\mathbf{J}_2 t) \end{bmatrix}, \quad \exp(\mathbf{J}_1 t) = \begin{bmatrix} 1 & t \\ 0 & 1 \end{bmatrix}$$

$$\exp(\mathbf{J}_2 t) = \exp(\alpha_2 t) \begin{bmatrix} \cos(\beta_2 t) & \sin(\beta_2 t) \\ -\sin(\beta_2 t) & \cos(\beta_2 t) \end{bmatrix}.$$

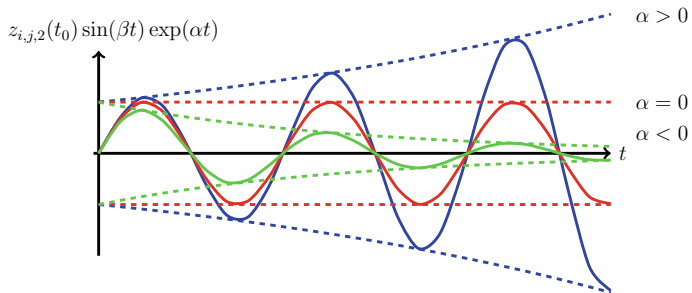


Fig. 3.6 Time behavior of $z_{i,j,2}(t_0) \sin(\beta t) \exp(\alpha t)$

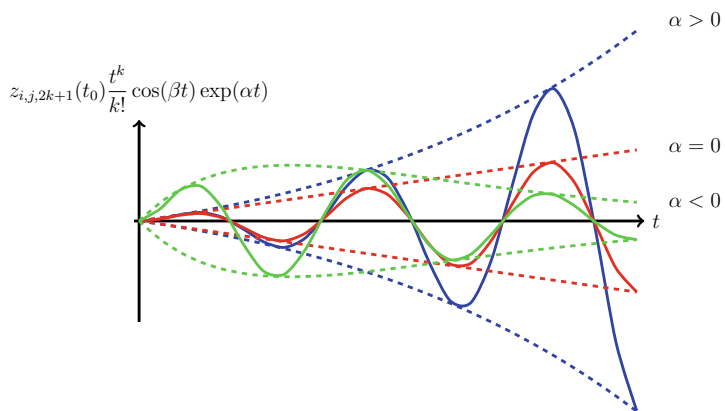


Fig. 3.7 Time behavior of $z_{i,j,2k+1}(t_0) \frac{t^k}{k!} \cos(\beta t) \exp(\alpha t)$ for $k > 0$

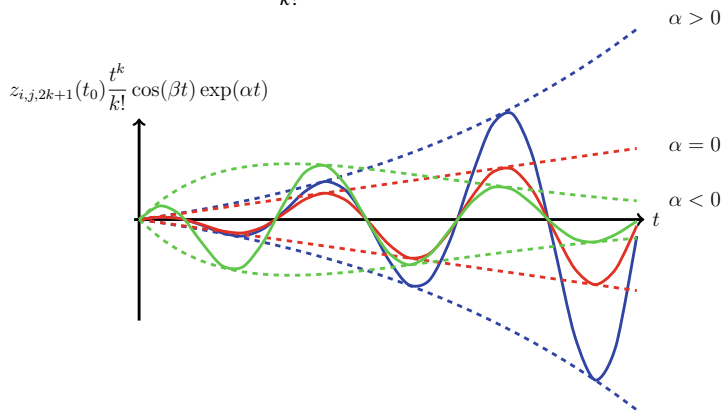


Fig. 3.8 Time behavior of $z_{i,j,2k+1}(t_0) \frac{t^k}{k!} \sin(\beta t) \exp(\alpha t)$ for $k > 0$

Since the numerical values specified in Exercise 3.2 lead to $\alpha_2 < 0$, the system (i.e., the linearization of the cart-pole around the static equilibrium) has one divergent mode (associated with the first line of \mathbf{J}_1), one constant mode (associated with the second line of \mathbf{J}_1), and two damped oscillating modes (associated with \mathbf{J}_2).

3.3 BIBS Stability

As previously described, the eigenvalues and the lengths of the chains of eigenvectors associated with matrix \mathbf{A} entirely describe the dynamics of LTI systems [1,2]. In particular, the trajectories of \mathbf{x} are convergent to the origin if and only if the real parts of the eigenvalues are all strictly negative. In addition, eigenvalues with null or positive real parts may lead to constant or divergent behaviors, depending on the length of the eigenvector chains. This section exploits these results to state a stability criterion that ensures trajectory boundedness [3,7].

Definition 3.1 Bounded-Input Bounded-State (BIBS) Stability. For LTI systems in the form (3.9) define

$$\chi_{\mathbf{u}}(t, \mathbf{x}(t_0)) = \exp(\mathbf{A}(t - t_0))\mathbf{x}(0) + \int_{t_0}^t \exp(\mathbf{A}(t - \tau))\mathbf{B}\mathbf{u}(\tau)d\tau.$$

Then, the system is BIBS-stable if

$\forall \varepsilon > 0 \exists \delta_\varepsilon : \forall \delta\mathbf{u}(\cdot) : \|\delta\mathbf{u}(t)\| \leq \delta_\varepsilon \implies \|\chi_{\mathbf{u}+\delta\mathbf{u}}(t, \mathbf{x}(t_0)) - \chi_{\mathbf{u}}(t, \mathbf{x}(t_0))\| \leq \varepsilon$
for all $t \geq t_0$.

The definition of BIBS stability links the perturbation of the input \mathbf{u} , i.e., $\delta\mathbf{u}$, with the evolution of the state \mathbf{x} , see Fig. 3.9.

The remainder of this section demonstrates that having as negative the real part of all eigenvalues implies BIBS stability. Without loss of generality, assume $\mathbf{x}(t_0) = \mathbf{0}$ and calculate the perturbed and unperturbed trajectories

$$\begin{aligned} \chi_{\mathbf{u}+\delta\mathbf{u}}(t, \mathbf{x}(t_0)) &= \int_{t_0}^t \exp(\mathbf{A}(t - \tau)) \mathbf{B} (\mathbf{u}(\tau) + \delta\mathbf{u}(\tau)) d\tau \\ \chi_{\mathbf{u}}(t, \mathbf{x}(t_0)) &= \int_{t_0}^t \exp(\mathbf{A}(t - \tau)) \mathbf{B} \mathbf{u}(\tau) d\tau \end{aligned}$$

whose difference is

$$\chi_{\mathbf{u}+\delta\mathbf{u}}(t, \mathbf{x}(t_0)) - \chi_{\mathbf{u}}(t, \mathbf{x}(t_0)) = \int_{t_0}^t \exp(\mathbf{A}(t - \tau)) \mathbf{B} \delta\mathbf{u}(\tau) d\tau.$$

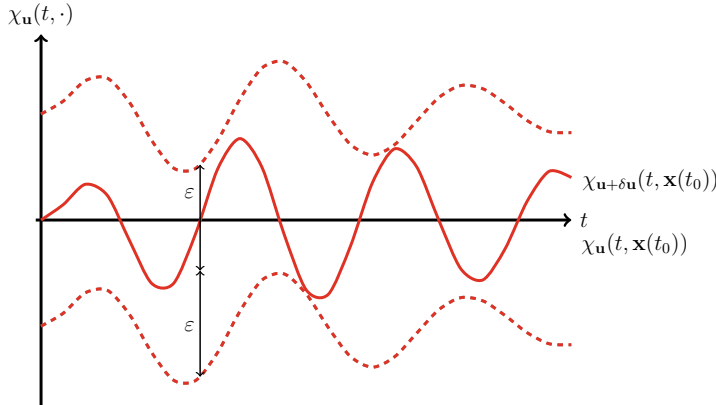


Fig. 3.9 The case of a BIBS-stable system

The latter is bounded as

$$\begin{aligned} \|\chi_{\mathbf{u}+\delta\mathbf{u}}(t, \mathbf{x}(t_0)) - \chi_{\mathbf{u}}(t, \mathbf{x}(t_0))\| &= \left\| \int_{t_0}^t \exp(\mathbf{A}(t-\tau)) \mathbf{B} \delta\mathbf{u}(\tau) d\tau \right\| \leq \\ &\leq \int_{t_0}^t \|\exp(\mathbf{A}(t-\tau)) \mathbf{B} \delta\mathbf{u}(\tau)\| d\tau \leq \int_{t_0}^t \|\exp(\mathbf{A}(t-\tau))\| d\tau \|\mathbf{B}\| \delta_\varepsilon \leq \\ &\leq \int_{t_0}^t \max_{\substack{i=1, \dots, p \\ j=1, \dots, g_i}} \sum_{k=0}^{q_{i,j}} \left| \frac{t^k}{k!} \exp(\alpha_i t) \right| d\tau \|\mathbf{B}\| \delta_\varepsilon. \end{aligned}$$

Therefore, LTI systems (3.9) are BIBS-stable if for all $\varepsilon > 0$ there exists $\delta_\varepsilon > 0$ such that

$$\delta_\varepsilon \leq \frac{\varepsilon}{\|\mathbf{B}\| \int_{t_0}^t \max_{\substack{i=1, \dots, p \\ j=1, \dots, g_i}} \sum_{k=0}^{q_{i,j}} \left| \frac{t^k}{k!} \exp(\alpha_i t) \right| d\tau}.$$

The integral appearing at the denominator of the right-hand side is finite if

$$\max_{\substack{i=1, \dots, p \\ j=1, \dots, a_i}} \sum_{k=0}^{q_{i,j}} \left| \frac{t^k}{k!} \exp(\alpha_i t) \right|$$

is absolutely integrable which, in turn, is true if the real part of all the eigenvalues of \mathbf{A} is strictly negative. Such a matrix is called Hurwitz.

Example 3.4 (Cart-pole Stability) The cart-pole is not BIBS-stable in agreement with the results of Example 3.3.

3.4 ADAS Analysis

This section investigates the stability properties of the linear plants defined in Chap. 2. The computation of eigenvectors and eigenvalues is instrumental to achieve this goal.

3.4.1 Active Suspensions

Equations (2.7) and (2.16) model the dynamics of the suspension system with active components for the single corner and the half car, respectively.

Single-Corner model

Let (2.11) be a linearization of (2.7) in which

$$\mathbf{A} = \begin{bmatrix} 0 & 1 & 0 & 0 \\ -k_s \frac{m_s + m_u}{m_s m_u} & -\beta_s \frac{m_s + m_u}{m_s m_u} & \frac{k_t}{m_u} & 0 \\ 0 & 0 & 0 & 1 \\ \frac{k_s}{m_u} & \frac{\beta_s}{m_u} & -\frac{k_t}{m_u} & 0 \end{bmatrix}. \quad (3.16)$$

Numerical computations of the eigenvalues of \mathbf{A} show that, for a typical passenger car, there are two couples of complex conjugate roots whose real part is non-positive. These two couples differ mainly by their natural pulsation, where the higher can be intuitively linked to the tire's natural frequency, and the lower is associated with the suspension's natural pulsation. To understand the influence of the suspension parameters (stiffness and damping ratio), Fig. 3.10 presents the loci of the eigenvalues obtained by letting β_s and k_s vary from 0 to a bounded positive value. In more detail, Fig. 3.10 shows that in the absence of a damper, i.e., for $\beta_s = 0$, the modes are purely oscillatory, whereas, for any $\beta_s > 0$, the eigenvalues have a negative real part. The left picture of Fig. 3.10 shows that two eigenvalues become real for sufficiently large values of β_s . On the other hand, assuming $k_s = 0$, the plant possesses a null real eigenvalue that can be physically associated with the dynamics of the position of the sprung mass relative to the unsprung one. Indeed, in the absence of a suspension spring, the cabin-wheel relative position is obtained as an integration of the suspension speed. For any sufficiently small $k_s > 0$, the composition of two convergent and two damped oscillatory modes represents the dynamics. Therefore, the plant behaves as in the case of strong damping. This study helps us to gain insight into the meaning of the entries of \mathbf{K}_s , designed in Sect. 5.4.1.

Remark 3.5 The locus of the eigenvalues can be considered a generalization of the *root contour*, at zero feedback gain, for MIMO systems. Indeed, the eigenvalues are generally more informative than the poles, which correspond only to a subset of the eigenvalues, those related to the reachable and observable part of the plant (see Chap. 4).

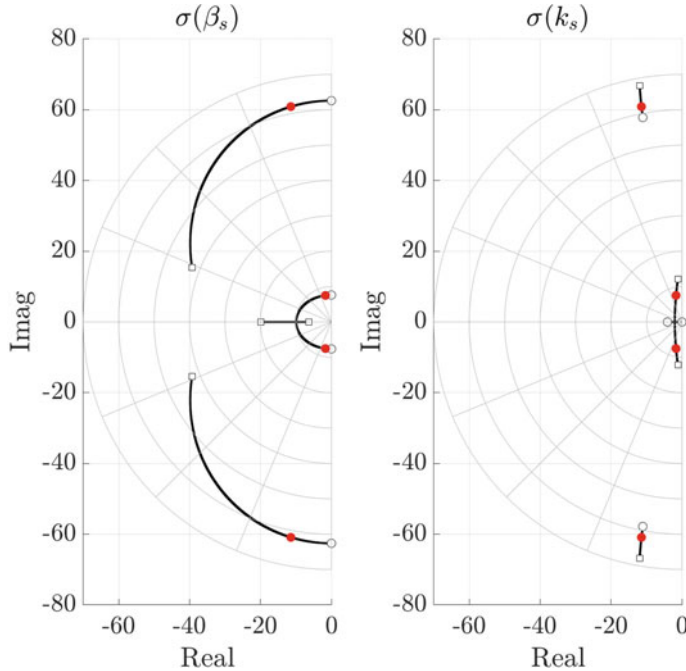


Fig. 3.10 Single-Corner model. Loci of the eigenvalues of (3.16) obtained with $k_t = 160000$ N/m, $m_u = 45$ kg, and $m_s = 250$ kg. The red points represent the eigenvalues for the nominal $\beta_s = \beta_{s0} := 1000$ N/(m/s) and $k_s = k_{s0} := 16000$ N/m. (Left) Locus for $\beta_s \in [0, 4\beta_{s0}]$ where the white circle and squares are the eigenvalues for $\beta_s = 0$ and $\beta_s = 4\beta_{s0}$. (Right) Locus for $k_s \in [0, 4k_{s0}]$ where the white circle and squares are the eigenvalues for $k_s = 0$ and $k_s = 4k_{s0}$. Around the nominal conditions, increasing the damping coefficient (mainly) leads to a rotation of the eigenvalues whereas increasing the spring stiffness amplifies the eigenvalues norm

Let $\lambda_{1,2} = -\alpha_1 \pm i\beta_1$ and $\lambda_{3,4} = -\alpha_2 \pm i\beta_2$ be the eigenvalues at the nominal plant parameters $\beta_s = \beta_{s0} > 0$ and $k_s = k_{s0} > 0$ depicted, in red, in Fig. 3.10. Let $\mathbf{z} := \text{col}(z_1, \dots, z_4)$, then at the nominal conditions, the free evolution of \mathbf{z} is

$$\begin{aligned} \begin{bmatrix} z_1(t) \\ z_2(t) \end{bmatrix} &= e^{-\alpha_1 t} \begin{bmatrix} \cos(\beta_1 t) & \sin(\beta_1 t) \\ -\sin(\beta_1 t) & \cos(\beta_1 t) \end{bmatrix} \begin{bmatrix} z_1(0) \\ z_2(0) \end{bmatrix} \\ \begin{bmatrix} z_3(t) \\ z_4(t) \end{bmatrix} &= e^{-\alpha_2 t} \begin{bmatrix} \cos(\beta_2 t) & \sin(\beta_2 t) \\ -\sin(\beta_2 t) & \cos(\beta_2 t) \end{bmatrix} \begin{bmatrix} z_3(0) \\ z_4(0) \end{bmatrix}. \end{aligned}$$

Let $\mathbf{V} \in \mathbb{R}^{4 \times 4}$ be the matrix, in real form, of the eigenvectors associated with $\lambda_1, \dots, \lambda_4$ and define with $v_{i,j}$ the i -th element of \mathbf{V} . Then,

$$\tilde{x}_i(t) = \sum_{j=1}^4 v_{i,j} z_j(t) \quad i = 1, \dots, 4.$$

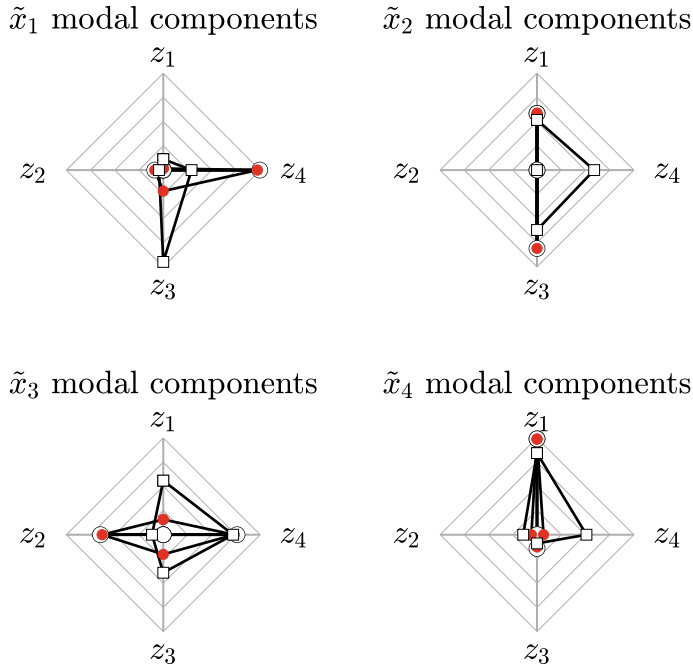


Fig. 3.11 Single-Corner model. State modal decomposition. Each state variable x_i is obtained as a linear combination, defined by the eigenvectors of \mathbf{A} , of the z_j , with $j = 1, \dots, 4$. The red markers identify the modal decomposition for the nominal values $\beta_s = \beta_{s0} := 1000 \text{ N/(m/s)}$ and $k_s = k_{s0} := 16000 \text{ N/m}$. The white circled markers represent the modal decomposition for $\beta_s = 0$ and $k_s = k_{s0}$ and the squared markers are relative to the decomposition for $\beta_s = 4\beta_{s0}$ and $k_s = k_{s0}$

Let $\lambda_{1,2}$ be the eigenvalues with higher pulsation. Then, with the support of Figs. 3.11 and 3.12, identify the influence of each component of \mathbf{z} on \tilde{x}_i . In more detail, at the nominal parameters (depicted with red circles), $\tilde{x}_1 \approx z_4$ meaning that the suspension length (see Eq. (2.5)) behaves approximately as a low-frequency oscillation. On the other hand, \tilde{x}_2 and \tilde{x}_3 representing the suspension speed (variation of height over time) and the tire deflection combine both slow and fast oscillations. Conversely, the tire speed (variation of length over time), denoted by \tilde{x}_4 , is well approximated by z_1 , i.e., by a fast oscillation. This behavior is motivated as follows. The tire stiffness is much higher than the suspension spring stiffness. This implies that the tire *nearly rigidly* transfers the load from the ground to the suspension. For this reason, the suspension speed is also affected by high-frequency content. Moreover, the suspension creates a low-frequency force (through a length variation) that compresses the tire. The time history of $\tilde{\mathbf{x}}$ shown in Fig. 3.13 corroborates these arguments.

Figures 3.11 and 3.12 also report the modal decomposition for the off-design conditions $\beta_s = \{0, 4\beta_{s0}\}$ and $k_s = \{0, 4k_{s0}\}$.

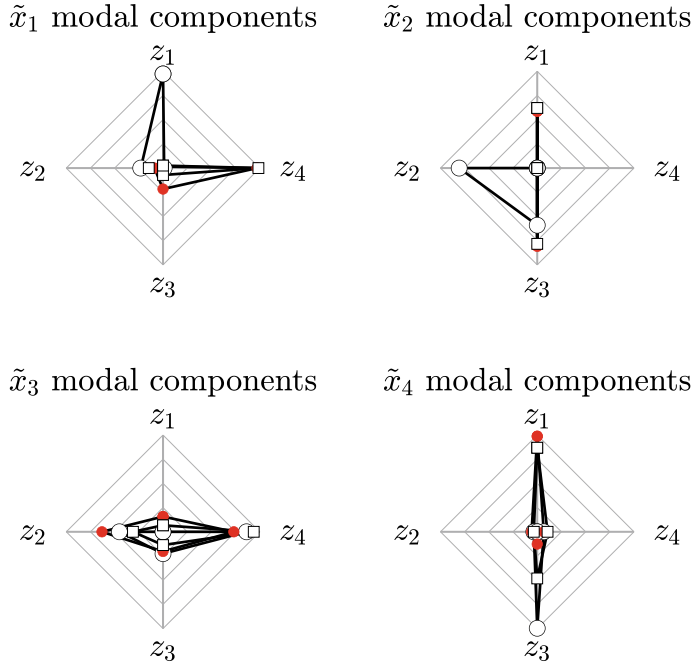


Fig. 3.12 Single-Corner model. State modal decomposition. Each state variable x_i is obtained as a linear combination, defined by the eigenvectors of A , of the modes z_i . The red markers identify the modal decomposition for the nominal values $\beta_s = \beta_{s0} := 1000 \text{ N/(m/s)}$ and $k_s = k_{s0} := 16000 \text{ N/m}$. The white circled markers represent the modal decomposition for $\beta_s = \beta_{s0}$ and $k_s = 0$ and the squared markers are relative to the decomposition for $\beta_s = \beta_{s0}$ and $k_s = 4k_{s0}$

Half-Car model

Equations (2.16) and (2.21) model and linearize the dynamics of a half car. The linear system is characterized by

$$\mathbf{A} = \begin{bmatrix} 0 & 1 & 0 & 0 & 0 & 0 \\ -\frac{2k}{m} & -\frac{2\beta}{m} & -\frac{k(d_l-d_r)}{m} & -\frac{\beta(d_l-d_r)}{m} & \frac{k(d_l-d_r)}{m} & \frac{\beta(d_l-d_r)}{m} \\ 0 & 0 & 0 & 1 & 0 & 0 \\ -\frac{k(d_l-d_r)}{J} & -\frac{\beta(d_l-d_r)}{J} & -\frac{k(d_l^2+d_r^2)}{J} & -\frac{\beta(d_l^2+d_r^2)}{J} & \frac{k(d_l^2+d_r^2)}{J} & \frac{\beta(d_l^2+d_r^2)}{J} \\ 0 & 0 & 0 & 0 & 0 & 1 \\ 0 & 0 & 0 & 0 & 0 & 0 \end{bmatrix}. \quad (3.17)$$

It is easy to see that \mathbf{A} is an upper triangular block matrix whose eigenvalues are those of the blocks on the main diagonal. In particular, similar to the single-corner linearized model, the half-car one is also described by four eigenvalues representing the vehicle dynamics associated with the block

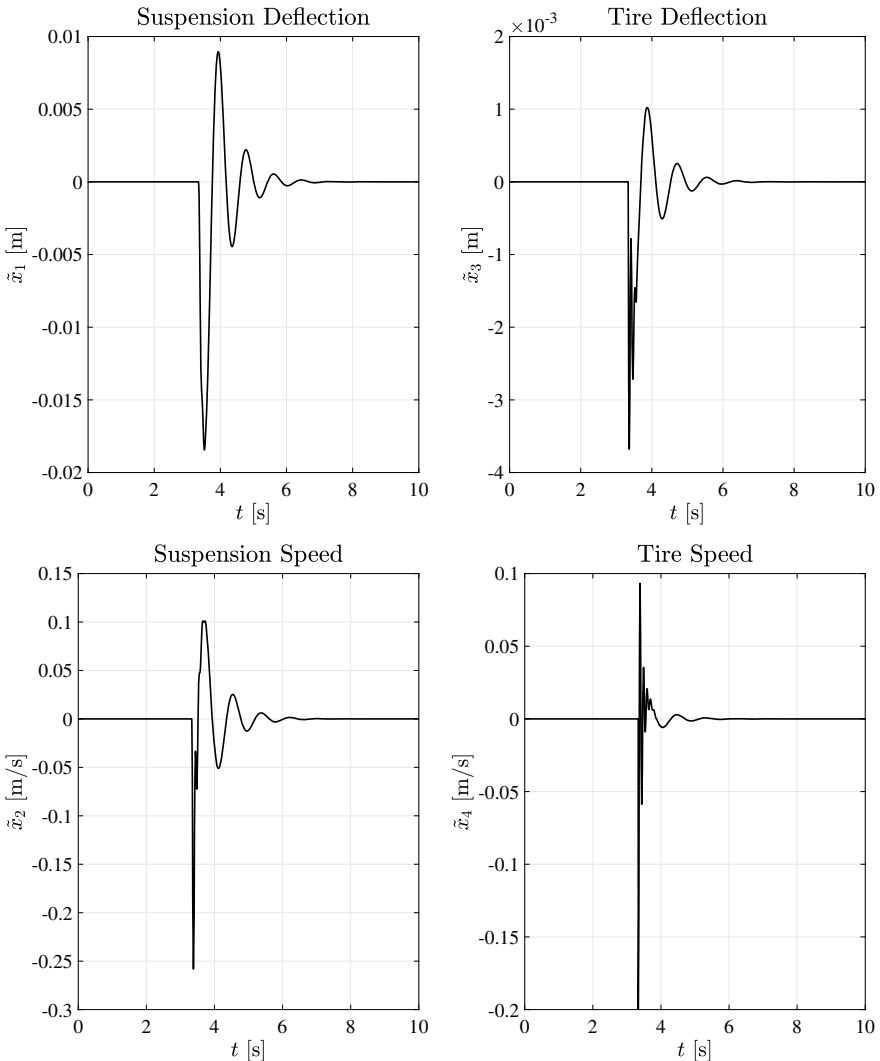


Fig. 3.13 Single-Corner model. Simulation of suspension dynamics in the case of a road acceleration pulse at time $t = 3.3$ s. The two complex conjugate modes are evident in the time behavior of the tire deflection and the suspension speed. Let x_{30} be the linearization condition found in Eq. (2.10). Then, $x_3 = x_{30} + \tilde{x}_3 = \ell_t - g(m_s + m_u)/k_t + \tilde{x}_3$, and the simulation is valid until $x_3 \leq \ell_t$ (see “Important” after Eq. (2.11)) or equivalently until $\tilde{x}_3 \leq g(m_s + m_u)/k_t$. It is worth noting that, for the vehicle under investigation, the value $g(m_u + m_s)/k_t$ is about 1.8 cm and that this value is more than ten times the maximum positive value of \tilde{x}_3 , keeping valid the model of Eq. (2.11)

$$\begin{bmatrix} 0 & 1 & 0 & 0 \\ -\frac{2k}{m} & -\frac{2\beta}{m} & -\frac{k(d_l-d_r)}{m} & -\frac{\beta(d_l-d_r)}{m} \\ 0 & 0 & 0 & 1 \\ -\frac{k(d_l-d_r)}{J} & -\frac{\beta(d_l-d_r)}{J} & -\frac{k(d_l^2+d_r^2)}{J} & -\frac{\beta(d_l^2+d_r^2)}{J} \end{bmatrix}.$$

But, in this case, two other eigenvalues describe the road bank angle kinematic chain

$$\begin{bmatrix} 0 & 1 \\ 0 & 0 \end{bmatrix}.$$

As for the first four eigenvalues, these constitute, for the plant evaluated at the nominal parameters $\beta = \beta_0 > 0$ and $k = k_0 > 0$, two couples of complex conjugate roots, one of them characterized by a larger pulsation and damping. As seen for the single-corner model and regarding Fig. 3.14, any increase of the damping coefficient β leads to a *rotation* of the roots towards more damped configurations. Indeed, for sufficiently large β , the eigenvalues become real (see the left plot of Fig. 3.14). On the other hand, any increase of the spring stiffness k leads to a rise

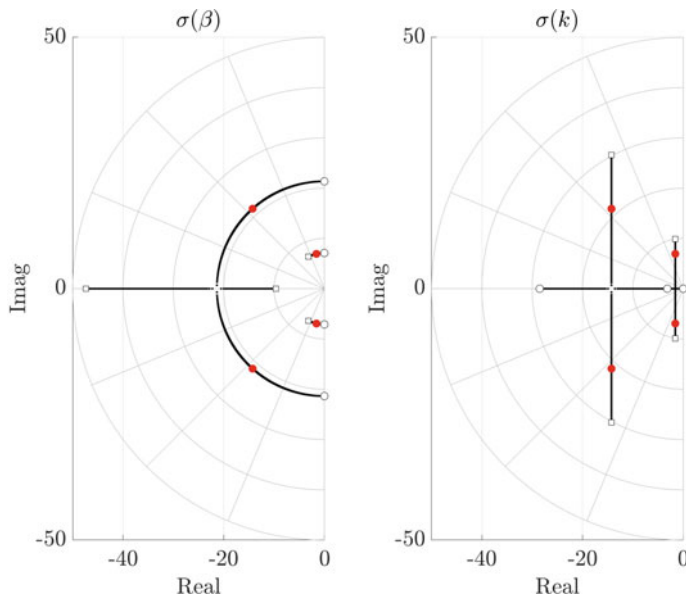


Fig. 3.14 Half-car model. Loci of the eigenvalues of (3.17) obtained with $m = 600 \text{ kg}$, $d_r = 1.10 \text{ m}$, and $d_l = 0.70 \text{ m}$. The red points represent the eigenvalues for $\beta = \beta_0 := 1000 \text{ N/(m/s)}$ and $k = k_0 := 16000 \text{ N/m}$. (Left) Locus for $\beta \in [0, 2\beta_0]$ where the white circle and squares are the eigenvalues for $\beta = 0$ and $\beta = 4\beta_0$. (Right) Locus for $k \in [0, 2k_0]$ where the white circle and squares are the eigenvalues for $k = 0$ and $k_s = 2k_0$. Around the nominal conditions, increasing the damping coefficient (mainly) leads to a rotation of the eigenvalues. Conversely, increasing the spring stiffness amplifies the eigenvalue norm

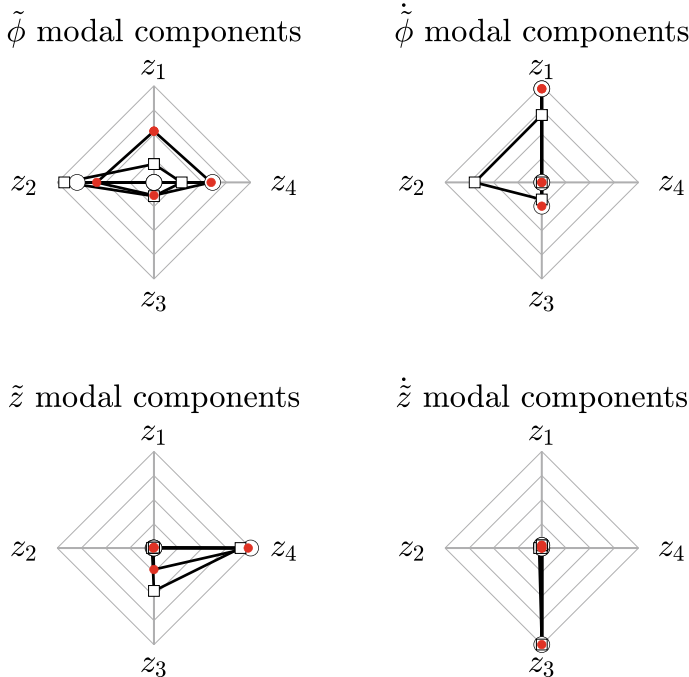


Fig. 3.15 Half-car model. State modal decomposition. Each state variable x_i is obtained as a linear combination, defined by the eigenvectors of A , of the modes z_i . The red markers identify the modal decomposition for the nominal values $\beta = \beta_0 := 1000 \text{ N/(m/s)}$ and $k = k_0 := 16000 \text{ N/m}$. The white circled markers represent the modal decomposition for $\beta = 0$ and $k = k_0$ and the squared markers are relative to the decomposition for $\beta = 2\beta_0$ and $k = k_0$

in the imaginary part of the eigenvalues. As shown in the right plot of Fig. 3.14, a sufficiently small k exists, so the eigenvalues become real.

Similar to the single-corner model, the behavior of the half car one reveals the superposition of high-pulsation, high-damping, and low-pulsation low-damping modes. Define $\mathbf{T} \in \mathbb{R}^{6 \times 6}$ as a Jordan transformation, and let $\mathbf{z} := \text{col}(z_1, \dots, z_6) = \mathbf{T}\mathbf{x}$. Assume the plant is at its nominal conditions and let z_1 and z_2 be the modes associated with the high-pulsation and high-damping eigenvalues. The remaining z_3 and z_4 represent the low-pulsation, low-damping ration modes. Then, the modal decomposition shown in Figs. 3.15 and 3.16 demonstrate that, at the nominal conditions (red points), the roll deflection and speed are mainly composed of the first two modes. In contrast, the low-pulsation and low-damping ration modes describe vertical displacement and velocity. This phenomenon is due to the difference between inertia and mass. Indeed, since $m \gg J$ the inertia of the vertical dynamics is higher than the roll dynamics' inertia, which implies higher oscillations with longer settling times. The time behavior shown in Fig. 3.17 supports these arguments.

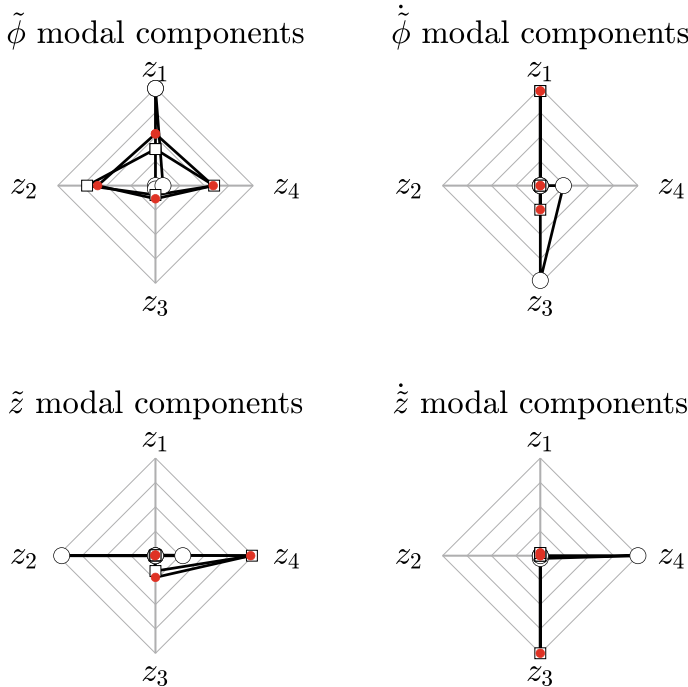


Fig.3.16 Half-car model. State modal decomposition. Each state variable x_i is obtained as a linear combination, defined by the eigenvectors of A , of the modes z_i . The red markers identify the modal decomposition for the nominal values $\beta = \beta_0 := 1000 \text{ N/(m/s)}$ and $k = k_0 := 16000 \text{ N/m}$. The white circled markers represent the modal decomposition for $\beta = \beta_0$ and $k = 0$ and the squared markers are relative to the decomposition for $\beta = \beta_0$ and $k_s = 2k_0$

To conclude, the last two eigenvalues of \mathbf{A} are those associated with the block

$$\begin{bmatrix} 0 & 1 \\ 0 & 0 \end{bmatrix}.$$

As described in Sect. 3.1.2, this matrix possesses one single eigenvalue, namely $\lambda_5 = 0$, with algebraic multiplicity $a_5 = 2$, geometric multiplicity $g_5 = 1$, and a chain of generalized eigenvectors of length $q_{5,1} = 2$. Consequently, the linearized dynamics associated with λ_5 are not BIBS-stable.

3.4.2 Electro-mechanical Brakes

The nonlinear model (2.28) linearized in (2.30) describes the dynamics of Electro-mechanical Brakes (EMBs). The following \mathbf{A} matrix is part of the linearized model:

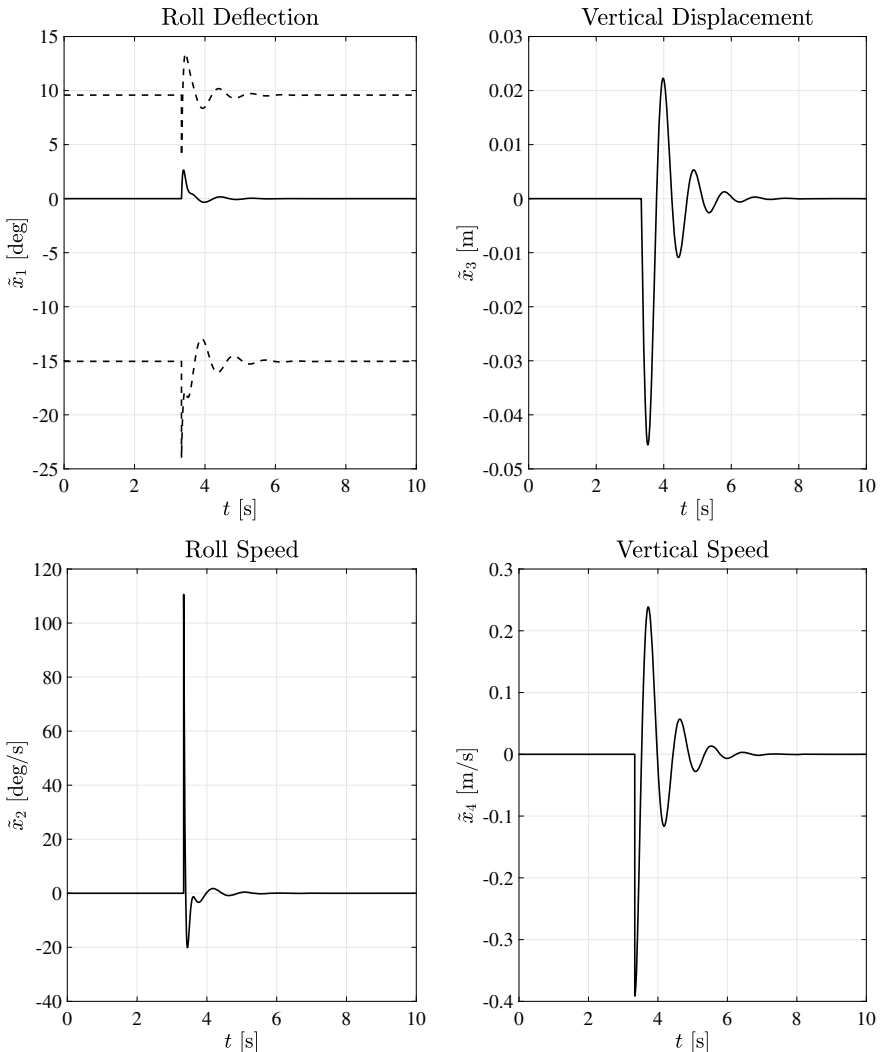


Fig. 3.17 Half-car model. Dynamics in the case of a side acceleration pulse at time $t = 3.3$ s. The oscillatory behavior induced by the two complex conjugate modes describes the vertical and rotational deflection and speed. The simulation is valid until $ks_1 + \beta s_2 \leq 0$ and $ks_3 + \beta s_4 \leq 0$ (see “Important” after Eq. (2.21)). These inequalities are translated into a lower bound $\underline{\phi}$ and an upper bound $\bar{\phi}$ for $\tilde{\phi}$. As a consequence, the simulation is valid until $\underline{\phi} \leq \tilde{\phi} \leq \bar{\phi}$. The dashed lines in the top right picture represent the maximum roll rotation that keeps the model (2.21) valid

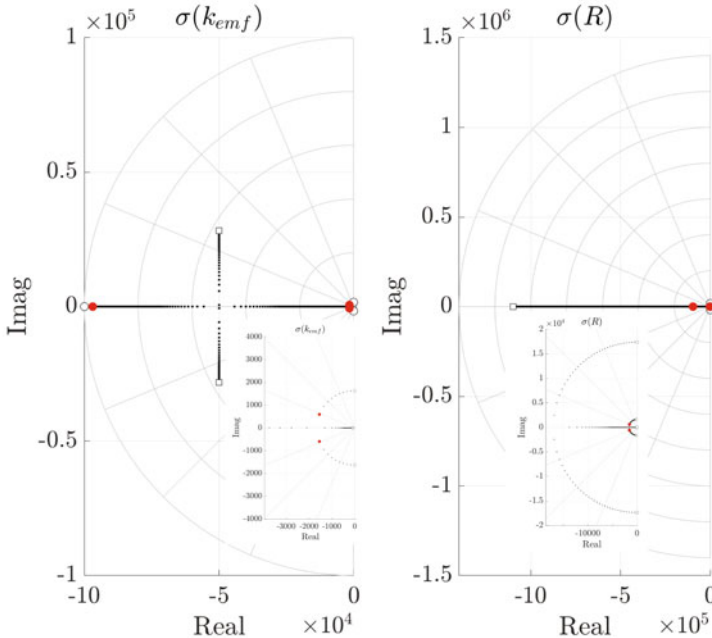


Fig. 3.18 Loci of the eigenvalues of (3.18) obtained with $J = 2.91e-4 \text{ kg m}^2$, $N = 2.63e-5 \text{ m/rad}$, $k = 6.97e-2 \text{ Nm/A}$, $L = 1e-6 \text{ H}$, $R = 0.1 \text{ Ohm}$, $k_{\text{emf}} = 1.25 \text{ V/(rad/s)}$, $\alpha_1 = 0.0327e4$, $\alpha_2 = 3.834e4$, $\alpha_3 = -1.518e4$, $r_0 = 1e4 \text{ N}$, $\theta_0 = 34.3436 \text{ rad}$, $\beta_0 = 3.0e-4$, $\beta_1 = 3e-4$, $\beta_2 = 0.01$, and $\kappa = 1e3$. (Left) Locus for $k_{\text{emf}} \in [0, 10k_{\text{emf}0}]$ where the white circles and squares are the eigenvalues for $k_{\text{emf}} = 0$ and $k_{\text{emf}} = 10k_{\text{emf}0}$. (Right) Locus for $k_{\text{emf}} = k_{\text{emf}0}$ and $R \in [0, 10R_0]$ where the white circles and squares are the eigenvalues for $R = 0$ and $R = 10R_0$

$$\mathbf{A} = \begin{bmatrix} 0 & 1 & 0 \\ -N \frac{N\alpha_1 + 2N\alpha_2\theta_0 + 3N\alpha_3(N\theta_0)^2}{J} & 0 & \frac{k}{J} \\ 0 & -\frac{k_{\text{emf}}}{L} & -\frac{R}{L} \end{bmatrix}. \quad (3.18)$$

For the plant evaluated at the nominal parameters $R = R_0 > 0$ and $k_{\text{emf}} = k_{\text{emf}0} > 0$, numerical computations provide one real and two complex conjugate eigenvalues, all with negative real parts. Let $\lambda_{1,2}$ be the two complex eigenvalues and λ_3 be the real one. As depicted in Fig. 3.18, $|\lambda_3| \gg |\text{Real}(\lambda_{1,2})|$ thus implying that the third mode, of kind $e^{\lambda_3 t}$, vanishes much faster than the oscillatory modes. On the other hand, $|\text{Real}(\lambda_{1,2})| \approx 3|\text{Imag}(\lambda_{1,2})|$ means high damping of the oscillations associated with $\lambda_{1,2}$. With the support of the modal decomposition depicted in Figs. 3.19 and 3.20, it is possible to claim that the oscillatory modes are (mainly) affecting the mechanical dynamics. On the other hand, the third mode principally describes the electric current dynamics.

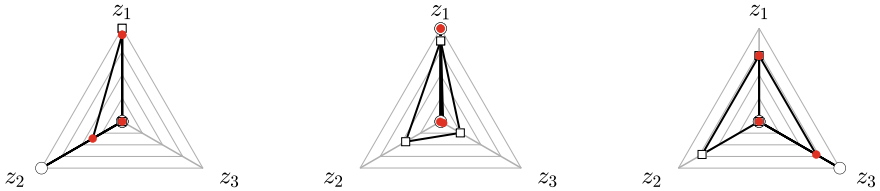


Fig. 3.19 EMB modal decomposition. Each state variable x_i is obtained as a linear combination, defined by the eigenvectors of \mathbf{A} , of the modes z_i . The red markers identify the modal decomposition for the nominal values of $k_{\text{emf}} = k_{\text{emf}0} := 1.25 \text{ V/(rad/s)}$ and $R = R_0 := 0.05 \text{ Ohm}$, the white circled markers represent the modal decomposition for $R = R_0$ and $k_{\text{emf}} = 0$, and the squared markers are relative to the decomposition for $R = R_0$ and $k_{\text{emf}} = 10k_{\text{emf}0}$

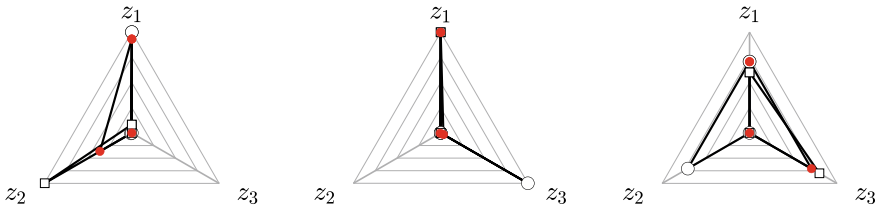


Fig. 3.20 EMB modal decomposition. Each state variable x_i is obtained as a linear combination, defined by the eigenvectors of \mathbf{A} , of the modes z_i . The red markers identify the modal decomposition for the nominal values of $k_{\text{emf}} = k_{\text{emf}0} := 1.25 \text{ V/(rad/s)}$ and $R = R_0 := 0.05 \text{ Ohm}$, the white circled markers represent the modal decomposition for $R = 0$ and $k_{\text{emf}} = k_{\text{emf}0}$, and the squared markers are relative to the decomposition for $R = 10R_0$ and $k_{\text{emf}} = k_{\text{emf}0}$

Figure 3.21 highlights time scales and modal decompositions. In more detail, the simulation shows the behavior of the linearized plant subject to a change in the input voltage \tilde{u} . A higher voltage leads to a higher current which, in turn, creates a positive shaft torque. This extra torque increases the shaft speed, and so does the angular position. Then, the raised position leads to a higher load torque that counterbalances the motor torque. Consequently, an asymptotic equilibrium is reached with damped oscillations.

As for the eigenvalue displacement induced by the variation of parameters, Fig. 3.18 shows that, for $R = 0$, the plant possesses complex conjugate eigenvalues and single real eigenvalues, all with a null real part. Indeed, setting $R = 0$ implies that the linearized model has no dissipative terms (Ri is conceived as “electric friction”). On the other hand, setting $k_{\text{emf}} = 0$ decouples the electric subsystem from the mechanical one. Therefore, the friction Ri still damps the electric circuit while the mechanical part oscillates due to the load torque feedback.

3.4.3 Wheel Speed Controls

Section 2.3 presented the linearized model of the longitudinal dynamics of a ground vehicle. To investigate the properties of the linearized model, define

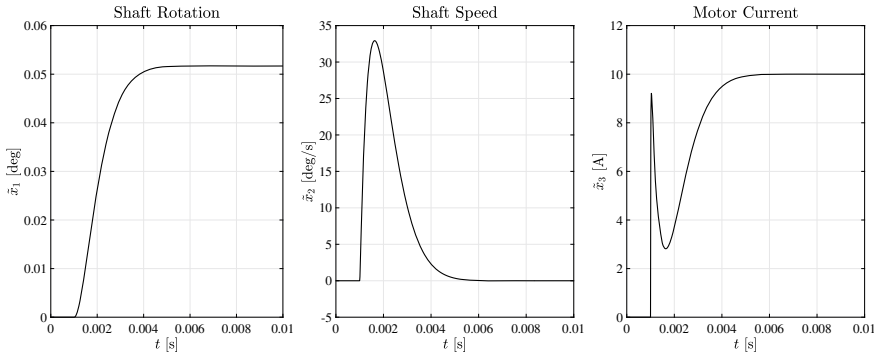


Fig. 3.21 Simulation of the linearized EMB. The plant starts at the linearization conditions and, at $t = 1e - 3$ is forced by a constant input voltage. The system evolves according to the modes shown in Fig. 3.18, for the nominal parameters. As predicted by the modal decomposition, the dynamics of the electric current are influenced by a combination of fast and slow modes, whereas the trajectories of position and speed are mainly described by the slow mode

$$\bar{\mu}_r = \mu_r - c_r, \bar{\mu}_f = \mu_f - c_r,$$

$$\mathbf{A}_s = \begin{bmatrix} \frac{N_r}{m} \frac{\partial \bar{\mu}_r}{\partial v} + \frac{N_f}{m} \frac{\partial \bar{\mu}_f}{\partial v} - \frac{\rho S v C_D}{m} & \frac{N_r}{m} \frac{\partial \bar{\mu}_r}{\partial \omega_r} & \frac{N_f}{m} \frac{\partial \bar{\mu}_f}{\partial \omega_f} \\ -\frac{r_r N_r}{J_r} \frac{\partial \bar{\mu}_r}{\partial v} & -\frac{r_r N_r}{J_r} \frac{\partial \bar{\mu}_r}{\partial \omega_r} & 0 \\ -\frac{r_f N_f}{J_f} \frac{\partial \bar{\mu}_f}{\partial v} & 0 & -\frac{r_f N_f}{J_f} \frac{\partial \bar{\mu}_f}{\partial \omega_f} \end{bmatrix}_{\mathbf{x}=\mathbf{x}_0},$$

and

$$\mathbf{A}_{lt} = \begin{bmatrix} \frac{\bar{\mu}_r}{m} \frac{\partial N_r}{\partial v} + \frac{\bar{\mu}_f}{m} \frac{\partial N_f}{\partial v} & \frac{\bar{\mu}_r}{m} \frac{\partial N_r}{\partial \omega_r} + \frac{\bar{\mu}_f}{m} \frac{\partial N_f}{\partial \omega_r} & \frac{\bar{\mu}_r}{m} \frac{\partial N_r}{\partial \omega_f} + \frac{\bar{\mu}_f}{m} \frac{\partial N_f}{\partial \omega_f} \\ -\frac{r_r \bar{\mu}_r}{J_r} \frac{\partial N_r}{\partial v} & -\frac{r_r \bar{\mu}_r}{J_r} \frac{\partial N_r}{\partial \omega_r} & -\frac{r_r \bar{\mu}_r}{J_r} \frac{\partial N_r}{\partial \omega_f} \\ -\frac{r_f \bar{\mu}_f}{J_f} \frac{\partial N_f}{\partial v} & -\frac{r_f \bar{\mu}_f}{J_f} \frac{\partial N_f}{\partial \omega_r} & -\frac{r_f \bar{\mu}_f}{J_f} \frac{\partial N_f}{\partial \omega_f} \end{bmatrix}_{\mathbf{x}=\mathbf{x}_0}.$$

The term \mathbf{A}_s collects the terms independent of the load transfer variation, whose effects are embedded in \mathbf{A}_{lt} . Then, split Eq. (2.47) as

$$\mathbf{A} = \mathbf{A}_s + \mathbf{A}_{lt}.$$

Numerical evaluations of \mathbf{A}_s reveal that, by neglecting the load transfer, the linearized dynamics possess three real negative eigenvalues. Two of them are much more prominent in magnitude than the third. This difference is because $m \gg J_r, J_f$ implies that the first row of \mathbf{A}_s is numerically negligible for the rest of the matrix entries. Consequently, \mathbf{A}_s becomes numerically similar to a lower triangular matrix whose eigenvalues are the elements on the main diagonal. Then, the modal decomposition associated with \mathbf{A}_s shows that the eigenvalue with the smallest magnitude (the closest to zero) mainly affects the car's longitudinal speed and represents the effects of air drag and rolling resistance. In addition, the remaining two high-magnitude eigenvalues mostly describe the wheel speed dynamics. Indeed, from a

physical viewpoint, since the wheel inertias are much smaller than the vehicle mass, the wheel dynamics evolve on a much faster time scale, see Fig. 3.24.

A second critical comment concerns the eigenvalues as a function of the linearization speed, namely v_0 . In more detail, assuming a driving linearization condition, i.e., $\lambda_0 \in (0, 1)$ and $\omega_0 = v_0/(r(1 - \lambda_0))$, it is

$$\begin{aligned} \frac{\partial \mu(\lambda(v, \omega r), \Theta)}{\partial v} \Big|_{v=v_0, \omega=\omega_0} &= \frac{\partial \mu(\lambda, \Theta)}{\partial \lambda} \Big|_{\lambda=\lambda_0} \frac{\partial \lambda(v, \omega r)}{\partial v} \Big|_{v=v_0, \omega=\omega_0} \\ &= \frac{\partial \mu(\lambda, \Theta)}{\partial \lambda} \Big|_{\lambda=\lambda_0} \frac{\lambda_0 - 1}{v_0} \\ \frac{\partial \mu(\lambda(v, \omega r), \Theta)}{\partial \omega} \Big|_{v=v_0, \omega=\omega_0} &= \frac{\partial \mu(\lambda, \Theta)}{\partial \lambda} \Big|_{\lambda=\lambda_0} \frac{\partial \lambda(v, \omega r)}{\partial \omega} \Big|_{v=v_0, \omega=\omega_0} \\ &= \frac{\partial \mu(\lambda, \Theta)}{\partial \lambda} \Big|_{\lambda=\lambda_0} \frac{r(1 - \lambda_0)^2}{v_0}, \end{aligned}$$

implying that the magnitude of all the non-trivial entries of \mathbf{A}_s increases to infinite for $v_0 \rightarrow 0$.

As for \mathbf{A}_{lt} , the load transfer couples the front and rear wheel dynamics through the derivatives $\bar{\mu}_r \partial N_r / \partial \omega_f$ and $\bar{\mu}_f \partial N_f / \partial \omega_r$. Indeed, for $\bar{\mu}_r, \bar{\mu}_f \neq 0$, any wheel speed variation corresponds to a load transfer variation that changes the friction force on the other wheel. For some positions of the gravity center and driving distributions (rear/front torques), this cross-coupling modifies the two real negative high-magnitude eigenvalues making these roots complex conjugate.

Figure 3.22 shows the locus of the eigenvalues of \mathbf{A} with $v_0 \in [10, 100]$ km/h for a four-wheel drive vehicle. The magnification highlights the presence of complex conjugate eigenvalues, as the previous analysis foresaw. Moreover, the modal decomposition visualized in Fig. 3.23 associates the eigenvalue with the smallest amplitude to the vehicle speed dynamics (Fig. 3.24).

This section ends with a study of the eigenvalues of \mathbf{A} evaluated at $(\mathbf{x}', \mathbf{u}', \mathbf{w}')$, which is not an equilibrium triplet. This study is motivated by the time scale separation between the vehicle and the wheel dynamics. Indeed, let $\tilde{\boldsymbol{\omega}} := \text{col}(\tilde{\omega}_r, \tilde{\omega}_f)$ and $\tilde{\mathbf{x}} := \text{col}(\tilde{v}, \tilde{\boldsymbol{\omega}})$, assume $\tilde{\mathbf{u}}, \tilde{\mathbf{w}} = \mathbf{0}$, and divide \mathbf{A} into sub-matrices such that

$$\begin{bmatrix} \dot{\tilde{v}} \\ \dot{\tilde{\boldsymbol{\omega}}} \end{bmatrix} = \begin{bmatrix} A_{11} & A_{12} \\ A_{21} & A_{22} \end{bmatrix} \begin{bmatrix} \tilde{v} \\ \tilde{\boldsymbol{\omega}} \end{bmatrix}.$$

Then, since the vehicle speed can be considered quasi-static during the fast wheel transients, i.e., $\dot{\tilde{v}} \approx 0$, the wheel dynamics can be approximated as

$$\dot{\tilde{\boldsymbol{\omega}}} = \mathbf{A}_{22} \tilde{\boldsymbol{\omega}} + \mathbf{A}_{21} \tilde{v},$$

in which \tilde{v} is conceived as a quasi-constant disturbance. Moreover, for sufficiently small v_0 , the entries of \mathbf{A}_{lt} are negligible for those of \mathbf{A}_s . Then,

$$\mathbf{A}_{22} \approx \begin{bmatrix} -\frac{r_r N_r}{J_r} \frac{\partial \bar{\mu}_r}{\partial \omega_r} & 0 \\ 0 & -\frac{r_f N_f}{J_f} \frac{\partial \bar{\mu}_f}{\partial \omega_f} \end{bmatrix}_{\mathbf{x}=\mathbf{x}'}$$

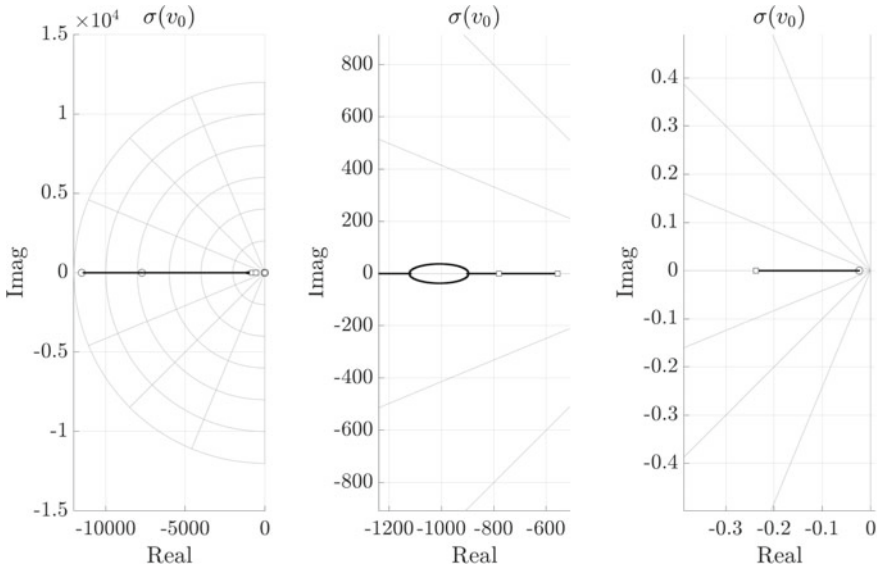


Fig. 3.22 A car’s longitudinal dynamics. Locus of the eigenvalues of (2.47) for $v_0 \in [10, 100]$ km/h. (Left) The eigenvalues are distinct negative and real for an extensive range of vehicle linearization speeds. The circles denote the position of the eigenvalues at $v = 10$ km/h, whereas the squares are those at $v = 100$ km/h. (Mid) Magnification of the complex conjugate eigenvalues, describing the wheel dynamics, and due to the load transfer. (Right) Zoom in the variation due to the linearization speed of the eigenvalue describing the longitudinal vehicle dynamics. The locus has been obtained by adopting the following parameters: $m = 600$ kg, $\bar{a} = 0.4$, $\bar{h} = 0.2$, $J_r = J_f = 1$ kg m², $r_r = r_f = 0.3$ m, $c_{r0} = c_{r1} = c_{r2} = 0$, $\rho = 1.225$ kg/m³, $S = 1.92$ m², and $C_D = 2.2$

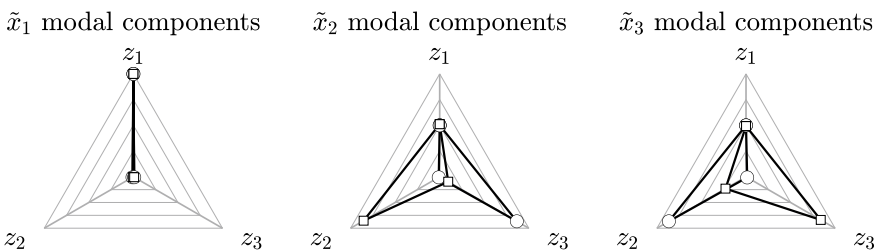


Fig. 3.23 A car’s longitudinal dynamics. State modal decomposition. Each state variable x_i is obtained as a linear combination, defined by the eigenvectors of \mathbf{A} , of the modes z_i . The white circled markers represent the modal decomposition for $v = 10$ km/h, and the squared markers are relative to the decomposition for $v = 100$ km/h

at low vehicle speeds, implying that the two wheels evolve independently of each other. Then, without loss of generality, assume that \mathbf{x}' is such that $\lambda'_r := \lambda(v', \omega'_r r) \in (\lambda^*, 1)$. In these conditions, the derivative $\partial\mu(\lambda, \Theta)/\partial\lambda$ evaluated at $\lambda_r = \lambda'_r$ is negative. Figure 2.5 shows the slope change before and after λ^* . Consequently, one

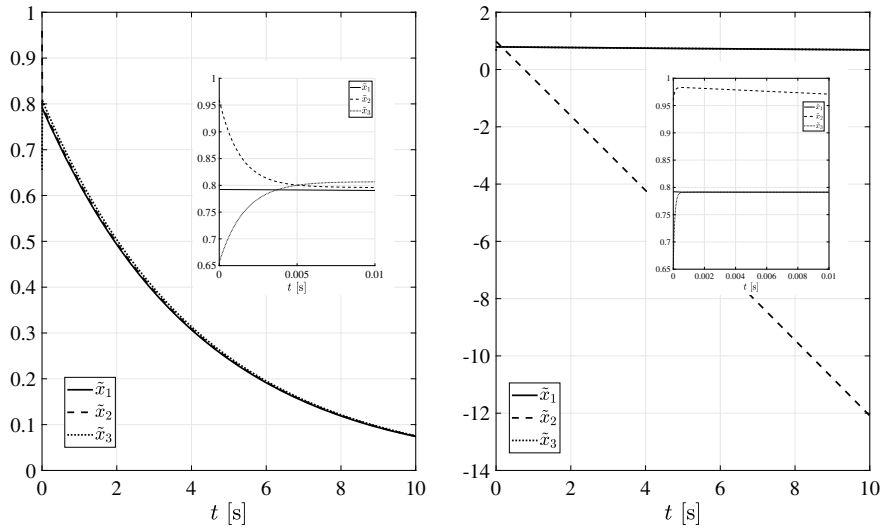


Fig. 3.24 A car’s longitudinal dynamics. Time behavior of linearized states. (Left) The vehicle dynamics are linearized at $v_0 = 100$ km/h and the state \mathbf{x}_0 represents an equilibrium for (2.41). (Right) Linearization at $v_0 = 10$ km/h with the rear wheel speed such that $\lambda_r \in (\lambda^*, 1)$

of the eigenvalues of \mathbf{A}_{22} becomes positive. This instability phenomenon is associated with the excessive skidding typically experienced when starting at traffic lights. The same arguments apply to \mathbf{x}' such that $\lambda'_r \in (-1, -\lambda^*)$ (braking) and for the front wheel.

3.4.4 Adaptive Cruise Control

The following matrix \mathbf{A} is part of Eq. (2.55) representing the linearization of the dynamics of a platoon of three vehicles modeled in Eq. (2.53):

$$\mathbf{A} = \begin{bmatrix} 0 & -1 & 0 & 0 \\ 0 & -\rho S_B C_{D_B} v_0 / m_B & 0 & 0 \\ 0 & 1 & 0 & -1 \\ 0 & 0 & 0 & -\rho S_C C_{D_C} v_0 / m_C \end{bmatrix}. \quad (3.19)$$

The structure of this matrix is sufficiently simple to compute the eigenvalues by hand. Indeed, the solutions to

$$\det(\mathbf{A} - \lambda \mathbf{I}) = \lambda^2(\lambda + \rho S_B C_{D_B} v_0 / m_B)(\lambda + \rho S_C C_{D_C} v_0 / m_C) = 0$$

are

$$\begin{aligned} \lambda_1 &= 0 & a_1 &= 2 \\ \lambda_2 &= -\rho S_B C_{D_B} v_0 / m_B & a_2 &= 1 \\ \lambda_3 &= -\rho S_C C_{D_C} v_0 / m_C & a_3 &= 1 \end{aligned} \quad (3.20)$$

where a_1 , a_2 , and a_3 denote the algebraic multiplicities. Note that λ_1 is independent of v_0 , whereas λ_2 and λ_3 increase linearly with the linearization speed. The increase of λ_2 and λ_3 is physically associated with the rising of the aerodynamics drag with speed. On the other hand, the eigenvectors can also be computed by hand. As for

λ_1 , the geometric multiplicity is $g_1 = 2$, and no chains of generalized eigenvectors exist. In more detail

$$\mathbf{v}_{1,1} = \text{col}(1, 0, 0, 0)$$

$$\mathbf{v}_{1,2} = \text{col}(0, 0, 1, 0).$$

Furthermore, the eigenvectors relating to λ_2 and λ_3 are given by

$$\mathbf{v}_2 = \text{col}(1, \rho S_B C_{D_B} v_0 / m_B, -1, 0)$$

$$\mathbf{v}_3 = \text{col}(0, 0, 1, \rho S_C C_{D_C} v_0 / m_C).$$

As a consequence,

$$\begin{aligned} \mathbf{T}^{-1} &:= [\mathbf{v}_{1,1} \ \mathbf{v}_{1,2} \ \mathbf{v}_2 \ \mathbf{v}_3] \\ &= \begin{bmatrix} 1 & 0 & 1 & 0 \\ 0 & 0 & \frac{\rho S_B C_{D_B} v_0}{m_B} & 0 \\ 0 & 1 & -1 & 1 \\ 0 & 0 & 0 & \frac{\rho S_C C_{D_C} v_0}{m_C} \end{bmatrix}, \end{aligned}$$

whereas

$$\mathbf{J} = \begin{bmatrix} 0 & 0 & 0 & 0 \\ 0 & 0 & 0 & 0 \\ 0 & 0 & -\rho S_B C_{D_B} v_0 / m_B & 0 \\ 0 & 0 & 0 & -\rho S_C C_{D_C} v_0 / m_C \end{bmatrix}.$$

Define $z_1, z_2, z_3, z_4 \in \mathbb{R}$ and let $\mathbf{z} := \text{col}(z_1, z_2, z_3, z_4)$. Then, the dynamics of the platoon, with $\mathbf{u}, \mathbf{w} = \mathbf{0}$, are described by $\mathbf{x}(t) = \mathbf{T}^{-1}\mathbf{z}(t)$, where $\mathbf{z}(t)$ is the solution to $\dot{\mathbf{z}} = \mathbf{J}\mathbf{z}$, $\mathbf{z}(0) = \mathbf{z}_0$. In particular,

$$\begin{bmatrix} \tilde{x}_1(t) \\ \tilde{x}_2(t) \\ \tilde{x}_3(t) \\ \tilde{x}_4(t) \end{bmatrix} = \begin{bmatrix} 1 & 0 & 1 & 0 \\ 0 & 0 & \frac{\rho S_B C_{D_B} v_0}{m_B} & 0 \\ 0 & 1 & -1 & 1 \\ 0 & 0 & 0 & \frac{\rho S_C C_{D_C} v_0}{m_C} \end{bmatrix} \begin{bmatrix} z_{10} \\ z_{20} \\ \exp(-\frac{\rho S_B C_{D_B} v_0}{m_B} t) z_{30} \\ \exp(-\frac{\rho S_C C_{D_C} v_0}{m_C} t) z_{40} \end{bmatrix},$$

which states that, with zero input and no disturbance, $x_1(t)$ is the sum of a constant (representing the initial position error) and a vanishing term (induced by the stable dynamics of the speed v_B). The states $x_2(t)$ and $x_4(t)$ are asymptotically stable (the speed of B and C are stabilized by the aerodynamic drag). The state $x_3(t)$ is composed of one constant contribution plus two vanishing terms (the distance between B and C converges to a constant value according to the initial speed difference $v_B(0) - v_C(0)$). The simulations shown in Fig. 3.25 confirm these results.

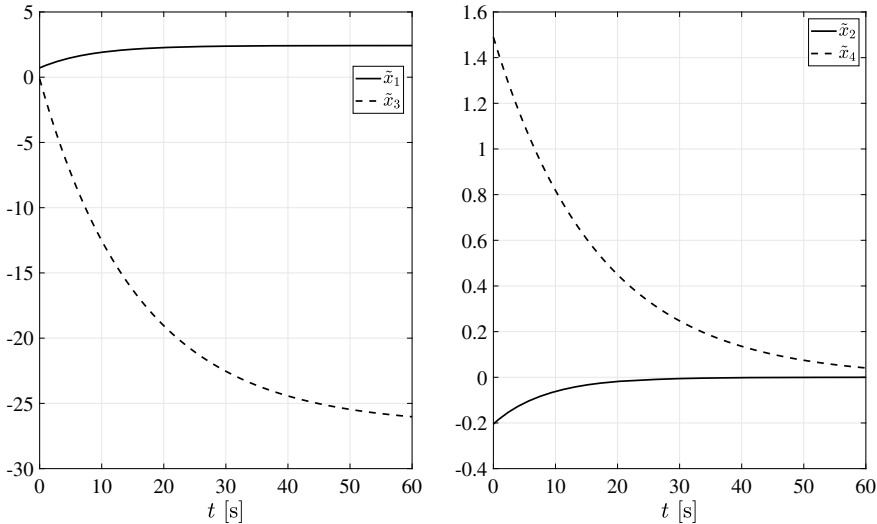


Fig. 3.25 Adaptive cruise control: Time behavior of linearized states. These simulations are obtained with $\rho = 1.225 \text{ kg/m}^3$, $S_B = 3.4 \text{ m}^2$, $C_{D_B} = 2.2$, $m_B = 2400 \text{ kg}$, $S_C = 0.96 \text{ m}^2$, $C_{D_C} = 1.10$, $m_C = 600 \text{ kg}$, and $v_0 = 100 \text{ km/h}$. The initial conditions are generated randomly. (Left) The inter-vehicle distance is approximated with the states \tilde{x}_1 and \tilde{x}_3 . Then, this simulation shows that the distance from vehicle B to vehicle A and from vehicle C to vehicle B converge to a constant. (Right) The dynamics of the states \tilde{x}_2 and \tilde{x}_4 approximate to the variation of the speeds v_B and v_C from v_0 . As detailed in Sect. 3.4.4, the states \tilde{x}_2 and \tilde{x}_4 are asymptotically vanishing. This simulation confirms the results of the study conducted in Sect. 3.4.4

3.4.5 Automatic Steering System

Equation (2.66) models the steering system described in Sect. 2.5. Equation (2.68) provides the linearization of Eq. (2.66) and relies on

$$\mathbf{A} = \begin{bmatrix} 0 & 1 \\ A_{21} & 0 \end{bmatrix}, \quad (3.21)$$

where

$$A_{21} = B^{-1}(\delta_0) \left(\frac{\partial J_r(\delta)}{\partial \delta} d_{r0} + \frac{\partial J_l(\delta)}{\partial \delta} d_{l0} - (J_r^2(\delta_0) + J_l^2(\delta_0))c \right) \Big|_{\delta=\delta_0}.$$

Assume the linearization point is on a straight trajectory at δ_0 , d_{l0} , $d_{r0} = 0$, then $A_{21} = -(J(J_l^2(0) + J_r^2(0)) + mr^2)^{-1}(J_r^2(0) + J_l^2(0))c$. Therefore, since $A_{21} < 0$, the eigenvalues of (3.21) are

$$\lambda_{1,2} = \pm j\sqrt{|A_{21}|},$$

whose algebraic multiplicity is 1. In agreement with Sect. 3.1, since the eigenvalues are complex conjugated, compute the eigenvector associated with $\lambda_1 = j\sqrt{|A_{21}|}$ only, namely \mathbf{v}_1 . Then, exploit the real and imaginary parts of \mathbf{v}_1 to build the change

of coordinates. In more detail, let $\mathbf{v}_1 := \mathbf{a} + j\mathbf{b}$ with $\mathbf{a} = \text{col}(a_1, a_2)$ and $\mathbf{b} = \text{col}(b_1, b_2)$, then the eigenvector is obtained as a solution to

$$\begin{aligned} (\mathbf{A} - \lambda_1 \mathbf{I})\mathbf{v}_1 &= \begin{bmatrix} -j\sqrt{A_{21}} & 1 \\ A_{21} & -j\sqrt{A_{21}} \end{bmatrix}(\mathbf{a} + j\mathbf{b}) \\ &= \begin{bmatrix} -j\sqrt{A_{21}} & 1 \\ A_{21} & -j\sqrt{A_{21}} \end{bmatrix}\left(\begin{bmatrix} a_1 \\ a_2 \end{bmatrix} + j\begin{bmatrix} b_1 \\ b_2 \end{bmatrix}\right) \\ &= \begin{bmatrix} -j\sqrt{A_{21}}(a_1 + jb_1) + (a_2 + jb_2) \\ A_{21}(a_1 + jb_1) - j\sqrt{A_{21}}(a_2 + jb_2) \end{bmatrix} \\ &= \begin{bmatrix} (\sqrt{A_{21}}b_1 + a_2) - j(\sqrt{A_{21}}a_1 + b_2) \\ (A_{21}a_1 + \sqrt{A_{21}}b_2) + j(A_{21}b_1 - \sqrt{A_{21}}a_2) \end{bmatrix} = \begin{bmatrix} 0 \\ 0 \end{bmatrix}. \end{aligned}$$

Now, rewrite the latter equality as

$$\begin{bmatrix} A_{21} & \sqrt{A_{21}} & 0 & 0 \\ -\sqrt{A_{21}} & -1 & 0 & 0 \\ 0 & 0 & 1 & \sqrt{A_{21}} \\ 0 & 0 & -\sqrt{A_{21}} & A_{21} \end{bmatrix} \begin{bmatrix} a_1 \\ a_2 \\ b_1 \\ b_2 \end{bmatrix} = \begin{bmatrix} 0 \\ 0 \\ 0 \\ 0 \end{bmatrix},$$

from which

$$\begin{bmatrix} a_1 \\ a_2 \end{bmatrix} = \begin{bmatrix} 1 \\ \sqrt{A_{21}} \end{bmatrix}, \quad \begin{bmatrix} b_1 \\ b_2 \end{bmatrix} = \begin{bmatrix} 1 \\ -\sqrt{A_{21}} \end{bmatrix}.$$

Use these two vectors to design the change of coordinates $\mathbf{T} \in \mathbb{R}^{2 \times 2}$ with

$$\mathbf{T}^{-1} := \begin{bmatrix} 1 & 1 \\ \sqrt{A_{21}} & -\sqrt{A_{21}} \end{bmatrix}.$$

The Jordan canonical form is

$$\mathbf{J} = \mathbf{T}\mathbf{A}\mathbf{T}^{-1} = \begin{bmatrix} 0 & \sqrt{A_{21}} \\ -\sqrt{A_{21}} & 0 \end{bmatrix}.$$

Let $\mathbf{z} := \mathbf{T}\mathbf{x}$ and assume $z_1, z_2 : \mathbb{R} \rightarrow \mathbb{R}$ such that $\mathbf{z}(t) = \text{col}(z_1(t), z_2(t))$, then exploit \mathbf{J} to write

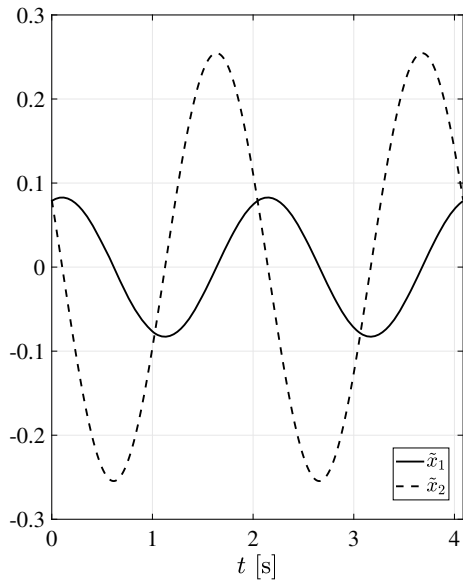
$$\begin{bmatrix} z_1(t) \\ z_2(t) \end{bmatrix} = \begin{bmatrix} \cos(\sqrt{A_{21}}t) & \sin(\sqrt{A_{21}}t) \\ -\sin(\sqrt{A_{21}}t) & \cos(\sqrt{A_{21}}t) \end{bmatrix} \begin{bmatrix} z_1(0) \\ z_2(0) \end{bmatrix}.$$

In practice, the modes associated with matrix (3.21) describe a non-damped oscillation, see Fig. 3.26. These modes are purely oscillatory because Eq. (2.66) does not consider any friction effect.

3.4.6 Latero-directional Controls

Section 2.6 described the latero-directional dynamics of a 3-DOF ground vehicle. In more detail, the nonlinear plant (2.78) is linearized in Eq. (2.83) on a straight line traveled at a constant speed, $v_0 > 0$, without sideslip ($v_y, \omega = 0$).

Fig. 3.26 Steering system: free evolution associated with (3.21). The pinion position and speed oscillate because Eq. (2.66) neglects friction torques. Concerning (2.66), this simulation has been obtained with
 $a = 0.20 \text{ m}$, $b = 1.80 \text{ m}$,
 $c = 0.15 \text{ m}$, $d = 0.50 \text{ m}$,
 $r = 0.004 \text{ m}$, $\ell = 0.70 \text{ m}$,
 $J = 2 \text{ kg}\cdot\text{m}^2$, $m = 10 \text{ kg}$,
and $c_\delta = 20 \text{ Nm}$



Concerning Eq. (2.83), define

$$\begin{aligned} \frac{1}{m} \frac{\partial f_x}{\partial v_x} &= \frac{1}{v_0} \frac{\partial \bar{f}_x}{\partial v_x}, \\ \frac{1}{m} \frac{\partial f_y}{\partial v_y} &= \frac{1}{v_0} \frac{\partial \bar{f}_y}{\partial v_y}, \quad \frac{1}{m} \frac{\partial f_y}{\partial \omega} = \frac{1}{v_0} \frac{\partial \bar{f}_y}{\partial \omega}, \\ \frac{1}{m} \frac{\partial \tau}{\partial v_y} &= \frac{1}{v_0} \frac{\partial \bar{\tau}}{\partial v_y}, \quad \frac{1}{m} \frac{\partial \tau}{\partial \omega} = \frac{1}{v_0} \frac{\partial \bar{\tau}}{\partial \omega}. \end{aligned}$$

Then, the following block diagonal matrix describes the linearized dynamics:

$$\mathbf{A} = \begin{bmatrix} \frac{1}{v_0} \frac{\partial \bar{f}_x}{\partial v_x} - \frac{\rho S C_D}{m} v_0 & 0 & 0 \\ 0 & \frac{1}{v_0} \frac{\partial \bar{f}_y}{\partial v_y} & \frac{1}{v_0} \frac{\partial \bar{f}_y}{\partial \omega} - v_0 \\ 0 & \frac{m}{J v_0} \frac{\partial \bar{\tau}}{\partial v_y} & \frac{m}{J v_0} \frac{\partial \bar{\tau}}{\partial \omega} \end{bmatrix}_{\mathbf{x}=\mathbf{x}_0, \mathbf{u}=\mathbf{u}_0}. \quad (3.22)$$

This matrix has three eigenvalues

$$\begin{aligned} \lambda_1 &= \frac{1}{v_0} \frac{\partial \bar{f}_x}{\partial v_x} - \frac{\rho S C_D}{m} v_0 \\ \lambda_{2,3} &= \frac{1}{2v_0} \left(\frac{\partial \bar{f}_y}{\partial v_y} + \frac{m}{J} \frac{\partial \bar{\tau}}{\partial \omega} \right) \pm \frac{1}{2v_0} \sqrt{\left(\frac{\partial \bar{f}_y}{\partial v_y} - \frac{m}{J} \frac{\partial \bar{\tau}}{\partial \omega} \right)^2 + \frac{4m}{J} \frac{\partial \bar{\tau}}{\partial v_y} \left(\frac{\partial \bar{f}_y}{\partial \omega} - v_0^2 \right)}. \end{aligned}$$

To study λ_1 , note that

$$\begin{aligned}\frac{\partial \bar{f}_x}{\partial v_x} = & -\frac{g}{[1 - \bar{h}(\mu_{r0} - \mu_{f0})]^2} \left[(\bar{a} + \bar{h}\mu_{f0}) \frac{\partial \mu(\lambda, \Theta)}{\partial \lambda} \Big|_{\lambda=\lambda_{r0}} (1 - \lambda_{r0}) \right. \\ & \left. + (\bar{b} - \bar{h}\mu_{r0}) \frac{\partial \mu(\lambda, \Theta)}{\partial \lambda} \Big|_{\lambda=\lambda_{f0}} (1 - \lambda_{f0}) \right] < 0,\end{aligned}$$

thus implying $\lambda_1 < 0$ for all $v_0 > 0$. In particular, for the speed variation, $\lim_{v_0 \rightarrow 0} \lambda_1 = -\infty$ due to the raised sensitivity of the slip ratio function $\lambda(\cdot, \cdot)$. In addition, $\lim_{v_0 \rightarrow \infty} \lambda_1 = -\infty$ because of the increased sensitivity of the drag resistance.

To investigate $\lambda_{2,3}$, it is worth observing that

$$\frac{\partial \bar{f}_y}{\partial v_y} = -g \frac{2}{\pi} \frac{\partial \mu(\beta, \Theta_0)}{\partial \beta} \Big|_{\beta=0} < 0$$

and

$$\frac{\partial \bar{f}_y}{\partial \omega} = g \ell \bar{h} \frac{\mu_{r0} \bar{a} + \mu_{f0} \bar{b}}{1 - (\mu_{r0} - \mu_{f0}) \bar{h}} \frac{2}{\pi} \frac{\partial \mu(\beta, \Theta_0)}{\partial \beta} \Big|_{\beta=0} > 0$$

because, by assumption, at least one between μ_{r0} and μ_{f0} is greater than zero (see Sect. 2.6). On the other hand,

$$\frac{\partial \bar{\tau}}{\partial v_y} = h \frac{N_{r0} - N_{f0}}{m} (\mu_{r0} - \mu_{f0}) \frac{2}{\pi} \frac{\partial \mu(\beta, \Theta_0)}{\partial \beta} \Big|_{\beta=0}$$

is null for four-wheel drive vehicles with a 50-50 balance. In general, the sign of $\partial \bar{\tau} / \partial v_y$ is determined by the traction distribution (front/rear) and by the location of the gravity center.

As for $\partial \bar{\tau} / \partial \omega$, define

$$\frac{\partial \bar{\tau}}{\partial \omega} = \frac{\partial \bar{\tau}_S}{\partial \omega} + \frac{\partial \bar{\tau}_L}{\partial \omega}$$

where the derivative $\partial \bar{\tau}_S / \partial \omega$, denoting the torque obtained neglecting the load transfer, is

$$\begin{aligned}\frac{\partial \bar{\tau}_S}{\partial \omega} = & -\frac{g \ell^2}{1 - \bar{h}(\mu_{r0} - \mu_{f0})} \left[\frac{2}{\pi} \frac{\partial \mu(\beta, \Theta_0)}{\partial \beta} \Big|_{\beta=0} (\bar{b}^2 (\bar{a} + \bar{h}\mu_{f0}) + \bar{a}^2 (\bar{b} - \bar{h}\mu_{r0})) \right. \\ & \left. + \bar{c}^2 \left(\mu_{f0} (\bar{b} - \bar{h}\mu_{r0})(1 - \lambda_{f0}) + \mu_{r0} (\bar{a} + \bar{h}\mu_{f0})(1 - \lambda_{r0}) \right) \right]\end{aligned}$$

which is negative for any configuration of the gravity center and any traction distribution. Conversely, $\partial \bar{\tau}_L / \partial \omega$ represents the torque induced by the load transfer, and it reads as

$$\begin{aligned}\frac{\partial \bar{\tau}_L}{\partial \omega} = & \frac{g \bar{h} \ell^3}{2(1 - \bar{h}(\mu_{r_0} - \mu_{f_0}))^2} \left[\frac{2}{\pi} \frac{\partial \mu(\beta, \Theta_0)}{\partial \beta} \Big|_{\beta=0} \bar{h} \right. \\ & \times \left(\bar{a} \mu_{r_0}^2 + \bar{b} \mu_{f_0}^2 + \mu_{f_0} \mu_{r_0} + \bar{h}(\mu_{f_0}^2 - \mu_{r_0}^2)(\bar{a} \mu_{r_0} + \bar{b} \mu_{f_0}) \right) \\ & + \bar{c}^2 (\bar{h}(\mu_{f_0}^2 - \mu_{r_0}^2) + (\bar{a} - \bar{b})(\mu_{f_0} - \mu_{r_0})) \\ & \left. \times \left(\frac{\partial \mu(\lambda, \Theta_0)}{\partial \lambda} \Big|_{\lambda=\lambda_{f_0}} (1 - \lambda_{f_0}) - \frac{\partial \mu(\lambda, \Theta_0)}{\partial \lambda} \Big|_{\lambda=\lambda_{r_0}} (1 - \lambda_{r_0}) \right) \right],\end{aligned}$$

whose sign depends on mass configurations and driving distributions.

Assume $\partial \bar{\tau} / \partial \omega < 0$, then $\lambda_{2,3}$ have positive/negative real parts and eventually possess an imaginary part according to the sign of $\partial \bar{\tau} / \partial v_y$ and the magnitude of v_0 :

- $\partial \bar{\tau} / \partial v_y < 0$. Define

$$v_1(v_0) = \sqrt{\frac{\partial \bar{f}_y}{\partial \omega} - \left(\frac{\partial \bar{\tau}}{\partial v_y} \right)^{-1} \frac{\partial \bar{f}_y}{\partial v_y} \frac{\partial \bar{\tau}}{\partial \omega}},$$

then $\lambda_{2,3}$ are distinct negative reals for $v_0 > 0$ such that $v_1(v_0) > v_0$. At $v_0 = v_1^* > 0$: $v_1^* = v_1(v_1^*)$, it is $\lambda_2 < 0$ and $\lambda_3 = 0$. Lastly, $\lambda_2 < 0$, $\lambda_3 > 0$ for $v_0 > 0$: $v_0 > v_1(v_0)$;

- $\partial \bar{\tau} / \partial v_y = 0$. In this case, $\lambda_{2,3}$ are two distinct negative real roots whose magnitude decreases with v_0 ;

Fig. 3.27 Plot of $v_1(v_0)$ for a rear-wheel-drive vehicle with $\bar{a} = 0.3$. For $v_0 > v_1^*$, one of the eigenvalues is positive

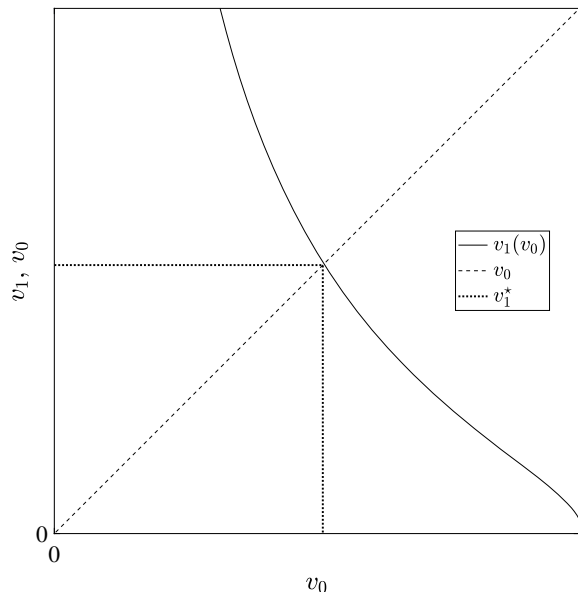
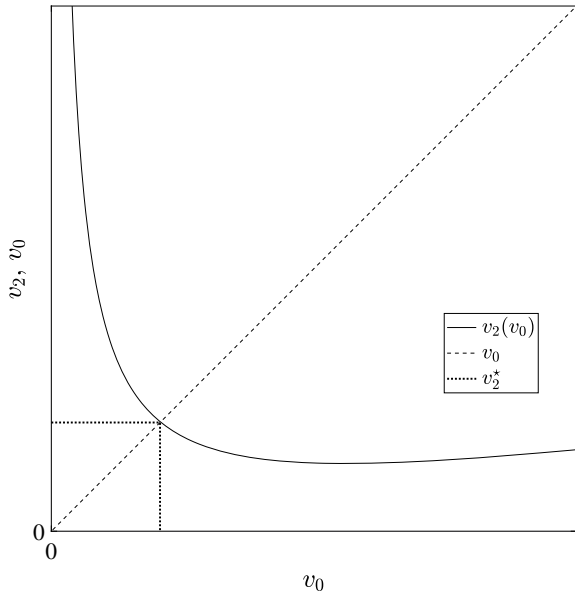


Fig. 3.28 Plot of $v_2(v_0)$ for a rear-wheel-drive vehicle with $\bar{a} = 0.7$. For $v_0 > v_2^*$, two eigenvalues are complex conjugate with negative real parts



- $\partial\bar{\tau}/\partial v_y > 0$. Define

$$v_2(v_0) = \sqrt{\frac{\partial \bar{f}_y}{\partial \omega} + \left(\frac{\partial \bar{\tau}}{\partial v_y}\right)^{-1} \frac{J}{4m} \left(\frac{\partial \bar{f}_y}{\partial v_y} - \frac{m}{J} \frac{\partial \bar{\tau}}{\partial \omega}\right)^2},$$

then $\lambda_{2,3}$ are distinct negative reals for $v_0 > 0 : v_0 < v_2(v_0)$. At $v_0 = v_2^* > 0 : v_2^* = v_2(v_2^*)$, it is $\lambda_2 = \lambda_3 < 0$. To conclude, $\lambda_{2,3}$ are complex conjugated with negative real parts for $v_0 > 0 : v_0 > v_2(v_0)$.

Figure 3.29 graphically represents the behavior of λ_2, λ_3 as a function of v_0 , for $\partial\bar{\tau}/\partial v_y$ negative, null, and positive.

Infobox 3.3 (Cornering stiffness, Understeering Gradient, and Critical Speed)
According to the notation adopted in this book, the “cornering stiffness” of rear and front wheels is defined as

$$C_r = -\frac{4}{\pi} \frac{N_{r0}}{m} \left. \frac{\partial \mu(\beta, \Theta)}{\partial \beta} \right|_{\beta=0}, \quad C_f = -\frac{4}{\pi} \frac{N_{f0}}{m} \left. \frac{\partial \mu(\beta, \Theta)}{\partial \beta} \right|_{\beta=0},$$

and the “understeering gradient” is

$$\eta := -g \frac{C_f \bar{a} - C_r \bar{b}}{C_f C_r}.$$

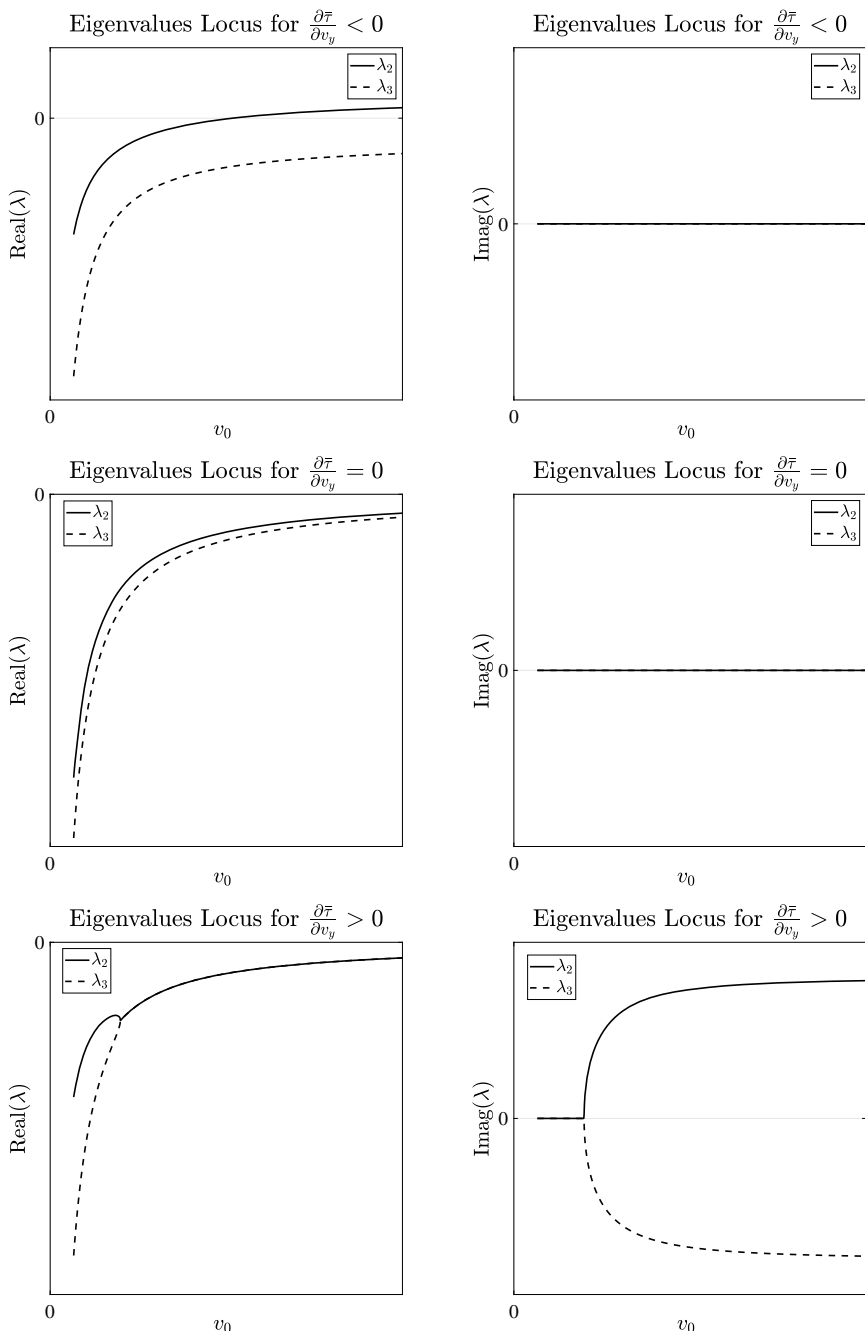


Fig. 3.29 Locus of the eigenvalues of \mathbf{A} for $\partial \bar{\tau} / \partial v_y$ negative, null, and positive as a function of v_0

Then,

$$\frac{\partial \bar{f}_y}{\partial v_y} = - (C_r + C_f) \text{ and } \frac{\partial \bar{f}_y}{\partial \omega} = -\ell (C_f \bar{a} - C_r \bar{b}),$$

which cohere with [4,6,8]. In more detail, vehicles with $\eta > 0$ are named “understeering”, those with $\eta = 0$ are called “neutral steering”, and cars with $\eta < 0$ are said to be “oversteering”.

Then, for $\bar{c} = 0$, the following equalities are true

$$\frac{\partial \bar{\tau}}{\partial v_y} = -\ell (C_f \bar{a} - C_r \bar{b}), \quad \frac{\partial \bar{\tau}}{\partial \omega} = -\ell^2 (C_f \bar{a}^2 + C_r \bar{b}^2)$$

as described in [4,6,8]. Moreover, assume $\eta < 0$ and let

$$v_{cr} := \sqrt{-\frac{g\ell}{\eta}}$$

be the so-called “critical speed”. Then, for $\bar{c} = 0$ we have $v_1^* = v_{cr}$.

The computation of the eigenvalues of \mathbf{A} reveals that λ_2, λ_3 , obtained for $\bar{c} = 0$, have a negative/positive real part and eventually have an imaginary part as a function of the sign of η and the magnitude of v_0 . A direct comparison with the results presented in this section reveals that the classification of λ_2, λ_3 remains unaltered (for $\bar{c} = 0$) if we substitute η for $\partial \bar{\tau} / \partial v_y$ and v_{cr} for v_1^* .

With the eigenvalues of (3.22) at hand, compute the eigenvectors through the procedure described in Sect. 3.1.2. Let $\mathbf{v}_1 \in \mathbb{R}^3$ be the eigenvector associated with λ_1 , then $(\mathbf{A} - \lambda_1 \mathbf{I})\mathbf{v}_1 = \mathbf{0}$ is solved with $\mathbf{v}_1 = \text{col}(1, 0, 0)$.

Define $\mathbf{v}_2 = \text{col}(v_{21}, v_{22}, v_{23})$ and $\mathbf{v}_3 = \text{col}(v_{31}, v_{32}, v_{33})$, with $v_{ij} \in \mathbb{R}$ for $i = 2, 3$ and $j = 1, 2, 3$, as the eigenvectors associated with λ_2 and λ_3 . Then $v_{21}, v_{31} = 0$ due to the block diagonal structure of (3.22). Therefore, the change of coordinates is

$$\mathbf{T}^{-1} := \begin{bmatrix} 1 & 0 & 0 \\ 0 & v_{22} & v_{32} \\ 0 & v_{23} & v_{33} \end{bmatrix}, \quad (3.23)$$

which reveals that λ_1 describes the longitudinal dynamics. This latter is independent of the latero-directional one, whose behavior is captured by $\lambda_{2,3}$. Since the longitudinal dynamics can be obtained as a composition of the results presented in Sects. 3.4.4 and 3.4.3, the remainder of this section studies the free evolution of \tilde{v}_y and $\tilde{\omega}$ only. To this end, define $p_x, p_y, \psi \in \mathbb{R}$ such that

$$\begin{bmatrix} \dot{p}_x \\ \dot{p}_y \\ \dot{\psi} \end{bmatrix} = \begin{bmatrix} v_0 \cos \psi - \tilde{v}_y \sin \psi \\ v_0 \sin \psi + \tilde{v}_y \cos \psi \\ \tilde{\omega} \end{bmatrix}$$

where \tilde{v}_y and $\tilde{\omega}$ are described through the free evolution associated with Eq. (3.22). Figure 3.30 shows the behavior of a ground vehicle with $\partial \bar{\tau} / \partial v_y \geq 0$. Compare these results with those presented in Figure 3.31, obtained for $\partial \bar{\tau} / \partial v_y < 0$ and speeds lower and higher than v_1^* .

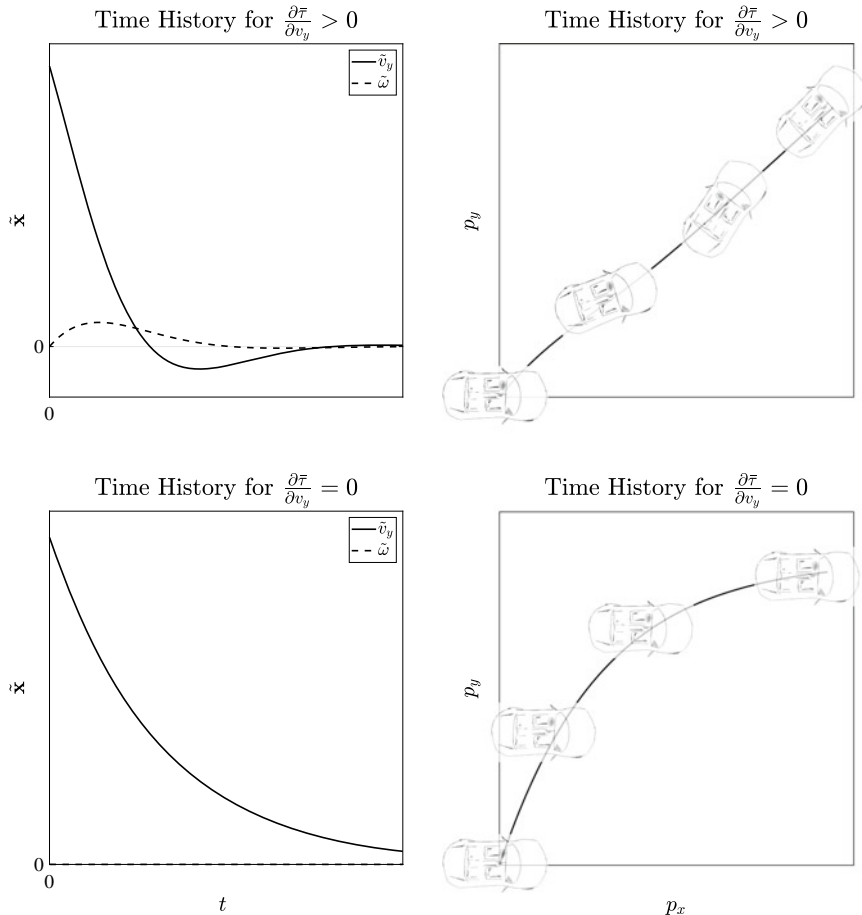


Fig. 3.30 Behavior of vehicles characterized by $\eta \geq 0$. When $\eta = 0$, the dynamics of \tilde{v}_y and $\tilde{\omega}$ are decoupled; for this reason, the vehicle skids laterally until the friction force reduces \tilde{v}_y to zero. On the other hand, vehicles with $\eta > 0$ are naturally stable, assessed by a self-aligning behavior that reduces \tilde{v}_y to zero

Lane controls

Section 2.6.1 extended the models presented in Sect. 2.6 to describe the plant dynamics involved in the lane control problem formulation. In more detail, the states ρ and ψ_r , denoting the distance to the lane and the vehicle–lane relative yaw, were added to the states describing the latero-directional dynamics. As for the linearized model, Eq. 2.93 reports the matrix

$$\mathbf{A}_L := \begin{bmatrix} \begin{bmatrix} 0 & -v_0 \\ 0 & 0 \end{bmatrix} & \begin{bmatrix} 0 & -1 & -x_A \\ 0 & 0 & 1 \end{bmatrix} \\ \mathbf{0} & \mathbf{A} \end{bmatrix}, \quad (3.24)$$

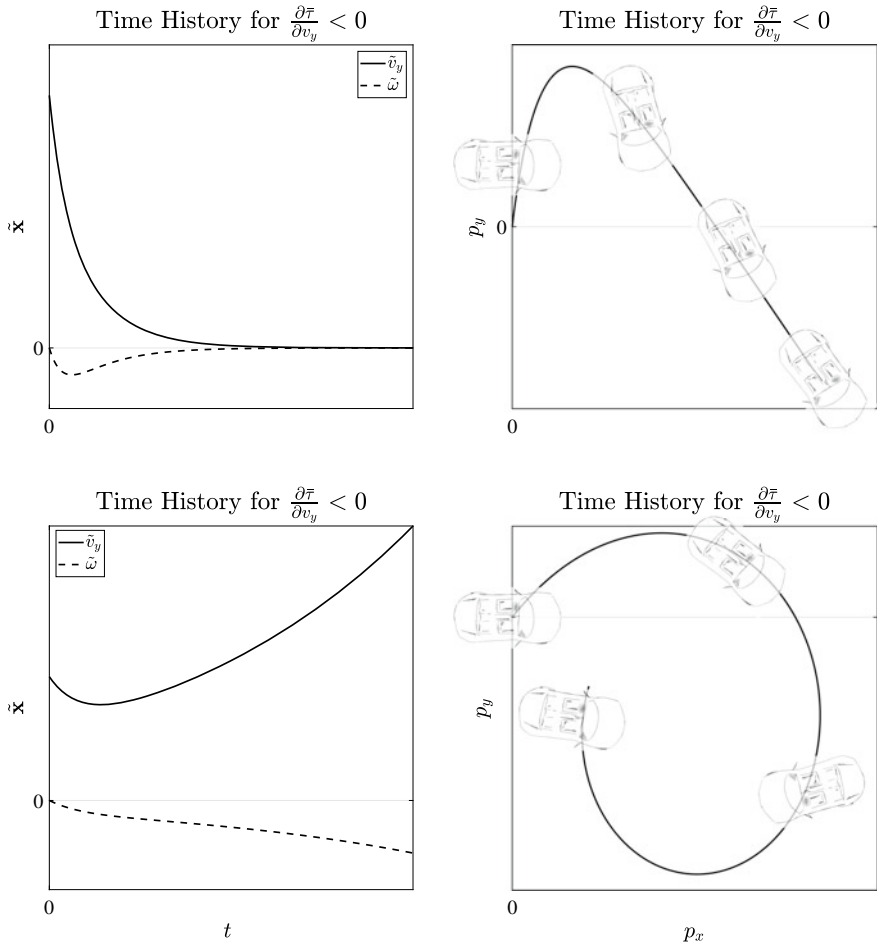


Fig. 3.31 Behavior of vehicles characterized by $\partial\bar{\tau}/\partial v_y < 0$. The top pictures show the dynamics of a vehicle traveling at $v_0 < v_1^*$: in this case, the trajectory evolves in a direction that is opposite with respect to that of the initial conditions, but, thanks to the low speed, the self-alignment motion is still dominant. On the other hand, the bottom pictures show the behavior of a vehicle running at $v_0 > v_1^*$: the asymptotic path becomes nonlinear and the lateral and rotational speeds \tilde{v}_y and $\tilde{\omega}$ are not bounded. The result is a spiral with an increasing sideslip angle. Lastly, at $v_0 = v_1^*$ both \tilde{v}_y and $\tilde{\omega}$ are asymptotically constant thus leading to circular paths at constant sideslip angles (not reported in this figure)

in which $v_0 > 0$ represents the linearization speed, $x_A \in \mathbb{R}$ denotes the position of the virtual point that should keep a reference distance to the lane, and \mathbf{A} is given in Eq. (3.22). The investigation of the eigenvalues of (3.24) starts by noting that \mathbf{A}_L is a block diagonal matrix. Thanks to this property, the eigenvalues are those of the blocks on the main diagonal. Let $\lambda_1, \lambda_2, \lambda_3$ be the eigenvalues of \mathbf{A} found in this section, then the eigenvalue of

$$\begin{bmatrix} 0 & -v_0 \\ 0 & 0 \end{bmatrix}$$

is $\lambda_4 = 0$. From a physical viewpoint, this means that the distance to the lane and the vehicle–lane relative angle are integrals of their initial conditions and the vehicle speeds (both linear and angular). Define with $a_4 \in \mathbb{N}$ the algebraic multiplicity of λ_4 and consider \mathbf{A}_L . Therefore $a_4 = 2$ for any driving conditions but for $\partial\bar{\tau}/\partial v_y < 0$ and $v_0 = v_1^*$. Let $g_4 \in \mathbb{N}$ be the geometric multiplicity associated with λ_4 . Then, since $\ker(\mathbf{A}_L - \lambda_4 \mathbf{I})$ has dimension 1, $1 = g_4 < a_4$, implying the existence of a chain of generalized eigenvectors. Assume $v_0 \neq v_1^*$ and let $\mathbf{v}_{4,1}, \mathbf{v}_{4,2} \in \mathbb{R}^5$ be the eigenvectors associated with λ_4 . It follows that

$$\mathbf{v}_{4,1} = \text{col}(1, 0, 0, 0, 0)$$

solves $(\mathbf{A}_L - \lambda_4 \mathbf{I})\mathbf{v}_{4,1} = \mathbf{0}$. Moreover, according to Eq. (3.6), $\mathbf{v}_{4,2} = \text{col}(0, -v_0^{-1}, 0, 0, 0)$ solves $(\mathbf{A}_L - \lambda_4 \mathbf{I})\mathbf{v}_{4,2} = \mathbf{v}_{4,1}$. As a consequence, the transformation that leads to the Jordan canonical form is given by

$$\mathbf{T}_L^{-1} := \begin{bmatrix} \begin{bmatrix} 1 & 0 \\ 0 & -v_0^{-1} \\ \mathbf{0} \end{bmatrix} & \mathbf{0} \\ & \mathbf{T}^{-1} \end{bmatrix}$$

with \mathbf{T}^{-1} provided in Eq. (3.23). Since \mathbf{T}_L^{-1} is a block diagonal matrix, the dynamics of $\tilde{\rho}$ and $\tilde{\psi}_r$ are described by λ_4 only.

Consider now the case of $\partial\bar{\tau}/\partial v_y < 0$ and $v_0 : v_0 : v_0 = v_1(v_0)$, for which $\lambda_3 = \lambda_4 = 0$ and $a_3 = 3$. Let $\mathbf{v}_{3,1}, \mathbf{v}_{3,2}, \mathbf{v}_{3,3} \in \mathbb{R}^5$ be the eigenvectors associated with λ_3 . Then, find $\mathbf{v}_{3,1}$ through Eq. (3.6) applied to $\mathbf{A}_L - \lambda_3 \mathbf{I}$, i.e.,

$$\mathbf{v}_{3,1} = \text{col}(1, 0, 0, 0, 0)$$

$$\mathbf{v}_{3,2} = \text{col}(0, -v_1^{-1}, 0, 0, 0)$$

$$\mathbf{v}_{3,3} = \text{col}\left(0, v_1^{-1}(\kappa x_A - 1), 0, 1, -\kappa\right)$$

with $\kappa := \frac{\partial\bar{\tau}_y}{\partial v_y} \left(\frac{\partial\bar{\tau}_y}{\partial\omega} \right)^{-1}$. These eigenvectors, jointly with those found for λ_1 and λ_2 , generate the change of coordinates

$$\mathbf{T}_L^{-1} = \begin{bmatrix} 1 & 0 & 0 & 0 & 0 \\ 0 & v_1^{-1} & v_1^{-1}(\kappa x_A - 1) & 0 & 0 \\ 0 & 0 & 0 & 1 & 0 \\ 0 & 0 & 1 & 0 & v_{22} \\ 0 & 0 & -\kappa & 0 & v_{23} \end{bmatrix}.$$

The terms v_{22} and v_{23} are those of Eq. (3.23). In this case, unlike $v_0 \neq v_1^*$, $\lambda_3 = 0$ influences the dynamics of states $\tilde{\rho}$, $\tilde{\psi}_r$, \tilde{v}_y , and $\tilde{\omega}$.

Self-Park Assist

The Self-Park Assist (SPA) control problem is formulated on the model introduced in Sect. 2.6.2. The nonlinear dynamics (2.95) is linearized in (2.96), whose matrix \mathbf{A} is reported hereafter

$$\mathbf{A} = \begin{bmatrix} 0 & -v_0 \\ 0 & 0 \end{bmatrix}.$$

The theoretical tools presented in this section are exploited to compute the eigenvalues and eigenvectors of this matrix. In particular, \mathbf{A} possesses only one eigenvalue, namely $\lambda_1 = 0$, whose algebraic multiplicity is $a_1 = 2$. On the other hand, the geometric multiplicity of λ_1 is $g_1 = 1$, thus leading to the following chain of generalized eigenvectors:

$$\mathbf{v}_{1,1} = \text{col}(1, 0), \quad \mathbf{v}_{1,2} = \text{col}(0, -v_0^{-1}).$$

Let $\mathbf{T}^{-1} := [\mathbf{v}_{1,1} \ \mathbf{v}_{1,2}]$ and define $\mathbf{z} = \mathbf{T}\tilde{\mathbf{x}}$. Then, the free evolution of $\tilde{\mathbf{x}}$ is provided by a linear combination of

$$\mathbf{z}(t) = \begin{bmatrix} 1 & t \\ 0 & 1 \end{bmatrix} \mathbf{z}(0).$$

In more detail, since $\tilde{\mathbf{x}}(t) = \mathbf{T}^{-1}\mathbf{z}(t)$, $\mathbf{z}(0) = \mathbf{T}\mathbf{x}(0)$, and $\tilde{\mathbf{x}} = \text{col}(\tilde{\rho}, \tilde{\psi}_r)$, we have

$$\begin{bmatrix} \tilde{\rho}(t) \\ \tilde{\psi}_r(t) \end{bmatrix} = \begin{bmatrix} 1 & -tv_0 \\ 0 & 1 \end{bmatrix} \begin{bmatrix} \tilde{\rho}(0) \\ \tilde{\psi}_r(0) \end{bmatrix}.$$

From a physical viewpoint, this result means that the assumption of vehicle path and lane straight and parallel has led to a constant vehicle–lane relative angle. Moreover, $\tilde{\rho}$ increases linearly over time if the vehicle path and lane are not parallel at the linearization point, i.e., if $\tilde{\psi}_r(0) \neq 0$.

3.5 Summary

The boundedness of state trajectories is related to the eigenvalues of \mathbf{A} . The investigation of the trajectories of linear systems via a suitable change of coordinates led to this relation. This coordinate transformation modifies the original system into the so-called *Jordan canonical form*. This form decomposes the dynamics of an LTI system into independent sub-parts. These parts evolve according to the nature of the eigenvalues and the length of the chain of eigenvectors. Then, the boundedness of trajectories is formally linked to the real part of the eigenvalues through the definition of the BIBS stability.

These theoretical tools have been applied to investigate the linear dynamics presented in Chap. 2. These applications demonstrate how a combination of modes

describes the free evolutions of the linearized plants. Moreover, some case studies have introduced a numerical evaluation of eigenvalues and eigenvectors and their variation concerning some plant parameters. Finally, for the case of latero-directional dynamics, an analytical investigation shows how gravity center locations, traction configurations, and linearization speeds affect eigenvalues and eigenvectors.

3.6 Exercises

Exercise 3.1 Let $a, b \in \mathbb{R}$ and compute the eigenvalues and eigenvectors of the matrix

$$\mathbf{A} = \begin{bmatrix} 1 & b \\ 0 & a \end{bmatrix}.$$

Moreover, determine the solutions to the differential problem $\dot{\mathbf{x}} = \mathbf{Ax}$, $\mathbf{x}(0) = \mathbf{x}_0$, with $\mathbf{x}, \mathbf{x}_0 \in \mathbb{R}^2$.

Exercise 3.2 For $a, b \in \mathbb{R}$, find the eigenvalues and eigenvectors of the matrix

$$\mathbf{A} = \begin{bmatrix} b & a \\ -a & b \end{bmatrix}.$$

Let $\mathbf{x}, \mathbf{x}_0 \in \mathbb{R}^2$ be states and initial conditions associated with the differential problem $\dot{\mathbf{x}} = \mathbf{Ax}$, $\mathbf{x}(0) = \mathbf{x}_0$. Then, find the solutions to this problem.

Exercise 3.3 Find the solutions to the differential problem $\dot{\mathbf{x}} = \mathbf{Ax}$, $\mathbf{x}(0) = \mathbf{x}_0$, where $\mathbf{x}, \mathbf{x}_0 \in \mathbb{R}^3$ and

$$\mathbf{A} = \begin{bmatrix} b & a/2 & -a/2 \\ -a & b & 0 \\ a & 0 & b \end{bmatrix}.$$

For $a, b \in \mathbb{R}$, determine the eigenvalues and eigenvectors of \mathbf{A} .

Exercise 3.4 For $a, b \in \mathbb{R}$, calculate the eigenvalues and eigenvectors of the matrix

$$\mathbf{A} = \begin{bmatrix} b & a/2 & -a/2 \\ 0 & b + a/2 & a/2 \\ 0 & -a/2 & b - a/2 \end{bmatrix}.$$

Then, exploit these findings to solve the differential problem $\dot{\mathbf{x}} = \mathbf{Ax}$, $\mathbf{x}(0) = \mathbf{x}_0$, where $\mathbf{x}, \mathbf{x}_0 \in \mathbb{R}^3$.

Exercise 3.5 Let $\mathbf{x}, \mathbf{x}_0 \in \mathbb{R}^4$ be states and initial conditions of an LTI system described by $\dot{\mathbf{x}} = \mathbf{A}\mathbf{x}$, $\mathbf{x}(0) = \mathbf{x}_0$. Then, for $a \in \mathbb{R}$, find the eigenvalues and eigenvectors of

$$\mathbf{A} = \begin{bmatrix} 1 & a/2 + 1/2 & a/2 - 1/2 & 0 \\ -1 & 1 & 0 & -a - 1 \\ 1 & 0 & 1 & a - 1 \\ 0 & 1/2 & 1/2 & 1 \end{bmatrix}$$

and use them to compute $\mathbf{x}(t)$.

References

1. Antsaklis P, Michel AN (2006) Linear systems. Birkhäuser Basel
2. Antsaklis P, Michel AN (2007) A linear systems primer. Birkhäuser Basel
3. Bacciotti A (2019) Stability and control of linear systems. Springer International Publishing
4. Chen W, Xiao H, Wang Q, Zhao L, Zhu M (2016) Integrated vehicle dynamics and control. Wiley, New York
5. Grujitch LT (2013) Tracking control of linear systems. CRC Press
6. Kiencke U, Nielsen L (2000) Automotive control systems: for engine, driveline, and vehicle
7. Kisačanin B, Agarwal GC (2001) Linear control systems: with solved problems and MATLAB examples. Springer, US
8. Rajamani R (2012) Vehicle dynamics and control. Springer, US



Control System Architecture

4

Goal G1 requires the controller to keep states \mathbf{x} , inputs \mathbf{u} , and regulated outputs \mathbf{e} bounded for all times under the assumption of bounded exogenous signals (i.e., bounded disturbances, noises, and references). Chapter 3 has linked the boundedness of these signals to BIBS stability through the eigenvalues of the linearized system. This chapter incrementally obtains the controller architecture starting from the simplest control system, i.e., a *stabilizer* based on a *state feedback*; see Sect. 4.2. Section 4.3 enhances the basic controller by presenting the robust output regulation of set points in the case of unknown but constant disturbances. Unfortunately, the whole state, often not available at measurement, is necessary to implement the state-feedback stabilizer. Therefore, Sect. 4.5 proposes stabilizing linear plants by employing feasible *output feedback* to overcome this limitation. To achieve this result, the concept of *state observer* described in Sect. 4.4 plays a fundamental role. Furthermore, Sect. 4.6 relies on the state-feedback stabilizer to solve the tracking of time-varying references by utilizing the feed-forward. Finally, this chapter describes the control system architecture for each case study illustrated in Chap. 2.

4.1 Closed-Loop System

This section exploits Eqs. (1.16) and (1.17) to identify an overall linear system whose properties are directly associated with achieving control goals G1 and G2.

We impose $\mathbf{D}_O = \mathbf{0}$ and $\mathbf{C}_O = \mathbf{I}$ to simplify the presentation of topics. Infobox 4.6 shows how to remove this assumption.

Let $\mathbf{e}_x := \mathbf{x}_O - \tilde{\mathbf{x}}$ and $\chi := \text{col}(\tilde{\mathbf{x}}, \eta, \mathbf{e}_x, \mathbf{x}_{FF})$. Then, exploit $\mathbf{x}_O = \mathbf{e}_x + \tilde{\mathbf{x}}$, Eq. (1.16), and Eq. (1.17) to compute the closed-loop dynamics

$$\begin{aligned}\dot{\chi} &= \mathbf{A}_\chi \chi + \mathbf{B}_{\chi_w} \tilde{\mathbf{w}} + \sum_{i=0}^{r_{\max}} \mathbf{B}_{\chi_i} \frac{d^i}{dt^i} \mathbf{r} \\ \tilde{\mathbf{u}} &= \mathbf{C}_\chi \chi + \sum_{i=0}^{r_{\max}} \mathbf{D}_{FF_i} \frac{d^i}{dt^i} \mathbf{r},\end{aligned}\quad (4.1a)$$

where

$$\mathbf{A}_\chi = \begin{bmatrix} \mathbf{A} + \mathbf{B}_1 \mathbf{K}_S & \mathbf{B}_1 \mathbf{K}_I & \mathbf{B}_1 \mathbf{K}_S & \mathbf{B}_1 \mathbf{C}_{FF} \\ \mathbf{C}_e + \mathbf{D}_{e_1} \mathbf{K}_S & \mathbf{D}_{e_1} \mathbf{K}_I & \mathbf{D}_{e_1} \mathbf{K}_S & \mathbf{D}_{e_1} \mathbf{C}_{FF} \\ \mathbf{A}_O + \mathbf{K}_O \mathbf{C} - \mathbf{A} + \mathbf{M} \mathbf{K}_S & \mathbf{M} \mathbf{K}_I & \mathbf{A}_O + \mathbf{M} \mathbf{K}_S & \mathbf{M} \mathbf{C}_{FF} \\ \mathbf{0} & \mathbf{0} & \mathbf{0} & \mathbf{A}_{FF} \end{bmatrix}, \quad (4.1b)$$

$$\mathbf{B}_{\chi_w} = \begin{bmatrix} \mathbf{B}_2 \\ \mathbf{D}_{e_2} \\ \mathbf{K}_O \mathbf{D}_2 - \mathbf{B}_2 \\ \mathbf{0} \end{bmatrix}, \quad \mathbf{B}_{\chi_i} = \begin{bmatrix} \mathbf{B}_1 \mathbf{D}_{FF_i} \\ \mathbf{D}_{e_1} \mathbf{D}_{FF_i} \\ \mathbf{M} \mathbf{D}_{FF_i} \\ \mathbf{B}_{FF_i} \end{bmatrix}, \quad (4.1c)$$

and

$$\mathbf{C}_\chi = [\mathbf{K}_S \ \mathbf{K}_I \ \mathbf{K}_S \ \mathbf{C}_{FF}] \quad (4.1d)$$

with $\mathbf{M} = \mathbf{B}_O + \mathbf{K}_O \mathbf{D}_1 - \mathbf{B}_1$.

First, observe that the boundedness of χ and \mathbf{r} (and all its time derivatives up to order r_{\max}) implies the boundedness of $\tilde{\mathbf{u}}$. On the one hand, \mathbf{r} is bounded by the assumption, but, on the other hand, the BIBS stability of system (4.1a) implies the boundedness of χ as described in Sect. 3.3. In turn, the BIBS stability of system (4.1a) is related to the eigenvalues of \mathbf{A}_χ (which must be Hurwitz). Moreover, the BIBS stability of system (4.1a) is twofold because, \mathbf{e} being part of χ , the boundedness of the latter implies the boundedness of the former. Consequently, to achieve G1 and G2, the control system is designed to make \mathbf{A}_χ Hurwitz.

The remaining sections describe the design of the controller matrices with an incremental approach. First, in more detail, Sect. 4.2 states the conditions the plant must satisfy to guarantee the existence of \mathbf{K}_S such that $\mathbf{A} + \mathbf{B}_1 \mathbf{K}_S$ is Hurwitz. Then, Sect. 4.3 introduces the integral action and designs \mathbf{K}_I which makes Hurwitz the sub-matrix

$$\begin{bmatrix} \mathbf{A} + \mathbf{B}_1 \mathbf{K}_S & \mathbf{B}_1 \mathbf{K}_I \\ \mathbf{C}_e + \mathbf{D}_{e_1} \mathbf{K}_S & \mathbf{D}_{e_1} \mathbf{K}_I \end{bmatrix}.$$

Section 4.4 describes the conditions the plant must satisfy to allow \mathbf{K}_O to exist such that $\mathbf{A} - \mathbf{K}_O \mathbf{C}$ is Hurwitz. Moreover, Sect. 4.5 designs \mathbf{A}_O and \mathbf{B}_O , which make the following sub-matrix Hurwitz:

$$\begin{bmatrix} \mathbf{A} + \mathbf{B}_1 \mathbf{K}_S & \mathbf{B}_1 \mathbf{K}_I & \mathbf{B}_1 \mathbf{K}_S \\ \mathbf{C}_e + \mathbf{D}_{e_1} \mathbf{K}_S & \mathbf{D}_{e_1} \mathbf{K}_I & \mathbf{D}_{e_1} \mathbf{K}_S \\ \mathbf{A}_O + \mathbf{K}_O \mathbf{C} - \mathbf{A} + \mathbf{M} \mathbf{K}_S & \mathbf{M} \mathbf{K}_I & \mathbf{A}_O + \mathbf{M} \mathbf{K}_S \end{bmatrix}.$$

Finally, Sect. 4.6 designs the feed-forward control (with \mathbf{A}_{FF} Hurwitz) and allows the tracking of time-varying references.

4.2 State-Feedback Stabilizer

As introduced in Sect. 4.1, the achievement of the control goals G1 and G2 is obtained through a design strategy whose first step consists of making Hurwitz the matrix $\mathbf{A} + \mathbf{B}_1 \mathbf{K}_S$. But, first, it is essential to understand which assumptions the plant must verify to let such \mathbf{K}_S exist. The so-called *reachability decomposition* represents the tool to perform these analyses. To keep the notation lighter, refer to the linearized vectors $\tilde{\mathbf{x}}$, $\tilde{\mathbf{y}}$, $\tilde{\mathbf{u}}$, and $\tilde{\mathbf{w}}$ by hiding the accent~ $\tilde{\cdot}$.

Let

$$\begin{aligned} \dot{\mathbf{x}} &= \mathbf{A}\mathbf{x} + \mathbf{B}_1\mathbf{u} + \mathbf{B}_2\mathbf{w} & \mathbf{x}(t_0) &= \mathbf{x}_0 \\ \mathbf{y} &= \mathbf{C}\mathbf{x} + \mathbf{D}_1\mathbf{u} + \mathbf{D}_2\mathbf{w} \end{aligned} \quad (4.2)$$

be the LTI system obtained by picking the first two equations of system (1.16). Then,

$$\chi_u(t, \mathbf{x}(t_0)) = \exp(\mathbf{A}(t - t_0))\mathbf{x}(t_0) + \int_{t_0}^t \exp(\mathbf{A}(t - \tau))\mathbf{B}_1\mathbf{u}(\tau)d\tau. \quad (4.3)$$

represents the integral curve of (4.2) with $\mathbf{w} \equiv \mathbf{0}$. Assume that the initial condition is identically null, i.e., $\mathbf{x}(t_0) = \mathbf{0}$, and denote with $\mathcal{R}(t)$ the set of *reachable states from the origin* thanks to any control $\mathbf{u} : [t_0, t] \rightarrow \mathbb{R}^p$ ([1], Sect. 3)

$$\mathcal{R}(t) := \left\{ \mathbf{x} \in \mathbb{R}^n : \mathbf{x} = \chi_u(t, \mathbf{0}) \right\}.$$

Note

In practice, the set $\mathcal{R}(t)$ represents the set of states reached from the origin thanks to the whole set of time-varying control signals $\tau \mapsto \mathbf{u}(\tau)$ with $\tau \in [t_0, t]$ (not just one particular control law!).

Remark 4.1 The reachability set \mathcal{R} is a subspace of \mathbb{R}^n , i.e., is a set closed to multiplication by scalar and addition. Therefore, a basis $\{\mathbf{b}_1, \dots, \mathbf{b}_{\ell_R}\}$ exists, which spans $\mathcal{R}(\infty)$, where ℓ_R represents the dimension of \mathcal{R} . Moreover, it is impossible to reach the states which do not belong to $\mathcal{R}(\infty)$ starting from the origin. Equivalently, the control $\mathbf{u}(\cdot)$ can not influence the dynamics of states out of \mathcal{R} .

Theorem 4.1 (Reachability [6]) *Let (4.2), then the matrix*

$$\mathbf{R} := [\mathbf{B}_1 \ \mathbf{AB}_1 \ \mathbf{A}^2\mathbf{B}_1 \cdots \mathbf{A}^{n-1}\mathbf{B}_1] \in \mathbb{R}^{n \times np}$$

*is such that $\text{im}(\mathbf{R}) = \mathcal{R}$. The matrix \mathbf{R} is called **reachability matrix**.*

Infobox 4.1 (Proof of Theorem 4.1) *The proof of Theorem 4.1 is founded on the Cayley–Hamilton theorem, which allows writing*

$$\exp(\mathbf{At}) = \sum_{i=0}^{n-1} \Phi_i(t) \mathbf{A}^i$$

where $\Phi_i : \mathbb{R} \rightarrow \mathbb{R}$ for any $i = 1, \dots, n - 1$. Then, write

$$\begin{aligned} \mathbf{x}(t) &= \int_0^t \exp(\mathbf{A}(t-\tau)) \mathbf{B}_1 \mathbf{u}(\tau) d\tau \\ &= \int_0^t \sum_{i=0}^{n-1} \Phi_i(t-\tau) \mathbf{A}^i \mathbf{B}_1 \mathbf{u}(\tau) d\tau \\ &= \sum_{i=0}^{n-1} \mathbf{A}^i \mathbf{B}_1 \int_0^t \Phi_i(t-\tau) \mathbf{u}(\tau) d\tau \\ &= \mathbf{R} \begin{bmatrix} \int_0^t \Phi_0(t-\tau) \mathbf{u}(\tau) d\tau \\ \vdots \\ \int_0^t \Phi_{n-1}(t-\tau) \mathbf{u}(\tau) d\tau \end{bmatrix}. \end{aligned}$$

Conceive the vector of the convolution integrals as a degree of freedom and obtain $\mathbf{x}(t)$ as a linear combination of the elements of \mathbf{R} . So, $\mathbf{x}(t)$ must belong to the image of \mathbf{R} to allow the equality be verified, i.e., to allow for the existence of a family of control laws $\mathbf{u}(t)$ that verify the equality.

Infobox 4.2 (Reachability and Controllability) *Control system theory developed the concept of the **controllability set**. In particular, consider the LTI system (4.2), then $\bar{\mathbf{x}} \in \mathbb{R}^n$ belongs to the controllability set, namely $\mathcal{C}(t)$, if there exists a control law $\tau \in [t_0, t] \mapsto \mathbf{u}(\tau)$ such that*

$$\mathbf{0} = \exp(\mathbf{A}(t-t_0)) \bar{\mathbf{x}} + \int_{t_0}^t \exp(\mathbf{A}(t-\tau)) \mathbf{B}_1 \mathbf{u}(\tau) d\tau.$$

Since $\exp(\mathbf{A}(t - t_0))$ is invertible, the latter equality can be re-arranged as

$$\bar{\mathbf{x}} = -\exp(-\mathbf{A}(t - t_0)) \int_{t_0}^t \exp(\mathbf{A}(t - \tau)) \mathbf{B}_1 \mathbf{u}(\tau) d\tau.$$

Now, note that $\exp(-\mathbf{A}(t - t_0))$ is full-rank and

$$\int_{t_0}^t \exp(\mathbf{A}(t - \tau)) \mathbf{B}_1 \mathbf{u}(\tau) d\tau \in \mathcal{R}.$$

Therefore, since $\bar{\mathbf{x}} \in \mathcal{C}$ implies $\bar{\mathbf{x}} \in \mathcal{R}$ and vice versa, the reachability and controllability subspaces are equivalent (only for continuous-time LTI systems). For this reason, the terms **reachability** and **controllability** are interchangeable (for instance this book adopts the former while MATLAB® uses the latter, e.g., in the command `ctrb`).

Important

An LTI system, or its couple (\mathbf{A}, \mathbf{B}) equivalently, is said to be **completely reachable** if $\text{rank}(\mathbf{R}) = n$, i.e., if $\mathcal{R} \equiv \mathbb{R}^n$.

Note

Intuitively, the reachability matrix form is derived as follows. Assume that $\mathbf{x}(t_0) = \mathbf{0}$ and take a constant control action, \mathbf{u} . Select p particular control inputs as

$$\mathbf{u}_1 = \begin{bmatrix} 1 \\ 0 \\ 0 \\ \vdots \\ 0 \\ 0 \end{bmatrix}, \quad \mathbf{u}_2 = \begin{bmatrix} 0 \\ 1 \\ 0 \\ \vdots \\ 0 \\ 0 \end{bmatrix}, \quad \dots, \quad \mathbf{u}_p = \begin{bmatrix} 0 \\ 0 \\ 0 \\ \vdots \\ 0 \\ 1 \end{bmatrix}.$$

Evaluate the first-order time derivatives $\dot{\mathbf{x}}_i(t_0) = \mathbf{B}_1 \mathbf{u}_i$ for each control input, collecting them in the matrix

$$\mathbf{X}^{(1)} := \left[\frac{d\mathbf{x}_1}{dt} \frac{d\mathbf{x}_2}{dt} \dots \frac{d\mathbf{x}_p}{dt} \right] = \mathbf{B}_1 [\mathbf{u}_1 \mathbf{u}_2 \dots \mathbf{u}_p],$$

where it is essential to remark that $[\mathbf{u}_1 \mathbf{u}_2 \dots \mathbf{u}_p] = \mathbf{I}$ (hidden hereafter).

On the other hand, $\frac{d^k \mathbf{x}_i}{dt^k}(t_0) = \mathbf{A}^{k-1} \mathbf{B}_1 \mathbf{u}_i$ for $k = 2, \dots, n$ and $i = 1, \dots, p$ represent the higher-order time derivatives of \mathbf{x} at time t_0 . For each $k = 2, \dots, n$, build the matrices $\mathbf{X}^{(k)}$ and organize them in a matrix as

$$[\mathbf{X}^{(1)} \mathbf{X}^{(2)} \dots \mathbf{X}^{(n)}] = [\mathbf{B}_1 \mathbf{A} \mathbf{B}_1 \dots \mathbf{A}^{n-1} \mathbf{B}_1].$$

In conclusion, the reachability matrix represents the basis for describing state time derivatives up to order n .

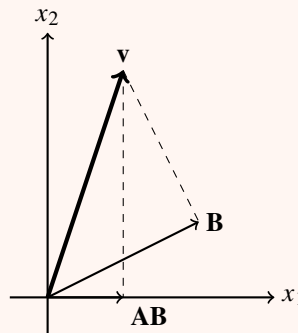
Example 4.1 (*Reachability study*) Let the system $\dot{\mathbf{x}} = \mathbf{Ax} + \mathbf{Bu}$, where $\mathbf{x} \in \mathbb{R}^2$, $u \in \mathbb{R}$, and

$$\mathbf{A} = \begin{bmatrix} 0 & a \\ 0 & 0 \end{bmatrix}, \quad \mathbf{B} = \begin{bmatrix} b_1 \\ b_2 \end{bmatrix},$$

with $a, b_1, b_2 > 0$. The reachability matrix is then given by

$$\mathbf{R} = [\mathbf{B} \ \mathbf{AB}] = \left[\begin{pmatrix} b_1 \\ b_2 \end{pmatrix} \begin{pmatrix} ab_2 \\ 0 \end{pmatrix} \right].$$

Draw the vectors \mathbf{B} and \mathbf{AB} on the plane $x_1 - x_2$.



The vectors \mathbf{B} and \mathbf{AB} are linearly independent because they have different directions and thus they represent a valid base for the representation of any vector \mathbf{v} in the space $x_1 - x_2$. More formally, the vectors \mathbf{B} and \mathbf{AB} span the whole state space \mathbb{R}^2 implying a fully reachable system.

Example 4.2 (*Reachability study*) Consider the system defined in Example 4.1 and assume $b_2 = 0$. The reachability matrix becomes

$$\mathbf{R} = [\mathbf{B} \ \mathbf{AB}] = \left[\begin{pmatrix} b_1 \\ 0 \end{pmatrix} \begin{pmatrix} 0 \\ 0 \end{pmatrix} \right],$$

which implies that the vectors \mathbf{B} and \mathbf{AB} do not span the whole state space; equivalently, they cannot represent any vector $\mathbf{v} \in \mathbb{R}^2$ but only those in the x_1 direction. Consequently, the system is not fully reachable and the reachable subspace is spanned by \mathbf{B} (which represents the x_1 direction). The non-reachable subspace is identified by the direction orthogonal to \mathbf{B} , i.e., by $\mathbf{w} = \text{col}(0, 1)$.

Example 4.3 (*Cart-pole reachability study*) Let

$$\mathbf{A} = \begin{bmatrix} 0 & 1 & 0 & 0 \\ 0 & 0 & A_{23} & A_{42} \\ 0 & 0 & 0 & 1 \\ 0 & 0 & A_{43} & A_{44} \end{bmatrix}, \quad \mathbf{B}_1 = \begin{bmatrix} 0 \\ B_{12} \\ 0 \\ B_{14} \end{bmatrix}$$

be defined as in Example 1.2, with the assumptions made in Example 3.2. The reachability matrix is obtained as

$$\mathbf{R} = \begin{bmatrix} \begin{pmatrix} 0 \\ B_{12} \\ 0 \\ B_{14} \end{pmatrix} \begin{pmatrix} B_{12} \\ A_{24}B_{14} \\ B_{14} \\ A_{44}B_{14} \end{pmatrix} \begin{pmatrix} B_{12} \\ A_{23}B_{14} + A_{24}A_{44}B_{14} \\ A_{44}B_{14} \\ A_{43}B_{14} + A_{44}^2B_{14} \end{pmatrix} \\ \begin{pmatrix} B_{12} \\ A_{23}A_{44}B_{14} + A_{24}(A_{43}B_{14} + A_{44}^2B_{14}) \\ A_{43}B_{14} + A_{44}^2B_{14} \\ A_{43}A_{44}B_{14} + A_{44}(A_{43}B_{14} + A_{44}^2B_{14}) \end{pmatrix} \end{bmatrix}.$$

The substitution of the numerical values listed in Example 3.2 leads to a full-rank matrix \mathbf{R} that implies a fully reachable system.

Since \mathcal{R} is a subspace of \mathbb{R}^n , its orthogonal complement exists, namely \mathcal{R}^\perp , such that $\mathcal{R} \oplus \mathcal{R}^\perp = \mathbb{R}^n$. Since the image of \mathbf{R} corresponds to \mathcal{R} , then $\ker(\mathbf{R}^\top) = \mathcal{R}^\perp$. Therefore, the matrices $\text{im}(\mathbf{R})$ and $\ker(\mathbf{R}^\top)$ can be exploited to identify a change of coordinate, namely $\mathbf{z} = \mathbf{T}_R \mathbf{x}$, which highlights the reachable part of system (4.2). In particular, the transformation matrix \mathbf{T}_R is called *reachability transformation* and is defined as ([2], Sect. 6)

$$\mathbf{T}_R^{-1} = [\text{im}(\mathbf{R}) \ \ker(\mathbf{R}^\top)],$$

which, applied to system (4.2), leads to

$$\begin{aligned} \dot{\mathbf{z}} &= \mathbf{T}_R \mathbf{A} \mathbf{T}_R^{-1} \mathbf{z} + \mathbf{T}_R \mathbf{B}_1 \mathbf{u} + \mathbf{T}_R \mathbf{B}_2 \mathbf{w} \quad \mathbf{z}(t_0) = \mathbf{T}_R \mathbf{x}_0 \\ \mathbf{y} &= \mathbf{C} \mathbf{T}_R^{-1} \mathbf{z} + \mathbf{D}_1 \mathbf{u} + \mathbf{D}_2 \mathbf{w}. \end{aligned} \tag{4.4}$$

A study of $\bar{\mathbf{A}} := \mathbf{T}_R \mathbf{A} \mathbf{T}_R^{-1}$, $\bar{\mathbf{B}}_1 := \mathbf{T}_R \mathbf{B}_1$, $\bar{\mathbf{B}}_2 := \mathbf{T}_R \mathbf{B}_2$, and $\bar{\mathbf{C}} := \mathbf{C} \mathbf{T}_R^{-1}$ reveals that

$$\bar{\mathbf{A}} = \begin{bmatrix} \bar{\mathbf{A}}_{11} & \bar{\mathbf{A}}_{12} \\ \mathbf{0} & \bar{\mathbf{A}}_{22} \end{bmatrix} \quad \bar{\mathbf{B}}_1 = \begin{bmatrix} \bar{\mathbf{B}}_{11} \\ \mathbf{0} \end{bmatrix} \quad \bar{\mathbf{B}}_2 = \begin{bmatrix} \bar{\mathbf{B}}_{21} \\ \bar{\mathbf{B}}_{22} \end{bmatrix} \quad \bar{\mathbf{C}} = [\bar{\mathbf{C}}_1 \ \bar{\mathbf{C}}_2]$$

so that, if the state is defined as $\mathbf{z} = \text{col}(\mathbf{z}_R, \mathbf{z}_{NR})$, the dynamics of (4.4) become (see Fig. 4.1)

$$\begin{aligned} \dot{\mathbf{z}}_R &= \bar{\mathbf{A}}_{11} \mathbf{z}_R + \bar{\mathbf{A}}_{12} \mathbf{z}_{NR} + \bar{\mathbf{B}}_{11} \mathbf{u} + \bar{\mathbf{B}}_{21} \mathbf{w} \\ \dot{\mathbf{z}}_{NR} &= \bar{\mathbf{A}}_{22} \mathbf{z}_{NR} + \bar{\mathbf{B}}_{22} \mathbf{w} \\ \mathbf{y} &= \bar{\mathbf{C}}_1 \mathbf{z}_R + \bar{\mathbf{C}}_2 \mathbf{z}_{NR} + \mathbf{D}_1 \mathbf{u} + \mathbf{D}_2 \mathbf{w} \\ \begin{bmatrix} \mathbf{z}_R(t_0) \\ \mathbf{z}_{NR}(t_0) \end{bmatrix} &= \mathbf{T}_R \mathbf{x}_0. \end{aligned} \tag{4.5}$$

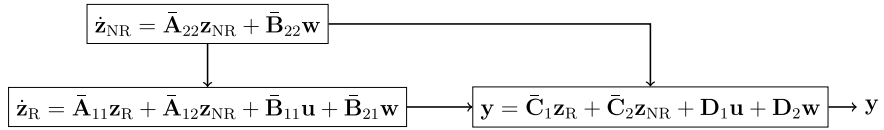


Fig. 4.1 Reachability decomposition

Equation (4.5) clearly shows that the dynamics of \mathbf{z}_{NR} are not (and cannot be) influenced by the control $\mathbf{u}(\cdot)$. It is important to note that the properties of $\bar{\mathbf{A}}_{22}$ determine the dynamics of

$$\dot{\mathbf{z}}_{NR} = \bar{\mathbf{A}}_{22}\mathbf{z}_{NR} + \bar{\mathbf{B}}_{22}\mathbf{w} \quad \mathbf{z}_{NR}(t_0) = \mathbf{z}_{NR_0}.$$

Important

According to the nature of the eigenvalues and eigenvectors of $\bar{\mathbf{A}}_{22}$, the dynamics of the non-reachable subpart of the state \mathbf{z}_{NR} , can be either BIBS-stable or not and we can do nothing to modify it.

Example 4.4 (*Reachability decomposition*) The reachability matrix associated with the couple

$$\mathbf{A} = \begin{bmatrix} 0 & 1 & 1 \\ -1 & 0 & 1 \\ 1 & 1 & 0 \end{bmatrix} \quad \mathbf{B} = \begin{bmatrix} 0 \\ 1 \\ 0 \end{bmatrix},$$

is

$$\mathbf{R} = [\mathbf{B} \ \mathbf{AB} \ \mathbf{A}^2\mathbf{B}] = \begin{bmatrix} 0 & 1 & 1 \\ 1 & 0 & 0 \\ 0 & 1 & 1 \end{bmatrix}.$$

Since $\text{rank}(\mathbf{R}) = 2$, the reachable subspace has dimensions two, whereas the non-reachable one is one-dimensional. Thus, one possible basis for the representation of the reachable subspace is

$$\{\mathbf{b}_1, \mathbf{b}_2\} = \left\{ \begin{pmatrix} 0 \\ 1 \\ 0 \end{pmatrix}, \begin{pmatrix} 1 \\ 0 \\ 1 \end{pmatrix} \right\}.$$

In addition, a basis for the representation of the non-reachable subspace is

$$\mathbf{b}_3 := \ker \left(\begin{bmatrix} \mathbf{b}_1^\top \\ \mathbf{b}_2^\top \end{bmatrix} \right) = \ker \left(\begin{bmatrix} 0 & 1 & 0 \\ 1 & 0 & 1 \end{bmatrix} \right) = \begin{pmatrix} 1 \\ 0 \\ -1 \end{pmatrix}.$$

So, the reachability decomposition relies on the transformation matrix

$$\mathbf{T}_R^{-1} = [\mathbf{b}_1 \ \mathbf{b}_2 \ \mathbf{b}_3] = \left[\begin{pmatrix} 0 \\ 1 \\ 0 \end{pmatrix} \begin{pmatrix} 1 \\ 0 \\ 1 \end{pmatrix} \begin{pmatrix} 1 \\ 0 \\ -1 \end{pmatrix} \right].$$

Finally, matrices $\bar{\mathbf{A}} = \mathbf{T}_R \mathbf{A} \mathbf{T}_R^{-1}$ and $\bar{\mathbf{B}} = \mathbf{T}_R \mathbf{B}$ are

$$\bar{\mathbf{A}} = \begin{bmatrix} 0 & 0 & | & -2 \\ 1 & 1 & | & 0 \\ \hline 0 & 0 & | & -1 \end{bmatrix} \quad \bar{\mathbf{B}} = \begin{bmatrix} 1 \\ 0 \\ \hline 0 \end{bmatrix}.$$

Example 4.5 (*Cart-pole reachability decomposition*) Example 4.6 shows that the cart-pole plant of Example 1.2 is fully reachable. Consequently, the origin trivially represents the non-reachable subspace, which is zero-dimensional. Thus, the transformation $\mathbf{T}_R^{-1} = \mathbf{I}$ means that the linear system of Example 4.6 is already in the reachability form.

As for the reachable subsystem, assume $\mathbf{z}_{NR} = \mathbf{0}$, write

$$\dot{\mathbf{z}}_R = \bar{\mathbf{A}}_{11}\mathbf{z}_R + \bar{\mathbf{B}}_1\mathbf{u} \quad \mathbf{z}_R(t_0) = \mathbf{z}_{R0}, \quad (4.6)$$

and note that system (4.6) is completely reachable by construction.

Theorem 4.2 (Existence of a stabilizing state feedback ([1], Sect. 4)) *Let $\dot{\mathbf{x}} = \mathbf{Ax} + \mathbf{Bu}$ be a fully reachable LTI system. Then, there exists a matrix \mathbf{K}_R such that $\mathbf{A} + \mathbf{BK}_R$ is Hurwitz.*

Infobox 4.3 (Proof sketch of Theorem 4.2) *To reduce the complexity of this proof, assume that the input is scalar, i.e., $u \in \mathbb{R}$. Introduce the following system [6]:*

$$\dot{\mathbf{z}} = \bar{\mathbf{A}}\mathbf{z} + \bar{\mathbf{B}}u$$

with

$$\bar{\mathbf{A}} := \begin{bmatrix} 0 & 1 & \dots & 0 & 0 \\ 0 & 0 & \ddots & 0 & 0 \\ \vdots & \vdots & \dots & \ddots & 0 \\ 0 & 0 & \dots & \dots & 1 \\ -\alpha_0 & -\alpha_1 & \dots & -\alpha_{n-2} & -\alpha_{n-1} \end{bmatrix}, \quad \bar{\mathbf{B}} := \begin{bmatrix} 0 \\ 0 \\ \vdots \\ 0 \\ 1 \end{bmatrix},$$

and where $\alpha_0, \dots, \alpha_{n-1}$ are the coefficients of the polynomial

$$\det(\bar{\mathbf{A}} - \lambda\mathbf{I}) := \alpha_0 + \alpha_1\lambda + \dots + \alpha_{n-1}\lambda^{n-1} + \lambda^n.$$

On the one hand, it is worth noting that these coefficients are directly linked to the eigenvalues of $\bar{\mathbf{A}}$ which are the roots of $\det(\bar{\mathbf{A}} - \lambda\mathbf{I}) = 0$. So, any change in

$\alpha_0, \dots, \alpha_{n-1}$ results in a change of the eigenvalues of the plant. On the other hand, the couple $(\bar{\mathbf{A}}, \bar{\mathbf{B}})$ is fully reachable and therefore the matrix

$$\mathbf{R}_z := [\bar{\mathbf{B}} \cdots \bar{\mathbf{A}}^{n-1} \bar{\mathbf{B}}]$$

is full-rank. Now, any feedback $u := \mathbf{K}_R \mathbf{z}$ with the matrix

$$\mathbf{K}_R := [k_0 \cdots k_{n-1}]$$

leads to a closed-loop system $\dot{\mathbf{z}} = (\bar{\mathbf{A}} + \bar{\mathbf{B}} \mathbf{K}_R) \mathbf{z}$ with

$$\bar{\mathbf{A}} + \bar{\mathbf{B}} \mathbf{K}_R := \begin{bmatrix} 0 & 1 & \cdots & 0 & 0 \\ 0 & 0 & \ddots & 0 & 0 \\ \vdots & \vdots & \cdots & \ddots & 0 \\ 0 & 0 & \cdots & \cdots & 1 \\ k_0 - \alpha_0 & k_1 - \alpha_1 & \cdots & k_{n-2} - \alpha_{n-2} & k_{n-1} - \alpha_{n-1} \end{bmatrix}.$$

As a consequence, the roots of $\det(\bar{\mathbf{A}} + \bar{\mathbf{B}} \mathbf{K}_R - \lambda \mathbf{I}) = 0$ can be modified, and their real parts can be made negative. The last step of this proof demonstrates that, for any scalar-input system $\dot{\mathbf{x}} = \mathbf{A}\mathbf{x} + \mathbf{B}u$, fully reachable, a change of coordinates \mathbf{T} exists such that $\mathbf{z} = \mathbf{T}\mathbf{x}$, $\bar{\mathbf{A}} := \mathbf{T}\mathbf{A}\mathbf{T}^{-1}$, and $\bar{\mathbf{B}} := \mathbf{T}\mathbf{B}$. To show the existence of \mathbf{T} , note that if (\mathbf{A}, \mathbf{B}) is fully reachable, the matrix

$$\mathbf{R}_x := [\mathbf{B} \cdots \mathbf{A}^{n-1} \mathbf{B}]$$

is full-rank. On the other hand, \mathbf{R}_z is rewritten as

$$\mathbf{R}_z := \mathbf{T}[\mathbf{B} \cdots \mathbf{A}^{n-1} \mathbf{B}],$$

which, compared with \mathbf{R}_x , leads to $\mathbf{R}_z = \mathbf{T}\mathbf{R}_x$. Then, define $\mathbf{T} = \mathbf{R}_z \mathbf{R}_x^{-1}$. A suitable choice of the reachability subspaces, associated with each control input, extends this proof strategy to plants with multidimensional inputs [7]. In detail, in the \mathbf{z} coordinates, the $\bar{\mathbf{A}} + \bar{\mathbf{B}} \mathbf{K}_R$ matrix is a block diagonal matrix whose blocks have the structure of the plant exploited in this proof.

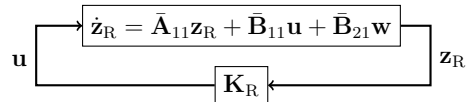
Important

The direct consequence of Theorem 4.2 is that there exists a **state-feedback control law** $\mathbf{u} = \mathbf{K}_R \mathbf{z}_R$ which makes the reachable system (4.6) BIBS-stable in the closed loop.

The substitution of $\mathbf{u} = \mathbf{K}_R \mathbf{z}_R$ into Eq. (4.6) leads to

$$\dot{\mathbf{z}}_R = (\bar{\mathbf{A}}_{11} + \bar{\mathbf{B}}_{11} \mathbf{K}_R) \mathbf{z}_R + \bar{\mathbf{B}}_{21} \mathbf{w} \quad \mathbf{z}_R(t_0) = \mathbf{z}_{R0}, \quad (4.7)$$

Fig. 4.2 The stabilizer is based on a state-feedback architecture



whose block scheme is depicted in Fig. 4.2. Moreover, the dynamics of (4.5) subject to $\mathbf{u} = \mathbf{K}_R \mathbf{z}_R$ are given by

$$\begin{aligned}\dot{\mathbf{z}}_R &= (\bar{\mathbf{A}}_{11} + \mathbf{B}_1 \mathbf{K}_R) \mathbf{z}_R + \bar{\mathbf{A}}_{12} \mathbf{z}_{NR} + \bar{\mathbf{B}}_{21} \mathbf{w} \\ \dot{\mathbf{z}}_{NR} &= \bar{\mathbf{A}}_{22} \mathbf{z}_{NR} + \bar{\mathbf{B}}_{22} \mathbf{w} \\ \mathbf{y} &= (\bar{\mathbf{C}}_1 + \mathbf{D}_1 \mathbf{K}_R) \mathbf{z}_R + \bar{\mathbf{C}}_2 \mathbf{z}_{NR} + \bar{\mathbf{D}}_2 \mathbf{w} \\ \begin{bmatrix} \mathbf{z}_R(t_0) \\ \mathbf{z}_{NR}(t_0) \end{bmatrix} &= \mathbf{T} \mathbf{x}_0\end{aligned}\quad (4.8)$$

in which the exogenous \mathbf{z}_{NR} influences the dynamics of the reachable part. Since the reachable subsystem is BIBS-stable, thanks to the stability properties of $\bar{\mathbf{A}}_{11} + \mathbf{B}_1 \mathbf{K}_R$, the state \mathbf{z}_R is bounded if \mathbf{z}_{NR} is so too. On the other hand, the state \mathbf{z}_{NR} is bounded if $\bar{\mathbf{A}}_{22}$ is Hurwitz.

Important

An LTI system is said to be stabilizable if the non-reachable state is BIBS-stable, i.e., if $\bar{\mathbf{A}}_{22}$ is Hurwitz.

From now on, this book adopts the following assumption.

Assumption 4.1 The plant (1.16) is stabilizable.

To conclude, with reference to (4.1a), use Assumptions 4.1, Theorem 4.2, and

$$\mathbf{u} = [\mathbf{K}_R \ \mathbf{0}] \begin{bmatrix} \mathbf{z}_R \\ \mathbf{z}_{NR} \end{bmatrix} = [\mathbf{K}_R \ \mathbf{0}] \mathbf{T}_R \mathbf{x}$$

to guarantee that $\mathbf{K}_S := [\mathbf{K}_R \ \mathbf{0}] \mathbf{T}_R$ makes $\mathbf{A} + \mathbf{B}_1 \mathbf{K}_S$ Hurwitz.

Before moving to the next section, it is worth noting that the control law $\mathbf{u} = \mathbf{K}_S \mathbf{x}$ applied to system (4.2) makes BIBS-stable the closed loop

$$\dot{\mathbf{x}} = (\mathbf{A} + \mathbf{B}_1 \mathbf{K}_S) \mathbf{x} + \mathbf{B}_2 \mathbf{w}$$

which, under Assumption 1.1, achieves goal G1. Ideally, this law solves all those problems in which the main control goal is stabilizing the linearization point (e.g., vibration suppression via active suspensions, yaw damper, and lane keeping). But:

- Its performance could be improved to achieve asymptotic tracking, i.e., to have $\lim_{t \rightarrow \infty} \mathbf{e}(t) = \mathbf{0}$, at least for constant \mathbf{w} . Indeed, this scenario (called *set-point regulation*) represents one of the most common operations in automotive applications (e.g., speed control, vehicle height regulation, roll control, and lane changing). Section 4.3 extends the control architecture to deal with this requirement.

- It is not implementable because it requires a perfect knowledge of \mathbf{x} . Section 4.5 overcomes this problem through the adoption of the observer described in Section 4.4.
- The control law can be extended to feedback also the non-reachable part, namely as $\mathbf{u} = [\mathbf{K}_R \ \mathbf{K}_{NR}] \mathbf{z}$. Indeed, even if it does not contribute to stability, \mathbf{z}_{NR} can improve the performance of the closed-loop plant. Section 5.1 provides an optimal design criterion for \mathbf{K}_{NR} .

4.3 Integral Action

As anticipated in Sect. 4.1 and reiterated at the end of Sect. 4.2, this section increments the controller design complexity by introducing the integral control action [8]. First, this section aims to design \mathbf{K}_S and \mathbf{K}_I by exploiting the results of Sect. 4.2. Second, the benefits associated with the control action are highlighted. Indeed, concerning plant (4.1a) with assumption $\mathbf{e}_x \equiv \mathbf{0}$, the integral action asymptotically steers to zero the regulated output for any constant reference \mathbf{r} and despite the presence of unknown but constant disturbances \mathbf{d} .

Let

$$\begin{bmatrix} \dot{\mathbf{x}} \\ \dot{\boldsymbol{\eta}} \end{bmatrix} = \begin{bmatrix} \mathbf{A} & \mathbf{0} \\ \mathbf{C}_e & \mathbf{0} \end{bmatrix} \begin{bmatrix} \mathbf{x} \\ \boldsymbol{\eta} \end{bmatrix} + \begin{bmatrix} \mathbf{B}_1 \\ \mathbf{D}_{e_1} \end{bmatrix} \mathbf{u} + \begin{bmatrix} \mathbf{B}_2 \\ \mathbf{D}_{e_2} \end{bmatrix} \mathbf{w} \quad (4.9)$$

be the LTI system obtained by picking the first and the last equations of system (1.16) with $\dot{\boldsymbol{\eta}} := \mathbf{e}$. Then, as done in Sect. 4.2, first study the reachability of system (4.9) through the matrix

$$\mathbf{R}_e := \begin{bmatrix} \mathbf{B}_1 & \mathbf{AB}_1 & \cdots & \mathbf{A}^{n-1}\mathbf{B}_1 & \mathbf{A}^n\mathbf{B}_1 & \cdots & \mathbf{A}^{n+m-1}\mathbf{B}_1 \\ \mathbf{D}_{e_2} & \mathbf{C}_e\mathbf{B}_1 & \cdots & \mathbf{C}_e\mathbf{A}^{n-2}\mathbf{B}_1 & \mathbf{C}_e\mathbf{A}^{n-1}\mathbf{B}_1 & \cdots & \mathbf{C}_e\mathbf{A}^{n+m-2}\mathbf{B}_1 \end{bmatrix}.$$

Then, if system (4.9) is stabilizable there exists a couple $(\mathbf{K}_S, \mathbf{K}_I)$ that makes Hurwitz

$$\begin{bmatrix} \mathbf{A} + \mathbf{B}_1\mathbf{K}_S & \mathbf{B}_1\mathbf{K}_I \\ \mathbf{C}_e + \mathbf{D}_{e_1}\mathbf{K}_S & \mathbf{D}_{e_1}\mathbf{K}_I \end{bmatrix}. \quad (4.10)$$

Therefore, define

$$\mathbf{u} = \mathbf{K}_S \mathbf{x} + \mathbf{K}_I \boldsymbol{\eta} \quad (4.11)$$

and demonstrate that it asymptotically steers \mathbf{e} to zero if \mathbf{w} is constant, as follows. Substitute the control law (4.11) into system (4.9)

$$\begin{bmatrix} \dot{\mathbf{x}} \\ \dot{\boldsymbol{\eta}} \end{bmatrix} = \begin{bmatrix} \mathbf{A} + \mathbf{B}_1\mathbf{K}_S & \mathbf{B}_1\mathbf{K}_I \\ \mathbf{C}_e + \mathbf{D}_{e_1}\mathbf{K}_S & \mathbf{D}_{e_1}\mathbf{K}_I \end{bmatrix} \begin{bmatrix} \mathbf{x} \\ \boldsymbol{\eta} \end{bmatrix} + \begin{bmatrix} \mathbf{B}_2 \\ \mathbf{D}_{e_2} \end{bmatrix} \mathbf{w} \quad (4.12)$$

and assume this system is BIBS-stable. Then, a bounded $t \mapsto \mathbf{w}(t)$ leads to limited trajectories $t \mapsto (\mathbf{x}(t), \boldsymbol{\eta}(t))$. In particular, the integral curve of system (4.12) evaluated at \mathbf{w} constant is such that

$$\lim_{t \rightarrow \infty} \begin{bmatrix} \mathbf{x}(t) \\ \boldsymbol{\eta}(t) \end{bmatrix} = - \begin{bmatrix} \mathbf{A} + \mathbf{B}_1\mathbf{K}_S & \mathbf{B}_1\mathbf{K}_I \\ \mathbf{C}_e + \mathbf{D}_{e_1}\mathbf{K}_S & \mathbf{D}_{e_1}\mathbf{K}_I \end{bmatrix}^{-1} \begin{bmatrix} \mathbf{B}_2 \\ \mathbf{D}_{e_2} \end{bmatrix} \mathbf{w} \quad (4.13)$$

which is well defined and bounded because matrix (4.10) is Hurwitz (and thus invertible) by assumption. As a consequence $\lim_{t \rightarrow \infty} \dot{\eta}(t) = \lim_{t \rightarrow \infty} \mathbf{e}(t) = \mathbf{0}$.

Example 4.6 (PI control) Let

$$\begin{aligned}\dot{x} &= ax + b_1 u + b_2 d \\ y &= cx\end{aligned}$$

be an LTI system with $x, y, u, d, a, b_1, b_2, c \in \mathbb{R}$, $b_1, b_2, c \neq 0$, and $\dot{d} = 0$. The goal is to asymptotically steer $x \rightarrow 0$ despite the presence of d . Start solving this problem by noting that the couple (a, b_1) is fully reachable. So, design $u = k_S x + k_I \eta$ with $\dot{\eta} = y$. Then, the controller takes the form

$$\begin{aligned}\dot{\eta} &= y \\ u &= k_S x + k_I \eta,\end{aligned}$$

representing a standard Proportional–Integral (PI) controller.

Example 4.7 (Cart-pole set-point regulation) The cart-pole model defined in Example 1.2 is described by

$$\dot{\mathbf{x}} = \mathbf{A}\mathbf{x} + \mathbf{B}_1 u + \mathbf{B}_2 d,$$

in which $\mathbf{x} := \text{col}(p - p_0 - v_0(t - t_0), v - v_0, \theta - \theta_0, 0)$, $u = f_x - f_{x0}$, $d = w$, and

$$\mathbf{A} := \begin{bmatrix} 0 & 1 & 0 & 0 \\ 0 & A_{22} & A_{23} & A_{24} \\ 0 & 0 & 0 & 1 \\ 0 & A_{42} & A_{43} & A_{44} \end{bmatrix}, \quad \mathbf{B}_1 := \begin{bmatrix} 0 \\ B_{12} \\ 0 \\ B_{14} \end{bmatrix}, \quad \mathbf{B}_2 := \begin{bmatrix} 0 \\ B_{22} \\ 0 \\ B_{24} \end{bmatrix}.$$

Let $p_R(t)$ be the reference position and $e := p - p_R(t)$ the tracking error, define $\dot{\eta} = e$, $\mathbf{C}_e = [1 \ 0 \ 0 \ 0]$, and $\mathbf{w} := \text{col}(w, p_R(t))$. Extend the plant as

$$\begin{bmatrix} \dot{\mathbf{x}} \\ \dot{\eta} \end{bmatrix} = \begin{bmatrix} \mathbf{A} & \mathbf{0} \\ \mathbf{C}_e & 0 \end{bmatrix} \mathbf{x} + \begin{bmatrix} \mathbf{B}_1 \\ 0 \end{bmatrix} u + \begin{bmatrix} \mathbf{B}_2 & \mathbf{0} \\ 0 & -1 \end{bmatrix} \mathbf{w}.$$

Then, since this system is fully reachable, there exists a control law $u = [\mathbf{K}_S \ k_I] \text{col}(\mathbf{x}, \eta)$ that makes Hurwitz

$$\begin{bmatrix} \mathbf{A} & \mathbf{0} \\ \mathbf{C}_e & 0 \end{bmatrix} + \begin{bmatrix} \mathbf{B}_1 \\ 0 \end{bmatrix} [\mathbf{K}_S \ k_I].$$

4.4 State Observer

Section 4.2 showed that the control law $\mathbf{u} = \mathbf{K}_S \mathbf{x}$ guarantees the stability of the closed-loop plant. However, the same section pointed out that this control law could not be implemented because \mathbf{x} may be unknown. So then, is it possible to “estimate” \mathbf{x} starting from the available information \mathbf{y} and \mathbf{u} ? This section introduces a further dynamic system, called *observer*, which answers this question [6]. The design of this system is achieved through a change of coordinates (dual to the reachability one) which reveals which parts of \mathbf{x} can be “estimated” and which cannot.

Let (4.2) be the plant and assume $\mathbf{u}(\tau), \mathbf{w}(\tau) \equiv \mathbf{0}$ for all $\tau \in [t_0, t]$. As a consequence, the integral curve is only given by free evolution, i.e.,

$$\mathbf{x}(t) = \exp(\mathbf{A}(t - t_0))\mathbf{x}(t_0), \quad (4.14)$$

which leads to

$$\mathbf{y}(t) = \mathbf{C} \exp(\mathbf{A}(t - t_0))\mathbf{x}(t_0). \quad (4.15)$$

It is interesting to understand if (and eventually, which part of) $\mathbf{x}(t_0)$ can be reconstructed from the output $\mathbf{y}(\tau)$ with $\tau \in [t_0, t]$. With this aim, define the *unobservability subspace at time $t > t_0$* , namely $\mathcal{E}(t)$, as ([1], Sect. 3)

$$\mathcal{E}(t) = \left\{ \mathbf{x} \in \mathbb{R}^n : \mathbf{C} \exp(\mathbf{A}(t - t_0))\mathbf{x} \equiv \mathbf{0}, \forall \tau \in [t_0, t] \right\}.$$

Note

In practice, $\mathcal{E}(t)$ represents the set of initial conditions that lead to a null output for any time belonging to the interval $[t_0, t]$. If $\mathbf{x} \in \mathcal{E}(t)$, then $\mathbf{C} \exp(\mathbf{A}(t - t_0))\mathbf{x} = \mathbf{C} \exp(\mathbf{A}(t - t_0))\mathbf{0} = \mathbf{0}$. Hence, \mathbf{x} is not “distinguishable” from the origin because it produces the same (null) output.

Theorem 4.3 (Unobservability [6]) *Let (4.2) be the plant, then its unobservability subspace corresponds to $\ker(\mathbf{O})$, where*

$$\mathbf{O} := \begin{bmatrix} \mathbf{C} \\ \mathbf{CA} \\ \vdots \\ \mathbf{CA}^{n-1} \end{bmatrix}$$

is called **observability matrix**.

Infobox 4.4 (Proof sketch of Theorem 4.3) *Theorem 4.3 is proved with the joint use of the arguments of the proof of Theorem 4.1, detailed in Infobox 4.1, and of the concept of duality, presented in Sect. 5.2.*

Important

An LTI system, or its couple (\mathbf{A}, \mathbf{C}) equivalently, is said to be **completely observable** if $\ker(\mathbf{O}) \equiv \{\mathbf{0}\}$.

Note

Intuitively, the observability matrix is derived through the following procedure. First, let the output be $\mathbf{y} = \mathbf{Cx}$ and assume $\mathbf{u} \equiv \mathbf{0}$. Then consider n particular vectors, namely \mathbf{x}_i with $i = 1, \dots, n$, as

$$\mathbf{x}_1 = \begin{bmatrix} 1 \\ 0 \\ 0 \\ \vdots \\ 0 \\ 0 \end{bmatrix}, \quad \mathbf{x}_2 = \begin{bmatrix} 0 \\ 1 \\ 0 \\ \vdots \\ 0 \\ 0 \end{bmatrix}, \quad \dots, \quad \mathbf{x}_n = \begin{bmatrix} 0 \\ 0 \\ 0 \\ \vdots \\ 0 \\ 1 \end{bmatrix}.$$

Next, collect the outputs $\mathbf{y}_i = \mathbf{Cx}_i$ in

$$\mathbf{Y}^{(0)} := [\mathbf{y}_1 \ \mathbf{y}_2 \ \dots \ \mathbf{y}_n] = \mathbf{C} [\mathbf{x}_1 \ \mathbf{x}_2 \ \dots \ \mathbf{x}_n].$$

and note that $[\mathbf{x}_1 \ \mathbf{x}_2 \ \dots \ \mathbf{x}_n] = \mathbf{I}$. Compute $\frac{d^k \mathbf{y}_i}{dt^k} = \mathbf{CA}^k \mathbf{x}_i$, for $i = 1, \dots, n$ and $k = 0, \dots, n-1$. Now, collect terms $\frac{d^k \mathbf{y}_i}{dt^k}$ in matrices $\mathbf{Y}^{(k)}$ and sequentially collect these matrices in

$$\begin{bmatrix} \mathbf{Y}^{(0)} \\ \mathbf{Y}^{(1)} \\ \vdots \\ \mathbf{Y}^{(n-1)} \end{bmatrix} = \begin{bmatrix} \mathbf{C} \\ \mathbf{CA} \\ \vdots \\ \mathbf{CA}^{n-1} \end{bmatrix}.$$

Thus, intuitively speaking, the kernel of the observability matrix represents the basis for the description of the states that make null the first $n-1$ time derivatives of \mathbf{y} .

By looking at this rough explanation and assuming (\mathbf{A}, \mathbf{C}) is fully observable, one can be tempted to use $\text{col}(\mathbf{y}, d\mathbf{y}/dt, \dots, d^{n-1}\mathbf{y}/dt^{n-1})$ to estimate \mathbf{x} by employing the pseudo-inverse of \mathbf{O} as

$$\hat{\mathbf{x}} = (\mathbf{O}^\top \mathbf{O})^{-1} \mathbf{O}^\top \begin{bmatrix} \mathbf{y} \\ d\mathbf{y}/dt \\ \vdots \\ d^{n-1}\mathbf{y}/dt^{n-1} \end{bmatrix}.$$

This procedure is feasible only if \mathbf{y} is noise-free. Indeed, assume a scalar output $y = \mathbf{Cx} + \nu(t)$ affected by the noise $\nu(t) := \sum_{i=1}^{\infty} \bar{\nu}_i \sin(i \omega t)$ with $\omega > 0$

and $\bar{\nu}_i \geq 0$ such that $\sum_i^\infty \bar{\nu}_i^2$ is finite. So, for any $k \geq 1$, the k th-order time derivative of y is

$$\frac{d^k y}{dt^k} = \mathbf{C}\mathbf{A}^k \mathbf{x} + \frac{d^k \nu}{dt^k}.$$

The application of the pseudo-inverse of \mathbf{O} to $\text{col}(y, dy/dt, \dots, d^{n-1}y/dt^{n-1})$ leads to

$$\begin{aligned} \hat{\mathbf{x}} &= (\mathbf{O}^\top \mathbf{O})^{-1} \mathbf{O}^\top \left(\mathbf{O}\mathbf{x} + \begin{bmatrix} \nu \\ d\nu/dt \\ \vdots \\ d^{n-1}\nu/dt^{n-1} \end{bmatrix} \right) \\ &= \mathbf{x} + (\mathbf{O}^\top \mathbf{O})^{-1} \mathbf{O}^\top \begin{bmatrix} \nu \\ d\nu/dt \\ \vdots \\ d^{n-1}\nu/dt^{n-1} \end{bmatrix}. \end{aligned}$$

This expression demonstrates that $\hat{\mathbf{x}}$ is proportionally affected by the magnitude of the time derivatives of ν . For any $k \geq 1$ these magnitudes are upper bounded by

$$\left\| \frac{d^k \nu}{dt^k} \right\|_\infty = \sum_{i=1}^{\infty} \bar{\nu}_i (i\omega)^k,$$

which is an increasing function of i and k (for all $i \in \mathbb{N} : i\omega > 1$).

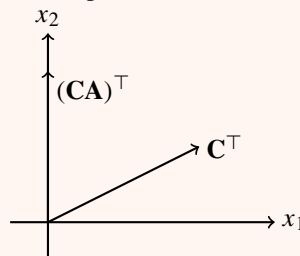
Example 4.8 (Observability study) Let $\dot{\mathbf{x}} = \mathbf{Ax}$, $y = \mathbf{Cx}$, with $\mathbf{x} \in \mathbb{R}^2$, and $y \in \mathbb{R}$ be the plant model. Define \mathbf{A} and \mathbf{C} as

$$\mathbf{A} = \begin{bmatrix} 0 & a \\ 0 & 0 \end{bmatrix}, \quad \mathbf{C} = \begin{bmatrix} c_1 & c_2 \end{bmatrix},$$

with $a, c_1, c_2 > 0$. Therefore, the observability matrix is

$$\mathbf{O} = \begin{bmatrix} \mathbf{C} \\ \mathbf{CA} \end{bmatrix} = \begin{bmatrix} c_1 & c_2 \\ 0 & c_1 a \end{bmatrix}.$$

Now, draw the rows of \mathbf{O} in the plane $x_1 - x_2$ as



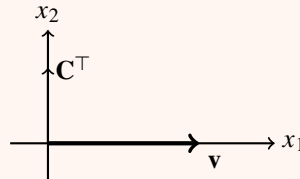
Since \mathbf{C}^\top and $(\mathbf{CA})^\top$ span the whole state space \mathbb{R}^2 , the unique vector with null projections on \mathbf{C}^\top and $(\mathbf{CA})^\top$ is the trivial $\mathbf{v} = \mathbf{0}$. So then, since the set

of states which create a null output is only constituted by $\mathbf{0}$, the system is fully observable.

Example 4.9 (Observability Study) Let the plant be defined in Example 4.8 and consider $c_1 = 0$. The observability matrix becomes

$$\mathbf{O} = \begin{bmatrix} \mathbf{C} \\ \mathbf{CA} \end{bmatrix} = \begin{bmatrix} 0 & c_2 \\ 0 & 0 \end{bmatrix},$$

whose row vectors are drawn as



Then, since \mathbf{C}^\top does not span the whole state space \mathbb{R}^2 , the system is not fully observable. Indeed, the unobservable set is composed of vectors, like $\mathbf{v} = \text{col}(s, 0)$ with $s \in \mathbb{R}$, which have a null projection in direction \mathbf{C}^\top .

Example 4.10 (Cart-pole observability) The couple (\mathbf{A}, \mathbf{C}) of the linearized cart-pole model of Example 1.2 are reported as

$$\mathbf{A} = \begin{bmatrix} 0 & 1 & 0 & 0 \\ 0 & A_{22} & A_{23} & A_{24} \\ 0 & 0 & 0 & 1 \\ 0 & A_{42} & A_{43} & A_{44} \end{bmatrix} \quad \mathbf{C} = \begin{bmatrix} 0 & 1 & 0 & 0 \\ 0 & 0 & 1 & 0 \end{bmatrix}.$$

The observability matrix associated with this couple is then obtained as

$$\mathbf{O} = \begin{bmatrix} \mathbf{C} \\ \mathbf{CA} \\ \mathbf{CA}^2 \\ \mathbf{CA}^3 \end{bmatrix} = \begin{bmatrix} 0 & 1 & 0 & 0 \\ 0 & 0 & 1 & 0 \\ 0 & A_{22} & A_{23} & A_{24} \\ 0 & 0 & 0 & 1 \\ 0 & o_{52} & o_{53} & o_{54} \\ 0 & A_{42} & A_{43} & A_{44} \\ 0 & o_{72} & o_{73} & o_{74} \\ 0 & o_{82} & o_{83} & o_{84} \end{bmatrix},$$

where

$$\begin{aligned}
 o_{52} &= A_{22}^2 + A_{24}A_{42} \\
 o_{53} &= A_{22}A_{23} + A_{24}A_{43} \\
 o_{54} &= A_{22}A_{24} + A_{23} + A_{24}A_{44} \\
 o_{72} &= o_{52}A_{22} + o_{54}A_{42} \\
 o_{73} &= o_{52}A_{23} + o_{54}A_{43} \\
 o_{74} &= o_{52}A_{24} + o_{53} + o_{54}A_{44} \\
 o_{82} &= A_{42}A_{22} + A_{44}A_{42} \\
 o_{83} &= A_{42}A_{23} + A_{44}A_{43} \\
 o_{84} &= A_{42}A_{24} + A_{43} + A_{44}^2.
 \end{aligned}$$

Since the first column of \mathbf{O} is null and the transpose of the first, second, and fourth rows span \mathbb{R}^3 , the kernel of \mathbf{O} is one-dimensional and given by

$$\ker(\mathbf{O}) = \text{col}(1, 0, 0, 0).$$

Consequently, the system of Example 1.2 is not fully observable.

Let \mathcal{E} be an unobservability subspace, then its orthogonal complement \mathcal{E}^\perp is such that $\mathcal{E} \oplus \mathcal{E}^\perp = \mathbb{R}^n$. In terms of basis, if $\ker(\mathbf{O})$ represents a basis for \mathcal{E} , then $(\ker(\mathbf{O}))^\perp = \text{im}(\mathbf{O}^\top)$ defines a basis for \mathcal{E}^\perp . The remainder of this section relies on these bases to determine a change of coordinates that decomposes the state into unobservable and observable subparts. The so-called “decomposition of observability” ([2], Sect. 6) is defined by introducing the transformation $\mathbf{z} = \mathbf{T}_O \mathbf{x}$ where

$$\mathbf{T}_O^{-1} = [\ker(\mathbf{O}) \text{ im}(\mathbf{O}^\top)] \quad (4.16)$$

which applied to system (4.2) leads to

$$\begin{aligned}
 \dot{\mathbf{z}} &= \mathbf{T}_O \mathbf{A} \mathbf{T}_O^{-1} \mathbf{z} + \mathbf{T}_O \mathbf{B}_1 \mathbf{u} + \mathbf{T}_O \mathbf{B}_2 \mathbf{w} \quad \mathbf{z}(t_0) = \mathbf{T}_O \mathbf{x}_0 \\
 \mathbf{y} &= \mathbf{C} \mathbf{T}_O^{-1} \mathbf{z} + \mathbf{D}_1 \mathbf{u} + \mathbf{D}_2 \mathbf{w}.
 \end{aligned} \quad (4.17)$$

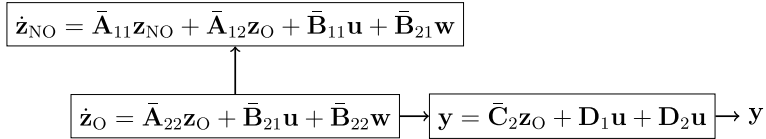
A study of $\bar{\mathbf{A}} := \mathbf{T}_O \mathbf{A} \mathbf{T}_O^{-1}$, $\bar{\mathbf{B}}_1 := \mathbf{T}_O \mathbf{B}_1$, $\bar{\mathbf{B}}_2 := \mathbf{T}_O \mathbf{B}_2$, and $\bar{\mathbf{C}} := \mathbf{C} \mathbf{T}_O^{-1}$ reveals that

$$\bar{\mathbf{A}} = \begin{bmatrix} \bar{\mathbf{A}}_{11} & \bar{\mathbf{A}}_{12} \\ \mathbf{0} & \bar{\mathbf{A}}_{22} \end{bmatrix} \quad \bar{\mathbf{B}}_1 = \begin{bmatrix} \bar{\mathbf{B}}_{11} \\ \bar{\mathbf{B}}_{12} \end{bmatrix} \quad \bar{\mathbf{B}}_2 = \begin{bmatrix} \bar{\mathbf{B}}_{21} \\ \bar{\mathbf{B}}_{22} \end{bmatrix} \quad \bar{\mathbf{C}} = [\bar{\mathbf{0}} \quad \bar{\mathbf{C}}_2].$$

So, define $\mathbf{z} = \text{col}(\mathbf{z}_{NO}, \mathbf{z}_O)$ to make the dynamics of system (4.17) become

$$\begin{aligned}
 \dot{\mathbf{z}}_{NO} &= \bar{\mathbf{A}}_{11} \mathbf{z}_{NO} + \bar{\mathbf{A}}_{12} \mathbf{z}_O + \bar{\mathbf{B}}_{11} \mathbf{u} + \bar{\mathbf{B}}_{21} \mathbf{w} \\
 \dot{\mathbf{z}}_O &= \bar{\mathbf{A}}_{22} \mathbf{z}_O + \bar{\mathbf{B}}_{21} \mathbf{u} + \bar{\mathbf{B}}_{22} \mathbf{w} \\
 \mathbf{y} &= \bar{\mathbf{C}}_2 \mathbf{z}_O + \mathbf{D}_1 \mathbf{u} + \mathbf{D}_2 \mathbf{w} \\
 \begin{bmatrix} \mathbf{z}_{NO}(t_0) \\ \mathbf{z}_O(t_0) \end{bmatrix} &= \mathbf{T}_O \mathbf{x}_0.
 \end{aligned} \quad (4.18)$$

Equation (4.18) shows that \mathbf{z}_O represents the subpart of the system available at the output. It is worth noting that \mathbf{z}_{NO} does not influence the dynamics of \mathbf{z}_O . Therefore, assuming $\mathbf{u}, \mathbf{w} \equiv 0$, the output \mathbf{y} is null for any time if and only if $\mathbf{z}_O \equiv \mathbf{0}$. Figure 4.3 depicts system (4.18).

**Fig. 4.3** Observability decomposition

Example 4.11 (*Observability decomposition*) The observability matrix associated with the couple

$$\mathbf{A} = \begin{bmatrix} 0 & 1 & 1 \\ -1 & 0 & 1 \\ 1 & 1 & 0 \end{bmatrix} \quad \mathbf{C} = [1 \ 0 \ 0],$$

is

$$\mathbf{O} = \begin{bmatrix} \mathbf{C} \\ \mathbf{CA} \\ \mathbf{CA}^2 \end{bmatrix} = \begin{bmatrix} 1 & 0 & 0 \\ 0 & 1 & 1 \\ 0 & 1 & 1 \end{bmatrix}.$$

The kernel of \mathbf{O} provides a basis for the unobservable subspace

$$\mathbf{b}_1 := \ker(\mathbf{O}) = \ker \left(\begin{bmatrix} 1 & 0 & 0 \\ 0 & 1 & 1 \\ 0 & 1 & 1 \end{bmatrix} \right) = \begin{pmatrix} 0 \\ 1 \\ -1 \end{pmatrix}.$$

In addition, the image of \mathbf{O} leads to the basis of the observable subspace

$$\{\mathbf{b}_2, \mathbf{b}_3\} := \left\{ \begin{pmatrix} 1 \\ 0 \\ 0 \end{pmatrix}, \begin{pmatrix} 0 \\ 1 \\ 1 \end{pmatrix} \right\}.$$

Finally, the observability decomposition is obtained through the transformation matrix $\mathbf{T}_O^{-1} = [\mathbf{b}_1 \ \mathbf{b}_2 \ \mathbf{b}_3]$, which leads to

$$\bar{\mathbf{A}} = \mathbf{T}_O \mathbf{A} \mathbf{T}_O^{-1} = \begin{bmatrix} -1 & -1 & 0 \\ 0 & 0 & 2 \\ 0 & 0 & 1 \end{bmatrix}, \quad \mathbf{C} = \mathbf{C} \mathbf{T}_O^{-1} = [0 \ 1 \ 0].$$

Example 4.12 (*Cart-pole observability decomposition*) As described in Example 4.10, the system of Example 1.2 is not fully observable. The kernel of \mathbf{O} provides the basis of the unobservable subspace $\mathbf{b}_1 := \ker(\mathbf{O}) = \text{col}(1, 0, 0, 0)$, whereas the basis of the observable subspace is

$$\{\mathbf{b}_2, \mathbf{b}_3, \mathbf{b}_4\} := \left\{ \begin{pmatrix} 0 \\ 1 \\ 0 \\ 0 \end{pmatrix}, \begin{pmatrix} 0 \\ 0 \\ 1 \\ 0 \end{pmatrix}, \begin{pmatrix} 0 \\ 0 \\ 0 \\ 1 \end{pmatrix} \right\}.$$

Finally, the observability transformation is $\mathbf{T}_O^{-1} = [\mathbf{b}_1 \ \mathbf{b}_2 \ \mathbf{b}_3 \ \mathbf{b}_4] = \mathbf{I}$ meaning that the system of Example 1.2 is already in the form of observability.

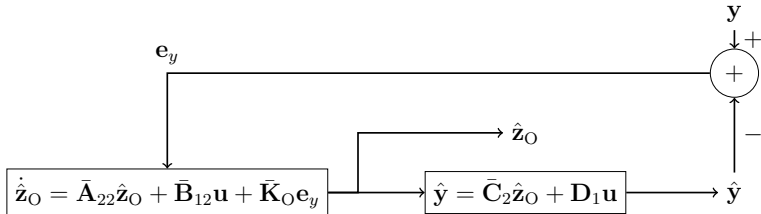


Fig. 4.4 State observer

Now, focus on the observable subsystem of (4.18)

$$\begin{aligned}\dot{\mathbf{z}}_O &= \bar{\mathbf{A}}_{22} \mathbf{z}_O + \bar{\mathbf{B}}_{12} \mathbf{u} + \bar{\mathbf{K}}_O \mathbf{e}_y & \mathbf{z}_O(t_0) &= \mathbf{z}_{O0} \\ \mathbf{y} &= \bar{\mathbf{C}}_2 \mathbf{z}_O + \mathbf{D}_2 \mathbf{w},\end{aligned}\quad (4.19)$$

which is completely observable, by definition, and for which the following result can be stated.

Theorem 4.4 (Existence of a stabilizing output feedback ([1], Sect. 4)) *Let*

$$\begin{aligned}\dot{\mathbf{x}} &= \mathbf{Ax} \\ \mathbf{y} &= \mathbf{Cx}\end{aligned}$$

be a completely observable LTI system. Then, there exists a matrix \mathbf{K}_O such that $\mathbf{A} - \mathbf{K}_O \mathbf{C}$ is Hurwitz.

Infobox 4.5 (Proof sketch of Theorem 4.4) *Theorem 4.4 is proved through the same strategy adopted to prove Theorem 4.2 (see Infobox 4.3) with the support of the concept of duality presented in Sect. 5.2.*

Important

A direct consequence of Theorem 4.4 is that it is possible to design a BIBS-stable dynamic system that provides an estimation of \mathbf{z}_O in the following form [4]:

$$\begin{aligned}\dot{\mathbf{z}}_O &= \bar{\mathbf{A}}_{22} \hat{\mathbf{z}}_O + \bar{\mathbf{B}}_{12} \mathbf{u} + \bar{\mathbf{K}}_O (\mathbf{y} - \hat{\mathbf{y}}) & \hat{\mathbf{z}}_O(t_0) &= \mathbf{0} \\ \hat{\mathbf{y}} &= \bar{\mathbf{C}}_2 \hat{\mathbf{z}}_O + \mathbf{D}_1 \mathbf{u}.\end{aligned}\quad (4.20)$$

Let $\mathbf{e}_O := \mathbf{z}_O - \hat{\mathbf{z}}_O$ be the estimation error; then, the estimator (4.20), whose scheme is illustrated in Fig. 4.4, makes \mathbf{e}_O bounded. Indeed

$$\dot{\mathbf{e}}_O = (\bar{\mathbf{A}}_{22} - \bar{\mathbf{K}}_O \bar{\mathbf{C}}_2) \mathbf{e}_O + (\bar{\mathbf{B}}_{22} + \bar{\mathbf{K}}_O \mathbf{D}_2) \mathbf{w} \quad \mathbf{e}_O(t_0) = \mathbf{z}_O(t_0) - \hat{\mathbf{z}}_O(t_0), \quad (4.21)$$

whose state asymptotically converges to the neighborhood of the origin, provided that $\bar{\mathbf{A}}_{22} - \bar{\mathbf{K}}_O \bar{\mathbf{C}}_2$ is Hurwitz.

Infobox 4.6 (Reduced order observer) *The implementation of observer (4.20) requires the computation of a dynamic system of the same order as the plant. This section proposes a strategy to reduce the observer dimension [2, 6]. Let*

$$\begin{aligned}\dot{\mathbf{z}}_O &= \bar{\mathbf{A}}_{22}\mathbf{z}_O + \bar{\mathbf{B}}_{12}\mathbf{u} + \bar{\mathbf{B}}_{22}\mathbf{w} \\ \mathbf{y} &= \bar{\mathbf{C}}_2\mathbf{z}_O + \mathbf{D}_1\mathbf{u} + \mathbf{D}_2\mathbf{w}\end{aligned}$$

be the observable part of system (4.18). Define \mathbf{N} such that

$$\mathbf{T} := \begin{bmatrix} \bar{\mathbf{C}}_2 \\ \mathbf{N} \end{bmatrix}$$

constitutes a change of coordinates. Introduce $\zeta = \mathbf{T}\mathbf{z}_O$, with $\zeta := \text{col}(\zeta_1, \zeta_2)$ and $\zeta_1 \in \mathbb{R}^q$. Then, the dynamics of ζ are

$$\begin{aligned}\dot{\zeta}_1 &= \underline{\mathbf{A}}_{11}\zeta_1 + \underline{\mathbf{A}}_{12}\zeta_2 + \underline{\mathbf{B}}_{11}\mathbf{u} + \underline{\mathbf{B}}_{21}\mathbf{w} \\ \dot{\zeta}_2 &= \underline{\mathbf{A}}_{21}\zeta_1 + \underline{\mathbf{A}}_{22}\zeta_2 + \underline{\mathbf{B}}_{12}\mathbf{u} + \underline{\mathbf{B}}_{22}\mathbf{w} \\ \mathbf{y} &= \zeta_1 + \mathbf{D}_1\mathbf{u} + \mathbf{D}_2\mathbf{w},\end{aligned}$$

where $\underline{\mathbf{A}}_{ij}$ and $\underline{\mathbf{B}}_{ij}$, with $i, j \in \{1, 2\}$, denote subparts of $\underline{\mathbf{A}} := \mathbf{T}\bar{\mathbf{A}}_{22}\mathbf{T}^{-1}$, $\underline{\mathbf{B}}_1 := \mathbf{T}\bar{\mathbf{B}}_1$, and $\underline{\mathbf{B}}_2 := \mathbf{T}\bar{\mathbf{B}}_2$. As a consequence, since $\hat{\zeta}_1 := \mathbf{y} - \mathbf{D}_1\mathbf{u} = \zeta_1 + \mathbf{D}_2\mathbf{w}$ provides a direct (noisy) estimation of ζ_1 , only ζ_2 needs to be estimated. To this end, conceive

$$\mu := \dot{\hat{\zeta}}_1 - \underline{\mathbf{A}}_{11}\hat{\zeta}_1 - \underline{\mathbf{B}}_{11}\mathbf{u} = \underline{\mathbf{A}}_{12}\zeta_2 + (\underline{\mathbf{B}}_{21} - \underline{\mathbf{A}}_{11}\mathbf{D}_2)\mathbf{w} + \mathbf{D}_2\dot{\mathbf{w}}$$

as a potential output and rewrite the plant as

$$\begin{aligned}\dot{\zeta}_2 &= \underline{\mathbf{A}}_{22}\zeta_2 + \underline{\mathbf{A}}_{21}\zeta_1 + \underline{\mathbf{B}}_{12}\mathbf{u} + \underline{\mathbf{B}}_{22}\mathbf{w} \\ \mu &= \underline{\mathbf{A}}_{12}\zeta_2 + (\underline{\mathbf{B}}_{21} - \underline{\mathbf{A}}_{11}\mathbf{D}_2)\mathbf{w} + \mathbf{D}_2\dot{\mathbf{w}}.\end{aligned}$$

Since the couple $(\underline{\mathbf{A}}_{22}, \underline{\mathbf{A}}_{12})$ is fully observable, $\underline{\mathbf{K}}_O$ exists such that $\underline{\mathbf{A}}_{22} - \underline{\mathbf{K}}_O\underline{\mathbf{A}}_{12}$ is Hurwitz and

$$\dot{\hat{\zeta}}_2 = (\underline{\mathbf{A}}_{22} - \underline{\mathbf{K}}_O\underline{\mathbf{A}}_{12})\hat{\zeta}_2 + \underline{\mathbf{A}}_{21}\hat{\zeta}_1 + \underline{\mathbf{B}}_{12}\mathbf{u} + \underline{\mathbf{K}}_O\mu$$

converges to a neighborhood of ζ_2 . To make this observer implementable, introduce a change of variables that removes the derivative of $\hat{\zeta}_1$ (appearing in μ). Let $\hat{\mathbf{v}} := \hat{\zeta}_2 - \underline{\mathbf{K}}_O\hat{\zeta}_1$, exploit $\hat{\zeta}_2 = \hat{\mathbf{v}} + \underline{\mathbf{K}}_O\hat{\zeta}_1$, and rewrite the observer as

$$\begin{aligned}\dot{\hat{\mathbf{v}}} &= (\underline{\mathbf{A}}_{22} - \underline{\mathbf{K}}_O\underline{\mathbf{A}}_{12})\hat{\mathbf{v}} + ((\underline{\mathbf{A}}_{22} - \underline{\mathbf{K}}_O\underline{\mathbf{A}}_{12})\underline{\mathbf{K}}_O + \underline{\mathbf{A}}_{21} - \underline{\mathbf{K}}_O\underline{\mathbf{A}}_{11})\hat{\zeta}_1 \\ &\quad + (\underline{\mathbf{B}}_{12} - \underline{\mathbf{K}}_O\underline{\mathbf{B}}_{11})\mathbf{u}.\end{aligned}$$

Then, the estimation of \mathbf{z}_O is obtained as

$$\hat{\mathbf{z}}_O = \mathbf{T}^{-1} \begin{bmatrix} \hat{\zeta}_1 \\ \hat{\zeta}_2 \end{bmatrix} = \begin{bmatrix} \mathbf{I} & \mathbf{0} \\ \underline{\mathbf{K}}_O & \mathbf{I} \end{bmatrix} \begin{bmatrix} \hat{\zeta}_1 \\ \hat{\mathbf{v}} \end{bmatrix}.$$

To conclude this section, let us focus on the estimation of the non-observable states. First, introduce the subsequent definition.

Important

The LTI system of Eq. (4.18) is said to be **detectable** if $\bar{\mathbf{A}}_{11}$ is Hurwitz.

Then, adopt the next assumption.

Assumption 4.2 The system (4.2) is detectable.

Therefore, the non-observable states \mathbf{z}_{NO} are estimated by the so-called *identity observer* which simply consists of a copy of the plant

$$\dot{\hat{\mathbf{z}}}_{NO} = \bar{\mathbf{A}}_{11}\hat{\mathbf{z}}_{NO} + \bar{\mathbf{A}}_{12}\hat{\mathbf{z}}_O + \bar{\mathbf{B}}_{12}\mathbf{u} \quad \hat{\mathbf{z}}_{NO}(t_0) = \hat{\mathbf{z}}_{NO_0}. \quad (4.22)$$

To analyze this algorithm, let $\mathbf{e}_{NO} := \hat{\mathbf{z}}_{NO} - \mathbf{z}_{NO}$ be the estimation error. Then, compute its dynamics exploiting Eqs. (4.18) and (4.22) as

$$\dot{\mathbf{e}}_{NO} = \bar{\mathbf{A}}_{11}\mathbf{e}_{NO} - \bar{\mathbf{A}}_{12}\mathbf{e}_O - \bar{\mathbf{B}}_{22}\mathbf{w} \quad \mathbf{e}_{NO}(t_0) = \hat{\mathbf{z}}_{NO}(t_0) - \mathbf{z}_{NO}(t_0). \quad (4.23)$$

It is worth noting that the dynamics of \mathbf{e}_{NO} are bounded because $\bar{\mathbf{A}}_{11}$ is Hurwitz, but the identity observer cannot tune them. Adopt the following strategy to estimate the state:

$$\hat{\mathbf{x}} = \mathbf{T}_O^{-1} \begin{bmatrix} \hat{\mathbf{z}}_{NO} \\ \hat{\mathbf{z}}_O \end{bmatrix}. \quad (4.24)$$

4.5 Output-Feedback Stabilizer

As described at the end of Sect. 4.2, the state feedback $\mathbf{u} = \mathbf{K}_S \mathbf{x}$ could not be implementable because \mathbf{x} may be unavailable. On the other hand, Sect. 4.4 provides a strategy to estimate \mathbf{x} . Consequently, an implementable control law is ([2], Sect. 9)

$$\mathbf{u}_S = \mathbf{K}_S \hat{\mathbf{x}}, \quad (4.25)$$

which matches the architecture of Eq. (1.17). Concerning Eq. (4.1a), this section demonstrates that using control law (4.25), as well as the integral action defined in Sect. 4.3, makes Hurwitz the matrix

$$\begin{bmatrix} \mathbf{A} + \mathbf{B}_1 \mathbf{K}_S & \mathbf{B}_1 \mathbf{K}_I & \mathbf{B}_1 \mathbf{K}_S \\ \mathbf{C}_e + \mathbf{D}_{e_1} \mathbf{K}_S & \mathbf{D}_{e_1} \mathbf{K}_I & \mathbf{D}_{e_1} \mathbf{K}_S \\ \mathbf{A}_O + \mathbf{K}_O \mathbf{C} - \mathbf{A} + \mathbf{M} \mathbf{K}_S & \mathbf{M} \mathbf{K}_I & \mathbf{A}_O + \mathbf{M} \mathbf{K}_S \end{bmatrix}, \quad (4.26)$$

where $\mathbf{M} = \mathbf{B}_O + \mathbf{K}_O \mathbf{D}_I - \mathbf{B}_1$.

First, introduce a change of coordinates to exploit the observability decomposition. Let \mathbf{T}_O be as in Eq. (4.16) and define $\mathbf{T} = \text{blkdiag}(\mathbf{I}, \mathbf{I}, \mathbf{T}_O)$. Premultiply and post-multiply Eq. (4.26) by \mathbf{T} and \mathbf{T}^{-1}

$$\begin{bmatrix} \mathbf{A} + \mathbf{B}_1 \mathbf{K}_S & \mathbf{B}_1 \mathbf{K}_I & \mathbf{B}_1 \mathbf{K}_S \mathbf{T}_O^{-1} \\ \mathbf{C}_e + \mathbf{D}_{e_1} \mathbf{K}_S & \mathbf{D}_{e_1} \mathbf{K}_I & \mathbf{D}_{e_1} \mathbf{K}_S \mathbf{T}_O^{-1} \\ \mathbf{T}_O (\mathbf{A}_O + \mathbf{K}_O \mathbf{C} - \mathbf{A} + \mathbf{M} \mathbf{K}_S) & \mathbf{T}_O \mathbf{M} \mathbf{K}_I & \mathbf{T}_O (\mathbf{A}_O + \mathbf{M} \mathbf{K}_S) \mathbf{T}_O^{-1} \end{bmatrix}. \quad (4.27)$$

Second, use observers (4.20) and (4.22) to define

$$\dot{\hat{\mathbf{z}}} = \mathbf{A}_z \hat{\mathbf{z}} + \mathbf{B}_z \mathbf{u} + \mathbf{K}_z \mathbf{y}, \quad (4.28)$$

where $\hat{\mathbf{z}} = \text{col}(\hat{\mathbf{z}}_{\text{NO}}, \hat{\mathbf{z}}_O)$ and

$$\mathbf{A}_z = \begin{bmatrix} \bar{\mathbf{A}}_{11} & \bar{\mathbf{A}}_{12} \\ \mathbf{0} & \bar{\mathbf{A}}_{22} - \bar{\mathbf{K}}_O \bar{\mathbf{C}}_2 \end{bmatrix}, \quad \mathbf{B}_z = \mathbf{T}_O \mathbf{B}_1 - \bar{\mathbf{K}}_O \mathbf{D}_1, \quad \mathbf{K}_z = \begin{bmatrix} \mathbf{0} \\ \bar{\mathbf{K}}_O \end{bmatrix}.$$

Then, define $\mathbf{x}_O := \hat{\mathbf{x}}$ and compare Eqs. (1.17a) and (4.28) to identify $\mathbf{A}_O = \mathbf{T}_O^{-1} \mathbf{A}_z \mathbf{T}_O$, $\mathbf{B}_O = \mathbf{T}_O^{-1} \mathbf{B}_z$, and $\mathbf{K}_O = \mathbf{T}_O^{-1} \mathbf{K}_z$. As a consequence, $\mathbf{M} = \mathbf{0}$ and $\mathbf{A}_O = \mathbf{A} - \mathbf{K}_O \mathbf{C}$, which reduce matrix (4.27) to

$$\begin{bmatrix} \mathbf{A} + \mathbf{B}_1 \mathbf{K}_S & \mathbf{B}_1 \mathbf{K}_I & \mathbf{B}_1 \mathbf{K}_S \mathbf{T}_O^{-1} \\ \mathbf{C}_e + \mathbf{D}_{e1} \mathbf{K}_S & \mathbf{D}_{e1} \mathbf{K}_I & \mathbf{D}_{e1} \mathbf{K}_S \mathbf{T}_O^{-1} \\ \mathbf{0} & \mathbf{0} & \mathbf{A}_z \end{bmatrix}. \quad (4.29)$$

This matrix is Hurwitz because its eigenvalues correspond to the union of the eigenvalues of the main diagonal blocks. Indeed, \mathbf{A}_z is Hurwitz thanks to Assumption 4.2 and the design of observer (4.20). Moreover,

$$\begin{bmatrix} \mathbf{A} + \mathbf{B}_1 \mathbf{K}_S & \mathbf{B}_1 \mathbf{K}_I \\ \mathbf{C}_e + \mathbf{D}_{e1} \mathbf{K}_S & \mathbf{D}_{e1} \mathbf{K}_I \end{bmatrix}$$

is Hurwitz thanks to Assumption 4.1 and the design of stabilizer (4.11).

Important

The triangular structure of (4.29) lets the design of matrices \mathbf{K}_S and \mathbf{K}_I be independent of $\bar{\mathbf{K}}_O$. This design feature is called the *separation principle*.

4.5.1 Minimal Stabilizer

The output-feedback stabilizer (4.24), (4.25), and (4.28) requires implementing a dynamic system of the same order as the plant. Moreover, Assumptions 4.1 and 4.2 allow the state feedback to be simpler to assure the stability of the reachable and observable subpart of \mathbf{x} only. In particular, thanks to the introduction of a change of coordinates called *ultimate Kalman decomposition* ([2], Sect. 6), this section highlights that the goal G1 is achieved with observer (4.20) (eventually reduced as in Infobox 4.6) and by a suitable subpart of \mathbf{K}_R .

The concepts of reachability and unobservability and their relative decompositions can be jointly exploited to find a transformation, namely $\mathbf{z} = \mathbf{T}_K \mathbf{x}$, which highlights the reachable, unreachable, unobservable, and observable subsystems of (4.2). Let us identify the following subspaces:

- reachable and unobservable $\mathcal{X}_{R,\text{NO}} := \mathcal{R} \cap \mathcal{E}$ with basis $X_{R,\text{NO}}$;
- reachable and observable $\mathcal{X}_{R,O} := \mathcal{X}_{R,\text{NO}}^\perp \cap \mathcal{R}$ with basis $X_{R,O}$;
- unreachable and unobservable $\mathcal{X}_{NR,\text{NO}} := \mathcal{X}_{R,\text{NO}}^\perp \cap \mathcal{E}$ with basis $X_{NR,\text{NO}}$;

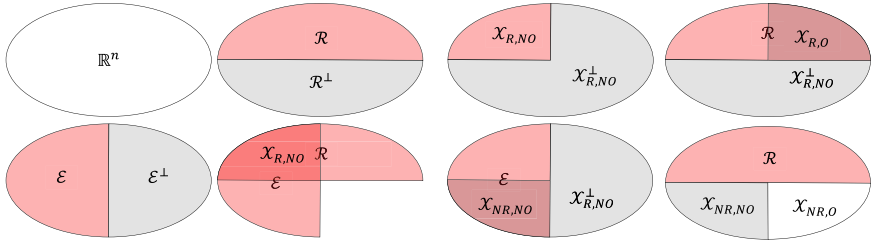


Fig. 4.5 Graphical representation of the sequence of intersections exploited to find the ultimate Kalman decomposition of LTI systems

- unreachable and observable $\mathcal{X}_{NR,O} := (\mathcal{R} \cup \mathcal{X}_{NR,NO})^\perp$ with basis $X_{NR,O}$,

whose derivation is supported by the Venn diagram of Fig. 4.5.

The transformation \mathbf{T}_K is then defined as

$$\mathbf{T}_K^{-1} = [X_{R,NO} \ X_{R,O} \ X_{NR,NO} \ X_{NR,O}],$$

which, applied to system (4.2), leads to

$$\begin{aligned} \dot{\mathbf{z}} &= \mathbf{T}_K \mathbf{A} \mathbf{T}_K^{-1} \mathbf{z} + \mathbf{T}_K \mathbf{B}_1 \mathbf{u} + \mathbf{T}_K \mathbf{B}_2 \mathbf{w} \quad \mathbf{z}(t_0) = \mathbf{T}_K \mathbf{x}_0 \\ \mathbf{y} &= \mathbf{C} \mathbf{T}_K^{-1} \mathbf{z} + \mathbf{D}_1 \mathbf{u} + \mathbf{D}_2 \mathbf{w}. \end{aligned} \quad (4.30)$$

A study of $\bar{\mathbf{A}} := \mathbf{T}_K \mathbf{A} \mathbf{T}_K^{-1}$, $\bar{\mathbf{B}}_1 := \mathbf{T}_K \mathbf{B}$, and $\bar{\mathbf{C}} := \mathbf{C} \mathbf{T}_K^{-1}$ reveals that

$$\begin{aligned} \bar{\mathbf{A}} &= \begin{bmatrix} \bar{\mathbf{A}}_{11} & \bar{\mathbf{A}}_{12} & \bar{\mathbf{A}}_{13} & \bar{\mathbf{A}}_{14} \\ \mathbf{0} & \bar{\mathbf{A}}_{22} & \mathbf{0} & \bar{\mathbf{A}}_{24} \\ \mathbf{0} & \mathbf{0} & \bar{\mathbf{A}}_{33} & \bar{\mathbf{A}}_{34} \\ \mathbf{0} & \mathbf{0} & \mathbf{0} & \bar{\mathbf{A}}_{44} \end{bmatrix}, \quad \bar{\mathbf{B}}_1 = \begin{bmatrix} \bar{\mathbf{B}}_{11} \\ \bar{\mathbf{B}}_{12} \\ \mathbf{0} \\ \mathbf{0} \end{bmatrix}, \quad \bar{\mathbf{B}}_2 = \begin{bmatrix} \bar{\mathbf{B}}_{21} \\ \bar{\mathbf{B}}_{22} \\ \bar{\mathbf{B}}_{23} \\ \bar{\mathbf{B}}_{24} \end{bmatrix} \\ \bar{\mathbf{C}} &= [\mathbf{0} \ \bar{\mathbf{C}}_2 \ \mathbf{0} \ \bar{\mathbf{C}}_4]. \end{aligned}$$

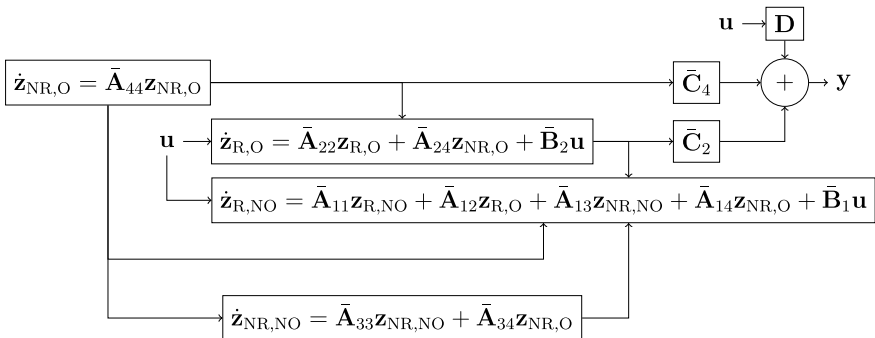


Fig. 4.6 The ultimate Kalman decomposition highlights the reachable and observable parts of systems. The input affects only the reachable parts, whereas the observable ones contribute only to the output

Let the state \mathbf{z} be divided in four parts as

$$\mathbf{z} = \text{col} (\mathbf{z}_{R,NO}, \mathbf{z}_{R,O}, \mathbf{z}_{NR,NO}, \mathbf{z}_{NR,O}),$$

then the dynamics of \mathbf{z} is given by (Fig. 4.6)

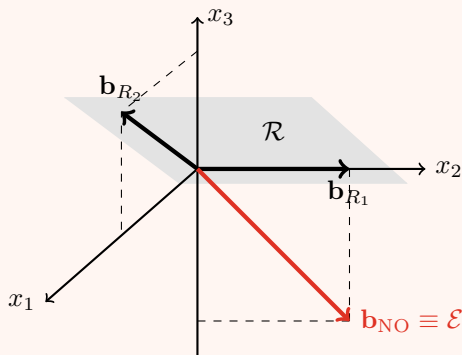
$$\begin{aligned}\dot{\mathbf{z}}_{R,NO} &= \bar{\mathbf{A}}_{11}\mathbf{z}_{R,NO} + \bar{\mathbf{A}}_{12}\mathbf{z}_{R,O} + \bar{\mathbf{A}}_{13}\mathbf{z}_{NR,NO} + \bar{\mathbf{A}}_{14}\mathbf{z}_{NR,O} + \bar{\mathbf{B}}_{11}\mathbf{u} + \bar{\mathbf{B}}_{21}\mathbf{w} \\ \dot{\mathbf{z}}_{R,O} &= \bar{\mathbf{A}}_{22}\mathbf{z}_{R,O} + \bar{\mathbf{A}}_{24}\mathbf{z}_{NR,O} + \bar{\mathbf{B}}_{12}\mathbf{u} + \bar{\mathbf{B}}_{22}\mathbf{w} \\ \dot{\mathbf{z}}_{NR,NO} &= \bar{\mathbf{A}}_{33}\mathbf{z}_{NR,NO} + \bar{\mathbf{A}}_{34}\mathbf{z}_{NR,O} + \bar{\mathbf{B}}_{23}\mathbf{w} \\ \dot{\mathbf{z}}_{NR,O} &= \bar{\mathbf{A}}_{44}\mathbf{z}_{NR,O} + \bar{\mathbf{B}}_{24}\mathbf{w} \\ \mathbf{y} &= \bar{\mathbf{C}}_2\mathbf{z}_{R,O} + \bar{\mathbf{C}}_4\mathbf{z}_{NR,O} + \mathbf{D}_1\mathbf{u} + \mathbf{D}_2\mathbf{w}.\end{aligned}$$

Example 4.13 (*Ultimate Kalman decomposition*) Let matrices \mathbf{A} , \mathbf{B} , and \mathbf{C} be those of Examples 4.4 and 4.11. Then, the basis of reachable and unobservable subspaces are

$$\{\mathbf{b}_{R_1}, \mathbf{b}_{R_2}\} = \left\{ \begin{pmatrix} 0 \\ 1 \\ 0 \end{pmatrix}, \begin{pmatrix} 1 \\ 0 \\ 1 \end{pmatrix} \right\}, \quad \mathbf{b}_{NO} = \begin{pmatrix} 0 \\ 1 \\ -1 \end{pmatrix}.$$

As illustrated in the following picture, the intersection of the reachable and non-observable subspaces is trivial and corresponds to the origin, i.e., $\mathcal{X}_{R,NO} = \mathcal{R} \cap \mathcal{E} = \{0\}$. Consequently, the ultimate Kalman decomposition does not highlight any reachable but non-observable subsystem. Moreover, since $\mathcal{X}_{R,NO}^\perp = \mathbb{R}^3$, $\mathcal{X}_{R,O} = \mathcal{X}_{R,NO}^\perp \cap \mathcal{R} = \mathcal{R}$ and $\mathcal{X}_{NR,NO} = \mathcal{X}_{R,NO}^\perp \cap \mathcal{E} = \mathcal{E}$. In conclusion, since $\mathcal{R} \cup \mathcal{X}_{NR,NO} = \mathbb{R}^3$, the subspace $\mathcal{X}_{NR,O} = \{0\}$ and then

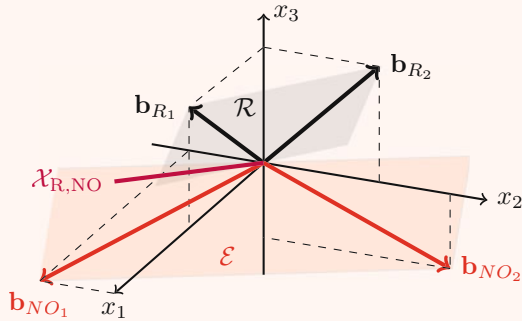
$$\mathbf{T}_K^{-1} = [\mathbf{b}_{R_1} \ \mathbf{b}_{R_2} \ \mathbf{b}_{NO}].$$



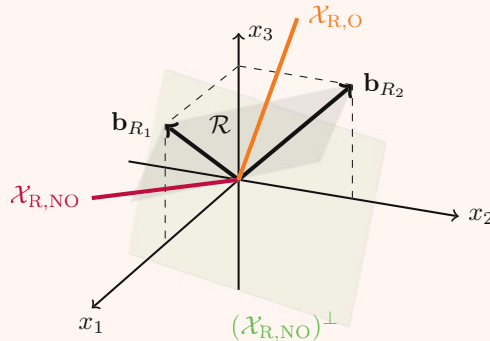
The application of \mathbf{T}_K to matrices \mathbf{A} , \mathbf{B} , and \mathbf{C} defined in Examples 4.4 and 4.11, leads to

$$\bar{\mathbf{A}} = \begin{bmatrix} 0 & 0 & 0 \\ 1 & 1 & 0 \\ 0 & 0 & -1 \end{bmatrix}, \quad \bar{\mathbf{B}} = \begin{bmatrix} 1 \\ 0 \\ 0 \end{bmatrix}, \quad \mathbf{C} = [0 \ 1 \ 0].$$

Example 4.14 (Ultimate Kalman decomposition) Assume that the reachability and unobservability subspaces of an LTI system have basis $im(\mathbf{R}) = [\mathbf{b}_{\mathbf{R}1} \ \mathbf{b}_{\mathbf{R}2}]$ and $ker(\mathbf{O}) = [\mathbf{b}_{NO_1} \ \mathbf{b}_{NO_2}]$, respectively. The following figure depicts the subspaces geometry.

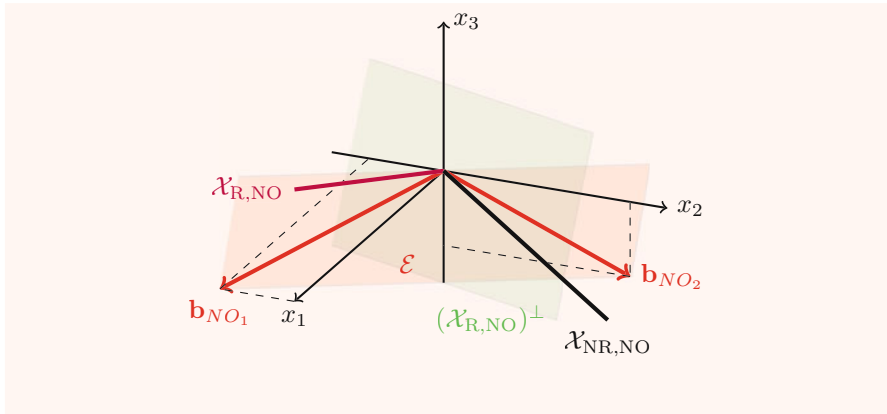


The intersection $X_{R,NO} = \mathcal{R} \cap \mathcal{E}$ represents the unique line that belongs to both \mathcal{R} and \mathcal{E} . Moreover, the orthogonal to $X_{R,NO}$, drawn as a green plane in the following figure, intersects the reachable set and provides $X_{R,O} = (X_{R,NO})^\perp \cap \mathcal{R}^+$, whose basis is $X_{R,O}$.



Finally, the intersection between $(X_{R,NO})^\perp$ and \mathcal{E} generates $X_{NR,NO}$, whose basis is $X_{NR,NO}$. Then, the transformation matrix is

$$\mathbf{T}_K^{-1} = [X_{R,NO} \ X_{R,O} \ X_{NR,NO}].$$



Example 4.15 (Ultimate Kalman decomposition) The following matrices identify an LTI system:

$$\mathbf{A} = \begin{bmatrix} 7 & 5 & -1 \\ -3 & -1 & -1 \\ 2 & 2 & 0 \end{bmatrix}, \quad \mathbf{B} = \begin{bmatrix} 2 \\ -1 \\ 1 \end{bmatrix}, \quad \mathbf{C} = [1 \ 1 \ -1].$$

This system is neither fully reachable nor fully observable because the reachability and observability matrices,

$$\mathbf{R} = \begin{bmatrix} 2 & 8 & 24 \\ -1 & -6 & -20 \\ 1 & 2 & 4 \end{bmatrix}, \quad \mathbf{O} = \begin{bmatrix} 1 & 1 & -1 \\ 2 & 2 & -2 \\ 4 & 4 & -4 \end{bmatrix},$$

have rank = 2 and rank = 1, respectively. Define $\text{im}(\mathbf{R}) = [\mathbf{b}_{R_1} \ \mathbf{b}_{R_2}]$ and $\text{ker}(\mathbf{O}) = [\mathbf{b}_{NO_1} \ \mathbf{b}_{NO_2}]$ with

$$[\mathbf{b}_{R_1} \ \mathbf{b}_{R_2}] = \begin{bmatrix} 1 & 0 \\ 0 & 1 \\ 1 & 1 \end{bmatrix}, \quad [\mathbf{b}_{NO_1} \ \mathbf{b}_{NO_2}] = \begin{bmatrix} 1 & 0 \\ 0 & 1 \\ 1 & 1 \end{bmatrix}.$$

Since these two bases are equal, the reachable and unobservable subspaces coincide, i.e., $\mathcal{R} \equiv \mathcal{E}$ and thus $\mathcal{X}_{R,NO} = \mathcal{R} \cap \mathcal{E} = \mathcal{R}$. As a consequence $\mathcal{X}_{R,O} = (\mathcal{X}_{R,NO})^\perp \cap \mathcal{R} = \{0\}$ as well as $\mathcal{X}_{NR,NO} = (\mathcal{X}_{R,NO})^\perp \cap \mathcal{E} = \{0\}$. Therefore, the only non-trivial subspace further than $\mathcal{X}_{R,NO}$ is $\mathcal{X}_{NR,O} = (\mathcal{X}_{R,NO})^\perp$. In this case, $X_{NR,O} = \text{col}(1, 1, -1)$ represents a basis for $\mathcal{X}_{NR,O}$. Finally, the transformation matrix is

$$\mathbf{T}_K^{-1} = \begin{bmatrix} 1 & 0 & 1 \\ 0 & 1 & 1 \\ 1 & 1 & -1 \end{bmatrix}$$

which applied to matrices \mathbf{A} , \mathbf{B} , and \mathbf{C} leads to

$$\bar{\mathbf{A}} = \begin{bmatrix} 6 & 4 & 11 \\ -4 & -2 & -5 \\ 0 & 0 & 2 \end{bmatrix}, \quad \bar{\mathbf{B}} = \begin{bmatrix} 2 \\ -1 \\ 0 \end{bmatrix}, \quad \mathbf{C} = [0 \ 0 \ 3].$$

Example 4.16 (*Cart-pole ultimate Kalman decomposition*) The bases of reachability and unobservability subspaces of the cart-pole, modeled in Example 1.2, have been studied in Examples 4.3 and 4.12. In more detail, they are

$$im(\mathbf{R}) = \mathbf{I} \in \mathbb{R}^{4 \times 4}, \quad ker(\mathbf{O}) = \begin{bmatrix} 1 \\ 0 \\ 0 \\ 0 \end{bmatrix}.$$

Then, the $X_{R,NO}$ represents the intersection between line $ker(\mathbf{O})$ and the whole 4D space. This intersection leads to

$$X_{R,NO} = \begin{bmatrix} 1 \\ 0 \\ 0 \\ 0 \end{bmatrix}, \quad X_{R,NO}^\perp = \begin{bmatrix} 0 & 0 & 0 \\ 1 & 0 & 0 \\ 0 & 1 & 0 \\ 0 & 0 & 1 \end{bmatrix}.$$

Also, the intersections of $X_{R,NO}^\perp$ with \mathcal{R} and \mathcal{E} lead to

$$X_{R,O} = \begin{bmatrix} 0 & 0 & 0 \\ 1 & 0 & 0 \\ 0 & 1 & 0 \\ 0 & 0 & 1 \end{bmatrix}, \quad X_{NR,NO} = \begin{bmatrix} 0 \\ 0 \\ 0 \\ 0 \end{bmatrix}.$$

Finally, $X_{NR,O}$ is orthogonal to the union of \mathcal{R} with $X_{NR,NO}$, whose basis is $Im(\mathcal{R} \cup X_{NR,NO}) = \mathbf{I} \in \mathbb{R}^{4 \times 4}$. Then, the basis of its orthogonal is represented by the origin, i.e., $X_{NR,O} = \mathbf{0}$. The ultimate Kalman decomposition is finally obtained as

$$\mathbf{T}_K^{-1} = [X_{R,NO} \ X_{R,O}] = \left[\begin{pmatrix} 1 \\ 0 \\ 0 \\ 0 \end{pmatrix} \begin{pmatrix} 0 & 0 & 0 \\ 1 & 0 & 0 \\ 0 & 1 & 0 \\ 0 & 0 & 1 \end{pmatrix} \right].$$

The subsystem

$$\begin{aligned} \dot{\mathbf{z}}_{R,O} &= \bar{\mathbf{A}}_{22}\mathbf{z}_{R,O} + \bar{\mathbf{A}}_{24}\mathbf{z}_{NR,O} + \bar{\mathbf{B}}_{12}\mathbf{u} + \bar{\mathbf{B}}_{22}\mathbf{w} \\ \dot{\mathbf{z}}_{NR,O} &= \bar{\mathbf{A}}_{44}\mathbf{z}_{NR,O} + \bar{\mathbf{B}}_{24}\mathbf{w} \\ \mathbf{y} &= \bar{\mathbf{C}}_2\mathbf{z}_{R,O} + \bar{\mathbf{C}}_4\mathbf{z}_{NR,O} + \mathbf{D}_1\mathbf{u} + \mathbf{D}_2\mathbf{w} \end{aligned} \tag{4.31}$$

is of interest because it is the only part that influences the output and, thanks to Assumption 1.3, the regulated output.

Infobox 4.7 (Transfer matrix) *Transfer functions only consider the reachable and observable part of LTI systems [1, 6]. Indeed, the term $\mathbf{z}_{NR,O}$ is regarded as an external input for system (4.31), which is not involved in the input–output relation between \mathbf{u} and \mathbf{y} . So, the transfer matrix is*

$$\mathbf{G}(s) := \frac{\mathbf{Y}(s)}{\mathbf{U}(s)} = \bar{\mathbf{C}}_2 (s\mathbf{I} - \bar{\mathbf{A}}_{22})^{-1} \bar{\mathbf{B}}_{12} + \mathbf{D}_1.$$

It is worth noting that $\mathbf{z}_{R,O}$ and $\mathbf{z}_{NR,O}$ influence the output. $\mathbf{z}_{NR,O}$ represents a known signal (thanks to the existence of the observer) whose dynamics cannot be modified by the control action. Since the couple $(\bar{\mathbf{A}}_{22}, \bar{\mathbf{B}}_{12})$ is fully reachable by definition, a matrix $\mathbf{K}_{R,O}$ exists such that $\bar{\mathbf{A}}_{22} + \bar{\mathbf{B}}_{12}\mathbf{K}_{R,O}$ is Hurwitz, thus implying that the state $\mathbf{z}_{R,O}$ is bounded if $\mathbf{z}_{NR,O}$ is so too. In turn, this is true if Assumption 4.1 is verified. Then, the minimal stabilizer becomes

$$\begin{bmatrix} \dot{\mathbf{z}}_{R,O} \\ \dot{\mathbf{z}}_{NR,O} \end{bmatrix} = \left(\begin{bmatrix} \bar{\mathbf{A}}_{22} & \bar{\mathbf{A}}_{24} \\ \mathbf{0} & \bar{\mathbf{A}}_{44} \end{bmatrix} - \bar{\mathbf{K}}_O [\bar{\mathbf{C}}_2 \bar{\mathbf{C}}_4] \right) \begin{bmatrix} \mathbf{z}_{R,O} \\ \mathbf{z}_{NR,O} \end{bmatrix} + \begin{bmatrix} \bar{\mathbf{B}}_{12} \\ \mathbf{0} \end{bmatrix} \mathbf{u} + \bar{\mathbf{K}}_O \mathbf{y}$$

$$\mathbf{u}_S = \mathbf{K}_{R,O} \mathbf{z}_{R,O}. \quad (4.32)$$

Important

The overall closed-loop system can be made BIBS-stable if matrices $\bar{\mathbf{A}}_{11}$, $\bar{\mathbf{A}}_{33}$, and $\bar{\mathbf{A}}_{44}$ are Hurwitz, i.e., if the plant is detectable and stabilizable.

Example 4.17 (*Cart-pole stabilizer*) The ultimate Kalman decomposition of Example 4.16 applied to the plant of Example 1.2 shows that the first state is reachable but not observable. In contrast, the last three states are reachable and observable. Formally, the system, in the ultimate Kalman decomposition, is

$$\begin{bmatrix} \dot{\mathbf{z}}_{R,NO} \\ \dot{\mathbf{z}}_{R,O} \end{bmatrix} = \begin{bmatrix} \bar{a}_{11} & \bar{\mathbf{A}}_{12} \\ \mathbf{0} & \bar{\mathbf{A}}_{22} \end{bmatrix} \begin{bmatrix} \mathbf{z}_{R,NO} \\ \mathbf{z}_{R,O} \end{bmatrix} + \begin{bmatrix} 0 \\ \bar{\mathbf{B}}_2 \end{bmatrix} \mathbf{u}$$

$$\mathbf{y} = [0 \ \bar{\mathbf{C}}_2] \begin{bmatrix} \mathbf{z}_{R,NO} \\ \mathbf{z}_{R,O} \end{bmatrix}$$

in which the contribution of the disturbances has been neglected. The output-feedback stabilizer is given by

$$\dot{\mathbf{z}}_{R,O} = (\bar{\mathbf{A}}_{22} - \mathbf{K}_O \bar{\mathbf{C}}_2 + \bar{\mathbf{B}}_2 \mathbf{K}_S) \hat{\mathbf{z}}_{R,O} + \mathbf{K}_O \mathbf{y}$$

$$\mathbf{u} = \mathbf{K}_{R,O} \hat{\mathbf{z}}_{R,O}.$$

4.5.2 Robustness to Disturbance and Noise

Previous sections demonstrate that controller (4.24), (4.25), and (4.28), extended with the integral action (4.11), makes the closed-loop plant BIBS-stable. Moreover, assuming a fully reachable and observable plant, the eigenvalues of system (4.2) can

be assigned through the design of the matrices \mathbf{K}_S , \mathbf{K}_I , and \mathbf{K}_O . Thus, one could be tempted to push on the feedback gains to make the control system as reactive as desired and to reduce the asymptotic bound of the regulated output (see control goal G2). But unfortunately, the presence of measurement noises deeply impacts the design of \mathbf{K}_S , \mathbf{K}_I , and \mathbf{K}_O , as well as the asymptotic values of the state and regulated output. In particular, let

$$\begin{aligned}\dot{\mathbf{x}} &= \mathbf{Ax} + \mathbf{B}_1\mathbf{u} + \mathbf{B}_2\mathbf{d} \\ \dot{\hat{\mathbf{x}}} &= (\mathbf{A} - \mathbf{K}_O\mathbf{C})\hat{\mathbf{x}} + (\mathbf{B}_1 - \mathbf{K}_O\mathbf{D}_1)\mathbf{u} + \mathbf{K}_O\mathbf{y} \\ \dot{\boldsymbol{\eta}} &= \mathbf{C}_e\mathbf{x} + \mathbf{D}_{e1}\mathbf{u} + \mathbf{E}\boldsymbol{\nu} \\ \mathbf{u} &= \mathbf{K}_S\hat{\mathbf{x}} + \mathbf{K}_I\boldsymbol{\eta} \\ \mathbf{y} &= \mathbf{Cx} + \mathbf{D}_1\mathbf{u} + \boldsymbol{\nu}\end{aligned}\tag{4.33}$$

be a fully observable and reachable LTI plant, subject to disturbances and measurement noises, controlled by an output-feedback stabilizer plus an integral action where \mathbf{d} denotes the exogenous disturbance and $\boldsymbol{\nu}$ is the measurement noise. Define the estimation error as $\mathbf{e}_x = \hat{\mathbf{x}} - \mathbf{x}$, let

$$\mathbf{A}_{cl} := \begin{bmatrix} \mathbf{A} + \mathbf{B}_1\mathbf{K}_S & \mathbf{B}_1\mathbf{K}_I \\ \mathbf{C}_e + \mathbf{D}_{e1}\mathbf{K}_S & \mathbf{D}_{e1}\mathbf{K}_I \end{bmatrix},$$

and use the expressions of \mathbf{y} and \mathbf{u} to rewrite system (4.33) as

$$\begin{bmatrix} \dot{\mathbf{x}} \\ \dot{\boldsymbol{\eta}} \end{bmatrix} = \mathbf{A}_{cl} \begin{bmatrix} \mathbf{x} \\ \boldsymbol{\eta} \end{bmatrix} + \begin{bmatrix} \mathbf{B}_1\mathbf{K}_S \\ \mathbf{D}_{e1}\mathbf{K}_S \end{bmatrix} \mathbf{e}_x + \begin{bmatrix} \mathbf{B}_2 & \mathbf{0} \\ \mathbf{0} & \mathbf{E} \end{bmatrix} \begin{bmatrix} \mathbf{d} \\ \boldsymbol{\nu} \end{bmatrix}$$

$$\dot{\mathbf{e}}_x = (\mathbf{A} - \mathbf{K}_O\mathbf{C})\mathbf{e}_x - \mathbf{B}_2\mathbf{d} + \mathbf{K}_O\boldsymbol{\nu},$$

whose solution is

$$\begin{bmatrix} \mathbf{x}(t) \\ \boldsymbol{\eta}(t) \end{bmatrix} = \int_0^t e^{\mathbf{A}_{cl}(t-\tau)} \left(\begin{bmatrix} \mathbf{B}_1\mathbf{K}_S \\ \mathbf{D}_{e1}\mathbf{K}_S \end{bmatrix} \mathbf{e}_x(\tau) + \begin{bmatrix} \mathbf{B}_2 & \mathbf{0} \\ \mathbf{0} & \mathbf{E} \end{bmatrix} \begin{bmatrix} \mathbf{d}(\tau) \\ \boldsymbol{\nu}(\tau) \end{bmatrix} \right) d\tau$$

$$\mathbf{e}_x(t) = \int_0^t e^{(\mathbf{A} - \mathbf{K}_O\mathbf{C})(t-\tau)} (-\mathbf{B}_2\mathbf{d}(\tau) + \mathbf{K}_O\boldsymbol{\nu}(\tau)) d\tau,$$

where, without loss of generality, $(\mathbf{x}(0), \boldsymbol{\eta}(0)) := (\mathbf{0}, \mathbf{0})$ and $\mathbf{e}_x(0) := \mathbf{0}$. Then, assume that the norms of disturbance and noise are uniformly bounded by \bar{d} and $\bar{\nu}$ respectively, i.e., $\|\mathbf{d}(t)\| \leq \bar{d}$ and $\|\boldsymbol{\nu}(t)\| \leq \bar{\nu}$ for all $t \geq 0$. Then, the norm of $\mathbf{x}(t)$, $\boldsymbol{\eta}(t)$, and $\mathbf{e}_x(t)$ are bounded as

$$\begin{aligned}\left\| \begin{bmatrix} \mathbf{x}(t) \\ \boldsymbol{\eta}(t) \end{bmatrix} \right\| &\leq \frac{1}{\underline{\sigma}(\mathbf{A}_{cl})} \left(\bar{\sigma} \left(\begin{bmatrix} \mathbf{B}_1\mathbf{K}_S \\ \mathbf{D}_{e1}\mathbf{K}_S \end{bmatrix} \right) \bar{e} + \bar{\sigma}(\mathbf{B}_2) \bar{d} + \bar{\sigma}(\mathbf{E}) \bar{\nu} \right) \\ \|\mathbf{e}_x(t)\| &\leq \bar{e},\end{aligned}\tag{4.34}$$

with $\bar{e} = [\underline{\sigma}(\mathbf{A} - \mathbf{K}_O\mathbf{C})]^{-1} (\bar{\sigma}(\mathbf{B}_2)\bar{d} + \bar{\sigma}(\mathbf{K}_O)\bar{\nu})$. A more aggressive observer feedback \mathbf{K}_O cannot attenuate the effects of $\boldsymbol{\nu}$ on \mathbf{e}_x . Indeed, a larger \mathbf{K}_O (possibly) leads to larger $\underline{\sigma}(\mathbf{A} - \mathbf{K}_O\mathbf{C})$ and $\bar{\sigma}(\mathbf{K}_O)$. Then, increasing \mathbf{K}_O such that

$\underline{\sigma}(\mathbf{A} - \mathbf{K}_O \mathbf{C}) \approx \underline{\sigma}(\mathbf{K}_O \mathbf{C})$ leads to $\bar{e} \approx [\underline{\sigma}(\mathbf{K}_O \mathbf{C})]^{-1} (\bar{\sigma}(\mathbf{B}_2) \bar{d} + \bar{\sigma}(\mathbf{K}_O))$, which cannot be arbitrarily reduced with a suitable design of \mathbf{K}_O because of $\underline{\sigma}(\mathbf{K}_O) \leq \bar{\sigma}(\mathbf{K}_O)$. The same argument demonstrates that increasing \mathbf{K}_S does not attenuate the effects of ν on $\|(\mathbf{x}(t), \boldsymbol{\eta}(t))\|$. Conversely, more aggressive feedback \mathbf{K}_O , \mathbf{K}_S , and \mathbf{K}_I could attenuate the effects of \mathbf{d} on the norm of \mathbf{x} and $\boldsymbol{\eta}$ because, according to the first of Eqs. (4.34), the disturbance amplification is inversely proportional to $\bar{\sigma}(\mathbf{B}_2)/\underline{\sigma}(\mathbf{A}_{Cl})$.

In conclusion, the BIBS stability properties guaranteed by the output feedback (4.11), (4.24), (4.25), and (4.28) make the state and the estimation error bounded even in the presence of disturbances and noises. Unfortunately, $\|(\mathbf{x}(t), \boldsymbol{\eta}(t))\|$ and $\|\mathbf{e}_x(t)\|$ cannot be arbitrarily reduced through high-gain policy. In detail, more aggressive \mathbf{K}_S and \mathbf{K}_I could attenuate the effects of disturbances. Conversely, increasing \mathbf{K}_S , \mathbf{K}_I , and \mathbf{K}_O may not lead to any noise attenuation. Chapter 5 presents an optimal criterion for designing \mathbf{K}_S , \mathbf{K}_I , and \mathbf{K}_O .

4.5.3 Limitations on the Stabilization of Nonlinear Systems

The output-feedback controller (4.11), (4.24), (4.25), and (4.28) guarantees $\tilde{\mathbf{x}} = \mathbf{0}$ to be a globally (i.e., for any initial condition) exponentially stable equilibrium point for the linearized plant (1.14). On the other hand, it is worth remembering that system (1.14) represents a linearization of system (1.1) in the neighborhood of \mathbf{x}_0 . Then, it seems natural to try to transfer the stability properties of the origin of the linearized system to the equilibrium of the nonlinear one. Let

$$\begin{aligned}\dot{\mathbf{x}} &= \mathbf{f}(\mathbf{x}, \mathbf{u}, \mathbf{w}) & \mathbf{x}(t_0) &= \mathbf{x}_0 \\ \mathbf{y} &= \mathbf{h}(\mathbf{x}, \mathbf{u}, \mathbf{w}) \\ \mathbf{e} &= \mathbf{h}_e(\mathbf{x}, \mathbf{u}, \mathbf{w})\end{aligned}\tag{4.35}$$

be a nonlinear plant which is assumed completely observable and reachable, as for the definitions of earlier in this section. Then, for systems such as (4.35), which are locally completely reachable and observable, it is possible to transfer the stability properties of the origin of the linearized system to the equilibrium point of the nonlinear system. This result is constrained by the domains of the initial conditions and exogenous signals whose size depends on the controller parameters ([5], Sect. 4.3).

In detail, assume a control system (4.35) with (4.11), (4.24), (4.25), and (4.28) designed on the equilibrium tuple $(\mathbf{x}_0, \mathbf{u}_0, \mathbf{w}_0, \mathbf{y}_0)$. First, change the coordinates to

$$\tilde{\mathbf{x}} := \mathbf{x} - \mathbf{x}_0, \quad \tilde{\mathbf{u}} := \mathbf{u} - \mathbf{u}_0, \quad \tilde{\mathbf{w}} := \mathbf{w} - \mathbf{w}_0, \quad \tilde{\mathbf{y}} := \mathbf{y} - \mathbf{y}_0$$

and rewrite system (4.35) as

$$\begin{aligned}\dot{\tilde{\mathbf{x}}} &= \tilde{\mathbf{f}}(\tilde{\mathbf{x}}, \tilde{\mathbf{u}}, \tilde{\mathbf{w}}) & \tilde{\mathbf{x}}(t_0) &= \tilde{\mathbf{x}}_0 \\ \tilde{\mathbf{y}} &= \tilde{\mathbf{h}}(\tilde{\mathbf{x}}, \tilde{\mathbf{u}}, \tilde{\mathbf{w}}) \\ \mathbf{e} &= \tilde{\mathbf{h}}_e(\tilde{\mathbf{x}}, \tilde{\mathbf{u}}, \tilde{\mathbf{w}}),\end{aligned}\tag{4.36}$$

in which

$$\begin{aligned}\tilde{\mathbf{f}}(\tilde{\mathbf{x}}, \tilde{\mathbf{u}}, \tilde{\mathbf{w}}) &:= \mathbf{f}(\tilde{\mathbf{x}} + \mathbf{x}_0, \tilde{\mathbf{u}} + \mathbf{u}_0, \tilde{\mathbf{w}} + \mathbf{w}_0) \\ \tilde{\mathbf{h}}(\tilde{\mathbf{x}}, \tilde{\mathbf{u}}, \tilde{\mathbf{w}}) &:= \mathbf{h}(\tilde{\mathbf{x}} + \mathbf{x}_0, \tilde{\mathbf{u}} + \mathbf{u}_0, \tilde{\mathbf{w}} + \mathbf{w}_0) \\ \tilde{\mathbf{h}}_e(\tilde{\mathbf{x}}, \tilde{\mathbf{u}}, \tilde{\mathbf{w}}) &:= \mathbf{h}_e(\tilde{\mathbf{x}} + \mathbf{x}_0, \tilde{\mathbf{u}} + \mathbf{u}_0, \tilde{\mathbf{w}} + \mathbf{w}_0).\end{aligned}$$

Second, write the closed loop as

$$\begin{aligned}\dot{\tilde{\mathbf{x}}} &= \tilde{\mathbf{f}}(\tilde{\mathbf{x}}, \tilde{\mathbf{u}}, \tilde{\mathbf{w}}) \\ \dot{\eta} &= \tilde{\mathbf{h}}_e(\tilde{\mathbf{x}}, \tilde{\mathbf{u}}, \tilde{\mathbf{w}}) \\ \dot{\hat{\mathbf{x}}} &= \mathbf{A}\hat{\mathbf{x}} + \mathbf{B}_1\tilde{\mathbf{u}} + \mathbf{K}_O(\tilde{\mathbf{y}} - \hat{\mathbf{y}}) \\ \tilde{\mathbf{u}} &= \mathbf{K}_S\hat{\mathbf{x}} + \mathbf{K}_I\eta \\ \hat{\mathbf{y}} &= \mathbf{C}\hat{\mathbf{x}} + \mathbf{D}_1\tilde{\mathbf{u}}.\end{aligned}\tag{4.37}$$

Define $\mathbf{e}_x = \hat{\mathbf{x}} - \tilde{\mathbf{x}}$, exploit the formulation of $\tilde{\mathbf{u}}$ and $\tilde{\mathbf{y}}$, and add and subtract $\mathbf{A}\tilde{\mathbf{x}} + \mathbf{B}_1\tilde{\mathbf{u}}$ and $\mathbf{C}_e\tilde{\mathbf{x}} + \mathbf{D}_{e1}\tilde{\mathbf{u}}$ to the first and second line of Eq. (4.37), respectively. Let $\bar{\mathbf{x}} := \text{col}(\tilde{\mathbf{x}}, \eta, \mathbf{e}_x)$ and compute its dynamics as

$$\dot{\bar{\mathbf{x}}} = \bar{\mathbf{A}}\bar{\mathbf{x}} + \mathbf{G}(\bar{\mathbf{x}}, \tilde{\mathbf{w}}),\tag{4.38}$$

where

$$\bar{\mathbf{A}} := \begin{bmatrix} \mathbf{A} + \mathbf{B}_1\mathbf{K}_S & \mathbf{B}_1\mathbf{K}_I & \mathbf{B}_1\mathbf{K}_S \\ \mathbf{C}_{e1} + \mathbf{D}_{e1}\mathbf{K}_S & \mathbf{D}_{e1}\mathbf{K}_I & \mathbf{D}_{e1}\mathbf{K}_S \\ \mathbf{0} & \mathbf{0} & \mathbf{A} - \mathbf{K}_O\mathbf{C} \end{bmatrix}$$

and

$$\begin{aligned}\mathbf{G}(\bar{\mathbf{x}}, \tilde{\mathbf{w}}) &:= \begin{bmatrix} \tilde{\mathbf{f}}(\tilde{\mathbf{x}}, \tilde{\mathbf{u}}, \tilde{\mathbf{w}}) - \mathbf{A}\tilde{\mathbf{x}} - \mathbf{B}_1\tilde{\mathbf{u}} \\ \tilde{\mathbf{h}}_e(\tilde{\mathbf{x}}, \tilde{\mathbf{u}}, \tilde{\mathbf{w}}) - \mathbf{C}_e\tilde{\mathbf{x}} - \mathbf{D}_{e1}\tilde{\mathbf{u}} \\ \mathbf{A}\tilde{\mathbf{x}} + \mathbf{B}_1\tilde{\mathbf{u}} - \tilde{\mathbf{f}}(\tilde{\mathbf{x}}, \tilde{\mathbf{u}}, \tilde{\mathbf{w}}) \end{bmatrix} \\ &\quad + \begin{bmatrix} \mathbf{0} \\ \mathbf{0} \\ \mathbf{K}_O \end{bmatrix} (\tilde{\mathbf{h}}(\tilde{\mathbf{x}}, \tilde{\mathbf{u}}, \tilde{\mathbf{w}}) - \mathbf{C}\tilde{\mathbf{x}} - \mathbf{D}_1\tilde{\mathbf{u}}).\end{aligned}$$

Define with $n_{\bar{x}}$ and n_w the dimensions of $\bar{\mathbf{x}}$ and $\tilde{\mathbf{w}}$. Then, since \mathbf{f} , \mathbf{h} , and \mathbf{h}_e are assumed to be locally Lipschitz, for any $\epsilon > 0$, $\mathbf{K}_S \in \mathbb{R}^{p \times n}$, and $\mathbf{K}_I \in \mathbb{R}^{p \times m}$, there exist $L_1, L_2 > 0$ such that, for any $(\bar{\mathbf{x}}, \tilde{\mathbf{w}}) \in \mathbb{R}^{n_{\bar{x}}} \times \mathbb{R}^{n_w}$ such that $\|(\bar{\mathbf{x}}, \tilde{\mathbf{w}})\| \leq \epsilon$, \mathbf{G} is bounded as

$$\|\mathbf{G}(\bar{\mathbf{x}}, \tilde{\mathbf{w}})\| \leq (L_1 + L_2\bar{\sigma}(\mathbf{K}_O))(\|\bar{\mathbf{x}}\|^2 + \|\tilde{\mathbf{w}}\|).$$

To compute a bound for the trajectories of system (4.38), rely on the support function $V(\bar{\mathbf{x}}) := \bar{\mathbf{x}}^\top \mathbf{P}\bar{\mathbf{x}}$ in which $\mathbf{P} = \mathbf{P}^\top \succ 0$ represents the solution to the so-called Lyapunov equation.

$$\mathbf{P}\bar{\mathbf{A}} + \bar{\mathbf{A}}^\top \mathbf{P} = -2\lambda I$$

for some $\lambda > 0$. Then, exploit Eq. (4.38) to calculate the time derivative of V as

$$\dot{V} = \frac{\partial V}{\partial \bar{\mathbf{x}}} \dot{\bar{\mathbf{x}}} = \dot{\bar{\mathbf{x}}}^\top \mathbf{P}\bar{\mathbf{x}} + \bar{\mathbf{x}}^\top \mathbf{P}\dot{\bar{\mathbf{x}}} = -\lambda\|\bar{\mathbf{x}}\|^2 + 2\bar{\mathbf{x}}^\top \mathbf{P}\mathbf{G}(\bar{\mathbf{x}}, \tilde{\mathbf{w}})\tag{4.39}$$

As a consequence, exploiting $\|\bar{\mathbf{x}}\|^2 = 2V$ and assuming $\bar{w} > 0$ such that $\|\tilde{\mathbf{w}}(t)\| \leq \bar{w}$ for all $t \geq 0$, \dot{V} can be bounded from above as

$$\dot{V} \leq 2\alpha V + \|\bar{\mathbf{x}}\|(L_1 + L_2\bar{\sigma}(\mathbf{K}_O))\bar{w}, \quad (4.40)$$

where $\alpha := (L_1 + L_2\bar{\sigma}(\mathbf{K}_O))\epsilon^2 - \lambda/\bar{\sigma}(\mathbf{P})$. Let $q \in (0, \lambda/\bar{\sigma}(\mathbf{P}))$, then ϵ is chosen to have $\alpha \in (-\lambda/\bar{\sigma}(\mathbf{P}), -q]$, i.e., $\epsilon^2 \leq (\lambda/\bar{\sigma}(\mathbf{P}) - q)/(L_1 + L_2\bar{\sigma}(\mathbf{K}_O))$. Then, Eq. (4.40) represents a linear system whose solution is

$$V(t) \leq V(\bar{\mathbf{x}}(0))e^{2\alpha t} + \epsilon \frac{L_1 + L_2\bar{\sigma}(\bar{\mathbf{K}}_O)}{2\alpha} \bar{w}. \quad (4.41)$$

Use $\|\bar{\mathbf{x}}\| \leq \sqrt{V/\underline{\sigma}(\mathbf{P})}$ and $V(\bar{\mathbf{x}}(0)) \leq \|\bar{\mathbf{x}}_0\|^2\bar{\sigma}(\mathbf{P})$ to bound the trajectories of $\bar{\mathbf{x}}$ as

$$\begin{aligned} \|\bar{\mathbf{x}}(t)\| &\leq \sqrt{\bar{\sigma}(\mathbf{P})V(\bar{\mathbf{x}}(0))e^{2\alpha t} + \epsilon \frac{L_1 + L_2\bar{\sigma}(\bar{\mathbf{K}}_O)}{\alpha} \bar{w}} \\ &\leq \sqrt{\frac{\bar{\sigma}(\mathbf{P})}{\underline{\sigma}(\mathbf{P})}} \|\bar{\mathbf{x}}_0\| e^{\alpha t} + \sqrt{\epsilon \frac{L_1 + L_2\bar{\sigma}(\bar{\mathbf{K}}_O)}{\alpha} \bar{w}}. \end{aligned} \quad (4.42)$$

To assure $\|\bar{\mathbf{x}}(t)\| \leq \epsilon$ for all $t \geq 0$ (and thus to make valid this investigation), define $\rho \in (0, \epsilon/2)$ and impose the following bounds on $\bar{\mathbf{x}}_0$ and $\tilde{\mathbf{w}}$:

$$\|\bar{\mathbf{x}}_0\| \leq \rho \sqrt{\frac{\sigma(\mathbf{P})}{\bar{\sigma}(\mathbf{P})}}, \quad \bar{w} \leq \min \left\{ \frac{\rho^2}{\epsilon} \frac{\alpha}{L_1 + L_2\bar{\sigma}(\bar{\mathbf{K}}_O)}, \epsilon \right\}.$$

To conclude, this section demonstrates that if the nonlinear plant is locally completely observable and reachable and in form (4.35), then the control via linearization makes the equilibrium \mathbf{x}_0 locally exponentially stable with restrictions on initial conditions and exogenous signals. Therefore, the trajectories of system (4.38) are guaranteed to exist within a bounded domain containing \mathbf{x}_0 .

4.6 Feed-Forward Control

As described in Sect. 1.2, a feed-forward action completes the control system. The feed-forward forces the plant to *anticipate* the reference variation independently of the current state [3]. This section presents a design strategy applicable to BIBS-stable plants or plants made BIBS-stable by a stabilizer. Let the stabilizer be a pure state feedback to reduce the topic presentation complexity without losing generality. Thus, let

$$\mathbf{u} = \mathbf{K}_S \mathbf{x} + \mathbf{u}_{FF} \quad (4.43)$$

be the complete control law whose \mathbf{K}_S is designed according to Sect. 4.2. Assuming $\mathbf{d} = \mathbf{0}$, the goal is to create \mathbf{u}_{FF} to assure $\lim_{t \rightarrow \infty} \mathbf{e}(t) = \mathbf{0}$. To achieve this result, introduce a further hypothesis, Assumption 4.3. If this latter is not verified, the set of trackable references is reduced, as detailed in Infobox 4.9.

Let

$$\begin{aligned}\dot{\mathbf{x}} &= \mathbf{Ax} + \mathbf{B}_1\mathbf{u} + \mathbf{B}_2\mathbf{r} & \mathbf{x}(t_0) = \mathbf{x}_0 \\ \mathbf{e} &= \mathbf{C}_e\mathbf{x} + \mathbf{D}_1\mathbf{u} + \mathbf{D}_2\mathbf{r}\end{aligned}\quad (4.44)$$

be a stabilizable LTI system. Let e_i , with $i = 1, \dots, m$, be the i -th entry of \mathbf{e} . Then, for each $i = 1, \dots, m$, determine r_{\max_i} as the smallest integer such that

$$\frac{d^{r_{\max_i}}}{dt^{r_{\max_i}}} e_i \propto \mathbf{m}_i \mathbf{u}$$

for some $\mathbf{m}_i \neq \mathbf{0}$.

Assumption 4.3 (*Vector relative degree*) Let (4.44) be an LTI plant with $\mathbf{D}_1 = \mathbf{0}$ and $\sum_{i=1}^m r_{\max_i} = n$.

Then, substitute (4.43) into (4.44)

$$\begin{aligned}\dot{\mathbf{x}} &= (\mathbf{A} + \mathbf{B}_1\mathbf{K}_S)\mathbf{x} + \mathbf{B}_1\mathbf{u}_{\text{FF}} + \mathbf{B}_2\mathbf{r} & \mathbf{x}(t_0) = \mathbf{x}_0 \\ \mathbf{e} &= \mathbf{C}_e\mathbf{x} + \mathbf{D}_2\mathbf{r}.\end{aligned}\quad (4.45)$$

Let $\mathbf{c}_{e,i}$ be the i -th row of \mathbf{C}_e and define $\zeta = \mathbf{T}_\zeta \mathbf{x}$ with

$$\mathbf{T}_\zeta := \text{col}(\mathbf{c}_{e,1}, \dots, \mathbf{c}_{e,1}\mathbf{A}^{r_{\max_1}-1}, \dots, \mathbf{c}_{e,m}, \dots, \mathbf{c}_{e,m}\mathbf{A}^{r_{\max_m}-1}). \quad (4.46)$$

Apply the change of coordinates (4.46) to system (4.45) to obtain

$$\begin{aligned}\dot{\zeta} &= \mathbf{T}_\zeta(\mathbf{A} + \mathbf{B}_1\mathbf{K}_S)\mathbf{T}_\zeta^{-1}\zeta + \mathbf{T}_\zeta\mathbf{B}_1\mathbf{u}_{\text{FF}} + \mathbf{T}_\zeta\mathbf{B}_2\mathbf{r} & \zeta(t_0) = \mathbf{T}_\zeta\mathbf{x}_0 \\ \mathbf{e} &= \mathbf{C}_e\mathbf{T}_\zeta^{-1}\zeta + \mathbf{D}_2\mathbf{r}.\end{aligned}\quad (4.47)$$

Let

$$\zeta := \text{col}(\zeta_1, \dots, \zeta_m) \quad (4.48)$$

and for each $i = 1, \dots, m$, define

$$\zeta_i = \text{col}(\zeta_{i,1}, \dots, \zeta_{i,r_{\max_i}}). \quad (4.49)$$

Then, let $\mathbf{d}_{2,i}$ be the i -th row of \mathbf{D}_2 and compute the dynamics of ζ_i as

$$\begin{aligned}\dot{\zeta}_{i,1} &= \zeta_{i,2} + \mathbf{c}_{e,i}\mathbf{B}_2\mathbf{r} \\ \dot{\zeta}_{i,2} &= \zeta_{i,3} + \mathbf{c}_{e,i}\mathbf{A}\mathbf{B}_2\mathbf{r} \\ &\vdots \\ \dot{\zeta}_{i,r_{\max_i}-1} &= \zeta_{i,r_{\max_i}} + \mathbf{c}_{e,i}\mathbf{A}^{r_{\max_i}-1}\mathbf{B}_2\mathbf{r} \\ \dot{\zeta}_{i,r_{\max_i}} &= \mathbf{c}_{e,i}\mathbf{A}^{r_{\max_i}-1}((\mathbf{A} + \mathbf{B}_1\mathbf{K}_S)\mathbf{T}_\zeta^{-1}\zeta + \mathbf{B}_1\mathbf{u}_{\text{FF}} + \mathbf{B}_2\mathbf{r}) \\ e_i &= \zeta_{i,1} + \mathbf{d}_{2,i}\mathbf{r}.\end{aligned}\quad (4.50)$$

Exploit Eq. (4.50) to define the reference state ζ_i^* such that $\zeta_i = \zeta_i^* \implies e_i = 0$, i.e.,

$$\begin{aligned}\zeta_{i,1}^* &:= -\mathbf{d}_{2,i}\mathbf{r} \\ \zeta_{i,2}^* &:= -\mathbf{d}_{2,i}\frac{d}{dt}\mathbf{r} - \mathbf{c}_{e,i}\mathbf{B}_2\mathbf{r} \\ &\vdots \\ \zeta_{i,r_{\max_i}}^* &:= -\mathbf{d}_{2,i}\frac{d^{r_{\max_i}-1}}{dt^{r_{\max_i}-1}}\mathbf{r} - \sum_{k=0}^{r_{\max_i}-2} \mathbf{c}_{e,i}\mathbf{A}^k\mathbf{B}_2\frac{d^{r_{\max_i}-2-k}}{dt^{r_{\max_i}-2-k}}\mathbf{r}.\end{aligned}\tag{4.51}$$

To conclude, let $\zeta^* := \text{col}(\zeta_1^*, \dots, \zeta_m^*)$, define \mathbf{H} such that

$$\mathbf{H}\dot{\zeta}^* = \text{col}(\dot{\zeta}_{1,r_{\max_1}}^*, \dots, \dot{\zeta}_{m,r_{\max_m}}^*),$$

take

$$\bar{\mathbf{M}} := \begin{bmatrix} \mathbf{c}_{e,1}\mathbf{A}^{r_{\max_1}-1} \\ \vdots \\ \mathbf{c}_{e,m}\mathbf{A}^{r_{\max_m}-1} \end{bmatrix},$$

and exploit Eq. (4.50), for $i = 1, \dots, m$, to write

$$\mathbf{H}\dot{\zeta}^* = \bar{\mathbf{M}}((\mathbf{A} + \mathbf{B}_1\mathbf{K}_S)\mathbf{T}_\zeta^{-1}\zeta^* + \mathbf{B}_1\mathbf{u}_{FF} + \mathbf{B}_2\mathbf{r}).\tag{4.52}$$

Assumption 4.4 The matrix $\mathbf{M} := \bar{\mathbf{M}}\mathbf{B}_1$ has m rows linearly independent. As a consequence, the Moore–Penrose right pseudo-inverse $\mathbf{M}^+ := \mathbf{M}^\top(\mathbf{M}\mathbf{M}^\top)^{-1}$ is well defined.

If Assumption 4.4 is verified, define $r_{\max} = \max\{r_{\max_1}, \dots, r_{\max_m}\}$ and compute the feed-forward law as

$$\begin{aligned}\mathbf{u}_{FF} &= \sum_{i=1}^{r_{\max}} \mathbf{D}_{FF_i} \frac{d^i}{dt^i} \mathbf{r} \\ &:= \mathbf{M}^+ \left(\mathbf{H}\dot{\zeta}^* - \bar{\mathbf{M}} \left((\mathbf{A} + \mathbf{B}_1\mathbf{K}_S)\mathbf{T}_\zeta^{-1}\zeta^* + \mathbf{B}_2\mathbf{r} \right) \right).\end{aligned}\tag{4.53}$$

Remark 4.2 The feed-forward control (4.53) represents an algebraic sum of the reference and its time derivatives. It also constitutes a subpart of system (1.17e), whose remaining elements are detailed in Infobox 4.9.

Infobox 4.8 (*Implementation in the original coordinates*) Define $\mathbf{x}^* = \mathbf{T}^{-1}\zeta^*$, exploit $\mathbf{M}^+\bar{\mathbf{M}}\mathbf{B}_1 = (\bar{\mathbf{M}}\mathbf{B}_1)^+\bar{\mathbf{M}}\mathbf{B}_1 = \mathbf{I}$, and rewrite Eq. (4.53) as

$$\mathbf{u}_{FF} = \mathbf{M}^+ \left(\mathbf{H}\dot{\mathbf{x}}^* - \bar{\mathbf{M}} \left(\mathbf{A}\mathbf{x}^* + \mathbf{B}_2\mathbf{r} \right) \right) - \mathbf{K}_S\mathbf{x}^*.$$

Then, the overall control law, which is the sum of the state-feedback stabilizer and feed-forward, becomes

$$\mathbf{u} = \mathbf{K}_S(\mathbf{x} - \mathbf{x}^*) + \mathbf{M}^+ (\mathbf{H}\mathbf{T}\dot{\mathbf{x}}^* - \bar{\mathbf{M}}(\mathbf{A}\mathbf{x}^* + \mathbf{B}_2\mathbf{r})).$$

Example 4.18 Let

$$\dot{x} = ax + bu$$

$$y = x$$

$$e = cx - dr(t)$$

be an LTI system where $a, b, c, d > 0$, x is the state, y the output, e the controlled output, and $r(t)$ represents the known reference value. Since the goal is steering $e \rightarrow 0$, it must be $x^* = (d/c)r(t)$. Note that $r_{\max} = 1$ and Assumption 4.3 is verified. Therefore, define $u = k_Rx + v$, with $k_R : a + b_1k_R < 0$, and v as

$$v = -[c(a + bk_R)^{-1}b]^{-1}dr(t) + b^{-1}\dot{x}^*.$$

Infobox 4.9 (Zero dynamics and reference generator) This note shows how to solve the asymptotic tracking problem when Assumption 4.3 is not verified but $\mathbf{D}_1 = \mathbf{0}$. As detailed hereafter, a modified change of coordinates represents the right tool for the solution of the problem. Consequently, the feed-forward describes the output of a dynamic system called zero dynamics. Moreover, we design the reference to make the zero dynamics BIBS-stable under some stabilization conditions. Let \mathbf{T}_ζ be as in Eq. (4.46) and introduce \mathbf{T}_{ζ_\perp} such that $\mathbf{T} := \text{col}(\mathbf{T}_\zeta, \mathbf{T}_{\zeta_\perp})$ is invertible and $\mathbf{T}_{\zeta_\perp}\mathbf{B}_1 = \mathbf{0}$. Then, let $\text{col}(\zeta, \zeta_\perp) = \mathbf{T}\mathbf{x}$, define

$$\begin{bmatrix} \bar{\mathbf{A}}_{11} & \bar{\mathbf{A}}_{12} \\ \bar{\mathbf{A}}_{21} & \bar{\mathbf{A}}_{22} \end{bmatrix} = \mathbf{T}(\mathbf{A} + \mathbf{B}_1\mathbf{K}_S)\mathbf{T}^{-1},$$

and compute the dynamics of ζ , ζ_\perp as

$$\begin{aligned} \dot{\zeta} &= \bar{\mathbf{A}}_{11}\zeta + \bar{\mathbf{A}}_{12}\zeta_\perp + \mathbf{T}_\zeta\mathbf{B}_1\mathbf{u}_{FF} \\ \dot{\zeta}_\perp &= \bar{\mathbf{A}}_{21}\zeta + \bar{\mathbf{A}}_{22}\zeta_\perp \\ \mathbf{e} &= \mathbf{C}_e\mathbf{T}_\zeta^{-1}\zeta + \mathbf{D}_2\mathbf{r}. \end{aligned}$$

Exploit this system to generate the references ζ^* and ζ_\perp^* . Let $\zeta^* := \text{col}(\zeta_1^*, \dots, \zeta_m^*)$ with ζ_i^* defined as in Eq. (4.51), for $i = 1, \dots, m$. Then, $\zeta = \zeta^*$ and $\zeta_\perp = \zeta_\perp^*$ imply

$$\zeta_\perp^* = \bar{\mathbf{A}}_{21}\zeta^* + \bar{\mathbf{A}}_{22}\zeta_\perp^*,$$

which represents the zero dynamics. If the couple $(\bar{\mathbf{A}}_{22}, \bar{\mathbf{A}}_{21})$ is stabilizable, there exists \mathbf{K} such that $\bar{\mathbf{A}}_{22} + \bar{\mathbf{A}}_{21}\mathbf{K}$ is Hurwitz. Therefore, the reference \mathbf{r} generated as $\zeta^* = \mathbf{K}\zeta_\perp^* + \mathbf{v}$, where \mathbf{v} represents the actual reference to be tracked, makes BIBS-stable the dynamics ζ_\perp^* . To conclude, use the same steps exploited in

Eqs. (4.52)–(4.53) to obtain system (1.17e) with $\mathbf{x}_{FF} := \zeta^\star_\perp$, $\mathbf{A}_{FF} := \bar{\mathbf{A}}_{22} + \bar{\mathbf{A}}_{21}\mathbf{K}$, $\sum_{i=1}^{r_{\max}} \mathbf{B}_{FF_i} d^i \mathbf{r}/dt^i := \bar{\mathbf{A}}_{21}\mathbf{v}$,

$$\mathbf{C}_{FF} := \mathbf{M}^+ \mathbf{H} [\mathbf{K} (\bar{\mathbf{A}}_{22} + \bar{\mathbf{A}}_{21}\mathbf{K}) - \bar{\mathbf{A}}_{12} - \bar{\mathbf{A}}_{11}\mathbf{K}],$$

and

$$\sum_{i=1}^{r_{\max}} \mathbf{D}_{FF_i} \frac{d^i}{dt^i} \mathbf{r} := \mathbf{M}^+ \mathbf{H} [\dot{\mathbf{v}} + (\mathbf{K}\bar{\mathbf{A}}_{21} - \bar{\mathbf{A}}_{11}) \mathbf{v}].$$

Example 4.19 (Cart-pole: speed tracking) As shown in Example 4.17, the reachable and observable subsystem of (1.2) is

$$\dot{\mathbf{z}}_{R,O} = \mathbf{A}\mathbf{z}_{R,O} + \mathbf{B}u,$$

in which $\mathbf{d} = \mathbf{0}$ and

$$\mathbf{A} = \begin{bmatrix} A_{22} & A_{23} & A_{24} \\ 0 & 0 & 1 \\ A_{42} & A_{43} & A_{44} \end{bmatrix}, \quad \mathbf{B} = \begin{bmatrix} b_1 \\ 0 \\ b_3 \end{bmatrix}.$$

The goal is to design $u = \mathbf{K}_S \mathbf{z}_{R,O} + u_{FF}$ which makes the cart follow a known speed profile, namely $\dot{p}^\star(t)$. As the first step, define the stabilizing feedback $\mathbf{K}_s = [k_{S_1} \ k_{S_2} \ k_{S_3}]$. Then, let the speed error be $e := \mathbf{C}_e \mathbf{z}_{R,O} - \dot{p}^\star(t)$, where $\mathbf{C}_e := [1 \ 0 \ 0]$. Compute

$$\dot{e} = \mathbf{C}_e \dot{\mathbf{z}}_{R,O} - \ddot{p}^\star(t) = \mathbf{C}_e \mathbf{A} \mathbf{z}_{R,O} + \mathbf{C}_e \mathbf{B} u - \ddot{p}^\star(t)$$

and observe that $\bar{m} := \mathbf{C}_e \mathbf{B} = b_1 \neq 0$. Define with $n_{R,O}$ the dimension of $\mathbf{z}_{R,O}$, then $r_{\max} = 1 < n_{R,O}$ implies that Assumption 4.3 is not verified. Thus, proceed according to Infobox 4.9 and identify

$$\mathbf{T}_\zeta = [1 \ 0 \ 0], \quad \mathbf{T}_{\zeta\perp} = \begin{bmatrix} 0 & 1 & 0 \\ -b_3 & 0 & b_1 \end{bmatrix}$$

such that $\mathbf{T} := \text{col}(\mathbf{T}_\zeta, \mathbf{T}_{\zeta\perp})$ is full-rank and $\mathbf{T}_{\zeta\perp} \mathbf{B} = \mathbf{0}$. Compute

$$\begin{aligned} \begin{bmatrix} \bar{\mathbf{A}}_{11} & \bar{\mathbf{A}}_{12} \\ \bar{\mathbf{A}}_{21} & \bar{\mathbf{A}}_{22} \end{bmatrix} &:= \mathbf{T}(\mathbf{A} + \mathbf{B}\mathbf{K}_s)\mathbf{T}^{-1} \\ &= \mathbf{T} \begin{bmatrix} A_{22} + b_1 k_{S_1} & A_{23} + b_1 k_{S_2} & A_{24} + b_1 k_{S_3} \\ 0 & 0 & 1 \\ A_{42} + b_2 k_{S_1} & A_{43} + b_2 k_{S_2} & A_{44} + b_2 k_{S_3} \end{bmatrix} \mathbf{T}^{-1} \end{aligned}$$

with

$$\begin{aligned}\bar{A}_{11} &= A_{22} + b_1 k_{S_1} + \frac{(A_{24} + b_1 k_{S_3}) b_3}{b_1} \\ \bar{A}_{12} &= \begin{bmatrix} A_{23} + b_1 k_{S_2} & \frac{A_{24} + b_1 k_{S_3}}{b_1} \\ 0 & \frac{1}{b_1} \end{bmatrix} \\ \bar{A}_{21} &= \begin{bmatrix} \frac{b_3}{b_1} \\ (A_{42} + b_2 k_{S_1}) b_1 - (A_{22} + b_1 k_{S_1}) b_3 - \frac{b_3 ((A_{24} + b_1 k_{S_3}) b_3 - (A_{44} + b_2 k_{S_3}) b_1)}{b_1} \end{bmatrix} \\ \bar{A}_{22} &= \begin{bmatrix} 0 & \frac{1}{b_1} \\ (A_{43} + b_2 k_{S_2}) b_1 - (A_{23} + b_1 k_{S_2}) b_3 - \frac{(A_{24} + b_1 k_{S_3}) b_3 - (A_{44} + b_2 k_{S_3}) b_1}{b_1} \end{bmatrix}.\end{aligned}$$

Note that couple $(\bar{A}_{22}, \bar{A}_{21})$ is fully reachable, and thus \mathbf{K} exists such that $\bar{A}_{22} + \bar{A}_{21}\mathbf{K}$ is Hurwitz. Define $\text{col}(\zeta, \zeta_\perp) = \mathbf{Tz}_{R,O}$ whose dynamics are

$$\begin{aligned}\dot{\zeta} &= \bar{A}_{11}\zeta + \bar{A}_{12}\zeta_\perp + b_{21}u_{FF} \\ \dot{\zeta}_\perp &= \bar{A}_{21}\zeta + \bar{A}_{22}\zeta_\perp \\ \mathbf{e} &= \zeta - p^*(t).\end{aligned}$$

Let $v : \mathbb{R} \rightarrow \mathbb{R}$ be a continuous and bounded function and define the reference generator as

$$\begin{aligned}\dot{\zeta}_\perp^* &= (\bar{A}_{22} + \bar{A}_{21}\mathbf{K})\zeta_\perp^* + \bar{A}_{21}v(t) \\ \zeta^* &= \mathbf{K}\zeta_\perp^* + v(t).\end{aligned}$$

To conclude, the feed-forward control law is

$$\begin{aligned}u_{FF} &= b_1^{-1} (\dot{\zeta}^* - \bar{A}_{11}\zeta^* - \bar{A}_{12}\zeta_\perp^*) \\ &= b_1^{-1} (\mathbf{K}(\bar{A}_{22} + \bar{A}_{21}\mathbf{K}) - \bar{A}_{11}\mathbf{K} - \bar{A}_{12}) \zeta_\perp^* \\ &\quad + b_1^{-1} (\dot{v}(t) + (\mathbf{K}\bar{A}_{21} - \bar{A}_{11}) v(t)).\end{aligned}$$

4.7 ADAS Architecture

This section translates into practice the theoretical achievements presented in Sects. 4.2–4.6. In particular, this section aims to define the system architecture to achieve the control goals described in Chap. 2 through reachability and observability analyses.

4.7.1 Active Suspensions

As for the Active Suspensions, Sect. 2.1 presents two case studies named Single Corner and Half Car. The former regards the vertical displacement control of the cabin and tires, whereas the latter focuses on the translation and rotation of the cabin only.

Single-Corner model

The study of eigenvalues carried out in Sect. 3.4 reveals that system (2.11) is BIBS-stable in the open loop. So then, in this context, the stabilizer aims to modify the eigenvalues of matrix (3.16) to change the behavior of the open-loop plant.

On the other hand, the AS should make the suspension length track a reference value; see Sect. 2.1.1. To accomplish this task, assume the reference length to be a constant and implement an integral action designed according to the theory presented in Sect. 4.3.

As for the observer, note that $\tilde{\mathbf{x}}$ is not directly available at the output, i.e., \mathbf{C} is not invertible. Then, the state needs to be estimated by an observer. Consequently, the control architecture of AS, designed on the Single Corner (2.7), consists of a dynamic output-feedback scheme.

To design the stabilizer, check if the couple $(\mathbf{A}, \mathbf{B}_1)$, identified in model (2.11), is stabilizable. Then, since $\tilde{\mathbf{x}} \in \mathbb{R}^4$ and according to the theoretical tools introduced in Sect. 4.2, the reachability matrix is

$$\mathbf{R} = [\mathbf{B}_1 \cdots \mathbf{A}^3 \mathbf{B}_1] \\ = \frac{1}{m_u} \begin{bmatrix} 0 & 0 & -1 & \frac{\bar{m}\beta_s}{m_u} \\ \bar{m} & -\frac{\bar{m}^2\beta_s}{m_u} & \frac{\bar{m}^3\beta_s^2 - k_t m_u}{m_u^2} & \frac{\bar{m}(2k_t\beta_s m_u + k_s m_u^2 - \bar{m}^3\beta_s^3)}{m_u^3} \\ 0 & -1 & \frac{\bar{m}\beta_s}{m_u} & \frac{k_t m_u - \bar{m}^2\beta_s^2}{m_u^2} \\ -1 & \frac{\bar{m}\beta_s}{m_u} & \frac{k_t m_u - \bar{m}^2\beta_s^2}{m_u^2} & \frac{\bar{m}^3\beta_s^3 - k_t\beta_s m_u(1+\bar{m})}{m_u^3} - \frac{k_s}{m_s} \end{bmatrix},$$

in which $\bar{m} = (m_s + m_u)/m_s$. The columns of \mathbf{R} represent linearly independent vectors; hence, the system is fully reachable.

To design the observer, compute the observability matrix as prescribed in Sect. 4.4. Let \mathbf{C} be the matrix defined in model (2.11), then

$$\mathbf{O} = \begin{bmatrix} \mathbf{C} \\ \vdots \\ \mathbf{C}\mathbf{A}^3 \end{bmatrix} \\ = \begin{bmatrix} 1 & 0 & 0 & 0 \\ -\frac{k_s}{m_s} & -\frac{\beta_s}{m_s} & 0 & 0 \\ 0 & 0 & 1 & 0 \\ \frac{\bar{m}\beta_s k_s}{m_s m_u} & \frac{\bar{m}\beta_s^2}{m_s m_u} & -\frac{\beta_s k_t + k_s m_u}{m_s m_u} & 0 \\ 0 & 0 & 0 & 1 \\ \vdots & \vdots & \vdots & \vdots \end{bmatrix},$$

in which only the first five lines have been reported. Indeed, since among them there are four linearly independent rows (first, second, third, and fifth), the full observability of the couple (\mathbf{A}, \mathbf{C}) is guaranteed independently of the remaining lines.

For the design of the integral action, refer to Sect. 4.3 and use model (2.11) to compute

$$\begin{aligned}\dot{\eta} &= \mathbf{C}_e \mathbf{x} - r + \nu_p \\ u_I &= k_I \eta.\end{aligned}$$

The existence of k_I making stable the closed-loop system is checked through the extended system introduced in Sect. 4.3. In particular, with the matrices \mathbf{A} , \mathbf{B}_1 , and \mathbf{C}_e at hand, define

$$\mathbf{A}_e = \begin{bmatrix} \mathbf{A} & \mathbf{0} \\ \mathbf{C}_e & 0 \end{bmatrix}, \quad \mathbf{B}_e = \begin{bmatrix} \mathbf{B}_1 \\ 0 \end{bmatrix}.$$

Then, since the couple $(\mathbf{A}_e, \mathbf{B}_e)$ is fully reachable, there exists \mathbf{K}_e that makes $\mathbf{A}_e + \mathbf{B}_e \mathbf{K}_e$ Hurwitz. The matrix \mathbf{K}_S and the scalar k_I are subparts of \mathbf{K}_e such that $\mathbf{K}_e = [\mathbf{K}_S \ k_I]$.

To conclude, adopting the notation of Eq. (1.17), the overall control system is

$$\begin{aligned}\dot{\mathbf{x}}_O &= (\mathbf{A} + \mathbf{K}_O \mathbf{C}) \mathbf{x}_O + \mathbf{B}_1 \tilde{\mathbf{u}} + \mathbf{K}_O \tilde{\mathbf{y}} \\ \dot{\eta} &= \mathbf{C}_e \mathbf{x} - \tilde{r} + \nu_p \\ \tilde{\mathbf{u}} &= \mathbf{K}_S \mathbf{x}_O + k_I \eta.\end{aligned}\tag{4.54}$$

Half-Car model

In this context, the main objective of the control system is to asymptotically track the constant reference height and apparent roll angle despite unknown lateral accelerations and road variations. Examples of these applications are trains on planar railways that tilt the coaches when cornering or vehicles that keep the underbody horizontal despite ground irregularities. In this scenario, the control system changes the open-loop eigenvalues of the plant (thus resulting in a harder/softer suspension system) and tracks the desired height and apparent roll angle. For these reasons, the control architecture comprises state feedback and integral action. Moreover, a state observer makes the stabilizer implementable.

Section 4.2 showed that a state-feedback stabilizer exists if the plant is stabilizable. Check this property through the reachability matrix. In detail, use the couple $(\mathbf{A}, \mathbf{B}_1)$ introduced in (2.21) to compute

$$\begin{aligned}\mathbf{R} &= [\mathbf{B}_1 \ \mathbf{AB}_1 \cdots \mathbf{A}^5 \mathbf{B}_1] \\ &= \begin{bmatrix} 0 & 0 & 1/m & 0 & x & \cdots & x \\ 1/m & 0 & -2\beta/m^2 & -\beta(d_l - d_r)/(Jm) & x & \cdots & x \\ 0 & 0 & 0 & 1/J & x & \cdots & x \\ 0 & 1/J & -\beta(d_l - d_r)/(Jm) & -\beta(d_l^2 + d_r^2)/J^2 & x & \cdots & x \\ 0 & 0 & 0 & 0 & 0 & \cdots & 0 \\ 0 & 0 & 0 & 0 & 0 & \cdots & 0 \end{bmatrix},\end{aligned}$$

where x denotes a possibly nontrivial entry. It is clear that, since the last two rows are null, the system is not fully reachable. Moreover, the non-reachable states are the fifth and sixth, i.e., those corresponding to the kinematic chain of the road bank angle. As detailed in Sect. 3.4.1, the dynamics of these states are not Hurwitz due to the presence of a generalized chain of eigenvectors. Then, the system is not stabilizable.

From a physical viewpoint, the road bank angle is not adjustable via the suspension actuators. Motivated by these arguments, assume that ϕ_g and ω_g are bounded (which has physical sense), and design the stabilizer for the first four states only. Note that the system is already in the reachability form (see Sect. 4.2). Thus, define $\mathbf{z}_R \in \mathbb{R}^4$ and $\mathbf{z}_{NR} \in \mathbb{R}^2$ such that $\text{col}(\mathbf{z}_R, \mathbf{z}_{NR}) = \mathbf{x}$. Let $\bar{\mathbf{A}}_{11} \in \mathbb{R}^{4 \times 4}$, $\bar{\mathbf{A}}_{12} \in \mathbb{R}^{4 \times 2}$, $\bar{\mathbf{A}}_{22} \in \mathbb{R}^{2 \times 2}$, and $\bar{\mathbf{B}}_{11} \in \mathbb{R}^{4 \times 1}$ such that

$$\mathbf{A} = \begin{bmatrix} \bar{\mathbf{A}}_{11} & \bar{\mathbf{A}}_{12} \\ \mathbf{0} & \bar{\mathbf{A}}_{22} \end{bmatrix}, \quad \mathbf{B}_1 = \begin{bmatrix} \bar{\mathbf{B}}_{11} \\ \mathbf{0} \end{bmatrix}.$$

Then, at least one matrix \mathbf{K}_R exists such that $\bar{\mathbf{A}}_{11} + \bar{\mathbf{B}}_{11}\mathbf{K}_R$ is Hurwitz. Use this matrix to define the state stabilizer as

$$u_S = \mathbf{K}_R \mathbf{z}_R.$$

To implement u_S , the state \mathbf{z}_R must be available whether measured or estimated. For this application, the observer is built on the couple (\mathbf{A}, \mathbf{C}) detailed in Eq. (2.21). First, the detectability of this couple is checked via the observability matrix

$$\mathbf{O} = \begin{bmatrix} \mathbf{C} \\ \mathbf{CA} \\ \vdots \\ \mathbf{CA}^5 \end{bmatrix} = \begin{bmatrix} 0 & 0 & g & 0 & 0 & 0 \\ x & x & x & x & x & x \\ 0 & 0 & 0 & 1 & 0 & 0 \\ 1 & 0 & d_l & 0 & -d_l & 0 \\ 1 & 0 & -d_r & 0 & d_r & 0 \\ 0 & 0 & 0 & g & 0 & 0 \\ x & x & x & x & x & x \\ x & x & x & x & x & x \\ 0 & 1 & 0 & d_l & 0 & -d_l \\ 0 & 1 & 0 & -d_r & 0 & d_r \\ x & x & x & x & x & x \\ \vdots & \vdots & \vdots & \vdots & \vdots & \vdots \\ x & x & x & x & x & x \end{bmatrix},$$

in which x denotes a possible nontrivial entry. This matrix is full-rank, thus implying that the state is fully observable. It follows that at least one matrix \mathbf{K}_O exists such that $\mathbf{A} - \mathbf{K}_O \mathbf{C}$ is Hurwitz. As a consequence, the procedure illustrated in Sect. 4.4 can be adopted to design the following observer:

$$\begin{aligned} \dot{\hat{\mathbf{x}}} &= \mathbf{A}\hat{\mathbf{x}} + \mathbf{B}_1 \mathbf{u} + \mathbf{K}_O (\mathbf{y} - \hat{\mathbf{y}}) \\ \hat{\mathbf{y}} &= \mathbf{C}\hat{\mathbf{x}} + \mathbf{D}_1 \mathbf{u}. \end{aligned}$$

With $\hat{\mathbf{x}}$ at hand, the stabilizer is implemented through $\mathbf{u}_S = [\mathbf{K}_R \mathbf{0}] \hat{\mathbf{x}}$.

As for the integral action, define the following system:

$$\dot{\boldsymbol{\eta}} = \mathbf{e}$$

$$\mathbf{u}_{IA} = \mathbf{K}_I \boldsymbol{\eta}.$$

To conclude, introduce

$$\mathbf{A}_e = \begin{bmatrix} \bar{\mathbf{A}}_{11} & \mathbf{0} \\ \mathbf{C}_e & 0 \end{bmatrix}, \quad \mathbf{B}_e = \begin{bmatrix} \bar{\mathbf{B}}_{11} \\ \mathbf{0} \end{bmatrix}, \quad (4.55)$$

then, as detailed in Sect. 4.3, matrices \mathbf{K}_R and \mathbf{K}_I are subparts of \mathbf{K}_e such that $\mathbf{A}_e + \mathbf{B}_e \mathbf{K}_e$ is Hurwitz.

4.7.2 Electro-mechanical Brakes

As described in Sect. 2.2, the EMB control system's main purpose is tracking a reference caliper force, despite the presence of external torques, e.g., those due to friction. On the other hand, as shown in Sect. 3.4.2, the open-loop modes are characterized by high-frequency oscillations. So, a further task of the EMB controller is modifying the system behavior by increasing the damping.

These arguments lead to designing a control system composed of a stabilizer and an integral action. As the first step, check the existence of a stabilizer through the reachability study illustrated in Sect. 4.2. Use matrices \mathbf{A} and \mathbf{B}_1 defined in (2.30) to compute

$$\mathbf{R} = [\mathbf{B}_1 \mathbf{AB}_1 \mathbf{A}^2\mathbf{B}_1] = \begin{bmatrix} 0 & 0 & \frac{k}{JL} \\ 0 & \frac{k}{JL} & -\frac{R}{L^2} \frac{k}{J} \\ 1 & \frac{R}{L^2} & \frac{R^2}{L^3} - \frac{k k_{\text{emf}}}{JL^2} \end{bmatrix}.$$

Since \mathbf{R} is full-rank, the system is completely reachable, and, as shown in Sect. 4.2, at least one matrix $\mathbf{K}_S \in \mathbb{R}^{1 \times 3}$ exists such that $\mathbf{A} + \mathbf{B}_1\mathbf{K}_S$ is Hurwitz. Therefore, the state-feedback stabilizer is $u_S = \mathbf{K}_S \mathbf{x}$.

This stabilizer is made implementable by substituting for \mathbf{x} its estimation, see Sect. 4.4. To obtain this estimate, proceed as follows. Exploit matrices \mathbf{A} and \mathbf{C} defined in Eq. (2.30), and check the detectability through the matrix

$$\begin{aligned} \mathbf{O} &= \begin{bmatrix} \mathbf{C} \\ \mathbf{CA} \\ \mathbf{CA}^2 \end{bmatrix} \\ &= \begin{bmatrix} N\alpha_1 + 2N\alpha_2(N\theta_0) + 3N\alpha_3(N\theta_0)^2 & 0 & 0 \\ 0 & 1 & 0 \\ 0 & N\alpha_1 + 2N\alpha_2(N\theta_0) + 3N\alpha_3(N\theta_0)^2 & 0 \\ -N \frac{N\alpha_1 + 2N\alpha_2(N\theta_0) + 3N\alpha_3(N\theta_0)^2}{J} & 0 & \frac{k}{J} \\ \mathbf{x} & \mathbf{x} & \mathbf{x} \\ \mathbf{x} & \mathbf{x} & \mathbf{x} \end{bmatrix} \end{aligned}$$

where \mathbf{x} denotes a possibly non-empty entry. Since $\ker(\mathbf{O})$ corresponds to the origin of the state space, the system is fully observable, and, as suggested in Sect. 4.4, there exists at least a matrix $\mathbf{K}_O \in \mathbb{R}^{3 \times 2}$ such that $\mathbf{A} - \mathbf{K}_O \mathbf{C}$ is Hurwitz. Then, the state observer is given by

$$\dot{\hat{\mathbf{x}}} = \mathbf{A}\hat{\mathbf{x}} + \mathbf{B}_1 u + \mathbf{K}_O(\mathbf{y} - \hat{\mathbf{y}})$$

$$\hat{\mathbf{y}} = \mathbf{C}\hat{\mathbf{x}}$$

Finally, estimate $\hat{\mathbf{x}}$ is exploited into the stabilizer as $u_S = \mathbf{K}_S \hat{\mathbf{x}}$.

As for the integral action, elaborate on e as follows:

$$\dot{\eta} = e$$

$$u_{IA} = k_I \eta.$$

To conclude, the matrix \mathbf{K}_S and the scalar k_I are designed according to the theory developed in Sect. 4.3. Specifically, define

$$\mathbf{A}_e = \begin{bmatrix} \mathbf{A} & \mathbf{0} \\ \mathbf{C}_e & 0 \end{bmatrix}, \quad \mathbf{B}_e = \begin{bmatrix} \mathbf{B}_1 \\ 0 \end{bmatrix}$$

and find a matrix $\mathbf{K}_e \in \mathbb{R}^{1 \times 4}$ such that $\mathbf{A}_e + \mathbf{B}_e \mathbf{K}_e$ is Hurwitz. Then, the matrix \mathbf{K}_S and the scalar k_I are such that $\mathbf{K}_e = [\mathbf{K}_S \ k_I]$.

4.7.3 Wheel Speed Controls

The wheel speed control architecture described in this section is founded on the model presented in Sect. 2.3 and investigated in Sect. 3.4.3. This latter shows that the vehicle speed dynamics can be neglected when considering the stabilization of the wheel dynamics. For this reason, the design of the control system is proposed on the sub-model

$$\begin{aligned} \dot{\tilde{\omega}} &= \mathbf{A}_{22}\tilde{\omega} + \mathbf{B}_{12}\mathbf{u} + \mathbf{A}_{21}\tilde{v}, \\ \mathbf{e} &= \tilde{\omega} - \mathbf{r} \end{aligned} \quad (4.56)$$

where \mathbf{A}_{21} and \mathbf{A}_{22} are identified in Sect. 3.4.3, while \mathbf{B}_{12} represents the last two rows of \mathbf{B}_1 .

Moreover, regardless of the condition (driving/braking), the magnitude of the eigenvalues of \mathbf{A}_{22} increases to infinity for vehicle speeds approaching zero.

Remark 4.3 Constant gain linear control systems cannot stabilize system (4.56) at any vehicle and wheel speed. To prove this, denote with $\mathbf{A}_{22}(\mathbf{x}^*)$ the matrix \mathbf{A}_{22} , evaluated at \mathbf{x}^* . Let $\lambda_r^*, \lambda_f^* \in [-1, 1]$ be the longitudinal slip ratios for the rear and front wheels associated with \mathbf{x}^* . Then, define $\mathbf{K}_S \in \mathbb{R}^{2 \times 2}$ such that $\mathbf{A}_{22}(\mathbf{x}^*) + \mathbf{B}_{12}\mathbf{K}_S$ is Hurwitz. Now, let \mathbf{x}^* such that $\lambda_r^*, \lambda_f^* \in [-1, -\lambda^*) \cup (\lambda^*, 1]$, then the lower the vehicle speed, the more positive are the eigenvalues of $\mathbf{A}_{22}(\mathbf{x}^*)$ and the larger is the \mathbf{K}_S needed to make the closed loop Hurwitz. Thus, for any finite \mathbf{K}_S , there exists $v_{th} > 0$ such that the stabilization of system (4.56), with $\lambda_r^*, \lambda_f^* \in [-1, -\lambda^*) \cup (\lambda^*, 1]$, is achieved only for $v \geq v_{th}$. Conversely, if \mathbf{x}^* is such that $\lambda_r^*, \lambda_f^* \in (-\lambda^*, \lambda^*)$, then the linearized plant can be stabilized at any $v > 0$.

Note

Roughly, the stabilization policy adopted for this application relies on the election of $\lambda_r^*, \lambda_f^* \in (-\lambda^*, \lambda^*)$ and a linearization point as the worst case. Then, the control system properly operates for all the conditions for which the linearized system is more “stable” than the worst one.

The adoption of an integral action improves the control architecture. Indeed, the presence of unknown disturbances (such as the rolling resistance), and the neglected vehicle acceleration, could impact the tracking of the reference wheel speed. Moreover, since the reference wheel speed could vary accordingly to the vehicle speed (as in LaC and ABS), the tracking performance is improved using a feed-forward control system.

As for the stabilization of the couple $(\mathbf{A}_{22}, \mathbf{B}_{12})$, the reachability is checked with the computation of

$$\mathbf{R} = [\mathbf{B}_{12} \ \mathbf{A}_{22}\mathbf{B}_{12}],$$

where it is easy to see that, for four-wheel drive vehicles, \mathbf{B}_{12} has two linearly independent columns, and so $\mathbf{A}_{22}\mathbf{B}_{12}$ is not actually needed to assess the reachability of $(\mathbf{A}_{22}, \mathbf{B}_{12})$.

As for the observation of $\tilde{\omega}$, the sensor suite described in Sect. 2.3 is composed of two tone-wheels. The linearized sensor model (2.46) leads to $\mathbf{C} = \mathbf{I}$ (fully accessible state). Hence, the system is fully observable, and one can even take $\mathbf{A}_0, \mathbf{B}_0, \mathbf{K}_0, \mathbf{C}_0 = \mathbf{0}$ and $\mathbf{D}_0 = \mathbf{I}$ in the presence of reliable and accurate sensors.

For what concerns the integral action, adopt the scheme depicted in Sect. 4.3 with

$$\begin{aligned}\dot{\boldsymbol{\eta}} &= \mathbf{e} \\ \mathbf{u}_{IA} &= \mathbf{K}_I \boldsymbol{\eta}.\end{aligned}$$

As described in Sect. 3.4.3, the vehicle speed dynamics are much slower than the wheel dynamics. This means that the vehicle speed can be conceived as a quasi-constant disturbance affecting the dynamics of the wheels. In this context, the integral action quasi-perfectly cancels the undesired effect of the vehicle's acceleration.

Matrices \mathbf{K}_S and \mathbf{K}_I are such that $\mathbf{K}_e := [\mathbf{K}_S \ \mathbf{K}_I]$ makes Hurwitz $\mathbf{A}_e + \mathbf{B}_e \mathbf{K}_e$ with

$$\mathbf{A}_e = \begin{bmatrix} \mathbf{A}_{22} & \mathbf{0} \\ \mathbf{I} & 0 \end{bmatrix}, \quad \mathbf{B}_e = \begin{bmatrix} \mathbf{B}_{12} \\ 0 \end{bmatrix}.$$

As the last ingredient of the control system architecture, the feed-forward logic is designed for LaC and ABS.

As detailed in Sect. 4.6, assume \mathbf{x}_0 is the linearization point, let e_1, e_2 be the elements of \mathbf{e} , define u_1, u_2 such that $\mathbf{u} = \text{col}(u_1, u_2)$, split \mathbf{r} into r_1 and r_2 , and let A_{ij} be the entries of $\mathbf{A}_{22}(\mathbf{x}_0) + \mathbf{B}_{12}\mathbf{K}_S$, A_{21_i} be the elements of \mathbf{A}_{21} , and B_{12_i} be the entries of the main diagonal of \mathbf{B}_{12} . Then, using Eq. (2.46) we have

$$\begin{aligned}\frac{de_1}{dt} &= [\bar{A}_{11} \ \bar{A}_{12}] \tilde{\omega} + B_{12_1} u_1 + A_{21_1} \tilde{v} - \dot{r}_1 \quad \implies r_{\max_1} = 1 \\ \frac{de_2}{dt} &= [\bar{A}_{21} \ \bar{A}_{22}] \tilde{\omega} + B_{12_2} u_2 + A_{21_2} \tilde{v} - \dot{r}_2 \quad \implies r_{\max_2} = 1.\end{aligned}$$

Then, since Assumption 4.3 is verified, we proceed as detailed in Sect. 4.6. In more detail, note that the transformation (4.46) is $\mathbf{T} = \mathbf{I}$. Therefore, the plant is already in the desired form. Then, assume $\mathbf{e} \equiv \mathbf{0}$ and define

$$\mathbf{u}_{FF} = \mathbf{B}_{12}^{-1} (\dot{\mathbf{r}} - (\mathbf{A}_{22} + \mathbf{B}_{12}\mathbf{K}_S) \mathbf{r} - \mathbf{A}_{21} \tilde{v}).$$

References r_1 and r_2 can be specialized for the LaC and ABS. Indeed, for LaC, assume $\lambda' \in (0, \lambda^*)$, define $k_d = 1/(1 - \lambda')$, and let $r_1 = r_r^{-1} k_d \tilde{v}$ and $r_2 = r_f^{-1} k_d \tilde{v}$. For ABS, choose $\lambda' \in (-\lambda^*, 0)$, let $k_b = (1 + \lambda')$, and define $r_1 = r_r^{-1} k_b \tilde{v}$ and $r_2 = r_f^{-1} k_b \tilde{v}$. To conclude, since $\dot{\tilde{v}}$ is negligible, the derivatives \dot{r}_1, \dot{r}_2 are not included

in the computation of the control law. Substitute r_1 and r_2 into the previous equation to see that the feed-forward controller becomes

$$\mathbf{u}_{FF} = - \left((\mathbf{B}_{12}^{-1} \mathbf{A}_{22} + \mathbf{K}_S) \begin{bmatrix} r_r^{-1} \\ r_f^{-1} \end{bmatrix} k_{\#} + \mathbf{B}_{12}^{-1} \mathbf{A}_{21} \right) \tilde{v}$$

where $\# \in \{d, b\}$. The overall control policy is a composition of stabilizer, integral action, and simplified feed-forward

$$\begin{aligned} \dot{\eta} &= \mathbf{e} \\ \mathbf{u} &= \mathbf{K}_S(\tilde{\omega} - \mathbf{r}) + \mathbf{K}_I \eta + \mathbf{u}_{FF}. \end{aligned}$$

To conclude, TC represents the strategy of regulating the wheel speed to a (possibly) time-varying reference. Moreover, LaC and ABS represent opposite extrema, the former for $\lambda' \in (0, \lambda^*)$ and the latter for $\lambda' \in (-\lambda^*, 0)$.

4.7.4 Adaptive Cruise Control

The model proposed in Sect. 2.4 describes the dynamics of a platoon of three heterogeneous vehicles. The mathematical model (2.55), representing the linearization of Eq. (2.53), is hereafter exploited to design an ACC. Before introducing any technical detail, it is worth noting that a design made on model (2.55) would lead to a *centralized* algorithm, i.e., a control strategy that needs the state of the whole platoon. Roughly, one can imagine the leader collecting the information on speed and distance from the followers, computing and sending the control laws back to the followers. This solution, despite being appealing, requires a communication network connecting the vehicles. Conversely, *distributed* algorithms compute the control laws based on local information only. In practice, a distributed ACC consists of algorithms deployed only to the followers and using only local sensors. This section focuses on this second scenario, i.e., the design of a local control system.

Plant (2.53) is slightly reorganized to design a distributed ACC. In particular, vehicle B is the target to deploy the control law. Then, restrict the state to the first two elements by defining $\mathbf{x}_d = \text{col}(d_B, v_B)$, let $u_d := f_B$ be the control input, and take $\mathbf{y}_d := \text{col}(y_{dB}, y_{vB})$ as the local sensor suite, which is associated with the vector of noises $\nu_d := \text{col}(\nu_{dB}, \nu_{vB})$. Moreover, define $\mathbf{w}_d = \text{col}(\mathbf{d}, \nu_d)$ as the vector of exogenous signals and let $e_d := e_{dB}$ be the regulated output restricted to vehicle B.

Now, since $\dot{\mathbf{x}}_d$, \mathbf{y}_d , and e_d are independent of the states of vehicle C, the nonlinear model describing the local scenario is obtained by selecting the first two rows of each function appearing in Eq. (2.53). Similarly, the linearized model is retrieved by restricting the matrices in Eq. (2.55) to the first two rows/columns as follows. Let \mathbf{x}_{d0} , u_{d0} , \mathbf{w}_{d0} , \mathbf{y}_{d0} , and e_{d0} be associated with the linearization point. Define $\tilde{\mathbf{x}}_d = \mathbf{x}_d - \mathbf{x}_{d0}$, $\tilde{u}_d = u_d - u_{d0}$, $\tilde{\mathbf{w}}_d = \mathbf{w}_d - \mathbf{w}_{d0}$, $\tilde{\mathbf{y}}_d = \mathbf{y}_d - \mathbf{y}_{d0}$, and $\tilde{e}_d = e_d - e_{d0}$. Then

$$\begin{aligned} \dot{\tilde{\mathbf{x}}}_d &= \mathbf{A}_d \tilde{\mathbf{x}}_d + \mathbf{B}_{d1} \tilde{u}_d + \mathbf{B}_{d2} \tilde{\mathbf{w}}_d \\ \tilde{\mathbf{y}}_d &= \mathbf{C}_d \tilde{\mathbf{x}}_d + \mathbf{D}_{d2} \tilde{\mathbf{w}}_d \\ \tilde{e}_d &= \mathbf{C}_{de} \tilde{\mathbf{x}}_d + \mathbf{D}_{de} \tilde{\mathbf{w}}_d, \end{aligned}$$

where

$$\begin{aligned}\mathbf{A}_d &= \begin{bmatrix} 0 & -1 \\ 0 & -\rho S_B C_{D_B} v 0 / m_B \end{bmatrix} \\ \mathbf{B}_{d1} &= \begin{bmatrix} 0 \\ m_B^{-1} \end{bmatrix}, \quad \mathbf{B}_{d2} = \begin{bmatrix} 0 & 0 & 0 & 0 \\ 0 & g & \rho S_B C_{D_B} v 0 / m_B & 0 \\ 0 & 0 & 0 & 0 \end{bmatrix} \\ \mathbf{C}_d &= \begin{bmatrix} 1 & 0 \\ 0 & 1 \end{bmatrix}, \quad \mathbf{D}_{d2} = \begin{bmatrix} 0 & 0 & 0 & 1 & 0 \\ 0 & 0 & 0 & 0 & 1 \end{bmatrix} \\ \mathbf{C}_{de} &= [1 \ 2v_0/k], \quad \mathbf{D}_{de} = [0 \ 0 \ 0 \ 1 \ -2v_0/k].\end{aligned}$$

The eigenvalues of \mathbf{A}_d correspond to the roots λ_1 and λ_2 investigated in Sect. 3.4.4. As a consequence, the open-loop plant is not Hurwitz. With this model at hand, the ACC system is designed as follows.

ACC aims to regulate the speed to that of the leader while maintaining the safety distance. In performing this task, the control system also changes the vehicle dynamics, e.g., to avoid overshoots. Moreover, the controller should maintain the safety distance despite unknown constant disturbances (wind, road slope, etc.). In this context, the control architecture relies on a state-feedback stabilizer to which an integral action is added.

As the first step, matrices \mathbf{A}_d and \mathbf{B}_{d1} are exploited to build

$$\mathbf{R} = [\mathbf{B}_{d1} \ \mathbf{A}_d \mathbf{B}_{d1}] = \begin{bmatrix} 0 & -m_B^{-1} \\ m_B^{-1} & -\rho S_B C_{D_B} v 0 / m_B^2 \end{bmatrix},$$

which shows that the plant is fully reachable.

Now, since the couple $(\mathbf{A}_d, \mathbf{B}_{d1})$ is fully reachable, there exists at least one matrix $\mathbf{K}_S \in \mathbb{R}^{1 \times 2}$ such that $\mathbf{A}_d + \mathbf{B}_{d1} \mathbf{K}_S$ is Hurwitz. Consequently, the stabilizer is

$$u_S = \mathbf{K}_S \tilde{\mathbf{x}}_d.$$

For this application, the observer is optional because the state is fully available at the output. In the following, in the computation of the stabilization law, the state $\tilde{\mathbf{x}}_d$ is directly substituted by $\tilde{\mathbf{y}}_d$, i.e.,

$$u_S = \mathbf{K}_S \tilde{\mathbf{y}}_d.$$

The integral action completes the control system architecture. Define

$$\dot{\eta} = e_d$$

$$u_{IA} = k_I \eta.$$

Finally, use the theoretical tools presented in Sect. 4.3 to conclude the design. Hence, introduce

$$\mathbf{A}_e = \begin{bmatrix} \mathbf{A}_d & \mathbf{0} \\ \mathbf{C}_{de} & 0 \end{bmatrix}, \quad \mathbf{B}_e = \begin{bmatrix} \mathbf{B}_{d1} \\ 0 \end{bmatrix},$$

and find a matrix $\mathbf{K}_e \in \mathbb{R}^{1 \times 3}$ such that $\mathbf{A}_e + \mathbf{B}_e \mathbf{K}_e$ is Hurwitz. Then, the matrix \mathbf{K}_S and the scalar k_I are such that $\mathbf{K}_e = [\mathbf{K}_S \ k_I]$.

String stability

This section solves the ACC problem through a decentralized control system. It shows that this control policy guarantees the stability of the platoon (also called *string*). To demonstrate this result, let $\tilde{x}_1, \dots, \tilde{x}_4$ be the linearized state defined in (2.55). Denote with $\tilde{\mathbf{x}}_B := \text{col}(\tilde{x}_1, \tilde{x}_2)$ and $\tilde{\mathbf{x}}_C := \text{col}(\tilde{x}_3, \tilde{x}_4)$ the distributed states and, with reference to Fig. 2.6, assume that vehicles B and C are equipped with the control laws $u_B := \mathbf{K}_B \tilde{\mathbf{x}}_B$ and $u_C := \mathbf{K}_C \tilde{\mathbf{x}}_C$, respectively. Let \mathbf{A} and \mathbf{B}_1 be the matrices identified in Eq. (2.55). Then, define \mathbf{A}_B , \mathbf{A}_C , \mathbf{X} , \mathbf{B}_{1B} , and \mathbf{B}_{1C} such that

$$\mathbf{A} = \begin{bmatrix} \mathbf{A}_B & \mathbf{0} \\ \mathbf{X} & \mathbf{A}_C \end{bmatrix}, \quad \mathbf{B}_1 = \begin{bmatrix} \mathbf{B}_{1B} \\ \mathbf{B}_{1C} \end{bmatrix}.$$

With this notation at hand and neglecting $\tilde{\mathbf{w}}$, the dynamics of the closed loop become

$$\begin{aligned} \begin{bmatrix} \dot{\tilde{x}}_B \\ \dot{\tilde{x}}_C \end{bmatrix} &= \begin{bmatrix} \mathbf{A}_B & \mathbf{0} \\ \mathbf{X} & \mathbf{A}_C \end{bmatrix} \begin{bmatrix} \tilde{x}_B \\ \tilde{x}_C \end{bmatrix} + \begin{bmatrix} \mathbf{B}_{1B} \\ \mathbf{B}_{1C} \end{bmatrix} \begin{bmatrix} \mathbf{K}_B & \mathbf{0} \\ \mathbf{0} & \mathbf{K}_C \end{bmatrix} \begin{bmatrix} \tilde{x}_B \\ \tilde{x}_C \end{bmatrix} \\ &= \begin{bmatrix} \mathbf{A}_B + \mathbf{B}_{1B} \mathbf{K}_B & \mathbf{0} \\ \mathbf{X} & \mathbf{A}_C + \mathbf{B}_{1C} \mathbf{K}_C \end{bmatrix} \begin{bmatrix} \tilde{x}_B \\ \tilde{x}_C \end{bmatrix}. \end{aligned}$$

As a consequence, the dynamics of the closed-loop system are described by a block triangular matrix. Then, the stability of the string is guaranteed if $\mathbf{A}_B + \mathbf{B}_{1B} \mathbf{K}_B$ and $\mathbf{A}_C + \mathbf{B}_{1C} \mathbf{K}_C$ are Hurwitz. Finally, these matrices are Hurwitz thanks to the design of \mathbf{K}_B and \mathbf{K}_C proposed in this section.

4.7.5 Automatic Steering System

As introduced in Sect. 2.5, the control algorithm that governs the steering system has, as its primary purpose, the goal of making the wheels track a reference time-varying trajectory. Moreover, as detailed in Sect. 3.4.5, the system dynamics are described by pure oscillatory modes (due to the absence of friction). Consequently, the control system is also in charge of stabilizing the plant. In addition, the system state is not completely available at the output through the measurements.

Therefore, the control architecture is composed of a state-feedback algorithm (to stabilize the plant) fed by a state observer (to make the stabilizer implementable). In addition, an integral action (needed to make the system robust) and a feed-forward control law (necessary to improve the tracking performance during the transients) extend the dynamic output-feedback system.

On the one hand, in agreement with Sect. 4.2, a state-feedback stabilizer exists if the system is stabilizable or, even better, if the system is fully reachable. To check if the plant under investigation falls in one of these two categories, let \mathbf{A} and \mathbf{B}_1 be the matrices defined in Sect. 2.5. Then, compute

$$\mathbf{R} = [\mathbf{B}_1 \mathbf{A} \mathbf{B}_1] = \begin{bmatrix} 0 & B^{-1}(\delta_0) \\ B^{-1}(\delta_0) & 0 \end{bmatrix}.$$

Since $B^{-1}(\delta_0) > 0$ for any $\delta_0 \in \mathbb{R}$ the matrix \mathbf{R} is full-rank, thus making the system fully reachable. As a consequence, $\mathbf{K}_S \in \mathbb{R}^{1 \times 2}$ exists, which makes $\mathbf{A} + \mathbf{B}_1 \mathbf{K}_S$ Hurwitz.

On the other hand, Sect. 4.4 shows how to design an observer for detectable LTI plants. The observability check employs matrices \mathbf{A} and \mathbf{C} introduced in Sect. 2.5. In detail, compute

$$\mathbf{O} = \begin{bmatrix} \mathbf{C} \\ \mathbf{CA} \end{bmatrix} = \begin{bmatrix} 1 & 0 \\ 0 & 1 \end{bmatrix}.$$

The matrix \mathbf{O} is full-rank, thus making the linearized plant fully observable. As a consequence, there exists $\mathbf{K}_O \in \mathbb{R}^{2 \times 1}$ such that $\mathbf{A} - \mathbf{K}_O \mathbf{C}$ is Hurwitz. The matrices \mathbf{K}_S and \mathbf{K}_O are exploited to build the following output-feedback stabilizer:

$$\begin{aligned}\hat{\mathbf{x}} &= \mathbf{A}\hat{x} + \mathbf{B}_1 u_S + \mathbf{K}_O(\tilde{y} - \mathbf{C}\hat{x}) \\ u_S &= \mathbf{K}_S \hat{x}.\end{aligned}$$

As described before, an integral action extends the control system. In agreement with Sect. 4.3, the integral control relies on the following equations:

$$\begin{aligned}\dot{\eta} &= e \\ u_{IA} &= k_I \eta.\end{aligned}$$

The existence of k_I stabilizing the closed loop is guaranteed by the reachability check performed on the extended system built on the matrices \mathbf{A} , \mathbf{B}_1 , and \mathbf{C}_e . In particular, define

$$\mathbf{A}_e = \begin{bmatrix} \mathbf{A} & \mathbf{0} \\ \mathbf{C}_e & 0 \end{bmatrix}, \quad \mathbf{B}_e = \begin{bmatrix} \mathbf{B}_1 \\ 0 \end{bmatrix}.$$

Then, since the couple $(\mathbf{A}_e, \mathbf{B}_e)$ is fully reachable, there exists $\mathbf{K}_e \in \mathbb{R}^{1 \times 3}$ such that $\mathbf{A}_e + \mathbf{B}_e \mathbf{K}_e$ is Hurwitz. The feedback matrices are subparts of \mathbf{K}_e by defining $\mathbf{K}_e = [\mathbf{K}_S \ k_{IA}]$.

The last part of the control architecture is composed of a feed-forward law. To design this law, adopt the strategy defined in Sect. 4.6. Let $\tilde{\delta}$ and $\tilde{\omega}$ be the first and second elements of $\tilde{\mathbf{x}}$, and compute

$$\begin{aligned}\dot{e} &= \mathbf{C}_e(\mathbf{A}\tilde{\mathbf{x}} + \mathbf{B}_1\tilde{u}) - \dot{r}_\delta = \tilde{\omega} - \dot{r}_\delta \\ \ddot{e} &= \mathbf{C}_e \mathbf{A}(\mathbf{A}\tilde{\mathbf{x}} + \mathbf{B}_1\tilde{u}) - \ddot{r}_\delta = A_{21}\tilde{\delta} + B^{-1}(\delta_0)u - \ddot{r}_\delta.\end{aligned}$$

Let $u := \mathbf{K}_S \tilde{\mathbf{x}} + u_{FF}$ and assume $\mathbf{K}_S := [k_1 \ k_2]$, with $k_1, k_2 \in \mathbb{R}$. Then, assume $\nu = 0$ and obtain the feed-forward control law by imposing $e, \dot{e}, \ddot{e} = 0$. In detail,

$$u_{FF} = B(\delta_0) [\ddot{r}_\delta - A_{21}r_\delta - B^{-1}(\delta_0)(k_1r_\delta + k_2\dot{r}_\delta)].$$

4.7.6 Latero-directional Controls

The automatic control systems developed on model (2.78) embrace the Electronic Stability Program (ESP) and Torque Vectoring (TV). On the one hand, the extension of system (2.78), represented by Eq. (2.92), is used as a model for the design of Lane Keeping (LK) and Lane Changing (LC). On the other hand, the specialization of system (2.78) provided in Eq. (2.95) constitutes the starting point for the development of Self-Park Assist (SPA).

ESP architecture

The main purpose of ESP is that of improving the stability of (2.83), which represents the linearization of (2.78) evaluated on a straight trajectory traveled at constant speed $v_0 > 0$. As described in Sect. 3.4.6, there exist speed-dependent conditions (dependent on v_0) in which the vehicle, when perturbed, departs from the equilibrium trajectory. In this context, ESP changes the closed-loop eigenvalues via a state-feedback algorithm.

In agreement with the theory depicted in Sect. 4.2, stabilizability is essential to design a state-feedback controller. So, for the investigation of the reachability properties of system (2.83), note that there are two categories of control inputs, i.e., the toe of the wheels (whether 4WS or 2WS) and the yaw torque provided by differential driving/braking actions. This section assumes a 2WS vehicle in which the driver has full authority over the steering system. Then, assuming that the rear wheels are non-steerable (with null toe angle), their speed represents the unique available control input. In this scenario, let $\bar{\omega} := (\omega_2 + \omega_3)/2$, $\Delta\omega := (\omega_3 - \omega_2)/2$, and $\mathbf{w}_{\text{ESP}} := \text{col}(\mathbf{d}, \delta_1, \delta_2, \omega_1, \bar{\omega}, \omega_4, \nu, r)$. Then, use \mathbf{B}_1 and \mathbf{B}_2 to define $\mathbf{B}_{1,\text{ESP}}$, $\mathbf{B}_{2,\text{ESP}}$ such that $\mathbf{B}_1\mathbf{u} + \mathbf{B}_2\mathbf{w} = \mathbf{B}_{1,\text{ESP}}\Delta\omega + \mathbf{B}_{2,\text{ESP}}\mathbf{w}_{\text{ESP}}$. In particular,

$$\mathbf{B}_{1,\text{ESP}} = \text{col}(0, 0, k) \quad (4.57)$$

where

$$k := \frac{\partial\mu(\lambda, \Theta_0)}{\partial\lambda} \Big|_{\lambda=\lambda_{r_0}} \frac{r(1-\lambda_{r_0})^2}{v_0} \frac{c}{J} \left(2N_{20} + \frac{\bar{h}(\mu_{f0} - \mu_{r0})(N_{20} - N_{10})}{1 - \bar{h}(\mu_{r0} - \mu_{f0})} \right) > 0$$

for standard configurations.

Now, using matrix \mathbf{A} provided in (3.22), the reachability study is performed on the couple $(\mathbf{A}, \mathbf{B}_{1,\text{ESP}})$ through

$$\begin{aligned} \mathbf{R} &= [\mathbf{B}_{1,\text{ESP}} \ \mathbf{AB}_{1,\text{ESP}} \ \mathbf{A}^2\mathbf{B}_{1,\text{ESP}}] \\ &= \begin{bmatrix} 0 & 0 & 0 \\ 0 & k \left(\frac{1}{v_0} \frac{\partial \bar{f}_y}{\partial \omega} - v_0 \right) & \frac{k}{v_0} \left(\frac{\partial \bar{f}_y}{\partial v_y} + \frac{m}{J} \frac{\partial \bar{\tau}}{\partial \omega} \right) \left(\frac{1}{v_0} \frac{\partial \bar{f}_y}{\partial \omega} - v_0 \right) \\ k & k \frac{m}{Jv_0} \frac{\partial \bar{\tau}}{\partial \omega} & k \frac{m}{Jv_0} \left(\frac{\partial \bar{\tau}}{\partial v_y} \left(\frac{1}{v_0} \frac{\partial \bar{f}_y}{\partial \omega} - v_0 \right) + \frac{m}{Jv_0} \left(\frac{\partial \bar{\tau}}{\partial \omega} \right)^2 \right) \end{bmatrix}. \end{aligned}$$

The investigation of \mathbf{R} leads to the conclusion that the system is not fully reachable. This result is inferred because the dynamics of v_x cannot be modified by acting on $\Delta\omega$. Moreover, let $v_{lc}(v_0) := \sqrt{\partial \bar{f}_y / \partial \omega}$, then, it is easy to see that, as far as $v_{lc}(v_0) \neq v_0$, the non-reachable part corresponds to the longitudinal speed dynamics. These dynamics are Hurwitz, as demonstrated in Sect. 3.4.6, and so the couple $(\mathbf{A}, \mathbf{B}_{1,\text{ESP}})$ is stabilizable for $v_0 > 0$: $v_{lc}(v_0) \neq v_0$ (which is true for any $v_0 > 0$ for typical vehicle configurations).

On the other hand, at $v_0 = \sqrt{\partial \bar{f}_y / \partial \omega}$, the only reachable state is ω . In this case, the study of the eigenvalues of \mathbf{A} outlined in Sect. 3.4.6 shows that the roots $\lambda_{2,3}$ are real and negative. So, the system is again stabilizable.

Let $v_{\max} > 0$ be the maximum expected speed for the considered vehicle, then pick the most forward configuration of the gravity center and define $\bar{\Delta} = \bar{a} - \bar{b}$. Then, choose $v_0 := \arg \max_{v \in [0, v_{\max}]} \text{real}(\lambda_3)$ as the linearization speed. As detailed in Sect. 3.4.6 (see Fig. 3.29), this configuration represents the worst (the least stable) condition.

For $v_0 \neq \sqrt{\partial \bar{f}_y / \partial \omega}$, identify the reachable state as $\mathbf{z}_R := \text{col}(v_y, \omega)$. Then, for the design of the state feedback, refer to the dynamics $\dot{\mathbf{z}}_R = \bar{\mathbf{A}}\mathbf{z}_R + \bar{\mathbf{B}}_1\Delta\omega$ in which

$$\begin{aligned}\bar{\mathbf{A}} &= \left[\begin{array}{cc} \frac{1}{v_0} \frac{\partial \bar{f}_y}{\partial v_y} & \frac{1}{v_0} \frac{\partial \bar{f}_y}{\partial \omega} - v_0 \\ \frac{m}{Jv_0} \frac{\partial \bar{\tau}}{\partial v_y} & \frac{m}{Jv_0} \frac{\partial \bar{\tau}}{\partial \omega} \end{array} \right]_{\mathbf{x}=\mathbf{x}_0, \mathbf{u}=\mathbf{u}_0} \\ \bar{\mathbf{B}}_1 &= \frac{\partial \mu(\lambda, \Theta_0)}{\partial \lambda} \Big|_{\lambda=\lambda_{r_0}} \left[\begin{array}{c} \frac{r(1-\lambda_{r_0})^2}{v_0} \frac{c}{J} \\ k \end{array} \right].\end{aligned}$$

The state must be available, whether at measurement or estimated to implement a state-feedback control law. In this context, the sensor suite described in Sect. 2.6 is exploited for the state estimation provided that the plant is detectable; see Sect. 4.4. Concerning model (2.83), the observability study relies on the couple (\mathbf{A}, \mathbf{C}) through

$$\mathbf{O} = \begin{bmatrix} \mathbf{C} \\ \mathbf{CA} \\ \mathbf{CA}^2 \end{bmatrix} = \begin{bmatrix} 0 & 0 & 1 \\ 0 & \frac{m}{Jv_0} \frac{\partial \bar{\tau}}{\partial v_y} & \mathbf{x} \\ 0 & \frac{m}{Jv_0^2} \frac{\partial \bar{\tau}}{\partial v_y} \left(\frac{\partial \bar{f}_y}{\partial v_y} + \frac{m}{J} \frac{\partial \bar{\tau}}{\partial \omega} \right) & \mathbf{x} \end{bmatrix}$$

where \mathbf{x} denotes the presence of an entry, possibly nontrivial. The study of the kernel of \mathbf{O} shows that the system is not fully observable because the first column is null. Also the second column becomes null for $\partial \bar{\tau} / \partial v_y = 0$. On the one hand, for $\partial \bar{\tau} / \partial v_y = 0$, it is

$$\ker(\mathbf{O}) = \begin{bmatrix} 1 & 0 & 0 \\ 0 & 1 & 0 \end{bmatrix},$$

which implies that v_x and v_y are not observable. On the other hand, as described in Sect. 3.4.6, the system has negative real part eigenvalues for $\partial \bar{\tau} / \partial v_y = 0$. So, the couple (\mathbf{A}, \mathbf{C}) is detectable.

Furthermore, it is easy to see that, if $\partial \bar{\tau} / \partial v_y \neq 0$, the gyroscope output represents a necessary and sufficient measurement for the observation of \mathbf{z}_R . It is also important to note that v_x does not affect the dynamics of \mathbf{z}_R (so there is no need to know this for the computation of the stabilization control). For these reasons, design the following observer:

$$\begin{aligned}\dot{\hat{\mathbf{z}}}_R &= \bar{\mathbf{A}}\hat{\mathbf{z}}_R + \bar{\mathbf{B}}_1\Delta\omega + \mathbf{K}_O(\tilde{y}_\omega - \hat{\tilde{y}}_\omega) \\ \hat{\tilde{y}}_\omega &= \bar{\mathbf{C}}\hat{\mathbf{z}}_R\end{aligned}$$

where $\bar{\mathbf{C}} := [0 \ 1]$. Adopting the design technique proposed in Sect. 4.2, the feedback control law is $u_S = \mathbf{K}_S\hat{\mathbf{z}}_R$.

TV architecture

TV's main purpose is to improve the turning performance by making the vehicle tracking the reference side-speed and yaw rate. This section assumes that TV relies on the same ESP control input. However, other configurations are possible (e.g., an active steering system, four-wheel steering, and front-rear differential).

In this context, the ESP control architecture is extended with a feed-forward block to make the actual vehicle yaw rate track a time-varying reference. Let $r \in \mathbb{R}$ be the reference yaw rate, and define $e = \omega - r$ as the tracking error. Then, concerning the couple $\bar{\mathbf{A}}, \bar{\mathbf{B}}_1$ identified in the ESP investigation, the feed-forward control is designed (see Sect. 4.6) by computing the relative degree of the system

$$\begin{aligned}\dot{\mathbf{z}}_R &= \bar{\mathbf{A}}\mathbf{z}_R + \bar{\mathbf{B}}_1(u_S + u_{FF}) \\ e &= \bar{\mathbf{C}}_e\mathbf{z}_R - r,\end{aligned}$$

with $\bar{\mathbf{C}}_e = [0 \ 1]$. It is easy to see that the relative degree $r_{\max} = 1$ is less than the dimension of \mathbf{z}_R . As a consequence, inspired by Infobox 4.9, define

$$\mathbf{T}_\zeta = \bar{\mathbf{C}}_e, \quad \mathbf{T}_{\zeta_\perp} = [1 \ 0], \quad \mathbf{T} = \text{col}(\mathbf{T}_{\zeta_\perp}, \mathbf{T}_\zeta)$$

and introduce the state $\zeta = \text{col}(\zeta_\perp, \zeta) := \mathbf{T}\mathbf{z}_R$. Note that, since $\mathbf{T} = \mathbf{I}$, it is $\zeta = \mathbf{z}_R$ whose dynamics are symbolically written as

$$\begin{aligned}\dot{\zeta} &= \bar{A}_{11}\zeta_\perp + \bar{A}_{12}\zeta + \bar{\mathbf{C}}_e\bar{\mathbf{B}}_1u_{FF} \\ \dot{\zeta}_\perp &= \bar{A}_{21}\zeta_\perp + \bar{A}_{22}\zeta \\ e &= \zeta - r.\end{aligned}$$

Hence, let $u_S := \mathbf{K}_S\mathbf{z}_R$ and $\zeta^* := \text{col}(\zeta_\perp^*, r)$, then the feed-forward control law is provided, by imposing $e \equiv 0$, by

$$\begin{aligned}\dot{\zeta}_\perp^* &= \bar{A}_{11}\zeta_\perp^* + \bar{A}_{12}r \\ u_{FF} &= (\bar{\mathbf{C}}_e\bar{\mathbf{B}}_1)^{-1}(\dot{r} - \bar{\mathbf{C}}_e(\bar{\mathbf{A}} + \bar{\mathbf{B}}_1\mathbf{K}_S)\zeta^*).\end{aligned}$$

Infobox 4.10 provides a guide for selecting the reference yaw rate. To conclude, for robustness reasons, an integral action is added to asymptotically nullify the tracking error in the case of constant reference and disturbance. Since the yaw rate is directly available at measurement via $y_\omega = \omega + \nu_\omega$, the integral action can be implemented as

$$\dot{\eta} = y_\omega - r$$

$$u_{IA} = k_{IA}\eta.$$

Infobox 4.10 (Latero-directional Reference Generator) *Advanced latero-directional controllers, designed on Eq. (2.83) and relying on a feed-forward architecture, need a reference for the states v_y and ω , nominally r_{v_y} and r_ω . For example, a reference yaw rate must feed the TV controller. Hereafter, a possible design criterion for r_{v_y} and r_ω is provided, where the main idea is assuming the steering wheel angle as a known disturbance. This angle is then used to generate r_{v_y} and r_ω . These references feed the automatic control system in agreement with the number of control inputs. In particular, only r_ω feeds the TV detailed*

in Sect. 4.7.6 because the input is scalar. So then, only one reference can be tracked according to the theory developed in Sect. 4.6.

Denote the steering wheel angle with $\delta_s \in \mathbb{R}$ (assumed to be at the driver's disposal). A steering system kinematics associates the wheel toe angles to the steering wheel angle. In detail, assume two functions $f_i : \mathbb{R} \rightarrow \mathbb{R}$, such that $\delta_i = f_i(\delta_s)$ for $i = 1, 4$ (remember that $\delta_2, \delta_3 = 0$ by assumptions made for ESP). With this description at hand, linearize model (2.78) around a constant-speed straight path to define $\mathbf{B}_s \in \mathbb{R}^{3 \times 1}$ such that

$$\mathbf{B}_1 \tilde{\mathbf{u}} = \mathbf{B}_s \delta_s + \mathbf{B}'' \text{col}(\tilde{\omega}_1, \dots, \tilde{\omega}_4).$$

Now, assume $\tilde{\omega}_1, \dots, \tilde{\omega}_4 = 0$ and study the linearized system

$$\dot{\tilde{\mathbf{x}}} = \mathbf{A} \tilde{\mathbf{x}} + \mathbf{B}_s \delta_s$$

where $\tilde{\mathbf{x}} := \text{col}(\tilde{v}_x, \tilde{v}_y, \tilde{\omega})$. In more detail, if \mathbf{A} is Hurwitz, this system is BIBS-stable. Consequently, if \mathbf{A} is Hurwitz and for constant δ_s , the state asymptotically converges to

$$\tilde{\mathbf{x}}_\infty = -\mathbf{A}^{-1} \mathbf{B}_s \delta_s.$$

A detailed analysis of \mathbf{B}_s reveals that $\mathbf{B}_s = \text{col}(0, b_1, b_2)$ where $b_1, b_2 \in \mathbb{R}$. First, note that δ_s has no impact on \tilde{v}_x due to the structure of \mathbf{A} (see model (2.83)). Hence, focus on the asymptotic values of $\tilde{v}_y, \tilde{\omega}$, whose expressions are obtained through Eq. (2.83) as

$$\begin{bmatrix} \tilde{v}_y \\ \tilde{\omega} \end{bmatrix}_\infty = \frac{v_0 J/m}{\frac{\partial \bar{\tau}}{\partial v_y} \left(\frac{\partial \bar{f}_y}{\partial \omega} - v_0^2 \right) - \frac{\partial \bar{f}_y}{\partial v_y} \frac{\partial \bar{\tau}}{\partial \omega}} \begin{bmatrix} \frac{m}{J} \frac{\partial \bar{\tau}}{\partial \omega} & v_0^2 - \frac{\partial \bar{f}_y}{\partial \omega} \\ -\frac{m}{J} \frac{\partial \bar{\tau}}{\partial v_y} & \frac{\partial \bar{f}_y}{\partial v_y} \end{bmatrix} \begin{bmatrix} b_1 \\ b_2 \end{bmatrix} \delta_s$$

and where the partial derivatives are evaluated at $(\mathbf{x}, \mathbf{u}) = (\mathbf{x}_0, \mathbf{u}_0)$. From the last equation, it is evident that the behavior of $\tilde{v}_{y\infty}, \tilde{\omega}_\infty$ is deeply affected by the sign of $\partial \bar{\tau} / \partial v_y$.

With the definitions of $v_1(\cdot)$ at hand (see Sect. 3.4.6), the denominator is nullified for $\partial \bar{\tau} / \partial v_y < 0$, at $v_0 = v^* > 0$, such that $v^* = v_1(v^*)$. This implies that $\tilde{v}_{y\infty}$ and $\tilde{\omega}_\infty$ are bounded for $v_0 < v^*$, but $\lim_{v_0 \rightarrow v^*} |\tilde{v}_{y\infty}/\delta_s|, |\tilde{\omega}_\infty/\delta_s| = \infty$. For $v_0 > v^*$, bounded values of $\tilde{v}_{y\infty}$ and $\tilde{\omega}_\infty$ do not represent valid references due to the instability of \mathbf{A} . On the other hand, if $\partial \bar{\tau} / \partial v_y = 0$, $\tilde{v}_{y\infty}$ and $\tilde{\omega}_\infty$ represent valid references for any $v_0 > 0$. Finally, assume $\partial \bar{\tau} / \partial v_y > 0$ and

$$\frac{\partial \bar{\tau}}{\partial v_y} \frac{\partial \bar{f}_y}{\partial \omega} - \frac{\partial \bar{f}_y}{\partial v_y} \frac{\partial \bar{\tau}}{\partial \omega} < 0,$$

then $\tilde{v}_{y\infty}$ and $\tilde{\omega}_\infty$ denote valid asymptotic solutions for any $v_0 > 0$ also for oversteering vehicles. For $\partial \bar{\tau} / \partial v_y \geq 0$ there exists a speed, namely $\bar{v}_0 > 0$, such

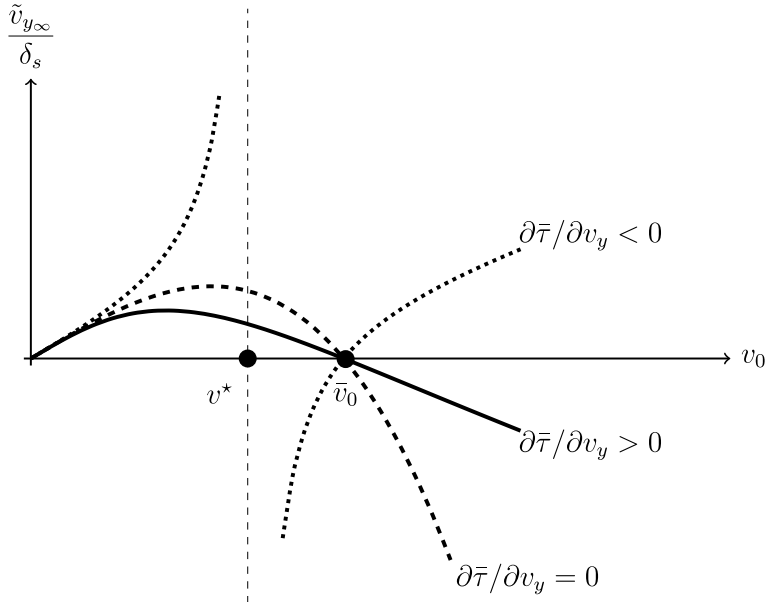


Fig. 4.7 Lateral speed sensitivity $\tilde{v}_{y_\infty}/\delta_s$. Asymptotic values of \tilde{v}_{y_∞} represent valid reference candidates, only at sufficiently low speeds, for models of understeered vehicles ($\partial\bar{\tau}/\partial v_y < 0$). On the other hand, models of neutral and oversteered vehicles can be used to design reference lateral speeds at any $v_0 > 0$

that $\tilde{v}_y/\delta_s = 0$. This speed is found by solving the implicit equality (remember that $\partial\bar{\tau}/\partial\omega$, $\partial\bar{f}_y/\partial\omega$, b_1 , and b_2 are functions of v_0)

$$\frac{m}{J} \frac{\partial\bar{\tau}}{\partial\omega} b_1 + \left(v_0^2 - \frac{\partial\bar{f}_y}{\partial\omega} \right) b_2 = 0.$$

Figures 4.7 and 4.8 depict sensitivities $\tilde{v}_{y_\infty}/\delta_s$ and $\tilde{\omega}_\infty/\delta_s$ for $b_1, b_2 > 0$ (common for front steering wheel vehicles). These pictures clearly show that neutral and oversteered reference vehicles represent plausible design choices. From these pictures one can see that for neutral and oversteering reference vehicles, and for $v_0 < \bar{v}_0$, the lateral speed \tilde{v}_{y_∞} is positive for positive δ_s . On the other hand, \tilde{v}_{y_∞} becomes negative for positive δ_s at $v_0 > \bar{v}_0$. The behavior change for $v_0 > \bar{v}_0$ is representative of high-speed turns usually performed in drift and rally competitions.

Lane control architecture

The LK control's main purpose is to (stably) maintain a constant distance from the lane. In this context and in agreement with the theory presented in Sect. 4.2, a stabilizer is required because, as detailed in Sect. 3.4.6, the plant is not Hurwitz. Also, a state observer is necessary to implement the stabilizer. Indeed, although

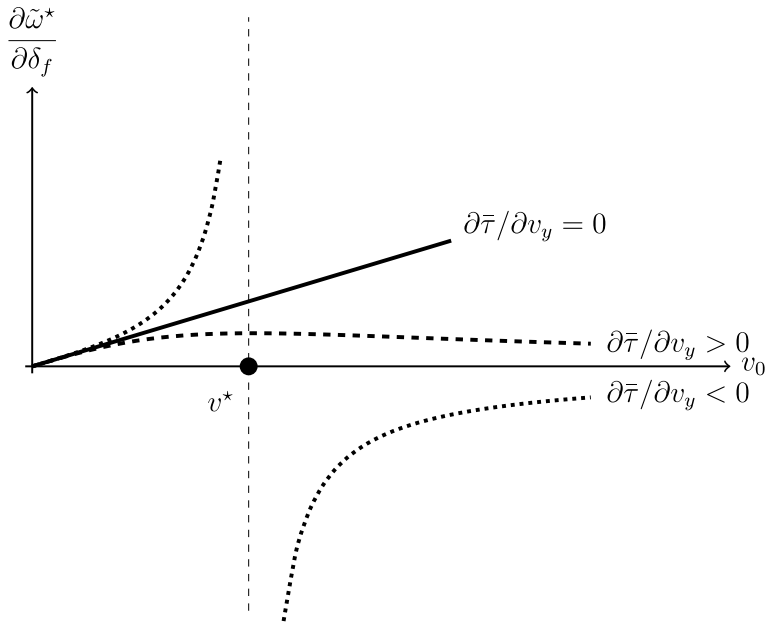


Fig. 4.8 Yaw sensitivity $\tilde{\omega}_\infty/\delta_s$. The reference yaw rate generated through a model representing a neutral or oversteered vehicle remains bounded for bounded v_0 . On the other hand, models of understeered vehicles provide valid reference yaw rates only at sufficiently low speeds

proprioceptive sensors could provide information about the distance and the heading to the lane, the vehicle speeds are not directly available at measurement. Moreover, an integral control action extends the controller architecture. This latter is needed to robustly maintain the desired distance to the lane. The control system architecture components are detailed in this section, which assumes a front-wheel steering vehicle.

The stabilization of plant (2.93) requires the design of a state-feedback controller that makes negative the real part of the eigenvalues of matrix (3.24). In addition, Sect. 2.6.1 shows that model (2.93) represents an extension of Eq. (2.83), i.e., the model adopted to design ESP. In particular, the extended state contains the vehicle speeds, the distance to the lane, and the vehicle–lane relative angle. The states of the ESP model force the dynamics of these last two variables through the top right part of matrix (3.24). On the one hand, this implies that, potentially, the same control input adopted for ESP, i.e., $\Delta\omega$, could be used to stabilize system (3.24) too. On the other hand, taking the steering wheel angle as a further control input improves the reachability. Indeed, the lateral force induced by tilting the front wheels affects the lateral motion more directly than the $\Delta\omega$ can do. For these reasons, a possible stabilization strategy relies on the rear wheel differential speed and the steering wheel rotation.

Let \mathbf{B}_{ESP} and \mathbf{B}_δ be those of Eq. (4.57) and Infobox 4.10, then define $\mathbf{u}_L = \text{col}(\Delta\omega, \delta_s)$ and

$$\mathbf{B}_L = \begin{bmatrix} \mathbf{0} & \mathbf{0} \\ \mathbf{B}_{\text{ESP}} & \mathbf{B}_\delta \end{bmatrix}.$$

Use \mathbf{A}_L , defined in Eq. (3.24), and \mathbf{B}_L to compute

$$\begin{aligned} \mathbf{R} &= [\mathbf{B}_L \mathbf{A}_L \mathbf{B}_L \mathbf{A}_L^2 \mathbf{B}_L] \\ &= \begin{bmatrix} 0 & 0 & -kx_A & -b_1 - b_2 x_A & \mathbf{x} \mathbf{x} \\ 0 & 0 & k & b_2 & \mathbf{x} \mathbf{x} \\ 0 & 0 & 0 & 0 & 0 \mathbf{0} \\ 0 & b_1 & k \left(\frac{1}{v_0} \frac{\partial \bar{f}_y}{\partial \omega} - v_0 \right) \frac{1}{v_0} \frac{\partial \bar{f}_y}{\partial v_y} b_1 + \left(\frac{1}{v_0} \frac{\partial \bar{f}_y}{\partial \omega} - v_0 \right) b_2 & \mathbf{x} \mathbf{x} \\ k & b_2 & k \frac{m}{Jv_0} \frac{\partial \bar{\tau}}{\partial \omega} & \frac{m}{Jv_0} \frac{\partial \bar{\tau}}{\partial v_y} b_1 + \frac{m}{Jv_0} \frac{\partial \bar{\tau}}{\partial \omega} b_2 & \mathbf{x} \mathbf{x} \end{bmatrix}, \end{aligned}$$

in which \mathbf{x} denotes a possibly nontrivial entry. Not surprisingly, the couple $(\mathbf{A}_L, \mathbf{B}_L)$ is not fully reachable. Indeed, \mathbf{u}_L cannot modify the longitudinal speed. Nevertheless, despite this deficiency, already investigated in the ESP study, the system is stabilizable because the first four columns of \mathbf{R} are linearly independent, for any $v_0 > 0$.

Therefore, in agreement with the reachability decomposition introduced in Sect. 4.2, \mathbf{x}_L can be transformed to highlight its reachable and non-reachable subparts. The transformation matrix at the base of this change of coordinates is

$$\mathbf{T}_R^{-1} := \begin{bmatrix} 1 & 0 & 0 & 0 & 0 \\ 0 & 1 & 0 & 0 & 0 \\ 0 & 0 & 0 & 0 & 1 \\ 0 & 0 & 1 & 0 & 0 \\ 0 & 0 & 0 & 1 & 0 \end{bmatrix},$$

where the first four columns represent a basis for \mathbf{R} . Consequently, define $\mathbf{z}_R \in \mathbb{R}^4$ and $z_{NR} \in \mathbb{R}$ and let $\mathbf{z} := \text{col}(\mathbf{z}_R, z_{NR})$ such that $\mathbf{z} = \mathbf{T}_R \mathbf{x}$. The application of this change of coordinates to system (2.93) leads to the identification of

$$\dot{\mathbf{z}}_R = \bar{\mathbf{A}} \mathbf{z}_R + \bar{\mathbf{B}} \mathbf{u}_L.$$

Matrices $\bar{\mathbf{A}} \in \mathbb{R}^{4 \times 4}$ and $\bar{\mathbf{B}} \in \mathbb{R}^{4 \times 2}$ are such that

$$\mathbf{T}_R \mathbf{A}_L \mathbf{T}_R^{-1} = \begin{bmatrix} \bar{\mathbf{A}} & \mathbf{0} \\ \mathbf{0} & \mathbf{x} \end{bmatrix}, \quad \mathbf{T}_R \mathbf{B}_L = \begin{bmatrix} \bar{\mathbf{B}} \\ \mathbf{0} \end{bmatrix}$$

with \mathbf{x} a nontrivial entry. The state-feedback stabilizer is then obtained, as described in Sect. 4.2, via a matrix $\mathbf{K}_R \in \mathbb{R}^{2 \times 4}$ such that $\bar{\mathbf{A}} + \bar{\mathbf{B}} \mathbf{K}_R$ is Hurwitz, as

$$\mathbf{u}_L = \mathbf{K}_R \mathbf{z}_R.$$

Study the observability matrix associated with the couple $(\mathbf{A}_L, \mathbf{C}_L)$ to identify the state's subpart that can be estimated. Then, compute

$$\mathbf{O} = \begin{bmatrix} \mathbf{C}_L \\ \mathbf{C}_L \mathbf{A}_L \\ \mathbf{C}_L \mathbf{A}_L^2 \end{bmatrix} = \begin{bmatrix} 1 & 0 & 0 & 0 & 0 \\ 0 & 1 & 0 & 0 & 0 \\ 0 & 0 & 0 & 0 & 1 \\ 0 & -v_0 & 0 & -1 & -x_A \\ 0 & 0 & 0 & \frac{m}{Jv_0} \frac{\partial \bar{\tau}}{\partial v_y} & \frac{m}{Jv_0} \frac{\partial \bar{\tau}}{\partial \omega} \\ 0 & v_0^2 & 0 & \times & \times \\ 0 & 0 & 0 & \times & \times \end{bmatrix},$$

where \times denotes a possible nontrivial entry. It is easy to see that the third state (i.e., v_x) is not observable, whereas, thanks to the proprioceptive sensors, the rest of the state is observable for any $v_0 > 0$ and any $\partial \bar{\tau} / \partial v_y$. Let $\tilde{\mathbf{y}}_L := \text{col}(\tilde{y}_\rho, \tilde{y}_\psi, \tilde{y})$ and

$$\bar{\mathbf{C}} := \begin{bmatrix} 1 & 0 & 0 & 0 \\ 0 & 1 & 0 & 0 \\ 0 & 0 & 0 & 1 \end{bmatrix}$$

and write the observer as

$$\begin{aligned} \dot{\hat{\mathbf{z}}}_R &= \bar{\mathbf{A}} \hat{\mathbf{z}}_R + \bar{\mathbf{B}} \mathbf{u}_L + \mathbf{K}_O (\tilde{\mathbf{y}}_L - \hat{\mathbf{y}}_L) \\ \hat{\mathbf{y}}_L &= \bar{\mathbf{C}} \hat{\mathbf{z}}_R. \end{aligned}$$

Last but not least, the integral action represents a component of the LK controller.

In agreement with model (2.93), the errors to be nullified are the distance to the lane and the relative heading angle. Let $r_L \in \mathbb{R}$ be the reference distance, and note that $y_\rho = \rho + \nu_\rho$ and $y_\psi = \psi_r + \nu_\psi$ provide a measure of the actual distance to the lane and the relative heading. Hence, the integral action is implemented as

$$\begin{aligned} \dot{\boldsymbol{\eta}} &= \begin{bmatrix} y_\rho - r_L \\ y_\psi \end{bmatrix} \\ \mathbf{u}_L &= \mathbf{K}_I \boldsymbol{\eta}. \end{aligned}$$

To design \mathbf{K}_I , adopt the procedure described in Sect. 4.3, i.e., define

$$\mathbf{A}_e = \begin{bmatrix} \bar{\mathbf{A}} & \mathbf{0} \\ \bar{\mathbf{C}}_e & \mathbf{0} \end{bmatrix}, \quad \mathbf{B}_e = \begin{bmatrix} \bar{\mathbf{B}} \\ \mathbf{0} \end{bmatrix}, \quad \bar{\mathbf{C}}_e = [\mathbf{I} \ \mathbf{0}].$$

Then, find matrices $\mathbf{K}_R, \in \mathbb{R}^{2 \times 4}$ and $\mathbf{K}_I, \in \mathbb{R}^{2 \times 1}$ such that $\mathbf{A}_e + \mathbf{B}_e [\mathbf{K}_R \ \mathbf{K}_I]$ is Hurwitz.

In Sect. 5.4.6, the capabilities of the LK are tested in a lane-changing scenario, modeled via a step-wise constant reference distance $r_L(t)$. In the case of $r_L(t)$ being continuous, a feed-forward law can improve the control architecture and performance during the transients. The resulting scheme represents an LC control.

Self-Park Assist

Section 2.6.2 presented the model describing the control problem associated with SPA. In this context, the control system stabilizes the states (distance to the lane

and relative heading) at the origin. Then, to accomplish this task, the control system architecture relies on a stabilizer working in cooperation with a feed-forward action. Moreover, in this context, the assumption of a SLAM algorithm providing an estimation of the distance to the lane and of the relative heading makes the state available at the output. This implies that there is no need for an observer. A feed-forward controller improves the parking performance. In this scenario, the feed-forward law pre-compensates for the disturbance introduced by the (known) lane curvature.

As for the state-feedback stabilizer, the theory developed in Sect. 4.2 demonstrated that this controller exists if the plant is stabilizable, i.e., if the non-reachable subpart's eigenvalues have negative real parts. Matrices \mathbf{A} and \mathbf{B}_1 detailed in Eq. (2.96) are exploited to compute

$$\mathbf{R} = [\mathbf{B}_1 \ \mathbf{AB}_1] = \begin{bmatrix} -v_0 x_A / \ell & -v_0^2 \ell \\ v_0 / \ell & 0 \end{bmatrix},$$

which is full-rank for all $v_0 \neq 0$ and all $x_A \in \mathbb{R}$. This implies that the plant under investigation is fully reachable, and there exists at least one matrix $\mathbf{K}_S \in \mathbb{R}^{1 \times 2}$ such that $\mathbf{A} + \mathbf{B}_1 \mathbf{K}_S$ is Hurwitz. As a consequence, the stabilization control is

$$u_S = \mathbf{K}_S \mathbf{x}.$$

To conclude, follow the next steps to design the feed-forward controller. First, in agreement with the theoretical tools provided in Sect. 4.6, compute the derivative

$$\dot{e} = -v_0 \tilde{\psi} - v_0 \frac{x_A}{\ell} u$$

and note that the system does not verify Assumption 4.3 for all $v_0 \neq 0$. Then, the technique described in Infobox 4.9 must be adopted. Define $\zeta = \text{col}(\zeta, \zeta_{\perp})$ with $\zeta, \zeta_{\perp} \in \mathbb{R}$, and $\mathbf{T} = \text{col}(\mathbf{C}_e, \mathbf{T}_{\zeta_{\perp}})$ with $\mathbf{T}_{\zeta_{\perp}} \in \mathbb{R}^{1 \times 2}$ such that \mathbf{T} is invertible and $\mathbf{T}_{\zeta_{\perp}} \mathbf{B}_1 = 0$. A valid choice is $\mathbf{T}_{\zeta_{\perp}} := [1 \ x_A]$. Use \mathbf{T} , \mathbf{A} , \mathbf{B}_1 , and \mathbf{B}_2 to define $\bar{A}_{ij} \in \mathbb{R}$, $\bar{\mathbf{B}}_{2i} \in \mathbb{R}^{1 \times 3}$, $i, j = 1, 2$, and $B_{11} \in \mathbb{R}$, such that

$$\mathbf{T} \mathbf{A} \mathbf{T}^{-1} = \begin{bmatrix} \bar{A}_{11} & \bar{A}_{12} \\ \bar{A}_{21} & \bar{A}_{22} \end{bmatrix}, \quad \mathbf{T} \mathbf{B}_1 = \begin{bmatrix} B_{11} \\ 0 \end{bmatrix}, \quad \mathbf{T} \mathbf{B}_2 = \begin{bmatrix} \bar{\mathbf{B}}_{21} \\ \bar{\mathbf{B}}_{22} \end{bmatrix}.$$

Then, define $\mathbf{w}^* = \text{col}(d^*, \mathbf{0})$ and compute the feed-forward control law as:

$$\begin{aligned} \dot{\zeta}_{\perp}^* &= \bar{A}_{22} \zeta_{\perp}^* + \bar{\mathbf{B}}_{22} \mathbf{w}^* \\ u_{FF} &= -\bar{B}_{11}^{-1} [\bar{A}_{12} \zeta_{\perp}^* + \bar{\mathbf{B}}_{21} \mathbf{w}^*]. \end{aligned}$$

It is worth stressing that, in this context, the knowledge of d^* (thought as generated by a planner) is exploited to pre-compensate for the disturbance effects. Moreover, let $\mathbf{K}_S := [k_1 \ k_2]$ with $k_1, k_2 \in \mathbb{R}$, then for $\mathbf{T}_{\zeta_{\perp}} := [1 \ x_A]$, it is $\bar{A}_{12} = -(v_0/x_A + k_2 v_0/\ell)$, $\bar{A}_{22} = -v_0/x_A$, $\bar{B}_{11} = -v_0 x_A / \ell$, $\bar{\mathbf{B}}_{21} = \mathbf{0}$, and $\bar{\mathbf{B}}_{22} = [-v_0 x_A \ \mathbf{0}]$.

4.8 Summary

This chapter has described every block composing the control system architecture of Fig. 1.5. The control system comprises a stabilizer, an integral action, an observer (that feeds the stabilizer), and a feed-forward control. The output-feedback stabilizer, obtained as a composition of the observer and the stabilizer, is in charge of making the plant BIBS-stable. This stability property guarantees the boundedness of the state and control. Moreover, the integral action leads to an asymptotic cancellation of constant disturbances and makes the regulation of constant set points possible. On the other hand, the feed-forward control helps to track a time-varying reference. All these control blocks are designed based on common concepts of reachability, stabilizability, observability, and detectability. In more detail, two fundamental theorems are introduced and exploited to assure the existence of matrices that make the controlled plant BIBS-stable. All these theoretical tools are finally applied to define the control system architecture for each case study proposed in Chap. 2.

4.9 Exercises

Exercise 4.1 Is the couple

$$\mathbf{A} = \begin{bmatrix} 0 & 1 \\ 0 & -1 \end{bmatrix} \quad \mathbf{B} = \begin{bmatrix} 1 & 1 \\ 0 & 1 \end{bmatrix}$$

fully reachable? Which column of \mathbf{B} can be eliminated without modifying the original reachability properties?

Exercise 4.2 Is the couple

$$\mathbf{A} = \begin{bmatrix} 0 & 1 \\ 0 & -1 \end{bmatrix} \quad \mathbf{B} = \begin{bmatrix} 1 \\ 0 \end{bmatrix}$$

stabilizable? How large is the non-reachable subspace?

Exercise 4.3 Is the couple

$$\mathbf{A} = \begin{bmatrix} -1 & 0 & 0 \\ 1 & 0 & 0 \\ 0 & 1 & 0 \end{bmatrix} \quad \mathbf{B} = \begin{bmatrix} 0 \\ 0 \\ 1 \end{bmatrix}$$

fully reachable? How large is the unstable part of the non-reachable subspace?

Exercise 4.4 Is the couple

$$\mathbf{A} = \begin{bmatrix} 0 & 1 & 0 & 0 \\ 0 & 0 & 1 & 0 \\ 0 & 0 & 0 & 0 \\ 0 & 0 & 1 & 0 \end{bmatrix} \quad \mathbf{B} = \begin{bmatrix} 1 \\ 0 \\ 0 \\ 1 \end{bmatrix}$$

fully reachable? Which column could be added to \mathbf{B} to achieve full reachability? Which elements of \mathbf{A} could be changed to make the original couple (\mathbf{A}, \mathbf{B}) stabilizable?

Exercise 4.5 Is the couple

$$\mathbf{A} = \begin{bmatrix} 0 & 1 \\ 0 & 0 \end{bmatrix} \quad \mathbf{C} = \begin{bmatrix} 0 & 1 \end{bmatrix}$$

fully observable? How large is the unobservable subsystem?

Exercise 4.6 Is the couple

$$\mathbf{A} = \begin{bmatrix} 0 & 0 \\ 0 & 1 \end{bmatrix} \quad \mathbf{C} = \begin{bmatrix} 0 & 1 \end{bmatrix}$$

detectable? Which element of \mathbf{A} could be changed to obtain detectability?

Exercise 4.7 Is the couple

$$\mathbf{A} = \begin{bmatrix} 1 & 0 & 0 \\ 0 & 0 & 1 \\ 0 & 1 & 0 \end{bmatrix} \quad \mathbf{C} = \begin{bmatrix} 0 & 1 & 0 \end{bmatrix}$$

detectable? Which row could be added to \mathbf{C} to make the couple (\mathbf{A}, \mathbf{C}) fully observable?

Exercise 4.8 Is the couple

$$\mathbf{A} = \begin{bmatrix} 1 & 0 & 0 & 0 \\ 0 & 0 & 1 & 0 \\ 0 & 1 & 0 & 0 \\ 0 & 0 & 0 & -1 \end{bmatrix} \quad \mathbf{C} = \begin{bmatrix} 1 & 0 & 0 & 0 \\ 0 & 1 & 0 & 0 \\ 0 & 0 & 0 & 1 \end{bmatrix}$$

fully observable? Which element of \mathbf{C} could be changed to lose full observability while keeping detectability?

References

1. Antsaklis P, Michel AN (2006) Linear systems. Birkhäuser Basel
2. Antsaklis P, Michel AN (2007) A linear systems primer. Birkhäuser Basel
3. Grujitch LT (2013) Tracking control of linear systems. CRC Press
4. Kailath T, Sayed AH, Hassibi B (2000) Linear estimation. Prentice Hall
5. Khalil HK (2002) Nonlinear systems, 3rd edn. Prentice Hall Inc., Upper Saddle River, New Jersey, p 07458
6. Kisačanin B, Agarwal GC (2001) Linear control systems: with solved problems and MATLAB examples. Springer, US
7. Luenberger D (1967) Canonical forms for linear multivariable systems. IEEE Trans Automat Control 12(3):290–293
8. Young PC, Willems JC (1972) An approach to the linear multivariable servomechanism problem†. Int J Control 15(5):961–979



Optimal Control and Kalman Filter

5

Chapter 4 proved the existence of the matrices required to implement a linearization-based control system. Accordingly, this chapter presents a technique for designing these matrices.

In more detail, Sect. 5.1 designs the state feedback matrices through the so-called *optimal control technique* [2, 12, 13]. Then, Sect. 5.2 presents the concept of duality, through which Sect. 5.3 reuses all the results of Sect. 5.1 to design the observer matrix. The optimal control design technique is then adopted to solve the problems developed in Chaps. 2–4. Finally, the performance of the controllers is evaluated in simulation.

5.1 Robust Stationary Optimal Control

Sections 4.2 and 4.3 detailed the feedback control structure as the composition of an ideal state feedback plus an integral action. In more detail, let

$$\begin{aligned}\dot{\mathbf{x}} &= \mathbf{A}\mathbf{x} + \mathbf{B}_I\mathbf{u} & \mathbf{x}(t_0) &= \mathbf{x}_0 \\ \mathbf{e} &= \mathbf{C}_e\mathbf{x} + \mathbf{D}_{eI}\mathbf{u}\end{aligned}\tag{5.1}$$

be a stabilizable LTI system, then there exist two matrices \mathbf{K}_S and \mathbf{K}_I such that

$$\begin{aligned}\dot{\boldsymbol{\eta}} &= \mathbf{e} \\ \mathbf{u} &= \mathbf{K}_S\mathbf{x} + \mathbf{K}_I\boldsymbol{\eta}\end{aligned}\tag{5.2}$$

makes plant (5.1) BIBS-stable. This section provides an optimal criterion for the design of \mathbf{K}_S and \mathbf{K}_I .

Let $\mathbf{x}_e := \text{col}(\mathbf{x}, \boldsymbol{\eta})$,

$$\mathbf{A}_e := \begin{bmatrix} \mathbf{A} & \mathbf{0} \\ \mathbf{C}_e & \mathbf{0} \end{bmatrix}, \quad \mathbf{B}_e := \begin{bmatrix} \mathbf{B}_1 \\ \mathbf{D}_{e1} \end{bmatrix},$$

and substitute Eq. (5.2) into Eq. (5.1) to obtain

$$\dot{\mathbf{x}}_e = \mathbf{A}_e \mathbf{x}_e + \mathbf{B}_e \mathbf{u} \quad \mathbf{x}_e(t_0) = \mathbf{x}_{e0}. \quad (5.3)$$

To keep the notation clean, this chapter drops the subscripts from \mathbf{x}_e , \mathbf{A}_e , and \mathbf{B}_e .

Then, to introduce a robust optimality criterion [3, 9], alter system (5.3) and define a cost function $J > 0$ as follows:

$$\dot{\mathbf{x}} = (\mathbf{A} + 2\alpha\mathbf{I})\mathbf{x} + \mathbf{B}\mathbf{u} \quad \mathbf{x}(t_0) = \mathbf{x}_0 \quad (5.4a)$$

$$\boldsymbol{\epsilon} = \mathbf{C}\mathbf{x} + \mathbf{D}\mathbf{u} \quad (5.4b)$$

$$J = \int_{t_0}^{\infty} \boldsymbol{\epsilon}^\top \mathbf{Q} \boldsymbol{\epsilon} + \mathbf{u}^\top \mathbf{R} \mathbf{u} dt \quad (5.4c)$$

in which $\alpha \geq 0$, $\boldsymbol{\epsilon}$ denotes any linear combination of states and control to be penalized, $\mathbf{Q} = \mathbf{Q}^\top \succeq \mathbf{0}$ and $\mathbf{R} = \mathbf{R}^\top \succeq \mathbf{0}$ constitute the cost to pay if $\boldsymbol{\epsilon}(t) \neq \mathbf{0}$ and $\mathbf{u}(t) \neq \mathbf{0}$.

Important

The error $\boldsymbol{\epsilon}$ is not necessarily a measurable output and therefore does not need to be either a part of \mathbf{y} or obtainable from \mathbf{y} . The matrices \mathbf{C} and \mathbf{D} are not necessarily those defined in model (1.16).

Problem 5.1 Let (5.4) be an optimization problem, then design a control law $\mathbf{u}(t)$ that minimizes the cost (5.4c) under the constraint (5.4a).

Note

Roughly, the tunable parameters appearing in problem (5.4) can be interpreted as follows.

To make the error $\boldsymbol{\epsilon}(t)$ stay close to the origin, increase \mathbf{Q} to associate the condition $\boldsymbol{\epsilon}(t) \neq \mathbf{0}$ with a higher cost. Conversely, to let $\boldsymbol{\epsilon}(t)$ possibly go far from the origin, take $\mathbf{Q} = \mathbf{0}$. Moreover, the cost \mathbf{Q} must be $\succeq \mathbf{0}$ to be well-posed. Indeed, a negative cost would mean a “gain” which could encourage $\boldsymbol{\epsilon}(t)$ to be infinite.

As for \mathbf{R} , the price to pay for using \mathbf{u} is directly proportional to $\bar{\mathbf{R}} := \mathbf{D}^\top \mathbf{Q} \mathbf{D} + \mathbf{R}$. Hence, increase the magnitude of \mathbf{R} to limit the control action. On the other hand, if the control law is for free (modeled with $\bar{\mathbf{R}} \succeq \mathbf{0}$), an

infinite-magnitude control law can be designed. Since this is unfeasible due to the finite power of actuators, the cost \mathbf{R} must be such that $\bar{\mathbf{R}} \succ \mathbf{0}$.

To conclude, α is introduced to design the control system on an apparently less stable plant. This trick makes the control robust to model uncertainties and extreme selection of gains \mathbf{Q} and \mathbf{R} .

The computation of \mathbf{u}^* that minimizes cost (5.4c) under constraint (5.4a) represents, in general, a challenging task. To face this complex assignment, a good practice consists of rewriting this constrained minimization problem as an unconstrained one using Lagrange multipliers. Introduce the trivial term $\boldsymbol{\lambda}^\top ((\mathbf{A} + 2\alpha\mathbf{I})\mathbf{x} + \mathbf{B}\mathbf{u} - \dot{\mathbf{x}})$ in Eq. (5.4c) to obtain

$$J = \int_{t_0}^{\infty} H(\mathbf{x}, \mathbf{u}, \boldsymbol{\lambda}) - \boldsymbol{\lambda}^\top \dot{\mathbf{x}} dt, \quad (5.5)$$

where

$$H(\mathbf{x}, \mathbf{u}, \boldsymbol{\lambda}) := \epsilon^\top \mathbf{Q} \epsilon + \mathbf{u}^\top \mathbf{R} \mathbf{u} + \boldsymbol{\lambda}^\top ((\mathbf{A} + 2\alpha\mathbf{I})\mathbf{x} + \mathbf{B}\mathbf{u}) \quad (5.6)$$

is called a Hamiltonian function and $\boldsymbol{\lambda} : \mathbb{R} \rightarrow \mathbb{R}^n$ represents the Lagrange multiplier, also called *co-state*. Integrate Eq. (5.5) by parts as

$$J = -\boldsymbol{\lambda}^\top \mathbf{x} \Big|_{t_0}^{\infty} + \int_{t_0}^{\infty} H(\mathbf{x}, \mathbf{u}, \boldsymbol{\lambda}) + \dot{\boldsymbol{\lambda}}^\top \mathbf{x} dt \quad (5.7)$$

and introduce the variation of J with respect to \mathbf{x} and \mathbf{u} as follows:

$$\begin{aligned} \delta J &= -\boldsymbol{\lambda}^\top(\infty)\delta\mathbf{x}(\infty) + \boldsymbol{\lambda}^\top(t_0)\delta\mathbf{x}(t_0) + \\ &\quad \int_{t_0}^{\infty} \frac{\partial H(\mathbf{x}, \mathbf{u}, \boldsymbol{\lambda})}{\partial \mathbf{u}} \delta\mathbf{u} + \left(\frac{\partial H(\mathbf{x}, \mathbf{u}, \boldsymbol{\lambda})}{\partial \mathbf{x}} + \dot{\boldsymbol{\lambda}}^\top \right) \delta\mathbf{x} dt. \end{aligned} \quad (5.8)$$

The J variation can be made independent of $\delta\mathbf{x}$ during the transient from t_0 to ∞ if

$$\dot{\boldsymbol{\lambda}} = -\left(\frac{\partial H(\mathbf{x}, \mathbf{u}, \boldsymbol{\lambda})}{\partial \mathbf{x}}\right)^\top, \quad \boldsymbol{\lambda}(\infty) = \mathbf{0} \quad (5.9)$$

is imposed. Condition (5.9) simplifies Eq. (5.8) as follows:

$$\delta J = \boldsymbol{\lambda}^\top(t_0)\delta\mathbf{x}(t_0) + \int_{t_0}^{\infty} \frac{\partial H(\mathbf{x}, \mathbf{u}, \boldsymbol{\lambda})}{\partial \mathbf{u}} \delta\mathbf{u} dt. \quad (5.10)$$

Then, if \mathbf{u} evaluated at \mathbf{u}^* is a minimizer for J , then it must be such that

$$\int_{t_0}^{\infty} \frac{\partial H(\mathbf{x}, \mathbf{u}, \boldsymbol{\lambda})}{\partial \mathbf{u}} \Big|_{\mathbf{u}=\mathbf{u}^*} \delta\mathbf{u}^\star d\tau = \mathbf{0}, \quad (5.11)$$

which leads to

$$\frac{\partial H(\mathbf{x}, \mathbf{u}, \boldsymbol{\lambda})}{\partial \mathbf{u}} \Big|_{\mathbf{u}=\mathbf{u}^*} = 2\mathbf{x}^\top \mathbf{C}^\top \mathbf{Q} \mathbf{D} + \boldsymbol{\lambda}^\top \mathbf{B} + 2[\mathbf{u}^*]^\top \bar{\mathbf{R}} = \mathbf{0} \quad (5.12)$$

where $\bar{\mathbf{R}} := \mathbf{D}^\top \mathbf{Q} \mathbf{D} + \mathbf{R}$. From Eq. (5.12), we find

$$\mathbf{u}^* = -\frac{1}{2}\bar{\mathbf{R}}^{-1}(2\mathbf{D}^\top \mathbf{Q} \mathbf{C} \mathbf{x} + \mathbf{B}^\top \boldsymbol{\lambda}). \quad (5.13)$$

Moreover, to make \mathbf{u}^* linearly dependent on $\boldsymbol{\lambda}$, design the Lagrange multiplier as a linear function of \mathbf{x} . Let $\boldsymbol{\lambda} := 2\mathbf{S}\mathbf{x}$ with $\mathbf{S} = \mathbf{S}^\top > \mathbf{0}$ and write Eq. (5.13) as

$$\begin{aligned} \mathbf{u}^* &= \mathbf{K}\mathbf{x} \\ \mathbf{K} &= -\bar{\mathbf{R}}^{-1}(\mathbf{D}^\top \mathbf{Q} \mathbf{C} + \mathbf{B}^\top \mathbf{S}). \end{aligned} \quad (5.14)$$

An expression for \mathbf{S} is found to conclude the optimal control design. Indeed, the solution of the stationary optimal control problem is found by noting that $\dot{\boldsymbol{\lambda}} = 2\mathbf{S}\dot{\mathbf{x}}$ must agree with Eq. (5.9) evaluated at \mathbf{u}^* , i.e., \mathbf{S} must verify ([1], Sect. 9)

$$\begin{aligned} \mathbf{S}\bar{\mathbf{R}}^{-1}\mathbf{B}^\top \mathbf{S} - \mathbf{S}(\mathbf{A} + \alpha\mathbf{I} - \mathbf{B}\bar{\mathbf{R}}^{-1}\mathbf{D}^\top \mathbf{Q}\mathbf{C}) \\ - (\mathbf{A} + \alpha\mathbf{I} - \mathbf{B}\bar{\mathbf{R}}^{-1}\mathbf{D}^\top \mathbf{Q}\mathbf{C})^\top \mathbf{S} - \mathbf{C}^\top \mathbf{Q}[\mathbf{I} - \mathbf{D}\bar{\mathbf{R}}^{-1}\mathbf{D}^\top \mathbf{Q}]\mathbf{C} = \mathbf{0}. \end{aligned} \quad (5.15)$$

Important

It is worth noting that the solution to Problem 5.1 must also stabilize the plant.

Expression (5.15), called Algebraic Riccati Equation (ARE), has one stabilising positive definite solution, namely \mathbf{S}_∞ , if $\mathbf{Q}, \mathbf{R} > \mathbf{0}$, the couple $(\mathbf{A} + \alpha\mathbf{I}, \mathbf{B})$ is stabilizable, and the couple $(\mathbf{A} + \alpha\mathbf{I}, \mathbf{C})$ is detectable (these three conditions must be jointly verified!).

Note

Let

$$\begin{aligned} \dot{x} &= (a + \alpha)x + bu \\ \varepsilon &= cx \\ 0 &= s^2 \frac{b^2}{r} - 2(a + \alpha)s - c^2q \end{aligned}$$

be a scalar plant with the associated ARE [10]. The solutions to the ARE are

$$s_{1,2} = \frac{(a + \alpha)r}{b^2} \pm \sqrt{\frac{(a + \alpha)^2 r^2}{b^4} + \frac{c^2qr}{b^2}},$$

with $s_1 \geq 0$ and $s_2 \leq 0$. The optimal control law is $u^* = ks_1$ with $k := -r^{-1}bs_1$. Then, the solution s_1 approaches zero for $r \rightarrow 0$ while

$$\lim_{r \rightarrow 0} k = -\lim_{r \rightarrow 0} \frac{bs_1}{r} = -\lim_{r \rightarrow 0} \left(\frac{a + \alpha}{b} + b\sqrt{\frac{(a + \alpha)^2}{b^4} + \frac{c^2q}{rb^2}} \right) = -\infty,$$

which confirms the intuition that if r is trivial, the control can be infinite. On the other hand, for $r \rightarrow \infty$ the solution s_1 goes to infinity but k remains finite

$$\begin{aligned} \lim_{r \rightarrow \infty} k &= -\lim_{r \rightarrow \infty} \frac{bs_1}{r} = -\lim_{r \rightarrow \infty} \left(\frac{a + \alpha}{b} + b\sqrt{\frac{(a + \alpha)^2}{b^4} + \frac{c^2q}{rb^2}} \right) \\ &= -\frac{a + \alpha + \sqrt{(a + \alpha)^2}}{b}. \end{aligned}$$

In practice, when $r \rightarrow \infty$, the cost associated with the control is so much higher than q (the cost associated with ϵ) that the latter can be neglected. In this configuration, the main objectives are reducing the control action and the stability of the closed-loop system. As a consequence, $k = 0$ for any $a \leq -\alpha$ because the system is already BIBS-stable with an eigenvalue less than or equal to $-\alpha$. On the other hand, for any $a > -\alpha$, the feedback gain is $k = -2(a + \alpha)/b$, which assures a closed-loop eigenvalue of less than or equal to $-(a + 2\alpha)$.

Infobox 5.1 *The stationary optimal control based on the quadratic cost function represents one of the most attractive control solutions of linear systems. Indeed, as described in Appendix C, this control strategy possesses surprising robustness to model uncertainties that, in the frequency domain, is translated into a phase margin of at least 60° and a gain margin between 1/2 and ∞.*

This section ends by investigating the solution to Problem 5.1 concerning the detectability of the couple $(A + \alpha I, C)$ and the stabilizability of the couple $(A + \alpha I, B)$. Let T_K be the transformation that changes Eqs. (5.4a)–(5.4b) into the ultimate Kalman decomposition form. Then, define $z = T_K x$ and determine the dynamics of z as follows:

$$\begin{aligned}\dot{z} &= A^* z + B^* u \quad x(t_0) = x_0 \\ \epsilon &= C^* z + D u,\end{aligned}$$

in which $z := \text{col}(z_{R,NO}, z_{R,O}, z_{NR,NO}, z_{NR,O})$, $A^* := T A T^{-1}$, $B^* := T B$, and $C^* := C T^{-1}$. Let S^* be partitioned in 16 parts as

$$S^* = \begin{bmatrix} S_{11}^* & S_{12}^* & S_{13}^* & S_{14}^* \\ (S_{12}^*)^\top & S_{22}^* & S_{23}^* & S_{24}^* \\ (S_{13}^*)^\top & (S_{23}^*)^\top & S_{33}^* & S_{34}^* \\ (S_{14}^*)^\top & (S_{24}^*)^\top & (S_{34}^*)^\top & S_{44}^* \end{bmatrix}.$$

Then, we demonstrate that S^* reduces to

$$S^* = \begin{bmatrix} \mathbf{0} & \mathbf{0} & \mathbf{0} & \mathbf{0} \\ \mathbf{0} & S_{22}^* & \mathbf{0} & S_{24}^* \\ \mathbf{0} & \mathbf{0} & \mathbf{0} & \mathbf{0} \\ \mathbf{0} & (S_{24}^*)^\top & \mathbf{0} & S_{44}^* \end{bmatrix}. \quad (5.16)$$

To prove Eq. (5.16), calculate the closed-loop $A^* - B^* \bar{R}^{-1} (B^*)^\top S^*$ and note that only S_{11}^* , S_{12}^* , S_{13}^* , $S_{23}^* = 0$ keep the ultimate Kalman decomposition. As a consequence, the solution of the ARE imposes S_{14}^* , S_{33}^* , $S_{34}^* = 0$.

The substitution of Eq. (5.16) into Eq. (5.14) leads to

$$u^* = -\bar{R}^{-1} [\mathbf{0} (B_2^*)^\top S_{22}^* \mathbf{0} (B_2^*)^\top S_{24}^*] \begin{bmatrix} z_{R,NO} \\ z_{R,O} \\ z_{NR,NO} \\ z_{NR,O} \end{bmatrix}. \quad (5.17)$$

Finally, the closed-loop dynamics are given by

$$\begin{bmatrix} \dot{\mathbf{z}}_{R,NO} \\ \dot{\mathbf{z}}_{R,O} \\ \dot{\mathbf{z}}_{NR,NO} \\ \dot{\mathbf{z}}_{NR,O} \end{bmatrix} = \begin{bmatrix} \mathbf{A}_{11}^* + \alpha\mathbf{I} & \mathbf{A}_{12}^* - \mathbf{B}_1^*\bar{\mathbf{R}}^{-1}(\mathbf{B}_2^*)^\top \mathbf{S}_{22}^* & \mathbf{A}_{13}^* & \mathbf{A}_{14}^* - \mathbf{B}_1^*\bar{\mathbf{R}}^{-1}(\mathbf{B}_2^*)^\top \mathbf{S}_{24}^* \\ \mathbf{0} & \mathbf{A}_{22}^* + \alpha\mathbf{I} - \mathbf{B}_2^*\bar{\mathbf{R}}^{-1}(\mathbf{B}_2^*)^\top \mathbf{S}_{22}^* & \mathbf{0} & \mathbf{A}_{24}^* - \mathbf{B}_2^*\bar{\mathbf{R}}^{-1}(\mathbf{B}_2^*)^\top \mathbf{S}_{24}^* \\ \mathbf{0} & \mathbf{0} & \mathbf{A}_{33}^* + \alpha\mathbf{I} & \mathbf{A}_{34}^* \\ \mathbf{0} & \mathbf{0} & \mathbf{0} & \mathbf{A}_{44}^* + \alpha\mathbf{I} \end{bmatrix} \begin{bmatrix} \mathbf{z}_{R,NO} \\ \mathbf{z}_{R,O} \\ \mathbf{z}_{NR,NO} \\ \mathbf{z}_{NR,O} \end{bmatrix},$$

which must be stabilizable and detectable to allow the ARE to have a stabilizing solution. Since $\mathbf{A}_{22}^* + \alpha\mathbf{I} - \mathbf{B}_2^*\bar{\mathbf{R}}^{-1}(\mathbf{B}_2^*)^\top \mathbf{S}_{22}^*$ can be made Hurwitz because $(\mathbf{A}_{22}^* + \alpha\mathbf{I}, \mathbf{B}_2^*)$ is fully reachable and observable, $\alpha > 0$ is upper bounded by the smallest absolute value of the real part of the eigenvalues of \mathbf{A}_{11}^* , \mathbf{A}_{33}^* , and \mathbf{A}_{44}^* .

Example 5.1 (Non detectable model) Consider a point with mass $m > 0$ that moves on a straight path. Define $\mathbf{x} = \text{col}(p, v)$ as the state in which $p, v \in \mathbb{R}$ are positions and speed, respectively. Let $u \in \mathbb{R}$ be the force acting on the mass and $y \in \mathbb{R}$ be the speed measurement. Then, the following linear system models the plant dynamics:

$$\begin{aligned} \dot{\mathbf{x}} &= \mathbf{Ax} + \mathbf{Bu} \quad \mathbf{x}(0) = \mathbf{x}_0 \\ e &= \mathbf{Cx}, \end{aligned}$$

where

$$\mathbf{A} = \begin{bmatrix} 0 & 1 \\ 0 & 0 \end{bmatrix}, \quad \mathbf{B} = \begin{bmatrix} 0 \\ m^{-1} \end{bmatrix}, \quad \mathbf{C} = \begin{bmatrix} 0 & 1 \end{bmatrix}.$$

It is worth noting that the couple (\mathbf{A}, \mathbf{B}) is fully reachable, whereas the couple (\mathbf{A}, \mathbf{C}) is not fully observable. Moreover, the unobservable part of the system is not BIBS-stable, thus leading to a non-detectable system. Let $\alpha = 0$, $r > 0$, $q \geq 0$, and

$$\mathbf{S} := \begin{bmatrix} s_{11} & s_{12} \\ s_{12} & s_{22} \end{bmatrix},$$

then the ARE associated with this problem becomes

$$\frac{1}{r m^2} \begin{bmatrix} s_{12}^2 & s_{12}s_{22} \\ s_{12}s_{22} & s_{22}^2 \end{bmatrix} - \begin{bmatrix} 0 & s_{11} \\ s_{11} & 2s_{12} + q \end{bmatrix} = \begin{bmatrix} 0 & 0 \\ 0 & 0 \end{bmatrix}$$

which leads to a positive semi-definite \mathbf{S}

$$\mathbf{S} = \begin{bmatrix} s_{11} & s_{12} \\ s_{12} & s_{22} \end{bmatrix} = \begin{bmatrix} 0 & 0 \\ 0 & m\sqrt{qr} \end{bmatrix}.$$

Also, the optimal control law is $u = \mathbf{Kx}$ with

$$\mathbf{K} = -\frac{1}{r} [0 \ m^{-1}] \begin{bmatrix} 0 & 0 \\ 0 & m\sqrt{qr} \end{bmatrix} = -[0 \ \sqrt{q/r}].$$

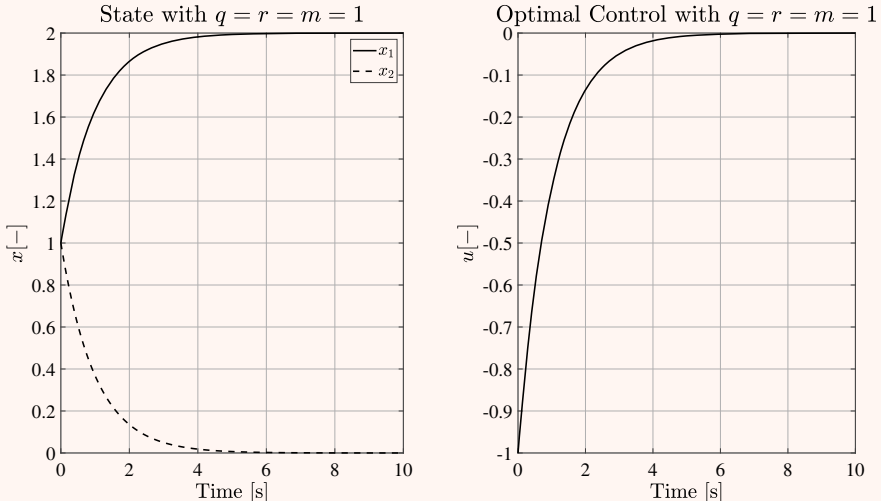
Finally, the closed-loop system has dynamics described by

$$\mathbf{A} + \mathbf{BK} = \begin{bmatrix} 0 & 1 \\ 0 & -\sqrt{q/r}/m \end{bmatrix}$$

which is not BIBS-stable. The time evolution of the state is obtained utilizing the Lagrange formula (3.13) that, applied to $\mathbf{A} + \mathbf{BK}$, leads to

$$\begin{aligned}x_1(t) &= \frac{m}{\sqrt{q/r}} \left(1 - e^{-t\sqrt{q/r}/m}\right) x_2(0) + x_1(0) \\x_2(t) &= e^{-t\sqrt{q/r}/m} x_2(0).\end{aligned}$$

The following figures depict the time evolution of the states and control.



Example 5.2 (Non stabilizable model) With reference to the plant of Example 5.1, assume that $\mathbf{C} = [1 \ 0]$ and $\mathbf{B} = \text{col}(1, 0)$. Due to these variations, the plant becomes fully observable but not fully reachable. Moreover, the non-reachable subsystem is characterized by a null eigenvalue, so the system is not stabilizable. Assuming $\alpha = 0$, the ARE associated with the optimal control problem becomes

$$\begin{bmatrix} s_{11}^2/r - q & s_{11}(s_{12}/r - 1) \\ s_{11}(s_{12}/r - 1) & s_{12}(s_{12}/r - 2) \end{bmatrix} = \begin{bmatrix} 0 & 0 \\ 0 & 0 \end{bmatrix},$$

which has no solutions for $q > 0$. Therefore, assume $q = 0$ to obtain $s_{11} = 0$, $s_{22} \in \mathbb{R}$, and $s_{12} \in \{0, 2r\}$. Observe that

$$\begin{aligned}\det(\mathbf{S} - \lambda I) &= \det \left(\begin{bmatrix} -\lambda & s_{12} \\ s_{12} & s_{22} - \lambda \end{bmatrix} \right) = \lambda^2 - \lambda s_{22} - s_{12}^2 = 0 \implies \\ \lambda_{1,2} &= \frac{s_{22} \pm \sqrt{s_{22}^2 + 4s_{12}^2}}{2}.\end{aligned}$$

The roots $\lambda_{1,2}$ are opposite in sign and different from zero for any $s_{22} \in \mathbb{R}$. Hence, the ARE is solved by an \mathbf{S} which is semi-positive definite. The optimal control is obtained as $u = \mathbf{Kx}$ with

$$\mathbf{K} = -\frac{1}{r} \begin{bmatrix} 1 & 0 \end{bmatrix} \begin{bmatrix} 0 & s_{12} \\ s_{12} & s_{22} \end{bmatrix} = -\frac{1}{r} \begin{bmatrix} 0 & s_{12} \end{bmatrix}.$$

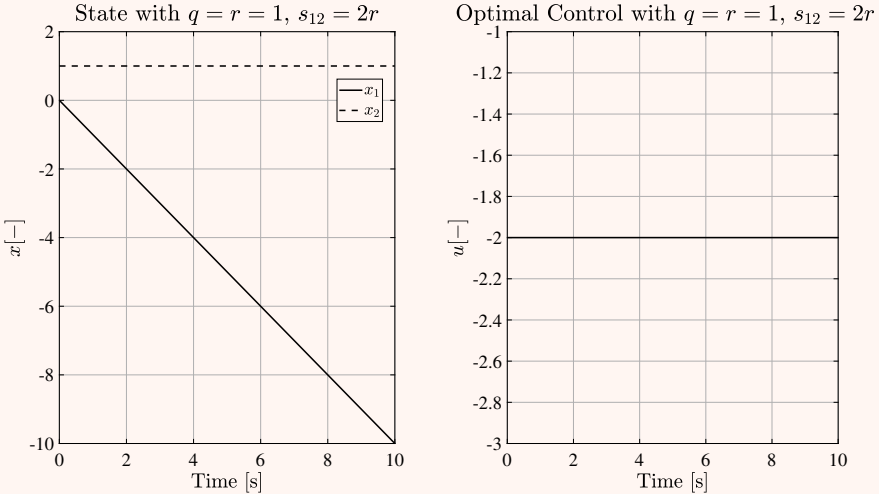
Finally, the closed-loop transition matrix becomes

$$\mathbf{A} + \mathbf{B}\mathbf{K} = \begin{bmatrix} 0 & 1 - s_{12}/r \\ 0 & 0 \end{bmatrix}$$

which indeed is not BIBS-stable. In conclusion, the time evolution of the state is described as

$$\begin{aligned} x_1(t) &= (1 - s_{12}/r)x_2(0)t + x_1(0) \\ x_2(t) &= x_2(0) \end{aligned}$$

which leads to the control $u(t) = -x_2(t)s_{12}/r$.



Example 5.3 (Observable and reachable model) With reference to the plant of Example 5.1, assume that $\mathbf{C} = [1 \ 0]$ which makes (\mathbf{A}, \mathbf{C}) fully observable. The reachability of (\mathbf{A}, \mathbf{B}) assures that there exists a stabilizing optimal control $u = -r^{-1}\mathbf{B}^\top \mathbf{S}\mathbf{x}$, with \mathbf{S} solving the following ARE:

$$\begin{bmatrix} s_{12}^2/(m^2r) - q & s_{12}s_{22}/(m^2r) - s_{11} \\ s_{12}s_{22}/(m^2r) - s_{11} & s_{22}^2/(m^2r) - 2s_{12} \end{bmatrix} = \begin{bmatrix} 0 & 0 \\ 0 & 0 \end{bmatrix}.$$

Let

$$s_{11} = \sqrt{2m} q^{3/4} r^{1/4}, \quad s_{12} = m\sqrt{rq}, \quad s_{22} = \sqrt{2} m^{3/2} r^{3/4} q^{1/4}$$

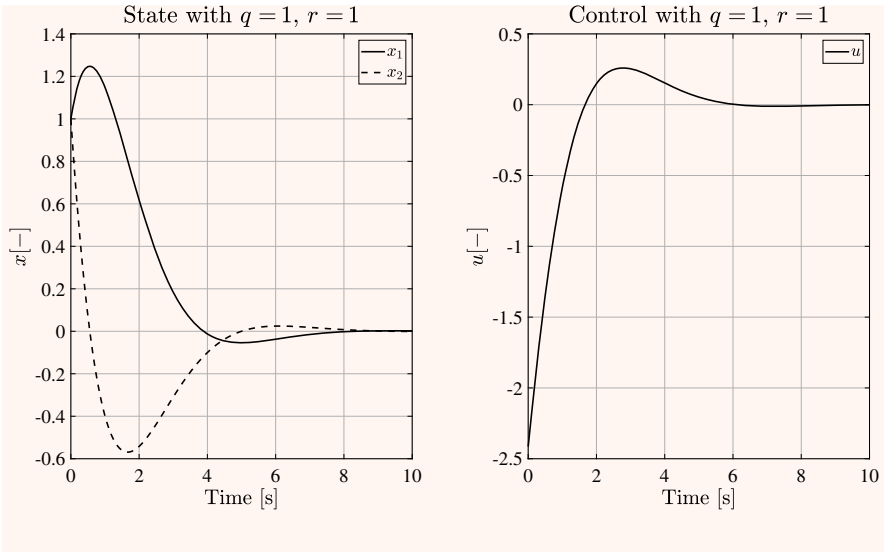
be the solution of the ARE, then the state-feedback control is $u = \mathbf{K}\mathbf{x}$ with

$$\mathbf{K} = -\frac{1}{r}[0 \ m^{-1}] \begin{bmatrix} s_{11} & s_{12} \\ s_{12} & s_{22} \end{bmatrix} = -\frac{1}{rm} \begin{bmatrix} s_{11} & s_{12} \\ s_{12} & s_{22} \end{bmatrix}.$$

Finally, the closed-loop system has dynamics described by the matrix

$$\mathbf{A} + \mathbf{B}\mathbf{K} = \begin{bmatrix} 0 & \frac{1}{rm} \\ -\frac{s_{12}}{rm} & -\frac{s_{22}}{rm} \end{bmatrix}$$

which is BIBS-stable.



Example 5.4 (*Cart-pole set point regulator design*) Constants $\mathbf{K}_{R,O}$ and k_I , defined in Sects. 4.5.1 and 4.3, are designed through the stationary optimal control technique. Let the system be (see Example 4.17)

$$\begin{bmatrix} \dot{\mathbf{z}}_{R,O} \\ \dot{\eta} \end{bmatrix} = \begin{bmatrix} \bar{\mathbf{A}}_{22} & \mathbf{0} \\ \bar{\mathbf{C}}_e & 0 \end{bmatrix} \begin{bmatrix} \mathbf{z}_{R,O} \\ \eta \end{bmatrix} + \begin{bmatrix} \bar{\mathbf{B}}_2 \\ 0 \end{bmatrix} u$$

$$\epsilon = \begin{bmatrix} \mathbf{I} & \mathbf{0} \\ \mathbf{0} & 1 \end{bmatrix} \begin{bmatrix} \mathbf{z}_{R,O} \\ \eta \end{bmatrix}$$

and define the cost function

$$J = \int_0^\infty \epsilon^\top \mathbf{Q} \epsilon + u^2 R dt,$$

in which $\mathbf{Q} = \mathbf{Q}^\top \succ 0$ and $R > 0$. Assume

$$\mathbf{S} := \begin{bmatrix} \mathbf{S}_{11} & \mathbf{S}_{12} \\ \mathbf{S}_{12}^\top & s_{22} \end{bmatrix},$$

in which $\mathbf{S}_{12} \in \mathbb{R}^{1 \times 3}$ and $\mathbf{S}_{11} \in \mathbb{R}^{3 \times 3}$. Then, the stationary optimal control law is

$$u^* = -R^{-1} [\bar{\mathbf{B}}_2^\top \ 0] \mathbf{S} \begin{bmatrix} \mathbf{z}_{R,O} \\ \eta \end{bmatrix} = -R^{-1} \bar{\mathbf{B}}_2^\top \mathbf{S}_{11} \mathbf{z}_{R,O} - R^{-1} \bar{\mathbf{B}}_2^\top \mathbf{S}_{12}^\top \eta.$$

where $\mathbf{K}_{R,O} = -R^{-1} \bar{\mathbf{B}}_2^\top \mathbf{S}_{11}$ and $k_I = -R^{-1} \bar{\mathbf{B}}_2^\top \mathbf{S}_{12}^\top$. The matrices \mathbf{S}_{12} and \mathbf{S}_{11} can be found via numerical solvers. As an example, exploit the following MATLAB® listing.

% Plant

```
Ac = [barA22 zeros(3,1); barCe 0];
Bc = [barB2; 0];
Cc = eye(4);
```

% Costs

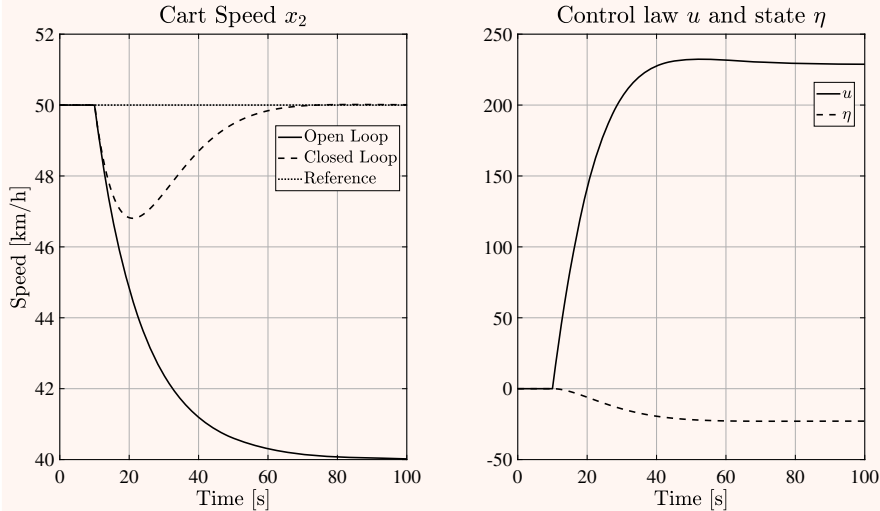
$Q = \text{any } 4 \times 4 \text{ matrix positive definite}$

$R = \text{any positive scalar}$

% Solve the ARE

$[K, S, e] = lqr(Ac, Bc, Q, R, \text{zeros}(4, 1));$ *%WARNING! The control law is $u = -Kx$. S is the positive definite solution of the ARE.*

The following results have been obtained by imposing $\mathbf{Q} = 100 \mathbf{I}$ and $R = 1$. The cart starts the simulation at the equilibrium speed of 50 km/h. At $t = 10s$, a constant wind of -10 km/h appears and brakes the system. Thanks to the control action, the target speed is recovered after a transient. In this period, the variable η integrates the tracking error.



5.1.1 Gain Selection

Matrices \mathbf{Q} and \mathbf{R} represent tunable gains at the disposal of the designer. The desire to limit the error $\epsilon(t)$ and the control $\mathbf{u}(t)$ drives a rule of thumb for designing these matrices (other approaches are found in [4, 5, 11, 14]). Let

$$\boldsymbol{\epsilon} := \text{col}(\epsilon_1, \dots, \epsilon_m), \quad \mathbf{u} := \text{col}(u_1, \dots, u_p)$$

and define $\epsilon_{i\max}, u_{j\max} > 0$, for $i = 1, \dots, m$ and $j = 1, \dots, p$. Conceive

- $|\epsilon_i(t)| \leq \epsilon_{i\max} \in \mathbb{R}_{>0}$, for $i = 1, \dots, m$ and
- $|u_i(t)| \leq u_{i\max} \in \mathbb{R}_{>0}$, for $i = 1, \dots, p$

as soft constraints the controlled plant should verify. Then, the matrices \mathbf{Q} and \mathbf{R} are defined as

$$\mathbf{Q}^{-1} = q \begin{bmatrix} \epsilon_{1\max}^2 & 0 & \dots & 0 \\ 0 & \epsilon_{2\max}^2 & \dots & 0 \\ \vdots & \vdots & \ddots & \vdots \\ 0 & 0 & \dots & \epsilon_{m\max}^2 \end{bmatrix}$$

$$\mathbf{R}^{-1} = p \begin{bmatrix} u_{1\max}^2 & 0 & \dots & 0 \\ 0 & u_{2\max}^2 & \dots & 0 \\ \vdots & \vdots & \ddots & \vdots \\ 0 & 0 & \dots & u_{p\max}^2 \end{bmatrix}.$$

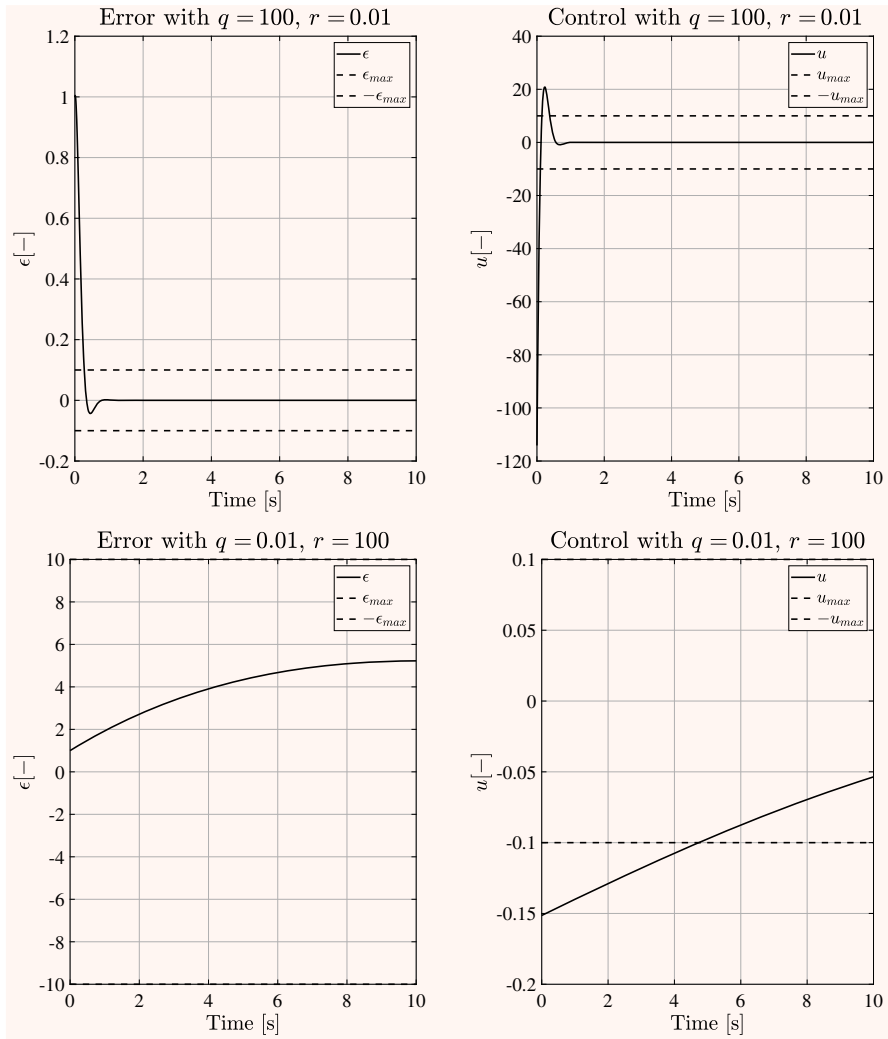
It is worth noting that the above-defined \mathbf{Q} and \mathbf{R} do not guarantee that $\boldsymbol{\epsilon}$ and \mathbf{u} remain bounded within the prescribed constraints. Parameters m and p are normalization weights that make matrices \mathbf{Q} and \mathbf{R} independent of the dimensions of vectors $\boldsymbol{\epsilon}$ and \mathbf{u} .

Example 5.5 (Tuning of \mathbf{Q} and \mathbf{R}) With reference to the model of Example 5.3, impose $m = 1$ and try different settings, one for each combination of $\epsilon_{\max}, u_{\max} \in \{0.1, 10\}$. First of all, note that

$$\frac{s_{12}}{mr} = \sqrt{q/r}, \quad \frac{s_{22}}{mr} = \sqrt{2m} (q/r)^{1/4}.$$

Then, the closed-loop system behaves the same for any q/r constant. For this reason, the plots for $\epsilon_{\max} = u_{\max}$ are not shown.

Moreover, concerning the time evolution of $\boldsymbol{\epsilon}$ and \mathbf{u} of Example 5.3, observe that increasing q and decreasing r leads to a faster response that relies on larger control values, which can rapidly steer the error to zero. Conversely, reducing q and increasing r induces the controller to tolerate larger errors with a “lazier” control action.



5.2 Duality

Section 5.1 presented a constructive procedure for designing the state-feedback control gain \mathbf{K}_S . It is possible to apply the same approach for the design of the observer matrix \mathbf{K}_O through the duality properties of linear systems.

Let

$$\begin{aligned}\dot{\mathbf{x}} &= \mathbf{A}\mathbf{x} + \mathbf{B}\mathbf{u} \\ \mathbf{y} &= \mathbf{C}\mathbf{x} + \mathbf{D}\mathbf{u}\end{aligned}\tag{5.18}$$

be an LTI system with $\mathbf{x} \in \mathbb{R}^n$, $\mathbf{u} \in \mathbb{R}^p$, and $\mathbf{y} \in \mathbb{R}^q$. Then, the *dual system* associated with the *primary system* (5.18) is defined as

$$\begin{aligned}\dot{\chi} &= \mathbf{A}^\top \chi + \mathbf{C}^\top v \\ \mu &= \mathbf{B}^\top \chi + \mathbf{D}^\top v\end{aligned}\tag{5.19}$$

with $\chi \in \mathbb{R}^n$, $v \in \mathbb{R}^q$, and $\mu \in \mathbb{R}^p$.

The primary and the dual systems are two equivalent representations of the same mathematical model and, thus, any property possessed by the primary system can be translated into an equivalent property of its dual.

Lemma 5.1 *Let the primary system (5.18) be fully reachable. Then, the dual system is fully observable and vice versa.*

Proof The reachability subset of the primary system (5.18) has as one of its bases the image of the reachability matrix

$$\mathbf{R}_p := [\mathbf{B} \ \mathbf{AB} \ \mathbf{A}^2\mathbf{B} \ \dots \ \mathbf{A}^{n-1}\mathbf{B}],$$

whereas the unobservability subspace of the dual system \mathcal{E}_d has as one of its bases the kernel of the observability matrix

$$\mathbf{O}_d := \begin{bmatrix} \mathbf{B}^\top \\ \mathbf{B}^\top \mathbf{A}^\top \\ \mathbf{B}^\top (\mathbf{A}^\top)^2 \\ \vdots \\ \mathbf{B}^\top (\mathbf{A}^\top)^{n-1} \end{bmatrix}.$$

If the primary system is fully reachable, then $\text{im}(\mathbf{R}_p) = \mathbb{R}^n$, whereas if the dual system is fully observable, then $\ker(\mathbf{O}_d) = \{\mathbf{0}\}$ or equivalently $(\ker(\mathbf{O}_d))^\perp = \mathbb{R}^n$. In particular,

$$(\ker(\mathbf{O}_d))^\perp = \text{im}(\mathbf{O}_d^\top) = \text{im}(\mathbf{R}_p),$$

which demonstrates that if the primary system is fully reachable, the dual system is fully observable and vice versa. \square

Lemma 5.2 *Let the primary system (5.18) be fully observable. Then, the dual system is fully reachable and vice versa.*

Proof The reachability subset of the dual system (5.18) has as one of its bases the image of the reachability matrix

$$\mathbf{R}_d := [\mathbf{C}^\top \ \mathbf{A}^\top \mathbf{C}^\top \ (\mathbf{A}^\top)^2 \mathbf{C}^\top \ \dots \ (\mathbf{A}^\top)^{n-1} \mathbf{C}^\top],$$

whereas the unobservability subspace of the primary system \mathcal{E}_p has as one of its bases the kernel of the observability matrix

$$\mathbf{O}_p := \begin{bmatrix} \mathbf{C} \\ \mathbf{CA} \\ \mathbf{CA}^2 \\ \vdots \\ \mathbf{CA}^{n-1} \end{bmatrix}.$$

If the dual system is fully reachable, then $\text{im}(\mathbf{R}_d) = \mathbb{R}^n$, whereas if the primary system is fully observable, then $\ker(\mathbf{O}_p) = \{\mathbf{0}\}$ or equivalently $(\ker(\mathbf{O}_p))^\perp = \mathbb{R}^n$. In particular,

$$(\ker(\mathbf{O}_p))^\perp = \text{im}(\mathbf{O}_p^\top) = \text{im}(\mathbf{R}_d),$$

which demonstrates that if the dual system is fully reachable, the primary system is fully observable and vice versa. \square

Lemma 5.3 *Let the primary model (5.18) be BIBS-stable. Then also the dual model (5.19) is BIBS-stable and vice versa.*

Proof If the primary model is BIBS-stable, the real part of the eigenvalues of the matrix \mathbf{A} is strictly negative. Let $\sigma_{\mathbf{A}}$ be the set of the eigenvalues of \mathbf{A} and let $\text{Real}(\sigma_{\mathbf{A}})$ denote the real part of each eigenvalue of \mathbf{A} . Since \mathbf{A} and its transpose have the same eigenvalues, it is

$$\text{Real}(\sigma_{\mathbf{A}}) < 0 \iff \text{Real}(\sigma_{\mathbf{A}^\top}) < 0.$$

This section extends the duality properties also to control and observation problems so that the existence of a solution to one problem implies the existence of a solution to its dual.

Let the primary system (5.18) be fully observable. Then in agreement with the results of Sect. 4.4, $\mathbf{K}_{\mathbf{O}_p}$ exists such that the state estimation error $\mathbf{e}_x := \hat{\mathbf{x}} - \mathbf{x}$ is governed by the dynamics

$$\dot{\mathbf{e}}_x = (\mathbf{A} - \mathbf{K}_{\mathbf{O}_p} \mathbf{C}) \mathbf{e}_x \quad (5.20)$$

whose dual is

$$\dot{\varepsilon} = (\mathbf{A}^\top - \mathbf{C}^\top \mathbf{K}_{\mathbf{O}_p}^\top) \varepsilon \quad (5.21)$$

Now, since system (5.19) is fully reachable, there exists $\mathbf{K}_{\mathbf{S}_d}$ such that $\mathbf{v} := \mathbf{K}_{\mathbf{S}_d} \chi$ leads to

$$\dot{\chi} = (\mathbf{A}^\top + \mathbf{C}^\top \mathbf{K}_{\mathbf{S}_d}) \chi. \quad (5.22)$$

Compare Eqs. (5.21) and (5.22) to note that matrices $\mathbf{A}^\top - \mathbf{C}^\top \mathbf{K}_{\mathbf{O}_p}^\top$ and $\mathbf{A}^\top + \mathbf{C}^\top \mathbf{K}_{\mathbf{S}_d}$ coincide if

$$\mathbf{K}_{\mathbf{O}_p} = -\mathbf{K}_{\mathbf{S}_d}^\top.$$

Then, the solution to the observation problem associated with the primary system is implied by the solution to the control problem associated with the dual system.

5.3 Kalman Filter

Section 5.2 has shown that the control and observation properties (and problems) associated with linear systems are dual. Therefore, the solution of the observation problem of the primary system is implied by the solution of the control problem of the dual system. Also, Sect. 5.1 shows how to solve an optimal control problem by designing a state-feedback gain. This section formulates and solves the optimal observation problem for the primary system through the statement and the solution of the optimal control problem for the dual system. Let

$$\begin{aligned}\dot{\mathbf{x}} &= \mathbf{Ax} + \mathbf{B}_1\mathbf{u} + \mathbf{B}_2\mathbf{w} \\ \mathbf{y} &= \mathbf{Cx} + \mathbf{D}_1\mathbf{u} + \mathbf{D}_2\mathbf{w}\end{aligned}\quad (5.23)$$

be a detectable LTI system for which the observer has to be designed. In agreement with Sect. 4.4, define an identity observer as

$$\begin{aligned}\dot{\hat{\mathbf{x}}} &= \mathbf{A}\hat{\mathbf{x}} + \mathbf{B}_1\mathbf{u} \\ \hat{\mathbf{y}} &= \mathbf{C}\hat{\mathbf{x}} + \mathbf{D}_1\mathbf{u}.\end{aligned}\quad (5.24)$$

Let $\mathbf{e}_x := \hat{\mathbf{x}} - \mathbf{x}$ and $\tilde{\mathbf{y}} := \hat{\mathbf{y}} - \mathbf{y}$, and compute the dynamics of the estimation error as

$$\begin{aligned}\dot{\mathbf{e}}_x &= \mathbf{A}\mathbf{e}_x - \mathbf{B}_2\mathbf{w} \\ \tilde{\mathbf{y}} &= \mathbf{C}\mathbf{e}_x - \mathbf{D}_2\mathbf{w}.\end{aligned}\quad (5.25)$$

Let

$$\begin{aligned}\dot{\chi} &= \mathbf{A}^\top\chi + \mathbf{C}^\top v \\ \mu &= \mathbf{B}_2^\top\chi + \mathbf{D}_2^\top v\end{aligned}\quad (5.26)$$

be the dual model associated with system (5.25). Define and solve the robust optimal control problem for plant (5.26) through the steps depicted in Sect. 5.1. In more detail, let $\alpha > 0$, alter model (5.26) as

$$\begin{aligned}\dot{\chi} &= (\mathbf{A}^\top + 2\alpha\mathbf{I})\chi + \mathbf{C}^\top v \quad \chi(t_f) = \chi_f \\ \mu &= \mathbf{B}_2^\top\chi + \mathbf{D}_2^\top v,\end{aligned}\quad (5.27a)$$

and define the following cost function:

$$J_d = \int_{t_0}^{\infty} \mu^\top \mathbf{Q}_d \mu + v^\top \mathbf{R}_d v dt, \quad (5.27b)$$

where $\mathbf{Q}_d \succeq 0$ and $\mathbf{R}_d \succeq \mathbf{0}$. Apply steps (5.5)–(5.15) to the constrained optimization problem (5.27) to obtain $v^* = \mathbf{K}_{S_d}\chi$, where

$$\begin{aligned}\mathbf{K}_{S_d} &= -\bar{\mathbf{R}}_d^{-1} \left(\mathbf{D}_2 \mathbf{Q}_d \mathbf{B}_2^\top + \mathbf{C} \mathbf{S} \right) \\ \mathbf{0} &= \mathbf{S} \mathbf{C}^\top \bar{\mathbf{R}}_d^{-1} \mathbf{C} \mathbf{S} - \mathbf{S} (\mathbf{A}^\top + \alpha \mathbf{I} - \mathbf{C}^\top \bar{\mathbf{R}}_d^{-1} \mathbf{D}_2 \mathbf{Q}_d \mathbf{B}_2^\top) \\ &\quad - (\mathbf{A}^\top + \alpha \mathbf{I} - \mathbf{C}^\top \bar{\mathbf{R}}_d^{-1} \mathbf{D}_2 \mathbf{Q}_d \mathbf{B}_2^\top)^\top \mathbf{S} - \mathbf{B}_2 \mathbf{Q}_d [\mathbf{I} - \mathbf{D}_2^\top \bar{\mathbf{R}}_d^{-1} \mathbf{D}_2 \mathbf{Q}_d] \mathbf{B}_2^\top\end{aligned}\quad (5.28)$$

and $\bar{\mathbf{R}}_d = \mathbf{D}_2 \mathbf{Q}_d \mathbf{D}_2^\top + \mathbf{R}_d$. Then, as described in Sect. 5.2, the observer for model (5.23) is given by [9]

$$\begin{aligned}\dot{\hat{\mathbf{x}}} &= \mathbf{A}\hat{\mathbf{x}} + \mathbf{B}_1\mathbf{u} - \mathbf{K}_{S_d}^\top(\mathbf{y} - \hat{\mathbf{y}}) \quad \hat{\mathbf{x}}(t_0) = \hat{\mathbf{x}}_0 \\ \hat{\mathbf{y}} &= \mathbf{C}\hat{\mathbf{x}} + \mathbf{D}_1\mathbf{u},\end{aligned}\tag{5.29}$$

where \mathbf{K}_{S_d} is defined in Eq. (5.28). Solution (5.28) can be specialized by noting that, in most practical cases, $\mathbf{B}_2 := [\mathbf{B}_{21} \ \mathbf{0}]$ and $\mathbf{D}_2 := [\mathbf{0} \ \mathbf{I} \ \mathbf{0}]$ (remember from Sect. 1.2 that $\mathbf{w} := \text{col}(\mathbf{d}, \nu, \mathbf{r})$). Let \mathbf{Q}_d be divided into nine parts as follows:

$$\mathbf{Q}_d = \begin{bmatrix} \mathbf{Q}_{d_{11}} & \mathbf{Q}_{d_{12}} & \mathbf{Q}_{d_{13}} \\ \mathbf{Q}_{d_{12}}^\top & \mathbf{Q}_{d_{22}} & \mathbf{Q}_{d_{23}} \\ \mathbf{Q}_{d_{13}}^\top & \mathbf{Q}_{d_{23}}^\top & \mathbf{Q}_{d_{33}} \end{bmatrix}.$$

Then,

$$\begin{aligned}\bar{\mathbf{R}}_d &= \mathbf{Q}_{d_{22}} + \mathbf{R}_d \\ \mathbf{D}_2 \mathbf{Q}_d \mathbf{B}_2^\top &= \mathbf{Q}_{d_{12}}^\top \mathbf{B}_{21}^\top \\ \mathbf{B}_2 \mathbf{Q}_d \mathbf{B}_2^\top &= \mathbf{B}_{21} \mathbf{Q}_{d_{11}} \mathbf{B}_{21}^\top.\end{aligned}$$

Infobox 5.2 (Kalman Filter) *It has been demonstrated [6,7] that the dynamic observer constituted by the composition of Eqs. (5.28)–(5.29) represents an optimal observer in stochastic terms. In detail, this observer minimizes the expectation of the squared estimation error*

$$E[(\mathbf{x}(t) - \hat{\mathbf{x}}(t))^\top \mathbf{M}(\mathbf{x}(t) - \hat{\mathbf{x}}(t))],$$

for some $\mathbf{M} = \mathbf{M}^\top \succ 0$, if the following conditions are verified. Let $\delta(\cdot) : \mathbb{R} \rightarrow \mathbb{R}$ be the unit impulse, then:

- $\mathbf{d}(t)$ and $\nu(t)$ are white stochastic processes with covariance kernel

$$E[\mathbf{d}(t)\mathbf{d}^\top(\tau)] = \mathbf{Q}_{d_{11}}\delta(t - \tau) \quad \forall t, \tau \geq t_0$$

$$E[\nu(t)\mathbf{v}^\top(\tau)] = \mathbf{Q}_{d_{22}}\delta(t - \tau) \quad \forall t, \tau \geq t_0;$$

- the processes $\mathbf{d}(t)$ and $\nu(t)$ are correlated by

$$E[\mathbf{d}(t)\nu^\top(\tau)] = \mathbf{Q}_{d_{12}}\delta(t - \tau) \quad \forall t, \tau \geq t_0;$$

- the state vector \mathbf{x}_0 is a random variable with mean and covariance given by

$$E[\mathbf{x}_0] = \bar{\mathbf{x}}_0, \quad E[(\mathbf{x}_0 - \bar{\mathbf{x}}_0)(\mathbf{x}_0 - \bar{\mathbf{x}}_0)^\top] = \mathbf{P}_0;$$

- the stochastic processes $\mathbf{d}(t)$ and $\nu(t)$ are not correlated with respect to the random variable \mathbf{x}_0 , i.e.,

$$E[\mathbf{x}_0 \nu^\top(t)] = \mathbf{0}, \quad E[\mathbf{x}_0 \mathbf{d}^\top(t)] = \mathbf{0} \quad \forall t \geq t_0.$$

Note

Roughly, the gain matrix \mathbf{K}_{S_d} represents a compromise between two opposite approaches. On the one hand, the observer exploits model $\dot{\mathbf{x}} = \mathbf{Ax}$ to make a prediction, but on the other hand, the observer corrects the prediction made with $\dot{\mathbf{x}} = \mathbf{Ax}$ through an output-feedback loop. These two pieces of information, i.e., model $\dot{\mathbf{x}} = \mathbf{Ax}$ and measurement \mathbf{y} , are corrupted by the unknowns \mathbf{d} and ν , respectively. So, the gain \mathbf{K}_{S_d} represents a compromise between the model's reliability and the measurement's trustworthiness. Suppose the model is "perfect" or the measurement is totally unreliable. In this case, the gain \mathbf{K}_{S_d} can be "any" in the family of matrices stabilizing the couple $(\mathbf{A}^\top + \alpha\mathbf{I}, \mathbf{C}^\top)$. Conversely, if the model is inconsistent or the measurement is perfect, \mathbf{K}_{S_d} should become infinite. To confirm this intuition, it is worth noting that the matrix \mathbf{K}_{S_d} is directly proportional to \mathbf{Q}_{d11} (through \mathbf{S}) and $(\mathbf{Q}_{d22} + \mathbf{R}_d)^{-1}\mathbf{C}$. So, high (low) magnitudes of $(\mathbf{Q}_{d22} + \mathbf{R}_d)^{-1}\mathbf{CB}_{21}\mathbf{Q}_{d11}\mathbf{B}_{21}^\top$ mean that the model is less (more) reliable than the output. Also, the term $\mathbf{Q}_{d22}^{-1}\mathbf{C}$ can be interpreted as a signal-to-noise ratio between the output \mathbf{y} and the noise ν . To conclude, the designer can tune \mathbf{Q}_{d11} and \mathbf{R}_d to balance the exploitation of the model and the measurement and to make $\bar{\mathbf{R}}_d$ invertible.

Example 5.6 (Optimal observer) Design an optimal observer for the following LTI system:

$$\dot{\mathbf{x}} = \mathbf{Ax} + \mathbf{B}_2 \mathbf{w}$$

$$\mathbf{y} = \mathbf{Cx} + \mathbf{Dw},$$

where

$$\begin{aligned} \mathbf{A} &= \begin{bmatrix} 0 & 1 \\ -1 & 0 \end{bmatrix}, & \mathbf{B} &= \begin{bmatrix} 1 & 0 \\ 0 & 0 \end{bmatrix} \\ \mathbf{C} &= [1 \ 0], & \mathbf{D} &= [0 \ 1]. \end{aligned}$$

First, write the dual

$$\dot{\chi} = \mathbf{A}^\top \chi + \mathbf{C}^\top v$$

$$\mu = \mathbf{B}^\top \chi + \mathbf{D}^\top v$$

and introduce the cost

$$J = \int_0^\infty \mu^\top \begin{bmatrix} q & 0 \\ 0 & 0 \end{bmatrix} \mu + rv^2 dt.$$

Second, let $\mathbf{S} := [s_{ij}]$, with $s_{ij} \in \mathbb{R}$ for $i, j = 1, 2$. Impose $s_{21} = s_{12}$ and find s_{11} , s_{12} , and s_{22} by solving the following ARE:

$$\begin{bmatrix} 0 \\ 0 \\ 0 \end{bmatrix} = \begin{bmatrix} -s_{11}^2/r + q + 2s_{12} \\ s_{22} - s_{11} - s_{11}s_{12}/r \\ -s_{12}^2/r - 2s_{12} \end{bmatrix}.$$

In particular, the solutions are $s_{12} = 0$, $s_{11} = \sqrt{(q + 2s_{12})r}$, and $s_{22} = s_{11} + s_{11}s_{12}/r$. Also, the observer matrix given by the first of Eq. (5.28) is

$$\mathbf{K}_O = -\mathbf{K}_{S_d}^\top = \frac{1}{r} \begin{bmatrix} s_{11} \\ s_{12} \end{bmatrix}.$$

Then, write the observer as

$$\begin{bmatrix} \dot{\hat{x}}_1 \\ \dot{\hat{x}}_2 \end{bmatrix} = \begin{bmatrix} -s_{11}/r & 1 \\ -1 - s_{12}/r & 0 \end{bmatrix} \begin{bmatrix} \dot{\hat{x}}_1 \\ \dot{\hat{x}}_2 \end{bmatrix} + \frac{1}{r} \begin{bmatrix} s_{11} \\ s_{12} \end{bmatrix} y.$$

It is worth noting that the eigenvalues of

$$\begin{bmatrix} -s_{11}/r & 1 \\ -1 - s_{12}/r & 0 \end{bmatrix},$$

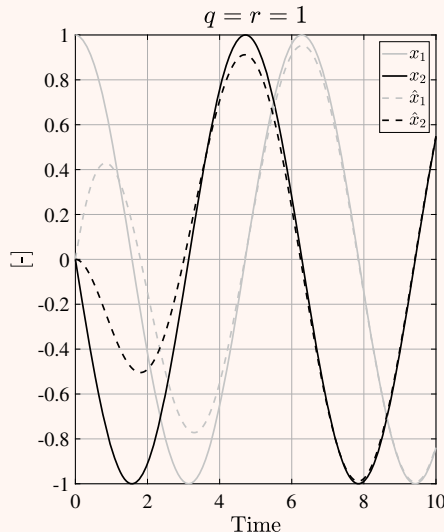
given as the solution to

$$\lambda^2 + \lambda s_{11}/r + 1 + s_{12}/r = 0,$$

are

$$\lambda_{1,2} = \frac{-s_{11} \pm \sqrt{s_{11}^2 - 4(r + s_{12})}}{2r}$$

whose real part is negative for $s_{11} > 0$ and $s_{12} > -r$. Finally, the following figure shows that the estimation asymptotically tracks the state.



Example 5.7 (Tuning of \mathbf{Q}_{d11}) This example investigates the tuning of \mathbf{Q}_{d11} interpreted in the sense of Kalman as a covariance matrix. To make clear as to how \mathbf{Q}_{d11} affects the estimation performance, deal with the scalar system

$$\dot{x} = ax + bu + w$$

$$y = cx + \nu$$

with covariances

$$E[w(t)w(\tau)] = q_{d11}\delta(t - \tau)$$

$$E[\nu(t)\nu(\tau)] = q_{d22}\delta(t - \tau)$$

$$E[w(t)\nu(\tau)] = 0.$$

The observer is given as

$$\dot{\hat{x}} = a\hat{x} + bu + k_O(y - \hat{y})$$

$$\hat{y} = c\hat{x}$$

with the gain

$$k_O = sc/q_{d22}$$

$$s = \frac{aq_{d22}}{c^2} + \sqrt{\frac{a^2q_{d22}^2}{c^4} + \frac{q_{d22}q_{d11}}{c^2}},$$

obtained thanks to the solution of an optimal observation problem. The feedback gain is directly proportional to q_{d11} and this is interpreted (in the sense of Kalman) as: “model $\dot{x} = ax + bu$ becomes increasingly uncertain as q_{d11} increases; thus, it is better to rely on the output y by increasing the feedback gain k_O .”

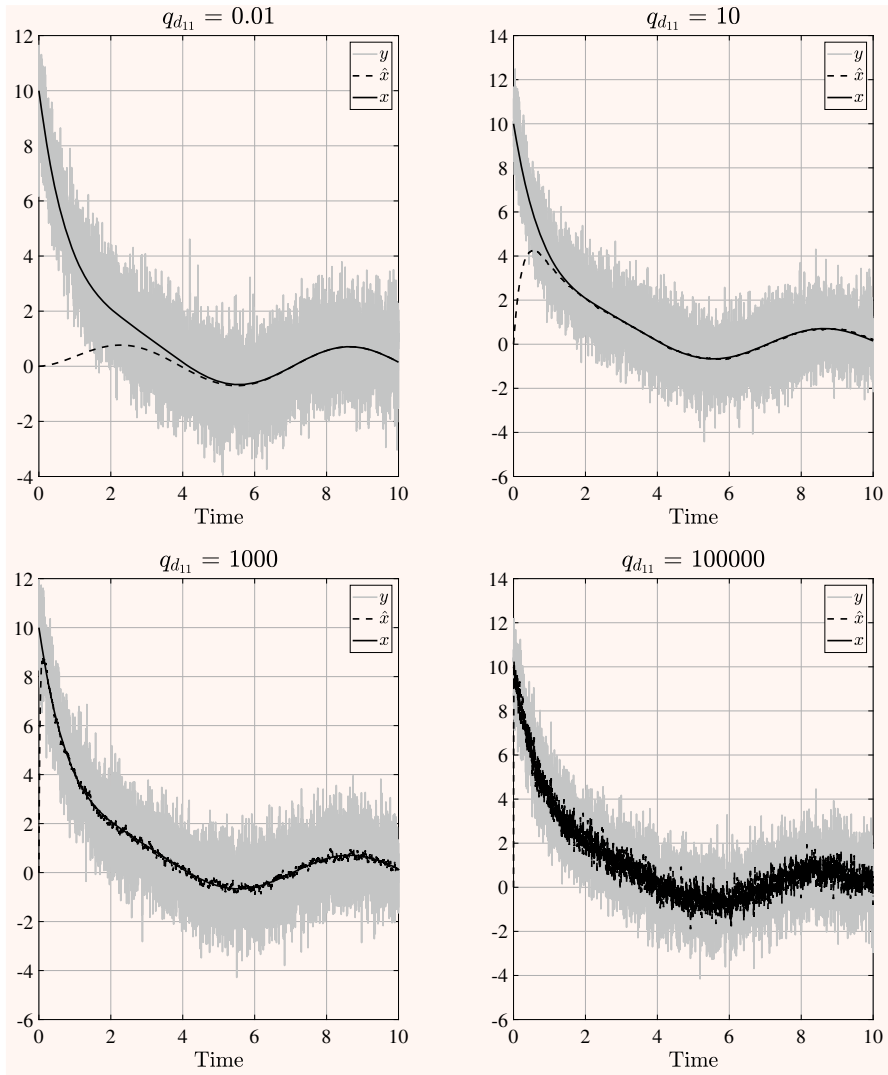
On the other hand, the dynamics of the observation error $e := x - \hat{x}$ are

$$\dot{e} = (a - k_Oc)e + k_O\nu,$$

whose eigenvalue is

$$\lambda = a - k_Oc = -\sqrt{a^2 + \frac{q_{d11}}{q_{d22}}c^2},$$

which is strictly negative and whose norm is directly proportional to q_{d11} . So, a larger q_{d11} leads to a larger k_O which, on the one hand, makes the observer more reactive (thanks to a more negative λ). But, conversely, a larger q_{d11} magnifies the effects of the measurement noise ν . For this reason, the compromise between the observer’s reactivity and the noise sensitivity could guide an intuitive tuning for q_{d11} . The following figures report observation performance for different settings, obtained by imposing $a = -1$, $b = c = q_{d22} = 1$, and $u = \sin t$.



Example 5.8 (Cart-pole observer design) Design an observer for

$$\begin{aligned}\dot{\mathbf{z}}_{R,O} &= \bar{\mathbf{A}}_{22}\mathbf{z}_{R,O} + \bar{\mathbf{B}}_{12}u + \bar{\mathbf{B}}_{22}d \\ \mathbf{y} &= \bar{\mathbf{C}}_2\mathbf{z}_{R,O} + \nu,\end{aligned}$$

which is the dynamics of the reachable and observable part of the model presented in Example 1.2. First, define the dual system

$$\begin{aligned}\dot{\chi} &= \bar{\mathbf{A}}_{22}^\top \chi + \bar{\mathbf{C}}_2^\top v \\ \mu &= [\bar{\mathbf{B}}_{22} \ \mathbf{0} \ \mathbf{0}]^\top \chi + [\mathbf{0} \ \mathbf{I} \ \mathbf{0}]^\top v\end{aligned}$$

and introduce the cost function

$$J_d = \int_0^\infty \mu^\top \mathbf{Q}_d \mu + v^\top \mathbf{R}_d v dt,$$

in which $\mathbf{Q}_d = \mathbf{Q}_d^\top \succeq 0$ and $\mathbf{R}_d = \mathbf{R}_d^\top \succeq 0$. The optimal control law for the dual is obtained as

$$v^* = -\bar{\mathbf{R}}_d^{-1} \bar{\mathbf{C}}_2 \mathbf{S} \chi$$

while the observer is

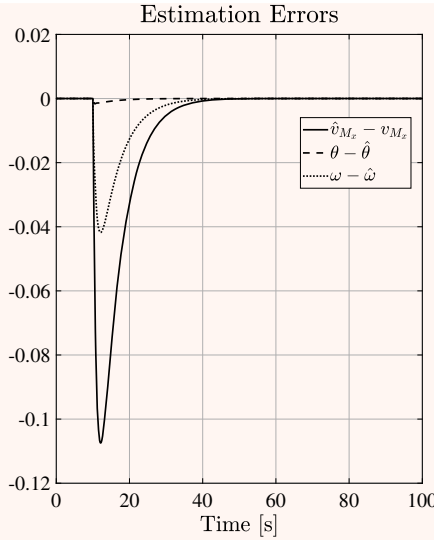
$$\begin{aligned}\dot{\hat{\mathbf{z}}}_{R,O} &= \bar{\mathbf{A}}_{22} \hat{\mathbf{z}}_{R,O} + \bar{\mathbf{B}}_{12} u + \mathbf{S} \bar{\mathbf{C}}_2^\top \bar{\mathbf{R}}_d^{-1} (\mathbf{y} - \hat{\mathbf{y}}) \\ \hat{\mathbf{y}} &= \bar{\mathbf{C}}_2 \hat{\mathbf{z}}_{R,O}.\end{aligned}$$

The matrix \mathbf{S} can be found through numerical solvers. For example, exploit the following MATLAB® listing:

```
% Plant
% Costs
Qn = barB22*Qd11*barB22; % any 3x3 semi-positive definite matrix
Rn = Qd22+Rd % any 2x2 positive definite matrix
% Solve the ARE
[K,S,e] = lqr(barA22.',barC2.',Qn,Rn,zeros(3,2)); %WARNING! The control law is u = -Kc*x. S is the positive definite solution of the ARE.
% Use duality results
Ko = K.';


```

With $\mathbf{Q}_{d11} = 1$, $\mathbf{Q}_{d22} = \mathbf{I}$, and $\mathbf{R}_d = \mathbf{0}$ the observer demonstrates the performance depicted in the following figure, under the same simulation conditions of Example 5.4. In more detail, in agreement with the results of Examples 4.10 and 4.12 and thanks to the definition of the plant in Example 1.1, $\mathbf{z}_{R,O} := \text{col}(v_{M_x}, \theta, \omega)$.



It is worth noting that the estimation errors are not vanishing and this is due to the model mismatch. Indeed, since the model is highly nonlinear, the linearization matrices $\bar{\mathbf{A}}_{22}$ and $\bar{\mathbf{B}}_{22}$ do not accurately approximate the plant.

5.4 ADAS Design

This section aims to set up optimal control and observation problems. Then, concerning the control architectures identified in Sect. 4.7, matrices \mathbf{K}_S , \mathbf{K}_I , and \mathbf{K}_O are designed numerically. Lastly, the performance of the control systems is investigated in simulations.

5.4.1 Active Suspensions

As described in Sect. 2, the AS can be applied to control the cabin's vertical movement (single corner) and rotation (half car). In the following, these two case studies are investigated.

Single-Corner model

Section 4.7.1 identified the control architecture (4.54) in which the matrices \mathbf{K}_S , \mathbf{K}_O , and the scalar k_I have to be designed.

Start with the design of \mathbf{K}_S and k_I and let \mathbf{A} , \mathbf{B}_1 , and \mathbf{C}_e be given by Eq. (2.11). Then, define $\mathbf{x}_e = \text{col}(\mathbf{x}, \eta)$,

$$\mathbf{A}_e = \begin{bmatrix} \mathbf{A} & \mathbf{0} \\ \mathbf{C}_e & \mathbf{0} \end{bmatrix}, \quad \mathbf{B}_e = \begin{bmatrix} \mathbf{B}_1 \\ \mathbf{0} \end{bmatrix}$$

and exploit the theory detailed in Sect. 5.1 to set up the following optimal control problem:

$$\begin{aligned}\dot{\mathbf{x}}_e &= \mathbf{A}_e \mathbf{x}_e + \mathbf{B}_e u \\ \boldsymbol{\epsilon} &= \mathbf{C}_\epsilon \mathbf{x}_e + \mathbf{D}_\epsilon u \\ J &= \int_{t_0}^{\infty} \boldsymbol{\epsilon}^\top \mathbf{Q} \boldsymbol{\epsilon} + R u^2 dt.\end{aligned}\tag{5.30}$$

Matrices \mathbf{C}_ϵ and \mathbf{D}_ϵ represent two degrees of freedom with the unique constraint of having the couple $(\mathbf{A}_e, \mathbf{C}_\epsilon)$ detectable. In more detail, investigate the following three scenarios:

1. **Comfort.** In this scenario, the focus is on the reduction of cabin acceleration. Thus, let $\epsilon_1 := \ddot{z}_s$ and use model (2.11) to write

$$\epsilon_1 = \left[-\frac{k_s}{m_s} - \frac{\beta_s}{m_s} \ 0 \ 0 \ 0 \right] \mathbf{x}_e + m_s^{-1} u.$$

2. **Race.** Rigid suspensions are often needed in high-performance vehicles. Let x_{10} be the equilibrium suspension length defined in Eq. (2.10). Then, in this scenario, the regulated output is defined as $\epsilon_2 = \tilde{x}_1 := x_1 - x_{10}$, i.e.,

$$\epsilon_2 = [1 \ 0 \ 0 \ 0 \ 0] \mathbf{x}_e.$$

3. **Off-road.** Let x_{30} be the tire length at the equilibrium, as found in Eq. (2.10). Then, when the task is to keep the tire contact patch as constant as possible, choose $\epsilon_3 = \tilde{x}_3 := x_3 - x_{30}$. In other terms, define

$$\epsilon_3 = [0 \ 0 \ 1 \ 0 \ 0] \mathbf{x}_e.$$

Driven by these criteria, impose $\boldsymbol{\epsilon} = \text{col}(\epsilon_1, \epsilon_2, \epsilon_3, x_4, \eta)$ and

$$\mathbf{C}_\epsilon = \begin{bmatrix} -\frac{k_s}{m_s} & -\frac{\beta_s}{m_s} & 0 & 0 & 0 \\ 1 & 0 & 0 & 0 & 0 \\ 0 & 1 & 0 & 0 & 0 \\ 0 & 0 & 1 & 0 & 0 \\ 0 & 0 & 0 & 1 & 0 \\ 0 & 0 & 0 & 0 & 1 \end{bmatrix}, \quad \mathbf{D}_\epsilon = \begin{bmatrix} m_s^{-1} \\ 0 \\ 0 \\ 0 \\ 0 \end{bmatrix}.$$

Note that since \mathbf{A} is Hurwitz, the couple $(\mathbf{A}_e, \mathbf{C}_\epsilon)$ is detectable. Then, \mathbf{Q} can be any semi-definite positive matrix (indeed, even if $\mathbf{Q} = \mathbf{0}$ the optimal control problem remains well-posed). Then, for any $\epsilon_{i_{\max}} \in \mathbb{R}$, with $i = 1, \dots, 6$, let

$$\mathbf{Q} := 1/6 \text{diag}(|\epsilon_{1_{\max}}|^{-2}, \dots, |\epsilon_{6_{\max}}|^{-2})$$

and evaluate these three settings:

1. **Comfort.** The main goal is the maximization of passenger comfort. Thus, a possible setting is $|\epsilon_{1_{\max}}| \ll |\epsilon_{2_{\max}}|, |\epsilon_{3_{\max}}|$.
2. **Race.** In this latter case, the variation of the suspension length should be minimized, thus motivating a tuning like $|\epsilon_{2_{\max}}| \ll |\epsilon_{1_{\max}}|, |\epsilon_{3_{\max}}|$.

3. **Off-road.** In these driving conditions, the main goal is to keep the tires on the ground at a nominal compression. For this reason, a plausible gain selection could be $|\epsilon_{3\max}| \ll |\epsilon_{1\max}|, |\epsilon_{2\max}|$.

As for the selection of R , use model (2.11) and remember that $\bar{R} = R + \mathbf{D}_\epsilon^\top \mathbf{Q} \mathbf{D}_\epsilon$ and write $\bar{R} = R + (1/3)m_s^{-2} |\epsilon_{1\max}|^{-2}$, which must be positive. Consequently, for the “comfort” scenario, while holding R constant, the smaller the desired cabin accelerations (i.e., the smaller $|\epsilon_{1\max}|$), the more powerful the requested control law. On the other hand, for the settings “off-road” and “race”, one can assume $|\epsilon_{1\max}| \gg R$. As a result, the power of the control action can be lowered via a reduction of R .

The second goal is the design of \mathbf{K}_O . Supported by the theoretical arguments developed in Sect. 5.3, the matrix \mathbf{K}_O is uniquely determined once the matrices \mathbf{Q}_d and \mathbf{R}_d are defined. So, concerning what was achieved in Sect. 4.7.1, remember that the couple (\mathbf{A}, \mathbf{C}) defined in Eq. (2.11) is fully observable with A Hurwitz. Thus, any $\mathbf{Q}_d \succeq 0$ and $\bar{\mathbf{R}}_d > 0$ make the optimal observation problem (5.27) well-posed. Moreover, let $\mathbf{Q}_d := \text{diag}(q_1, q_2, r_1, r_2, 0)$ and $\mathbf{R}_d = \mathbf{0}$ where q_1, r_1, r_2 can be interpreted, as suggested by Kalman [8], as covariances of disturbance and sensor noises. In more detail, assume $q_1, q_2, r_1, r_2 > 0$ such that

$$\begin{aligned} E[\ddot{z}_r(t)\ddot{z}_r(\tau)] &= q_1\delta(t-\tau) \quad E[f_d(t)f_d(\tau)] = q_2\delta(t-\tau) \\ E[\nu_p(t)\nu_p(\tau)] &= r_1\delta(t-\tau) \quad E[\nu_a(t)\nu_a(\tau)] = r_2\delta(t-\tau) \end{aligned}$$

for any $t, \tau \in \mathbb{R}$. On the one hand, the values r_1 and r_2 can be determined by sensor datasheets (when available) or laboratory experiments. On the other hand, the value of q_1 can be thought of as proportional to the ground roughness. For example, low q_1 could be associated with modern asphalts whereas high q_1 could represent cobblestone roads. As for q_2 , the larger the expected aerodynamic downforce, the higher q_2 , and vice versa.

AS control performance is presented in the following paragraphs for each of the three scenarios.

Comfort. AS is used to improve comfort, i.e., to reduce the acceleration felt by the occupant.

At $t = 0$, the vehicle is left falling from $z_s(0) = \ell_t + \ell_s$. Indeed, at $t = 0$, the accelerometer provides $y_2 \approx 0$. Moreover, the road disturbance $z_r(t)$ emulates a bump appearing at time $t \approx 5$ s (more details in Infobox 5.3). As for the observer initial conditions, this has been set as $\hat{\mathbf{x}}(0) = \tilde{\mathbf{x}}(0)$.

Figure 5.1a highlights the benefits of the AS control policy. This figure superposes the behavior of the open- and closed-loop nonlinear states. Figure 5.1d shows the reduction of the cabin vibrations obtained by adopting AS. The control law, see Fig. 5.1b, is computed via linear combinations of the estimations illustrated in Fig. 5.1e–h. These estimates, obtained by elaborating the measurements shown in Fig. 5.1c and d, are compared with the actual linearized states to show the observer’s performance. This simulation demonstrates that the open-loop low-frequency oscillations are profoundly attenuated thanks to the adoption of the AS control. It is worth noting that the vehicle is in free-fall for a few tenths of a second after the bump. Indeed, the measured acceleration becomes approximately null, see Fig. 5.1d. In this

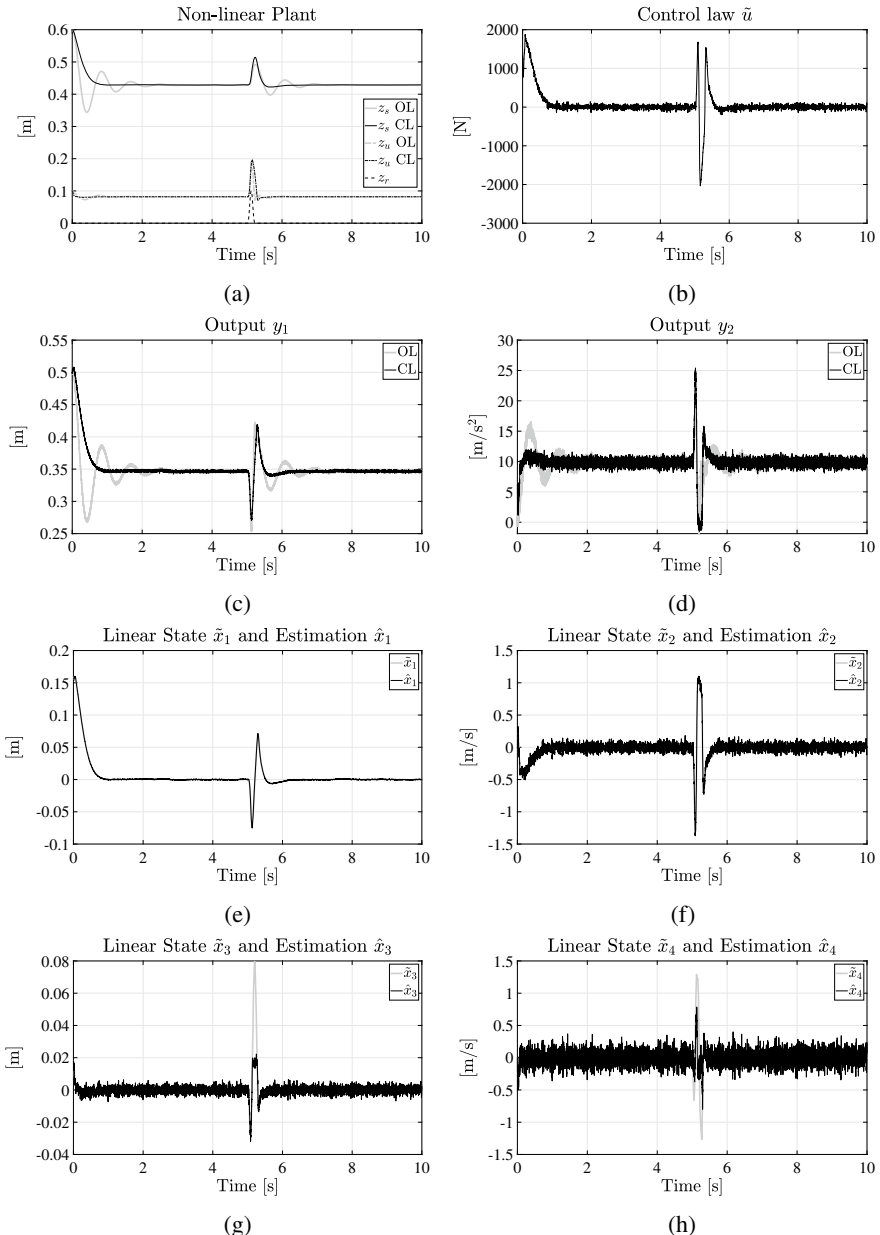


Fig. 5.1 The Active Suspension Control is applied, in an urban environment, adopting the “comfort” setting. The bump simulated in this experiment has been modeled as described in Infobox 5.3 with $v(t) = v_0 = 30 \text{ km/h}$, $h = 10 \text{ cm}$, and $\ell = 2 \text{ m}$

Table 5.1 Active suspension control settings

Symbol	Unit	Value		
		Comfort	Race	Off-road
ϵ_1	m/s^2	$0.1g$	$10g$	$10g$
$\epsilon_{2\max}$	m	10^4	10^{-1}	10^4
$\epsilon_{3\max}$	m/s	10^4	10^4	$5 \cdot 10^{-3}$
$\epsilon_{4\max}$	m	10^2	$2.5 \cdot 10^{-3}$	$2.5 \cdot 10^{-3}$
$\epsilon_{5\max}$	m/s	10^{-1}	10^{-2}	$5 \cdot 10^{-3}$
$\epsilon_{6\max}$	m s	10^{-1}	10^{-2}	10^{-2}
u_{\max}	N	10^3	10^3	10^3
r_1	m^2	$(10^{-3})^2$	$(10^{-3})^2$	$(10^{-3})^2$
r_2	m^2/s^4	$(0.05g)^2$	$(0.05g)^2$	$(0.05g)^2$
q_1	m^2/s^4	1	1	1
q_2	N^2	1	1	1

time interval, the linearized model does not efficiently approximate the nonlinear one, and, as can be seen in Fig. 5.1g–h, this makes poor the estimation of \tilde{x}_3 and \tilde{x}_4 .

The simulation shown in Fig. 5.1 has been obtained with the parameters listed in Table 5.1.

Infobox 5.3 (Bump/pothole profile simulation) *Adopting a sufficiently smooth time function to simulate the ground profile, namely $z_r(t)$, leads to a bounded $\ddot{z}_r(t)$ and maintains the coherency of the kinematic chain $z_r \rightarrow \dot{z}_r \rightarrow \ddot{z}_r$. Denote with $p \in \mathbb{R}$ the vehicle position and define with $g(\cdot) : \mathbb{R} \rightarrow \mathbb{R}$ a function such that $g(p)$ corresponds to the road profile. Assume $v(t) \in \mathbb{R}$ is the vehicle speed, then the asperity time-profile is given by*

$$\begin{aligned}\dot{p}(t) &= v(t) \\ z_r(t) &= g(p(t)).\end{aligned}$$

Therefore, if $g(\cdot)$ and $v(\cdot)$ are sufficiently smooth, the asperity speed and acceleration are given by

$$\begin{aligned}\dot{z}_r(t) &= \left. \frac{\partial g(s)}{\partial s} \right|_{s=p(t)} v(t) \\ \ddot{z}_r(t) &= \left. \frac{\partial^2 g(s)}{\partial s^2} \right|_{s=p(t)} v^2(t) + \left. \frac{\partial g(s)}{\partial s} \right|_{s=p(t)} \dot{v}(t).\end{aligned}$$

Among all the possible choices, polynomials represent suitable candidates for emulating the ground profile. Indeed, they can be proficiently used to describe a bump or a pothole. Let $\ell > 0$ be the bump/pothole length (along the vehicle motion direction). Moreover, let $h \in \mathbb{R}$ such that $h > 0$ represents the bump

height and $h < 0$ models the pothole depth. Assume $v(t)$ to be sufficiently continuous, then model a symmetric bump/pothole of length ℓ , thickness h , located at $p_g \in \mathbb{R}$, with continuous $z_r(t)$, $\dot{z}_r(t)$, and $\ddot{z}_r(t)$, adopt a polynomial of the eighth order, i.e., define

$$g(p) = \begin{cases} 0 & p - p_g \notin [0, \ell] \\ \sum_{i=0}^8 c_i (p - p_g)^i & p - p_g \in [0, \ell]. \end{cases}$$

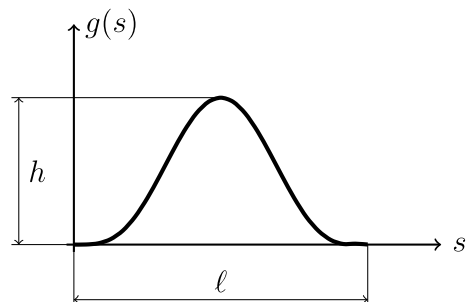
The coefficients $c_i \in \mathbb{R}$, with $i = 0, \dots, 8$, are found by imposing boundary conditions on $g(s)$, $\partial g(s)/\partial s$, $\partial^2 g(s)/\partial s^2$, and $\partial^3 g(s)/\partial s^3$, for $s \in \{0, \ell\}$, plus the constraint $g(\ell/2) = h$. Simple computations show that $c_i = 0$, for $i = 0, \dots, 3$, whereas the remaining coefficients are obtained from

$$\begin{bmatrix} c_4 \\ c_5 \\ c_6 \\ c_7 \\ c_8 \end{bmatrix} = \begin{bmatrix} \ell^4 & \ell^5 & \ell^6 & \ell^7 & \ell^8 \\ (\ell/2)^4 & (\ell/2)^5 & (\ell/2)^6 & (\ell/2)^7 & (\ell/2)^8 \\ 4\ell^3 & 5\ell^4 & 6\ell^5 & 7\ell^6 & 8\ell^7 \\ 12\ell^2 & 20\ell^3 & 30\ell^4 & 42\ell^5 & 56\ell^6 \\ 24\ell & 60\ell^2 & 120\ell^3 & 210\ell^4 & 336\ell^5 \end{bmatrix}^{-1} \begin{bmatrix} 0 \\ h \\ 0 \\ 0 \\ 0 \end{bmatrix}.$$

Figure 5.2 shows the profile of a bump obtained with this formulation.

Race. In this scenario, the controller is in charge of keeping the desired suspension length, despite an external (constant) disturbance due to the unknown downforce f_d . As shown in Fig. 5.3, the vehicle starts the simulation under the effects of f_d while, after 5 s, the reference suspension length is changed (shorter set point). Then, in the first part of the simulation, the control system demonstrates its ability to deal with constant disturbances. At the same time, in the second part of the simulated timespan, the controller highlights the capacity to track constant references. Indeed, the value of the control action \tilde{u} at time $t = 5$ s before the reference variation has a mean of about 735 N, necessary to compensate for the downforce. After the reference has changed, the control law changes to compress the spring and lower the vehicle, i.e., $\tilde{u} \approx k_s \tilde{r} - f_d$ at time 10 s. It is also worth noting that, at time $t = 0$, the vehicle starts with tire and suspension at their unloaded lengths. For this reason, the vehicle suddenly drops in the first few seconds, which induces oscillations damped through the control system. Figure 5.3e–h highlight the poor observation performance due to

Fig. 5.2 Bump profile



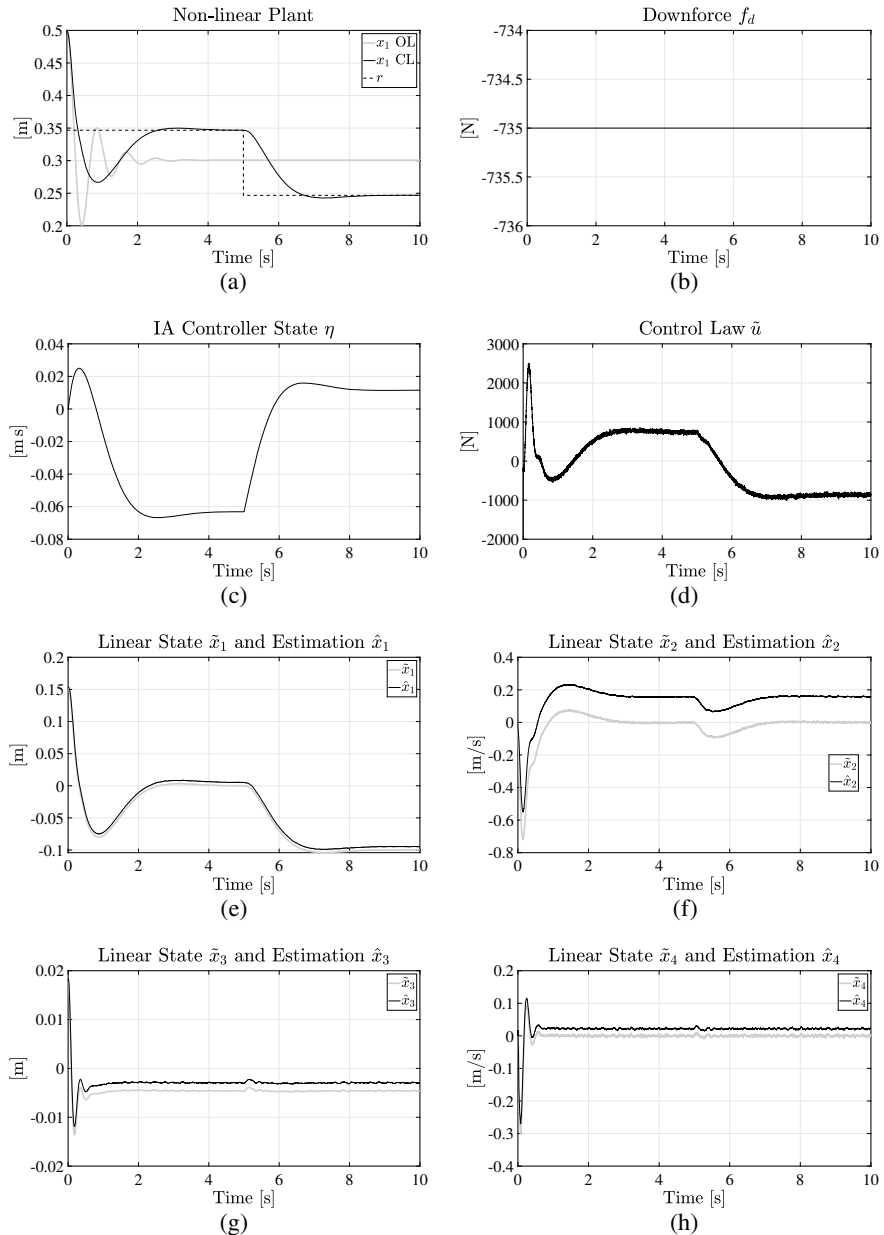


Fig. 5.3 The Active Suspension Control is applied, in a sports scenario, adopting the “Race” setting. The vehicle travels at 120 km/h and exhibits a downforce of about -735 N. The controller’s internal state η faces this external disturbance, regulating the suspension length at the desired value

the model mismatch. Indeed, in this case, the presence of an unknown and constant disturbance creates a persistent difference between the actual model and the observer design model. Despite this error, the closed-loop eigenvalues are modified as desired. Indeed, the initial oscillations are damped in the closed loop.

Off-road. When driving off-road, keeping the tire on the ground could be important, thus guaranteeing good traction performance. In this context, the main goal is reducing the tire deflections and, as a second achievement, regulating the suspension length (usually to a longer extension to increase the clearance between the terrain and the underbody). The simulation results presented in Fig. 5.4 have been obtained by adopting the tuning suggested for the setting “Off-Road”, whose numerical details are listed in Table 5.1. A comparison between open- and closed-loop behaviors highlights the improvements associated with the AS control system. The system starts at time $t = 0$ with both the tire and the suspension spring at their 0-load length. Then, after 5 s, the reference suspension length is changed concurrently with the injection of a road profile disturbance. In particular, the suspension is required to be 10 cm longer while the vehicle is perturbed by a bump of height 50 cm and base 2 m. The aerodynamic downforce is neglected because the vehicle speed is 3 km/h. The simulation shows that, despite the estimation errors due to the presence of the unknown road bump (Fig. 5.4e–g), the tire dynamics are improved thanks to the AS system. In particular, the oscillations characterizing the open-loop behavior are successfully damped, as depicted in Fig. 5.4b. On the other hand, the integral action allows the asymptotical tracking of the reference suspension length, see Fig. 5.4a. Indeed, the controller state η increases to the necessary value such that $\tilde{u} \approx k_s \tilde{r}$ asymptotically, see Fig. 5.4c–d.

Half-Car model

When applied to the half-car model, AS is used to regulate the vehicle height (distance from the ground) and the cabin attitude, e.g., the apparent roll angle, as modeled in Sect. 2.1. The vertical and rotational dynamics are tightly coupled when considering an asymmetric weight distribution. This leads to an interesting and challenging control problem, i.e., regulating a MIMO system. Section 4.7.1 identified a control system architecture composed of an output-feedback stabilizer (state feedback plus observer) and an integral action to solve this problem. Section 4.7.1 also highlighted that the system modeling the dynamics of a half car contains some non-reachable states. These states correspond to the kinematic chain describing the road bank angle. The rest of the states, denoted with \mathbf{z}_R , model the dynamics of height and roll angle. This state was extended with $\boldsymbol{\eta}$, representing the integral of the regulated output \mathbf{e} . Then, the control law is

$$\mathbf{u} = \mathbf{K}_R \hat{\mathbf{z}}_R + \mathbf{K}_I \boldsymbol{\eta}.$$

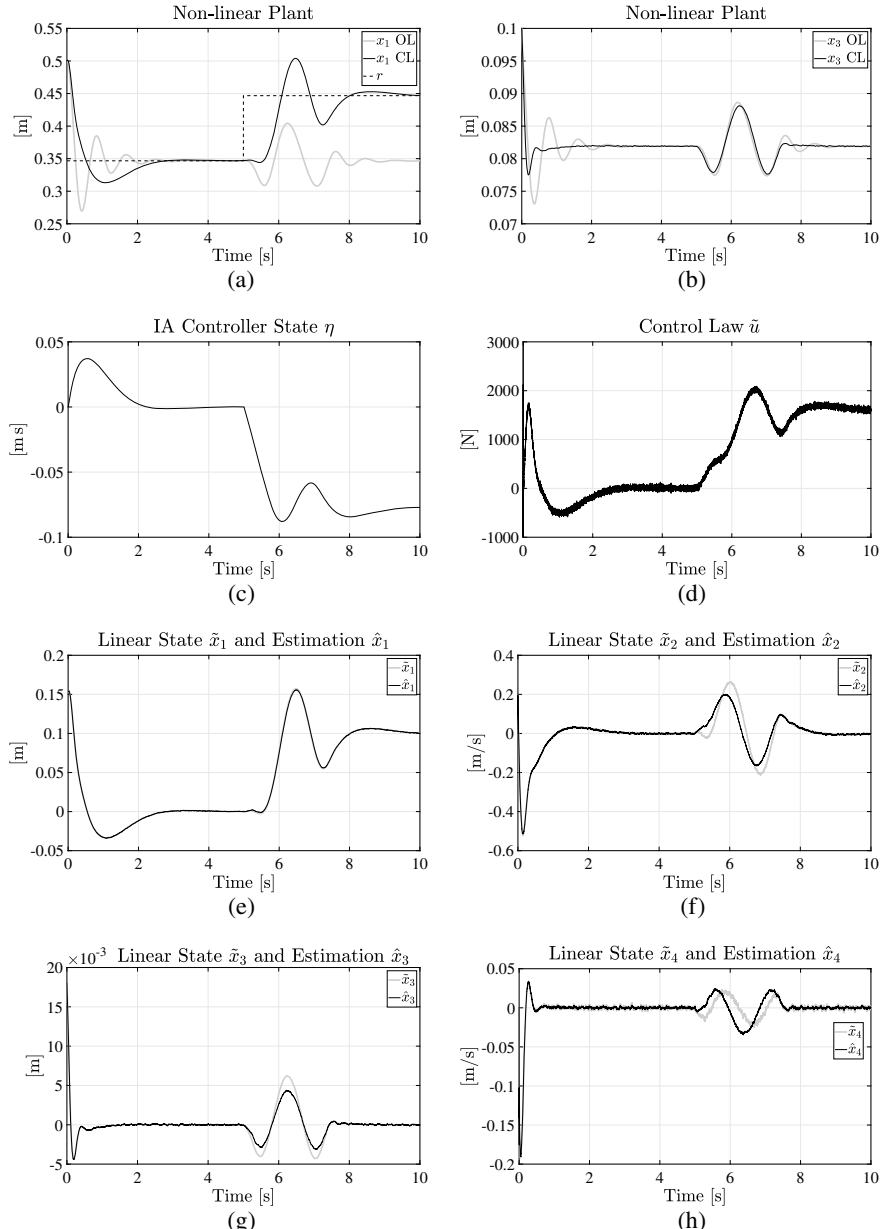


Fig. 5.4 The behavior of the single-corner model with and without the Active Suspension system. In an off-road scenario, the model is perturbed by a high-profile low-speed bump appearing at time $t = 5$ s. At the same time, a change in the suspension reference length is commanded. Thanks to the control tuning, the tire deflection is reduced while the reference suspension length is asymptotically tracked

Let $\mathbf{x}_e := \text{col}(\mathbf{z}_R, \boldsymbol{\eta})$ be the extended state, use matrices \mathbf{A}_e and \mathbf{B}_e defined in Eq. (4.55), and write the following equations:

$$\begin{aligned}\dot{\mathbf{x}}_e &= \mathbf{A}_e \mathbf{x}_e + \mathbf{B}_e \mathbf{u} \\ J &= \int_0^{\infty} \mathbf{x}_e^\top \mathbf{Q} \mathbf{x}_e + \mathbf{u}^\top \mathbf{R} \mathbf{u} dt,\end{aligned}$$

where $\mathbf{Q} = \mathbf{Q}^\top$, $\mathbf{R} = \mathbf{R}^\top \succ 0$ represent tunable parameters. In agreement with the theory developed in Sect. 5.1, the control that minimizes J and stabilizes the dynamics of \mathbf{x}_e can be written as a state-feedback law $\mathbf{u} = \mathbf{K}_e \mathbf{x}_e$ where $\mathbf{K}_e := [\mathbf{K}_R \mathbf{K}_I]$. The matrix \mathbf{K}_e is found as a solution to the ARE associated with the tuple $(\mathbf{A}_e, \mathbf{B}_e, \mathbf{Q}, \mathbf{R})$.

As for the selection of \mathbf{Q} and \mathbf{R} , adopt the following strategy.

First, in agreement with Sect. 5.1.1, let $x_{i_{\max}} > 0$, with $i = 1, \dots, 6$, be the maximum tolerable errors and define

$$\mathbf{Q}^{-1} = 6 \text{diag}(x_{1_{\max}}^2, \dots, x_{6_{\max}}^2).$$

Note that the open-loop system (see Sect. 3.4) is characterized by two oscillatory modes, one at a high frequency corresponding to the rotational dynamics and one at a low frequency representing the vertical translation dynamics. Then, the improvement introduced by the control consists of a higher damping for the rotational dynamics and higher pulsation and damping for the translational dynamics. To reach this goal, choose $x_{1_{\max}} \geq x_{3_{\max}}$, $x_{2_{\max}} \geq x_{4_{\max}}$, and $x_{2_{\max}} \geq x_{1_{\max}}$. Roughly, $x_{1_{\max}} \geq x_{3_{\max}}$ is used to increase the vertical dynamics pulsation more than the rotational dynamics pulsation, $x_{2_{\max}} \geq x_{4_{\max}}$ induces damping higher on the vertical dynamics than on the rotational one, and $x_{2_{\max}} \geq x_{1_{\max}}$ increases the damping of the vertical dynamics. Moreover, the weights $x_{5_{\max}}$ and $x_{6_{\max}}$ penalize $\boldsymbol{\eta}$, whose dynamics are described by two null eigenvalues (two integrals) in the open loop. Then, $x_{5_{\max}}$ and $x_{6_{\max}}$ are designed to be sufficiently small and smaller than $x_{1_{\max}}, \dots, x_{4_{\max}}$ to decrease (increase the norm of) the real part of the eigenvalues closest to the origin.

Second, define $\mathbf{R}^{-1} = 2 \text{diag}(u_{1_{\max}}^2, u_{2_{\max}}^2)$ with $u_{1_{\max}}, u_{2_{\max}} > 0$. As for the selection of $u_{1_{\max}}, u_{2_{\max}}, u_{1_{\max}} \geq u_{2_{\max}}$ makes the vertical control more aggressive than the rotational one.

Third, unlike the single-corner model, the half-car one is characterized by nonlinearities that make the control system less effective. To deal with this issue, as described in Sect. 5.1, the control law design can be improved by introducing the parameter α . Positive values of α induce more aggressive feedback gains that typically result in closed-loop eigenvalues with a more negative real part.

The control system design is completed with the computation of the observer gain \mathbf{K}_O . Exploiting the theoretical tools developed in Sect. 5.3 and relying on the observer's structure defined in Section 4.7.1, the matrix \mathbf{K}_O is computed by solving

the following dual control problem:

$$\begin{aligned}\dot{\chi} &= (\mathbf{A}^\top + 2\alpha\mathbf{I})\chi + \mathbf{C}^\top v \\ \mu &= \mathbf{B}_2^\top \chi + \mathbf{D}_2^\top v \\ J_d &= \int_{t_0}^{\infty} \mu^\top \mathbf{Q}_d \mu + v^\top \mathbf{R}_d v dt.\end{aligned}$$

The simulation reported in Figs. 5.5 and 5.6 has been obtained with $\alpha = 1/2$, $x_{1\max} = 10^{-1/2}$ m, $x_{2\max} = 5000^{-1/2}$ m/s, $x_{3\max} = 1$ rad, $x_{4\max} = 20^{-1/2}$ rad/s, $x_{5\max} = 5000^{-1/2}$ m · s, $x_{6\max} = 5000^{-1/2}$ rad · s, $u_{1\max} = 500$ N, and $u_{1\max} = 1000$ Nm. Furthermore, as for the observer design, the following parameters have been chosen: $\alpha = 10$, $q_i = 100^{-1}$, with $i = 1, \dots, 4$, $r_1 = r_2 = (0.05g)^2$ m²/s⁴, $r_3 = 0.01$ (deg/s)², $r_4 = r_5 = 1$ mm², and

$$\mathbf{Q}_d = \text{diag}(q_1, \dots, q_4, r_1, \dots, r_5, \mathbf{0}), \mathbf{R}_d = \mathbf{0}.$$

In Fig. 5.5, the control system is tested in two different conditions. At the beginning ($t = 0$), the vehicle starts from a lifted configuration and is left free to evolve. This experiment highlights the improvements induced by the control system in terms of damping. In particular, at $t = 0$, the control law compresses the suspension springs to “pull down” the vehicle; see Fig. 5.5e. Moreover, for $t \in [0, 5]$ s, Fig. 5.5a and b show that the modes characterizing the closed-loop system have damping higher than the open loop.

On the other hand, from $t = 5$ onwards, the vehicle is subject to $f_{w_l}, f_{w_r} \approx 600$ N (emulating a lateral acceleration of $\approx 0.2g$). The robustness to external disturbance and the asymptotic tracking performance is tested in this second part of the simulation. As can be seen in Fig. 5.5a and b, the open loop vehicle is lifted and tilted (rollover-related behavior) by the exogenous disturbance. As a result, the passengers feel an uncomfortable lateral acceleration, see Fig. 5.5g and h. As depicted in Fig. 5.5c and d, the unwanted vertical displacement and lateral acceleration are accumulated into the controller’s states η_1 and η_2 . These states are used to compute the control laws depicted in Fig. 5.5e and f. Thanks to these control laws, the errors e_1 and e_2 are asymptotically restored to zero; see Fig. 5.5g and h. It is worth noting that, as expected, the controlled vehicle rolls inward to reduce the occupants’ lateral acceleration; see Fig. 5.5b.

Finally, the behavior of the observer’s states is reported in Fig. 5.6. The observer has been set to have no errors at $t = 0$. As can be seen, for $t \in [0, 5)$, the observer tracks the linearized state with good accuracy. However, external disturbances create a mismatch between the actual model and that used to design the observer. For this reason, for $t \geq 5$ s, the estimation performance is poor. In particular, the observer fixes the disagreement between the model and the measurements mainly by the allocation of the inertial effects to the road bank speed and acceleration; see Fig. 5.6e and f. Consequently, all the remaining states are adjusted to keep the estimated output close to the actual one. Despite these estimation errors, the overall control system performance is satisfactory.

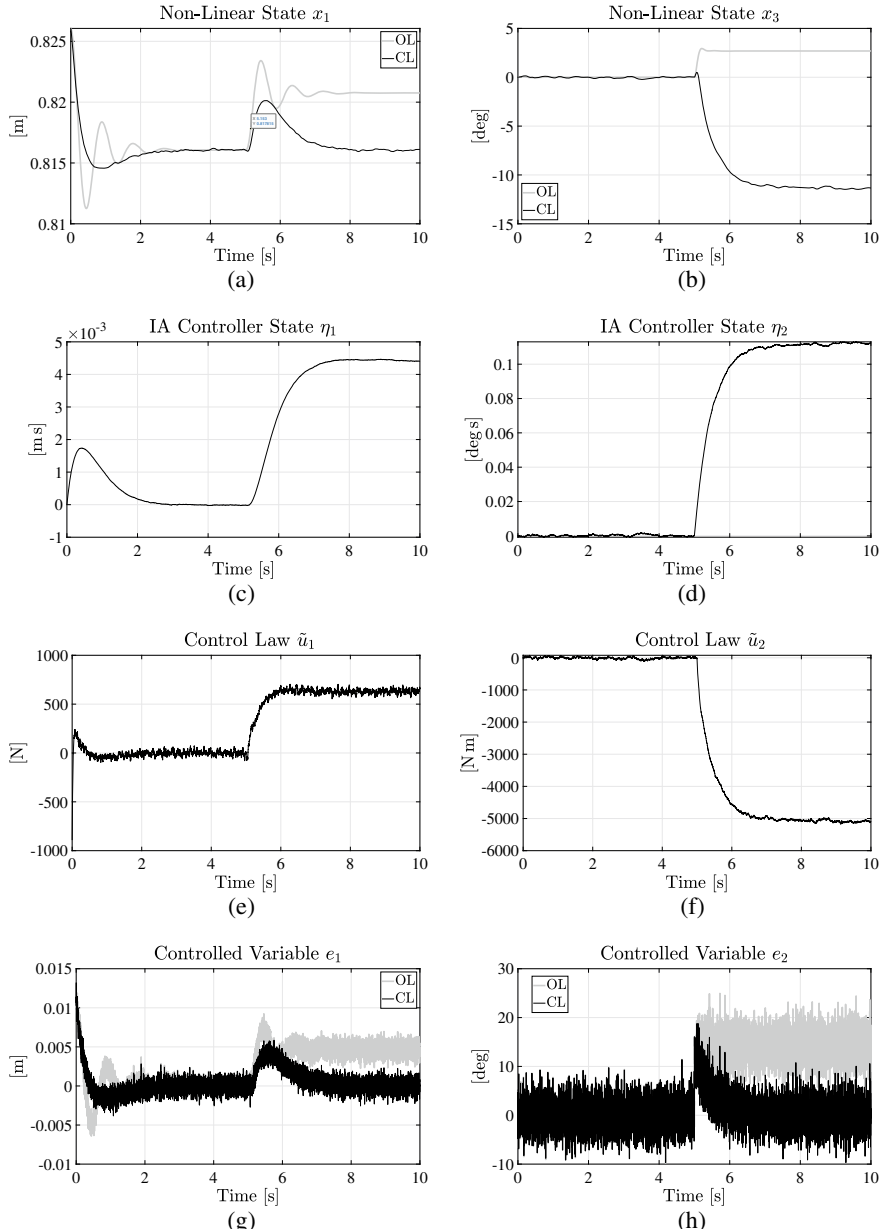


Fig. 5.5 Active suspensions applied to the half-car model. The purpose of this application consists of regulating the vehicle height and roll angle. In particular, to increase the comfort when cornering, the desired roll angle is designed to minimize the lateral acceleration felt by the passengers. Accordingly to this goal, the control action tilts (rolling) the vehicle inward the turn

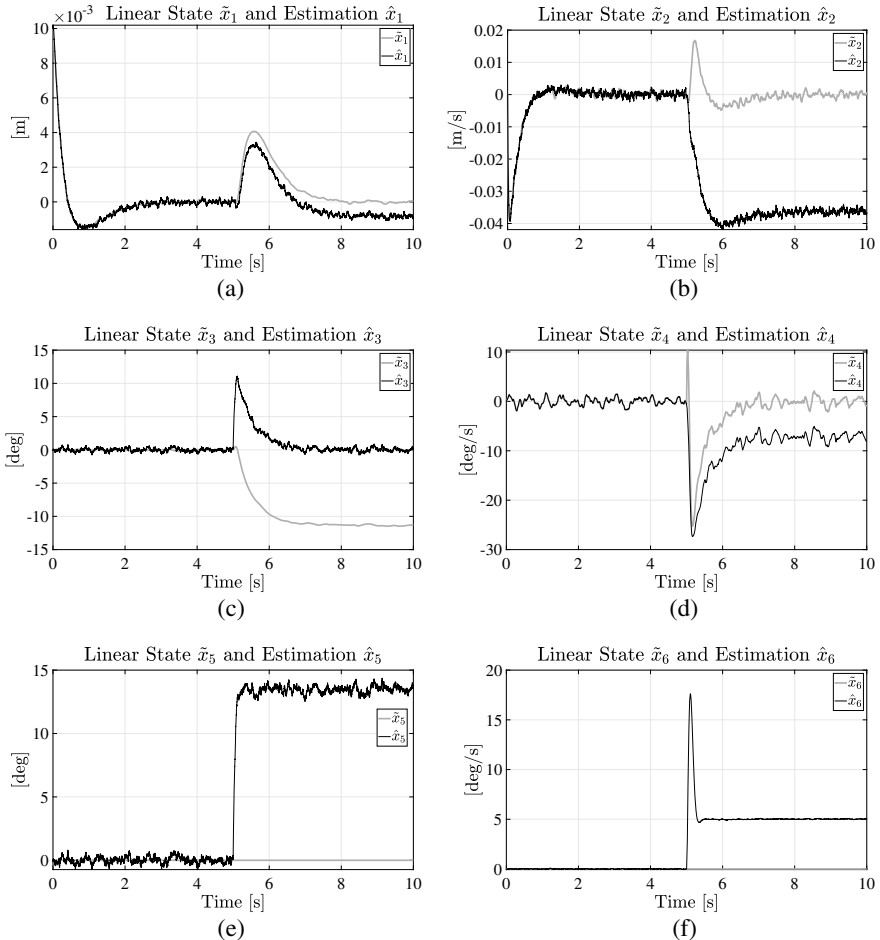


Fig. 5.6 Performance of the state observer designed on the half-car model. The estimation performance is good until the actual and design models are coherent. When an external disturbance appears, the observer is deceived by the mismatch between the actual and the design models. Indeed, at $t = 5$, a side force appears to emulate a cornering at $\approx 0.2g$. The observer allocates this effect to a road bank variation and, based on the design model, adjusts the remaining states accordingly

5.4.2 Electro-mechanical Brakes

The architecture suitable to control an EMB, described in Sect. 4.7.2, comprises a state-feedback stabilizer, a state observer, and an integral action. As for the design of the state-feedback stabilizer and the integral action, proceed as suggested in Sect. 4.3. Let \mathbf{x} , η , \mathbf{A}_e , and \mathbf{B}_e be as identified in Sect. 4.7.2. Define $\mathbf{x}_e = \text{col}(\mathbf{x}, \eta)$ and set the following optimization problem:

$$\dot{\mathbf{x}}_e = (\mathbf{A}_e + 2\alpha\mathbf{I})\mathbf{x}_e + \mathbf{B}_e u$$

$$J = \int_{t_0}^{\infty} \mathbf{x}_e^\top \mathbf{Q} \mathbf{x}_e + R u^2 dt$$

in which α , $\mathbf{Q} = \mathbf{Q}^\top \in \mathbb{R}^{4 \times 4}$ and R are designed hereafter. Let $x_{i_{\max}} > 0$, with $i = 1, \dots, 4$, be the maximum allowable state errors, and choose (see Sect. 5.1.1)

$$\mathbf{Q}^{-1} = 4 \operatorname{diag}(x_{1_{\max}}^2, \dots, x_{4_{\max}}^2).$$

One way to achieve the control goal described in Sect. 4.7.2, i.e., the asymptotic tracking of a constant reference caliper force, is that of imposing $x_{1_{\max}} \gg x_{2_{\max}}, x_{3_{\max}}, x_{4_{\max}}$. Roughly, the variables $x_{2_{\max}}$ and $x_{3_{\max}}$ are used to make the system more reactive, while $x_{4_{\max}}$ is necessary to stabilize the dynamics of η . The design of the state-feedback stabilizer and the integral action is completed with the selection of $\alpha \geq 0$, which, de facto, makes the real part of the eigenvalues more negative, thus increasing the damping of the oscillatory modes.

The observer matrix \mathbf{K}_O is considered the solution of an optimal control problem, dual to the observation of \mathbf{x} . The observer gain is uniquely defined once the parameters \mathbf{Q}_d and \mathbf{R}_d are specified by adopting the guidelines presented in Sect. 5.3. On the one hand, let $r_{d1}, r_{d2} > 0$ be noise covariances and set $\mathbf{R}_d = \mathbf{0}$. On the other hand, let $q > 0$ denote the uncertainty of the knowledge of the friction force, then $\mathbf{Q}_d := \operatorname{diag}(q, r_1, r_2 \mathbf{0})$.

The controller performance is shown in Fig. 5.7. Assuming that the system is in equilibrium at the beginning of the simulation, the controller tracks a reference caliper force, modeled as a piecewise constant function. At the time $t = 0.01$ s, the reference is increased by 1000 N and kept constant for the rest of the simulation. As can be seen, the controller reacts to this request by increasing the voltage (Fig. 5.7f). This, in turn, increases the current (Fig. 5.7c) that generates a higher torque on the motor shaft. Then, the shaft increases its speed (Fig. 5.7b) and angular position (Fig. 5.7a). To let x_1 asymptotically approach the desired position (associated with the desired caliper force), the controller has to accelerate and brake the shaft. This explains the positive and negative behavior of voltage and current. These electric profiles generate an increasing and decreasing positive shaft speed that, once integrated, leads to the shaft rotation (without oscillations). Figure 5.7d shows that the desired force is practically tracked in less than 0.03 s. At the same time, both η and the estimate \hat{x}_1 slowly converge to their asymptotic values, see Fig. 5.7e and g. This behavior is due to the non-linearities generated by the friction forces. Indeed, these latter affect the system, especially at low speeds. On the one hand, even if the friction-induced model mismatch is small, it is sufficient to induce a wrong estimation \hat{x}_1 . On the other hand, at low speed, the controller action is counterbalanced by strong friction forces, which justifies the slow transient of η .

The results presented in Fig. 5.7 have been obtained with the following settings: $x_{1_{\max}} = 1$ rad, $x_{2_{\max}} = (1e5)^{-1/2}$ rad/s, $x_{3_{\max}} = (1e4)^{-1/2}$ A, $x_{4_{\max}} = (1e4)^{-1/2}$ Nm, $R = 1e4$ V, $\alpha = 50$, $q = 1$ (Nm)², $r_1 = 1e4$ N², and $r_2 = (0.05\bar{\omega})^2$ rad²/s². The parameter $\bar{\omega} = 100$ rad/s (≈ 5730 deg/s) represents the expected maximum shaft speed, which is coherent with the maximum speed reported in Fig. 5.7b.

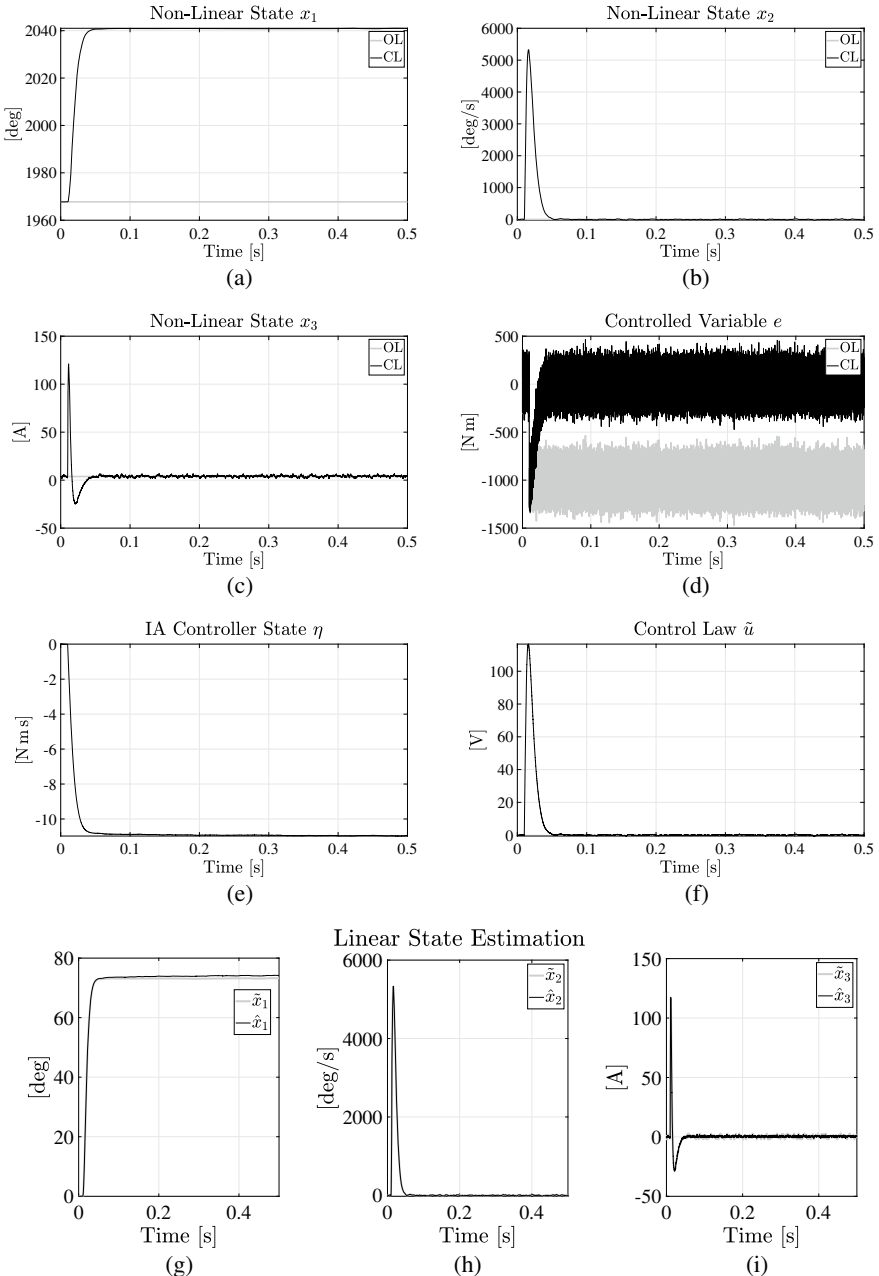


Fig. 5.7 Simulation of a controlled EMB. The system starts in equilibrium. Then, the desired reference caliper force is increased by 1 kN after 0.01 s. The controller reacts to this request by commanding an input voltage variation that has the final effect of increasing the shaft position. Despite the desired force being practically tracked in less than 0.03 s, the non-linearities affecting the system at low speed have an asymptotic impact on the observer's performance

5.4.3 Wheel Speed Controls

The control architecture that regulates the wheel speeds, described in Sect. 4.7.3, is founded on the linearized model derived in Sect. 2.3. In particular, this section focuses on the design of LaC. Still, it is worth noting that ABS and, more in general, TC are designed with criteria analogous to that detailed hereafter.

One of the main features of the plant under consideration is the dependency of the eigenvalues, of the open-loop system, on the vehicle speed; see Sect. 3.4.3. This dependency has a deep impact on the choice of the linearization condition. As Sect. 4.7.3 suggests, the linearization should be evaluated at some “worst” conditions to robustly stabilize the longitudinal dynamics of vehicles. To define these conditions, assume $\lambda' \in (0, \lambda^*)$ and exploit the results presented in Sect. 3.4.3. In particular, use Fig. 3.22 to conclude that the higher the speed v_0 , the closer the eigenvalues to the imaginary axis (i.e., the less stable the open-loop system). Since LaC is usually actuated at low speeds, v_0 can be the top speed at which LaC is turned off.

As the second design criterion, exploit the time scale separation highlighted in Sect. 3.4.3. Then, define $\mathbf{B}_{12} = \text{diag}(J_r^{-1}, J_f^{-1})$ and consider the wheel sub-system

$$\begin{aligned}\dot{\tilde{\omega}} &= \mathbf{A}_{22}\tilde{\omega} + \mathbf{B}_{12}\tilde{\mathbf{u}} + \mathbf{A}_{21}\tilde{v} \\ \tilde{\mathbf{e}} &= \tilde{\omega},\end{aligned}$$

where \tilde{v} represents a measurable disturbance.

With this criterion at hand, the design procedure follows what is stated in Sect. 5.1. First, extend the plant by defining $\mathbf{x}_e = \text{col}(\tilde{\omega}, \eta)$ and

$$\mathbf{A}_e = \begin{bmatrix} \mathbf{A}_{22} & \mathbf{0} \\ \mathbf{I} & \mathbf{0} \end{bmatrix}, \quad \mathbf{B}_e = \begin{bmatrix} \mathbf{B}_{12} \\ \mathbf{0} \end{bmatrix}.$$

Second, define $\mathbf{Q} = \mathbf{Q}^\top \succeq 0$, $\mathbf{R} = \mathbf{R}^\top \succ 0$, and $\alpha \geq 0$ to set up the following optimization problem:

$$\begin{aligned}\dot{\mathbf{x}}_e &= (\mathbf{A}_e + 2\alpha\mathbf{I})\mathbf{x}_e + \mathbf{B}_e\mathbf{u} \\ J &= \int_{t_0}^{\infty} \mathbf{x}_e^\top \mathbf{Q} \mathbf{x}_e + \mathbf{u}^\top \mathbf{R} \mathbf{u} dt.\end{aligned}$$

As for the selection of \mathbf{Q} and \mathbf{R} , Section 5.1.1 suggests defining $x_{i,\max} > 0$, with $i = 1, \dots, 4$, and $u_{1,\max}, u_{2,\max} > 0$ as the maximum allowable state and control errors. Then, take $\mathbf{Q}^{-1} = 4 \text{diag}(x_{1,\max}^2, \dots, x_{4,\max}^2)$ and $\mathbf{R}^{-1} = 2 \text{diag}(u_{1,\max}^2, u_{2,\max}^2)$. It is worth highlighting that, while $x_{3,\max}, x_{4,\max}$ are necessary to stabilize the integral of the regulated output, parameters $x_{3,\max}, x_{4,\max}$ are exploited to increase the damping. Then, since the open-loop system is already characterized by strongly damped modes, $x_{3,\max}, x_{4,\max}$ can be much smaller than $x_{1,\max}, x_{2,\max}$. Moreover, α is chosen positive to make the design robust, i.e., to tolerate a reduction of stability due to non-ideal road conditions. Furthermore, α is designed with the criterion that the higher α is, the more negative the real part of the closed-loop eigenvalues is, and the stronger the reduction of stability the control system can tolerate. Finally, the feed-forward scheme presented at the end of Sect. 4.7.3 completes the control system.

Figure 5.8 shows the performance of LaC. At time $t = 0$, vehicle and wheel speeds are zero. The nonlinear control \mathbf{u}_0 , whose entries are positive, accelerates the wheels, and, as a consequence, the wheels increase their speeds and generate a traction force that, in turn, accelerates the vehicle; see Fig. 5.8a–c. As the vehicle starts accelerating, its speed increases thus decreasing the slip ratios, see Fig. 5.8d and e. For the selected \mathbf{u}_0 , the slip ratio negotiated after the initial phases is much lower than the target ($\lambda' = 0.1$); see Fig. 5.8d and e. This acceleration performance is improved through LaC. Indeed, as depicted in black in Fig. 5.8, the control mainly increases the torque applied on the wheel shafts, thus resulting in a faster wheel rotation and a higher slip ratio. The integral action asymptotically stabilizes the wheel speed on a ramp corresponding to the reference slip ratio $\lambda' = 0.1$; see Fig. 5.8d and e.

The results presented in Fig. 5.8 have been obtained with $v_0 = 100 \text{ km/h}$, $\lambda' = 0.1$, $x_{1\max} = x_{1\max} = 1 \text{ rad/s}$, $x_{1\max} = x_{1\max} = 10^{-5/2} \text{ rad}$, $u_{1\max} = u_{1\max} = 10^3 \text{ Nm}$, and $\alpha = 5$.

5.4.4 Adaptive Cruise Control

Section 4.7.4 described the architecture of a decentralized ACC. In more detail, the control system is composed of a state-feedback stabilizer extended with integral action. Indeed, for this application, the state $\tilde{\mathbf{x}}_d$, being fully available at the output ($\tilde{\mathbf{y}}_d = \tilde{\mathbf{x}}_d + \boldsymbol{\nu}_d$), is used to stabilize the plant. Section 4.7.4 suggests the control law $\tilde{u}_d = \mathbf{K}_S \tilde{\mathbf{y}}_d + k_1 \eta$ with $\dot{\eta} = e_d$. To design the matrix \mathbf{K}_S and the scalar k_1 , adopt the following steps. First, define $\mathbf{x}_e = \text{col}(\tilde{\mathbf{x}}_d, \eta)$ as the extended state and introduce

$$\mathbf{A}_e := \begin{bmatrix} \mathbf{A}_d & \mathbf{0} \\ \mathbf{C}_{de} & 0 \end{bmatrix}, \quad \mathbf{B}_e := \begin{bmatrix} \mathbf{B}_{d1} \\ 0 \end{bmatrix}.$$

Second, let $\alpha \geq 0$, $R > 0$, and $\mathbf{Q} = \mathbf{Q}^\top \succeq 0$ be design parameters and find u that minimizes the cost

$$J = \int_{t_0}^{\infty} \mathbf{x}_e^\top \mathbf{Q} \mathbf{x}_e + R u^2 dt$$

subject to the constraint

$$\dot{\mathbf{x}}_e = (\mathbf{A}_e + 2\alpha \mathbf{I}) \mathbf{x}_e + \mathbf{B}_e u.$$

As for the design of \mathbf{Q} , introduce $x_{1\max}, x_{2\max}, x_{3\max} > 0$ and define $\mathbf{Q}^{-1} = 3 \text{ col}(x_{1\max}^2, x_{2\max}^2, x_{3\max}^2)$. The coefficient $x_{1\max}$ represents the maximum allowed error on the safety distance, $x_{2\max}$ is thought of as the maximum allowed error on the speed, and $x_{3\max}$ is associated with the maximum allowed value of the integral of the safety distance error. Now, in the open loop, the speed is asymptotically stable, but the safety distance is not Hurwitz (see Sect. 3.4.4). Then, $x_{1\max}$ and $x_{2\max}$ are designed to guarantee the stability of the safety distance and make speed dynamics faster. Also, $x_{3\max}$ is directly associated with the stability of η . The design is completed by

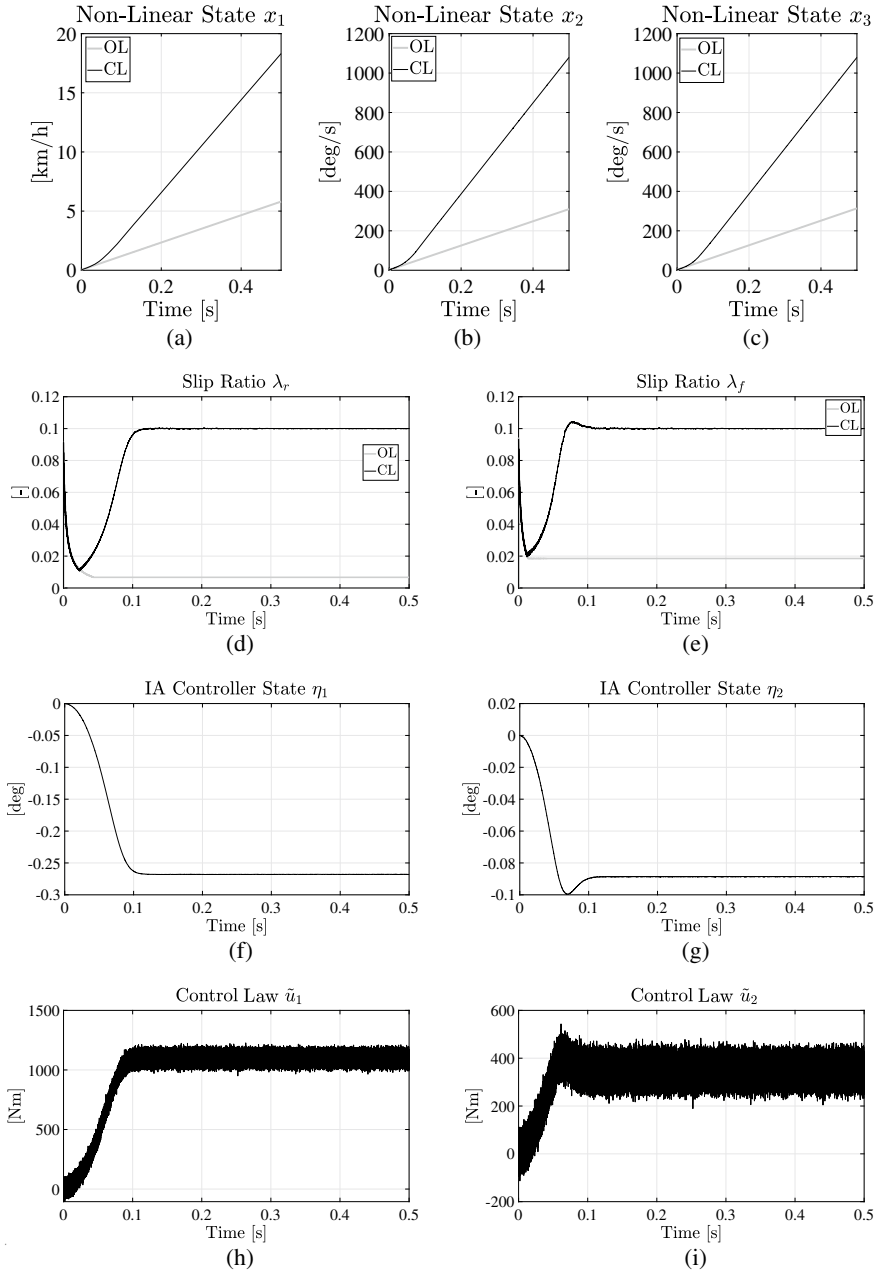


Fig. 5.8 Example of a Launch Control. The vehicle, conceived at rest at the beginning of the experiment, is accelerated to track the reference slip ratio $\lambda' = 0.1$ asymptotically. As can be seen in subplots (f) and (g), the integral action increases and induces an increment of the wheel torques, as also reported in subplots (h) and (i). These torques are designed to make the actual slip ratio asymptotically track the reference

selecting R and α . As for R , the design criterion is that the smaller R is, the stronger the control action is. Finally, α is used to make the control system robust against the non-linearities. In particular, the higher α is, the more negative the real part of the eigenvalues of the closed-loop system is.

Figure 5.9 graphically describes the performance of the ACC designed in this section. At the beginning of the simulation, the controlled vehicle follows a leader traveling at a constant speed of 100 km/h (see the dashed line in Fig. 5.9b). The initial speed of the follower is larger than that of the leader, thus leading to a safety distance longer than the actual one (see the dashed line in Fig. 5.9a). The control system reacts to these initial inconsistent conditions (the actual inter-vehicle distance is shorter than the safety one) by braking the car (see Fig. 5.9e). The system comes back to the design conditions in 15 s. As a consequence, the integral action comes back to zero (see Fig. 5.9d).

The leader brakes at $t = 15$ s and reduces the speed to 90 km/h. The difference between the leader and the follower speeds reduces the inter-vehicle distance. If not compensated, the speed difference leads to the linear error depicted in gray in Fig. 5.9c. In this context, ACC slows down the vehicle (see Fig. 5.9e) with a braking action proportional to the controller state η (see Fig. 5.9d). As shown in Fig. 5.9a, the control system keeps the actual inter-vehicle distance close to the safety one during the transient. The reference distance is tracked asymptotically. Accordingly, the vehicle speed is reduced and asymptotically converges to that of the leader; see Fig. 5.9b.

The simulation results shown in Fig. 5.9 have been obtained with $x_{1\max} = 2^{-1/2}$ m, $x_{2\max} = 3^{-1/2}$ m/s, $x_{3\max} = 1$ m/s, $R = 10^{-3}$ N, and $\alpha = 0.05$.

5.4.5 Automatic Steering System

Section 2.5 described how the Automatic Steering system allows the steering column to track a time-varying reference angle. The control system architecture proposed in Sect. 4.7.5 relies on a dynamic output-feedback stabilizer, an integral action, and a feed-forward law to accomplish this task.

To design the matrix $\mathbf{K}_S \in \mathbb{R}^{1 \times 2}$ and the coefficient $k_I \in \mathbb{R}$, which represent the gains of the stabilizer and the integral action, proceed as follows. First, use the arguments of Sect. 4.3, exploit matrices \mathbf{A}_e and \mathbf{B}_e determined in Sect. 4.7.5, and define $\mathbf{x}_e = \text{col}(\mathbf{x}, \eta)$. Let $\alpha \geq 0$, $\mathbf{Q} = \mathbf{Q}^\top \succeq 0$, and $R > 0$ be tunable parameters. Now, define the integral cost

$$J = \int_0^{\infty} \mathbf{x}_e^\top \mathbf{Q} \mathbf{x}_e + R u^2 dt$$

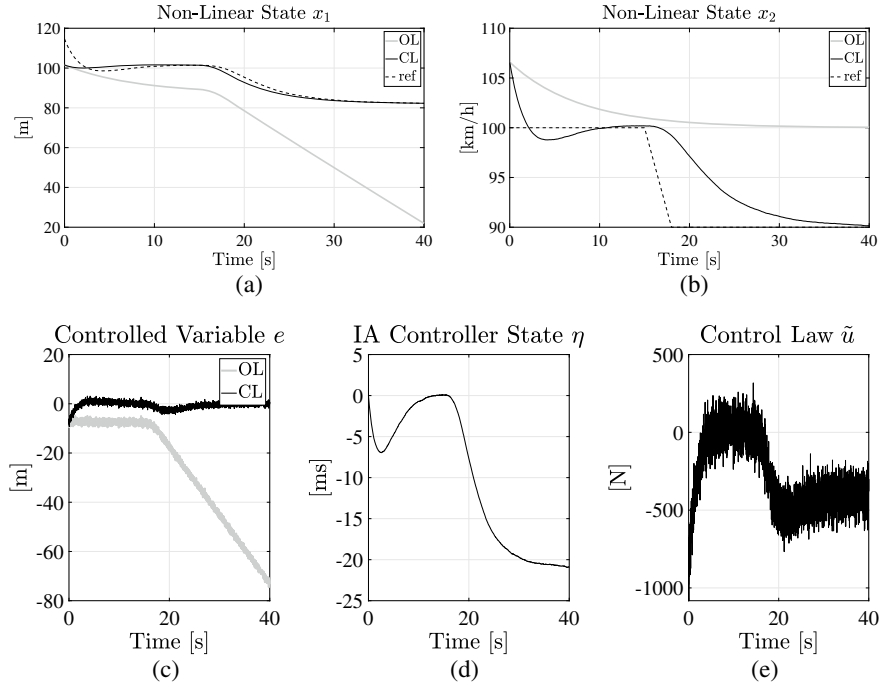


Fig. 5.9 Simulation of an Adaptive Cruise Control. In this test, the controlled vehicle follows a leader initially traveling at 100 km/h. At time $t = 15$ s, the leader brakes reducing its speed by 10 km/h. The ACC system reacts by braking the vehicle to asymptotically restore the right inter-vehicle distance. In reaching this goal, the follower's speed asymptotically tracks that of the leader

and the constraint

$$\dot{\mathbf{x}}_e = (\mathbf{A}_e + 2\alpha \mathbf{I})\mathbf{x}_e + \mathbf{B}_e u.$$

Then, Sect. 5.1 shows that $u = [\mathbf{K}_S \ k_I] \mathbf{x}_e$ minimizes J with $\mathbf{A}_e + \mathbf{B}_e [\mathbf{K}_S \ k_I]$ Hurwitz.

As for tuning this control law, let $x_{1\max}$, $x_{2\max}$, and $x_{3\max} > 0$ be the maximum allowed variation of the elements of \mathbf{x}_e from the equilibrium $\text{col}(\mathbf{x}_0, 0)$. Then, exploiting the procedure described in Sect. 5.1.1, define

$$\mathbf{Q}^{-1} = 3 \text{diag}(x_{1\max}^2, x_{2\max}^2, x_{3\max}^2).$$

One of the control system's tasks is stabilizing the open-loop plant by introducing a dissipative term. To achieve this goal, note that, roughly, the larger $x_{2\max}$ is, the stronger the damping the closed loop exhibits. Moreover, exploit α to make the system sufficiently fast. In particular, the higher α is, the more negative the real part of the eigenvalues is. Finally, the design of R completes the tuning of the control law, where the smaller R is, the stronger the feedback action is, so the more reactive the closed-loop plant is.

Design the observer through the duality arguments introduced in Sect. 5.2 and developed in Sect. 5.3. In more detail, let $\alpha_d \geq 0$ and define the dual system

$$\begin{aligned}\dot{\chi} &= (\mathbf{A}^\top + 2\alpha_d \mathbf{I})\chi + \mathbf{C}^\top v \\ \boldsymbol{\mu} &= \mathbf{B}_2^\top \chi + \mathbf{D}_2^\top v.\end{aligned}$$

Associate with this dual system the cost function

$$J_d = \int_{t_0}^{\infty} \boldsymbol{\mu}^\top \mathbf{Q}_d \boldsymbol{\mu} + R_d v^2 dt,$$

where \mathbf{Q}_d and R_d are designed by adopting the guidelines presented in Sect. 5.3. Denote with $r > 0$ the covariance of the encoder's noise. Let $q > 0$ be the uncertainty on exogenous torques, then \mathbf{Q}_d is defined as $\mathbf{Q}_d = \text{diag}(q, q, r, 0)$. Finally, the term $\alpha_d \geq 0$ is used to speed up the observer. Indeed, the higher α_d is, the more negative the real part of the eigenvalues of $\mathbf{A} - \mathbf{K}_O \mathbf{C}$ is.

The Automatic Steering system designed in this section has been tested in simulation. The simulation results are reported in Fig. 5.10. In particular, the system starts at $t = 0$ in equilibrium, and in the absence of disturbance; see Fig. 5.10a-d. The control system tracks a time-varying reference. The reference steering angle is $r_\delta(t) = 0$, for $t \in (0, 1)$, and $r_\delta(t) = A(1 - \cos(w(t - 1)))$, with $A = \pi/2$ and $w = 2\pi$, for $t \geq 1$. This time law only guarantees that $r_\delta(t)$ and $\dot{r}_\delta(t)$ are continuous at $t = 1$. The discontinuity of $\ddot{r}_\delta(t)$, at $t = 1$, leads to an abrupt change in \tilde{u} ; see Fig. 5.10e. From $t = 1$ to $t = 3$ s, the plant is not subject to any exogenous disturbance. In these circumstances, the observer perfectly estimates the linearized states; see Fig. 5.10f and g. At $t = 3$ a constant disturbance is introduced. Despite its effects being asymptotically canceled by the integral action, the disturbance leads to a tracking error; see Fig. 5.10c. This error is accumulated in the variable η ; see Fig. 5.10d, and generates the control bias visible in the last two seconds of Fig. 5.10e. As for the observation, the disturbance represents a model mismatch that the observer cannot compensate, as depicted in Fig. 5.10f and g.

The simulation results presented in Fig. 5.10 have been obtained with $\alpha = 5$, $x_{1\max} = 1/\sqrt{2}$ rad, $x_{2\max} = 1/\sqrt{3}$ rad/s, $x_{3\max} = 1$ rad s, $R = 1/10$ (Nm) 2 , $\alpha_d = 5$, $q = 0.01$ (Nm) 2 , $r = (\pi/180)^2$ rad 2 , and $R_d = 0$.

5.4.6 Latero-directional Controls

Section 4.7.6 presented the architecture of latero-directional controls. As for the controls designed on the model (2.78), the following paragraphs detail the design and tuning procedures adopted for ESP and TV.

ESP. The main goal of ESP is to improve vehicle stability. Section 4.7.6 introduced a stabilizer fed by a state observer to reach this goal. Let \mathbf{z}_R , $\Delta\omega$, $\tilde{\mathbf{A}}$, and $\tilde{\mathbf{B}}_1$ be the quantities defined in Sect. 4.7.6. Then, let $\alpha \geq 0$, $\mathbf{Q} = \mathbf{Q}^\top \succeq 0$, and $R > 0$ be tunable parameters and define the following cost function:

$$J = \int_0^{\infty} \mathbf{z}_R^\top \mathbf{Q} \mathbf{z}_R + R \Delta\omega^2 dt$$

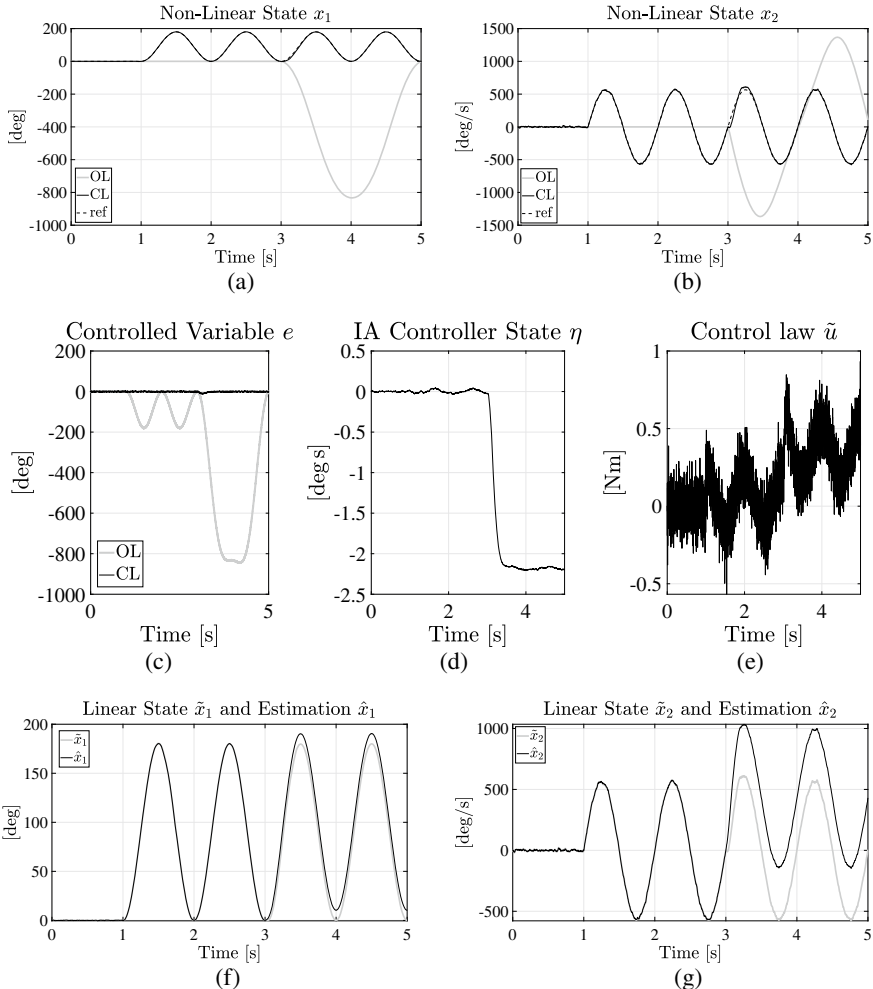


Fig. 5.10 Numerical test of an Automatic Steering System. At $t = 0$, the system starts in equilibrium, and at $t = 1$, a sinusoidal steering reference angle is introduced. After 3 s, the plant is affected by two external torques of 10 Nm each, acting on the wheels

under the constraint

$$\dot{\mathbf{z}}_R = (\bar{\mathbf{A}} + 2\alpha\mathbf{I})\mathbf{z}_R + \bar{\mathbf{B}}_1\Delta\omega.$$

In agreement with Sect. 5.1, the state feedback control law implements \mathbf{K}_S such that $\Delta\omega = \mathbf{K}_S\mathbf{z}_R$ minimizes J and $\bar{\mathbf{A}} + \bar{\mathbf{B}}_1\mathbf{K}_S$ is Hurwitz. Matrix \mathbf{K}_S can be tuned via the degrees of freedom α , \mathbf{Q} , and R . In particular, let $z_{1\max}, z_{2\max} > 0$ be the maximum tolerable amplitude for the entries of \mathbf{z}_R . Then, as suggested in Sect. 5.1.1, \mathbf{Q} can be defined such that $\mathbf{Q}^{-1} = 2\text{diag}(z_{1\max}^2, z_{2\max}^2)$. As a result, the smaller $z_{1\max}$ and $z_{2\max}$ are, the stronger the control action is. The remaining parameters α and R are

tuned by remembering that the larger α is, the more negative the real part of the eigenvalues of the closed-loop plant is. Moreover, the smaller R is, the stronger the control action is, and so the more negative the closed-loop eigenvalues' real part is.

The control system is also composed of a state observer. As described in Sect. 4.7.6, the model on which the observer is based is

$$\begin{aligned}\dot{\mathbf{z}}_R &= \bar{\mathbf{A}}\mathbf{z}_R + \bar{\mathbf{B}}_1\Delta\omega + \bar{\mathbf{B}}_2\mathbf{w}_{ESP} \\ y &= \bar{\mathbf{C}}\mathbf{z}_R + \bar{\mathbf{D}}\mathbf{w}_{ESP}\end{aligned}$$

where $\bar{\mathbf{B}}_2$ represents the last two rows of the matrix \mathbf{B}_{2ESP} identified in Sect. 4.7.6, and $\bar{\mathbf{D}}$ is such that $\bar{\mathbf{D}}\mathbf{w}_{ESP} = \nu$. Let $\alpha_d \geq 0$ be a tunable parameter, assume $\Delta\omega = 0$, and define the dual system

$$\begin{aligned}\dot{\chi} &= (\bar{\mathbf{A}}^\top + 2\alpha_d\mathbf{I})\chi + \bar{\mathbf{C}}^\top v \\ \mu &= \bar{\mathbf{B}}_2^\top\chi + \bar{\mathbf{D}}^\top v.\end{aligned}$$

Now, let $\mathbf{Q}_d = \mathbf{Q}_d^\top \succeq 0$ and $R_d \geq 0$ be tunable parameters, and introduce the cost function

$$J_d = \int_{t_0}^{\infty} \mu^\top \mathbf{Q}_d \mu + R_d v dt.$$

Then, as described in Sect. 5.3, the observer matrix \mathbf{K}_O is such that $\bar{\mathbf{A}}^\top - \bar{\mathbf{C}}^\top \mathbf{K}_O^\top$ is Hurwitz and $v := -\mathbf{K}_O^\top \chi$ minimizes J_d .

The parameter α_d is used to change the observer's dynamics. In particular, the larger α_d is, the more negative the real part of the eigenvalues of the observer is. Let $\mathbf{Q}_d := \text{blkdiag}(\mathbf{Q}_{d11}, r)$. Then, based on the interpretation suggested by Kalman (see Sect. 5.1), \mathbf{Q}_{d11} represents the covariance matrix of disturbance \mathbf{d} . In the context of the latero-directional dynamics, \mathbf{Q}_{d11} is representative of the expected variations of wind and tire-ground friction coefficients. So, the larger the \mathbf{Q}_{d11} entries are, the more uncertain the plant and the stronger the observer feedback are. Conversely, r represents the covariance of the noise affecting the gyroscope. The better the sensor, the lower r is, and the more the observer exploits the measurement via larger feedback actions.

Figure 5.11 shows the performance of ESP. The vehicle, modeled as a rear-traction car with a front-engine configuration, is assumed to travel at 250 km/h. This extreme condition makes the system unstable in the open loop and highlights the benefits associated with ESP. In more detail, the vehicle starts, at $t = 0$, with a non-trivial lateral speed and yaw rate. This initial state perturbation excites the modes (unstable in the open loop), and leads to the trajectories depicted in gray in Fig. 5.11a–c. In the open loop, the vehicle speed (Fig. 5.11a) decreases because of the nonlinear coupling with the latero-directional dynamics. Moreover, as correctly foreseen by the analysis outlined in Sect. 3.4.6, the vehicle starts spinning in a spiral motion (see gray lines in Fig. 5.11b and c). On the other hand, thanks to the control action of ESP, the vehicle state returns to the linearization conditions. Indeed, the black lines reported in Fig. 5.11a–c confirm that, asymptotically, the vehicle returns to a straight path at

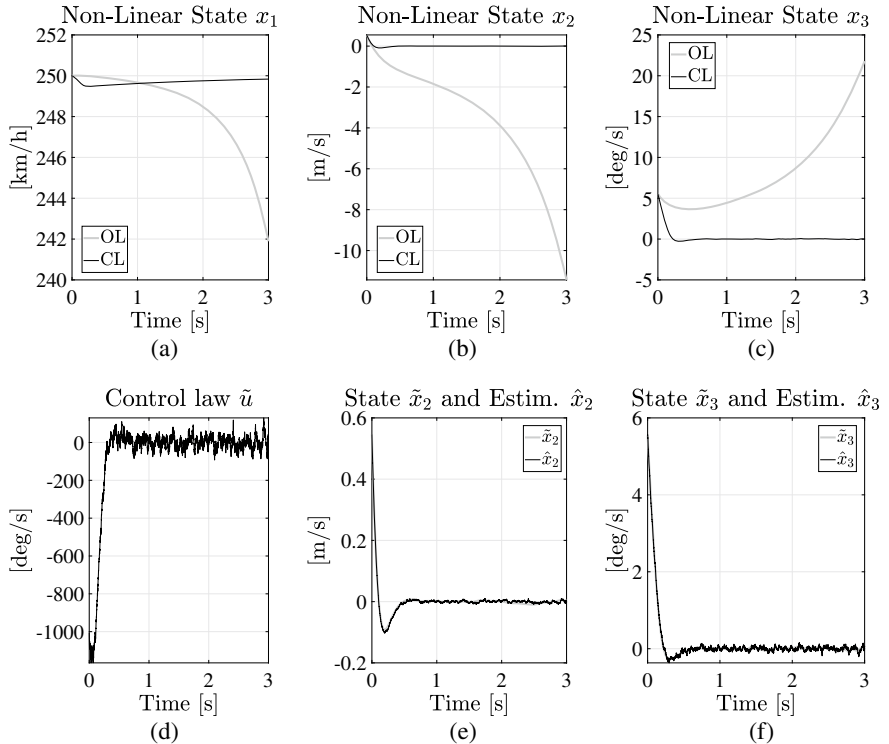


Fig. 5.11 ESP simulation. The vehicle, traveling at 250 km/h, is initialized with a non-trivial lateral speed and yaw rate. For the selected linearization conditions, the open loop has one eigenvalue with a positive real part. ESP makes stable the closed-loop plant

a constant speed asymptotically. To achieve this result, the controller relies on the state estimation reported in Fig. 5.11d and e. As seen in these diagrams, the observer tracks the evolution of the linearized state with good accuracy. Finally, the control law is shown in Fig. 5.11f. The stabilization action is evident in the first simulation instants when a wheel differential speed is commanded.

The simulation results shown in Fig. 5.11 have been obtained with $\alpha = 0$, $z_{1\max} = 1$ m/s, $z_{2\max} = 1$ rad/s, $R = 100$ rad/s, $\alpha_d = 0$, $\mathbf{Q}_{d11} = \text{diag}(100, 1)$, $r = (\pi/180)^2$ (rad/s) 2 , and $R_d = 0$.

TV. TV's main purpose is to improve the steering performance to make the vehicle track a time-varying reference yaw rate. The policy detailed in Infobox 4.10 can generate this reference. In addition, Sect. 4.7.6 describes the control system architecture as a composition of a stabilizer fed by a state observer, an integral control, and a feed-forward.

As for the design of the state feedback and the integral action, use the matrices $\bar{\mathbf{A}}$, $\bar{\mathbf{B}}_1$, and $\bar{\mathbf{C}}_e$ introduced in Sect. 4.7.6 to define

$$\mathbf{A}_e = \begin{bmatrix} \bar{\mathbf{A}} & \mathbf{0} \\ \bar{\mathbf{C}}_e & 0 \end{bmatrix}, \quad \mathbf{B}_e = \begin{bmatrix} \bar{\mathbf{B}}_e \\ 0 \end{bmatrix}.$$

Similarly, exploit the definitions of \mathbf{z}_R and η provided in Sect. 4.7.6 to let $\mathbf{x}_e := \text{col}(\mathbf{z}_R, \eta)$ be the extended state. Define $\alpha \geq 0$, $\mathbf{Q} = \mathbf{Q}^\top \succeq 0$, and $R > 0$ as tunable parameters and introduce the cost function

$$J = \int_0^\infty \mathbf{x}_e^\top \mathbf{Q} \mathbf{x}_e + R u^2 dt,$$

coupled with the constraint

$$\dot{\mathbf{x}}_e = (\mathbf{A}_e + 2\alpha \mathbf{I}) \mathbf{x}_e + \mathbf{B}_e u.$$

As described in Sect. 5.1, the control law that minimizes J and stabilizes the closed-loop plant is $u = \mathbf{K}_e \mathbf{x}_e$, with $\mathbf{K}_e \in \mathbb{R}^{1 \times 3}$. Let $\mathbf{K}_S \in \mathbb{R}^{1 \times 2}$ and $k_I \in \mathbb{R}$ be subparts of \mathbf{K}_e such that $\mathbf{K}_e = [\mathbf{K}_S \ k_I]$. Then (see Sect. 4.3 for details), the stabilizer is $u_S = \mathbf{K}_S \mathbf{z}_R$, while the integral action is $u_I = k_I \eta$.

The feedback matrix \mathbf{K}_e is tuned via the degrees of freedom α , \mathbf{Q} , and R . Roughly, the larger α is, the more negative the real part of the eigenvalues of the closed-loop system is. On the other hand, the smaller R is, the larger the magnitude of the eigenvalues of the closed loop is. As for \mathbf{Q} , the guideline depicted in Sect. 5.1.1 suggests starting with the definition of $x_{i_{\max}} > 0$, with $i = 1, 2, 3$. These quantities, conceived as maximum allowable values for the entries of \mathbf{x}_e , are exploited to define $\mathbf{Q}^{-1} = 3 \text{diag}(x_{1_{\max}}^2, x_{2_{\max}}^2, x_{3_{\max}}^2)$. To reduce the priority of the integral action, choose $x_{3_{\max}}$ to be much smaller than $x_{1_{\max}}$ and $x_{2_{\max}}$, which play a crucial role in stabilizing the vehicle (see ESP).

TV relies on the same state estimator designed for ESP. The following feed-forward law suggested in Sect. 4.7.6 completes the control system:

$$\begin{aligned} \dot{\zeta}_\perp^* &= \bar{A}_{11} \zeta_\perp^* + \bar{A}_{12} r \\ u_{FF} &= (\bar{\mathbf{C}}_e \bar{\mathbf{B}}_1)^{-1} (\dot{r} - \bar{\mathbf{C}}_e (\bar{\mathbf{A}} + \bar{\mathbf{B}}_1 \mathbf{K}_S) \text{col}(\zeta_\perp^*, r)), \end{aligned}$$

where r denotes the reference yaw rate. The policy detailed in Infobox 4.10 generates this reference by imposing $r = \tilde{\omega}_\infty$. In this context, since $\dot{\tilde{\omega}}_\infty$ is unknown (because the derivative of the steering wheel angle is considered unknown), the feed-forward control is approximated as

$$\begin{aligned} \dot{\zeta}_\perp^* &= \bar{A}_{11} \zeta_\perp^* + \bar{A}_{12} \tilde{\omega}_\infty \\ u_{FF} &= -(\bar{\mathbf{C}}_e \bar{\mathbf{B}}_1)^{-1} \bar{\mathbf{C}}_e (\bar{\mathbf{A}} + \bar{\mathbf{B}}_1 \mathbf{K}_S) \text{col}(\zeta_\perp^*, \tilde{\omega}_\infty). \end{aligned}$$

Figure 5.12 presents the performance of the TV designed in this section. In a simulation, the control system has been tested on a vehicle traveling at 90 km/h on a straight path; see Fig. 5.12a. The car starts the experiment with a non-trivial side-slip speed and yaw rate, as depicted in Fig. 5.12b and c. To correct these initial errors, the control system (which, in this context, acts as ESP) generates a positive torque

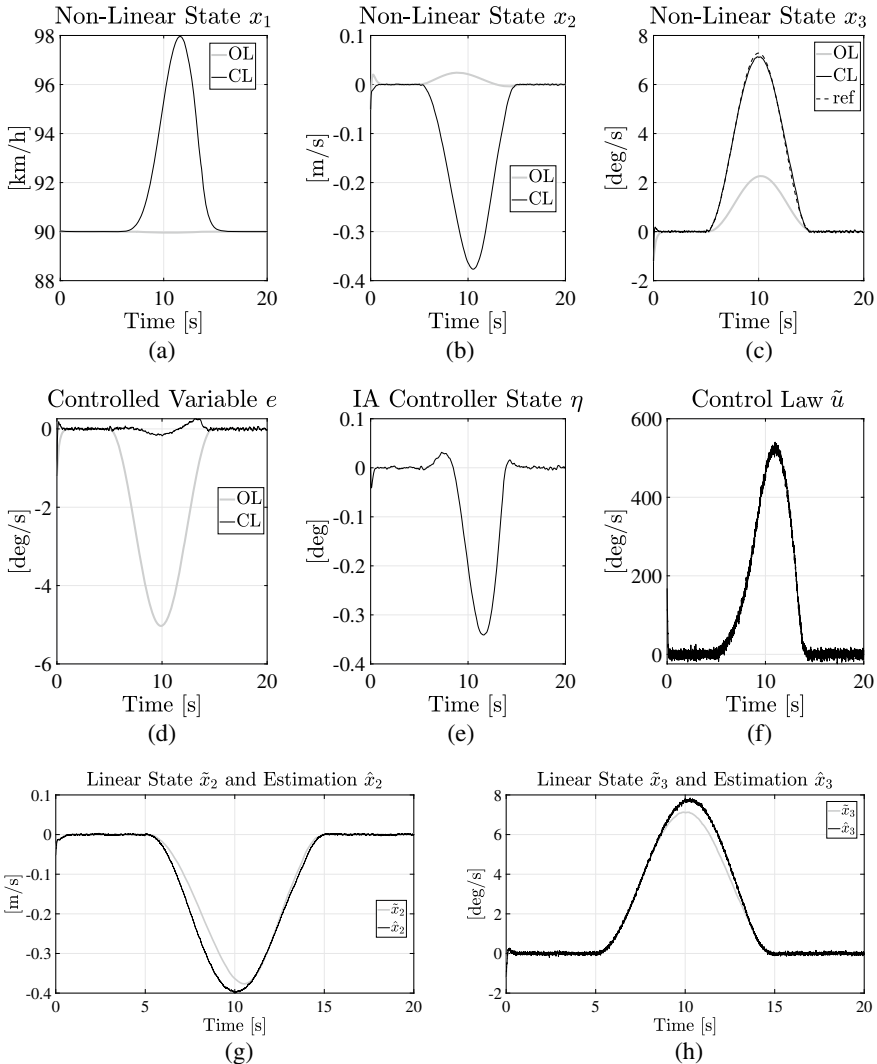


Fig. 5.12 TV numerical test. The vehicle is initialized on a straight path at 90 km/h but with a non-trivial side-slip angle. After 5 s, the driver rotates the steering wheel. This is translated into a reference yaw rate (higher than negotiated in the open loop) which is tracked by the control system

through a positive differential speed of the rear wheels; see Fig. 5.12f. After the initial transient, the vehicle returns to the nominal straight path at a constant speed. Then, the steering wheel is rotated at $t = 5$ s, and a reference yaw rate is generated (see dashed line in Fig. 5.12c). The trajectory of the open-loop system, shown in gray in Fig. 5.12c, demonstrates that the negotiated yaw rate is lower than the desired one. Conversely, TV adds an extra torque that improves the reference yaw rate tracking

(see the continuous black line in Fig. 5.12c). It is worth stressing that, in this case, the tracking of the reference cannot be perfect due to the approximation introduced into the feed-forward law. Moreover, the turning style changes in the presence of TV. Indeed, as can be appreciated in Fig. 5.12b, in the open loop, the vehicle keeps the nose outward (positive lateral speed), whereas, in the closed loop, the nose remains inward (negative side speed). The control policy depicted in Fig. 5.12f relies on integral action and state estimation to achieve this result. In particular, the error of Fig. 5.12d generates the internal state η of Fig. 5.12e. Also, the stabilizer takes as input the state estimations shown in Fig. 5.12g and h. The estimation becomes poorer at high yaw rates due to the non-linearities that make the linearized model inaccurate.

The simulation results of Fig. 5.12 have been obtained with $\alpha = 3.5$, $x_{1\max} = 10^{-1/2}$ m/s, $x_{2\max} = 10^{-1/2}$ rad/s, $x_{3\max} = 1$ rad, and $R = 1$ rad/s. For the tuning of the observer, the same setup of ESP has been adopted.

Lane controls

This section presents the design of an LK control system. In more detail, as described in Sect. 2.6.1, LK aims to provide stable and robust tracking of the lane distance while nullifying the vehicle–lane relative heading. Section 4.7.6 proposed a control system composed of a stabilizer (fed by a state observer) and an integral action to achieve this goal. Let $\mathbf{K}_R \in \mathbb{R}^{2 \times 4}$ be the stabilizer matrix and $\hat{\mathbf{z}}_R$ be the estimated state (in the observability coordinates). Then,

$$\tilde{\mathbf{u}}_S := \mathbf{K}_R \hat{\mathbf{z}}_R$$

represents the stabilization control law. Let $\mathbf{K}_I \in \mathbb{R}^{2 \times 2}$ be the integral feedback matrix and denote with $\boldsymbol{\eta}$ the integral of $\tilde{\mathbf{e}}_L$. Then, the integral action is

$$\tilde{\mathbf{u}}_I := \mathbf{K}_I \boldsymbol{\eta}.$$

The matrices \mathbf{K}_R and \mathbf{K}_I are designed as follows. Define $\mathbf{x}_e = \text{col}(\mathbf{z}_R, \boldsymbol{\eta})$, let $\alpha \geq 0$, $\mathbf{Q} = \mathbf{Q}^\top \succeq 0$, and $\mathbf{R} = \mathbf{R} > 0$ be tunable parameters, and define the cost function

$$J = \int_0^{\infty} \mathbf{x}_e^\top \mathbf{Q} \mathbf{x}_e + \mathbf{u}^\top \mathbf{R} \mathbf{u} dt$$

subject to the constraint

$$\dot{\mathbf{x}}_e = (\mathbf{A}_e + 2\alpha \mathbf{I}) \mathbf{x}_e + \mathbf{B}_e \mathbf{u},$$

where \mathbf{A}_e and \mathbf{B}_e are those defined in Section 4.7.6. Then, in agreement with Sect. 5.1, there exists $\mathbf{K}_e \in \mathbb{R}^{2 \times 6}$ such that the control law $\mathbf{u} = \mathbf{K}_e \mathbf{x}_e$ minimizes J while making $\mathbf{A}_e + \mathbf{B}_e \mathbf{K}_e$ Hurwitz. The matrices \mathbf{K}_R and \mathbf{K}_I are found as subparts of \mathbf{K}_e by imposing $\mathbf{K}_e = [\mathbf{K}_R \ \mathbf{K}_I]$. As for the tuning of \mathbf{K}_e , any increase in α results in closed-loop eigenvalues with a more negative real part. As a consequence, any increase in α leads to stronger feedback. As described in Sect. 5.1.1, the matrix $\mathbf{R} := (2 \text{diag}(u_{1\max}^2, u_{2\max}^2))^{-1}$, with $u_{1\max}, u_{2\max} > 0$, can be used to balance the control action. If the differential wheel speed represents a control input more advisable than the steering wheel rotation, then $u_{1\max}$ could be chosen to be larger than $u_{2\max}$ and vice versa. As for the selection of \mathbf{Q} , Sect. 5.1.1 suggests letting

$x_{i_{\max}} > 0$, with $i = 1, \dots, 6$, be the maximum tolerable errors for the entries of \mathbf{x}_e and defining $\mathbf{Q}^{-1} = 6 \operatorname{diag}(x_{1_{\max}}^2, \dots, x_{6_{\max}}^2)$. In the context of LK, $x_{1_{\max}}$, $x_{2_{\max}}$, $x_{5_{\max}}$, and $x_{6_{\max}}$ impact the stability of the distance to the lane, the relative heading, and their integrals. Moreover, $x_{3_{\max}}$ and $x_{4_{\max}}$ influence the lateral speed and yaw rate stability. Since the plant represents a chain of integrals (lateral speed, yaw rate \rightarrow distance, relative heading \rightarrow distance and relative heading integrals), a possible design criterion is to pick $x_{5_{\max}} > x_{1_{\max}} > x_{3_{\max}}$ and $x_{6_{\max}} > x_{2_{\max}} > x_{4_{\max}}$. This choice introduces a stabilizing damping action because, in the cost function, the derivative of each quantity is more penalized than the quantity itself. In practice, the controller minimizes the derivative of the quantities, as a priority. Once these are minimized, the quantities are also steered to zero (at low speed). Moreover, if it is more important to reduce the distance to the lane than to minimize the relative heading, taking $x_{5_{\max}} < x_{6_{\max}}$, $x_{1_{\max}} < x_{2_{\max}}$, and $x_{3_{\max}} < x_{4_{\max}}$ represents a valid option. On the other hand, $x_{5_{\max}} > x_{6_{\max}}$, $x_{1_{\max}} > x_{2_{\max}}$, and $x_{3_{\max}} > x_{4_{\max}}$ puts the priority on the reduction of the relative heading error.

As for the design of the observer, exploit the matrix \mathbf{B}_{L2} introduced in Sect. 2.6.1 and the transformation \mathbf{T}_R proposed in Sect. 4.7.6 to define $\bar{\mathbf{B}}_2$ as the last four rows of $\mathbf{T}_R \mathbf{B}_{L2}$. Let \mathbf{D}_2 be defined as in Sect. 2.6.1, $\bar{\mathbf{A}}$ and $\bar{\mathbf{C}}$ be the matrices delineated in Sect. 4.7.6, and follows what is described in Sect. 5.3. In more detail, let $\alpha_d \geq 0$, $\mathbf{Q}_d = \mathbf{Q}_d^\top \succeq 0$, and $\mathbf{R}_d = \mathbf{R}_d^\top \succeq 0$ be design parameters, and define the cost function

$$J_d = \int_{t_0}^{\infty} \boldsymbol{\mu}^\top \mathbf{Q}_d \boldsymbol{\mu} + \boldsymbol{v}^\top \mathbf{R}_d \boldsymbol{v} dt$$

subject to the constraint

$$\begin{aligned} \dot{\boldsymbol{\chi}} &= (\bar{\mathbf{A}}^\top + 2\alpha_d \mathbf{I}) \boldsymbol{\chi} + \bar{\mathbf{C}}^\top \boldsymbol{v} \\ \boldsymbol{\mu} &= \bar{\mathbf{B}}_2^\top \boldsymbol{\chi} + \mathbf{D}_2^\top \boldsymbol{v}. \end{aligned}$$

Then, in agreement with Sect. 5.1, $\mathbf{K}_O \in \mathbb{R}^{4 \times 3}$ exists such that $\bar{\mathbf{A}}^\top - \bar{\mathbf{C}}^\top \mathbf{K}_O^\top$ is Hurwitz and $\boldsymbol{v} = -\mathbf{K}_O^\top \boldsymbol{\chi}$ minimizes J_d . The observer proposed in Sect. 4.7.6 relies on \mathbf{K}_O , which is tuned as follows. In agreement with Sect. 5.3, the matrix \mathbf{Q}_{d22} represents the covariance matrix of the measurement noises $\boldsymbol{\nu}_L$. Also, $\mathbf{Q}_d := \text{blkdiag}(q_1, \mathbf{Q}_{d22}, 0)$ and q_1 denotes the covariance of the lane curvature. Finally, α_d is used to improve the observer performance (speed of convergence). Indeed, any increase in α_d results in closed-loop eigenvalues with a more negative real part.

Figure 5.13 shows the performance of the LK designed in this section. In this numerical experiment, the vehicle is governed to track a reference distance to the lane while minimizing the relative heading. At time $t = 0$, the reference distance is set to zero. The vehicle, traveling at 90 km/h, starts off in the lane with an initial heading error. The controller corrects this initial misalignment within the first ten seconds. At time $t = 10$, the reference lane distance is changed to 3 m and kept constant for the remainder of the test; see Fig. 5.13a. Moreover, a disturbance is introduced for $t \in [20, 32]$ s to simulate a turning. The lane curvature is linearly increased from 0 to 10^{-3} rad/m for $t \in [20, 21]$ s. Then, for $t \in (21, 31]$ s, the

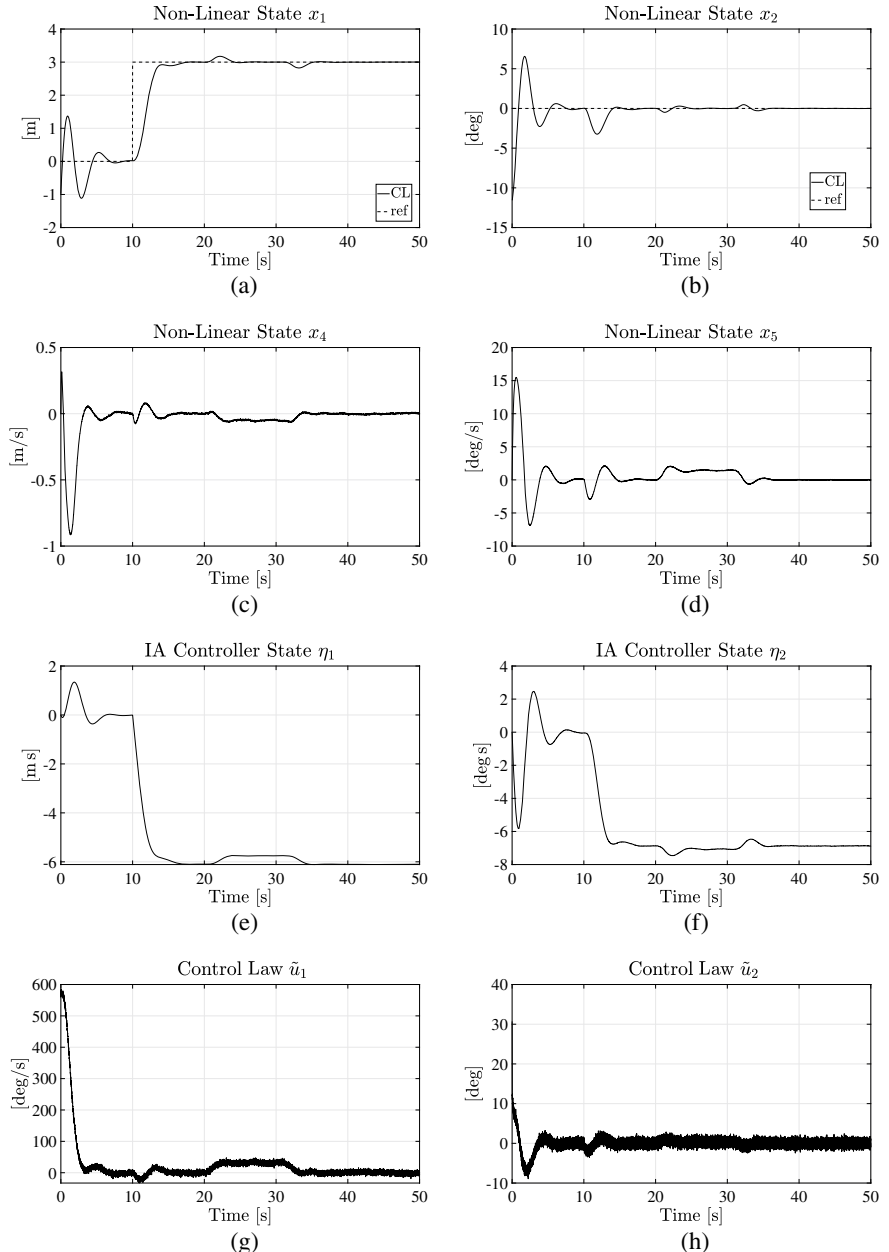


Fig. 5.13 Simulation of a vehicle equipped with an LK control system. The vehicle starts unaligned with the reference straight path. After the initial misalignment is corrected, at time $t = 10$ s, a change in the reference distance to the lane is commanded. Moreover, the lane curvature is progressively increased and decreased, for $t \in [20, 32]$ s, to simulate a turning

disturbance is kept constant, and, for $t \in [31, 32]$ s, linearly decreased back to 0. As shown in Fig. 5.13a and b, the tracking performance is satisfactory despite the exogenous disturbance. Figure 5.13c and d confirm that the states remain bounded. As for the controller states, Fig. 5.13e and f show that the integrals η_1 and η_2 , i.e., the first and second elements of $\boldsymbol{\eta}$, change to compensate for the variation of the reference lane distance. Moreover, for $t \in [20, 32]$ s, the integral η_1 varies to add an extra torque to cope with the lane curvature. Also, the integral η_2 varies in the presence of the disturbance. In this case, the steering wheel angle is modified to deal with the lateral accelerations requested to keep the vehicle at the right distance to the lane. The control law $\tilde{\mathbf{u}} := \text{col}(\tilde{u}_1, \tilde{u}_2)$ is shown in Fig. 5.13g and h. These diagrams highlight that the proposed control policy consists of a differential action on the rear wheel speed and a steering wheel law. On the one hand, the differential wheel speed mainly compensates for the relative heading errors. On the other hand, the steering wheel law aims at reducing the lane distance error.

The simulation results presented in Fig. 5.13 have been obtained with $\alpha = 0.25$, $x_{1\max} = 1$ m, $x_{2\max} = 1$ rad, $x_{3\max} = 100^{-1/2}$ m/s, $x_{4\max} = 100^{-1/2}$ rad/s, $x_{5\max} = 10$ m/s, $x_{6\max} = 10$ rad/s, $u_{1\max} = 10^{-3/2}$ rad/s, and $u_{2\max} = (\pi/180)^{1/2}$ rad/s. As for the observer, the parameters have been chosen as $\alpha_d = 25$ and $q_1 = 0.01$ (rad/m)². The sensor noises have been modeled with the following standard deviations: $\sigma_\rho = 0.01$ m, $\sigma_\psi = \pi/180$ rad, and $\sigma_\omega = \pi/180$ rad/s, thus leading to $\mathbf{Q}_{d22} = \text{diag}(\sigma_\rho^2, \sigma_\psi^2, \sigma_\omega^2)$. Finally, we set $\mathbf{R}_d = \mathbf{0}$.

Self-Park Assist

The SPA control system, whose architecture is delineated in Sect. 4.7.6, is designed in this section. The system comprises a stabilizer (with no need for a state observer) and a feed-forward law. As for the design of the stabilizer, use the matrices \mathbf{A} and \mathbf{B}_1 defined in Sect. 2.6.2, let $\mathbf{Q} = \mathbf{Q}^\top \succeq 0$ and $R > 0$ be tunable parameters, and introduce the cost function

$$J = \int_0^\infty \mathbf{x}^\top \mathbf{Q} \mathbf{x} + R u^2 dt$$

to which is associated the constraint

$$\dot{\mathbf{x}} = \mathbf{Ax} + \mathbf{B}_1 u.$$

As detailed in Sect. 5.1, $\mathbf{K}_S \in \mathbb{R}^{1 \times 2}$ exists such that $\mathbf{A} + \mathbf{B}_1 \mathbf{K}_S$ is Hurwitz and $u = \mathbf{K}_S \mathbf{x}$ minimizes J . Moreover, since the state is available at the output, the stabilizer is implemented as $u_S = \mathbf{K}_S \tilde{\mathbf{y}}$.

The matrix \mathbf{K}_S is tuned via the design of \mathbf{Q} and R . On the one hand, increasing R makes the control action less aggressive, while, on the other hand, \mathbf{Q} can be used to stabilize the closed-loop plant and to balance the minimization of the distance between the lane and the relative heading. In agreement with Sect. 5.1.1, let $x_{1\max}, x_{2\max} > 0$ be the maximum tolerable values for the elements of \mathbf{x} . Then, $x_{1\max} > x_{2\max}$ puts the priority on the minimization of the lane distance whereas, conversely, $x_{2\max} > x_{1\max}$ makes the controller more reactive to the relative heading errors.

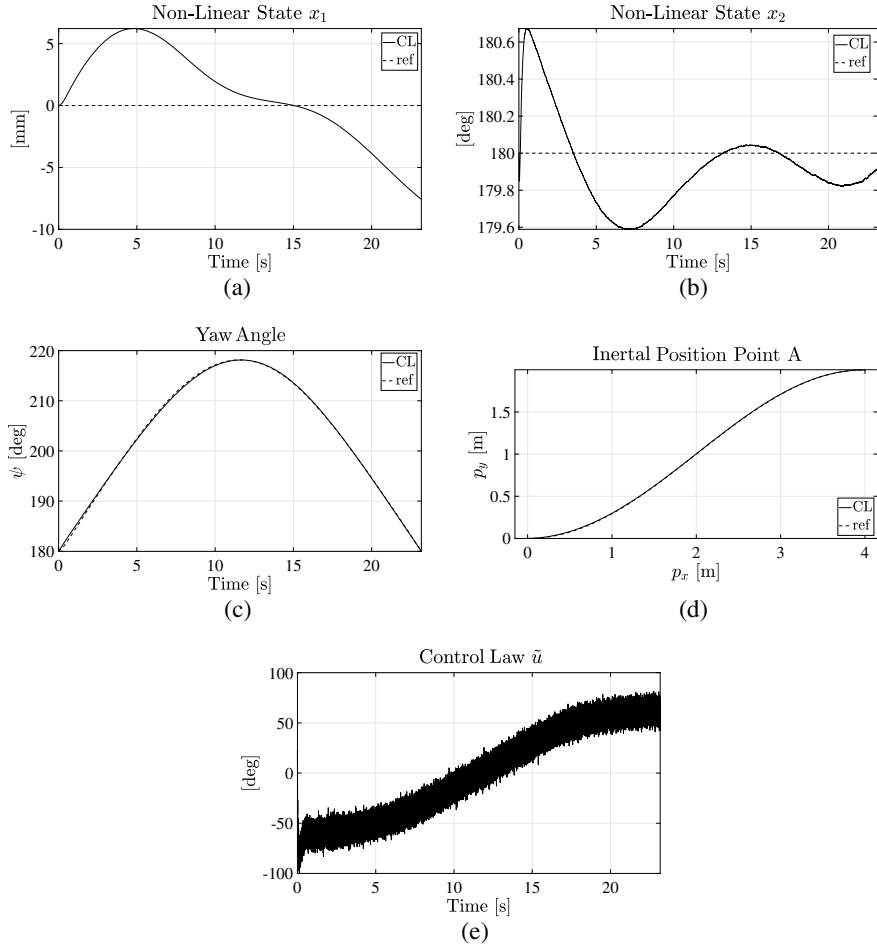


Fig. 5.14 Self-Park Assist numerical test. The vehicle traces a known reference provided by a path planner. The vehicle speed is assumed to be constant throughout the maneuver

Figure 5.14 graphically describes the performance of the SPA designed in this section. The vehicle is involved in a reverse parking maneuver, with the parking bay parallel to the road; see Fig. 5.14d. The simulation starts with the car aligned with the road. Then, assuming $v_0 = -1$ km/h and constant throughout the experiment, the path planner generates the curvature for the virtual reference lane; see Fig. 5.14b. The goal is to keep point A, located 1 cm behind the rear axle, as close as possible to the virtual lane. To accomplish this mission, in the first part of the simulation, the control system tilts the front wheels toward the right (negative toe) and gradually adjusts the wheel toe angle to reach positive values (see Fig. 5.14e). The maneuver is completed in less than 25 s, and the simulation is stopped when point A reaches the end of the parking bay. The overall performance is satisfactory and the tracking

errors are less than 1 cm (as for the lane distance) and 1 degree (as for the relative heading); see Fig. 5.14a and b.

The results shown in Fig. 5.14 have been obtained with these settings: $x_{1\max} = 0.01$ m, $x_{2\max} = \pi/180$ rad, and $R = \pi/4$ rad.

5.5 Summary

Control systems based on the linearization described in Chap. 1 rely on some key matrices, namely \mathbf{K}_S , \mathbf{K}_I , and \mathbf{K}_O . While Chap. 4 provides the existence conditions for these matrices, this chapter has introduced a design tool. In particular, the so-called *optimal control* technique has been exploited, also through the concept of *duality*, for designing \mathbf{K}_S , \mathbf{K}_I , and \mathbf{K}_O . In practice, the control matrices are those that make the closed-loop systems BIBS-stable while minimizing user-defined cost functions. These cost functions represent a compromise between the performance and the control effort (when used for the design of \mathbf{K}_S and \mathbf{K}_I). Also, the compromise between the accuracy of sensors and the design model is embedded in the cost functions used to design \mathbf{K}_O . The control systems developed in this chapter have been numerically tested in realistic simulation scenarios and have shown good performance.

5.6 Exercises

Exercise 5.1 Let

$$\begin{bmatrix} \dot{x}_1 \\ \dot{x}_2 \end{bmatrix} = \begin{bmatrix} 0 & 1 \\ 0 & 0 \end{bmatrix} \begin{bmatrix} x_1 \\ x_2 \end{bmatrix} + \begin{bmatrix} 0 \\ 1 \end{bmatrix} u$$

$$\varepsilon = [1 \ 0] \begin{bmatrix} x_1 \\ x_2 \end{bmatrix}$$

be an LTI system associated with the cost function $J = \int_0^\infty \varepsilon^2 + u^2 dt$. Design a state-feedback control, namely $u = \mathbf{K}_S \mathbf{x}$, through the optimal control strategy policy.

Exercise 5.2 Let

$$\begin{bmatrix} \dot{x}_1 \\ \dot{x}_2 \end{bmatrix} = \begin{bmatrix} 0 & 0 \\ 0 & -1 \end{bmatrix} \begin{bmatrix} x_1 \\ x_2 \end{bmatrix} + \begin{bmatrix} 1 \\ 0 \end{bmatrix} u$$

$$\varepsilon = [1 \ 0] \begin{bmatrix} x_1 \\ x_2 \end{bmatrix}$$

be an LTI system which is associated with the cost function $J = \int_0^\infty \varepsilon^2 + u^2 dt$. Design an optimal state-feedback control $u = \mathbf{K}_S \mathbf{x}$.

Exercise 5.3 Let

$$\begin{bmatrix} \dot{x}_1 \\ \dot{x}_2 \end{bmatrix} = \begin{bmatrix} 0 & 1 \\ -1 & 0 \end{bmatrix} \begin{bmatrix} x_1 \\ x_2 \end{bmatrix} + \begin{bmatrix} 0 \\ 1 \end{bmatrix} u$$

$$\varepsilon = \begin{bmatrix} 1 & 0 \end{bmatrix} \begin{bmatrix} x_1 \\ x_2 \end{bmatrix}$$

be an LTI system which is associated with the cost function $J = \int_0^\infty \varepsilon^2 + u^2 dt$. Design an optimal state-feedback control $u = \mathbf{K}_S \mathbf{x}$.

Exercise 5.4 Let

$$\begin{bmatrix} \dot{x}_1 \\ \dot{x}_2 \end{bmatrix} = \begin{bmatrix} -1 & 1 \\ 0 & 0 \end{bmatrix} \begin{bmatrix} x_1 \\ x_2 \end{bmatrix} + \begin{bmatrix} 0 \\ 1 \end{bmatrix} u$$

$$\varepsilon = \begin{bmatrix} 0 & 1 \end{bmatrix} \begin{bmatrix} x_1 \\ x_2 \end{bmatrix}$$

be an LTI system which is associated with the cost function $J = \int_0^\infty \varepsilon^2 + u^2 dt$. Design an optimal state-feedback control $u = \mathbf{K}_S \mathbf{x}$.

Exercise 5.5 Let

$$\begin{bmatrix} \dot{x}_1 \\ \dot{x}_2 \end{bmatrix} = \begin{bmatrix} 0 & 1 \\ 0 & -1 \end{bmatrix} \begin{bmatrix} x_1 \\ x_2 \end{bmatrix} + \begin{bmatrix} 1 \\ 0 \end{bmatrix} u$$

$$\varepsilon = \begin{bmatrix} 1 & 0 \end{bmatrix} \begin{bmatrix} x_1 \\ x_2 \end{bmatrix}$$

be an LTI system which is associated with the cost function $J = \int_0^\infty \varepsilon^2 + u^2 dt$. Design an optimal state-feedback control $u = \mathbf{K}_S \mathbf{x}$.

References

1. Antsaklis P, Michel AN (2007) A linear systems primer. Birkhäuser Basel
2. Berkovitz L (1974) Optimal control theory. Springer, New York
3. Bryson AE (1975) Applied optimal control: optimization, estimation and control. Taylor & Francis
4. Harvey C, Stein G (1978) Quadratic weights for asymptotic regulator properties. IEEE Trans Automat Control 23(3):378–387
5. Hiroe T, Morimoto T, Inoue S, Takamatsu H (1993) A new method for selecting weighting matrices of lq regulators and its application to an industrial turbine. In: Proceedings of 32nd IEEE conference on decision and control, vol 4, pp 3333–3334
6. Kailath T, Sayed AH, Hassibi B (2000) Linear estimation. Prentice Hall
7. Kalman R (1960) Three decades of driver assistance systems: review and future perspectives. J Basic Eng 82(1):35–45
8. Kalman RE (1964) When is a linear control system optimal? J Basic Eng 86(1):51–60

9. Kisačanin B, Agarwal GC (2001) Linear control systems: with solved problems and MATLAB examples. Springer, US
10. Kučera V (1973) A review of the matrix Riccati equation. *Kybernetika* 9(1):42–61
11. Kumar EV, Jerome J, Srikanth K (2014) Algebraic approach for selecting the weighting matrices of linear quadratic regulator. In: 2014 international conference on green computing communication and electrical engineering (ICGCCEE), pp 1–6
12. Locatelli A (2001) Optimal control. Birkhäuser Basel
13. Macki J, Strauss A (1982) Introduction to optimal control theory. Springer, New York
14. Stein G (1978) Generalized quadratic weights for asymptotic regulator properties. In: 1978 IEEE conference on decision and control including the 17th symposium on adaptive processes, pp 831–837



This book presents control systems founded on two main pillars: linearization (as for the control architecture) and optimization (as for the controller design). As detailed in Sects. 1.3.4 and 4.5.3, the control systems based on linearization can guarantee the stability of the closed loop only locally. This design choice implies that the system is constrained to operate in a small neighborhood of the linearization conditions. These limitations can be overcome with the adoption of nonlinear control algorithms. This chapter provides an overview of some nonlinear control techniques that could be conceived as improvements of the control via linearization or can be obtained through a generalization of the optimal control.

The control theory area is so wide that it is impossible to cover all the possible topics, even with rapid overviews. So, this section focuses only on the family of model-based control systems (to which also belongs control via linearization). In particular, some of the nonlinear control policies closest to the control via linearization are *gain scheduling*, *adaptive controls*, and *model predictive control*. Despite not being much adopted in the automotive field, special mention is given to *feedback linearization* because of its similarities with the control policy adopted in this book. As for the observer, the famous *Extended Kalman Filter* represents one of the most adopted nonlinear estimation schemes.

6.1 Gain Scheduling

This book presents the design of a control system for a single equilibrium point. The main idea behind gain scheduling is that a nonlinear controller can be obtained by suitable interpolation of local linear controllers, each of which is designed on

a different equilibrium point. As an example, Chap. 2 highlights the dependency, of most linearized plants, on the vehicle speed, namely v . Conceptually, a set of controllers can be designed for a given set of vehicle speeds $v_1, \dots, v_n, n \in \mathbb{N}$. Then, under some assumptions, the matrices $\mathbf{K}_S(v)$, $\mathbf{K}_I(v)$, and $\mathbf{K}_O(v)$ of the nonlinear controller are obtained via an interpolation of \mathbf{K}_S^k , \mathbf{K}_I^k , and \mathbf{K}_O^k designed at $v = v_k$, $k = 1, \dots, n$.

In more detail, inspired by the model presented in Sect. 1.2, let the plant be described by

$$\dot{\mathbf{x}} = \mathbf{f}(\mathbf{x}, \mathbf{u}, \mathbf{w})$$

$$\mathbf{y} = \mathbf{h}(\mathbf{x}, \mathbf{w})$$

in which, without loss of generality, the regulated output and the dependency of \mathbf{y} on \mathbf{u} have been omitted to make lighter the following arguments. Assume there exist a set \mathcal{P} and functions $\mathbf{x}_e(\cdot)$, $\mathbf{u}_e(\cdot)$, $\mathbf{w}_e(\cdot)$, and $\mathbf{y}_e(\cdot)$ such that for all $\mathbf{p} \in \mathcal{P}$

$$\mathbf{0} = \mathbf{f}(\mathbf{x}_e(\mathbf{p}), \mathbf{u}_e(\mathbf{p}), \mathbf{w}_e(\mathbf{p}))$$

$$\mathbf{y}_e(\mathbf{p}) = \mathbf{h}(\mathbf{x}_e(\mathbf{p}), \mathbf{w}_e(\mathbf{p})).$$

In words, \mathbf{p} represents a vector that parametrizes the equilibrium tuple. Let $n \in \mathbb{N}$ be the number of design setpoints, parametrized by \mathbf{p}_k , with $k = 1, \dots, n$, and linearize the plant by defining

$$\begin{aligned}\mathbf{A}^k &= \left. \frac{\partial \mathbf{f}(\mathbf{x}, \mathbf{u}_e(\mathbf{p}_k), \mathbf{w}_e(\mathbf{p}_k))}{\partial \mathbf{x}} \right|_{\mathbf{x}=\mathbf{x}_e(\mathbf{p}_k)} \\ \mathbf{B}_1^k &= \left. \frac{\partial \mathbf{f}(\mathbf{x}_e(\mathbf{p}_k), \mathbf{u}, \mathbf{w}_e(\mathbf{p}_k))}{\partial \mathbf{u}} \right|_{\mathbf{u}=\mathbf{u}_e(\mathbf{p}_k)} \\ \mathbf{B}_2^k &= \left. \frac{\partial \mathbf{f}(\mathbf{x}_e(\mathbf{p}_k), \mathbf{u}_e(\mathbf{p}_k), \mathbf{w})}{\partial \mathbf{w}} \right|_{\mathbf{w}=\mathbf{w}_e(\mathbf{p}_k)} \\ \mathbf{C}^k &= \left. \frac{\partial \mathbf{f}(\mathbf{x}, \mathbf{u}_e(\mathbf{p}_k), \mathbf{w}_e(\mathbf{p}_k))}{\partial \mathbf{x}} \right|_{\mathbf{x}=\mathbf{x}_e(\mathbf{p}_k)} \\ \mathbf{D}_2^k &= \left. \frac{\partial \mathbf{f}(\mathbf{x}_e(\mathbf{p}_k), \mathbf{u}_e(\mathbf{p}_k), \mathbf{w})}{\partial \mathbf{w}} \right|_{\mathbf{w}=\mathbf{w}_e(\mathbf{p}_k)}.\end{aligned}$$

Use these matrices and define $\tilde{\mathbf{y}}^k = \mathbf{y} - \mathbf{y}_e(\mathbf{p}_k)$ to design the controllers

$$\dot{\mathbf{x}}_O = \mathbf{F}^k \mathbf{x}_O + \mathbf{G}^k \tilde{\mathbf{y}}^k$$

$$\mathbf{u}_S = \mathbf{K}^k \mathbf{x}_O + \mathbf{H}^k \tilde{\mathbf{y}}^k,$$

such that, for all $k = 1, \dots, n$, \mathbf{F}^k and $\mathbf{A}^k + \mathbf{B}_1^k (\mathbf{K}^k + \mathbf{H}^k \mathbf{C}^k)$ are Hurwitz.

Remark 6.1 A direct comparison of this controller with Eq. (1.17a) leads to $\mathbf{F}^k = \mathbf{A}_O^k + \mathbf{B}_O^k \mathbf{K}_S^k \mathbf{C}_O^k$, $\mathbf{G}^k = \mathbf{B}_O^k \mathbf{K}_S^k \mathbf{D}_O^k + \mathbf{K}_O^k$, $\mathbf{K}^k = \mathbf{K}_S^k \mathbf{C}_O^k$, and $\mathbf{H}^k = \mathbf{K}_S^k \mathbf{D}_O^k$.

Assume that the dimensions of \mathbf{F}^k , \mathbf{G}^k , \mathbf{K}^k , and \mathbf{H}^k are uniform on k , and define interpolation policies $F(\cdot)$, $G(\cdot)$, $K(\cdot)$, and $H(\cdot)$ such that $F(\mathbf{p}_k) = \mathbf{F}^k$, $G(\mathbf{p}_k) = \mathbf{G}^k$, $K(\mathbf{p}_k) = \mathbf{K}^k$, and $H(\mathbf{p}_k) = \mathbf{H}^k$, for all $k = 1, \dots, n$.

Now, let $\mathbf{g}(\cdot)$ be such that $\mathbf{p} = \mathbf{g}(\mathbf{y})$, i.e., assume that \mathbf{p} is measurable. It is worth highlighting that \mathbf{p} can represent both the measurement of state variables or exogenous signals (e.g., disturbances and references). Then, define

$$\mathbf{f}_c(\mathbf{x}_O, \mathbf{y}) = F(\mathbf{g}(\mathbf{y}))\mathbf{x}_O + G(\mathbf{g}(\mathbf{y}))[\mathbf{y} - \mathbf{y}_e(\mathbf{g}(\mathbf{y}))]$$

$$\mathbf{h}_c(\mathbf{x}_O, \mathbf{y}) = K(\mathbf{g}(\mathbf{y}))\mathbf{x}_O + H(\mathbf{g}(\mathbf{y}))[\mathbf{y} - \mathbf{y}_e(\mathbf{g}(\mathbf{y}))]$$

and compute the so-called *gain-scheduled* controller

$$\dot{\mathbf{x}}_O = \mathbf{f}_c(\mathbf{x}_O, \mathbf{y})$$

$$\mathbf{u} = \mathbf{h}_c(\mathbf{x}_O, \mathbf{y}),$$

which is, de facto, nonlinear. The main advantage of the gain scheduling technique is associated with the linear nature of the control design tools. Conversely, proving that the gain-scheduled controller guarantees non-local stability can be hard. For further readings on this topic, see [149].

The gain scheduling technique has been widely adopted to solve ADAS control problems. For example, the active suspension system was investigated in [4, 50, 80, 81, 119, 158, 170, 198], electro-mechanical brakes were the focus of [106, 148], the wheel sleep control was of main interest in [77, 109, 133, 134], the improvement of vehicle lateral motion control and stability were studied in [16, 28, 36, 70, 78, 177, 192, 193], the adaptive cruise control problem was solved in [6, 65, 153], braking system performance was investigated in [191], lane controls were proposed in [10, 34, 139], the solution of the trajectory-tracking/path-following problem represented the main goal in [33, 112, 168, 176, 195], a vehicle speed servo control was conceived in [166], the management of the engine EGR valve is developed in [138], and steering control in the presence of human actions is investigated in [15, 184].

6.2 Indirect and Direct Adaptive Control

Indirect Adaptive Control (IAC) can be thought of as an extension of Gain Scheduling (GS). Indeed, consider a GS controller but assume that the scheduling parameter is not available at measurement. A solution to this issue is to implement a further (possibly) dynamic model that estimates the scheduling parameter. In particular, let

$$\dot{\mathbf{x}} = \mathbf{f}(\mathbf{x}, \mathbf{u}, \mathbf{w}, \mathbf{p})$$

$$\mathbf{y} = \mathbf{x}$$

be the plant in which, for the sake of simplicity, the state is assumed to be fully measurable. This plant is characterized by the presence of slow time-varying parameters $\mathbf{p} \in \mathcal{P}$, where \mathcal{P} represents a finite set. Let $(\mathbf{x}_0, \mathbf{u}_0, \mathbf{0}, \mathbf{p}_0)$ be a tuple of equilibrium in which \mathbf{p}_0 represents the nominal plant parameters. Introduce $\tilde{\mathbf{x}} = \mathbf{x} - \mathbf{x}_0$, $\tilde{\mathbf{u}} = \mathbf{u} - \mathbf{u}_0$, and

$$\mathbf{A}(\mathbf{p}_0) = \left. \frac{\partial \mathbf{f}(\mathbf{x}, \mathbf{u}_0, \mathbf{0}, \mathbf{p}_0)}{\partial \mathbf{x}} \right|_{\mathbf{x}=\mathbf{x}_0}$$

$$\mathbf{B}_1(\mathbf{p}_0) = \left. \frac{\partial \mathbf{f}(\mathbf{x}_0, \mathbf{u}, \mathbf{0}, \mathbf{p}_0)}{\partial \mathbf{u}} \right|_{\mathbf{u}=\mathbf{u}_0}.$$

Moreover, define the linearized plant as

$$\dot{\tilde{\mathbf{x}}} = \mathbf{A}(\mathbf{p}_0)\tilde{\mathbf{x}} + \mathbf{B}_1(\mathbf{p}_0)\tilde{\mathbf{u}}.$$

To design a robust controller, i.e., a controller able to stabilize the linearized plant for any $\mathbf{p} \in \mathcal{P}$, the design point could be identified by choosing the worst $\mathbf{p}_0 \in \mathcal{U}$ such that the real part of the eigenvalues of \mathbf{A} is the most positive. Section 5.1 embedded this criterion into the term $\alpha \geq 0$, creating a more unstable design system than the actual one. The outcome of this design path is that the feedback gain $\mathbf{K}_S(\mathbf{p}_0)$ is usually unnecessarily large for most real working conditions. In this context, an IAC could alleviate the problem with an online estimate of the plant parameters that update the control law and increases the gain only when necessary. For example, the vehicle mass and inertia are slow time-varying parameters usually not measurable online. An IAC could estimate these inertial quantities and update the controller, which has been designed as a parametrized algorithm.

Let the parameter estimation scheme be modeled as the following LTI dynamic plant:

$$\begin{aligned}\dot{\mathbf{x}}_A &= \mathbf{A}_A \mathbf{x}_A + \mathbf{B}_{ACOL}(\tilde{\mathbf{u}}, \tilde{\mathbf{y}}) \\ \hat{\mathbf{p}} &= \mathbf{C}_A \mathbf{x}_A.\end{aligned}$$

Then, the IAC is obtained by forcing the feedback gain to be $\mathbf{K}_S(\hat{\mathbf{p}})$.

The IAC can be specialized to generate the so-called Direct Adaptive Control (DAC) scheme. The major difference from the IAC is that the DAC exploits the definition of a reference model to compute the parameter estimation. For this reason, the DAC is also known as the Model Reference Adaptive Control (MRAC). In particular, let

$$\begin{aligned}\dot{\mathbf{x}}_R &= \mathbf{A}_R \mathbf{x}_R + \mathbf{B}_R \tilde{\mathbf{r}} \\ \tilde{\mathbf{y}}_R &= \mathbf{C}_R \mathbf{x}_R\end{aligned}$$

be the reference model that, fed by the reference signal $\tilde{\mathbf{r}}$, generates the reference output $\tilde{\mathbf{y}}_R$. Then, the adaptation law is written as

$$\begin{aligned}\dot{\mathbf{x}}_A &= \mathbf{A}_A \mathbf{x}_A + \mathbf{B}_{ACOL}(\tilde{\mathbf{y}}, \tilde{\mathbf{y}} - \tilde{\mathbf{y}}_R) \\ \hat{\mathbf{p}} &= \mathbf{C}_A \mathbf{x}_A,\end{aligned}$$

and the controller gain is $\mathbf{K}(\hat{\mathbf{p}})$, which represents an estimate of $\mathbf{K}_S(\mathbf{p}_0)$.

The basic adaptive controllers described in this paragraph have been improved over the years, and today, a large variety of nonlinear adaptive schemes exists. Good introductions to adaptive controls are [71, 90, 91, 152].

Adaptive controls have found many applications in the automotive sector, see [161]. Indeed, the control of active suspensions was investigated in [8, 31, 63, 64, 79, 82, 88, 89, 199], the electro-mechanical (regenerative) braking problem was solved in [29, 56, 116, 117], while wheel speed control was the main topic of [1, 11, 40, 87, 95, 142, 172]. The ACC problem was investigated in [9, 17, 51, 118, 125, 141, 173]. Adaptive steering systems were proposed in [30, 55, 86, 156, 164, 186] and vehicle latero-directional stability was investigated in [2, 3, 35, 41, 49, 154, 162, 169]. Adaptive algorithms for lane keeping/changing were investigated in [19, 45, 68, 128, 155, 174]. To conclude, the management of vehicles performing overtaking maneuvers was the main focus of [135].

6.3 Model Predictive Control

Model Predictive Control (MPC) represents a way to solve a generalization of the optimal control problem introduced in Sect. 5.1. To highlight the link between the stationary Linear Quadratic (LQ) optimal control, described in this book, and MPC, let the plant be modeled as

$$\begin{aligned}\dot{\mathbf{x}} &= \mathbf{f}(\mathbf{x}, \mathbf{u}, \mathbf{w}) \quad \mathbf{u} \in \mathcal{U} \\ \mathbf{y} &= \mathbf{x}\end{aligned}$$

in which the state is assumed to be entirely measurable to reduce the complexity of the arguments. It is worth noting that control is constrained to belong to the set \mathcal{U} . Let p represent the control vector length. Then, when $\mathcal{U} \subset \mathbb{R}^p$, the control law is constrained within saturation thresholds.

Assume that $(\mathbf{x}_e, \mathbf{u}_e, \mathbf{w}_e)$ is an equilibrium tuple such that $\mathbf{0} = \mathbf{f}(\mathbf{x}_e, \mathbf{u}_e, \mathbf{w}_e)$, let $\tilde{\mathbf{x}} := \mathbf{x} - \mathbf{x}_e$, $\tilde{\mathbf{u}} := \mathbf{u} - \mathbf{u}_e$, and $\tilde{\mathbf{w}} := \mathbf{w} - \mathbf{w}_e$, and denote with $\Delta t > 0$ the optimization horizon. Then, the goal is to find $\tilde{\mathbf{u}} : [t, t + \Delta t] \rightarrow \mathbb{R}^p$ that minimizes

$$J = \tilde{\mathbf{x}}^\top(t + \Delta t) \mathbf{S} \tilde{\mathbf{x}}(t + \Delta t) + \int_t^{t + \Delta t} \tilde{\mathbf{x}}^\top \mathbf{Q} \tilde{\mathbf{x}} + \tilde{\mathbf{u}}^\top \mathbf{R} \tilde{\mathbf{u}} d\tau$$

with $\mathbf{S} = \mathbf{S}^\top \succ 0$, $\mathbf{Q} = \mathbf{Q}^\top \succ 0$, $\mathbf{R} = \mathbf{R}^\top \succ 0$, and subject to the constraints $\dot{\mathbf{x}} = \mathbf{f}(\mathbf{x}, \mathbf{u}, \mathbf{w})$ and $\tilde{\mathbf{u}}(\tau) + \mathbf{u}_e \in \mathcal{U}$, for all $\tau \in [t, t + \Delta t]$.

Assume that $\tilde{\mathbf{u}}^*(\tau)$ represents the solution to this problem for $\tau \in [t, t + \Delta t]$. Then, MPC uses only the initial value $\tilde{\mathbf{u}}^*(t)$ to control the plant and discards the rest of the control law. Indeed, to solve the optimization problem, the state evolution is computed by exploiting the model of the plant. Unfortunately, unknown disturbances may force the system out of the forecast trajectories. This deviation makes the optimization process unreliable in the long term. For this reason, at each time instant, the model is updated with the most recent information (provided by the sensor suite), and the control law $\tilde{\mathbf{u}}^*(\tau)$ is re-computed. This strategy, in the field of MPC, is usually called *receding horizon*.

The solution to this constrained-optimization problem is hard and often not available in closed form. Indeed, the closed-form solution proposed in Chap. 5 was obtained under the simplifying assumptions of $\Delta t = \infty$ and $\mathcal{U} = \mathbb{R}^p$. So, in the context of MPC, both the plant and the cost function are usually discretized in time, and the solution is found as a finite time sequence of vectors $\mathbf{u}^*(\tau)$, with $\tau = t_1, \dots, t_N$, $t_1 = t$, $t_N = t + \Delta t$, and $N \in \mathbb{N}$.

The literature about MPC is large, and many variants of the (very) basic problem described above exist. For further readings, see [26, 54].

MPC represents a widespread technique that has a large number of applications in automotive case studies; see [189]. As an example, the active suspension system was investigated in [27, 57, 120, 167, 185], the control of electro-mechanical brakes was the main focus of [93, 106], the regenerative braking problem was addressed in [113], the wheel speed control problem (ABS/TC) was solved in [24, 73, 137, 147, 165], ACC was studied in [38, 53, 94, 98, 105], the latero-directional control problem

was solved in [14, 18, 37, 62, 74, 75, 102, 107], the control of a steering system was investigated in [46–48, 92, 123], lane controls were of main interest in [12, 114, 188, 197], and the trajectory-following/path-tracking problems were solved in [59, 129, 140, 151, 179, 180].

6.4 Feedback Linearization

Chapter 4 has detailed the control system architecture as feedback and feed-forward laws composition. The adopted design philosophy is that the feed-forward control is designed after the feedback scheme. This design procedure can be inverted and utilized to design a nonlinear control system. In particular, let

$$\dot{\mathbf{x}} = \mathbf{f}(\mathbf{x}) + \mathbf{g}(\mathbf{x})u \quad \mathbf{x}(t_0) = \mathbf{x}_0$$

$$\mathbf{y} = \mathbf{x}$$

$$e = h_e(\mathbf{x}) - r,$$

where, to keep arguments simple, the system is assumed to be SISO and with the state completely measurable. Moreover, the plant is *input-affine* (i.e., linear with respect to the input) and completely known (no disturbances). As the last assumption, the functions $\mathbf{f}(\cdot)$ and $h_e(\cdot)$ are assumed to be sufficiently smooth (to compute all the partial derivatives shown later). Define

$$\begin{aligned} L_f^0 h_e(\mathbf{x}) &= h_e(\mathbf{x}) \\ L_f^k h_e(\mathbf{x}) &= \frac{\partial L_f^{k-1} h_e(\mathbf{x})}{\partial \mathbf{x}} \mathbf{f}(\mathbf{x}) \quad k \geq 1 \end{aligned}$$

and

$$L_g L_f^k h_e(\mathbf{x}) = \frac{\partial L_f^k h_e(\mathbf{x})}{\partial \mathbf{x}} \mathbf{g}(\mathbf{x}) \quad k \geq 0.$$

Similar to what was presented in Sect. 4.6, let $n \in \mathbb{N}$ be the dimension of \mathbf{x} and compute $r_{\max} \leq n$ as the integer such that, for any $\mathbf{x} \in \mathbb{R}^n$, it is $L_g L_f^k h_e(\mathbf{x}) = 0$, $k = 0, \dots, r_{\max} - 2$, and $L_g L_f^{r_{\max}-1} h_e(\mathbf{x}) \neq 0$. As a consequence,

$$\begin{aligned} \frac{d}{dt} e &= L_f h_e(\mathbf{x}) - \frac{dr}{dt} \\ \frac{d^k}{dt^k} e &= L_f^2 h_e(\mathbf{x}) - \frac{d^k r}{dt^k} \quad k = 2, \dots, r_{\max} - 1 \\ \frac{d^{r_{\max}}}{dt^{r_{\max}}} e &= L_f^{r_{\max}} h_e(\mathbf{x}) + L_g L_f^{r_{\max}-1} h_e(\mathbf{x}) u - \frac{d^{r_{\max}} r}{dt^{r_{\max}}}. \end{aligned}$$

Define $\Phi : \mathbb{R}^n \rightarrow \mathbb{R}^{n-r_{\max}}$ such that $(\partial \Phi(\mathbf{x}) / \partial \mathbf{x}) \mathbf{g}(\mathbf{x}) = \mathbf{0}$ and let

$$\zeta := \begin{bmatrix} \zeta_\perp \\ \zeta \end{bmatrix} := \mathbf{T}(\mathbf{x}, r) := \begin{bmatrix} \Phi(\mathbf{x}) \\ h_e(\mathbf{x}) - r \\ \vdots \\ L_f^{r_{\max}-1} h_e(\mathbf{x}) - \frac{d^{r_{\max}-1} r}{dt^{r_{\max}-1}} \end{bmatrix}.$$

Moreover, introduce

$$\mathbf{f}_0(\boldsymbol{\zeta}_{\perp}, \boldsymbol{\zeta}) = \frac{\partial \Phi(\mathbf{x})}{\partial \mathbf{x}} \Big|_{\mathbf{x}=\mathbf{T}^{-1}(\boldsymbol{\zeta}, r)}.$$

Then, the dynamics of $\boldsymbol{\zeta}_{\perp}$ and $\boldsymbol{\zeta}$ are

$$\begin{aligned}\dot{\boldsymbol{\zeta}}_{\perp} &= \mathbf{f}_0(\boldsymbol{\zeta}_{\perp}, \boldsymbol{\zeta}) \\ \dot{\boldsymbol{\zeta}} &= \mathbf{A}\boldsymbol{\zeta} + \mathbf{B} \left(L_f^{r_{\max}} h_e(\mathbf{x}) + L_g L_f^{r_{\max}-1} h_e(\mathbf{x}) u - \frac{d^{r_{\max}} r}{dt^{r_{\max}}} \right) \\ e &= \mathbf{C}\boldsymbol{\zeta}\end{aligned}$$

with

$$\begin{aligned}\mathbf{A} &= \begin{bmatrix} 0 & 1 & 0 & \dots & 0 & 0 \\ 0 & 0 & 1 & \dots & 0 & 0 \\ & & & \ddots & & \\ 0 & 0 & 0 & \dots & 1 & 0 \\ 0 & 0 & 0 & \dots & 0 & 1 \\ 0 & 0 & 0 & \dots & 0 & 0 \end{bmatrix} & \mathbf{B} &= \begin{bmatrix} 0 \\ 0 \\ \vdots \\ 0 \\ 0 \\ 1 \end{bmatrix} \\ \mathbf{C} &= [1 \ 0 \ 0 \ \dots \ 0 \ 0].\end{aligned}$$

The control law is computed assuming $\boldsymbol{\zeta}, \dot{\boldsymbol{\zeta}} = \mathbf{0}$ as

$$u = \frac{1}{L_g L_f^{r_{\max}-1} h_e(\mathbf{x})} \left(\frac{d^{r_{\max}} r}{dt^{r_{\max}}} - L_f^{r_{\max}} h_e(\mathbf{x}) \right) + v,$$

where $v \in \mathbb{R}$ is used later to stabilize the closed-loop plant. This latter reads as

$$\begin{aligned}\dot{\boldsymbol{\zeta}}_{\perp} &= \mathbf{f}_0(\boldsymbol{\zeta}_{\perp}, \boldsymbol{\zeta}) \\ \dot{\boldsymbol{\zeta}} &= \mathbf{A}\boldsymbol{\zeta} + \mathbf{B}v \\ e &= \mathbf{C}\boldsymbol{\zeta}.\end{aligned}$$

Since the couple (\mathbf{A}, \mathbf{B}) is reachable, $\mathbf{K} \in \mathbb{R}^{1 \times r_{\max}}$ exists such that $\mathbf{A} + \mathbf{B}\mathbf{K}$ is Hurwitz. The overall *feedback linearization* control law is thus given by

$$u(\mathbf{x}, r) = \frac{1}{L_g L_f^{r_{\max}-1} h_e(\mathbf{x})} \left(\frac{d^{r_{\max}} r}{dt^{r_{\max}}} - L_f^{r_{\max}} h_e(\mathbf{x}) \right) + [\mathbf{0} \ \mathbf{K}] \mathbf{T}(\mathbf{x}, r).$$

The robustness concerning model mismatches, exogenous disturbances, and the eventual local existence of the change of coordinates has been extensively investigated in the literature; see [72, 84, 159].

In the automotive field, the feedback linearization control policy was adopted in the following case studies: active suspension control was studied in [7, 20, 25, 131, 163, 183], the control of electro-mechanical brakes was investigated in [106, 111], wheel speed controls were proposed in [106, 130, 136, 144], ACC was studied in [115, 171],

a vehicle speed controller was conceived in [196], the control of a steering system was the main topic of [61, 127], the latero-directional controls of ground vehicles were investigated in [66, 100, 101, 175, 194], solutions to the trajectory-tracking/path-following problems were proposed in [5, 44, 76], and the autonomous parking problem was investigated in [110, 126, 150].

6.5 Extended Kalman Filter

The Extended Kalman Filter (EKF) represents an extension of the Luenberger observer proposed in Sect. 4.4. In more detail, let the plant be

$$\begin{aligned}\dot{\mathbf{x}} &= \mathbf{f}(\mathbf{x}, \mathbf{u}, \mathbf{w}) & \mathbf{x}(t_0) &= \mathbf{x}_0 \\ \mathbf{y} &= \mathbf{h}(\mathbf{x}, \mathbf{u}, \mathbf{w}),\end{aligned}$$

which is associated with the identity observer

$$\begin{aligned}\dot{\hat{\mathbf{x}}} &= \mathbf{f}(\hat{\mathbf{x}}, \mathbf{u}, \mathbf{w}_0) & \hat{\mathbf{x}}(t_0) &= \hat{\mathbf{x}}_0 \\ \hat{\mathbf{y}} &= \mathbf{h}(\hat{\mathbf{x}}, \mathbf{u}, \mathbf{w}_0)\end{aligned}$$

where \mathbf{w}_0 denotes the known part of \mathbf{w} . Define the errors $\tilde{\mathbf{x}} = \mathbf{x} - \hat{\mathbf{x}}$, $\tilde{\mathbf{y}} = \mathbf{y} - \hat{\mathbf{y}}$, and $\tilde{\mathbf{w}} = \mathbf{w} - \mathbf{w}_0$. Compute the dynamics

$$\begin{aligned}\dot{\tilde{\mathbf{x}}} &= \mathbf{f}(\mathbf{x}, \mathbf{u}, \mathbf{w}) - \mathbf{f}(\hat{\mathbf{x}}, \mathbf{u}, \mathbf{w}_0) & \tilde{\mathbf{x}}(t_0) &= \mathbf{x}_0 - \hat{\mathbf{x}}_0 \\ \tilde{\mathbf{y}} &= \mathbf{h}(\mathbf{x}, \mathbf{u}, \mathbf{w}) - \mathbf{h}(\hat{\mathbf{x}}, \mathbf{u}, \mathbf{w}_0)\end{aligned}$$

and linearize it as

$$\begin{aligned}\dot{\tilde{\mathbf{x}}} &\approx \mathbf{A}(\hat{\mathbf{x}}, \mathbf{u}, \mathbf{w}_0)\tilde{\mathbf{x}} + \mathbf{B}_2(\hat{\mathbf{x}}, \mathbf{u}, \mathbf{w}_0)\tilde{\mathbf{w}} & \tilde{\mathbf{x}}(t_0) &= \hat{\mathbf{x}}_0 - \mathbf{x}_0 \\ \tilde{\mathbf{y}} &\approx \mathbf{C}(\hat{\mathbf{x}}, \mathbf{u}, \mathbf{w}_0)\tilde{\mathbf{x}} + \mathbf{D}_2(\hat{\mathbf{x}}, \mathbf{u}, \mathbf{w}_0)\tilde{\mathbf{w}}.\end{aligned}$$

Now, the strategy is to compute a feedback matrix $\mathbf{K}_O(t)$ such that $\mathbf{A}(\hat{\mathbf{x}}, \mathbf{u}, \mathbf{w}_0) - \mathbf{K}_O(t)\mathbf{C}(\hat{\mathbf{x}}, \mathbf{u}, \mathbf{w}_0)$ is Hurwitz for any $t \geq t_0$ and any tuple $(\hat{\mathbf{x}}, \mathbf{u}, \mathbf{w}_0)$. With $\mathbf{K}_O(t)$ at hand, EKF is implemented as

$$\dot{\hat{\mathbf{x}}} = \mathbf{f}(\hat{\mathbf{x}}, \mathbf{u}, \mathbf{w}_0) + \mathbf{K}_O(t)(\mathbf{y} - \hat{\mathbf{y}}) \quad \hat{\mathbf{x}}(t_0) = \hat{\mathbf{x}}_0.$$

In the context of the deterministic and continuous-time systems, the matrix $\mathbf{K}_O(t)$ is computed as the output of a dynamic system called a Differential Riccati Equation (DRE) in which the matrices $\mathbf{B}_2(\hat{\mathbf{x}}, \mathbf{u}, \mathbf{w}_0)$ and $\mathbf{D}_2(\hat{\mathbf{x}}, \mathbf{u}, \mathbf{w}_0)$ are involved. This latter represents a generalization of the ARE presented in Sect. 5.3.

EKF has been extensively investigated, and the literature proposes many improvements to the basic version reported above. More details can be found in [157].

This observation scheme has been widely adopted in the automotive sector, see [42, 60]. In more detail, vehicle speeds were the main target of EKF proposed in [58, 67] while [13, 22, 32, 52, 97, 99, 122, 124, 187] focused on the side-slip estimation. The vehicle state and parameters were estimated via an EKF in [39, 69, 83, 96, 103],

[104, 108, 121, 132, 181, 190], and the tire forces were estimated in [21, 23, 85, 143, 145, 182]. The estimation focused on the road cohesion coefficient in [43, 160]. In [178] an EKF was used to implement a fault-tolerant scheme. The localization problem was solved in [146].

References

1. Acosta Lúa C, Di Gennaro S, Sánchez Morales ME (2017) Nonlinear adaptive controller applied to an antilock braking system with parameters variations. *Int J Control, Autom Syst* 15(5):2043–2052
2. Ahmadi J, Sedigh AK, Kabgani M (2009) Adaptive vehicle lateral-plane motion control using optimal tire friction forces with saturation limits consideration. *IEEE Trans Veh Technol* 58(8):4098–4107
3. Ahmadian N, Khosravi A, Sarhadi P (2020) Adaptive yaw stability control by coordination of active steering and braking with an optimized lower-level controller. *Int J Adapt Control Signal Process* 34(9):1242–1258
4. Ahmed M, Svaricek F (2013) Adaptive robust gain scheduled control of vehicle semi-active suspension for improved ride comfort and road handling. In: 2013 IEEE international conference on mechatronics (ICM), pp 376–381
5. Akhtar A, Nielsen C, Waslander SL (2015) Path following using dynamic transverse feedback linearization for car-like robots. *IEEE Trans Robot* 31(2):269–279
6. Alcalá E, Puig V, Quevedo J, Escobet T (2018) Gain-scheduling LPV control for autonomous vehicles including friction force estimation and compensation mechanism. *IET Control Theory Appl* 12(12):1683–1693
7. Alique JR, Haber RE, Alique A (2003). Feedback linearization using neural networks: Application to an electromechanical process. In: International work-conference on artificial neural networks. Springer, Berlin, pp 758–765
8. Alleyne A, Hedrick J (1995) Nonlinear adaptive control of active suspensions. *IEEE Trans Control Syst Technol* 3(1):94–101
9. Althoff M, Maierhofer S, Pek C (2021) Provably-correct and comfortable adaptive cruise control. *IEEE Trans Intell Veh* 6(1):159–174
10. Amadio A, Savaresi SM (2018) A dual-level lane departure avoidance system based on differential torque. In: 2018 21st international conference on intelligent transportation systems (ITSC), pp 105–110
11. ASME, editor (2018). Intelligent adaptive control for anti-lock braking system, Volume 4A: dynamics, vibration, and control of international mechanical engineering congress and exposition. V04AT06A006
12. Bae S, Isele D, Nakhaei A, Xu P, Añon AM, Choi C, Fujimura K, Moura S (2022) Lane-change in dense traffic with model predictive control and neural networks. *IEEE Trans Control Syst Technol*, pp 1–14
13. Baffet G, Charara A, Lechner D (2009) Estimation of vehicle sideslip, tire force and wheel cornering stiffness. *Control Eng Pract* 17(11):1255–1264
14. Barbarisi O, Palmieri G, Scala S, Glielmo L (2009) LTV-MPC for yaw rate control and side slip control with dynamically constrained differential braking. *Eur J Control* 15(3):468–479
15. Baslamisli SC, Polat I, Emre Kose I (2008) Gain scheduled integrated vehicle control based on a parametric yaw roll model. In: 2008 IEEE intelligent vehicles symposium, pp 666–671
16. Baur M, Bascetta L (2021) High speed driving with the affine in the force input model. In: 2021 European control conference (ECC), pp 423–428

17. Bayuwinda A, Ploeg J, Lefeber E, Nijmeijer H (2020) Combined longitudinal and lateral control of car-like vehicle platooning with extended look-ahead. *IEEE Trans Control Syst Technol* 28(3):790–803
18. Beal CE, Gerdes JC (2013) Model predictive control for vehicle stabilization at the limits of handling. *IEEE Trans Control Syst Technol* 21(4):1258–1269
19. Beiji L, Bestaoui Y (2005) Motion generation and adaptive control method of automated guided vehicles in road following. *IEEE Trans Intell Transp Syst* 6(1):113–123
20. Beltrán-Carbajal F, Chávez-Conde E, Favela-Contreras A, Chávez-Bracamontes R (2011) Active nonlinear vehicle suspension control based on real-time estimation of perturbation signals. In: 2011 IEEE international conference on industrial technology, pp 437–442
21. Best M, Gordon T, Dixon P (2000) An extended adaptive Kalman filter for real-time state estimation of vehicle handling dynamics. *Veh Syst Dyn* 34(1):57–75
22. Biase FD, Lenzo B, Timpone F (2020) Vehicle sideslip angle estimation for a heavy-duty vehicle via extended Kalman filter using a rational tyre model. *IEEE Access* 8:142120–142130
23. Bolzern P, Cheli F, Falciola G, Resta F (1999) Estimation of the non-linear suspension tyre cornering forces from experimental road test data. *Veh Syst Dyn* 31(1):23–34
24. Borrelli F, Bemporad A, Fodor M, Hrovat D (2006) An MPC/hybrid system approach to traction control. *IEEE Trans Control Syst Technol* 14(3):541–552
25. Buckner GD, Schuetze KT, Beno JH (2000) Intelligent feedback linearization for active vehicle suspension control. *J Dyn Syst, Meas, Control* 123(4):727–733
26. Camacho EF, Alba CB (2013) Model predictive control. Springer Science & Business Media
27. Canale M, Milanese M, Novara C (2006) Semi-active suspension control using “fast” model-predictive techniques. *IEEE Trans Control Syst Technol* 14(6):1034–1046
28. Cao W, Zhu Z, Nan J, Yang Q, Gu G, He H (2022) An improved motion control with cyber-physical uncertainty tolerance for distributed drive electric vehicle. *IEEE Access* 10:770–778
29. Cesario N, Taglialatela F, Lavorgna M (2007) Adaptive control strategies for electro-mechanical brakes. Technical report, SAE Technical Paper
30. Cetin AE, Adli MA, Erol Barkana D, Kucuk H (2010) Implementation and development of an adaptive steering-control system. *IEEE Trans Veh Technol* 59(1):75–83
31. Chantranuwathana S, Peng H (2004) Adaptive robust force control for vehicle active suspensions. *Int J Adapt Control Signal Process* 18(2):83–102
32. Chen B-C, Hsieh F-C (2008) Sideslip angle estimation using extended Kalman filter. *Veh Syst Dyn* 46(sup1):353–364
33. Chen Y, Hu C, Wang J (2020) Impaired driver assistance control with gain-scheduling composite nonlinear feedback for vehicle trajectory tracking. *J Dyn Syst, Meas, Control* 142(7):071003
34. Chen Y, Wang J (2018) Personalized vehicle path following based on robust gain-scheduling control in lane-changing and left-turning maneuvers. In: 2018 annual american control conference (ACC), pp 4784–4789
35. Choi S (2000) The design of a look-down feedback adaptive controller for the lateral control of front-wheel-steering autonomous highway vehicles. *IEEE Trans Veh Technol* 49(6):2257–2269
36. Chokor A, Doumiati M, Talj R, Charara A (2019) Design of a new gain-scheduled LPV/ h_{infty} controller for vehicle’s global chassis control. In: 2019 IEEE 58th conference on decision and control (CDC), pp 7602–7608
37. Chowdhri N, Ferranti L, Iribarren FS, Shyrokau B (2021) Integrated nonlinear model predictive control for automated driving. *Control Eng Pract* 106:104654
38. Coskun S, Huang C, Zhang F (2021) Quadratic programming-based cooperative adaptive cruise control under uncertainty via receding horizon strategy. *Trans Inst Meas Control* 43(13):2899–2911
39. Cuadrado J, Dopico D, Barreiro A, Delgado E (2009) Real-time state observers based on multibody models and the extended Kalman filter. *J Mech Sci Technol* 23(4):894–900

40. Dincmen E (2017) A gain-switched self-optimizer for braking controller. *Int J Adapt Control Signal Process* 31(6):953–968
41. Dixit S, Montanaro U, Dianati M, Mouzakitis A, Fallah S (2021) Integral MRAC with bounded switching gain for vehicle lateral tracking. *IEEE Trans Control Syst Technol* 29(5):1936–1951
42. Doumiati M, Charara A, Victorino A, Lechner D (2012) Vehicle dynamics estimation using Kalman filtering: experimental validation. Wiley, New York
43. Doumiati M, Victorino AC, Charara A, Lechner D (2011) Onboard real-time estimation of vehicle lateral tire-road forces and sideslip angle. *IEEE/ASME Trans Mechatron* 16(4):601–614
44. D’Souza RS, Louwers R, Nielsen C (2021) Piecewise linear path following for a unicycle using transverse feedback linearization. *IEEE Trans Control Syst Technol* 29(6):2575–2585
45. El Hajjami L, Mellouli EM, Berrada M (2021) Robust adaptive non-singular fast terminal sliding-mode lateral control for an uncertain ego vehicle at the lane-change maneuver subjected to abrupt change. *Int J Dyn Control* 9(4):1765–1782
46. Ercan Z, Carvalho A, Gokasan M, Borrelli F (2017) Modeling, identification, and predictive control of a driver steering assistance system. *IEEE Trans Hum-Mach Syst* 47(5):700–710
47. Falcone P, Borrelli F, Asgari J, Tseng HE, Hrovat D (2007) Predictive active steering control for autonomous vehicle systems. *IEEE Trans Control Syst Technol* 15(3):566–580
48. Falcone P, Borrelli F, Tseng HE, Asgari J, Hrovat D (2008) Linear time-varying model predictive control and its application to active steering systems: stability analysis and experimental validation. *Int J Robust Nonlinear Control* 18(8):862–875
49. Ferrara A, Incremona GP, Regolin E (2019) Optimization-based adaptive sliding mode control with application to vehicle dynamics control. *Int J Robust Nonlinear Control* 29(3):550–564
50. Fialho I, Balas G (2002) Road adaptive active suspension design using linear parameter-varying gain-scheduling. *IEEE Trans Control Syst Technol* 10(1):43–54
51. Flores C, Spring J, Nelson D, Iliev S, Lu X-Y (2022) Enabling cooperative adaptive cruise control on strings of vehicles with heterogeneous dynamics and powertrains. *Veh Syst Dyn* 1–22
52. Gadola M, Chindamo D, Romano M, Padula F (2014) Development and validation of a Kalman filter-based model for vehicle slip angle estimation. *Veh Syst Dyn* 52(1):68–84
53. Gao B, Cai K, Qu T, Hu Y, Chen H (2020) Personalized adaptive cruise control based on online driving style recognition technology and model predictive control. *IEEE Trans Veh Technol* 69(11):12482–12496
54. García CE, Prett DM, Morari M (1989) Model predictive control: theory and practice—a survey. *Automatica* 25(3):335–348
55. Gartley E, Bevly DM (2008) Online estimation of implement dynamics for adaptive steering control of farm tractors. *IEEE/ASME Trans Mechatron* 13(4):429–440
56. Geraee S, Mohammadbagherpoor H, Shafiei M, Valizadeh M, Montazeri F, Feyzi MR (2018) Regenerative braking of electric vehicle using a modified direct torque control and adaptive control theory. *Comput Electr Eng* 69:85–97
57. Gohrle C, Schindler A, Wagner A, Sawodny O (2014) Design and vehicle implementation of preview active suspension controllers. *IEEE Trans Control Syst Technol* 22(3):1135–1142
58. Guo H, Chen H, Xu F, Wang F, Lu G (2013) Implementation of EKF for vehicle velocities estimation on fpga. *IEEE Trans Ind Electron* 60(9):3823–3835
59. Guo H, Shen C, Zhang H, Chen H, Jia R (2018) Simultaneous trajectory planning and tracking using an MPC method for cyber-physical systems: A case study of obstacle avoidance for an intelligent vehicle. *IEEE Trans Ind Electron* 14(9):4273–4283
60. Guo H, Yin Z, Cao D, Chen H, Lv C (2019) A review of estimation for vehicle tire-road interactions toward automated driving. *IEEE Trans Syst, Man, Cybern: Syst* 49(1):14–30
61. Guo L, Liao Q, Wei S (2009) Nonlinear stabilization of bicycle robot steering control system. In: 2009 international conference on mechatronics and automation, pp 3185–3189

62. Gutjahr B, Gröll L, Werling M (2017) Lateral vehicle trajectory optimization using constrained linear time-varying MPC. *IEEE Trans Intell Transp Syst* 18(6):1586–1595
63. Hac A (1987) Adaptive control of vehicle suspension. *Veh Syst Dyn* 16(2):57–74
64. Hakvoort W, Boerrigter G, Beijen M (2020) Active vibration isolation by model reference adaptive control. *IFAC-PapersOnLine* 53(2):9144–9149. 21st IFAC World Congress
65. Hidayatullah MR, Juang J-C (2021) Adaptive cruise control with gain scheduling technique under varying vehicle mass. *IEEE Access* 9:144241–144256
66. Hingwe P, Tomizuka M (1998) A variable look-ahead controller for lateral guidance of four wheeled vehicles. In: Proceedings of the 1998 American control conference. ACC (IEEE Cat. No.98CH36207), vol 1, pp 31–35
67. Hodgson D, Mecrow BC, Gadoue SM, Slater HJ, Barrass PG, Giaouris D (2013) Effect of vehicle mass changes on the accuracy of Kalman filter estimation of electric vehicle speed. *IET Electr Syst Transp* 3(3):67–78
68. Hu C, Qin Y, Cao H, Song X, Jiang K, Rath JJ, Wei C (2019) Lane keeping of autonomous vehicles based on differential steering with adaptive multivariable super-twisting control. *Mech Syst Signal Process*, 125:330–346. Exploring nonlinear benefits in engineering
69. Huang X, Wang J (2014) Real-time estimation of center of gravity position for lightweight vehicles using combined AKF-EKF method. *IEEE Trans Veh Technol* 63(9):4221–4231
70. Huang X, Zhang H, Zhang G, Wang J (2014) Robust weighted gain-scheduling h_∞ vehicle lateral motion control with considerations of steering system backlash-type hysteresis. *IEEE Trans Control Syst Technol* 22(5):1740–1753
71. Ioannou PA, Sun J (2012) Robust adaptive control. Courier Corporation
72. Isidori A (2016) Lectures in feedback design for multivariable systems. Advanced Textbooks in Control and Signal Processing, Springer International Publishing
73. Jacquet A, Chamaillard Y, Basset M, Gissinger G, Frank D, Garcia J (2008) Anti-lock braking system using predictive control and on-line tire/road characteristics estimation. *IFAC Proc Vol* 41(2):2099–2104. 17th IFAC World Congress
74. Jalali M, Khajepour A, Chen S-K, Litkouhi B (2017) Handling delays in yaw rate control of electric vehicles using model predictive control with experimental verification. *J Dyn Syst, Meas, Control* 139(12):121001
75. Jalali M, Khosravani S, Khajepour A, Chen S, Litkouhi B (2017b) Model predictive control of vehicle stability using coordinated active steering and differential brakes. *Mechatronics* 48:30–41
76. Jean J-H, Wu T-P, Lian F-L (2006) A visual servo controller for lateral navigation of mobile vehicles in path tracking applications. In: 2006 IEEE international conference on systems, man and cybernetics, vol 6, pp 4475–4480
77. Johansen T, Petersen I, Kalkkuhl J, Ludemann J (2003) Gain-scheduled wheel slip control in automotive brake systems. *IEEE Trans Control Syst Technol* 11(6):799–811
78. Kang CM, Lee S-H, Chung CC (2018) Linear parameter varying design for lateral control using kinematics of vehicle motion. In: 2018 Annual American control conference (ACC), pp 3239–3244
79. Kararsiz G, Paksoy M, Metin M, Basturk HI (2021) An adaptive control approach for semi-active suspension systems under unknown road disturbance input using hardware-in-the-loop simulation. *Trans Inst Meas Control* 43(5):995–1008
80. Karimi A, Emedi Z (2013). h_∞ gain-scheduled controller design for rejection of time-varying disturbances with application to an active suspension system. In: 52nd IEEE conference on decision and control, pp 7540–7545
81. Karlsson N, Ricci M, Hrovat D, Dahleh M (2000) A suboptimal nonlinear active suspension. In: Proceedings of the 2000 American control conference. ACC (IEEE Cat. No.00CH36334), vol 6, pp 4036–4040
82. Karnopp D, Margolis D (1984) Adaptive suspension concepts for road vehicles. *Veh Syst Dyn* 13(3):145–160

83. Katriniok A, Abel D (2016) Adaptive EKF-based vehicle state estimation with online assessment of local observability. *IEEE Trans Control Syst Technol* 24(4):1368–1381
84. Khalil H (2002) Nonlinear systems. Prentice Hall, Pearson Education
85. Kim J (2009) Identification of lateral tyre force dynamics using an extended kalman filter from experimental road test data. *Control Eng Pract* 17(3):357–367
86. Kim K, Lee J, Kim M, Yi K (2020) Adaptive sliding mode control of rack position tracking system for steer-by-wire vehicles. *IEEE Access* 8:163483–163500
87. Kirchner WT, Southward SC (2013) Adaptive vehicle traction control: combined longitudinal and lateral motion. *Int J Dyn Control* 1(3):239–253
88. Koch G, Diepold KJ, Lohmann B (2009) Multi-objective road adaptive control of an active suspension system. In: Motion and vibration control. Springer, Berlin, pp 189–200
89. Koch G, Kloiber T (2014) Driving state adaptive control of an active vehicle suspension system. *IEEE Trans Control Syst Technol* 22(1):44–57
90. Krstic M, Kokotovic PV, Kanellakopoulos I (1995) Nonlinear and adaptive control design. Wiley, New York
91. Landau ID, Lozano R, M'Saad M, Karimi A (2011) Adaptive control: algorithms, analysis and applications. Springer Science & Business Media
92. Lazcano AMR, Niu T, Akutain XC, Cole D, Shyrokau B (2021) MPC-based haptic shared steering system: a driver modeling approach for symbiotic driving. *IEEE/ASME Trans Mechatron* 26(3):1201–1211
93. Lee CF, Chris Line CM (2008) Explicit nonlinear MPC of an automotive electromechanical brake. *IFAC Proc Vol* 41(2):10758–10763. 17th IFAC World Congress
94. Lee Y, Lee DY, Lee SH, Kim Y (2021) A comparative study on model predictive control design for highway car-following scenarios: space-domain and time-domain model. *IEEE Access* 9:162291–162305
95. Lennon W, Passino K (1999) Intelligent control for brake systems. *IEEE Trans Control Syst Technol* 7(2):188–202
96. Leung KT, Whidborne JF, Purdy D, Barber P (2011) Road vehicle state estimation using low-cost gps/ins. *Mech Syst Signal Process* 25(6):1988–2004. Interdisciplinary Aspects of Vehicle Dynamics
97. Li L, Jia G, Ran X, Song J, Wu K (2014) A variable structure extended Kalman filter for vehicle sideslip angle estimation on a low friction road. *Veh Syst Dyn* 52(2):280–308
98. Li SE, Jia Z, Li K, Cheng B (2015) Fast online computation of a model predictive controller and its application to fuel economy-oriented adaptive cruise control. *IEEE Trans Intell Transp Syst* 16(3):1199–1209
99. Li X, Chan C-Y, Wang Y (2016) A reliable fusion methodology for simultaneous estimation of vehicle sideslip and yaw angles. *IEEE Trans Veh Technol* 65(6):4440–4458
100. Liaw D-C, Chung W-C (2008) A feedback linearization design for the control of vehicle's lateral dynamics. *Nonlinear Dyn* 52(4):313–329
101. Liaw D-C, Chung W-C, Song C-C, Hsieh C-S (2006) A feedback linearization design for the control of vehicle's lateral dynamics. In: *2006 SICE-ICASE international joint conference*, pp 4937–4942
102. Lim H, Kim C, Jo A (2021) Model predictive control-based lateral control of autonomous large-size bus on road with large curvature. Technical report, SAE Technical Paper
103. Lin C, Cheng X, Zhang H, Gong X (2016) Estimation of center of gravity position for distributed driving electric vehicles based on combined h_∞ -EKF method. *Energy Procedia* 88:970–977. CUE 2015 - Applied Energy Symposium and Summit 2015: Low carbon cities and urban energy systems
104. Lin C, Gong X, Xiong R, Cheng X (2017) A novel h_∞ and EKF joint estimation method for determining the center of gravity position of electric vehicles. *Appl Energy* 194:609–616
105. Lin X, Görges D (2020) Robust model predictive control of linear systems with predictable disturbance with application to multiobjective adaptive cruise control. *IEEE Trans Control Syst Technol* 28(4):1460–1475

106. Line C, Manzie C, Good MC (2008) Electromechanical brake modeling and control: from PI to MPC. *IEEE Trans Control Syst Technol* 16(3):446–457
107. Liu H, Zhang L, Wang P, Chen H (2022) A real-time NMPC strategy for electric vehicle stability improvement combining torque vectoring with rear-wheel steering. *IEEE Trans Transp Electrification* 8(3):3825–3835
108. Liu W, He H, Sun F (2016) Vehicle state estimation based on minimum model error criterion combining with extended kalman filter. *J Frankl Inst* 353(4):834–856
109. Liu Y, Sun J (1995) Target slip tracking using gain-scheduling for antilock braking systems. In: Proceedings of 1995 American control conference—ACC'95, vol 2, pp 1178–1182
110. Luca AD, Oriolo G, Samson C (1998) Feedback control of a nonholonomic car-like robot. In: Robot motion planning and control, pp 171–253
111. Lupberger S, Degel W, Odenthal D, Bajcinca N (2022) Nonlinear control design for regenerative and hybrid antilock braking in electric vehicles. *IEEE Trans Control Syst Technol* 30(4):1375–1389
112. Manav AC, Lazoglu I, Aydemir E (2022) Adaptive path-following control for autonomous semi-trailer docking. *IEEE Trans Veh Technol* 71(1):69–85
113. Mariani V, Rizzo G, Tiano F, Glielmo L (2022) A model predictive control scheme for regenerative braking in vehicles with hybridized architectures via aftermarket kits. *Control Eng Pract* 123:105142
114. Marino R, Scalzi S, Netto M (2012) Integrated driver and active steering control for vision-based lane keeping. *Eur J Control* 18(5):473–484
115. Mayr R (1994) Intelligent cruise control for vehicles based on feedback linearization. In: Proceedings of 1994 American control conference—ACC '94, vol 1, pp 16–20
116. Mei P, Karimi HR, Yang S, Xu B, Huang C (2022) An adaptive fuzzy sliding-mode control for regenerative braking system of electric vehicles. *Int J Adapt Control Signal Process* 36(2):391–410
117. Mengling W, Shun P, Maolin C (2017) The MRAC based clamping force control of the electro-mechanical braking device. In: 2017 2nd IEEE international conference on intelligent transportation engineering (ICITE), pp 48–51
118. Milanes V, Shladover SE, Spring J, Nowakowski C, Kawazoe H, Nakamura M (2014) Co-operative adaptive cruise control in real traffic situations. *IEEE Trans Intell Transp Syst* 15(1):296–305
119. Mohammadpour J, Scherer CW (2012) Control of linear parameter varying systems with applications. Springer Science & Business Media
120. Morato MM, Nguyen MQ, Sename O, Dugard L (2019) Design of a fast real-time LPV model predictive control system for semi-active suspension control of a full vehicle. *J Frankl Inst* 356(3):1196–1224
121. Naets F, Pastorino R, Cuadrado J, Desmet W (2014) Online state and input force estimation for multibody models employing extended Kalman filtering. *Multibody Syst Dyn* 32(3):317–336
122. Naets F, van Aalst S, Boulkroune B, Ghouti NE, Desmet W (2017) Design and experimental validation of a stable two-stage estimator for automotive sideslip angle and tire parameters. *IEEE Trans Veh Technol* 66(11):9727–9742
123. Nam H, Choi W, Ahn C (2019) Model predictive control for evasive steering of an autonomous vehicle. *Int J Automot Technol* 20(5):1033–1042
124. Nam K, Fujimoto H, Hori Y (2012) Lateral stability control of in-wheel-motor-driven electric vehicles based on sideslip angle estimation using lateral tire force sensors. *IEEE Trans Veh Technol* 61(5):1972–1985
125. Naus GJL, Vugts RPA, Ploeg J, van de Molengraft MJG, Steinbuch M (2010) String-stable CACC design and experimental validation: a frequency-domain approach. *IEEE Trans Veh Technol* 59(9):4268–4279
126. Oriolo G, De Luca A, Vendittelli M (2002) WMR control via dynamic feedback linearization: design, implementation, and experimental validation. *IEEE Trans Control Syst Technol* 10(6):835–852

127. Orosco-Guerrero R, Aranda-Bricaire E, Velasco-Villa M (2002) Modeling and dynamic feed-back linearization of a multi-steered n-trailer. IFAC Proc Vol 35(1):103–108. 15th IFAC World Congress
128. Oya M, Wang Q (2007) Adaptive lane keeping controller for four-wheel-steering vehicles. In: 2007 IEEE international conference on control and automation, pp 1942–1947
129. Park G, Choi SB (2021) A model predictive control for path tracking of electronic-four-wheel drive vehicles. *IEEE Trans Veh Technol* 70(11):11352–11364
130. Park K-S, Lim J-T (2008) Wheel slip control for abs with time delay input using feedback linearization and adaptive sliding mode control. In: 2008 international conference on control, automation and systems, pp 290–295
131. Pedro J, Dahunsi O (2011) Neural network based feedback linearization control of a servo-hydraulic vehicle suspension system. *Int J Appl Math Comput Sci* 21(1):137–147
132. Pei X, Hu X, Liu W, Chen Z, Yang B (2018) State estimation of vehicle's dynamic stability based on the nonlinear kalman filter. *Automot Innov* 1(3):281–289
133. Petersen I (2003) Wheel slip control in abs brakes using gain scheduled optimal control with constraints. Norwegian University of Science and Technology, Trondheim, Norway, Department of Engineering Cybernetics
134. Petersen I, Johansen TA, Kalkkuhl J, Lüdemann J (2003) Wheel slip control using gain-scheduled LQ - LPV/LMI analysis and experimental results. In: 2003 European control conference (ECC), pp 880–885
135. Petrov P, Nashashibi F (2014) Modeling and nonlinear adaptive control for autonomous vehicle overtaking. *IEEE Trans Intell Transp Syst* 15(4):1643–1656
136. Poursamad A (2009) Adaptive feedback linearization control of antilock braking systems using neural networks. *Mechatronics* 19(5):767–773
137. Pretagostini F, Shyrokau B, Berardo G (2019) Anti-lock braking control design using a nonlinear model predictive approach and wheel information. In: 2019 IEEE international conference on mechatronics (ICM), vol 1, pp 525–530
138. Qu S, He T, Zhu GG (2020) Engine egr valve modeling and switched LPV control considering nonlinear dry friction. *IEEE/ASME Trans Mechatron* 25(3):1668–1678
139. Quan YS, Kim JS, Chung CC (2022) Linear parameter varying models-based gain-scheduling control for lane keeping system with parameter reduction. *IEEE Trans Intell Transp Syst* 1–11
140. Raffo GV, Gomes GK, Normey-Rico JE, Kelber CR, Becker LB (2009) A predictive controller for autonomous vehicle path tracking. *IEEE Trans Intell Transp Syst* 10(1):92–102
141. Rajamani R, Zhu C (2002) Semi-autonomous adaptive cruise control systems. *IEEE Trans Veh Technol* 51(5):1186–1192
142. Rattasiri W, Wickramarachchi N, Halgamuge SK (2007) An optimized anti-lock braking system in the presence of multiple road surface types. *Int J Adapt Control Signal Process* 21(6):477–498
143. Ray LR (1997) Nonlinear tire force estimation and road friction identification: simulation and experiments. *Automatica* 33(10):1819–1833
144. Raza H, Xu Z, Yang B, Ioannou P (1997) Modeling and control design for a computer-controlled brake system. *IEEE Trans Control Syst Technol* 5(3):279–296
145. Reina G, Messina A (2019) Vehicle dynamics estimation via augmented extended Kalman filtering. *Measurement* 133:383–395
146. Rezaei S, Sengupta R (2007) Kalman filter-based integration of dgps and vehicle sensors for localization. *IEEE Trans Control Syst Technol* 15(6):1080–1088
147. Riva G, Formentin S, Corino M, Savaresi SM (2022) Model predictive control of high-performance braking systems: a force-based approach. *IEEE Control Syst Lett* 6:2383–2388
148. Riva G, Ruiz F, Formentin S, Savaresi SM (2021) Model-reference design of fixed-order controllers for brake-by-wire actuators. In: 2021 American control conference (ACC), pp 130–135
149. Rugh WJ, Shamma JS (2000) Research on gain scheduling. *Automatica* 36(10):1401–1425

150. Samani NN, Ghaisari J, Danesh M (2012) Autonomous parallel parking of a vehicle in a limited space using a rbf network and a feedback linearization controller. In: *2012 2nd international conference on computer and knowledge engineering (ICCKE)*, pp 117–122
151. Sánchez I, D'Jorge A, Raffo GV, González AH, Ferramosca A (2021) Nonlinear model predictive path following controller with obstacle avoidance. *J Intell Robot Syst* 102(1):1–18
152. Sastry S, Bodson M, Bartram JF (1990) Adaptive control: stability, convergence, and robustness
153. Shakouri P, Czeczot J, Ordys A (2015) Simulation validation of three nonlinear model-based controllers in the adaptive cruise control system. *J Intell Robot Syst* 80(2):207–229
154. Shirazi MM, Rad AB (2018) \mathcal{L}_1 adaptive control of vehicle lateral dynamics. *IEEE Trans Intell Veh* 3(1):92–101
155. Shu P, Sagara S, Wang Q, Oya M (2017) Improved adaptive lane-keeping control for four-wheel steering vehicles without lateral velocity measurements. *Int J Robust Nonlinear Control* 27(17):4154–4168
156. Shukla H, Roy S, Gupta S (2022) Robust adaptive control of steer-by-wire systems under unknown state-dependent uncertainties. *Int J Adapt Control Signal Process* 36(2):198–208
157. Simon D (2006) Optimal state estimation: Kalman, H infinity, and nonlinear approaches. Wiley, New York
158. Soliman AMA (2011) Adaptive lqr control strategy for active suspension system. In: Proceedings of the SAE 2011 world congress and exhibition, p 9
159. Sontag E (2013) Mathematical control theory: deterministic finite dimensional systems. Texts in applied mathematics. Springer, New York
160. Sun Y, Li L, Yan B, Yang C, Tang G (2016) A hybrid algorithm combining EKF and RLS in synchronous estimation of road grade and vehicle' mass for a hybrid electric bus. *Mech Syst Signal Process* 68–69:416–430
161. Swarnkar P, Jain SK, Nema R (2014) Adaptive control schemes for improving the control system dynamics: a review. *IETE Tech Rev* 31(1):17–33
162. Tagne G, Talj R, Charara A (2016) Design and comparison of robust nonlinear controllers for the lateral dynamics of intelligent vehicles. *IEEE Trans Intell Transp Syst* 17(3):796–809
163. Tahboub K (2005) Active nonlinear vehicle-suspension variable-gain control. In: Proceedings of the 2005 IEEE international symposium on, mediterranean conference on control and automation intelligent control, pp 569–574
164. Tanaka Y, Yamada N, Tsuji T, Suetomi T (2014) Vehicle active steering control system based on human mechanical impedance properties of the arms. *IEEE Trans Intell Transp Syst* 15(4):1758–1769
165. Tavernini D, Vacca F, Metzler M, Savitski D, Ivanov V, Gruber P, Hartavi AE, Dhaens M, Sorniotti A (2020) An explicit nonlinear model predictive ABS controller for electro-hydraulic braking systems. *IEEE Trans Ind Electron* 67(5):3990–4001
166. Tejado I, Milanés V, Villagrá J, Vinagre BM (2013) Fractional network-based control for vehicle speed adaptation via vehicle-to-infrastructure communications. *IEEE Trans Control Syst Technol* 21(3):780–790
167. Theunissen J, Sorniotti A, Gruber P, Fallah S, Ricco M, Kvasnica M, Dhaens M (2020) Regionless explicit model predictive control of active suspension systems with preview. *IEEE Trans Ind Electron* 67(6):4877–4888
168. Tian Y, Yao Q, Hang P, Wang S (2022) A gain-scheduled robust controller for autonomous vehicles path tracking based on LPV system with MPC and h_∞ . *IEEE Trans Veh Technol* 1–1
169. Tjonnas J, Johansen TA (2010) Stabilization of automotive vehicles using active steering and adaptive brake control allocation. *IEEE Trans Control Syst Technol* 18(3):545–558
170. Tran M, Hrovat D (1993) Application of gain scheduling to design of active suspensions. In: Proceedings of 32nd IEEE conference on decision and control, vol 2, pp 1030–1035
171. Trotta A, Cirillo A, Giorelli M (2019) A feedback linearization based approach for fully autonomous adaptive cruise control. In: *2019 18th European control conference (ECC)*, pp 2614–2619

172. Tyukin I, Prokhorov D, van Leeuwen C (2005) A new method for adaptive brake control. In: *Proceedings of the 2005, American control conference*, vol 3, pp 2194–2199
173. Vahidi A, Eskandarian A (2003) Research advances in intelligent collision avoidance and adaptive cruise control. *IEEE Trans Intell Transp Syst* 4(3):143–153
174. Waghchoure MR, Shukla A, Veepuri SKS, Dorle A (2022) A comprehensive rule-based control strategy for automated lane centering system. *SAE Int J Connect Autom Veh* 6(1). Cited by: 0
175. Wagner S, Prokop G (2016) Nonlinear controller design based on feedforward exact input-output linearization for active rear-wheel steering in passenger vehicles. In: 2016 European control conference (ECC), pp 963–970
176. Wang J, Zhang G, Wang R, Schnelle SC, Wang J (2017) A gain-scheduling driver assistance trajectory-following algorithm considering different driver steering characteristics. *IEEE Trans Intell Transp Syst* 18(5):1097–1108
177. Wang R, Zhang H, Wang J (2014) Linear parameter-varying controller design for four-wheel independently actuated electric ground vehicles with active steering systems. *IEEE Trans Control Syst Technol* 22(4):1281–1296
178. Wang Y, Xu L, Zhang F, Dong H, Liu Y, Yin G (2021) An adaptive fault-tolerant EKF for vehicle state estimation with partial missing measurements. *IEEE/ASME Trans Mechatron* 26(3):1318–1327
179. Wang Z, Wang J (2020) Ultra-local model predictive control: a model-free approach and its application on automated vehicle trajectory tracking. *Control Eng Pract* 101:104482
180. Wang Z, Zha J, Wang J (2021) Autonomous vehicle trajectory following: a flatness model predictive control approach with hardware-in-the-loop verification. *IEEE Trans Intell Transp Syst* 22(9):5613–5623
181. Wenzel TA, Burnham KJ, Blundell MV, Williams RA (2006) Dual extended Kalman filter for vehicle state and parameter estimation. *Veh Syst Dyn* 44(2):153–171
182. Wilkin MA, Manning WJ, Crolla DA, Levesley MC (2006) Use of an extended Kalman filter as a robust tyre force estimator. *Veh Syst Dyn* 44(sup1):50–59
183. Williams D, Haddad W (1994) Nonlinear control of vehicle yaw rate via roll moment distribution. In: *Proceedings of 1994 American control conference—ACC '94*, vol 2, pp 1959–1963
184. Wu J, Kong Q, Yang K, Liu Y, Cao D, Li Z (2022) Research on the steering torque control for intelligent vehicles co-driving with the penalty factor of human-machine intervention. *IEEE Trans Syst, Man, Cybern: Syst* 1–12
185. Wu J, Zhou H, Liu Z, Gu M (2020) Ride comfort optimization via speed planning and preview semi-active suspension control for autonomous vehicles on uneven roads. *IEEE Trans Veh Technol* 69(8):8343–8355
186. Yamaguchi Y, Murakami T (2009) Adaptive control for virtual steering characteristics on electric vehicle using steer-by-wire system. *IEEE Trans Ind Electron* 56(5):1585–1594
187. Yoon J-H, Peng H (2014) A cost-effective sideslip estimation method using velocity measurements from two gps receivers. *IEEE Trans Veh Technol* 63(6):2589–2599
188. Yoshida H, Shinohara S, Nagai M (2008) Lane change steering manoeuvre using model predictive control theory. *Veh Syst Dyn* 46(sup1):669–681
189. Yu S, Hirche M, Huang Y, Chen H, Allgöwer F (2021) Model predictive control for autonomous ground vehicles: A review. *Auton Intell Syst* 1(1):1–17
190. Yuan H, Song X (2022) A modified EKF for vehicle state estimation with partial missing measurements. *IEEE Signal Process Lett* 29:1594–1598
191. Yuan Y, Zhang J (2020) A novel initiative braking system with nondegraded fallback level for adas and autonomous driving. *IEEE Trans Ind Electron* 67(6):4360–4370
192. Zhang H, Wang J (2016) Vehicle lateral dynamics control through afs/dyc and robust gain-scheduling approach. *IEEE Trans Veh Technol* 65(1):489–494
193. Zhang H, Zhang X, Wang J (2014) Robust gain-scheduling energy-to-peak control of vehicle lateral dynamics stabilisation. *Veh Syst Dyn* 52(3):309–340

194. Zhang J, Yang W, Feng P (2019) A feedback linearization controller combined with a data-driven subspace-based prediction method for vehicle handling stabilization. *Proc Inst Mech Eng, Part C: J Mech Eng Sci* 233(4):1156–1180
195. Zhang W (2021) A robust lateral tracking control strategy for autonomous driving vehicles. *Mech Syst Signal Process* 150:107238
196. Zhang Y, Ioannou PA (2017) Combined variable speed limit and lane change control for highway traffic. *IEEE Trans Intell Transp Syst* 18(7):1812–1823
197. Zhao F, Wu W, Wu Y, Chen Q, Sun Y, Gong J (2021) Model predictive control of soft constraints for autonomous vehicle major lane-changing behavior with time variable model. *IEEE Access* 9:89514–89525
198. Zin A, Sename O, Gaspar P, Dugard L, Bokor J (2006) An LPV/ h_∞ active suspension control for global chassis technology: Design and performance analysis. In: 2006 American control conference, pp 2945–2950
199. Zuo L, Slotine J-J, Nayfeh S (2005) Model reaching adaptive control for vibration isolation. *IEEE Trans Control Syst Technol* 13(4):611–617



Control Problems in Future Vehicles

7

Since Karl Benz's patent of 1885 [13], automobiles have evolved through remarkable technological innovations, for example, electronic differentials, steering assistants, and many others [39]. Despite this constant and progressive evolution, the concept of automobiles as private human-driven machines remained unaltered. Although of great success, this model has led to a long-term unsustainable asset whose main criticalities are (among many others) [9,35]:

- **Machine under-exploitation:** when considering a typical day for employees, vehicles are mainly used to move from home to work and back. During working hours, however, cars and motorbikes remain parked and thus unexploited for the purpose they were designed. This implies a long time to recoup the costs of buying the vehicle.
- **Scarcely livable cities:** the need for two or more vehicles per family has led to inevitable traffic congestion to solve which many ways have been conceived. In many cases, this has not allowed for the introduction of safe and easy-to-travel bicycle lanes and sidewalks. Also, large city areas are often reserved for parking, thus precluding the introduction of green zones.
- **Time, stress, and safety:** queues in traffic congestion are a source of stress and wasted time. For example, people moving from home to work and vice versa lose a non-negligible amount of time waiting in queues, which could be used more efficiently: enjoying their family, reading a book, watching a movie, working, etc. Thus, the sense of frustration arising when realizing this waste of time increases the already high-stress level induced by driving on busy roads. Moreover, traveling for long times at low speeds is doubtless boring. This decreases driver attention and makes humans prone to errors, thus increasing the probability of accidents.
- **Pollution:** despite more and more stringent (inter-)national regulations to lower emissions of Internal Combustion Engine (ICE) cars, the increasing number of

vehicles makes the urban environment one of the main sources of pollution. This is even worse when considering congestion in which ICEs have poor efficiency, especially for those vehicles not equipped with the *start-and-stop* technology.

This viewpoint could also be revolutionized thanks to the pervasive use of electronics to implement automation. Indeed, when conceiving future mobility, people are seen as users of an optimized transportation service that could rely on the following three pillars [10,24]:

- **Sharing economy:** sharing a car as a public means of transport could positively impact the problems described above. Indeed, sharing a vehicle implies reducing the number of polluting sources. Also, this reduces congestion and travel times, benefiting the driver's health. Furthermore, vehicle-sharing avoids the costs of buying a personal automobile.
- **Autonomy:** in the context of a fully autonomous vehicle, the passengers would enjoy the travel time, which would be at their disposal. Moreover, a fully autonomous car could avoid human-triggered accidents, usually due to tiredness and lack of concentration. People do not have to spend time or even worry about finding a parking slot. Automation would rely on enabling technologies such as vehicle-to-vehicle and vehicle-to-network connectivity, intelligent control algorithms, and big data. Thanks to shared information spread among vehicles, traffic could be managed to reduce congestion and optimize overall fuel consumption, and so the pollution.
- **Electrification:** pure electrical vehicles seem to be a suitable answer to the pollution problem. Indeed, the availability of charging infrastructures, fed by renewable sources of energy, would deeply reduce the ecological footprint of future mobility.

The gap between *private ICE human-driven* and *shared electric self-driving* viewpoints cannot be filled in only one vehicle generation. It is reasonable to conceive an intermediate generation characterized by:

- **Human-machine collaboration:** before completely leaving commands to autopilots, there could be a phase, as interesting as challenging, in which humans and machines collaborate. As prescribed by the SAE classification, reported in Sect. 1.1.1, the driver could leave most of the driving duties to the car while being ready to take over control in case of exceptions [49]. The ability to keep the human brain focused on this supervisory task, how the driver should be awakened from his or her activities, and how the driver resumes driving represent topics under investigation [46]. Moreover, it is a non-written law that humans decide who goes first by finding an agreement through eye contact. Therefore, replicating this behavior in a mixed scenario of human and machine drivers represents a subject of great interest to the scientific community [11].
- **Plug-in hybrid electric power units:** although battery technology is progressively extending car autonomy, the battery energy density is still much less than the heat capacity of traditional fuels. This leads to using ICEs for long-duration constant-

speed journeys with the support of electric motors during acceleration phases and when ICEs are inefficient, as in urban traffic [23]. This hybrid solution tries to keep the benefits of the efficiency and autonomy of electric and ICE power units, respectively [47].

Aside from the ethical and philosophical aspects [34] (Who is held responsible in case of an accident with a self-driving vehicle? What about the privacy of people in shared cars?), this section focuses on control problems that arise when considering the scenarios described above [10].

Intelligence and Robustness. Vehicles with intelligent and robust control systems could turn the futuristic scenario of fully automated urban traffic into reality [5, 31]. In more detail, with the adjective *intelligent control*, the scientific community refers to systems that exploit the knowledge learned from sensing to make decisions [28]. Borrowed from information science, *Artificial Intelligence* (AI) represents a renewed way to conceive control systems. It consists of a strategy to learn from data, where *learning* means creating functions that best fit the data [53]. Specifically, *artificial neural networks* represent one of the most adopted schemes to generate (or approximate) a function [16].

AI is used for two main purposes: situation awareness and control [31]. As for situation awareness, AI algorithms are currently adopted for elaborating raw sensor data to provide higher-level information. For example, the raw data collected by visual cameras consist of integer numbers associated with each pixel composing the sensing area. These data are processed to infer the presence and estimate the position of pedestrians and vehicles, potholes and bumps, lane lines and marked crosswalks, traffic lights and signs (which also must be interpreted) [12], etc. This information can then be used to take control actions [31] such as braking and steering to avoid obstacles such as pedestrians or potholes, crossing an intersection, changing lanes in case of roadworks, and approaching highway exits.

As for control, AI algorithms are nowadays used in two non-mutually exclusive approaches. Both these strategies rely on the generation of approximating functions. In one case, these functions are used to represent the plant, whereas in the other case, they are used to describe the controller. The former philosophy is usually called *indirect*, and the latter *direct* [7]. Both of them have pros and cons. Roughly, the advantage of indirect methods mainly lies in the possibility of having a model (that could be eventually reduced) on which known control strategies can be designed (and so all the known theoretical arguments about stability and robustness can be carried on). On the other hand, direct methods provide data-driven control laws that could be potentially more sophisticated than the classic model-based laws, but for which it is harder to prove stability and robustness.

One of the crucial points of all the AI algorithms, both for situation awareness and control, is the use of sufficiently large and informative data for building the required functions. As an example, several thousands of pictures of traffic signs are needed to enable an AI scheme correctly classify signs [17] like no entry, speed limits, no parking, etc. Moreover, to perform correct and safe maneuvers, AI algorithms are trained on thousands of driving hours by thousands of different human and synthetic

drivers [19, 25]. Despite this considerable training effort, AI algorithms can be prone to errors because of their limited power of representation. This could confuse them in the presence of uncertain or new data: no two intersections are the same, no two roads are the same, etc. To take this argument to the extreme, assume a vehicle is equipped with a camera for marked crosswalks recognition. What would happen if the zebra markings are painted to look 3D [42]? Should the vehicle stop or keep traveling? And what if this happens in a queue?

In this context, the robustness to uncertainties plays a vital role. Indeed, vehicle, road, weather, traffic, and driver conditions vary in time and unpredictably. As an example, all-weather-condition control systems represent one of the goals of the industrial and academic communities in the upcoming years [30, 51].

On-board energy management. Automobiles have evolved and technologically improved over the years. With a unique energy source, i.e., fuel, one common development direction was doubtless that of energy saving [6]. More and more efficient ICEs have been designed to extend autonomy and meet anti-pollution regulations, such as the European emission standards [33]. With the introduction of hybrid electric vehicles and plug-in hybrid electric vehicles, the problem of optimization of onboard energy has become even more relevant [29, 47]. Indeed, researchers and engineers are trying to make the whole system more efficient and get maximum benefits from energy transfers among fluid dynamical, mechanical, electrical, and thermal processes. If one looks at F1 as a technology incubator, possible research directions are clear. Indeed, the power units for the years 2022–2025 [14] are composed of an ICE, fed by compressed air, whose exhaust gases feed a turbine. On the turbine-compressor shaft is installed a motor generator, usually called *Motor Generator Unit-Heat* (MGU-H), whose primary purpose is harvesting the extra kinetic energy produced by the turbine and not used by the compressor. This energy is stored within the battery and exploited to speed up the turbo-compressor when the driver presses the gas pedal. A secondary motor generator is installed on the ICE shaft and is usually called *Motor Generator Unit-Kinetic* (MGU-K). Similar to the MGU-H, the MGU-K retrieves (provides) energy from (to) the ICE shaft when required by the driver. Thanks to the MGU-K, the excess kinetic energy, e.g., during brakings, is transformed into electrical energy and stored in the battery. Moreover, in some conditions, the MGU-K is directly fed by the MGU-H. However, the control and optimization of energy fluxes within a system complex like F1 power units represent a non-trivial problem [4].

Exciting concepts such as *in-wheel* motors are catching on in the context of road vehicles. The idea is that each wheel can be equipped with an independent set of sensors and electro-mechanical actuators that embed all the chassis-related control functions such as driving, braking, steering, and height regulation. In this context, the energy fluxes that could be stored in a unique centralized battery or an onboard battery network have to be managed to optimize autonomy [21].

Distributed planning and control. The future availability of vehicle-to-vehicle and vehicle-to-infrastructure networks, and smart grids, could be instrumental in implementing traffic management systems [20]. The aggregated computational power of

each vehicle could be used to deploy distributed algorithms for the optimization of traffic with the goals of traveling time, pollution, and energy demand minimization [8, 36, 50]. For example, most automobiles nowadays are equipped with ACC. This system regulates the speed and distance to the preceding vehicle to meet safety standards. These standards are pretty conservative and guarantee that cars avoid crashes even when leading vehicles stop suddenly, despite the system's reaction delays. In current configurations, the main issue consists of the propagation of the information that, from the leader, reaches the last follower passing across the whole platoon. Conversely, control policies could rely on inter-vehicle connections in a fully connected vehicle string to simultaneously inform and brake the entire formation. This could result in a safety distance reduction which, in turn, implies a higher vehicle density and so better space exploitation [3]. Moreover, distributed optimization algorithms can arrange vehicles to reduce platoon air resistance thanks to a reduced safety distance. Indeed, if adequately distanced, not only can the follower take advantage of the leader's wake, but also the leader is pushed by the pressure waves of the follower [44].

As for the vehicle side, assuming a vehicle with n wheels, the *in-wheel motor* architecture provides $3n$ actuators (1 for the suspension, 1 for the wheel speed, and 1 for the steering, per wheel). Consequently, the implementation of architectures based on *in-wheel* motors requires the solution to the coordination and optimization of redundant actuators [52].

Safety and Security. Safety is an essential ingredient in future mobility based on autonomous vehicles [26]. The possibility that one of the vehicle's components experiences a malfunction cannot be nullified (e.g., computational units [27]), and this should not turn into an injury to occupants, pedestrians, or damage to other vehicles. To prevent this from happening, hardware redundancy has represented the solution for many years. Unfortunately, this solution implies extra hardware (often non-active for the entire vehicle's life), which means extra costs, weight, maintenance, consumption, pollution, etc. Software monitoring systems were introduced with the availability of onboard computational units [38]. The system's health is continuously monitored through *Fault Detection and Isolation* (FDI) algorithms whose main goals are discovering (detection) if the system is in trouble and determining (isolation) where the problem is. This information is used for informing the driver and reconfiguring the control system to steer the vehicle to a safe state. The scheme in which the FDI output is fed back to the controller is recognized in the literature as *Fault Detection, Isolation, and Reconfiguration* (FDIR) or *Fault Tolerant Control* (FTC), according to the kind of reconfiguration [22]. The FDI, FDIR, and FTC schemes are online systems that let the driver, human or artificial, safely conclude the driving task in the case of faults. On the other hand, another family of monitoring algorithms aims to prevent the systems from being in trouble through non-scheduled preventive maintenance. These supervisors are usually called *Digital Twins* (DT) and rely on the recognition of data paths that clue the trend to a fault, as previously investigated in controlled environments, e.g., during lab tests [43]. The main advantage of using DT consists of the optimization of maintenance that, thanks to the

DT, is undertaken only when necessary, with benefits for system efficiency, energy consumption, and pollution.

As mentioned before, future vehicles could be connected, directly or via infrastructures [2]. On the one hand, this network represents an incredible opportunity for improving urban traffic, but, on the other hand, it could represent a system weakness. Indeed, this network could be threatened by hacker attacks [15]. To prevent these events, some algorithms, initially borrowed from the FDI field, have been developed and specialized for detecting cyber attacks [41].

Estimation and prediction. Control systems of autonomous and semi-autonomous vehicles rely on the knowledge of vehicle and driver states and road conditions [48]. Therefore, information on vehicle and road conditions is necessary for accomplishing the driving tasks. Indeed, as seen in this book and many others on the same topic, the stabilization of a system consists of estimated-state feedback. The better this estimation, the better the control system performance. Thus, being the driver a part of the system, its inclusion in the estimation model seems to be a straightforward consequence of the need for estimate improvement. In this context, the driver models, already available in the literature [32], could be extended to be comprehensive of novel human–machine interactions that could arise in the transition from human-driven to self-driven vehicles. For example, innovative cockpit designs could lead to new interaction modalities. In more detail, once speed and steering controllers are assumed as a standard, what prevents manufacturers from substituting the steering wheel and pedals with a joystick [18]? Would the human reaction be the same as it is with the steering wheel and pedals [40]?

As for the interaction with the ground, adopting *in-wheel* motors would eliminate most of the transmission shafts, clutches, and gears. This leads to more accurate dynamic models that could be exploited to estimate road conditions better. Furthermore, an improved ground condition estimation, besides the precision of electric motors, implies a more accurate control of the wheel speed and ultimately of the tire forces, with great benefits for the control system adaptation reactivity [1].

Probably, one of the most crucial phases of the transition from human-driven to self-driven vehicles will be their coexistence. In this scenario, autonomous cars should be equipped with systems that estimate and predict pedestrian and vehicle intentions [37,45]. This seems to be an essential feature to reduce the number of possible accidents, especially in the case of non-collaborative behaviors (e.g., a human that intentionally jumps in front of an autonomous car).

References

1. Aksjonov A, Vodovozov V, Augsburg K, Petlenkov E (2018) Design of regenerative anti-lock braking system controller for 4 in-wheel-motor drive electric vehicle with road surface estimation. *Int J Automot Technol* 19(4):727–742
2. Arena F, Pau G (2019) An overview of vehicular communications. *Future Internet* 11(2)

3. Arnaout GM, Bowling S (2014) A progressive deployment strategy for cooperative adaptive cruise control to improve traffic dynamics. *Int J Autom Comput* 11(1):10–18
4. Balerna C, Neumann M-P, Robuschi N, Duhr P, Cerofolini A, Ravaglioli V, Onder C (2021) Time-optimal low-level control and gearshift strategies for the formula 1 hybrid electric powertrain. *Energies* 14(1)
5. Bensrhair A, Bapin T (2021) From AI to autonomous and connected vehicles: advanced driver-assistance systems (ADAS). Wiley, New York
6. Borek J, Groelke B, Eamhardt C, Vermillion C (2020) Economic optimal control for minimizing fuel consumption of heavy-duty trucks in a highway environment. *IEEE Trans Control Syst Technol* 28(5):1652–1664
7. Brunton S, Kutz J (2022) Data-driven science and engineering: machine learning, dynamical systems, and control. Cambridge University Press
8. Carron A, Seccamonte F, Ruch C, Fazzoli E, Zeilinger MN (2021) Scalable model predictive control for autonomous mobility-on-demand systems. *IEEE Trans Control Syst Technol* 29(2):635–644
9. Ceder AA (2021) Urban mobility and public transport: future perspectives and review. *Int J Urban Sci* 25(4):455–479
10. Chai Z, Nie T, Becker J (2021) Autonomous driving changes the future. Springer
11. De Clercq K, Dietrich A, Núñez Velasco JP, De Winter J, Happee R (2019) External human-machine interfaces on automated vehicles: effects on pedestrian crossing decisions. *Hum Factors* 61(8):1353–1370
12. de la Escalera A, Armingol J, Mata M (2003) Traffic sign recognition and analysis for intelligent vehicles. *Image Vis Comput* 21(3):247–258
13. Dietsche K-H, Kuhlgatz D (2014) History of the automobile. Springer Fachmedien Wiesbaden, Wiesbaden, pp 1–7
14. Ebbesen S, Salazar M, Elbert P, Bussi C, Onder CH (2018) Time-optimal control strategies for a hybrid electric race car. *IEEE Trans Control Syst Technol* 26(1):233–247
15. El-Rewini Z, Sadatsharan K, Selvaraj DF, Plathottam SJ, Ranganathan P (2020) Cybersecurity challenges in vehicular communications. *Veh Commun* 23:100214
16. Ferrari S, Stengel R (2005) Smooth function approximation using neural networks. *IEEE Trans Artif Neural Netw* 16(1):24–38
17. Gamez Serna C, Ruichek Y (2018) Classification of traffic signs: the European dataset. *IEEE Access* 6:78136–78148
18. Gil JJ, Díaz I, Ciáurriz P, Echeverría M (2013) New driving control system with haptic feedback: Design and preliminary validation tests. *Transp Res Part C: Emerg Technol* 33:22–36
19. Grigorescu S, Trasnea B, Cocias T, Macesanu G (2020) A survey of deep learning techniques for autonomous driving. *J Field Robot* 37(3):362–386
20. Gupta N, Prakash A, Tripathi R (2021) Internet of vehicles and its applications in autonomous driving. Springer, Berlin
21. Hung Y-H, Wu C-H (2015) A combined optimal sizing and energy management approach for hybrid in-wheel motors of EVs. *Appl Energy* 139:260–271
22. Isermann R (2006) Fault-diagnosis systems: an introduction from fault detection to fault tolerance. Springer, Berlin
23. Jurgen RK (2010) Electric and hybrid-electric vehicles-engines and powertrains. Technical report, SAE Technical Paper
24. Kane M, Whitehead J (2017) How to ride transport disruption—a sustainable framework for future urban mobility. *Aust Plan* 54(3):177–185
25. Kiran BR, Sobh I, Talpaert V, Mannion P, Sallab AAA, Yogamani S, Pérez P (2022) Deep reinforcement learning for autonomous driving: a survey. *IEEE Trans Intell Transp Syst* 23(6):4909–4926
26. Koopman P, Wagner M (2017) Autonomous vehicle safety: an interdisciplinary challenge. *IEEE Intell Transp Syst Mag* 9(1):90–96

27. Lee PA, Anderson T (1990) Fault tolerance. Springer Vienna, Vienna, pp 51–77
28. Lu Y (2019) Artificial intelligence: a survey on evolution, models, applications and future trends. *J Manag Anal* 6(1):1–29
29. Sabri MM, Danapalasingam K, Rahmat M (2016) A review on hybrid electric vehicles architecture and energy management strategies. *Renew Sustain Energy Rev* 53:1433–1442
30. Ma N, Pang G, Shi X, Zhai Y (2020) An all-weather lane detection system based on simulation interaction platform. *IEEE Access* 8:46121–46130
31. Ma Y, Wang Z, Yang H, Yang L (2020) Artificial intelligence applications in the development of autonomous vehicles: a survey. *IEEE/CAA J Automatica Sinica* 7(2):315–329
32. Macadam CC (2003) Understanding and modeling the human driver. *Veh Syst Dyn* 40(1–3):101–134
33. Martini G, Giechaskiel B, Dilara P (2009) Future european emission standards for vehicles: the importance of the UN-ECE particle measurement programme. *Biomarkers* 14(sup1):29–33 PMID: 19604055
34. Maurer M, Gerdes JC, Lenz B, Winner H (2016) Autonomous driving: technical, legal and social aspects. Springer Nature
35. Miskolczi M, Földes D, Munkácsy A, Jászberényi M (2021) Urban mobility scenarios until the 2030s. *Sustain Cities Soc* 72:103029
36. Mohseni F, Frisk E, Nielsen L (2021) Distributed cooperative mpc for autonomous driving in different traffic scenarios. *IEEE Trans Intell Veh* 6(2):299–309
37. Mozaffari S, Al-Jarrah OY, Dianati M, Jennings P, Mouzakitis A (2022) Deep learning-based vehicle behavior prediction for autonomous driving applications: a review. *IEEE Trans Intell Transp Syst* 23(1):33–47
38. Ng H, Chen R, Speyer J (2006) A vehicle health monitoring system evaluated experimentally on a passenger vehicle. *IEEE Trans Control Syst Technol* 14(5):854–870
39. Nunney M (2007) Light and heavy vehicle technology. Butterworth-Heinemann
40. Östlund J, Peters B (2002) Joystick versus conventional driving controls. In: Human factors in transportation, communication, health, and the workplace. The human factors and ergonomics society europe chapter annual meeting. Turin, Italy, pp 77–80
41. Petho Z, Torok A, Szalay Z (2021) A survey of new orientations in the field of vehicular cybersecurity, applying artificial intelligence based methods. *Trans Emerg Telecommun Technol* 32(10):e4325
42. Pichayapan P, Kaewmoracharoen M, Peansara T, Nanthavisit P (2020) Urban school area road safety improvement and assessment with a 3D piano-keyboard-styled pedestrian crossing approach: a case study of chiang mai university demonstration school. *Sustainability* 12(16)
43. Piromalis D, Kantaros A (2022) Digital twins in the automotive industry: the road toward physical-digital convergence. *Appl Syst Innovat* 5(4)
44. Schito P et al (2012) Numerical and experimental investigation on vehicles in platoon. *SAE Int J Commer Veh* 5(2012-01-0175):63–71
45. Sharma N, Dhiman C, Indu S (2022) Pedestrian intention prediction for autonomous vehicles: a comprehensive survey. *Neurocomputing* 508:120–152
46. Sun X, Cao S, Tang P (2021) Shaping driver-vehicle interaction in autonomous vehicles: how the new in-vehicle systems match the human needs. *Appl Ergon* 90:103238
47. Taghavipour A, Vajedi M, Azad NL (2019) Intelligent control of connected plug-in hybrid electric vehicles. Springer, Berlin
48. Van Brummelen J, O'Brien M, Gruyer D, Najjaran H (2018) Autonomous vehicle perception: the technology of today and tomorrow. *Transp Res Part C: Emerg Technol* 89:384–406
49. Walch M, Mühl K, Kraus J, Stoll T, Baumann M, Weber M (2017) From car-driver-handovers to cooperative interfaces: visions for driver–vehicle interaction in automated driving. Springer International Publishing, Cham, pp 273–294
50. Wang C, Zhang J, Xu L, Li L, Ran B (2019) A new solution for freeway congestion: Cooperative speed limit control using distributed reinforcement learning. *IEEE Access* 7:41947–41957

51. Wang Z, Cheng G, Zheng J (2019) Road edge detection in all weather and illumination via driving video mining. *IEEE Trans Intell Veh* 4(2):232–243
52. Zhang X (2021) Modeling and dynamics control for distributed drive electric vehicles. Springer, Berlin
53. Zhou M, Li H-X, Weijnen M (2015) Advances and challenges on intelligent learning in control systems, pp 241–264

This appendix recalls the base notions of matrices, vectors, linear spaces, and the operations between matrices and vectors exploited in this book. These notions are provided as well as MATLAB® listings.

A.1 Matrices and Vectors

Let $a_{ij} \in \mathbb{C}$, with $i = 1, \dots, n$, $j = 1, \dots, m$, and $n, m \in \mathbb{N}$, then

$$\mathbf{A} := \begin{bmatrix} a_{11} & a_{12} & \dots & a_{1n} \\ a_{21} & a_{22} & \dots & a_{2n} \\ \vdots & \vdots & \ddots & \vdots \\ a_{m1} & a_{m2} & \dots & a_{mn} \end{bmatrix} \quad (\text{A.1})$$

is called *matrix*. A matrix of m rows and n columns, whose entries belong to \mathbb{C} , represents an element of the space $\mathbb{C}^{m \times n}$, i.e., $\mathbf{A} \in \mathbb{C}^{m \times n}$. Matrices are called *square* if $n = m$.

```
% Declaration and assignment of a m-by-n matrix, A, of random real numbers
m = randi(10); % number of rows as a random integer between 1 and 10
n = randi(10); % number of columns as a random integer between 1 and 10
A = rand(m,n); % Matrix declaration and assignment
```

When $n = 1$, a matrix is said to be a *vector* (or column vector), and it is denoted with $\mathbf{x} \in \mathbb{C}^m$. Let \mathbf{A} be a matrix, then its *transpose*, namely \mathbf{A}^\top , is given by

$$\mathbf{A}^\top = \begin{bmatrix} a_{11} & a_{21} & \dots & a_{m1} \\ a_{12} & a_{22} & \dots & a_{m2} \\ \vdots & \vdots & \ddots & \vdots \\ a_{1n} & a_{2n} & \dots & a_{nm} \end{bmatrix} \quad (\text{A.2})$$

where $(\mathbf{A}^\top)^\top = \mathbf{A}$.

% Transpose of a matrix

`B = A.'`; % returns the nonconjugate transpose of A, that is, interchanges the row and column index for each element. If A contains complex elements, then A.' does not affect the sign of the imaginary parts.

A matrix \mathbf{A} is said to be *skew symmetric* if $\mathbf{A}^\top = -\mathbf{A}$.

Furthermore, a square matrix $\mathbf{A} \in \mathbb{C}^{n \times n}$ is said to be *diagonal* if $a_{ij} = 0$ for any $i, j = 1, \dots, n$ such that $i \neq j$, i.e., if

$$\mathbf{A} = \begin{bmatrix} a_{11} & 0 & \dots & 0 \\ 0 & a_{22} & \dots & 0 \\ \vdots & \vdots & \ddots & \vdots \\ 0 & 0 & \dots & a_{nn} \end{bmatrix}. \quad (\text{A.3})$$

% Diagonal matrix

`v = rand(1, m);` % creates a vector of m–columns of real random numbers
`D = diag(v);` % returns a square diagonal matrix with the elements of vector v on the main diagonal

A diagonal matrix with $a_{ii} = 1$ for all $i = 1, \dots, n$ is called *identity* and is denoted with \mathbf{I} . *Null matrices* and *null vectors*, both denoted with $\mathbf{0}$, are defined as matrices and vectors whose elements are (all) null.

% Null matrix

`X = zeros(m,n);` % returns an n–by–m matrix of zeros

A square matrix $\mathbf{A} \in \mathbb{C}^{n \times n}$ is said to be *upper (lower) triangular* if the elements below (above) the principal diagonal are all null, i.e.,

$$\mathbf{A}_{\text{up}} = \begin{bmatrix} a_{11} & a_{12} & \dots & a_{1n} \\ 0 & a_{22} & \dots & a_{2n} \\ \vdots & \vdots & \ddots & \vdots \\ 0 & 0 & \dots & a_{mn} \end{bmatrix} \quad \mathbf{A}_{\text{low}} = \begin{bmatrix} a_{11} & 0 & \dots & 0 \\ a_{21} & a_{22} & \dots & 0 \\ \vdots & \vdots & \ddots & \vdots \\ a_{m1} & a_{m2} & \dots & a_{mn} \end{bmatrix}.$$

A.2 Matrix Sum and Product

Let $\mathbf{A}, \mathbf{B} \in \mathbb{C}^{m \times n}$, with $m, n \in \mathbb{N}$, be matrices whose elements are a_{ij} and b_{ij} respectively. Then, the sum $\mathbf{A} + \mathbf{B}$ is defined as

$$\begin{aligned}\mathbf{A} + \mathbf{B} &= \begin{bmatrix} a_{11} & a_{12} & \dots & a_{1n} \\ a_{21} & a_{22} & \dots & a_{2n} \\ \vdots & \vdots & \ddots & \vdots \\ a_{m1} & a_{m2} & \dots & a_{mn} \end{bmatrix} + \begin{bmatrix} b_{11} & b_{12} & \dots & b_{1n} \\ b_{21} & b_{22} & \dots & b_{2n} \\ \vdots & \vdots & \ddots & \vdots \\ b_{m1} & b_{m2} & \dots & b_{mn} \end{bmatrix} = \\ &= \begin{bmatrix} a_{11} + b_{11} & a_{12} + b_{12} & \dots & a_{1n} + b_{1n} \\ a_{21} + b_{21} & a_{22} + b_{22} & \dots & a_{2n} + b_{2n} \\ \vdots & \vdots & \ddots & \vdots \\ a_{m1} + b_{m1} & a_{m2} + b_{m2} & \dots & a_{mn} + b_{mn} \end{bmatrix}.\end{aligned}$$

% Sum of matrices

`C = A+B;` % is the matrix sum of A and B. If A and B are an n-by-m matrices, then C is an n-by-m matrix

Let $\mathbf{A} \in \mathbb{C}^{m \times n}$, with $m, n \in \mathbb{N}$, and $\alpha \in \mathbb{C}$, then the product $\alpha\mathbf{A}$ is defined as

$$\alpha\mathbf{A} = \begin{bmatrix} \alpha a_{11} & \alpha a_{12} & \dots & \alpha a_{1n} \\ \alpha a_{21} & \alpha a_{22} & \dots & \alpha a_{2n} \\ \vdots & \vdots & \ddots & \vdots \\ \alpha a_{m1} & \alpha a_{m2} & \dots & \alpha a_{mn} \end{bmatrix}.$$

% Multiplication by a scalar

`alpha = rand(1);` % generates a random real number

`B = alpha*A;` % is the matrix product of alpha and A.

The operator “.” defines the dot matrix product, representative of the well-known rule *row-by-column*. In details, let $\mathbf{A} \in \mathbb{C}^{m \times n}$, $\mathbf{B} \in \mathbb{C}^{n \times p}$, and $\mathbf{C} \in \mathbb{C}^{m \times p}$, with $m, n, p \in \mathbb{N}$. Let a_{ik} , b_{kj} , and c_{ij} be the elements of \mathbf{A} , \mathbf{B} , and \mathbf{C} , with $i = 1, \dots, m$, $k = 1, \dots, n$, and $j = 1, \dots, p$. Then, $\mathbf{C} = \mathbf{A} \cdot \mathbf{B}$ if

$$c_{ij} = \sum_{k=1}^n a_{ik} b_{kj}. \quad (\text{A.4})$$

Remark A.1 It is worth noting that the matrix product is well-posed if the number of columns of \mathbf{A} is equal to the number of rows of \mathbf{B} .

% Matrices multiplications

`C = A*B;` % is the matrix product of A and B. If A is an m-by-n and B is a n-by-p matrix, then C is an m-by-p matrix

Let $\alpha \in \mathbb{C}$ and $\mathbf{A}, \mathbf{B}, \mathbf{C} \in \mathbb{C}^{m \times n}$, then the following equalities are true:

$$\begin{aligned}\mathbf{A} - \mathbf{B} &= \mathbf{A} + (-1)\mathbf{B} \\ (\mathbf{A} + \mathbf{B}) + \mathbf{C} &= \mathbf{A} + (\mathbf{B} + \mathbf{C}) \\ \alpha(\mathbf{A} \cdot \mathbf{B}) &= (\alpha\mathbf{A}) \cdot \mathbf{B} = \mathbf{A} \cdot (\alpha\mathbf{B}) \\ \mathbf{A} \cdot \mathbf{B} \cdot \mathbf{C} &= (\mathbf{A} \cdot \mathbf{B}) \cdot \mathbf{C} = \mathbf{A} \cdot (\mathbf{B} \cdot \mathbf{C}) \\ \mathbf{A} \cdot (\mathbf{B} + \mathbf{C}) &= \mathbf{A} \cdot \mathbf{B} + \mathbf{A} \cdot \mathbf{C} \\ (\mathbf{B} + \mathbf{C}) \cdot \mathbf{A} &= \mathbf{B} \cdot \mathbf{A} + \mathbf{C} \cdot \mathbf{A} \\ (\mathbf{A} \cdot \mathbf{B})^\top &= \mathbf{B}^\top \cdot \mathbf{A}^\top \\ (\mathbf{A} + \mathbf{B})^\top &= \mathbf{A}^\top + \mathbf{B}^\top.\end{aligned}$$

Anyway, it is worth noting that in general

- $\mathbf{A} \cdot \mathbf{B} \neq \mathbf{B} \cdot \mathbf{A}$.
- $\mathbf{A} \cdot \mathbf{B} = \mathbf{A} \cdot \mathbf{C} \not\Rightarrow \mathbf{B} = \mathbf{C}$.
- $\mathbf{A} \cdot \mathbf{B} = \mathbf{0} \not\Rightarrow \mathbf{B} = \mathbf{0}$ or $\mathbf{A} = \mathbf{0}$.

The identity matrix represents the neutral element for the dot product, such that

$$\mathbf{A} \cdot \mathbf{I} = \mathbf{A} \quad \mathbf{I} \cdot \mathbf{A} = \mathbf{A}.$$

Let $\mathbf{A} \in \mathbb{C}^{n \times n}$, then its k -th power is defined as

$$\mathbf{A}^k = \prod_{i=1}^k \mathbf{A} = \mathbf{A} \cdot \mathbf{A} \cdot \dots \cdot \mathbf{A} \quad k \text{ times.}$$

Let $\mathbf{A} \in \mathbb{R}^{m \times n}$ and $\mathbf{B} \in \mathbb{R}^{p \times q}$. Let a_{ij} be the entries of \mathbf{A} , with $i = 1, \dots, m$ and $j = 1, \dots, n$, then the *Kronecker product* is denoted by the operator \otimes and is such that

$$\mathbf{A} \otimes \mathbf{B} = \begin{bmatrix} a_{11}\mathbf{B} & a_{12}\mathbf{B} & \dots & a_{1n}\mathbf{B} \\ a_{21}\mathbf{B} & a_{22}\mathbf{B} & \dots & a_{2n}\mathbf{B} \\ \vdots & \vdots & \ddots & \vdots \\ a_{m1}\mathbf{B} & a_{m2}\mathbf{B} & \dots & a_{mn}\mathbf{B} \end{bmatrix}.$$

% Kronecker product

`K = kron(A,B)` % returns the Kronecker tensor product of matrices A and B. If A is an m-by-n matrix and B is a p-by-q matrix, then `kron(A,B)` is an m*p-by-n*q matrix formed by taking all possible products between the elements of A and the matrix B.

Let $\mathbf{A}_i, \mathbf{A} \in \mathbb{C}^{m \times n}$, with $i = 1, \dots, p$. Then \mathbf{A} is said to be a *linear combination* of $\{\mathbf{A}_1, \dots, \mathbf{A}_p\}$ if it can be obtained through

$$\mathbf{A} = \alpha_1 \mathbf{A}_1 + \cdots + \alpha_p \mathbf{A}_p$$

for some $\alpha_i \in \mathbb{C}$. The matrices in the set $\{\mathbf{A}_1, \dots, \mathbf{A}_p\}$ are said to be *linearly independent* if neither of them can be written as a linear combination of the remainder. Equivalently, $\mathbf{A}_1, \dots, \mathbf{A}_p$ are linearly independent if and only if

$$\alpha_1 \mathbf{A}_1 + \cdots + \alpha_p \mathbf{A}_p = \mathbf{0}$$

implies $\alpha_i = 0$ for any $i = 1, \dots, p$.

A.3 Vector Products

Let $\mathbf{u}_1, \mathbf{u}_2 \in \mathbb{C}^n$ be two vectors, then we define the *inner product* $\langle \mathbf{u}_1, \mathbf{u}_2 \rangle \in \mathbb{C}$ with

$$\langle \mathbf{u}_1, \mathbf{u}_2 \rangle := \mathbf{u}_1^\top \cdot \mathbf{u}_2 = \sum_k u_{1k} u_{2k}.$$

Let $\mathbf{u}_1, \mathbf{u}_2, \mathbf{u}_3 \in \mathbb{C}^n$ and $\alpha \in \mathbb{C}$, then the inner product between vectors satisfies the following properties:

- distribution with respect to the sum: $\langle \mathbf{u}_1 + \mathbf{u}_2, \mathbf{u}_3 \rangle = \langle \mathbf{u}_1, \mathbf{u}_3 \rangle + \langle \mathbf{u}_2, \mathbf{u}_3 \rangle$;
- distribution with respect to the scalar product: $\alpha \langle \mathbf{u}_1, \mathbf{u}_2 \rangle = \langle \alpha \mathbf{u}_1, \mathbf{u}_2 \rangle = \langle \mathbf{u}_1, \alpha \mathbf{u}_2 \rangle$;
- commutation: $\langle \mathbf{u}_1, \mathbf{u}_2 \rangle = \langle \mathbf{u}_2, \mathbf{u}_1 \rangle$;
- positive definition: $\langle \mathbf{u}_1, \mathbf{u}_1 \rangle > 0, \forall \mathbf{u}_1$.

The (Euclidean) norm of a vector is defined as $\|\mathbf{u}\| = \sqrt{\langle \mathbf{u}, \mathbf{u} \rangle}$. A vector is called *versor* if its norm is equal to 1, i.e., if $\|\mathbf{u}\| = 1$.

```
% Inner product and norm of vectors
u3 = dot(u1,u2); % returns the scalar dot product of the vectors u1 and
% u2 which must have the same length
n = norm(u); % returns the Euclidean norm of vector u. This norm is
% also called the 2-norm, vector magnitude, or Euclidean length.
```

A square matrix $\mathbf{A} \in \mathbb{C}^{n \times n}$ is said to be (*semi-*)*positive definite* if for any vector $\mathbf{x} \in \mathbb{C}^n, \mathbf{x} \neq \mathbf{0}$, the scalar $\langle \mathbf{x}, \mathbf{A} \cdot \mathbf{x} \rangle (\geq) > 0$.

Let $\mathbf{u} := \text{col}(u_1, u_2, u_3) \in \mathbb{R}^3$ and define the function $S : \mathbb{R}^3 \rightarrow \mathbb{R}^{3 \times 3}$ with

$$\mathbf{S}(\mathbf{u}) = \begin{bmatrix} 0 & -u_3 & u_2 \\ u_3 & 0 & -u_1 \\ -u_2 & u_1 & 0 \end{bmatrix}.$$

Let $\mathbf{u}_1, \mathbf{u}_2 \in \mathbb{R}^3$, then the *outer product* is defined as

$$\mathbf{u}_1 \times \mathbf{u}_2 = \mathbf{S}(\mathbf{u}_1) \cdot \mathbf{u}_2$$

The cross product is:

- non-commutative: $\mathbf{u}_1 \times \mathbf{u}_2 = -(\mathbf{u}_2 \times \mathbf{u}_1)$;
- distributive with respect to the sum: $\mathbf{u}_1 \times (\mathbf{u}_2 + \mathbf{u}_3) = \mathbf{u}_1 \times \mathbf{u}_2 + \mathbf{u}_1 \times \mathbf{u}_3$;
- distributive with respect to the product by a scalar: $\alpha(\mathbf{u}_1 \times \mathbf{u}_2) = (\alpha\mathbf{u}_1) \times \mathbf{u}_2 = \mathbf{u}_1 \times (\alpha\mathbf{u}_2)$;
- non-associative: $\mathbf{u}_1 \times (\mathbf{u}_2 \times \mathbf{u}_3) \neq (\mathbf{u}_1 \times \mathbf{u}_2) \times \mathbf{u}_3$.

```
% cross product of vectors
```

```
u3 = cross(u1,u2); % returns the cross product of the vectors u1 and u2  
which must have a length of 3.
```

A.4 Matrix Inverse

Let $\mathbf{A} \in \mathbb{R}^{n \times n}$, then the square matrix obtained from \mathbf{A} by the cancellation of the i -th row and the j -th column is denoted with $\mathbf{A}^{(ij)} \in \mathbb{R}^{n-1 \times n-1}$. It is worth observing that the i -th row and the j -th column share one common element, which is a_{ij} . The determinant $\det(\mathbf{A}) : \mathbb{R}^{n \times n} \mapsto \mathbb{R}$ is defined as

$$\det(\mathbf{A}) := \sum_j a_{ij} C_{ij} (-1)^{i+j}$$

where C_{ij} is the *cofactor* associated with a_{ij} . Iteratively, the cofactors C_{ij} are defined as

$$C_{ij} = \det\left(\mathbf{A}^{(ij)}\right).$$

The following properties hold true:

- $\det(\mathbf{A} \cdot \mathbf{B}) = \det(\mathbf{A}) \det(\mathbf{B})$;
- $\det(\mathbf{A}) = 0$ if the matrix \mathbf{A} has a row (column) which is a linear combination of the remaining rows (columns);
- $\det(\mathbf{A}) = \prod_{i=1}^n a_{ii}$ if the matrix is either triangular or diagonal.

If $\det(\mathbf{A}) = 0$ the matrix \mathbf{A} is said to be *singular*.

```
% Determinant of a matrix
```

```
d = det(A); % returns the determinant of square matrix A.
```

The **rank** of a square matrix $\mathbf{A} \in \mathbb{R}^{n \times n}$ is defined as a function $\rho : \mathbb{R}^{n \times n} \mapsto \mathbb{N}$ and corresponds to the maximum integer, namely p , for which there exists at least one sub-matrix of dimensions p (built selecting p rows and p columns of \mathbf{A}) whose determinant is not null. The following properties are valid:

- $\rho(\mathbf{A} \cdot \mathbf{B}) \leq \rho(\mathbf{A}) \cdot \rho(\mathbf{B})$;

- $\rho(\mathbf{A}^\top) = \rho(\mathbf{A})$.

Furthermore, if $\rho(\mathbf{A}) = n$ the matrix \mathbf{A} is said to be *full rank* or, equivalently, *invertible*.

Let $\mathbf{A} \in \mathbb{R}^{n \times n}$, the *adjoint matrix* is defined as

$$\text{Adj}(\mathbf{A}) = \begin{bmatrix} C_{11}(-1)^{1+1} & C_{12}(-1)^{1+2} & \dots & C_{1n}(-1)^{1+n} \\ C_{21}(-1)^{2+1} & C_{22}(-1)^{2+2} & \dots & C_{2n}(-1)^{1+n} \\ \vdots & \vdots & \ddots & \vdots \\ C_{n1}(-1)^{n+1} & C_{n2}(-1)^{n+2} & \dots & C_{nn}(-1)^{n+n} \end{bmatrix}^\top.$$

The *matrix inversion* is an operator which applies to square matrices. In particular, let $\mathbf{A} \in \mathbb{R}^{n \times n}$ be invertible. Then, its inverse is defined as

$$\mathbf{A}^{-1} = \frac{1}{\det(\mathbf{A})} \text{Adj}(\mathbf{A})$$

with

$$\mathbf{A}^{-1} \cdot \mathbf{A} = \mathbf{A} \cdot \mathbf{A}^{-1} = \mathbf{I}.$$

Finally, let $\mathbf{A}, \mathbf{B} \in \mathbb{R}^{n \times n}$, then $(\mathbf{A} \cdot \mathbf{B})^{-1} = \mathbf{B}^{-1} \cdot \mathbf{A}^{-1}$.

```
% Inverse of a matrix
Y = inv(X); % computes the inverse of square matrix X.
```

A.5 Matrix Pseudo-inverses (Moore–Penrose)

Let $\mathbf{A} \in \mathbb{R}^{m \times n}$ with $\rho(\mathbf{A}) = \min\{m, n\}$, then the *left* and *right pseudo-inverse of \mathbf{A}* are defined as follows:

$$\mathbf{A}^+ = \begin{cases} (\mathbf{A}^\top \cdot \mathbf{A})^{-1} \cdot \mathbf{A}^\top & \rho(\mathbf{A}) = n \text{ left pseudo-inverse} \\ \mathbf{A}^\top \cdot (\mathbf{A} \cdot \mathbf{A}^\top)^{-1} & \rho(\mathbf{A}) = m \text{ right pseudo-inverse} \end{cases}$$

```
% Pseudo-Inverse of a matrix
B = pinv(A); % returns the Moore–Penrose Pseudoinverse of matrix A.
```

A.6 Vector Spaces

Let $\mathbb{V}(\mathbb{C}) := \{\mathbf{x} \in \mathbb{C}^n\}$ with $n \in \mathbb{N}$. Then \mathbb{V} is a *vector space* if the following conditions hold true:

1. for any $\mathbf{u}_1, \mathbf{u}_2, \mathbf{u}_3 \in \mathbb{V}$ then

$$(\mathbf{u}_1 + \mathbf{u}_2) + \mathbf{u}_3 = \mathbf{u}_1 + (\mathbf{u}_2 + \mathbf{u}_3);$$

2. for any $\mathbf{u} \in \mathbb{V}$ the null vector $\mathbf{0}$ is such that

$$\mathbf{u} + \mathbf{0} = \mathbf{0} + \mathbf{u};$$

3. for any $\mathbf{u}_1 \in \mathbb{V}$ there exists $\mathbf{u}_2 \in \mathbb{V}$ such that

$$\mathbf{u}_1 + \mathbf{u}_2 = \mathbf{0} \implies \mathbf{u}_2 = -\mathbf{u}_1;$$

4. for any $\mathbf{u}_1, \mathbf{u}_2 \in \mathbb{V}$

$$\mathbf{u}_1 + \mathbf{u}_2 = \mathbf{u}_2 + \mathbf{u}_1;$$

5. for any $\mathbf{u} \in \mathbb{V}$ and for any $\alpha, \beta \in \mathbb{C}$

$$\alpha(\beta\mathbf{u}) = (\alpha\beta)\mathbf{u};$$

6. there exists a neutral element, namely 1, such that

$$1\mathbf{u} = \mathbf{u};$$

7. for any $\mathbf{u}_1, \mathbf{u}_2 \in \mathbb{V}$ and for any $\alpha \in \mathbb{C}$

$$\alpha(\mathbf{u}_1 + \mathbf{u}_2) = \alpha\mathbf{u}_1 + \alpha\mathbf{u}_2;$$

8. for any $\mathbf{u} \in \mathbb{V}$ and any $\alpha, \beta \in \mathbb{C}$

$$(\alpha + \beta)\mathbf{u} = \alpha\mathbf{u} + \beta\mathbf{u}.$$

A.7 Linear Functions and Matrices

Let $\mathbb{U}(\mathbb{C})$ and $\mathbb{V}(\mathbb{C})$ be two vector spaces, then a function $L : \mathbb{U} \rightarrow \mathbb{V}$ is said to be *linear* if for any $\mathbf{u}_1, \mathbf{u}_2 \in \mathbb{U}$ and for any $\alpha \in \mathbb{C}$ the following relations hold:

$$L(\mathbf{u}_1 + \mathbf{u}_2) = L(\mathbf{u}_1) + L(\mathbf{u}_2)$$

$$L(\alpha\mathbf{u}_1) = \alpha L(\mathbf{u}_1).$$

Let $\mathbf{x} \in \mathbb{U}$ and $\mathbf{y} \in \mathbb{V}$, then a linear transformation between the two vector spaces can be represented through a matrix $\mathbf{A} \in \mathbb{C}^{m \times n}$, as follows:

$$\mathbf{y} = \mathbf{A} \cdot \mathbf{x}.$$

References

- 1 Axler S (2015) Linear algebra done right. Springer International Publishing
- 2 Liesen J, Mehrmann V (2015) Linear algebra. Springer International Publishing
- 3 Shafarevich IR, Remizov A (2013) Linear algebra and geometry. Springer, Berlin

Linear Control Theory Applied with MATLAB®

B

The theoretical tools developed in this book can be applied, via software, to study and design linear time-invariant control systems. This appendix aims to review some of the most relevant MATLAB® functions that, properly used, represent the means to solve practical control problems. More in detail, the functions described hereafter are provided by the Control System Toolbox™, which is one of the extra add-ons provided by MATLAB®.

The first useful MATLAB® function is `eig`. This command is used to compute the eigenvalues and eigenvectors of matrices.

```
[V,D] = eig(A,'vector'); % returns vector matrix D of eigenvalues and matrix V whose columns are the corresponding right eigenvectors, so that A*V = V*D.
```

The reachability and observability studies are important, as well as the stability ones. The reachability and observability matrices in MATLAB® are computed through two separate commands.

`% Reachability`

```
R = ctrb(A,B); % returns the reachability matrix R = [B AB ... A^{n-1}*B]
```

`% Observability`

```
O = obsv(A,C); % returns the observability matrix O = [C; CA; ... ; C*A^{n-1}]
```

Section 5.1 describes how the solution to the optimal control and observation problems are linked to the solution of an Algebraic Riccati Equation (ARE). In particular, with Eq. (5.15) at hand, MATLAB® offers several functions to solve AREs. Probably the most basic one is `icare`.

```
[X,K,L] = icare(Am, Bm, Qm, Rm, Sm, Em, Gm); % computes the unique stabilizing solution X
% state-feedback gain K, and the % closed-loop eigenvalues L of the following continuous
% -time algebraic Riccati equation:
% Am.*X*Em+Em.*X*Am+Em.*X*Gm*X*Em-(Em.*X*Bm+Sm)*inv(Rm)*(Bm.*X*
Em+Sm.)*Qm=0
```

To make the notation of this book compatible with that used by MATLAB® programmers, a change of coordinates must be introduced. In particular, comparing Eq. (5.15)

$$(A^\top + \alpha I)S + S(A + \alpha I) - S\bar{R}^{-1}B^\top S - S\bar{R}^{-1}D^\top QC \\ - (B\bar{R}^{-1}D^\top QC)^\top S + C^\top QC - (C^\top QD)\bar{R}^{-1}(D^\top QC) = 0$$

with the MATLAB® expression

$$A_m^\top X E_m + E_m^\top X A_m + E_m^\top X (G_m - B_m R_m^{-1} B_m^\top) X E_m \\ - E_m^\top X B_m R_m^{-1} S_m^\top - S_m R_m^{-1} B_m^\top X E_m + Q_m - S_m R_m^{-1} S_m^\top = 0$$

leads to

$$A_m = (A + \alpha I), B_m = B, Q_m = C^\top QC, R_m = \bar{R} \\ S_m = (D^\top QC)^\top, E_m = I, G_m = 0.$$

Besides, it worth noting that $K_S = -K_m$. The same change of variables applies when using the command

```
[Km,S,P] = lqr(Am, Bm, Qm, Rm, Sm) % calculates the optimal gain matrix Km, the solution S
% of the associated algebraic Riccati equation and the closed-loop poles P using the
% continuous-time state-space matrices Am and Bm.
```

References

- 1 Dukkipati R (2009) Analysis and design of control systems using MATLAB. New Age Science
- 2 Kisačanin B, Agarwal GC (2001) Linear control systems: with solved problems and MATLAB examples. Springer US.
- 3 Ogata K (2008) MATLAB for control engineers. Pearson Prentice Hall

The dynamics of an LTI plant subject to the optimal stationary control based on a quadratic cost are described as

$$\begin{aligned}\dot{\mathbf{x}} &= \mathbf{Ax} + \mathbf{Bu} \\ \mathbf{e} &= \mathbf{Cx} \\ u &= -\mathbf{K}_R \mathbf{x}\end{aligned}\tag{C.1a}$$

in which $u \in \mathbb{R}$ for the sake of simplicity and without loss of generality. The control gain is $\mathbf{K}_R = \frac{1}{r} \mathbf{B}^\top \mathbf{S}$ where \mathbf{S} is solution of the following ARE:

$$\frac{1}{r} \mathbf{S} \mathbf{B} (\mathbf{B})^\top \mathbf{S} - \mathbf{S} \mathbf{A} - (\mathbf{A})^\top \mathbf{S} - \mathbf{C}^\top \mathbf{Q} \mathbf{C} = \mathbf{0}.\tag{C.1b}$$

The Laplace transform applied to Eq. (C.1a) leads to

$$\begin{aligned}\mathbf{X} &= \mathbf{G}(s)U \\ \mathbf{E} &= \mathbf{C}\mathbf{X} \\ U &= -\mathbf{K}_R \mathbf{X},\end{aligned}\tag{C.2}$$

in which the column vector $\mathbf{G}(s) := \Phi(s)\mathbf{B}$ represents the open-loop transfer matrix with $\Phi(s) := (s\mathbf{I} - \mathbf{A})^{-1}$. To analyse the stability of the closed loop refer to Fig. C.1, define $L(s) = \mathbf{K}_R \mathbf{G}(s)$, and determine the transfer function between the fictitious reference input U_R and the state \mathbf{X}

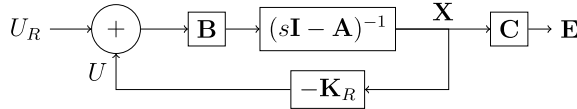


Fig. C.1: Control loop architecture

$$\frac{\mathbf{X}}{U_R} = \frac{\mathbf{G}(s)}{1 + L(s)} \quad (\text{C.3})$$

whose stability properties are provided by the so called *return difference* $1 + L(s)$. On the other hand, the ARE (C.1b) can be exploited to provide a lower bound for the norm of $L(s)$. In particular, after a premultiplication by $\mathbf{G}^\top(-s)$, a post multiplication by $\mathbf{G}(s)$, and some technicalities, one obtain

$$(1 + L(-s))(1 + L(s)) = 1 + \frac{1}{r}\mathbf{G}^\top(-s)\mathbf{C}^\top\mathbf{Q}\mathbf{C}\mathbf{G}(s), \quad (\text{C.4})$$

which, evaluated at $s = j\omega$, leads to

$$(1 + L(j\omega))^2 = 1 + \frac{1}{r}\mathbf{G}^\top(j\omega)\mathbf{C}^\top\mathbf{Q}\mathbf{C}\mathbf{G}(j\omega). \quad (\text{C.5})$$

Note that $\mathbf{G}^\top(j\omega)\mathbf{C}^\top\mathbf{Q}\mathbf{C}\mathbf{G}(j\omega)$ is a positive semi-definite quadratic form thanks to $\mathbf{C}^\top\mathbf{Q}\mathbf{C} \succeq 0$. As a consequence

$$|1 + L(j\omega)| = \sqrt{1 + \frac{1}{r}\mathbf{G}^\top(j\omega)\mathbf{C}^\top\mathbf{Q}\mathbf{C}\mathbf{G}(j\omega)} \geq 1. \quad (\text{C.6})$$

Equation (C.6), known as *return difference inequality*, implies that $L(j\omega)$ lives out of the unitary circle centered in the complex plane at $-1 + j0$, for any $\omega \in \mathbb{R}$, see Fig. C.2. Finally, in the worst case of $|1 + L(j\omega)| = 1$, when the phase of $L(j\omega)$ is $-\pi$, the gain margin ranges from $1/2$ to ∞ . On the other hand, even assuming $|1 + L(j\omega)| = 1$, the intersection with the unitary circle centered at the origin occurs at maximum at phases equal to $\pm 60^\circ$.

Note

The term $1 + L(j\omega)$ can be interpreted as $L(j\omega) - (-1 + j0)$, i.e., as a change of coordinate that moves the origin of the reference system from $0 + j0$ to $-1 + j0$.

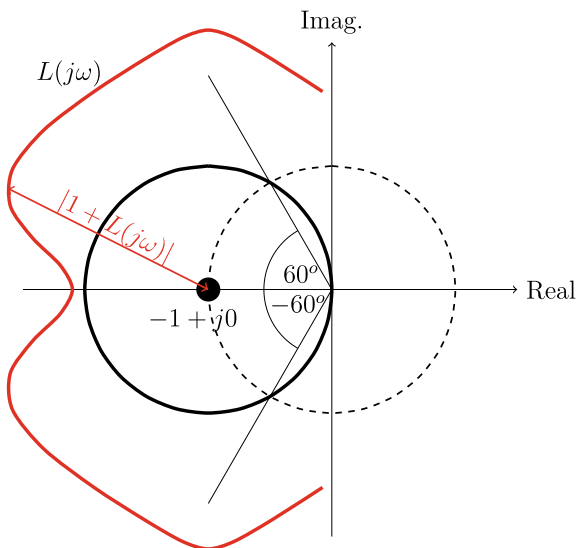


Fig. C.2: Graphical representation of the *return difference inequality*

References

- 1 Chen C, Holohan A (2014) A revisit of the stability robustness of linear quadratic regulators. In: 25th IET Irish signals systems conference 2014 and 2014 China-Ireland international conference on information and communications technologies (ISSC 2014/CIICT 2014), pp 310–315
- 2 Kalman RE (1964) When is a linear control system optimal? J Basic Eng 86(1):51–60

Index

A

Aerodynamic
downforce, 24
drag, 37
Algebraic Riccati Equation, 180

B

BIBS stability, 84
Bump model, 202
Burckhardt formula, 36

C

Control
adaptive, 235, 236
architecture, 16–18
closed-loop, 15
feedback, 15, 16
feed-forward, 15, 17, 149
linearized, 16
model predictive, 237
open-loop, 15
optimal, 177
output-feedback, 138
PID, 18
state-feedback, 126

Controllability, 120

Coordinates
change of, 67
Jordan, 74

Cost function, 178

Critical speed, 109

© The Editor(s) (if applicable) and The Author(s), under exclusive license to Springer
Nature Switzerland AG 2023

N. Mimmo, *Analysis and Design of Control Laws for Advanced Driver-Assistance Systems*, Advanced Textbooks in Control and Signal Processing,
<https://doi.org/10.1007/978-3-031-22520-8>

D

Detectable, 138
Disturbance, 7
Dual system, 189

E

Eigenvalue, 69
Eigenvector, 69, 70
chain length, 70
Equilibrium triplet, 12

G

Gain scheduling, 233

H

Hamiltonian function, 179

I

Incremental encoder, 33
Input, 7
control, 7
exogenous, 7
redundancy, 14
Integral action, 15, 128

K

Kalman
extended filter, 240
filter, 191
ultimate decomposition, 139

L

Linearization, 11
feedback, 238

M

Margin
gain, 181
phase, 181
Mass
sprung, 24, 28
unsprung, 24

Matrix, 261
Hurwitz, 85
invertible, 267
nilpotent, 79
Pseudo-inverse, 267
transfer, 145
triangular, 262

Modes, 77

Multiplicity
algebraic, 69
geometric, 70

N

Neutral steering, 109

O

Observability
complete, 131
decomposition, 134
matrix, 130, 131
Observer, 15, 16, 130
identity, 138
reduced-order, 137
Orthogonal complement, 68
Output, 7
controlled, 7
measurable, 7
readibility, 14
Oversteering, 109

P

Plant, 7
Pothole model, 202

R

Reachability, 119
complete, 121
matrix, 120, 121
transformation, 123

Reference, 7, 8

S

Sensor noise, 7
Separation principle, 139
Slip
longitudinal, 36
Stabilizable, 127
Stabilizer, 15, 17
State, 8
co-state, 179
Stiffness
aligning, 46
cornering, 107
Suspension, 23

U

Understeering, 109
gradient, 107

V

Vector, 261
relative degree, 150
Vector space, 267
basis, 68
image, 69
Kernel, 69

Z

Zero dynamics, 152